AD NUMBER: AD0858526

LIMITATION CHANGES

TO:

Approved for public release; distribution is unlimited.

FROM:

Distribution authorized to U.S. Gov't. agencies and their contractors; Export Controlled; 1 Jun 1969. Other requests shall be referred to Air Force Aero Propulsion Laboratory, Wright-Patterson AFB, OH 45433.

AUTHORITY

AFAPL ltr 12 Apr 1972

AFAPL-TR-69-44
PART III

PROPULSION SYSTEM INTEGRATION AND TEST PROGRAM (STEADY STATE)

PART III. NOZZLE INTERACTION DRAG TESTS

R. C. Westphal and R. H. Johnson
LOS ANGELES DIVISION OF NORTH AMERICAN ROCKWELL CORPORATION

TECHNICAL REPORT AFAPL-TR-69-44, PART III

June 1969

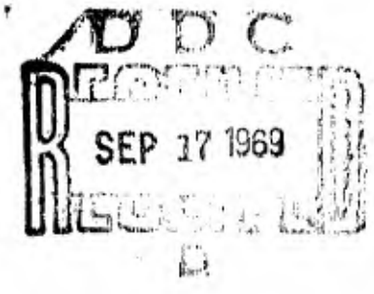

Air Force Aero Propulsion Laboratory
Air Force Systems Command
Wright-Patterson Air Force Base, Ohio

NOTICE

When Government drawings, specifications, or other data are used for any purpose other than in connection with a definitely related Government procurement operation, the United States Government thereby incurs no responsibility nor any obligation whatsoever; and the fact that the Government may have formulated, furnished, or in any way supplied the said drawings, specifications, or other data, is not to be regarded by implication or otherwise as in any manner licensing the holder or any other person or corporation, or conveying any rights or permission to manufacture, use, or sell any patented invention that may in any way be related thereto.

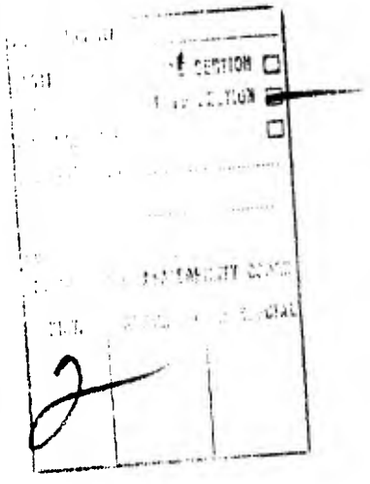

Copies of this report should not be returned unless return is required by security considerations, contractual obligations, or notice on a specific document.

AFAPL-TR-69-44
PART III

PROPULSION SYSTEM INTEGRATION AND TEST PROGRAM (STEADY STATE)

PART III. NOZZLE INTERACTION DRAG TESTS

R. C. Westphal and R. H. Johnson

FOREWORD

The effort described in this part of the report was conducted under Phase II, Task IIB of Air Force Contract F33615-67-C-1829, Project numbers 668A and 3066, "Propulsion System Integration and Test Program (Steady State)". The afterbody interaction tests described herein were conducted from 6 January 1969 through 13 January 1969 at the Trisonic Wind Tunnel of the Los Angeles Division, North American Rockwell Corporation.

The program was sponsored by the Air Force Aero Propulsion Laboratory, Wright-Patterson Air Force Base, Ohio. Squadron Leader Brian Brimelow (RAF), Air Force Aero Propulsion Laboratory, was the program monitor. This report was submitted by the authors on 30 January 1969.

This Technical Report consists of six parts. The titles of the six parts, along with the portion of the Phase II effort to which each is addressed, are shown below.

Part I.	Thrust Diverter/Vectoring System Flow Tests (Allison)	Task I
Part II.	Shared Exit Ejector Nozzle Static Tests	Task IIA
Part III.	Nozzle Interaction Drag Tests	Task IIB
Part IV.	Inlet Drag Tests	Task IIIA
Part V.	Low Speed Auxiliary Inlet Tests	Task IIIB
Part VI.	YTF-33 Turbofan Engine Tests	Task IIIC

Part III of the report has also been published as Los Angeles Division of North American Rockwell Corporation number NA-68-939, Part III, dated February 1969.

Publication of this report does not constitute Air Force approval of the report's findings or conclusions. It is published only for the exchange and stimulation of ideas.

Ernest C. Simpson
Chief, Turbine Engine Division

ABSTRACT

Near-wake and far-wake nozzle jet effects on forces on the aft end of a .09 scale simulated fighter airplane were tested at mach numbers of .6, .85, 1.27, 1.7 and 2.0. Cold air was used for producing the simulated engine exhaust jets. Model configuration changes included various boattail angles, inlet bluntness, wing sweep, and horizontal tail on and off. Data obtained include chord force, normal force, and pitching moment from an internal balance, external static pressure distributions and chord force determined from integrated pressures, and schlieren and shadowgraph photographs of exhaust plumes. At subsonic mach numbers, the far-wake jet effects on chord force of plug nozzles located forward on the afterbody were unfavorable. At supersonic mach numbers, the plug nozzle far-wake effects were favorable. Jet effects of the convergent-divergent nozzles located at the aft end of the model were favorable for all mach numbers.

(The reverse of this page is blank)

TABLE OF CONTENTS

(The reverse of this page is blank)

BLANK PAGE

LIST OF ILLUSTRATIONS

LIST OF TABLES

(The reverse of this page is blank)

BLANK PAGE

LIST OF SYMBOLS

A_9	convergent-divergent (C-D) nozzle exit area
A_M	fixed area at upstream end of the C-D nozzle shroud
C_c	afterbody chord force coefficient = $\frac{\text{chord force}}{qS}$
C_N	afterbody normal force coefficient = $\frac{\text{normal force}}{qS}$
C_M	afterbody pitching moment coefficient = $\frac{\text{pitching moment about airplane C.G.}}{qS\bar{c}}$
$\Delta C_{(\ )}$	afterbody force coefficient increment = $C_{(\ )}$ **(conf. of interest)** $- C_{(\ )}$ **(baseline conf.)**
C_P	pressure coefficient = $\frac{P - P_o}{q}$
$\bar{c}$	mean aerodynamic chord (.853 ft)
M	freestream mach number
P_T	plug nozzle or C-D nozzle total pressure
P_o	freestream static pressure
P_9	static pressure at C-D nozzle exit
P_S	local static pressure
q	freestream dynamic pressure
S	model wing area (S = 3.029 square feet)
α	model angle of attack (in degrees)
Λ or λ	leading edge wing sweep angle
ϕ	radial position on afterbody

Subscripts:

$(\ )_{C-D}$	refers to convergent-divergent (C-D) nozzle
$(\ )_{PLUG}$	refers to plug nozzle

$(\ )_{AB}$	refers to model afterbody, excluding plug and C-D nozzle areas
$(\ )_{BASE}$	refers to model base area between C-D nozzles
$(\ )_{TOT}$	refers to total value

Section I

INTRODUCTION

Accurate propulsion system component performance characteristic data are essential for performing a propulsion system optimization study. These data must be applicable to the environment in which the components will operate in service. Obtaining these data by analytical means is desirable because proven analysis techniques generally provide a wide range of data at relatively low cost. Analytical techniques for deriving component performance characteristics usually provide insight into the basic physical phenomena governing component losses. Often these techniques also provide a means of estimating the minimum losses which are likely to be attained and, in most cases, will suggest the design approach which can achieve the minimum loss condition.

If reliable analytical techniques are not available, data acquisition by test program is necessary. A number of loss phenomena associated with propulsion system optimization and integration studies have not been adequately simulated by analytical means, particularly in the areas where complex interactions between two or more components is prevalent. In addition, available analytical techniques often require the input of constant factors, highly dependent on configuration, the values of which must be determined empirically.

One of the primary objectives of the Propulsion System Integration and Test Program (Steady State) was to provide an overall approach to predicting the performance of a propulsion system in a multimission aircraft. In Phase I, available analytical techniques and test data were used in the performance analysis of the propulsion systems in two example vehicles. In a number of areas, the available data and techniques did not provide assurance that the performance predictions for propulsion system components operating in an installed environment were sufficiently accurate and general to define the vehicle performance over its full range of operating conditions.

Phase II of the program was set up to carry out test programs designed to provide the component performance definitions identified during the Phase I analysis effort as being necessary for a thorough propulsion system performance evaluation and not available from existing data or analysis techniques.

The purpose of this report is to describe the results of a wind tunnel test program designed to obtain nozzle exhaust interaction forces on the aft end of a vehicle.

Available test data indicate that the presence of a nozzle jet can have a significant influence on base and boattail drag levels. In addition, for a nozzle discharging upstream from part of the vehicle structure, drag phenomena, both favorable and unfavorable, are likely. The internal performance of certain nozzle types, operating below their design pressure ratios, can be strongly influenced by the external flow field around the nozzle discharge. In the Phase I vehicle studies, it was determined that the optimum vehicle designs could experience all of these interaction phenomena, therefore, this test was designed to achieve a better understanding of these interaction effects on an overall vehicle model.

Section II

SUMMARY

A wind tunnel investigation has been conducted to determine the differences in afterbody forces caused by exhaust jet interaction and afterbody configuration changes. All testing was conducted in the North American Rockwell Corporation (NR) Trisonic Wind Tunnel using a strut mounted .09 scale model similar to a tactical fighter type airplane. Testing was performed at freestream mach numbers of .6, .85, 1.27, 1.7 and 2.0. The model angle of attack was varied between zero and 10 degrees, the nozzle pressure ratio between off and 18.5, and the aft boattail angle between zero and 13.5 degrees. Although the entire vehicle shape was simulated, the model was constructed to measure only the forces and pressures on the aft portion of the model. Engine operation was simulated by ducting cold air to the model through a strut and exhausting the air at controlled pressure ratios through two pairs of nozzles built into the model. Two pairs of nozzles were used in order to obtain both near-wake and far-wake effects on one model. Nozzle thrust forces were not measured and were isolated from the external aft end model shell. Measured forces were obtained by both force measurements on a six component internal balance (only three components were used, normal force, chord force and pitching moment), and by integrating measured external pressures to obtain chord force.

This report presents the results from the tests. Comparisons of data and analytic predictions are made and discussed.

The results obtained include chord force, normal force and pitching moment balance data, integrated pressure chord force data, afterbody external pressure distributions, and schlieren and shadowgraph pictures of the engine exhaust plumes. Most of the afterbody force data are presented as increments from a baseline (common) configuration that was tested at all mach numbers. If tests were to be performed on an aerodynamic model that embodied the baseline afterbody configuration, the incremental forces herein could be applied to the data from the aerodynamic model to adjust for nozzle configuration and jet effects.

The baseline afterbody boattail angle was 6.7 degrees. This angle was varied between zero degrees and 13.5 degrees, but not at each mach number. At mach numbers of .614 and .85, the chord force increased by only 5 counts as the boattail angle changed from 6.7 to 13.5 degrees, jets off. At mach numbers of 1.27 and 1.7, the chord force varied about plus and minus 25 counts as the boattail angle ranged between 10.0 and 2.4 degrees, jets off. At mach number 2.0, the chord force decreased by about 25 counts as the boattail angle went from 6.7 to zero degrees, jets off. The above values agree fairly well with estimated configuration effects.

A simulated no-flow inlet was tested with a sharp fairing and with the fairing removed. The wing was tested at sweep angles of 30 and 70 degrees. The effect of inlet bluntness and wing sweep on force increments was

negligible at all mach numbers tested.

Jet effects were tested with two plug nozzles located forward on the afterbody, and with two convergent-divergent (C-D) nozzles located at the aft end of the model. The plug nozzle jet effects on chord force were unfavorable at mach numbers .6 and .85. Measured chord force increments from the baseline were about plus 15 counts. Estimated plug nozzle effects did not include far-wake effects on the afterbody and predicted favorable jet effects of about the same amount. At mach numbers 1.27, 1.7, and 2.0, plug nozzle jet effects were favorable and were reasonably close to predicted values. The worst agreement was at mach number 1.27.

The C-D nozzle jet effects on chord force were favorable at all mach numbers tested. At mach numbers .6 and .85, a reduction in chord force of up to about 15 counts was measured. The measured increments agreed quite well with estimates when the flow in the C-D nozzles was not separated. At the supersonic mach numbers, the C-D nozzle jet effects were estimated to be zero, but small reductions in chord force were measured.

At the subsonic mach numbers, the maximum plug nozzle jet effects caused an increment in normal force of about minus .02. The C-D nozzle jet effects were about one half the plug nozzle effects. From horizontal tail off data, it was determined that the jet effects were mostly on the horizontal tail. At the supersonic mach numbers, the jet effects on normal force were quite small.

The C-D nozzles were constructed with a sharp trailing edge to simulate full scale nozzles. In addition, the split between the metric and the nonmetric portion of the aft end of the model was located internally to avoid having a gap on the external surface near the trailing edge of the C-D nozzles. As a result, some large tare forces and other corrections were encountered on some runs with the C-D jets operating. Chord force data obtained with the internal balance for these runs is questionable. It appears, however, that slight changes in the construction details of the nozzle could result in a much improved situation.

Section III

APPARATUS AND PROCEDURE

MODEL DESCRIPTION

The model tested was similar to one of the tactical fighter airplanes developed during Phase I studies of this program. A drawing of the .09 scale model is shown in figure 1. In order to test both near-wake and far-wake jet effects on the same model, four nozzles have been used. Two are fixed geometry plug nozzles and two are variable geometry convergent-divergent (C-D) nozzles. The plug nozzles are located forward on the afterbody and were designed primarily to show far-wake jet effects. The convergent-divergent nozzles are located at the aft end of the model. Various nozzle shrouds were provided to test near-wake jet effects with different boattail angles. All nozzle configurations have a sharp trailing edge to represent as near as possible the full scale dimensions. Maintaining a sharp trailing edge is thought to be important to properly simulate the near-wake jet effects. A strut support, encompassing the vertical stabilizer, was added to support the model in the tunnel and to route high pressure air to the nozzles. The inlet openings have been faired over on the model. Two fairings were tested; a sharp fairing (as shown in figure 1) and a more blunt configuration which was the basic inlet with the sharp fairing removed. No air passed through the inlet. The bottom mold line of the model between the two aft nozzles was slightly modified to provide room for internal plumbing. The modification resulted in a slightly steeper boattail prior to the base. All other vehicle geometries have been held to those developed during Phase I studies. A sketch and photographs of the model installed in the tunnel are presented in figures 2, 3 and 4.

The fuselage of the model from station 40.32 aft has been constructed as a shell surrounding the internal plumbing as shown in figures 1 and 2. On this shell, which includes the horizontal stabilizer as well as the plug and C-D nozzles, measurements were made to determine the force changes induced by jet effects. The metric shell was carried far enough forward to include all significant changes due to jet effects on the afterbody of the model as shown in figure 5. An exploded view of the model showing the metric afterbody and its relation to the rest of the model is shown in figure 6.

To separate the nozzle internal thrust force from the external shell force as much as practical and still maintain a sharp trailing edge shroud required that the nozzles be manufactured in two pieces. This was accomplished by constructing the nozzles as an external shroud and an internal liner, as shown in figure 7. For the C-D nozzles, the split line between these two parts occurs on the inside of the nozzle. This internal split required the installation of an inflatable type seal which would prevent the nozzle flow from traveling forward, between the liner and shroud, and exit at the afterbody split (station 40.37). On the plug nozzle, the split between the shroud and liner occurs on the external portion of the nozzle. Because the split is not exposed to the internal nozzle flow, a seal arrangement was not required.

Afterbody configuration changes were accomplished by using a series of nozzle shrouds and liners to vary the C-D nozzle exit area and area ratios. The individual shrouds and liners used are shown in figure 8 with each of the afterbody configurations shown in figures 9 and 10. For the plug nozzle and three C-D nozzle configurations, conical closures were used for some tests. The C-D and plug nozzle cone configurations are sketched in figure 11. The main purpose of the cones was to provide a simple axisymmetric shape that could be easily tested and that was amenable to the available subsonic analytical tools. The A_9/A_M = .5 cone configuration was the common, or baseline, configuration tested at every mach number. The cones are attached to the non-metric portion of the model and forces on them are not measured. Figure 12 shows the external C-D shroud configurations along with the corresponding internal nozzle area ratios tested at the various mach numbers.

Additional configuration changes made during this investigation included the inlet fairings mentioned previously, and a variable sweep wing.

To provide independent control over each of the nozzle systems, each system was supplied with high pressure cold air from separately metered sources. This separation of flows allowed the plug and C-D nozzles to be operated at different weight flows and pressure ratios.

Because the purpose of this investigation was to determine jet effects on vehicle forces, the internal flow system was only required to generate a representative exhaust plume shape and not simulate thrust. For this reason, no provisions were made to measure nozzle thrust. The nozzle exit static pressure ratio was monitored, however, and may be used as a correlating parameter with the static nozzle test data reported in Part II of this report.

INSTRUMENTATION

Measurements of forces and moments were obtained using two electrical strain gage balances. A six component balance was located in the forebody of the model and was attached to the aft shell by using a sting type connector. Since the model was symmetrical and was not yawed, only three components were used. The other balance, a single component type, was located in the vertical support strut and attached directly to the aft shell. This single component balance was necessary to provide support and prevent excessive deflection between the forebody and aft shell.

Pressure instrumentation consisted of a total of 96 static and total pressure tap locations. The locations of these taps are shown in figure 13. Fifty-three of these were external static taps located on the aft shell and horizontal tail. Internal flow measurements and force corrections were based on the pressure data of the 43 taps located throughout the interior of the model. Two 9-tube boundary layer rakes were also provided but were not tested.

A system was provided to indicate grounding between the aft shell and the internal plumbing parts. If grounding existed, a light was turned on

and the tape data was marked. No grounding occurred during the time data were being obtained.

Photographs of the exhaust plumes were obtained with a shadowgraph system in the transonic test section and with a schlieren system in the supersonic test section of the tunnel.

TEST FACILITY AND INSTALLATION

The North American Rockwell Trisonic Wind Tunnel is an intermittent blow-down facility with a 7 foot by 7 foot tandem test section capable of mach numbers from .1 to 3.5.

A drawing of the model installed in the wind tunnel is shown in figure 14. The model internal air supply was routed from an external source through the sting assembly and support strut to the model. Angle of attack variation was accomplished by rotating the wind tunnel sector using a pitch and pause method of positioning for pre-selected values of angle of attack.

All instrumentation lines were routed through the strut and sting assembly and connected to leads located beneath the tunnel floor.

TEST PROCEDURE

Determination of exhaust interaction effects on vehicle drag required that nozzle pressure ratio (both plug and C-D), aft end geometry, freestream mach number and angle of attack be used as variables during this investigation. To accomplish this, angle of attack or nozzle pressure ratio was varied during a constant mach number run with configuration changes being made between runs. The run index is shown in table I. The index is grouped by mach number and major configuration changes for easy reference, rather than listed by consecutive blow number.

The ranges over which the variables were investigated are as follows:

A_9/A_M = .15 - 1.0
M = .60 - 2.0
Angle of attack = zero - 10 degrees
$(P_T/P_O)_{Plug}$ = cone - 10.0
$(P_T/P_O)_{C-D}$ = cone - 18.5

A_M is defined as the nozzle cross-sectional area at the shroud hinge line (station 50.31) and A_9 is the C-D nozzle exit area. The variables encompass the ranges expected in flight.

To permit angle of attack or nozzle pressure ratio to be varied through five values during a run required the wind tunnel run time to be of approximately 25 second duration. Tunnel Reynold's numbers associated with this run time are as follows:

M	R_N/ft
.6	$5.\times 10^6$
.85	$6.\times 10^6$
1.25	$7.\times 10^6$
1.70	$9.\times 10^6$
2.0	9.3×10^6

Data gathered during a run was stored on a magnetic tape which was then processed on an IBM 1800 data acquisition system.

DATA PRESENTATION

All force data resulting from this investigation, with the exception of the baseline configuration data, is presented in terms of an incremental force coefficient. This incremental coefficient is defined as the difference between the force coefficient of the afterbody configuration of interest and the force coefficient of the baseline afterbody configuration.

$$\Delta C = C_{\left|\begin{matrix}\text{conf. of}\\ \text{interest}\end{matrix}\right|} - C_{\left|\begin{matrix}\text{baseline}\\ \text{conf.}\end{matrix}\right|}$$

The baseline configuration has a value of $A_o/A_M = .5$, the cones are on the plug and C-D nozzles, and the model is at 3 degrees angle of attack.

The test results are presented in the model body axis (chord force, normal force, and pitching moment) rather than lift, drag, and pitching moment. A sketch indicating the positive direction for each of these forces is shown in figure 15. The normal force and chord force data can, of course, be resolved into lift and drag if required. Chord force is perhaps, somewhat more meaningful than drag since the afterbody data would be used in propulsion system analysis to correct the engine thrust. The thrust vector is more closely aligned with the chord force than the drag, especially at angle of attack. Also, for the present tests, external surface pressures on the afterbody were measured and integrated in the chord force direction. These values may be used to compare with the internal force balance data, also in the chord force direction.

Pressure distribution occurring on the external surfaces of the afterbody and horizontal tail are plotted in pressure coefficient form (C_P) versus model station. Internal pressures occurring in the nozzle are plotted as the ratio of nozzle static to freestream static pressure (P_S/P_o) versus model station. All of these data were plotted with an IBM CRT unit.

All data resulting from this test is reported, in tabulated form, in the wind test report, reference 1. For convenience, a tabulation of the data is presented in table II.

Section IV

RESULTS AND DISCUSSION

AFTERBODY INTERACTIONS

Afterbody forces have been determined for a range of C-D nozzle configurations and both C-D and plug nozzle pressure ratios. Interactions brought about by geometry changes or nozzle exhaust jets are indicated as incremental changes in the force data.

For those test blows with the jets off or with just the plug nozzle jet operating, the chord force increments obtained from the internal balance and from integrated external pressures are in good agreement. For these blows, the balance tare corrections are small. With the C-D nozzle on, however, the balance data was subjected to large tare forces plus a static correction which tends to make these data somewhat questionable. Chord force data requiring these corrections have been omitted from the main body of this report. The results presented are based on integrated pressures. A discussion of the jet-on chord force balance data, however, is presented in the Appendix for selected configurations and mach numbers.

Measurement of normal force and pitching moments with the force balance was unaffected by the operation of the jets. Therefore, all normal force and pitching moment data presented are based on force balance measurements.

JET OFF DATA

Angle of Attack and Configuration Effects

During development testing for an actual air breathing vehicle, wind tunnel tests would be performed to obtain aerodynamic data. In order to link the aerodynamic and the afterbody tests together, data from a common, or baseline, configuration would be obtained from both types of test. In this instance, there is no actual vehicle, and no aerodynamic tests were performed during the program. To provide a realistic exercise, however, a baseline configuration, $A_9/A_M = .5$ (see figure 11), was tested at each mach number. In addition to the baseline configuration, jet off data were obtained on a number of other model configurations. If desired, the jet effects may be referenced to some C-D nozzle area ratio other than $A_9/A_M = .5$, but not throughout the mach number range (see figure 12).

Chord Force

Figure 16 shows both force and integrated pressure chord force data at $M = .614$ for C-D area ratios of $A_9/A_M = .15$, .3, and .5. The main reasons for the differences between the levels of the force data and the pressure data are that the pressure data are not integrated over the horizontal tail and do not reflect skin friction forces. The effect of changing the C-D boattail angle is seen to be small. Figure 17 shows similar data for

M = .85. On figures 18 and 19, the C-D area ratios of A_9/A_M = .3, .5 and .8 show large differences in chord force at mach numbers of 1.27 and 1.7. On figure 20, increasing the C-D area ratio from A_9/A_M = .5 to A_9/A_M = 1.0 is seen to reduce the chord force by about 25 counts at M = 2.0. In all cases the effect of angle of attack is to reduce the chord force. The reduction was about 20 counts between 0 and 10 degrees angle of attack for all cases.

Normal Force

Normal force values presented in figures 21 through 25 were obtained from force balance measurements. No attempt was made to determine normal forces using pressure data.

Changes in afterbody normal force, brought about by changing the afterbody configuration, varied between approximately .007 and .010 subsonically and .003 and .010 supersonically. These changes in normal force were about the same for all angles of attack. The change in normal force however, showed large changes with angle of attack as would be expected with a fixed position horizontal tail.

Pitching Moment

Evaluation of the pitching moment is dependent on the value of the normal force, therefore, characteristics mentioned previously for the normal force were also exhibited in the pitching moment. An increasing normal force results in a decreasing pitching moment which is consistent with the sign convention of figure 15. The variation in the pitching moment values are shown in figure 26 through 30.

Baseline Summary

The values of chord force, normal force and pitching moment coefficient throughout the mach number range are summarized in figure 31, 32, and 33. Both force and pressure data are shown for chord force with normal force and pitching moment data being obtained from balance measurements. All values shown are for 3 degrees angle of attack. The values of chord force, normal force and pitching moment shown are the values used to obtain all incremental data shown herein unless otherwise stated. At M = .6, the wing sweep is 30 degrees. At all other mach numbers the wing sweep is 70 degrees. As a matter of interest, the afterbody chord force as measured by the balance, is approximately 40 percent of the total vehicle low angle of attack drag throughout the mach number range.

Incremental Configuration Effects

The effects on chord force of changing C-D nozzle area ratio (A_9/A_M), and hence the boattail angle, are summarized in figure 34. Both force data and integrated pressure data are shown and are seen to be about the same. Also shown are estimated values of chord force increments. For the subsonic mach numbers, the estimates were made by representing a portion of the model

with an equivalent body of revolution and calculating the pressure distribution using the Douglas-Neumann analysis. The calculated pressures were integrated to obtain the chord force increments. For supersonic mach numbers, the estimates were made using a wave drag analysis method. The actual model shapes were used in the analysis. The agreement between the measurements and estimates is fairly reasonable. Data and estimates are shown at zero angle of attack, where the estimates were made. Afterbody configuration effects have also been summarized for an angle of attack of 3 degrees. These data, representing the pressure data only, are presented in figure 35.

The measured C-D nozzle configuration effects on normal force and pitching moment increments are summarized in figure 36 and 37. The data, shown for 3 degrees angle of attack, indicates that the changes in normal force and pitching moment are relatively significant. No estimates were made for either normal force or pitching moment.

Repeat blows were made at M = .85 and 1.27. The data shown on figures 38 and 39 indicate good repeatability.

Inlet Fairing Effects

In tests of this type, where aft-end forces are being determined, it is important to know how exactly the rest of the model must also be represented. In an attempt to obtain some information on forebody effects on afterbody forces, two inlet shapes were tested. The basic shape consisted of a sharp fairing which extended forward of the inlet face as shown in figure 1. This sharp fairing was removable, leaving a much blunter solid inlet face. Both shapes were tested at all mach numbers with the jets off. The results are shown in figures 40 through 54. The effect of blunting the inlet face is seen to be negligible on the measured chord force, normal force and pitching moment.

Wing Sweep Effects

Two wing sweep angles, 30 and 70 degrees, were tested at M = .85. As shown in figure 55 through 57, the effect of changing sweep angle has a negligible effect on afterbody force coefficients.

JET EFFECTS

Prior to the test, estimates of chord force increments were made for various configurations and jet pressure ratios. These estimates are shown in figures 58 through 62. For the C-D nozzles, the original estimates assumed nozzles with sonic flow at the exit and plume shapes were calculated for this type of nozzle. Later, in order to reduce the tare forces and to be able to better control the nozzle pressure ratios, it was decided to test C-D nozzles. As a result, the nozzle exit static pressure was considerably different for a given total pressure. The chord force estimates shown at M = .614 and .85 were made assuming that the nozzle exit static pressure determined the plume shape, and hence the chord force increments. The estimates are shown at the corresponding total pressure ratios. At the lower

total pressure ratios, the exit static pressure ratio is considerably below unity, particularly at $A_9/A_M = .5$. The high chord force estimates are due to extrapolating to low pressures and ignoring the possibility of flow separation. Flow separation was noted during the test, however, for exit static pressure ratios less than approximately .6.

The estimation technique used to account for the plug nozzle effect could not simulate a far-wake jet effect. Therefore, only the near-wake jet effect of the plug nozzle is included in the estimated data. This lack of a far-wake effect in the estimates results in poor comparison with the data, as shown in figures 67 and 72. The estimated data indicates a decrease in chord force with increasing pressure ratio while the test data indicates just the opposite effect.

In the following sections, incremental force coefficients due to C-D nozzle jet effects are plotted versus both the ratio of the C-D nozzle total pressure to ambient static $(P_T/P_{o(C-D)})$ and the ratio of the C-D nozzle internal exit static pressure to ambient static pressure $(P_9/P_{o(C-D)})$. Plots versus total pressure ratio are presented only because the data were obtained using nozzle total pressure as a controlled setting.

The total pressure ratios do not correspond to engine power settings.

Presenting the data versus static pressure ratio is more general. If actual power settings and nozzle geometry are known, the exit static pressure ratio may be determined. The static pressure ratio is also the most predominate parameter in determining plume shape. Finally, the internal nozzle performance data, presented in Part II of this report, may be linked to the external force increments by way of the exit static pressure ratio.

Both estimated and measured data were converted from total pressure ratio to static pressure ratio by using the relations presented in figure 63. The curves on this figure were based on measured pressure data from the various C-D nozzle configurations.

For all C-D nozzle configurations tested, the nozzle flow separated for exit static pressure ratios below approximately .6. Once the flow separated, the static pressure ratio jumped to a value near unity. To identify separated points on the curves plotted versus total pressure ratio, only data points with attached flow have been faired through with a curve. On the curves plotted versus static pressure ratio, the separated points have been omitted.

Chord Force Increments

$M = .614$

C-D nozzle jet effects on chord force, as determined from integrated pressure data, are plotted versus total pressure ratio in figures 64 through 66. In figure 64, the cone was on the plug nozzle and the C-D nozzle pressure ratio was varied. A maximum chord force reduction due to jet effects of about 12 counts is noted. On figure 65, the plug nozzle pressure ratio

is held constant at 2.0 and the C-D pressure ratio is again varied. Operating the plug nozzle is seen to have an unfavorable effect. The plug nozzle at a pressure ratio of 5.0 is shown in figure 66. A chord force increase of as much as 12 counts is seen. The plug nozzle effect, with cones on the C-D nozzle, is shown in figure 67. An unfavorable measured chord force increment of 15 counts is noted. The estimated increment, shown by the dashed line, does not include far-wake effects and is seen to be a poor estimate. For all figures, the data points with cones on are plotted at a pressure ratio of 1.0.

Figure 68 shows the effect of C-D nozzle exit static pressure ratio on the chord force increment. For the various nozzle configurations shown, increasing the pressure ratio is seen to reduce the chord force, but not drastically. For example, a 10 count reduction in chord force required an increase in static pressure ratio from .6 to 2.1 for the A_9/A_M = .3 configuration. The solid data points represent chord force increments for configurations with conical fairings installed on the C-D nozzles. These values do not have a unique location on the static pressure ratio axis. They are therefore arbitrarily plotted at the pressure ratio that is estimated to produce a plume shape whose initial angle is the same as that of the cone. The estimated values shown correspond to those on figure 58, but plotted versus static pressure ratio. The measured points correspond to those in figures 64 through 66, plotted versus static pressure ratio. Note that the estimates compare reasonably well with the measurements when the plug nozzle is not operating.

M = .85

Figures 69 through 71 show the C-D nozzle total pressure ratio effect for plug nozzle pressure ratios of 2.0 and 5.0 with the cone installed. The curves appear similar to the M = .614 data with a maximum chord force reduction of about 7 counts. The plug nozzle far-wake effect is again seen to be unfavorable by 15 counts on figure 72, as opposed to the estimate.

The effect of C-D exit static pressure ratio is presented in figure 73. Estimated increments are also shown on figure 73. Comments on the M = .85 data and estimates are similar to those for M = .614.

M = 1.27

At M = 1.27 and the other supersonic mach numbers, fewer blows were made since C-D nozzle jet effects were estimated to be negligible. Figure 74 shows C-D nozzle jet effects on chord force with the plug nozzle operating at a pressure ratio of 3. At a C-D nozzle area ratio of A_9/A_M = .5, a chord force reduction of 20 counts is measured with both plug and C-D nozzle jets operating. Thus, the C-D nozzle jet effects are not negligible. At the higher C-D nozzle area ratio (lower boattail angle), the jet effect is less, as would be expected. Figure 75 shows plug nozzle jet effects. For subsonic mach numbers, the plug jet effect was unfavorable, however at this mach number, it is seen to be slightly favorable. Chord force increments versus C-D nozzle static pressure ratio are shown in figure 76. An

increasing pressure ratio is seen to reduce the chord force for all configurations. As mentioned, the estimated C-D jet effects were negligible and the estimate appears as a horizontal line in figure 76. Unlike the subsonic cases, large configuration effects are noted at M = 1.27 with either C-D or plug nozzles operating.

M = 1.7

Figure 77 shows C-D nozzle jet effects with the plug nozzle pressure ratio held constant at 5.0. Favorable, but smaller C-D nozzle jet effects are measured. The plug nozzle jet effects, with the C-D nozzle jet pressure ratio constant at 10.0, are shown in figure 78. The plug nozzle effects are again favorable. Figure 79 presents the incremental chord force versus C-D nozzle static pressure ratio. Slightly favorable near-wake jet effects are again shown as the pressure ratio increases. Large configuration effects are again noted. The estimates are seen to be in reasonable agreement with the measurements.

M = 2.0

The C-D nozzle jet effects are quite small, as seen in figure 80, with the plug nozzle pressure ratio held constant at 5.0. Plug nozzle jet effects are also small as noted in figure 81. The C-D nozzle pressure ratio was held constant at 15.0. C-D nozzle static pressure ratio effect is shown in figure 82. As was noted at the other two supersonic mach numbers, substantial configuration effects are present. Here the estimates agree very well with the measurements.

Chord Force Summary

For practical operation of a C-D nozzle, the exit static pressure ratio will very likely be near unity. It may be noted in figures 68, 73, 76, 79, and 82 that the chord force increment is a relatively weak function of the exit static pressure ratio for a given value of A_9/A_M. In fact, with little loss in accuracy, the value of chord force increment at P_9/P_o = 1.0 may be taken to represent a range of exit static pressure ratios of from .6 to 1.2. This has been done and the results are shown as the solid lines in figures 83 and 84 for various values of plug nozzle pressure ratios. Note that the chord force increment may be plotted versus A_9/A_M, which is convenient for a thrust minus drag evaluation. The dashed lines are taken from figure 35 and represent data with the jets off.

At the subsonic mach numbers, the jet effects are predominant. At the supersonic mach numbers, the configuration effects are predominant.

Normal Force Increments

M = .614

The effect of C-D nozzle total pressure ratio is shown in figures 85, 86 and 87. Values of normal force increment are presented for plug pressure ratios of cone, 2.0 and 5.0. Increasing C-D nozzle pressure ratio increases the

afterbody normal force with the A_9/A_M = .5 area ratio configuration experiencing the largest values of normal force. The effect of plug nozzle pressure ratio for the case with a cone installed in the C-D nozzles is shown in figure 88. All configurations show a decreasing normal force with increasing plug pressure ratio with changes of .012 being noted between a pressure ratio of 1.5 and 5.0. Blows conducted with the horizontal tail removed indicated that the major portion of the normal force and the incremental changes occurred on the tail itself. This data will be presented in a following section.

Incremental changes in normal force plotted versus C-D nozzle exit static pressure ratio are presented in figure 89, 90 and 91. An increasing pressure ratio is accompanied by an increasing normal force for all configurations.

M = .85

Changes in normal force increments due to C-D nozzle total pressure ratio are similar to the effects noted at M = .614 with the magnitude of the normal force being generally smaller than the M = .614 values. These data are shown in figures 92, 93 and 94. The effect of plug nozzle pressure ratio is presented in figure 95. This pressure ratio effect is also similar to that noted at M = .614 with the magnitude of the normal force again being slightly smaller. Exit static pressure ratio effects are shown in figure 96, 97 and 98. As with the M = .614 cases, increasing pressure ratio values increase the normal force.

M = 1.27

C-D nozzle jet effects on normal force are shown in figure 99. The changes in normal force are presented for a plug pressure ratio held constant at 3.0 while the C-D pressure ratio was varied. For A_9/A_M ratios of .5 and .8, the effect of increasing total pressure ratio is to reduce the normal force. The largest value of normal force and the greatest change due to pressure ratio occurred at A_9/A_M = .8. At A_9/A_M = .3 the effect of increasing C-D total pressure ratio is to increase the normal force slightly with a change of .001 being noted between pressure ratios of 3.0 and 12.0. Plug nozzle jet effects with the C-D pressure ratio held constant at 8.0, are shown in figure 100. An increasing pressure ratio increases the normal force slightly at A_9/A_M ratios of .3 and .5 while reducing the normal force at A_9/A_M = .8. Presenting the normal force increments versus nozzle exit static pressure ratio, figure 101, indicates the same trend described in the total pressure ratio plots. However, the slope of the A_9/A_M = .8 curve is very steep indicating a sensitivity to P_9/P_o.

M = 1.7

At this mach number, the plug pressure ratio was held constant at 5.0 when the C-D pressure ratio was varied. The resulting data is shown in figure 102. Slight decreases in normal force are shown with increasing total pressure ratio. Changes in normal force with increasing plug pressure ratio for a constant C-D pressure ratio of 10.0 is shown in figure 103. The effect

is seen to be a small increase in normal force. An increasing C-D nozzle exit static pressure ratio is seen to reduce the normal force a small amount in figure 104.

M = 2.0

Varying the C-D nozzle pressure ratio with the plug nozzle pressure ratio held constant at 5.0 produced the data shown in figure 105. Total pressure ratio is seen to produce a small decrease in normal force. The maximum decrease being .001. Plug nozzle jet effects are shown in figure 106. Normal force is seen to increase with increasing pressure ratio. Exit static pressure ratio effect of the C-D nozzle are shown in figure 107.

Pitching Moment Increments

In the discussion of pitching moment increments for jet off conditions, the statement was made that characteristics exhibited by the normal force would also be present in the pitching moment. That is, an increasing normal force would result in a decreasing pitching moment. This statement is not necessarily true while either the plug or C-D nozzle are operating. Disturbances caused by the exhaust jets may produce changes in the pressure distribution over the afterbody and horizontal tail. The load distributions over the afterbody and horizontal tail, therefore, will also change. Determination of the pitching moment is dependent on the normal loads and the point of application, which itself is dependent on the load distribution. Therefore, it is conceivable that a condition can exist where the normal force increases, but the location of the point of application is such that the pitching moment also increases. Comparison of the data of figures 85 and 108 show such a condition for the A_9/A_M values of .15 and .30.

Presentation of data for the pitching moment increments is identical to the method used for chord and normal force. That is, the increments are plotted versus C-D total pressure ratio, plug nozzle total pressure ratio and C-D nozzle exit static pressure ratio. Data for subsonic mach numbers is presented in figure 108 through 121. Supersonic conditions are shown in figure 122 through 130.

Angle of Attack Effects

At each mach number tested, angle of attack sweeps were made with both plug and C-D jets operating at a constant value. Figure 131 shows the chord force increments at M = .614 with both plug and C-D nozzle jets at a pressure ratio of 2.0. Also shown are data from other blows with the jets operating at the same pressure ratio for the same and for different C-D nozzle area ratios. Good repeatability is noted at the same area ratio. The area ratio (configuration) effects are small and about the same as they were with the jets off. Figure 132 shows similar data for M = .85. For blows 26 and 27, however, the data are questionalbe since the internal pressure readings for the left and right C-D nozzles were different. This could indicate that one, or both, of the nozzles had separated flow. Figures 133, 134 and 135 show data at mach numbers 1.27, 1.7 and 2.0. As for the M = .614 data, good repeatability is noted, and configuration incremental effects are comparable

to jet off increments.

Normal force increments are shown in figure 136 through 140. Changes caused by varying angle of attack are similar to the jet off data.

Figures 141 through 145 present the pitching moment increment versus angle of attack. The data is again similar to jet off results.

Horizontal Tail Effects

Three blows were made at M = .85 with the horizontal tail removed in an attempt to reconcile the differences between chord force data obtained with the force balance and integrated pressures. The results are shown in figure 146, 147 and 148. With the tail removed the difference between the force and pressure data should be the amount due to skin friction on the afterbody. The afterbody skin friction was estimated to be about 12 counts for the test conditions. This does not make up the difference. The remaining amount may be due to insufficient density of pressure taps on the afterbody. However, the differences in chord force between various configurations for the jet off blows, as indicated by the force and pressure data, are about the same.

Normal force and pitching moment effects are shown in figure 149 through 154. Changes in normal force and pitching moment due to angle of attack variation occur only on the horizontal tail. Also, changes brought about by plug nozzle pressure ratio changes occur almost entirely on the horizontal tail. C-D nozzle pressure ratio variations produced negligible changes for both conditions, tail on and off.

LOCAL FLOW DATA

The local flow data obtained during this test consisted of static pressures on the external afterbody and internal pressures near the C-D nozzle exit. In addition, photographic data in the form of schlieren and shadowgraphs of the exhaust plume and afterbody are also presented for selected configurations and mach numbers.

The plotted data is presented so that the pressure coefficients on the C-D nozzles and portions of the afterbody, on the plug nozzle afterbody, and on the inside of the C-D nozzle are shown on separate plots. Pressures on the lower surface of the horizontal tail are shown on the same plot as the plug nozzle afterbody. The pressure plotted at station 53.5 on the curves showing C-D nozzle internal pressures is actually the internal pressure between the shroud and nozzle liner located near the inflatable seal.

COMPARISON WITH ANALYTIC RESULTS

Prior to the test, an analysis was conducted to estimate the afterbody chord force. For the subsonic portion of the analysis, pressure coefficients were calculated on an equivalent axisymmetric afterbody. The details of this procedure are described in reference 2.

A comparison of the estimated and test pressure coefficients at equivalent C-D nozzle exit static pressure ratios are shown in figures 155 through 166. The estimated values are consistently higher than the measured values. This deviation results primarily from trying to approximate a complex afterbody shape with an equivalent axisymmetric shape. In addition, the analytic procedure makes no provision for wings, tails or support struts which all effect the local pressures.

On the plug nozzle afterbody, figures 167 through 172, the comparison between the estimated and test data shows large differences. These differences, can again be attributed to the geometry effects mentioned above. Although the levels of the estimated pressures differ from the measured values, the estimated afterbody chord force increments were in reasonable agreement with the measured values in many cases.

BASE PRESSURE DISTRIBUTIONS

On the model tested, a blunt base region was present between the C-D nozzles at station 50.3. The pressure coefficients in this region are presented in figure 173 through 177. For the subsonic mach numbers, the small base pressure coefficients in combination with the small base area (.00347 square feet) result in negligible chord force coefficients due to base pressure. For the supersonic mach numbers a minimum pressure coefficient value of minus .26 is obtained. This is equivalent to 2.96 counts of chord force.

Figure 178 presents a comparison between the estimated base pressure coefficients reported in reference 3 and the test data.

BOUNDARY LAYER THICKNESS ESTIMATES

Since it was not possible to make boundary layer thickness measurements during the test, estimates have been made.

Turbulent flow and freestream mach number along the model were assumed. The displacement thickness was calculated using the equation shown in figure 179. The ratio between the displacement thickness and the total boundary layer thickness was based on a one seventh power profile. The results are shown in figure 179 for the mach numbers and Reynolds numbers tested. The estimated boundary layer thickness at the afterbody split line is about 0.5 inches and at the end of the model, a little over 0.6 inches.

PHOTOGRAPHIC DATA

Photographic data taken at .6, .85 and 1.27 mach numbers were obtained using a shadowgraph system. The size of the model and the installation of the shadowgraph camera was such that only one nozzle system (plug or C-D) at a time could be photographed. To see the relationship between the two nozzle systems, a composite of two photographs was made and is shown in figure 180. Photographs of the plug nozzle exhaust plumes at .6 and .85 mach numbers are shown in figure 181. C-D nozzle exhaust plumes at .6 are 1.27 mach numbers are shown in figure 182 and 183.

At 1.7 and 2.0 mach number blows, a schlieren system was used to obtain photographic data. Figure 184 shows the complete model during a M = 1.70 blow. The outlined area in this figure shows that portion of the model presented in figures 185 through 188. Figures 185 and 186 show the exhaust plumes for a C-D nozzle pressure ratio variation. Plug nozzle pressure ratio variations are shown in figures 187 and 188. Angle of attack variations are shown in figure 189.

AFTERBODY PRESSURE DISTRIBUTIONS

Pressure distribution plots were made for each blow and for each variable during a blow. Only selected curves are presented here. The entire set of plots has been sent to the sponsoring agency. The specific configuration in the figures are identified by call-outs such as W1B1K1N1 P04 H1V1, etc. These call-outs are described in table I.

Wing Sweep Effects

The effect of wing sweep on afterbody pressures may be seen by comparing figures 190 and 191 (Λ = 30 degrees) with figures 192 and 193 (Λ = 70 degrees). In general, the effects are small, with the greatest change occurring along the row of pressure taps directly behind the wing (ϕ = 135 degrees). Pressure measurements along this row were consistently lower than any other position on the afterbody. Although no investigation was conducted to determine the cause of this phenomenon, a strong wing effect could be possible in view of the sweep effects noted above.

Inlet Fairing Effects

Inlet fairing effects on afterbody pressures are presented in figures 194 through 205. The sharp inlet is identified by an N1 in the vehicle description with an N2 being used to identify the blunt fairing.

Comparing the pressures for each inlet fairing indicates that the changes are negligible on the C-D afterbody at all mach numbers. On the plug nozzle afterbody some differences can be noted for the ϕ = 235 degree row of taps.

C-D Nozzle Pressure Ratio Effects

C-D nozzle jet effects (near-wake) on the vehicle afterbody are shown in figure 206 through 236. The data are shown for cases with the C-D nozzle conical fairing installed and a range of pressure ratios for which the nozzle flow was not separated. Data for separated nozzle flow were not included. Pressure ratios at which the nozzle flow was separated may be determined from plots showing the internal static pressure ratio (P_S/P_o) as shown in figures 212, 223 and 234. So that pressure ratio effect may be easily seen, plots have been included which show the effect on only one selected row of taps. All data are presented over a range of mach numbers for an angle of attack of 3 degrees and with the A_9/A_M = .50 configuration.

An increasing C-D nozzle pressure ratio, once the flow is attached, is seen to produce an increasing pressure on the nozzle shroud and afterbody

for subsonic and transonic mach numbers. At the supersonic mach numbers tested, the same effect is noted but is much less pronounced.

Plug Nozzle Pressure Ratio Effects

Plug nozzle pressure ratio effects on the vehicle afterbody are presented in figures 237 through 276. Operation of this nozzle produces a far-wake jet effect on that portion of the afterbody downstream of the nozzle exit and a near-wake effect on the plug nozzle afterbody. The data shown covers the range of mach numbers tested for an angle of attack of 3 degrees with a A_9/A_M = .5 configuration.

Subsonically, the effect of the plug nozzle pressure ratio on the afterbody is significant. An increasing pressure ratio is seen to produce lower pressures on the fuselage downstream of the nozzle exit (far-wake effect) and increasing pressures upstream of the nozzle exit. Supersonically, the effect of pressure ratio is seen to be small. On the bottom side of the horizontal tail, however, significant pressure changes are noted both subsonically and supersonically.

Afterbody Geometry Effects

Changes in afterbody pressures due to configuration changes, i.e., different values of A_9/A_M, may be determined by making comparisons between the data in figures 277 through 300. At each mach number, three values of A_9/A_M were tested. The particular value of A_9/A_M is indicated in the configuration title; P03, P02, etc. The meaning of these numbers in terms of A_9/A_M are determined from the run index. The data presented is for a constant angle of attack of 3 degrees with either the jets off or the conical closures installed.

Angle of Attack and Mach Number Effects

Angle of attack effects on afterbody pressures are presented in figure 301 through 320. Mach number effects may also be determined by comparing the data at constant angle of attack. All data is presented for A_9/A_M = .50 and with the conical closures installed in both the C-D and plug nozzles.

Section V

CONCLUSIONS AND RECOMMENDATIONS

Afterbody configurations producing a change in boattail angle from 6.7 to 13.5 degrees (A_9/A_M = .50 to .15), with the jets off, results in only a five count change in chord force at .614 and .85 mach numbers. At mach numbers of 1.27 and 1.7 the chord force decreases approximately 50 counts as the boattail angle ranged between 10 and 2.4 degrees, jets off. A chord force decrease of about 25 counts was noted at mach 2.0 as the boattail angles change from 6.7 to zero degrees, jets off. The above values agree fairly well with the estimated configuration effects.

A jet off configuration change that caused an increase in chord force, from the baseline configuration, caused a decrease in normal force and an increase in pitching moment. A decrease in chord force resulted in an increase in normal force and a decrease in pitching moment.

Jet effects were tested with two plug nozzles located forward on the afterbody, and with two convergent-divergent (C-D) nozzles located at the aft end of the model. The plug nozzle jet effects on chord force were unfavorable at mach numbers .6 and .85. Measured chord force increements from the baseline were about plus 15 counts. Estimated plug nozzle effects did not include far-wake effects on the afterbody and predicted favorable jet effects of about the same amount. At mach numbers 1.27, 1.7 and 2.0, plug nozzle jet effects on chord force were favorable and were reasonably close to predicted values. The worst agreement was at mach number 1.27. Plug nozzle jet effects produced significant changes in normal force and pitching moment at .614 and .85 mach numbers with a lesser effect being noted at the supersonic mach numbers. The major portion of these changes however, take place on the horizontal tail.

C-D nozzle jet effects produced a favorable chord force change at all mach numbers tested. At mach numbers .6 and .85, a reduction in chord force of up to about 15 counts was measured. The measured increments agreed quite well with estimates when the flow in the C-D nozzles was not separated. At the supersonic mach numbers, the C-D nozzle jet effects were estimated to be zero, but small reductions in chord force were measured. C-D nozzle jet effects on normal force and pitching moment were similar to those noted for the plug nozzle, i.e., the greatest changes occurred at the subsonic mach numbers.

A simulated no-flow inlet was tested with both a sharp and blunted inlet. In addition, the wing was tested at sweep angles of 30 and 70 degrees. Both of these configuration changes resulted in a negligible effect on chord force, normal force and pitching moment at the mach numbers tested.

The C-D nozzles were constructed with a sharp trailing edge to simulate full scale nozzles. In addition, the split between the metric and the non-metric portion of the aft end of the model was located internally to avoid having a gap on the external surface near the trailing edge of the C-D

nozzles. As a result, some large tare forces and other corrections were encountered on some runs with the C-D jets operating. Chord force data obtained with the internal balance for these runs is questionable. It appears, however, that slight changes in the construction details of the nozzle could result in a much improved situation. Normal force and pitching moment data were not affected. The integrated pressure data appears to give good results for chord force increments.

It is recommended that for future tests of this type, and with a similar afterbody nozzle arrangement, that the construction details be improved to significantly reduce the tare forces and static corrections required on the internal balance chord force data. A short development test to determine the best approach is suggested.

REFERENCES

1. Lemoine, P., et al, Trisonic Wind Tunnel Test to Determine the Afterbody Drag Effects on a .09 Scale IPS Exit Nozzle Model at Subsonic, Transonic and Supersonic Mach Numbers, Los Angeles Division of North American Rockwell Corporation, NA-69-298, 18 April 1969.

2. Sixteenth Monthly Technical Progress Report, Propulsion System Integration and Test Program (Steady State), Los Angeles Division of North American Rockwell Corporation, NA-67-791-15, 31 Oct 1968.

3. Fourteenth Monthly Technical Progress Report, Propulsion System Integration and Test Program (Steady State), Los Angeles Division of North American Rockwell Corporation, NA-67-791-13, 27 Aug 1968.

(The reverse of this page is blank)

BLANK PAGE

TABLE I TEST RUN INDEX

M	BLOW	CONFIGURATION	λ	A_9/A_M	α	P_T/P_0 C-D	P_T/P_0 PLUG
.60	17	N1P3H	30°	.15	0, 3, 5, 7, 10°	CONE	CONE
	18	N1P6H			3°	CONE	1.5, 2.0, 3.0, 4.0, 5.0
	53	N1P12H			3°	1.5, 2.0, 3.0, 5.0, 7.0	CONE
	52	N1P9H			3°	"	2.0
	51	N1P9H		.15	3°	"	5.0
	16	N1P2H		.30	0, 3, 5, 7, 10°	CONE	CONE
	15	N1P5H			3°	CONE	1.5, 2.0, 3.0, 4.0, 6.0
	38	N1P11H			3°	1.5, 2.0, 3.0, 6.0, 10.0	CONE
	39	N1P8H			3°	1.5, 2.0, 3.0, 6.0, 8.0	2.0
	40	N1P8H		.30	3°	1.5, 2.0, 3.0, 5.0, 6.0	5.0
	1	N1P1H		.60	0, 3, 5, 7, 10°	CONE	CONE
	33	N1P1H [NO GOOD]			"	"	"
	41	N1P1H [REPEAT]			"	"	"
	4	N2P1H			"	"	"
	5	N1P4H			3°	"	1.5, 2.0, 3.0, 4.0, 5.0
	36	N1P7H			0, 3, 5, 7, 10°	2.0	2.0
	37	N1P10H			3°	1.5, 2.0, 3.0, 5.0, 7.0	CONE
	35	N1P7H			3°	1.5, 2.0, 3.0, 5.0, 6.5	2.0
.60	34	N1P7H	30°	.60	3°	"	5.0
.85	20	N1P3H	70°	.15	0, 3, 5, 7, 10°	CONE	CONE
	19	N1P6H			3°	CONE	1.5, 2.0, 3.0, 4.0, 5.0
	54	N1P12H			3°	1.5, 2.0, 3.0, 5.0, 7.0	CONE
	55	N1P9H			3°	"	2.0
.85	56	N1P9H	70°	.15	3°	"	5.0

TABLE I TEST RUN INDEX

M	BLOW	CONFIGURATION	λ	A_9/A_M	α	P_T/P_0 C-D	P_T/P_0 PLUG
.85	13	NIP2H	70°	.30	0, 3, 5, 7, 10°	CONE	CONE
	14	NIP5H			3°	CONE	1.5, 2.0, 3.0, 4.0, 5.0
	47	NIP11H			3°	1.5, 2.0, 3.0, 5.0, 7.0	CONE
	43	NIP8H			3°	"	2.0
	44	NIP8H	70°	.30	3°	"	5.0
	2	NIP1H [NO GOOD]	30°	.50	0, 3, 5, 7, 10°	CONE	CONE
	3	NIP1H [REPEAT]	30°		"	"	"
	8	NIP1H	70°		"	"	"
	31	NIP1H [REPEAT]			"	"	"
	29	NIP1			"	"	"
	9	N2P1H			"	"	"
	6	NIP4H			3°	"	1.5, 2.0, 3.0, 4.0, 5.0
	30	NIP4			3°	"	"
	27	NIP7H			0, 3, 5, 7, 10°	3.0	2.0
	21	NIP10H			3°	1.5, 2.0, 3.0, 5.0, 7.0	CONE
	28	NIP10			3°	"	"
	26	NIP7H			3°	"	2.0
.85	25	NIP7H	70°	.50	3°	"	5.0
1.25	12	NIP2H	70°	.30	0, 3, 5, 7, 10°	CONE	CONE
	45	NIP8H		.30	3°	3.0, 5.0, 7.0, 10.0, 12.0	3.0
	46	NIP8H		.30	3°	8.0	1.5, 2.0, 3.0, 4.0, 5.0
	11	NIP1H		.50	0, 3, 5, 7, 10°	CONE	CONE
	32	NIP1H [NO GOOD]		.50	"	"	"
1.25	42	NIP1H [REPEAT]	70°	.50	"	"	"

TABLE I TEST RUN INDEX

M	BLOW	CONFIGURATION	λ	A_9/A_M	α	P_T/P_0 C-D	P_T/P_0 PLUG
1.25	10	N2P1H	70°	.50	0, 3, 5, 7, 10°	CONE	CONE
	24	N1P7H			"	10.0	3.0
	7	N1P4H			3°	CONE	1.5, 2.0, 3.0, 4.0, 5.0
	22	N1P7H			3°	8.0	"
	23	N1P7H		.60	3°	3.0, 5.0, 7.0, 10.0, 12.0	3.0
	50	N1P13H		.80	0, 3, 5, 7, 10°	1.0	CONE
	49	N1P14H		.80	3°	3.0, 5.0, 7.0, 9.0, 10.5	3.0
1.25	48	N1P14H	70°	.80	3°	8.0	1.5, 3.0, 4.0, 5.0, 7.0
1.70	66	N1P11H	70°	.30	0, 3, 5, 7°	1.0	CONE
	69	N1P8H		.30	3°	3.0, 5.0, 7.0, 10.0	5.0
	67	N1P8H		.30	3°	10.0	2.5, 5.0, 7.0, 10.0
	58	N1P1H		.50	0, 3, 5, 7°	CONE	CONE
	57	N2P1H			"	"	"
	63	N1P7H			"	15.0	5.0
	61	N1P7H			3°	1.0	2.5, 5.0, 7.0, 10.0
	62	N1P7H			3°	10.0	"
	65	N1P7H			3°	4.0, 7.0, 10.0, 15.0	5.0
	64	N1P7H [NO GLOD]		.50	"	"	"
	73	N1P13H		.80	0, 3, 5, 7°	1.0	CONE
	70	N1P14H		.80	3°	5.0, 7.0, 10.0, 13.0	5.0
1.70	72	N1P14H	70°	.80	3°	10.0	2.5, 5.0, 7.0, 10.0
2.0	86	N1P1H	70°	.50	0, 3, 5, 7°	CONE	CONE
2.0	87	N2P1H	70°	"	"	"	"

TABLE I TEST RUN INDEX

M	BLOW	CONFIGURATION	λ	A_9/A_M	α	P_T/P_0 C-D	P_T/P_0 PLUG
2.0	84	NIP7H	70°	.50	0, 3, 5, 7°	20.0	5.0
	82	NIP7H			3°	1.0	3.0, 5.0, 7.0, 10.0
	83	NIP7H			3°	15.0	"
	85	NIP7H		.50	3°	4.0, 6.0, 10.0, 16.0	6.0
	77	NIP13H		.80	0, 3, 5, 7°	1.0	CONE
	76	NIP14H		.80	3°	15.0	3.0, 5.0, 7.0, 10.0
	74	NIP14H		.80	3°	5.0, 10.0, 15.0, 18.0	6.0
	78	NIP16H		1.0	0, 3, 5, 7°	1.0	CONE
	79	NIP16H		1.0	3°	16.0	2.5, 5.0, 7.0, 10.0
2.0	81	NIP16H	70°	1.0	3°	5.0, 10.0, 15.0, 18.0	5.0
0.0	59	NIP7H	—	.50	—	1.0	1.6, 2.0, 3.0, 5.0, 7.0
	60	NIP7H	—	.50	—	1.6, 2.0, 3.0, 4.0, 5.0	1.0
	68	NIP8H	—	.30	—	1.6, 2.0, 3.0, 5.0, 7.0	1.0
	88	NIP8H [REPEAT]	—	.30	—	1.6, 2.5, 4.0, 6.0, 8.0	1.0
	71	NIP14H	—	.80	—	1.6, 2.0, 3.0, 5.0, 6.0	1.0
	75	NIP14H [REPEAT]	—	.80	—	"	"
	80	NIP16H	—	1.0	—	"	"
0.0	89	NIP9H	—	.15	—	1.5, 2.5, 4.0, 6.0, 8.0	"
		NOTE: N1 denotes sharp inlet fairing on					
		N2 " " " " off					
		H " horizontal tail on					
		1.0 " jet off					

TABLE II TABULATED DATA

BLOW	M	CONFIG	A_9/A_M	λ	α	$P_T/P_{0\ PLUG}$	$P_T/P_{0\ C-D}$	BALANCE DATA C_C	C_N	C_M	INTEGRATED PRESSURE DATA $C_{C\ AB}$	$C_{C\ C-D}$	$C_{C\ PLUG}$	$C_{C\ BASE}$	$C_{C\ TOT}$	NOTES
1	.61	N1P1H	.50	30°	0	CONE	CONE	99	213	-300	44	6.0	12	.8	62.8	
					3.2			95	439	-653	42	5	10	.7	57.7	
					5.2			94	588	-893	42	5	9	.7	56.7	
					7.2			87	745	-1152	40	4	8	.7	52.7	
					10.2			76	994	-1567	37	3	7	.7	47.7	
2	NO	GOOD														
3	.85	N1P1H	.50	30°	0	CONE	CONE	111	262	-407	63	8	12	.9	73.9	
					3.6			107	482	-760	51	7	10	.9	68.9	
					5.6			103	562	-890	49	6	9	.9	64.9	
					7.6			93	718	-1158	46	5	7	.8	58.8	
					10.6			81	916	-1506	42	4	7	.8	53.8	
4	.61	N2P1H	.60	30°	0	CONE	CONE	96	209	-290	42	4	12	.7	58.7	B
					3.2			93	486	-650	42	4	9	.7	53.7	
					5.3			88	690	-907	41	4	8	.7	53.7	
					7.3			79	728	-1141	39	3	7	.7	49.7	
					10.2			67	985	-1574	37	3	7	.7	48.7	
5	.61	N1P4H	.60	30°	2.9	1.49	CONE	97	412	-601	46	5	9	.7	60.7	
						1.97		103	392	-570	48	6	10	.8	64.8	
						2.97		104	354	-506	49	5	10	.7	64.7	
						3.96		108	323	-465	50	6	10	.8	66.8	
						4.98		107	302	-420	50	6	9	.7	65.7	

TABLE II TABULATED DATA

								BALANCE DATA			INTEGRATED PRESSURE DATA					
BLOW	M	CONFIG	A_0/A_M	λ	α	$P_T/P_{0\ PLUG}$	$P_T/P_{0\ C-D}$	C_C	C_N	C_M	$C_{C\ AB}$	$C_{C\ C-D}$	$C_{C\ PLUG}$	$C_{C\ BASE}$	$C_{C\ TOT}$	NOTES
6	.85	NIP4H	.50	70°	2.9	1.55	CONE	112	433	-703	54	8	11	1	74	
						2.01		114	412	-668	56	8	12	1	76	
						2.98		115	373	-604	57	8	11	1	77	
						4.03		116	340	-560	57	8	10	.9	75.9	
						5.00		114	308	-496	58	8	9	.9	75.9	
7	1.27	NIP4H	.50	70°	2.9	1.52	CONE	197	606	-825	48	38	16	3.2	105.2	
						3.12		198	503	-823	49	39	15	3.3	106.3	
						4.14		197	506	-822	49	39	13	3.3	104.3	
						5.20		195	506	-824	48	39	11	3.3	101.3	
						6.20		193	504	-823	49	39	10	3.3	101.3	
8	.85	NIPIH	.50	70°	0	CONE	CONE	112	255	-486	50	7	16	.9	73.9	BASE
					2.8			108	416	-695	49	6	13	.9	68.9	
					4.8			103	547	-906	47	6	12	.9	65.9	
					6.8			96	697	-1151	45	6	10	.9	61.9	
					9.8			84	949	-1569	41	4	8	.9	53.9	
9	.85	N2PIH	.50	70°	2.9	CONE	CONE	104	421	-706	47	6	12	.9	65.9	B
					4.9			97	544	-910	45	6	11	.9	62.9	
					6.9			90	672	-1129	43	5	9	.9	57.9	
					9.9			75	902	-1515	41	5	9	.9	55.9	

TABLE II TABULATED DATA

BLOW	M	CONFIG	A_9/A_M	λ	α	$P_T/P_{0\ PLUG}$	$P_T/P_{0\ C-D}$	BALANCE DATA C_C	C_N	C_M	INTEGRATED PRESSURE DATA $C_{C\ AB}$	$C_{C\ C-D}$	$C_{C\ PLUG}$	$C_{C\ BASE}$	$C_{C\ TOT}$	NOTES
10	1.28	N2P1H	.50	70°	0	CONE	CONE	195	168	-277	54	38	17	3.1	112.1	B
					2.8			197	441	-748	52	37	16	3.3	108.3	
					4.9			193	687	-1098	51	37	14	3.3	105.3	
					6.8			187	888	-1463	49	35	13	3.3	100.3	
					9.9			173	1194	-2113	46	32	11	3.3	92.3	
11	1.28	N1P1H	.50	70°	0	CONE	CONE	191	165	-266	54	37	17	3.0	111.0	BASE
					2.9			196	451	-763	53	37	16	3.1	109.1	
					4.9			194	666	-1124	51	37	15	3.3	106.3	
					6.9			188	899	-1534	49	36	13	3.4	101.4	
					9.9			176	1257	-2181	46	33	10	3.4	92.4	
12	1.28	N1P2H	.30	70°	0	CONE	CONE	212	183	-200	54	58	18	2.6	132.5	
					2.8			221	419	-681	53	62	16	2.8	133.8	
					4.8			219	626	-1039	51	63	15	3.0	132.0	
					6.8			213	845	-1419	49	63	13	3.0	128.0	
					9.8			201	1195	-2093	46	60	10	3.0	119.0	
13	.85	N1P2H	.30	70°	0	CONE	CONE	114	191	-328	52	9	15	.6	76.6	
					2.8			111	358	-595	50	8	13	.6	71.6	
					4.8			108	487	-803	49	8	12	.6	69.6	
					6.8			101	629	-1087	47	7	10	.6	64.6	
					9.8			87	881	-1454	43	6	8	.6	57.6	

TABLE II TABULATED DATA

								BALANCE DATA			INTEGRATED PRESSURE DATA					
BLOW	M	CONFIG	A_9/A_M	λ	α	P_T/P_0 PLUG	P_T/P_0 C-D	C_C	C_N	C_M	$C_{C\ AB}$	$C_{C\ C-D}$	$C_{C\ PLUG}$	$C_{C\ BASE}$	$C_{C\ TOT}$	NOTES
14	.86	NIP5H	.30	70°	2.9	2.04	CONE	117	359	-576	56	11	12	.7	79.7	
						3.0		118	326	-519	58	10	11	.6	79.6	
						4.0		119	296	-465	59	10	10	.6	79.6	
						5.0		118	267	-418	60	10	8	.6	78.6	
						2.0		116	360	-573	55	9	11	.6	75.6	
15	.61	NIP5H	.30	30°	2.9	1.51	CONE	105	379	-537	49	7	9	.6	65.6	
						1.97		106	353	-497	51	6	10	.6	67.6	
						2.92		109	316	-438	53	6	10	.7	69.7	
						3.94		112	280	-380	53	7	10	.7	70.7	
						4.96		112	260	-348	54	7	9	.6	70.6	
16	.61	NIP2H	.30	30°	0	CONE	CONE	98	174	-226	45	4	12	.5	61.5	
					2.7			96	376	-546	44	3	10	.5	57.5	
					4.8			96	514	-767	44	4	9	.5	57.5	
					6.7			88	682	-1041	41	2	8	.5	51.5	
					9.7			78	910	-1418	38	2	7	.5	47.5	
17	.61	NIP3H	.16	30°	0	CONE	CONE	101	146	-176	47	6	12	.3	65.3	
					2.9			103	352	-606	47	6	11	.3	64.3	
					4.9			102	502	-742	46	6	10	.4	62.4	
					6.9			91	654	-992	43	3	8	.3	54.3	
					9.9			82	880	-1366	39	4	7	.3	50.3	

TABLE II TABULATED DATA

								BALANCE DATA			INTEGRATED PRESSURE DATA					
BLOW	M	CONFIG	A_9/A_M	λ	α	$P_T/P_{0\ PLUG}$	$P_T/P_{0\ C-D}$	C_C	C_N	C_M	$C_{C\ AB}$	$C_{C\ C-D}$	$C_{C\ PLUG}$	$C_{C\ BASE}$	$C_{C\ TOT}$	NOTES
18	.61	NIP6H	.15	30°	2.9	1.54	CONE	107	340	-489	51	7	9	.3	67.3	
						1.98		111	318	-452	53	6	10	.4	69.4	
						2.96		112	276	-380	54	7	10	.4	71.4	
						3.98		114	248	-338	55	7	10	.4	72.4	
						5.06		116	222	-298	55	7	9	.4	71.4	
19	.86	NIP6H	.15	70°	2.9	1.54	CONE	121	341	-546	56	13	11	.5	80.5	
						2.01		123	318	-508	57	13	12	.5	82.5	
						2.99		123	280	-442	59	13	11	.5	83.5	
						4.03		124	251	-394	59	13	10	.4	82.4	
						5.02		124	226	-350	60	13	9	.4	82.4	
20	.85	NIP3H	.15	70°	0	CONE	CONE	118	148	-251	53	11	16	.4	80.4	
					2.9			118	318	-527	62	11	14	.5	77.5	
					4.9			118	443	-731	50	9	12	.4	71.4	
					6.8			104	581	-954	48	8	11	.4	67.4	
					9.8			92	808	-1330	44	8	8	.4	60.4	
21	.85	NIP10H	.60	70°	2.9	CONE	1.5	88	390	-676	45	0.0	14	.5	59.5	
							1.99	95	396	-692	46	1.5	13	.6	61.1	
							3.00	99	408	-709	46	2.6	13	.6	62.2	
							5.07	100	410	-718	45	.8	13	.6	59.4	
							7.08	100	417	-727	44	1.8	13	.5	59.3	

TABLE II TABULATED DATA

								BALANCE DATA			INTEGRATED PRESSURE DATA					
BLOW	M	CONFIG	A_9/A_M	λ	α	$P_T/P_{0\ PLUG}$	$P_T/P_{0\ C-D}$	C_C	C_N	C_M	$C_{C\ AB}$	$C_{C\ C-D}$	$C_{C\ PLUG}$	$C_{C\ BASE}$	$C_{C\ TOT}$	NOTES
22	1.27	NIP7H	.50	70°	2.85	1.63	8.29	171	471	-785	46	28	16	2.5	92.5	
						3.09		181	472	-786	49	33	15	2.5	99.5	
						4.16		181	475	-785	49	33	13	2.5	97.5	
						5.27		181	476	-787	48	38	11	2.5	99.5	
						6.88		179	476	-793	51	34	9	2.5	96.5	
23	1.27	NIP7H	.50	70°	2.81	3.0	3.1	178	474	-820	47	33	15	2.9	97.5	
							5.2	193	476	-802	49	36	15	2.9	102.9	
							7.2	192	462	-793	49	34	15	2.7	100.7	
							10.3	181	457	-779	48	30	15	2.3	95.3	
							12.5	175	455	-774	48	26	15	2.0	91.0	
24	1.27	NIP7H	.50	70°	.24	3.2	10.4	171	231	-367	49	28	16	2.0	95.0	
					3.1			175	491	-828	49	30	15	2.3	96.3	
					5.1			174	703	-1200	47	30	13	2.4	92.4	
					7.1			174	924	-1593	46	29	12	2.5	88.5	
					10.1			160	1276	-2242	42	26	9	2.6	79.6	
25	.85	NIP7H	.50	70°	2.9	5.1	1.5	96	280	-489	52	.3	8	.4	60.7	
							2.0	102	291	-515	54	2	8	.5	64.5	
							2.98	105	295	-523	54	4	8	.6	66.6	
							5.04	104	303	-537	53	2	8	.6	63.6	
							7.24	102	310	-552	52	-1	8	.5	59.5	

TABLE II TABULATED DATA

								BALANCE DATA			INTEGRATED PRESSURE DATA					
BLOW	M	CONFIG	A_9/A_M	λ	α	$P_T/P_{0\ PLUG}$	$P_T/P_{0\ C-D}$	C_C	C_N	C_M	$C_{C\ AB}$	$C_{C\ C-D}$	$C_{C\ PLUG}$	$C_{C\ BASE}$	$C_{C\ TOT}$	NOTES
26	.84	NIP7H	.60	70°	2.9	2.0	1.63	100	390	-666	51	1	12	.6	64.5	
							2.06	106	400	-684	52	3	11	.7	66.7	
							3.07	115	404	-692	53	4	12	.7	69.7	
							5.15	105	411	-698	52	3	12	.7	67.7	
							7.29	102	411	-707	50	0	11	.6	61.6	
27	.85	NIP7H	.50	70°	0	2.0	2.98	96	247	-412	52	3	13	.6	68.6	
					3.0			92	407	-681	49	2	10	.6	61.6	
					5.0			88	528	-895	48	2	9	.6	59.6	
					6.9			82	668	-1148	45	1	7	.6	53.6	
					9.9			70	907	-1673	41	1	5	.7	47.7	
28	.85	NIP10	.50	70°	2.9	CONE	1.56	65	91	-120	31	-5	16	0	42	T.O.
							2.06	71	95	-123	32	-3	16	.1	45.1	
							3.12	78	99	-132	33	-2	16	.2	47.2	
							5.21	75	94	-126	31	-4	16	.1	43.1	
							7.26	67	95	-133	29	-7	16	0	38	
29	.85	NIP1	.60	70°	0	CONE	CONE	87	94	-123	38	3	18	.5	59.5	T.O.
					2.9			85	93	-126	37	3	17	.5	57.5	
					4.9			82	94	-116	36	3	16	.4	55.4	
					6.9			78	95	-115	34	2	15	.4	51.4	
					9.9			72	98	-115	32	1	13	.3	46.3	

TABLE II TABULATED DATA

								BALANCE DATA			INTEGRATED PRESSURE DATA					
BLOW	M	CONFIG	A_9/A_M	λ	α	P_T/P_0 PLUG	P_T/P_0 C-D	C_C	C_N	C_M	$C_{C\ AB}$	$C_{C\ C-D}$	$C_{C\ PLUG}$	$C_{C\ BASE}$	$C_{C\ TOT}$	NOTES
30	.85	NIP4	.60	70°	2.9	1.39	CONE	87	97	-120	40	4	15	.6	59.6	T.O.
						1.99		89	98	-118	41	3	15	.6	59.6	
						3.06		90	96	-112	43	3	14	.6	60.6	
						4.09		90	87	-109	44	3	13	.6	60.6	
						5.14		90	85	-100	44	3	11	.6	58.6	
31	.85	NIPIH	.50	70°	0	CONE	CONE	113	253	-440		6	16	.9	22.9	R[8]
					3.0			111	425	-646		6	16	.9	22.9	
					5.0			104	553	-913		6	13	.9	19.9	
					6.9			98	699	-1152		5	12	.9	17.9	
					9.9			84	948	-1562		4	8	.9	12.9	
32	NO	GOOD														
33	NO	GOOD														
34	.61	NIP7H	.50	30°	2.9	5.1	1.53	82	282	-446	46	0	8	.5	54.5	
							2.03	88	276	-444	48	3	8	.6	59.6	
							3.03	105	293	-470	49	4	8	.7	61.7	
							5.08	91	296	-473	48	2	8	.6	58.6	
							6.60	84	299	-481	46	0	7	.5	53.5	

TABLE II TABULATED DATA

								BALANCE DATA			INTEGRATED PRESSURE DATA					
BLOW	M	CONFIG	A_0/A_M	λ	α	P_T/P_0 PLUG	P_T/P_0 C-D	C_C	C_N	C_M	$C_{C\ AB}$	$C_{C\ C-D}$	$C_{C\ PLUG}$	$C_{C\ BASE}$	$C_{C\ TOT}$	NOTES
35	.61	NIP7H	.50	30°	2.9	2.0	1.52	79	367	-579	44	1	9	.5	54.5	
							2.0	90	375	-594	46	3	9	.6	58.6	
							3.0	118	382	-603	46	3	9	.6	58.6	
							6.0	96	390	-620	46	2	9	.6	57.6	
							6.5	94	395	-632	45	0	9	.5	54.5	
36	.61	NIP7H	.50	30°	0	1.99	1.95	87	165	-255	47	3	11	.6	61.6	
					2.8			88	362	-583	47	3	9	.6	59.6	
					4.8			82	504	-827	45	2	8	.6	55.6	
					6.8			87	652	-1076	43	1	7	.5	51.5	
					9.8			68	878	-1474	39	0	6	.5	45.5	
37	.61	NIP10H	.50	30°	2.8	CONE	1.45	76	400	-651	39	-1	10	.4	48.4	
							1.95	83	406	-656	41	1	10	.5	52.5	
							2.93	87	414	-671	41	2	10	.6	53.6	
							4.93	89	427	-694	40	1	9	.5	50.5	
							6.84	88	432	-708	39	-2	9	.5	46.5	
38	.61	NIP11H	.30	30°	2.7	CONE	1.46	77	360	-585	43	-2	10	.3	51.3	
							1.95	82	369	-585	45	1	10	.5	56.5	
							2.92	68	376	-613	44	1	10	.5	55.5	
							4.90	93	386	-634	44	0	10	.4	54.4	
							9.69	113	417	-636	41	-7	9	.3	43.3	

TABLE II TABULATED DATA

								BALANCE DATA			INTEGRATED PRESSURE DATA					
BLOW	M	CONFIG	A_9/A_M	λ	α	$P_T/P_{0\ PLUG}$	$P_T/P_{0\ C-D}$	C_C	C_N	C_M	$C_{C\ AB}$	$C_{C\ C-D}$	$C_{C\ PLUG}$	$C_{C\ BASE}$	$C_{C\ TOT}$	NOTES
39	.61	N1P8H	.30	30°	2.8	2.0	1.50	85	329	-519	48	-1	9	.4	46.4	
							1.96	91	330	-515	50	2	9	.5	61.5	
							2.92	78	347	-545	50	2	9	.5	61.5	
							4.74	101	349	-553	49	1	9	.5	59.5	
							7.97	109	365	-575	47	-3	9	.4	53.4	
40	.61	N1P8H	.30	30°	2.7	5.0	1.49	90	229	-357	50	0	8	.4	58.4	
							1.99	96	232	-359	52	2	8	.5	62.5	
							2.96	88	246	-386	53	3	8	.6	64.6	
							4.91	108	259	-402	53	2	8	.6	63.6	
							6.36	109	261	-414	51	0	8	.5	59.5	
41	.61	N1P1H	.50	30°	0	CONE	CONE	95	222	-325	43	4	12	.7	59.7	REF BASE
					2.8			96	421	-618	42	4	10	.7	56.7	
					4.8			92	572	-870	41	4	9	.7	54.7	
					6.8			84	726	-1120	39	2	8	.6	49.6	
					9.8			74	962	-1514	35	2	7	.7	44.7	
42	1.27	N1P1H	.50	70°	0	CONE	CONE	192	178	-285	54	37	18	3	112	R[11]
					2.9			197	454	-768	63	38	17	3	111	
					4.9			194	667	-1128	51	38	14	3	106	
					6.9			189	897	-1530	49	36	13	3	101	
					9.9			177	1261	-2189	46	33	9	3	91	

TABLE II TABULATED DATA

								BALANCE DATA			INTEGRATED PRESSURE DATA					
BLOW	M	CONFIG	A_0/A_M	λ	α	P_T/P_0 PLUG	P_T/P_0 C-D	C_C	C_N	C_M	$C_{C\ AB}$	$C_{C\ C\text{-}D}$	$C_{C\ PLUG}$	$C_{C\ BASE}$	$C_{C\ TOT}$	NOTES
43	.85	NIP8H	.30	70°	2.9	2.0	1.60	87	332	-578	51	1	11	.3	63.3	
							2.00	94	335	-581	52	3	11	.3	66.3	
							3.00	88	349	-608	52	3	10	.4	65.4	
							4.99	103	359	-623	52	1	10	.4	63.4	
							7.05	97	363	-623	51	-1	10	.3	60.3	
44	.86	NIP8H	.30	70°	2.9	5.15	1.52	92	230	-402	55	3	8	.3	66.3	
							2.03	98	241	-427	57	5	8	.4	70.4	
							3.03	93	247	-436	57	5	7	.4	69.4	
							5.02	106	258	-456	57	3	7	.4	67.4	
							7.08	101	260	-459	55	0	7	.4	62.4	
45	1.27	NIP8H	.30	70°	3.0	3.17	3.18	186	463	-775	47	51	15	3	116	
							5.20	214	468	-776	49	57	15	3	124	
							7.25	208	469	-770	49	54	15	3	121	
							10.36	203	474	-769	48	47	15	2	112	
							12.59	199	474	-766	48	42	15	2	107	
46	1.27	NIP8H	.30	70°	2.9	1.64	8.3	188	470	-761	46	40	17	2	105	
						3.16		201	472	-769	48	51	15	2	116	
						4.24		201	477	-776	49	52	13	2	116	
						5.32		198	477	-777	48	52	11	2	113	
						6.95		196	477	-780	51	52	9	2	115	

TABLE II TABULATED DATA

BLOW	M	CONFIG	A_9/A_M	λ	α	$P_T/P_{0\ PLUG}$	$P_T/P_{0\ C-D}$	BALANCE DATA C_C	C_N	C_M	INTEGRATED PRESSURE DATA $C_{C\ AB}$	$C_{C\ C-D}$	$C_{C\ PLUG}$	$C_{C\ BASE}$	$C_{C\ TOT}$	NOTES
47	.85	NIPIIH	.30	70°	2.96	CONE	1.53	85	346	-612	45	-1	13	.2	57.2	
							2.05	92	357	-635	46	1	13	.3	60.3	
							3.04	84	361	-638	46	1	12	.3	59.3	
							5.03	97	368	-658	46	-1	12	.3	57.3	
							7.11	93	374	-668	45	-4.0	12	.2	53.2	
48	1.27	NIPI4H	.80	70°	2.88	1.61	8.3	158	528	-902	46	6	17	3	72	
						3.16		162	526	-897	48	7	15	3	73	
						4.25		162	525	-895	48	7	13	3	71	
						5.34		160	523	-893	48	7	11	3	69	
						7.05		157	517	-895	50	7	9	3	69	
49	1.27	NIPI4H	.80	70°	2.9	3.1	3.2	163	543	-935	46	6	15	3	70	
							5.28	167	539	-926	48	7	15	3	73	
							7.4	166	532	-917	48	7	15	3	73	
							8.9	165	528	-910	48	6	15	3	72	
							10.6	164	519	-896	48	6	15	3	72	
50	1.27	NIPI3H	.80	70°	0	CONE	CONE	155	209	-377	52	7	18	3	80	
					2.98			160	500	-879	52	7	17	3	79	
					5.0			157	725	-1273	50	7	15	3	75	
					7.0			151	971	-1702	49	5	13	3	70	
					9.9			137	1349	-2403	45	3	10	3	61	

TABLE II TABULATED DATA

BLOW	M	CONFIG	A_9/A_M	λ	α	$P_T/P_{0\ PLUG}$	$P_T/P_{0\ C-D}$	BALANCE DATA C_C	C_N	C_M	INTEGRATED PRESSURE DATA $C_{C\ AB}$	$C_{C\ C-D}$	$C_{C\ PLUG}$	$C_{C\ BASE}$	$C_{C\ TOT}$	NOTES
51	.61	NIP9H	.15	30°	3.3	5.0	1.5	127	222	-344	53	3	8	.3	64.3	
							1.97	127	222	-343	54	4	8	.4	66.4	
							2.88	146	228	-358	55	5	8	.4	68.4	
							4.85	149	253	-359	54	4	8	.4	66.4	
							6.89	139	292	-330	54	2	8	.3	64.3	
52	.61	NIP9H	.15	30°	2.8	2.0	1.45	81	279	-432	49	.3	9	.2	58.5	
							1.93	85	289	-444	52	3	9	.3	64.3	
							2.92	99	297	-462	50	2	9	.3	61.3	
							4.92	103	316	-470	51	2	9	.3	62.3	
							6.80	105	348	-432	50	0	9	.3	59.3	
53	.61	NIP12H	.15	30°	2.8	CONE	1.49	75	321	-514	44	-2	10	.1	52.1	
							1.96	79	327	-518	46	1	10	.3	57.3	
							2.86	98	335	-537	47	1	10	.3	58.3	
							4.9	97	360	-541	46	0	10	.3	56.3	
							6.87	96	386	-607	45	-2	10	.2	53.2	
54	.85	NIP12H	.15	70°	2.7	CONE	1.48	92	289	-517	49	4	13	.2	66.2	
							2.02	91	297	-526	51	6	13	.3	70.3	
							2.98	110	299	-535	50	6	13	.3	69.3	
							4.96	107	311	-539	50	4	13	.3	67.3	
							7.05	95	331	-524	49	2	13	.2	64.2	

TABLE II TABULATED DATA

								BALANCE DATA			INTEGRATED PRESSURE DATA					
BLOW	M	CONFIG	A_9/A_M	λ	α	P_T/P_0 PLUG	P_T/P_0 C-D	C_C	C_N	C_M	$C_{C\ AB}$	$C_{C\ C\text{-}D}$	$C_{C\ PLUG}$	$C_{C\ BASE}$	$C_{C\ TOT}$	NOTES
55	.85	N1P9H	.15	70°	2.9	2.0	1.48	95	291	-497	53	5	11	.3	69.3	
							2.04	94	299	-512	55	8	11	.3	74.3	
							3.01	115	304	-622	55	8	11	.3	74.3	
							5.01	111	317	-528	55	6	11	.3	72.3	
							7.1	98	339	-513	54	4	10	.3	68.3	
56	.85	N1P9H	.16	70°	2.9	5.1	1.47	92	195	-340	58	8	8	.3	74.3	
							2.03	97	192	-337	59	9	8	.3	76.3	
							2.99	117	200	-354	59	9	8	.3	76.3	
							4.98	114	216	-356	59	8	7	.3	74.3	
							7.08	104	239	-346	58	6	7	.3	71.3	
57	1.7	N2P1H	.50	70°	0	CONE	CONE	151	-68	134	36	29	15	2.3	82.3	B
					2.9			149	177	-305	34	29	14	2.3	79.3	
					4.9			143	369	-655	32	27	12	2.3	73.3	
					6.9			136	578	-1034	31	25	10	2.2	68.2	
					9.9			126	942	-1682	28	21	7	2.1	58.1	
58	1.7	N1P1H	.50	70°	0	CONE	CONE	148	-26	65	38	27	16	2	83.0	BASE
					2.9			152	233	-395	35	29	14	2	80.0	
					5.0			148	437	-756	33	28	13	2	86.0	
					7.0			141	648	-1134	30	27	11	2	70.0	
					10.0			129	1006	-1785	26	23	8	2	59.0	

TABLE II TABULATED DATA

BLOW	M	CONFIG	A_9/A_M	λ	α	P_T/P_0 PLUG	P_T/P_0 C-D	BALANCE DATA C_C	C_N	C_M	INTEGRATED PRESSURE DATA $C_{C\ AB}$	$C_{C\ C-D}$	$C_{C\ PLUG}$	$C_{C\ BASE}$	$C_{C\ TOT}$	NOTES
59	0	NIPTH	.50			1.0	1.55	13	.6	0	3	2	.9	.1	6.0	STATIC
							2.07	18	.7	.1	3	2	.9	.1	6.0	
							3.09	24	.5	.5	3	3	1	.1	7.1	
							5.16	37	.8	.2	4	3	1	.1	8.1	
							7.22	33	.9	-.2	6	4	2	.2	12.2	
60	0	NIPTH	.50			1.54	1.0	7	.1	.7	3	2	.8	.1	5.9	STATIC
						2.06		7	0	.8	3	2	.9	.1	6.0	
						3.09		7	0	.8	3	2	1	.1	6.1	
						4.14		7	-.1	1.3	3	2	1	.1	6.1	
						5.18		8	-.5	2	4	3	1	.1	8.1	
61	1.7	NIPTH	.50	70°	2.9	2.46	1.0	137	283	-478	38	24	16	3	81.0	
						4.93		150	287	-480	34	28	13	2	77.0	
						6.94		162	294	-485	33	30	11	3	77.0	
						9.98		151	294	-471	35	30	8	3	76.0	
62	1.7	NIPTH	.50	70°	2.9	2.48	10.0	139	285	-491	40	21	17	2	80.0	
						5.01		137	281	-480	34	25	13	2	74.0	
						7.03		138	285	-479	33	25	11	2	71.0	
						10.1		136	286	-468	35	25	8	2	70.0	

TABLE II TABULATED DATA

								BALANCE DATA			INTEGRATED PRESSURE DATA					
BLOW	M	CONFIG	A_9/A_M	λ	α	$P_T/P_{0\ PLUG}$	$P_T/P_{0\ C-D}$	C_C	C_N	C_M	$C_{C\ AB}$	$C_{C\ C-D}$	$C_{C\ PLUG}$	$C_{C\ BASE}$	$C_{C\ TOT}$	NOTES
63	1.7	NIP7H	.50	70°	0	5.0	10.2	139	22	-17	36	24	14	2	76	
					3.0			138	282	-483	34	25	13	2	74	
					5.0			134	481	-838	31	24	11	2	68	
					7.0			129	692	-1215	29	22	9	2	62	
64	NO	GOOD														
65	1.7	NIP7H	.50	70°	2.9	4.97	3.98	131	279	-481	41	24	16	3	84	
							6.98	142	274	-473	34	27	13	2	76	
							10.0	139	271	-465	34	25	13	2	74	
							15.15	131	271	-459	34	23	12	2	71	
66	1.7	NIP11H	.30	70°	0	CONE	1.0	180	-28	70	38	54	16	3	111	
					2.9			178	216	-361	35	54	14	3	106	
					4.9			174	410	-705	32	53	12	3	100	
					6.9			169	617	-1073	30	51	11	3	95	
67	1.7	NIP8H	.30	70°	2.8	2.46	10.0	156	261	-432	33	38	15	2	88	
						4.91		158	266	-436	34	40	13	2	89	
						6.91		156	270	-433	33	41	11	2	84	
						9.9		153	271	-422	34	40	8	2	84	

TABLE II TABULATED DATA

								BALANCE DATA			INTEGRATED PRESSURE DATA					
BLOW	M	CONFIG	A_9/A_M	λ	α	$P_T/P_{0\ PLUG}$	$P_T/P_{0\ C-D}$	C_C	C_N	C_M	$C_{C\ AB}$	$C_{C\ C-D}$	$C_{C\ PLUG}$	$C_{C\ BASE}$	$C_{C\ TOT}$	NOTES
68	0	NIP8H	.30			1.0	1.56	17	.1	-.5	3	3	.8	.1	6.9	STATIC
							2.06	24	0	0	3	3	.9	.1	7.0	
							3.09	36	.3	-.4	3	3	1	.1	7.1	
							5.15	30	.1	-.6	4	4	1	.1	9.1	
							7.27	16	.2	-.8	5	5	2	.2	12.2	
69	1.7	NIP8H	.30	70°	3.0	5.18	3.0	148	282	-479	35	44	13	2	94.0	
							6.0	163	276	-464	34	47	12	2	95.0	
							7.0	161	273	-453	34	44	12	2	92.0	
							10.1	156	273	-446	34	41	12	2	89.0	
70	1.7	NIP14H	.80	70°	3.0	4.96	5.2	124	298	-523	34	5	13	2	54.0	
							7.2	124	296	-521	34	5	12	2	53.0	
							10.3	123	294	-520	33	5	12	2	52.0	
							12.9	121	294	-520	33	5	12	2	52.0	
71	0	NIP14H	.80			1.0	1.6	10	.5	-1.2	3	1	1	.1	5.1	STATIC
							2.1	12	0	-.2	3	1	1	.1	5.1	
							3.2	14	-2	.2	4	1	1	.1	6.1	
							5.4	35	0	.9	5	2	2	.2	9.2	
							5.9	33	0	.5	5	2	2	.2	9.2	

TABLE II TABULATED DATA

BLOW	M	CONFIG	A_9/A_M	λ	α	P_T/P_0 PLUG	P_T/P_0 C-D	BALANCE DATA C_C	C_N	C_M	INTEGRATED PRESSURE DATA $C_{C\ AB}$	$C_{C\ C-D}$	$C_{C\ PLUG}$	$C_{C\ BASE}$	$C_{C\ TOT}$	NOTES
72	1.7	NIPI4H	.80	70°	2.9	2.5	10.2	120	297	-531	32	5	14	2	53	
						4.9		123	299	-526	33	5	12	2	52	
						6.9		121	299	-517	33	6	11	2	52	
						10.0		118	295	-496	34	6	8	2	50	
73	1.7	NIPI3H	.80	70°	0	CONE	1.0	124	-1	27	37	7	15	2	61	
					2.9			124	248	-486	34	6	14	2	56	
					4.9			121	457	-810	32	5	12	2	51	
					6.9			116	671	-1195	29	4	10	2	45	
74	2.0	NIPI4H	.80	70°	2.9	4.83	5.0	107	221	-386	28	4	12	2	54	
							10.2	110	218	-384	26	5	11	1	43	
							15.4	109	216	-384	27	5	11	1	44	
							18.6	108	217	-387	26	5	11	1	43	
75	0	NIPI4M	.80			1.0	1.6	11	0	-.1	3	.8	.9	.1	4.8	STATIC
							2.11	13	0	-.4	3	1	1	.1	5.1	
							3.16	14	0	-.2	4	1	1	.1	6.1	
							4.23	20	-.1	.3	4	1	1	.1	6.1	
							5.28	37	-.1	1.1	5	2	2	.2	9.2	
							5.9	35	.6	-.2	5	2	2	.2	9.2	

TABLE II TABULATED DATA

BLOW	M	CONFIG	A_0/A_M	λ	α	P_T/P_0 PLUG	P_T/P_0 C-D	BALANCE DATA C_C	C_N	C_M	INTEGRATED PRESSURE DATA $C_{C\ AB}$	$C_{C\ C-D}$	$C_{C\ PLUG}$	$C_{C\ BASE}$	$C_{C\ TOT}$	NOTES
76	2.0	NIPI4H	.80	70°	2.9	3.27	16.1	100	200	-355	30	4	13	2	49	
						4.77		106	203	-358	27	5	12	1	45	
						6.9		108	208	-360	27	5	11	1	44	
						10.0		109	215	-361	29	5	10	1	45	
77	2.0	NIPI3H	.80	70°	0	CONE	1.0	104	-66	128	32	5.0	14	2	54.0	
					3.0			108	167	-287	28	6	12	2	48	
					5.0			107	340	-648	27	5	11	2	45	
					7.0			102	524	-933	25	5	10	2	42	
78	2.0	NIPI6H	1.0	70°	0	CONE	1.0	105	5	2	29	0	13	1	43	
					2.9			107	238	-414	28	0	12	1	41	
					4.9			104	410	-725	27	0	11	1	39	
					6.9			100	597	-1068	25	0	10	1	36	
79	2.0	NIPI6H	1.0	70°	2.9	2.32	15.2	117	231	-419	37	0	16	2	55	
						4.89		102	242	-434	27	0	12	1	40	
						6.98		104	246	-434	27	0	11	1	39	
						9.98		104	249	-429	29	0	10	1	40	

TABLE II TABULATED DATA

BLOW	M	CONFIG	A_0/A_M	λ	α	P_T/P_0 PLUG	P_T/P_0 C-D	BALANCE DATA			INTEGRATED PRESSURE DATA					NOTES
								C_C	C_N	C_M	$C_{C\ AB}$	$C_{C\ C-D}$	$C_{C\ PLUG}$	$C_{C\ BASE}$	$C_{C\ TOT}$	
80	0	NIPI6H	1.0			1.0	1.62	9.6	1	0	3	0	.8	.1	3.9	STATIC
							2.13	8.9	4	-3	3	0	1	.1	4.1	
							3.18	10	1	0	4	0	1	.1	5.1	
							4.26	11	1	0	4	0	1	.1	5.1	
							5.35	15	0	5	5	0	2	.2	7.2	
							6.91	18	0	6	5	0	2	.2	7.2	
81	2.0	NIPI6H	1.0	70°	2.8	4.89	5.11	112	203	-366	30	0	13	2	45	
							10.0	104	201	-367	27	0	11	1	39	
							15.2	102	197	-362	27	0	11	1	39	
							18.6	102	193	-356	27	0	11	1	39	
82	2.0	NIP7H	.50	70°	2.9	3.3	1.0	114	202	-333	31	19	13	2	65	
						4.79		130	208	-341	27	24	11	2	64	
						7.04		136	216	-349	28	25	11	2	66	
						10.1		137	223	-351	29	25	11	2	67	
83	2.0	NIP7H	.50	70°	2.9	3.3	14.9	113	173	-289	29	18	12	1	60	
						4.78		119	178	-296	27	20	12	1	60	
						7.04		121	184	-300	28	21	11	1	61	
						10.1		122	192	-303	29	21	10	1	61	

TABLE II TABULATED DATA

BLOW	M	CONFIG	A_9/A_M	λ	α	$P_T/P_{0\ PLUG}$	$P_T/P_{0\ C-D}$	BALANCE DATA C_C	C_N	C_M	INTEGRATED PRESSURE DATA $C_{C\ AB}$	$C_{C\ C-D}$	$C_{C\ PLUG}$	$C_{C\ BASE}$	$C_{C\ TOT}$	NOTES
84	2.0	N1P7H	.50	70°	0	4.79	20.3	119	-30	81	29	18	13	1	61	
					2.9			121	187	-310	28	19	12	1	60	
					4.9			117	348	-602	26	18	11	1	56	
					6.9			111	524	-921	23	17	9	1	50	
85	2.0	N1P7H	.50	70°	2.9	4.96	4.0	112	201	-342	30	19	13	2	64	
							5.07	126	199	-340	27	23	11	2	63	
							10.0	125	192	-326	27	22	11	2	62	
							14.9	120	190	-319	27	21	11	1	60	
86	2.0	N1P1H	.50	70°	0	CONE	1.0	133	-74	150	30	25	13	2	70	
					2.84			133	140	-228	29	25	12	2	68	
					4.9			128	308	-527	27	25	11	2	65	
					6.9			121	489	-854	24	23	9.0	2	58.0	
87	2.0	N2P1H	.50	70°	0	CONE	1.0	133	-135	256	30	24	12	2	68	B
					2.9			132	90	-146	28	25	11	2	66	
					4.9			126	257	-445	27	24	10	2	63	
					6.9			117	433	-766	26	23	9	2	60	

TABLE II TABULATED DATA

BLOW	M	CONFIG	A_0/A_M	λ	α	P_T/P_0 PLUG	P_T/P_0 C-D	BALANCE DATA C_C	C_N	C_M	INTEGRATED PRESSURE DATA $C_{C\ AB}$	$C_{C\ C-D}$	$C_{C\ PLUG}$	$C_{C\ BASE}$	$C_{C\ TOT}$	NOTES
88	0	N1P8H	.20			1.0	1.66	15	1	-2	3	3	1	.1	7.1	STATIC
							2.04	24	0	0	3	3	1	.1	7.1	
							2.58	36	0	0	3	3	1	.1	7.1	
							2.87	41	1	0	3	3	1	.1	7.1	
							3.10	39	2	-1	3	3	1	.1	7.1	
							4.10	34	0	-1	4	4	1	.1	9.1	
							5.18	27	2	-2	4	4	1	.1	9.1	
							6.23	21	1	-2	4	5	1	.1	10.1	
							8.32	9	6	-2	5	5	2	.2	12.2	
89	0	N1P9H	.15			1.0	1.56	19	0	0	3	3	1	.1	7.1	STATIC
							2.06	33	0	1	3	3	1	.1	7.1	
							2.34	35	0	0	3	3	1	.1	7.1	
							3.07	25	-1	0	3	4	1	.1	8.1	
							4.17	10	-1	0	3	4	1	.1	8.1	
							5.18	-3	5	9	3	4	1	.1	8.1	
							7.24	-14	25	35	4	5	1	.1	10.1	

NOTES: B- DENOTES BLUNT FAIRING INSTALLED
BASE- BASE LINE CONFIGURATION BLOW
RI]- REPEAT OF BLOW WITHIN BRACKET
STATIC- WIND OFF BLOW
T.O. - DENOTES HORIZONTAL TAIL OFF

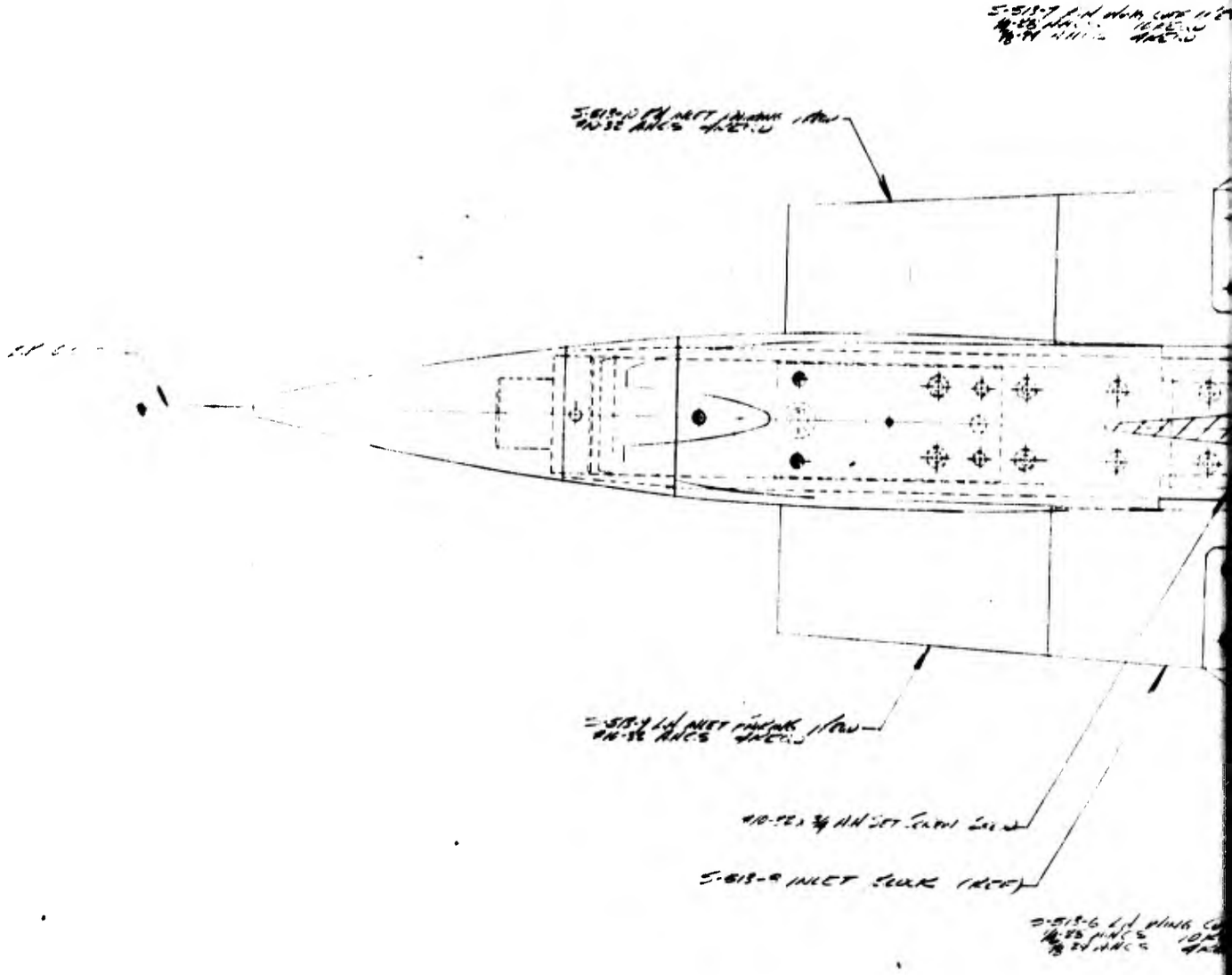

A.

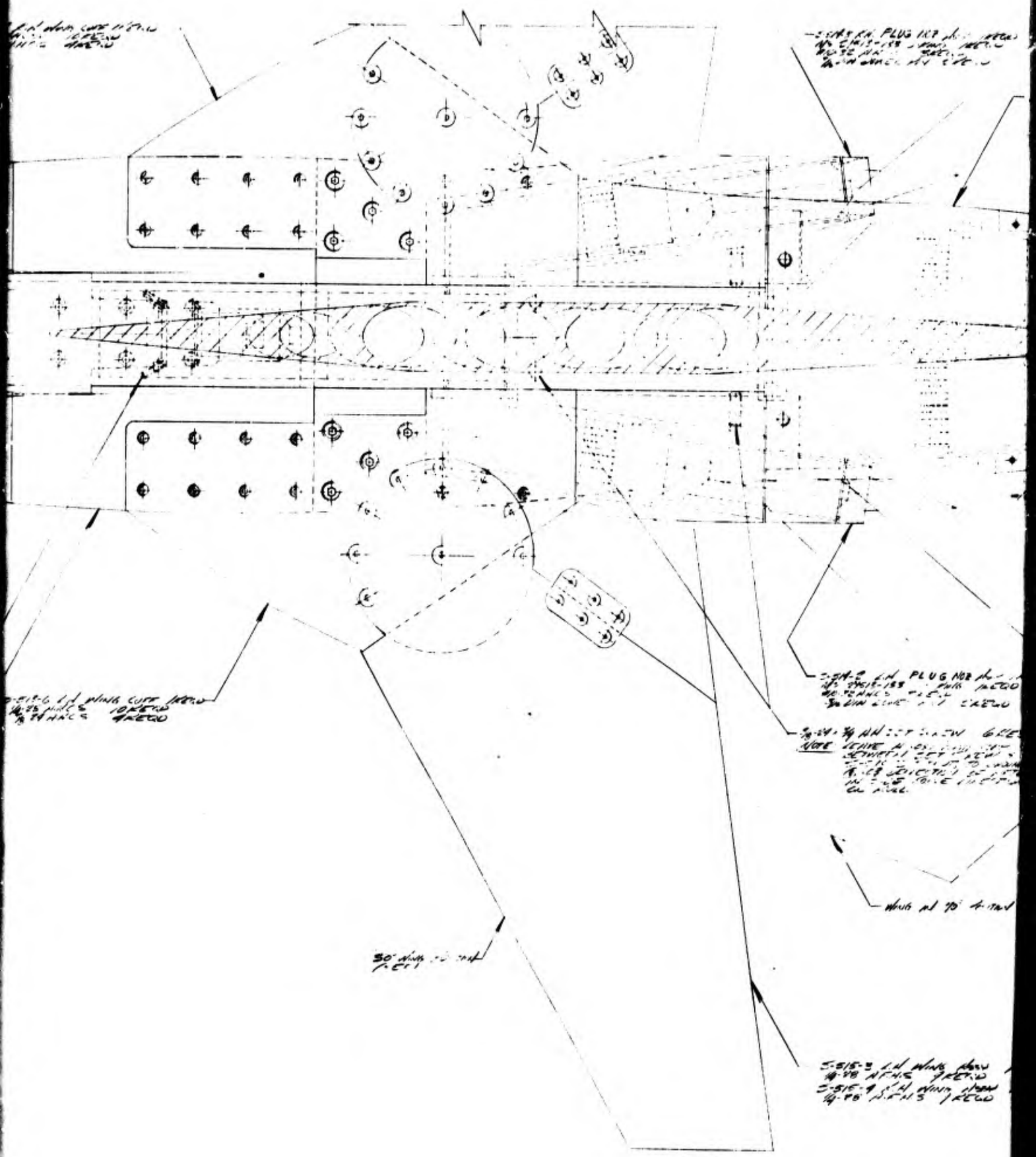

B.

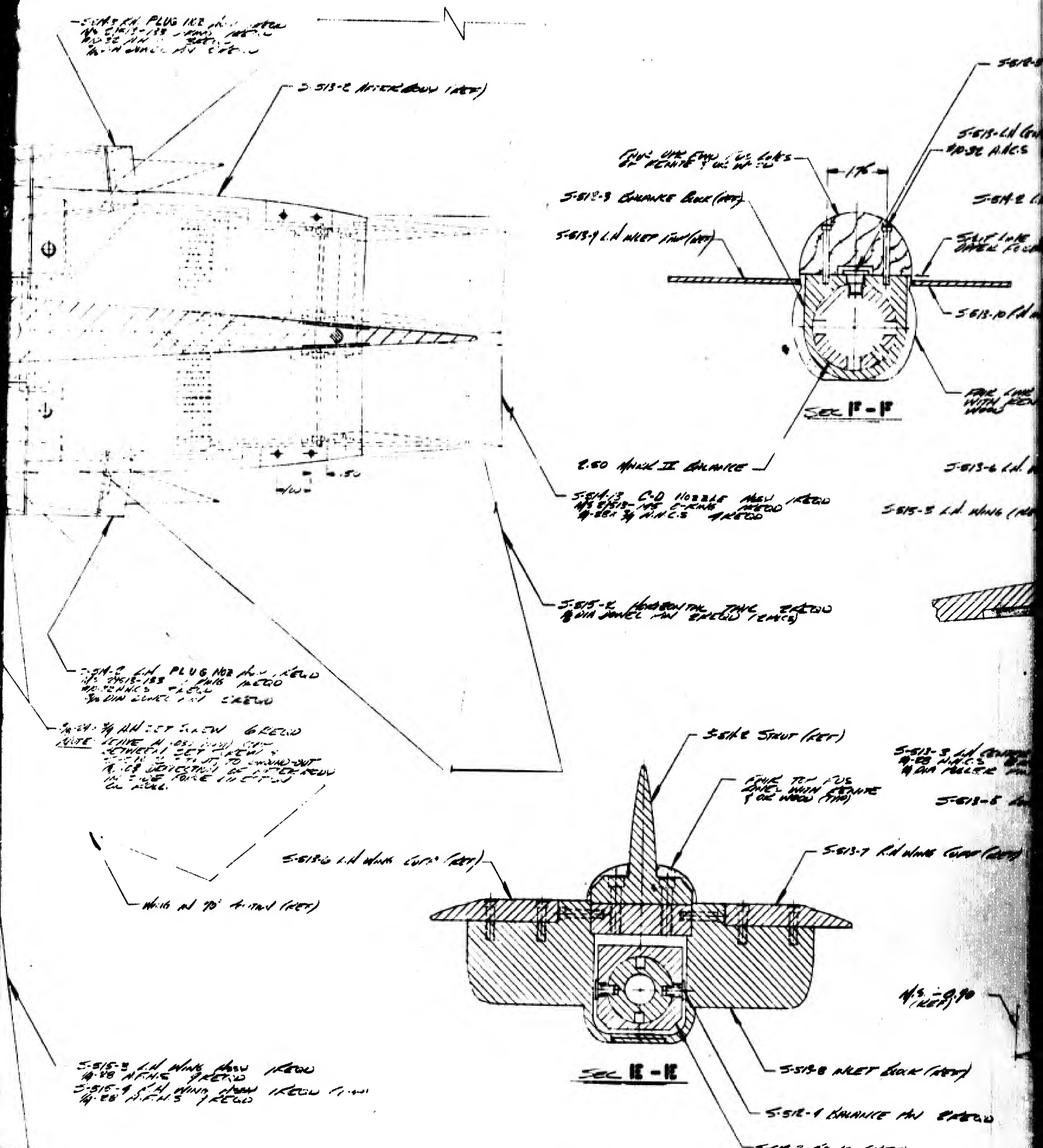
5-513-2 AFTERBODY (REF)
5-512-3 BALANCE BLOCK (REF)
SEC F - F
2.50 MARK II BALANCE
5-512 STRUT (REF)
5-513-6 L.H WING CUFF (REF)
5-513-7 R.H WING CUFF (REF)
SEC E - E
5-513-8 INLET BLOCK (REF)
5-512-4 BALANCE PIN 2 REQD
5-512-2 STING (REF)

C.

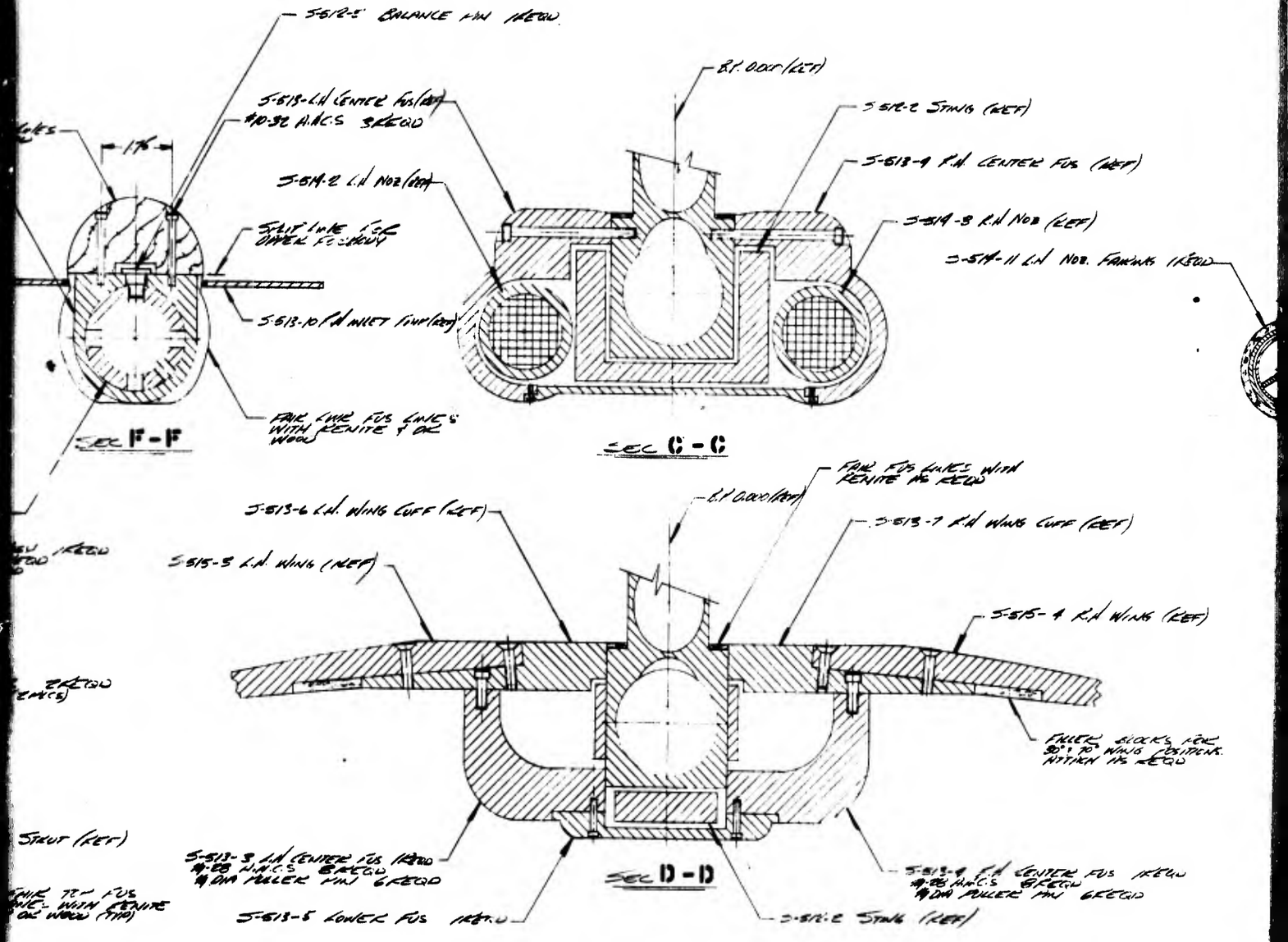
S-512-5 BALANCE PIN (REQD
S-513-L.H CENTER FUS (REF)
#10-32 H.N.C.S 3 REQD
S-514-2 L.H NO2 (REF)
SPLIT LINE FOR OUTER FUS SKIN
S-513-10 R.H INLET TIP (REF)
FAIR LINE FUS LINES WITH RENITE & DC WOOD
SEC F-F
B.P. 0.000 (REF)
S-512-2 STING (REF)
S-513-9 R.H CENTER FUS (REF)
S-514-3 R.H NO2 (REF)
S-514-11 L.H NO2. FAIRING (REQD
SEC C-C
FAIR FUS LINES WITH RENITE AS REQD
S-513-6 L.H. WING CUFF (REF)
B.P. 0.000 (REF)
S-513-7 R.H WING CUFF (REF)
S-515-3 L.H. WING (REF)
S-515-4 R.H WING (REF)
FILLER BLOCKS FOR 30° & 70° WING POSITIONS WITHIN AS REQD
S-513-3 L.H CENTER FUS (REQD
#10-32 H.N.C.S BACKED
1/4 DIA FILLER PIN 6 REQD
S-513-5 LOWER FUS (REQD
SEC D-D
S-513-9 R.H CENTER FUS (REQD
#10-32 H.N.C.S 6 REQD
1/4 DIA FILLER PIN 6 REQD
S-512-2 STING (REF)
S-513-7 R.H WING CUFF (REF)
S-513-8 INLET BLOCK (REF)
S-512-1 BALANCE PIN 2 REQD
S-512-2 STING (REF)
1/4 DIA x 3/8 FILLER PIN (REQD
M.S. -0.90 (REF)
M.S. 9.93
S-512-3 BALANCE BLOCK (REQD
5/16-24 x 100 H.N.C.S 10 REQD
5/16 DIA x 100 FILLER PIN 4 REQD
S-513-11 NOSE CONE (REQD
M.S. M.119 & CENTER OF BALANCE

D.

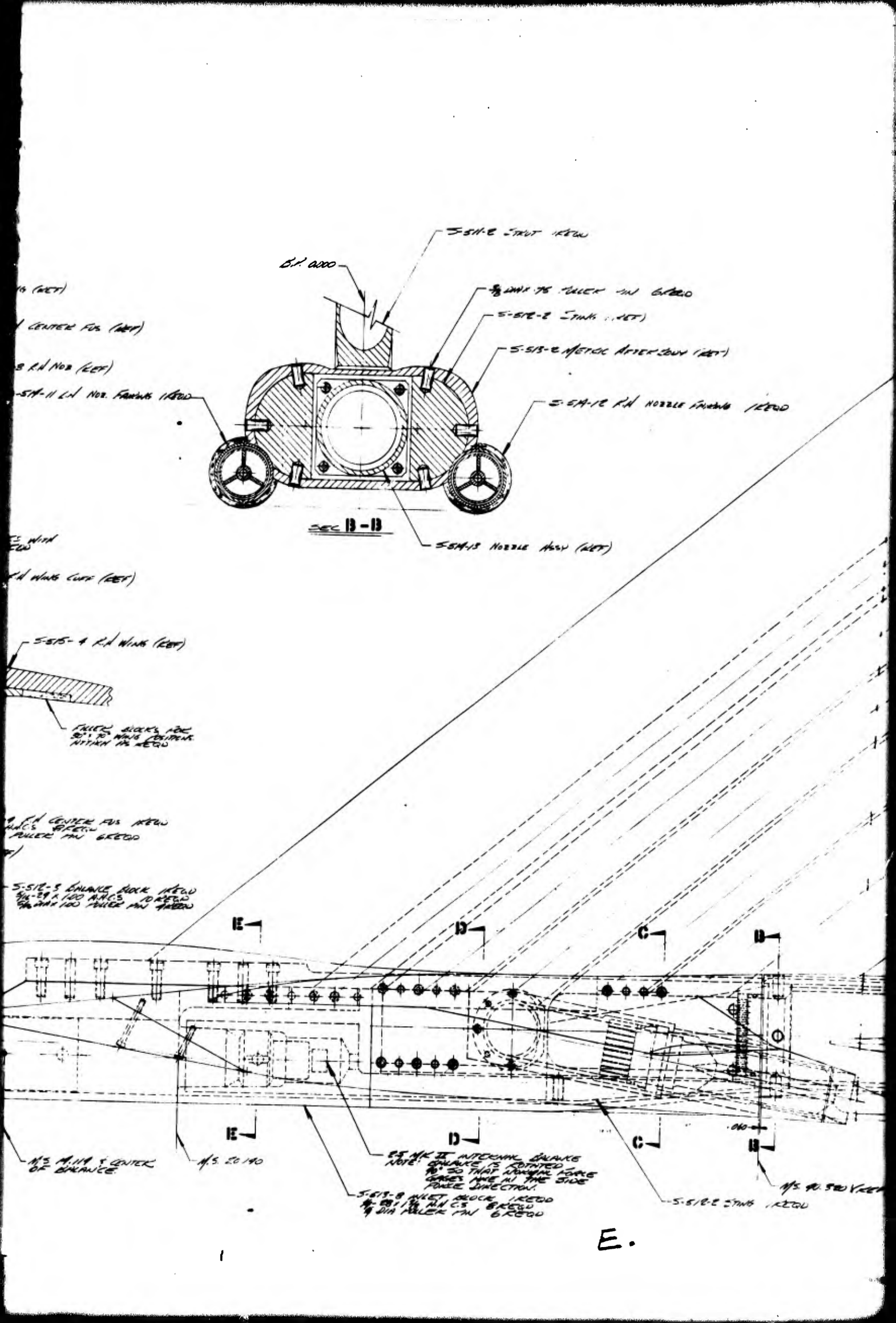
B.P. 0.000
SEC B-B
E
D
C
B
E.

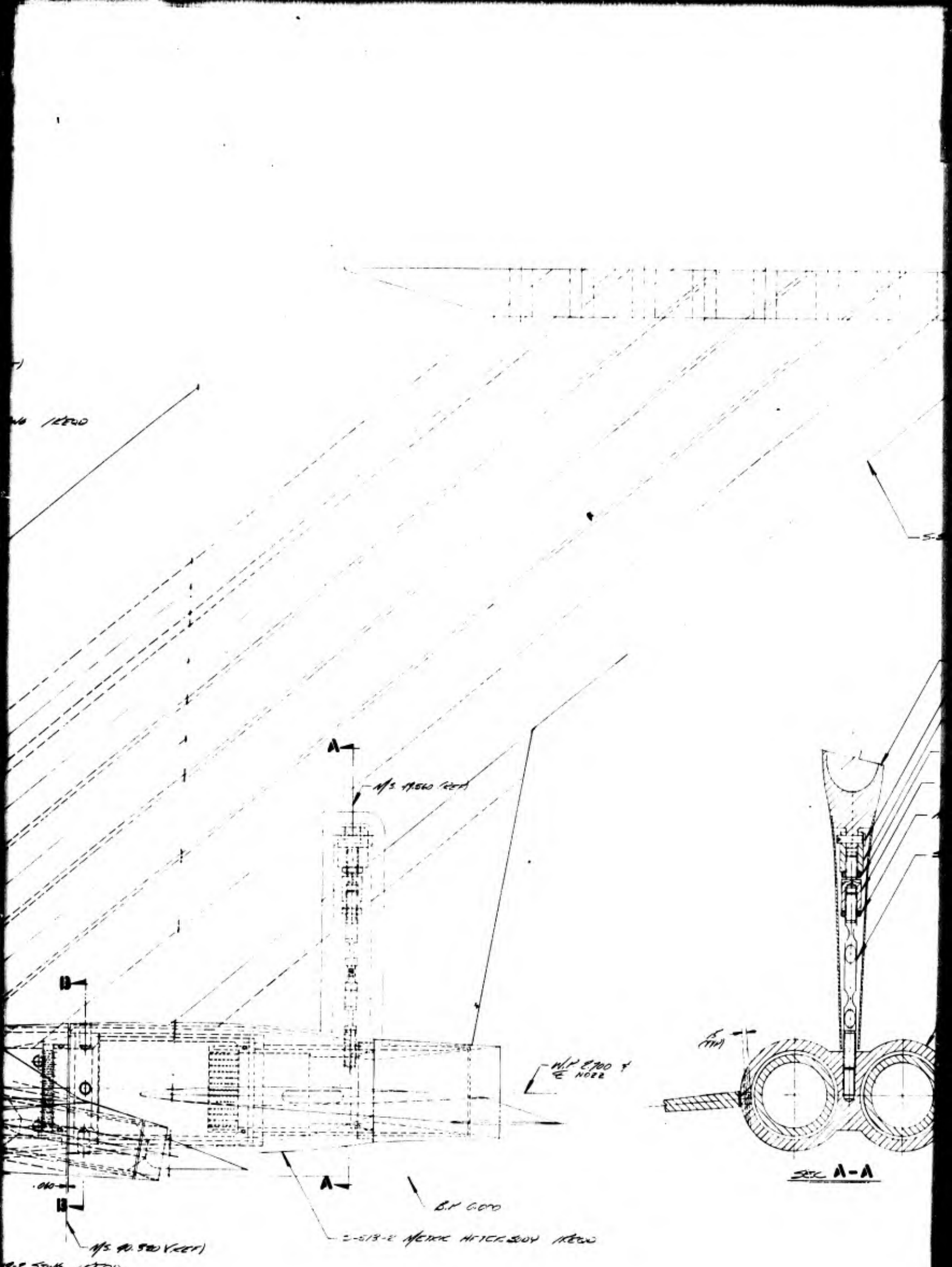

F.

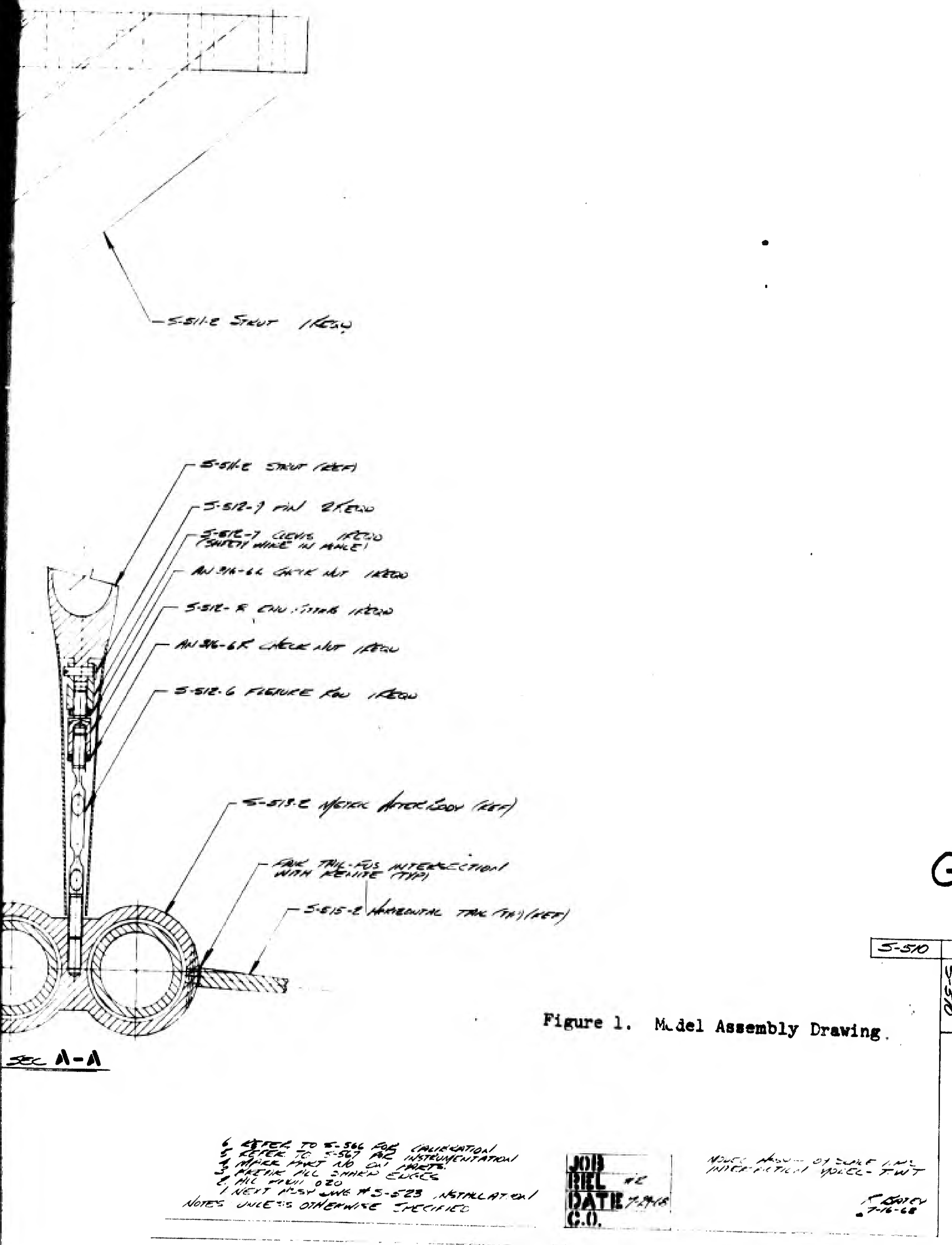

Figure 1. Model Assembly Drawing.

BLANK PAGE

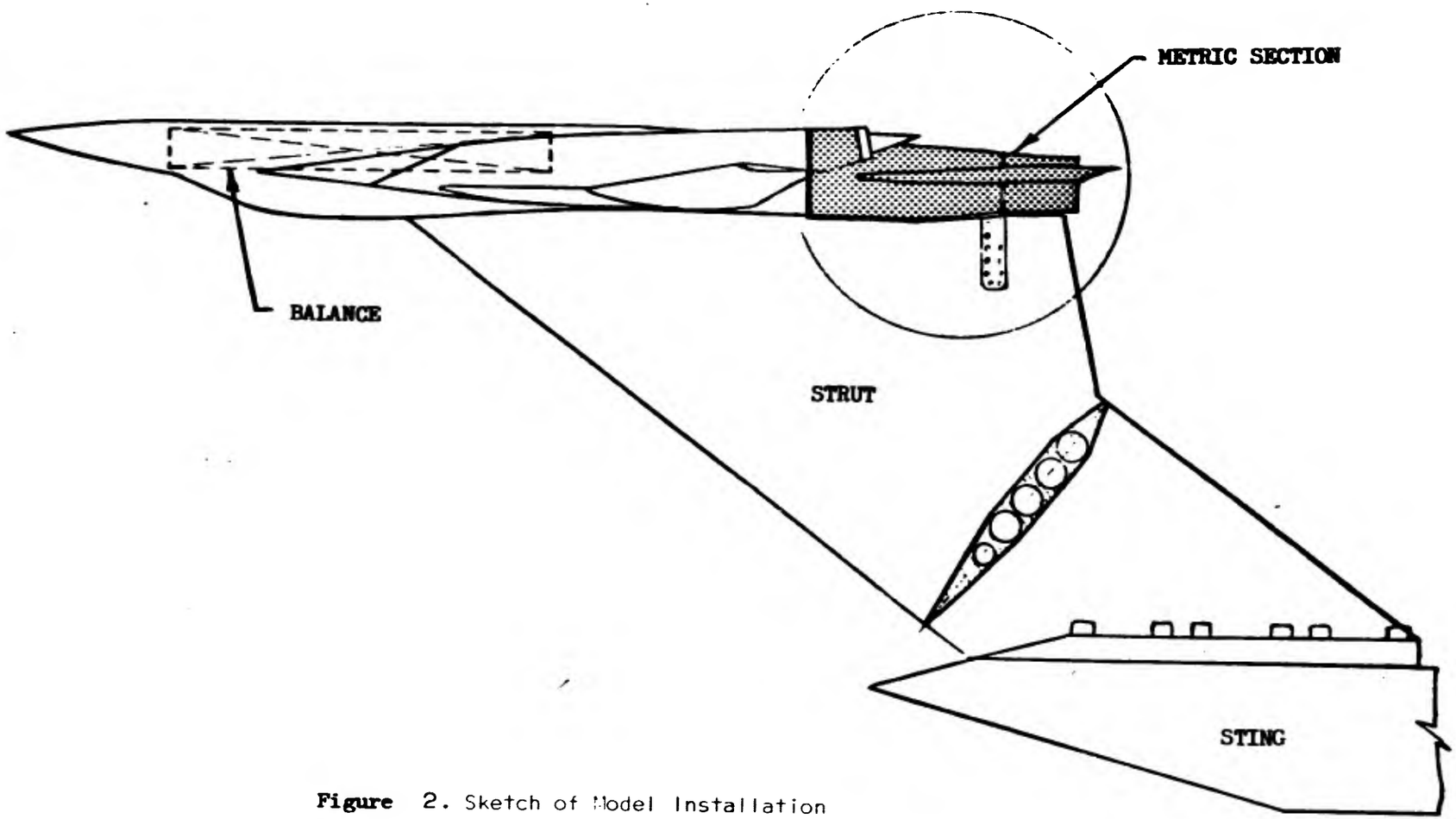

Figure 2. Sketch of Model Installation

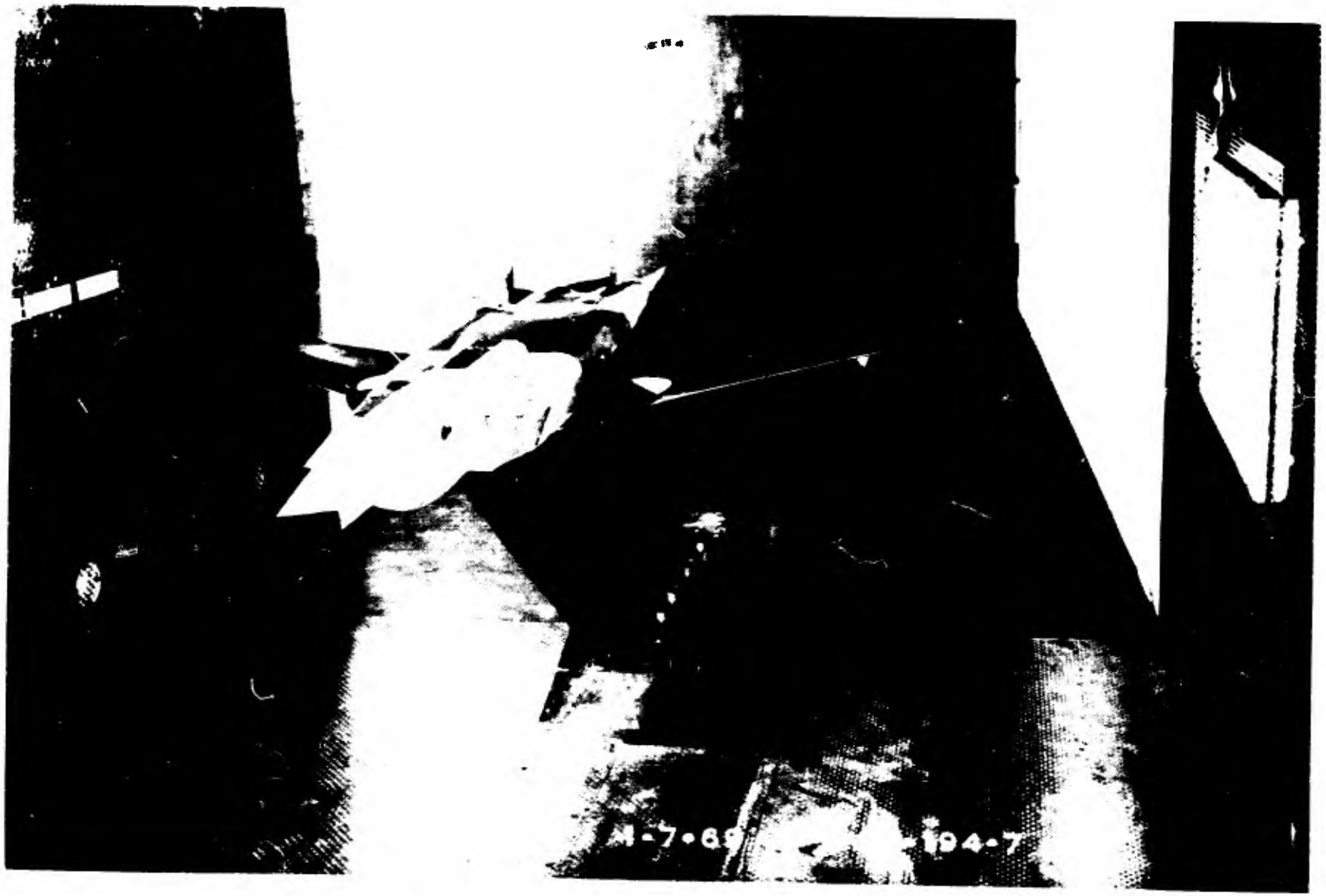

Figure 3. Interaction Model Installed In TWT

Figure 4. Interaction Model Installed In TWT

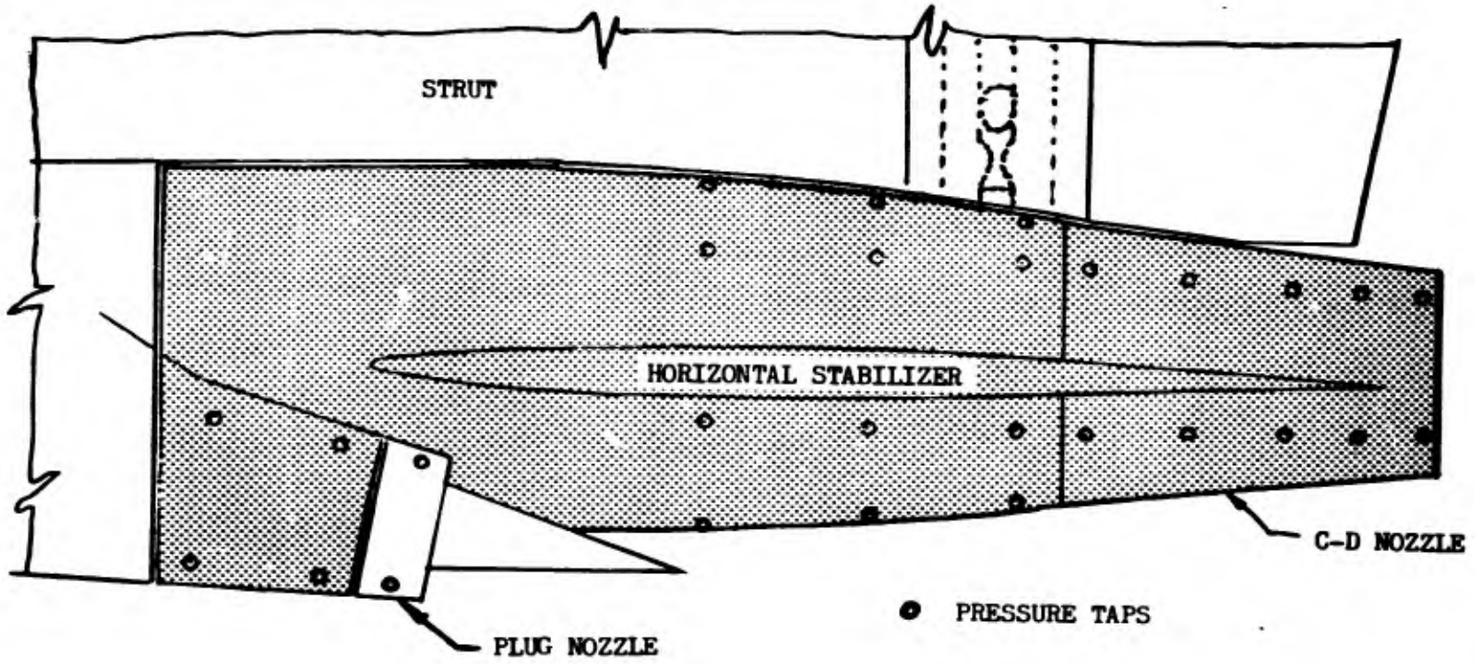

Figure 5. Pressure Instrumentation on Metric Section

Figure 6. Exploded View of Interaction Model

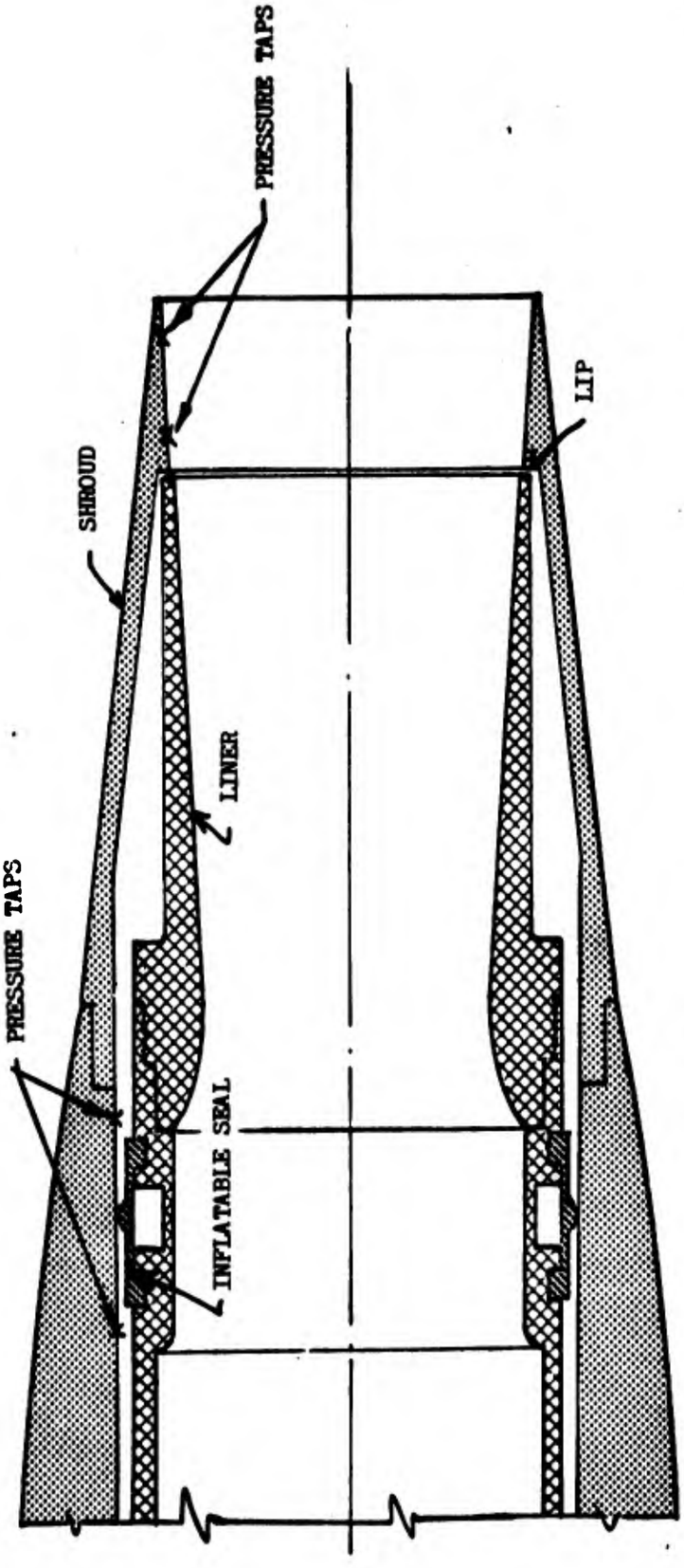

Figure 7. C-D Nozzle Details

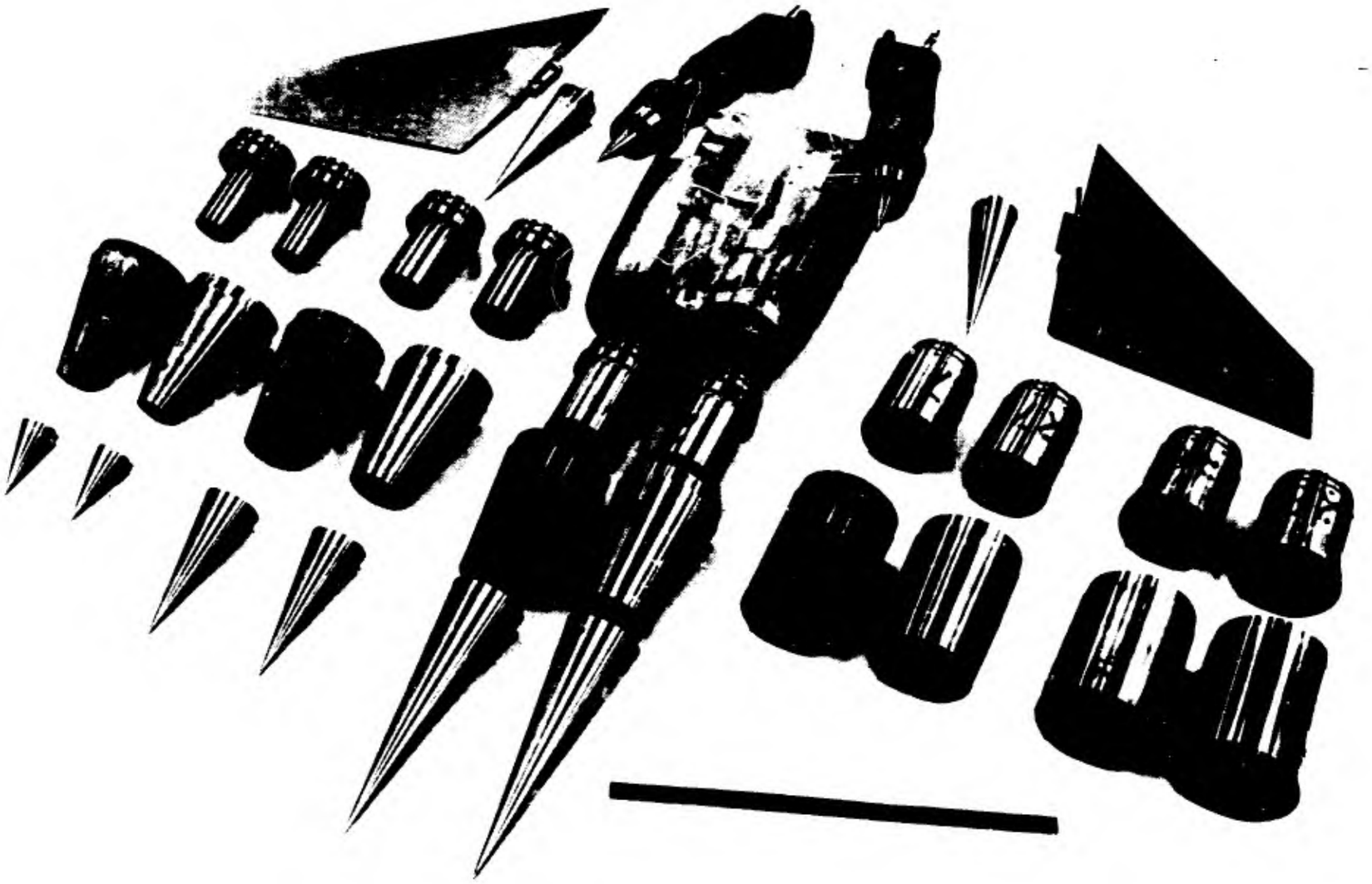

Figure 8. Exploded View of Aft Portion of Interaction Model

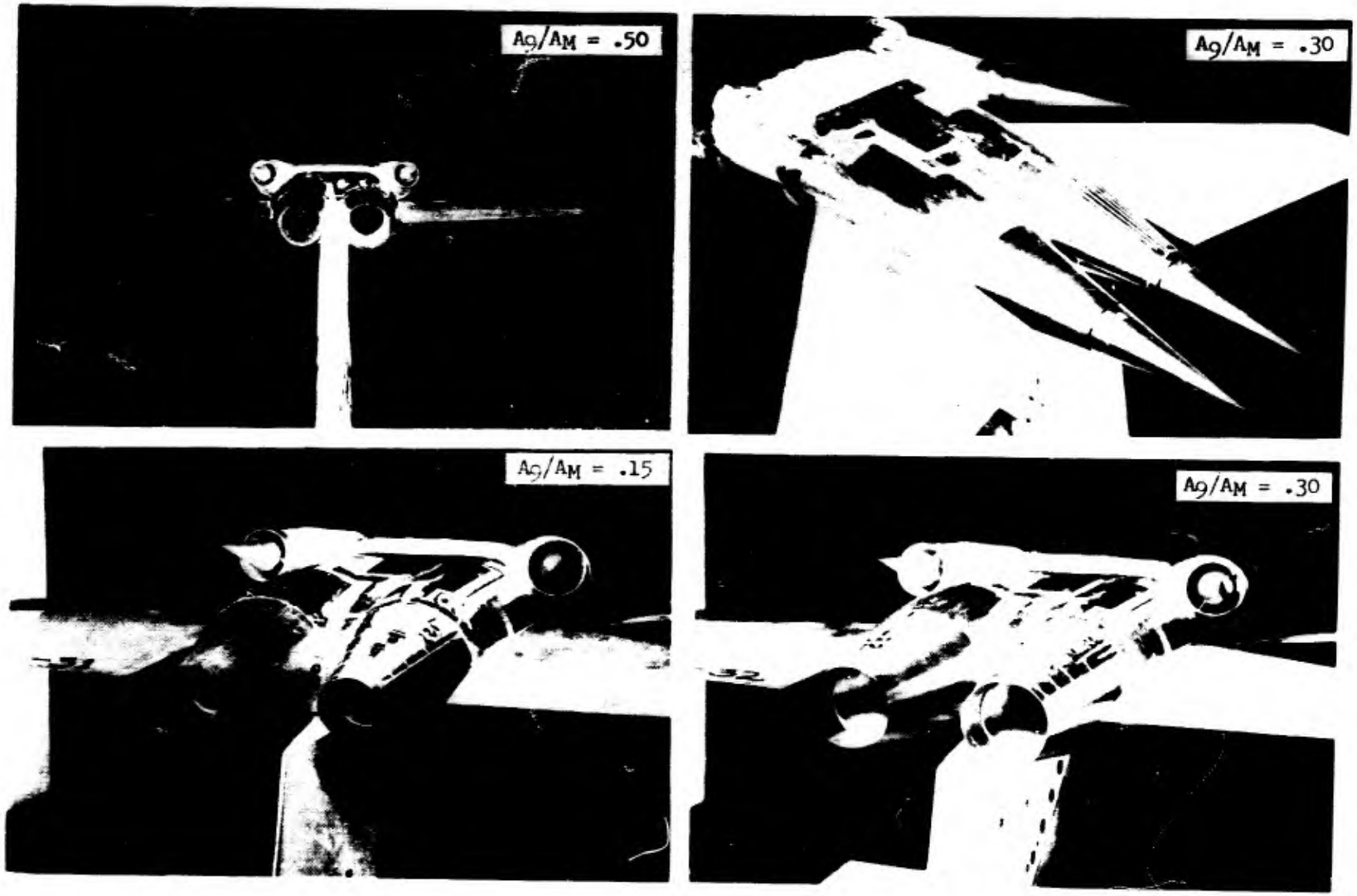

Figure 9. Rear View of Installed Nozzle Configurations

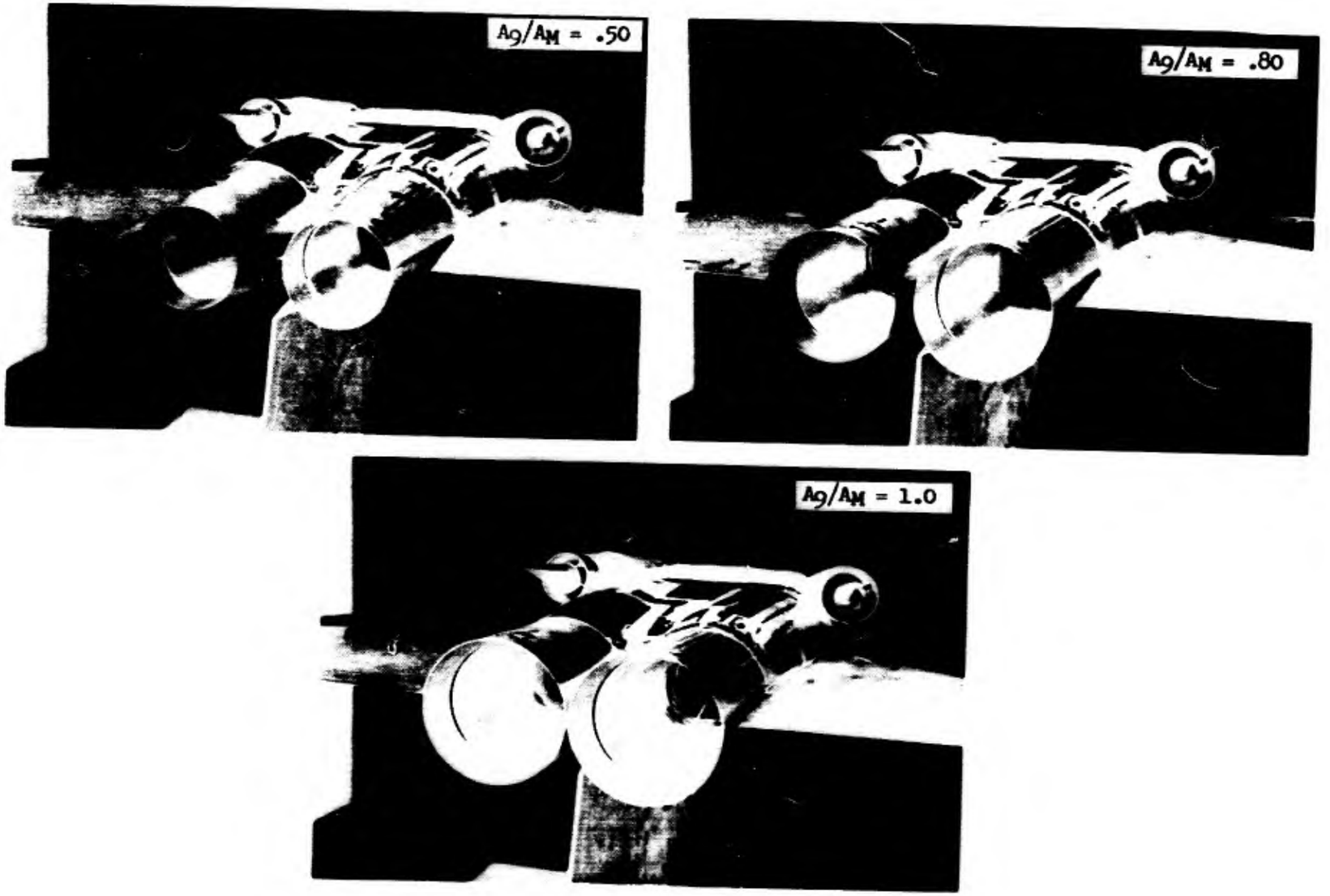

Figure 10. Rear View of Installed Nozzle Configurations

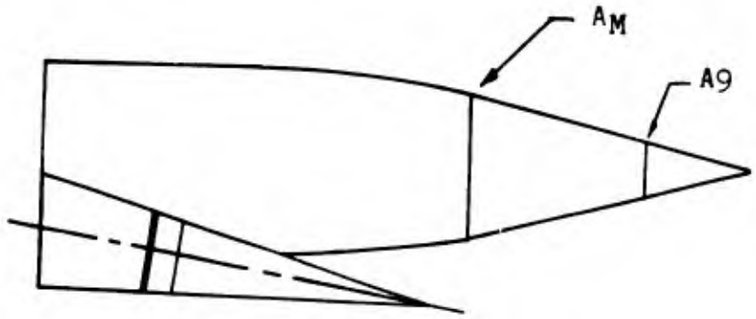

A_9/A_M =0.15

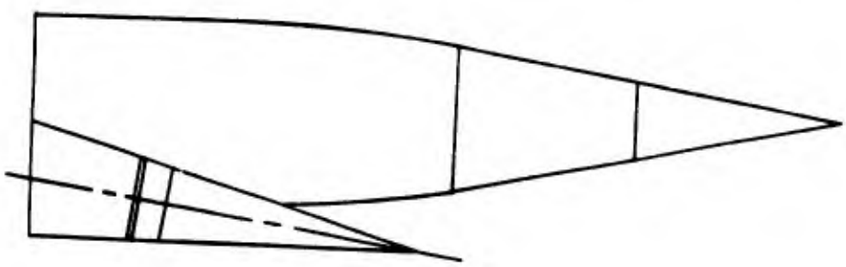

A_9/A_M = .30

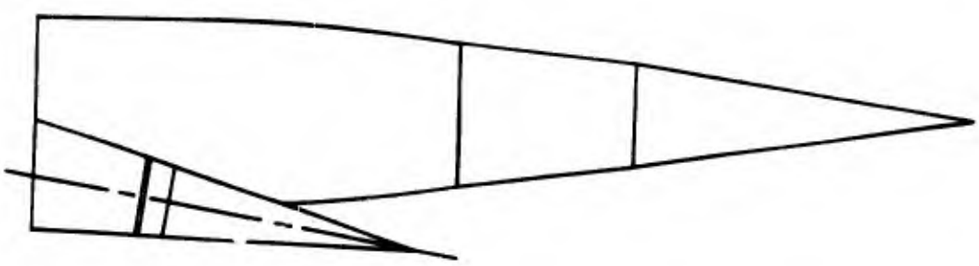

A_9/A_M=0.50 BASE LINE CONFIGURATION

Figure 11. Reference Cone Configurations

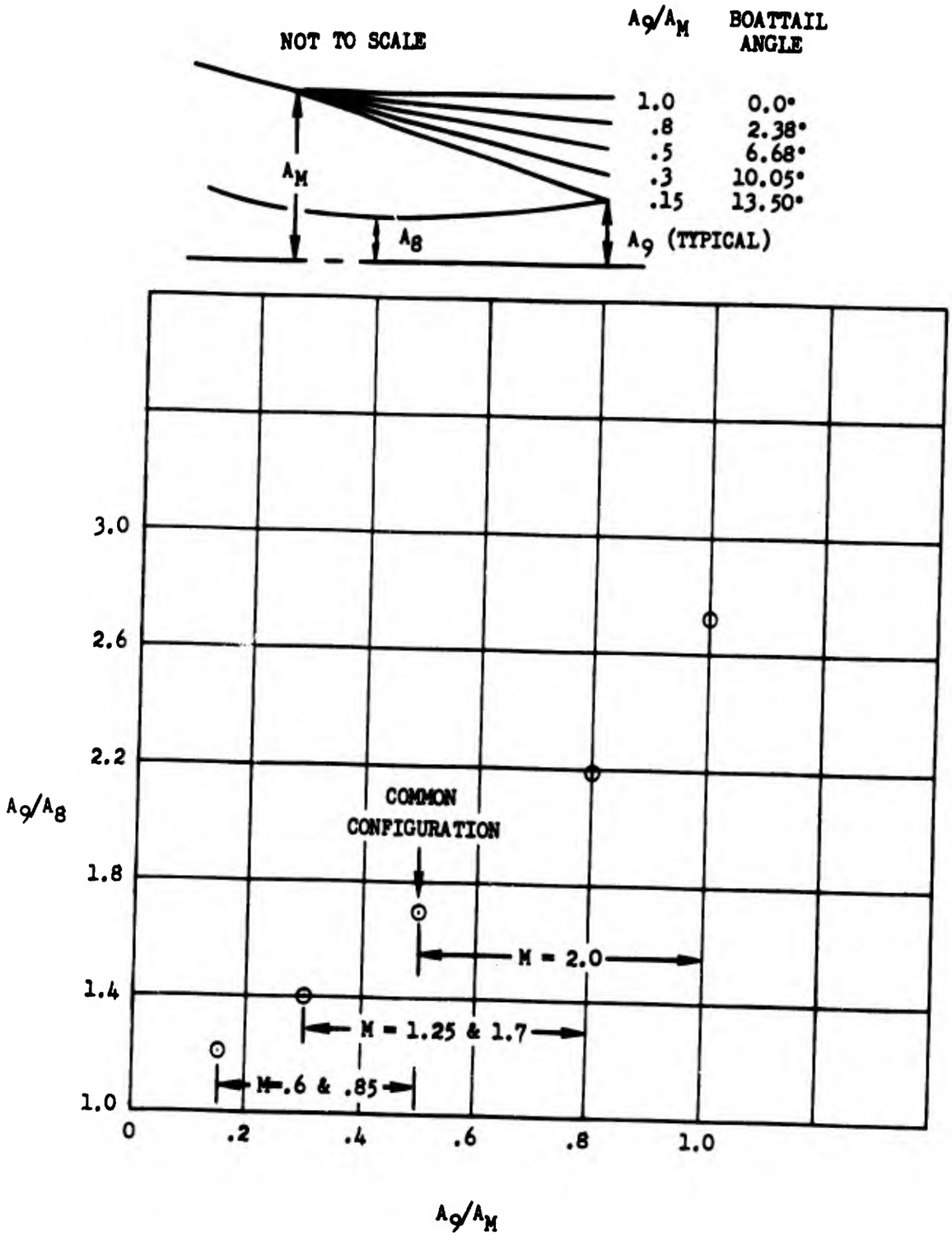

Figure 12. C-D Nozzle Configurations

(The reverse of this page is blank)

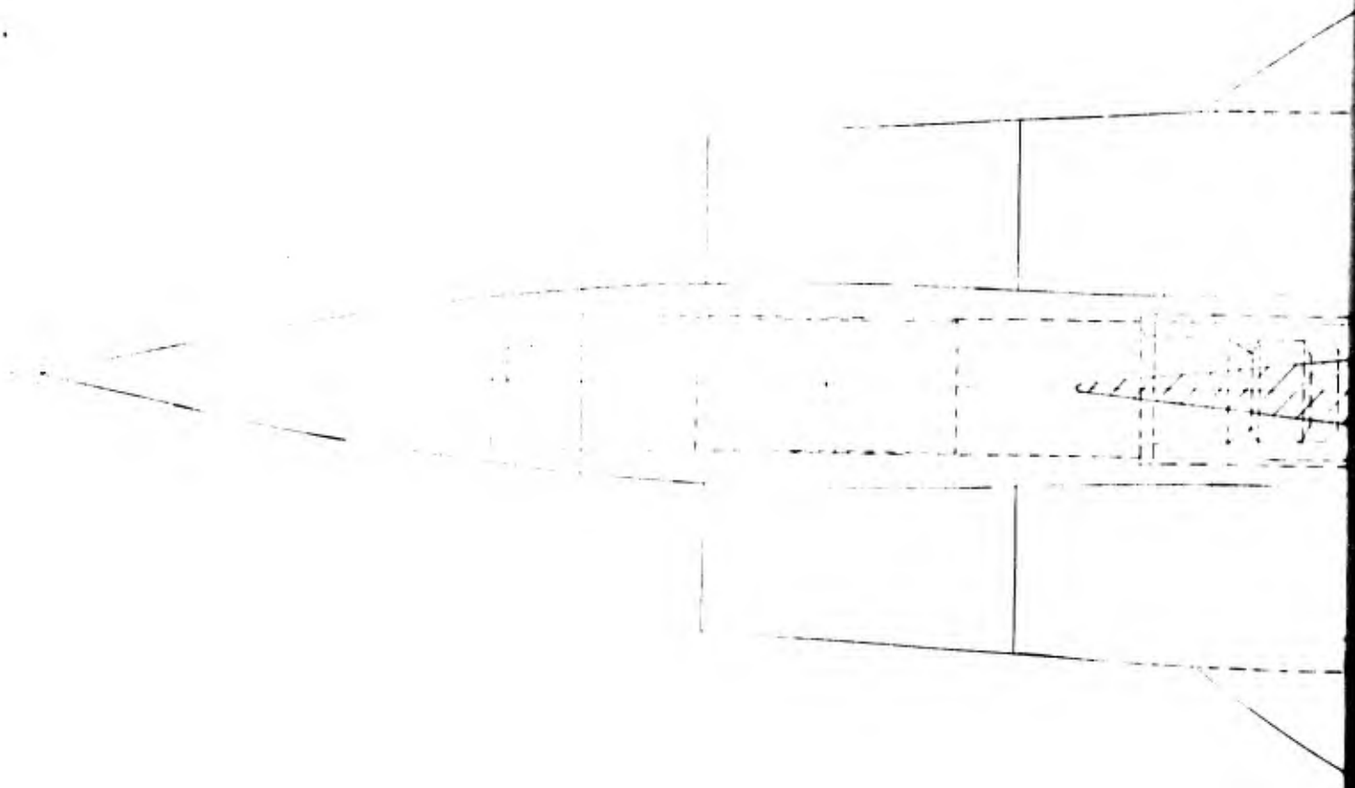

A.

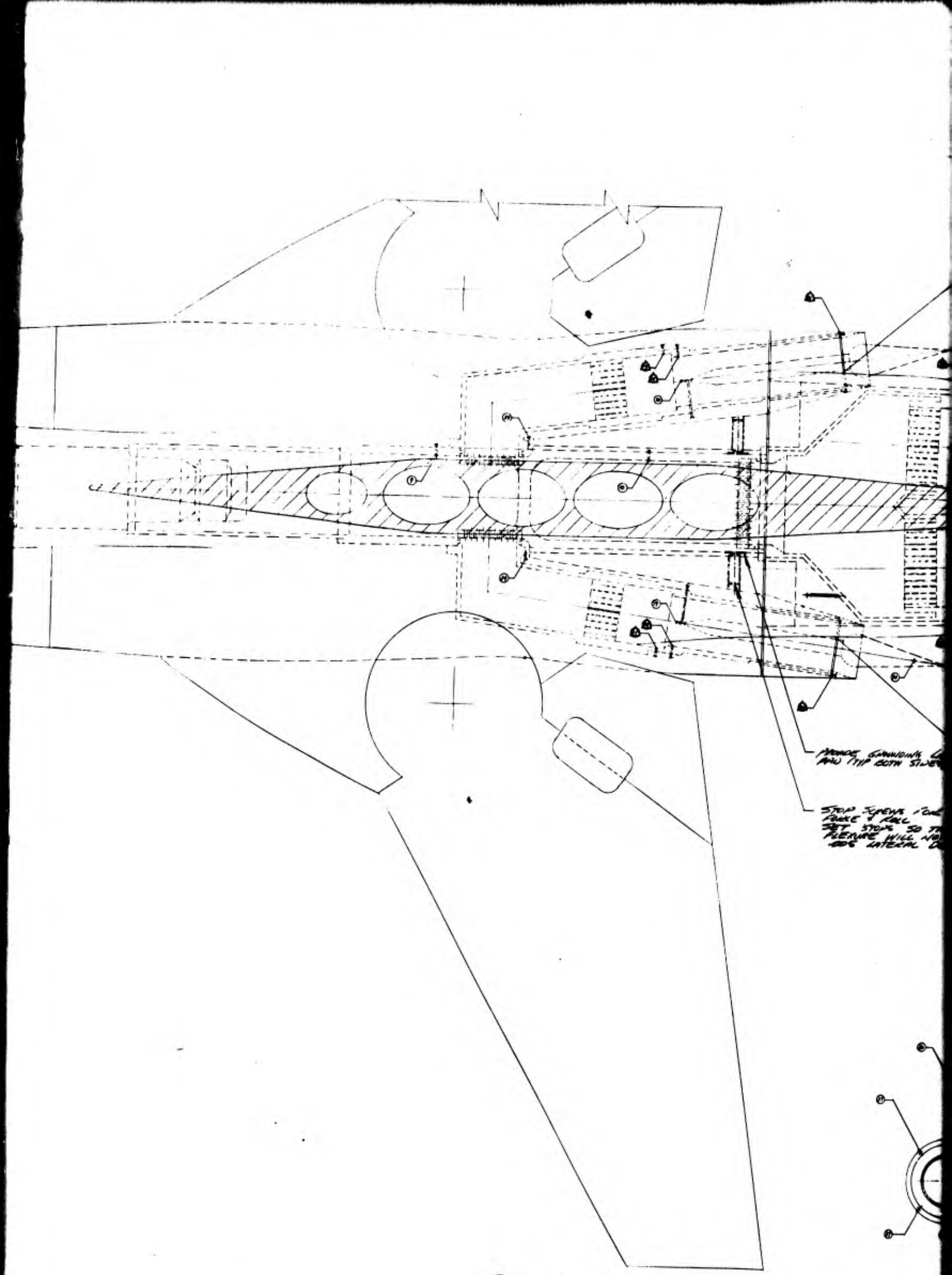

B.

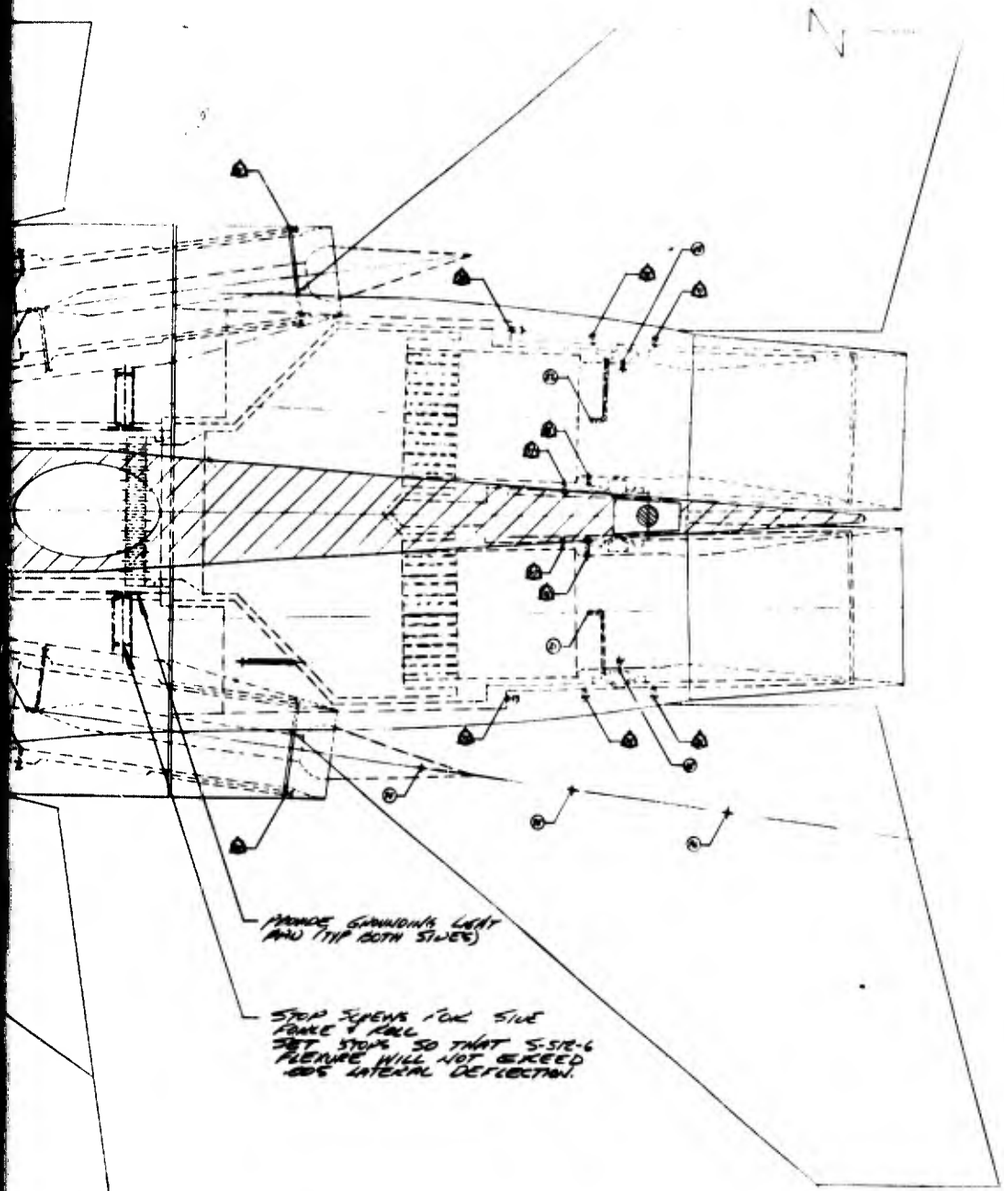
MOUNT GIMBLOINK LIGHT AND TYP BOTH SIDES
STOP SCREWS FOR SIDE ROLLER & ROLL SET STOP SO THAT S-SIZE-6 PLENUM WILL NOT EXCEED 60% LATERAL DEFLECTION.

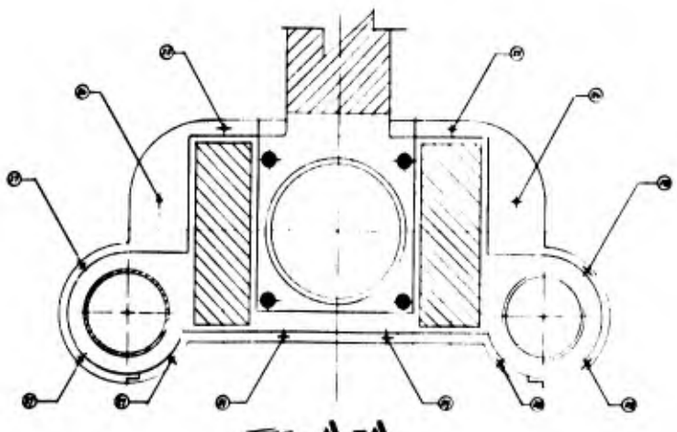

SEC A-A

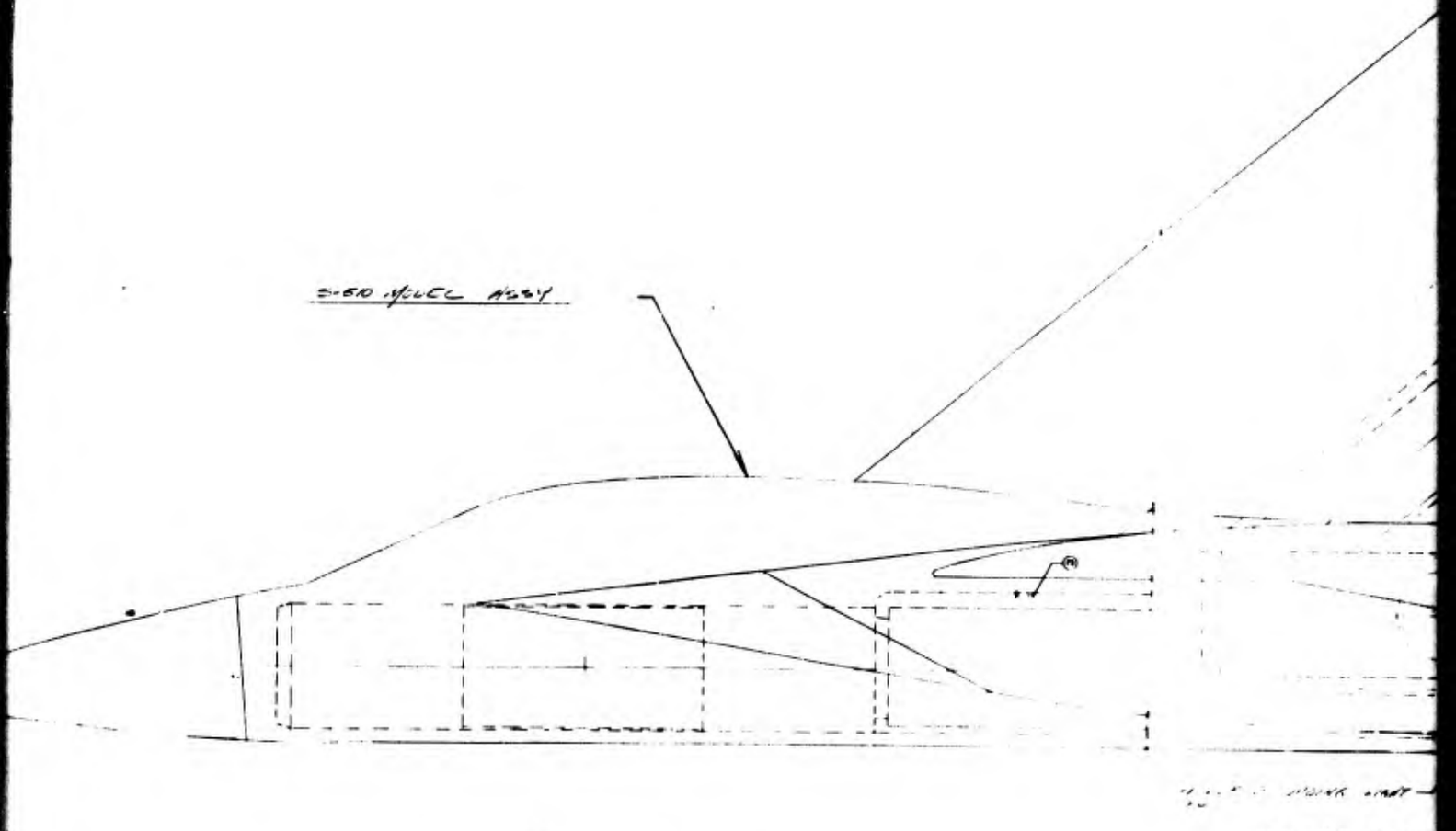

D.

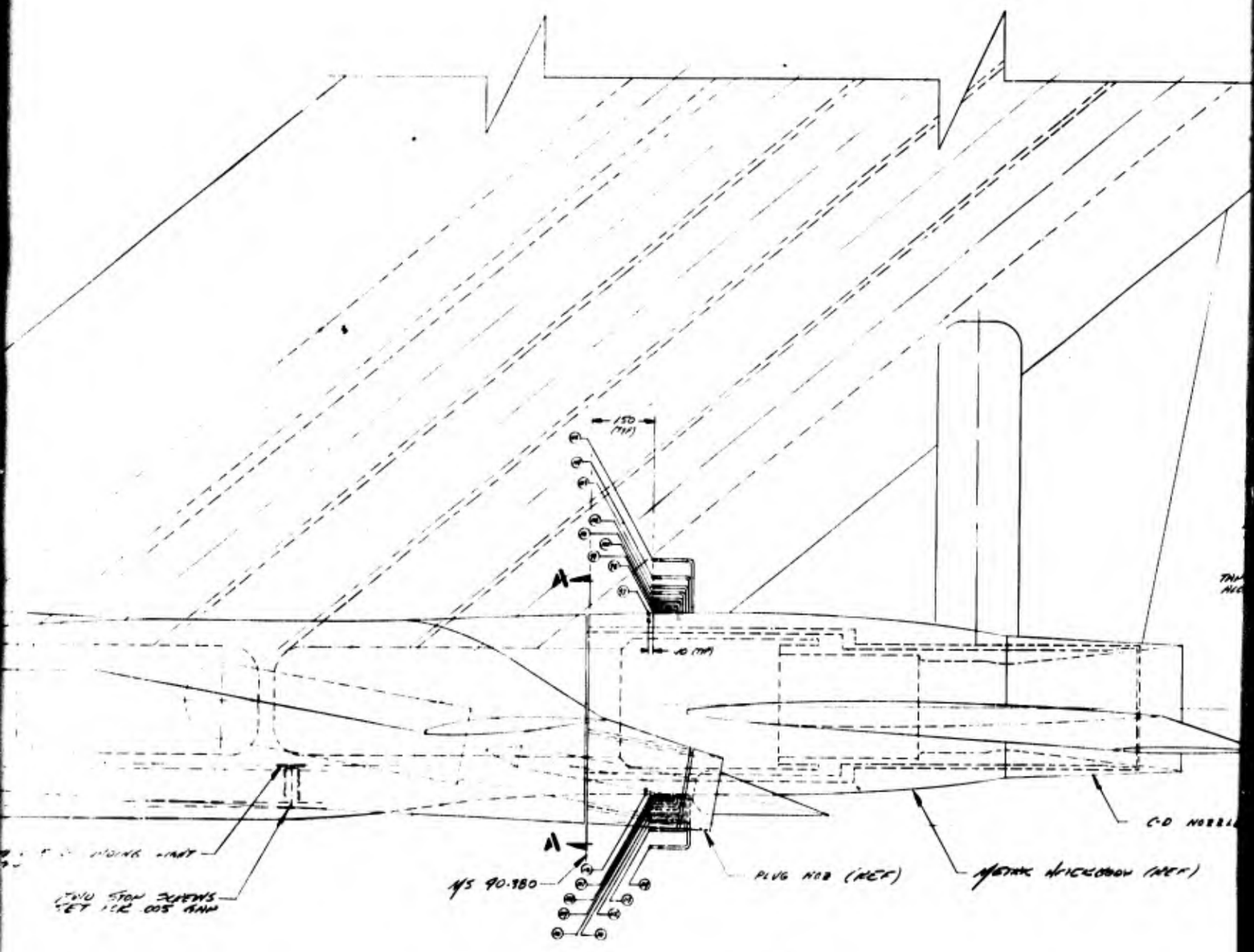

E.

PRESS TAP #	LOCATION
68	C-D NOZZLE SHROUD @ +.125", .865 FWD AT EXIT
69	" " " " .755 " " "
70	" " " " .160 " " "
71	" " " " .140 " " "
72	" " " " .130 " " "
73	" " " @ .065" .865 " " "
74	" " " " " .838 " " "
75	" " " " " .160 " " "
76	" " " " " .140 " " "
77	" " " " " .130 " " "
78	" " " @ .125" .865 " " "
79	" " " " " .838 " " "
80	" " " " " .160 " " "
81	" " " " " .140 " " "
82	" " " " " .130 " " "
83	" " " @ .065" .865 " " "
84	" " " " " .838 " " "
85	" " " " " .160 " " "
86	" " " " " .140 " " "
87	" " " " " .130 " " "
88	INTERNAL C-D NOZZLE @ .100" .80 FWD OF EXIT
89	" " " " .30 " " "
90	" " " @ .200" .80 " " "
91	" " " " .30 " " "
92	" " " @ .300" .80 " " "
93	" " " " .30 " " "
94	NOZZLE THIN LINE JUNCTURE
95	" " "
96	" " "
97	BODY SURF B.L. ABOVE STATIC TOTAL .05 ABOVE SL
98	" " " " " .10 " "
99	" " " " " .20 " "
100	" " " " " .30 " "
101	" " " " " .55 " "
102	" " " " " .60 " "
103	" " " " " .80 " "
104	" " " " " 1.00 " "
105	CANOPY SURF B.L. ABOVE STATIC TOTAL .05 ABOVE SL
106	" " " " " .10 " "
107	" " " " " .20 " "
108	" " " " " .30 " "
109	" " " " " .55 " "
110	" " " " " .60 " "
111	" " " " " .80 " "
112	" " " " " 1.00 " "
113	TOTAL PRESS ON SAT EXIT'S (MANIFOLD)

PRESS TAP #	
1	UPSTREAM AND
2	DOWNSTREAM A
3	UPSTREAM AND
4	DOWNSTREAM A
5	UPSTREAM AND
6	DOWNSTREAM A
7	TOTAL PRESSU
8	TOTAL PRESSU
9	NACEL FWD
10	NACEL AFT
11	UPSTREAM AND
12	DOWNSTREAM A
13	UPSTREAM AND
14	DOWNSTREAM A
15	UPSTREAM AND
16	DOWNSTREAM "
17	UPSTREAM AND
18	DOWNSTREAM "
19	TOTAL PRESSU
20	" "
21	" "
22	" "
23	NACEL CAVITY
24	NACEL CAVITY
25	FWD SEAT CA
26	" "
27	" "
28	" "
29	" "
30	PLUG NOZ
31	" "
32	R.H. INTERNA
33	R.H. INTERNA
34	L.H. INTERNA
35	R.H. "
36	L.H. INTERNA
37	R.H. "
38	AFTERBODY
39	"
40	"
41	"
42	"
43	"
44	"
45	"
46	"
47	"
48	"
49	"
50	"
51	"
52	"
53	"
54	"
55	"
56	AFTERBODY
57	"
58	PLUG FAIRING
59	" "
60	" "
61	" "
62	" "
63	" "
64	" "
65	" "
66	" "
67	" "

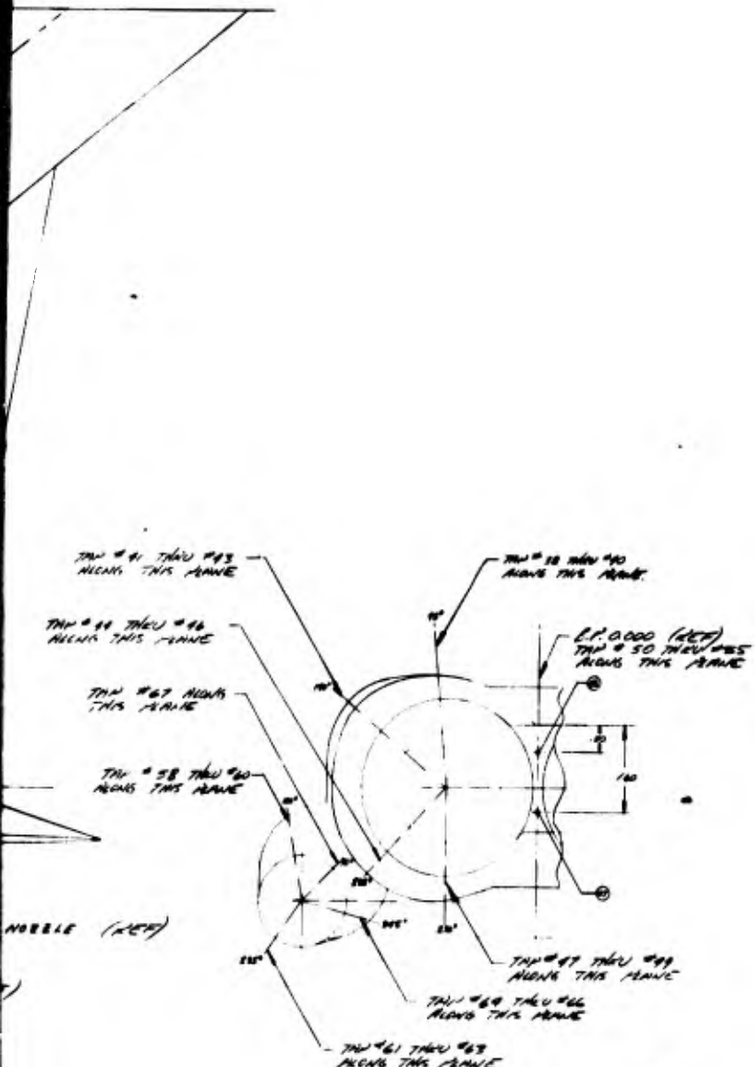

Figure 13. Pressure Instru

8. PROVIDE A .065 O.D. X .051 I.D. HARD LINE ALL THE WAY OUT FOR SEAL PRESSURE.
7. TUBE # 1 THRU #22 ARE TO BE HARD LINE ALL THE WAY OUT.
6. LEAK & CONTINUITY CHECK ALL PRESS. TAPS.
5. PROVIDE A GROUNDING LIGHT SYSTEM BETWEEN ALL STOP SCREWS.
4. CODE ALL TUBES WITH TUBE NO.
3. Δ DENOTES A MANIFOLD OF FOUR STATIC TAPS.
2. PRESS. TAPS WITH THE SAME NO. ARE TO BE MANIFOLDED
1. ALL TUBING TO BE .065 O.D. X .049 I.D. STN STL TUBING

NOTES: UNLESS OTHERWISE SPECIFIED

JOB	
REL	#1
DATE	10-24-68
C.O.	

INSTRU
INTE

F.

PRESS TAP #	LOCATION
60	C-D NOZZLE THROAT @ = 135°, .065 DIA AT EXIT
61	" " " " = 225, " " "
62	" " " " = 180, " " "
63	" " " " = 90, " " "
64	" " " " = 45, " " "
65	" " " @ = 315°, .065 " "
66	" " " " = 225, " " "
67	" " " " = 180, " " "
68	" " " " = 90, " " "
69	" " " @ = 45°, .065 " "
70	" " " " = 225, " " "
71	" " " " = 180, " " "
72	" " " " = 90, " " "
73	" " " @ = 315°, .065 " "
74	" " " " = 225, " " "
75	" " " " = 180, " " "
76	" " " " = 90, " " "
77	INTERNAL C-D NOZZLE @ = 135°, .80 DIA AT EXIT
78	" " " " = 225, .30 " " "
79	" " " " = 180, .30 " " "
80	" " " @ = 315°, .80 " " "
81	" " " " = 225, .30 " " "
82	" " " " = 180, .30 " " "
83	" " " @ = 90°, .80 " " "
84	" " " " = 45, .30 " " "
85	ABOVE TAPS ARE SURFACE
86	" " " "
87	" " " "
88	GRAIN SURF. @ L. ABOVE SURF.
89	" " " " TOTAL .45 ABOVE "
90	" " " " " .40 " "
91	" " " " " .50 " "
92	" " " " " .30 " "
93	" " " " " .75 " "
94	" " " " " .60 " "
95	" " " " " .80 " "
96	" " " " " .100 " "
97	CASTER SURF @ L. ABOVE STATIC
98	" " " " TOTAL .45 ABOVE "
99	" " " " " .40 " "
100	" " " " " .60 " "
101	" " " " " .30 " "
102	" " " " " .75 " "
103	" " " " " .60 " "
104	" " " " " .80 " "
105	" " " " " .100 " "
106	TOTAL PRESS. ON SET EVEN'S (REMAINING)

PRESS TAP #	LOCATION
1	UPSTREAM RING, MAIN FLOWMETER - 6" LINE
2	DOWNSTREAM RING, " " " " "
3	UPSTREAM RING, MAIN FLOWMETER - 8" LINE
4	DOWNSTREAM RING, " " " " "
5	UPSTREAM RING, MAIN FLOWMETER - 8" LINE
6	DOWNSTREAM RING, " " " " "
7	TOTAL PRESSURE - PROBE TO FWD WALL AFTERBODY
8	TOTAL PRESSURE - " " AFT " "
9	WALL FWD AFTERBODY STATIC - PORT
10	WALL AFT AFTERBODY STATIC - PORT
11	UPSTREAM RING, L.H. PLUG NOZ FLOWMETER
12	DOWNSTREAM RING, " " " " "
13	UPSTREAM RING, R.H. PLUG NOZ FLOWMETER
14	DOWNSTREAM RING, " " " " "
15	INTERCOM RING, L.H. C-D NOZZLE FLOWMETER
16	DOWNSTREAM " " " " "
17	UPSTREAM RING R.H. " " "
18	DOWNSTREAM " " " " "
19	TOTAL PRESSURE L.H. PLUG NOZZLE
20	" " R.H. " "
21	" " L.H. C-D NOZZLE
22	" " R.H. " "
23	MODEL BALANCE CAVITY - L.H. CWA
24	MODEL CAVITY PRESS.
25	FWD SHAFT CAVITY PRESS TAP
26	" " " " SIDE
27	" " " " L.H. END
28	" " " " R.H. END
29	" " " " BOTTOM
30	PLUG NOZ SHAFT PRESS - L.H. END
31	" " " " " - R.H. END
32	L.H. INTERNAL CAVITY
33	R.H. INTERNAL CAVITY
34	L.H. INTERNAL CAVITY UPSTREAM SEAL
35	R.H. " " " "
36	L.H. INTERNAL CAVITY DOWNSTREAM SEAL
37	R.H. " " " "
38	AFTERBODY STATIC @ = 15° M.S. 96.31
39	" " " = " M.S. 98.31
40	" " " = " M.S. 97.71
41	" " @ = 120° M.S. 96.31
42	" " " = " M.S. 98.31
43	" " " = " M.S. 97.71
44	" " @ = 225° M.S. 96.31
45	" " " = " M.S. 98.31
46	" " " = " M.S. 97.71
47	" " @ = 270° M.S. 96.31
48	" " " = " M.S. 98.31
49	" " " = " M.S. 97.71
50	" " @ AFT SHAFT M.S. 96.31
51	" " " " M.S. 97.81
52	" " @ CWA SHAFT M.S. 97.31
53	" " " " M.S. 97.71
54	" " " " M.S. 97.81
55	" " " " M.S. 98.01
56	AFTERBODY BASE PRESS @ 30 SECTOR 70
57	" " " 16 " "
58	PLUG FAIRING STATIC @ = 100°, .065 DIA AT EXIT
59	" " " " = " .45 " " "
60	" " " " = " .30 " " "
61	" " " @ = 235° .065 " " "
62	" " " " = " .45 " " "
63	" " " " = " .30 " " "
64	" " " @ = 315° .065 " " "
65	" " " " = " .45 " " "
66	" " " " = " .30 " " "
67	" " " @ = 45° .30 " " "

Figure 13. Pressure Instrumentation Drawing

5-713

5-713

6. PROVIDE A .065 O.D. x .051 I.D. HARD LINE ALL THE WAY OUT FOR SEAL PRESSURE.
7. TUBE # 1 THRU # 22 ARE TO BE HARD LINE ALL THE WAY OUT.
8. CLEAR & CONTINUITY CHECK ALL PRESS TAPS.
9. PROVIDE A GROUNDING LIGHT SYSTEM BETWEEN ALL STOP SCREWS.
4. CODE ALL TUBES WITH TUBE NO.
3. △ DENOTES A MANIFOLD OF FOUR STATIC TAPS.
2. PRESS TAPS WITH THE SAME NO. ARE TO BE MANIFOLDED.
1. ALL TUBING TO BE .065 O.D. x .049 I.D. STN STL TUBING.

NOTES: UNLESS OTHERWISE SPECIFIED.

JOB REL #1
DATE 10-24-68
C.O.

INSTRUMENTATION - .09 SCALE 1.M.S. INTERACTION MODEL - T.W.T.

R. BATES 10-16-68

65/66

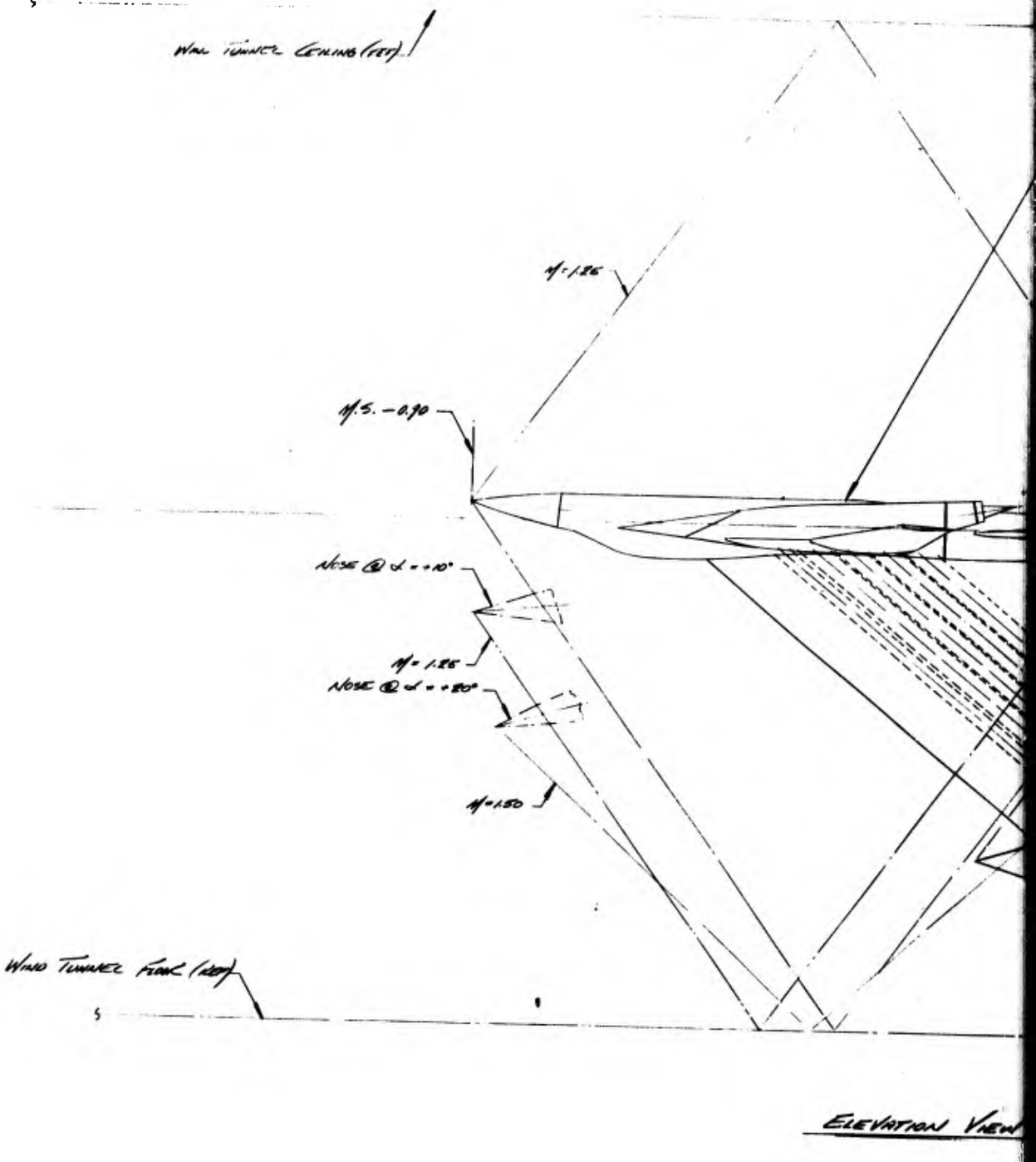

ELEVATION VIEW

A.

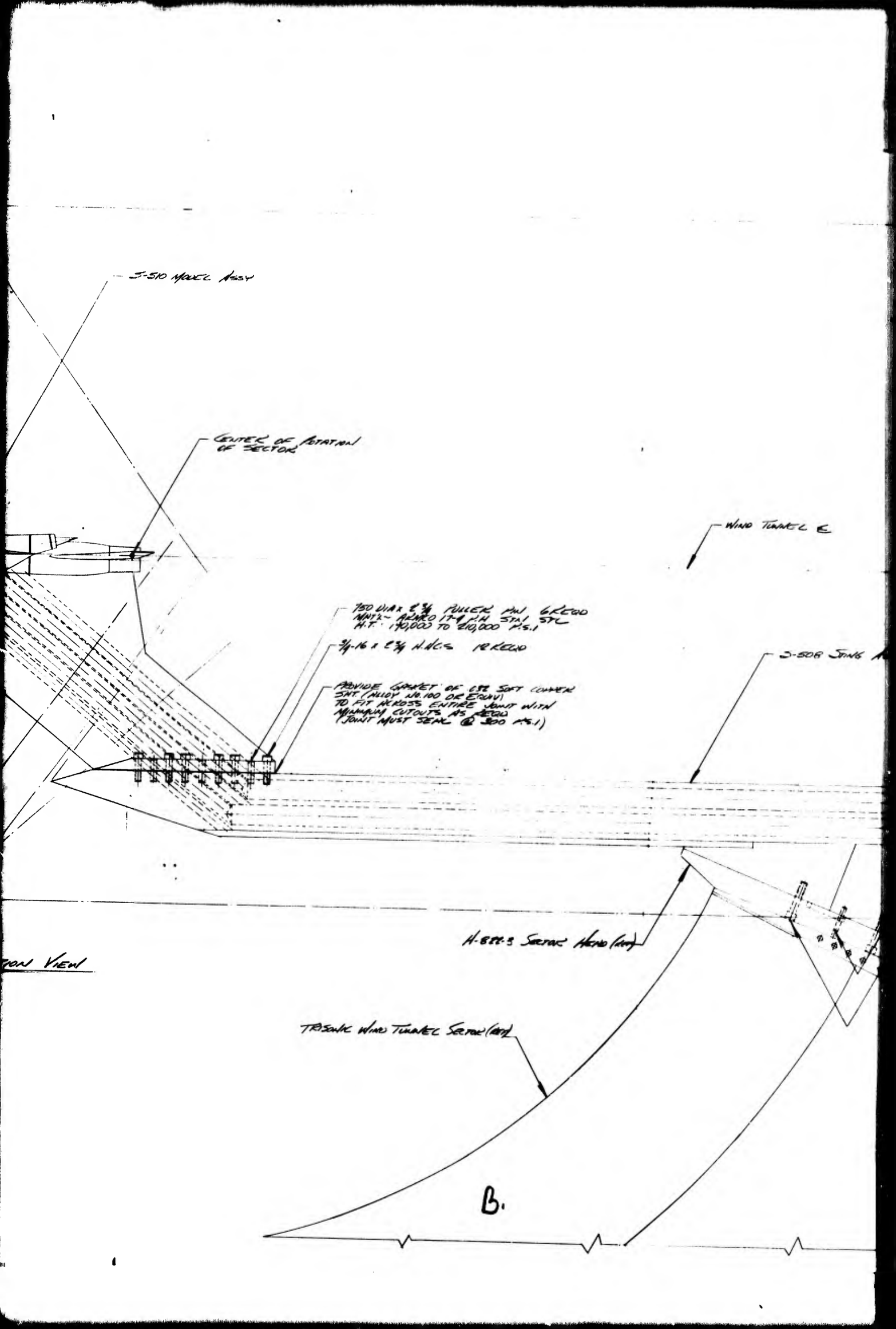
J-510 MODEL ASSY
CENTER OF ROTATION OF SECTOR
WIND TUNNEL ℄
750 DIA x ℄ 3/4 PULLER RH 6 REQD
NUT 2 - ALMCO 17-4 PH STA STL
H.T. 140,000 TO 210,000 P.S.I
3/4-16 x ℄ 3/4 H.H.C.S 18 REQD
PROVIDE GASKET OF 1/8 SOFT COPPER SHT (ALLOY NO. 100 OR EQUIV) TO FIT ACROSS ENTIRE JOINT WITH MINIMUM CUTOUTS AS REQD (JOINT MUST SEAL @ 300 P.S.I)
J-508 STING
H-877-3 SECTOR HEAD (REF)
TRANSONIC WIND TUNNEL SECTOR (REF)

TION VIEW

B.

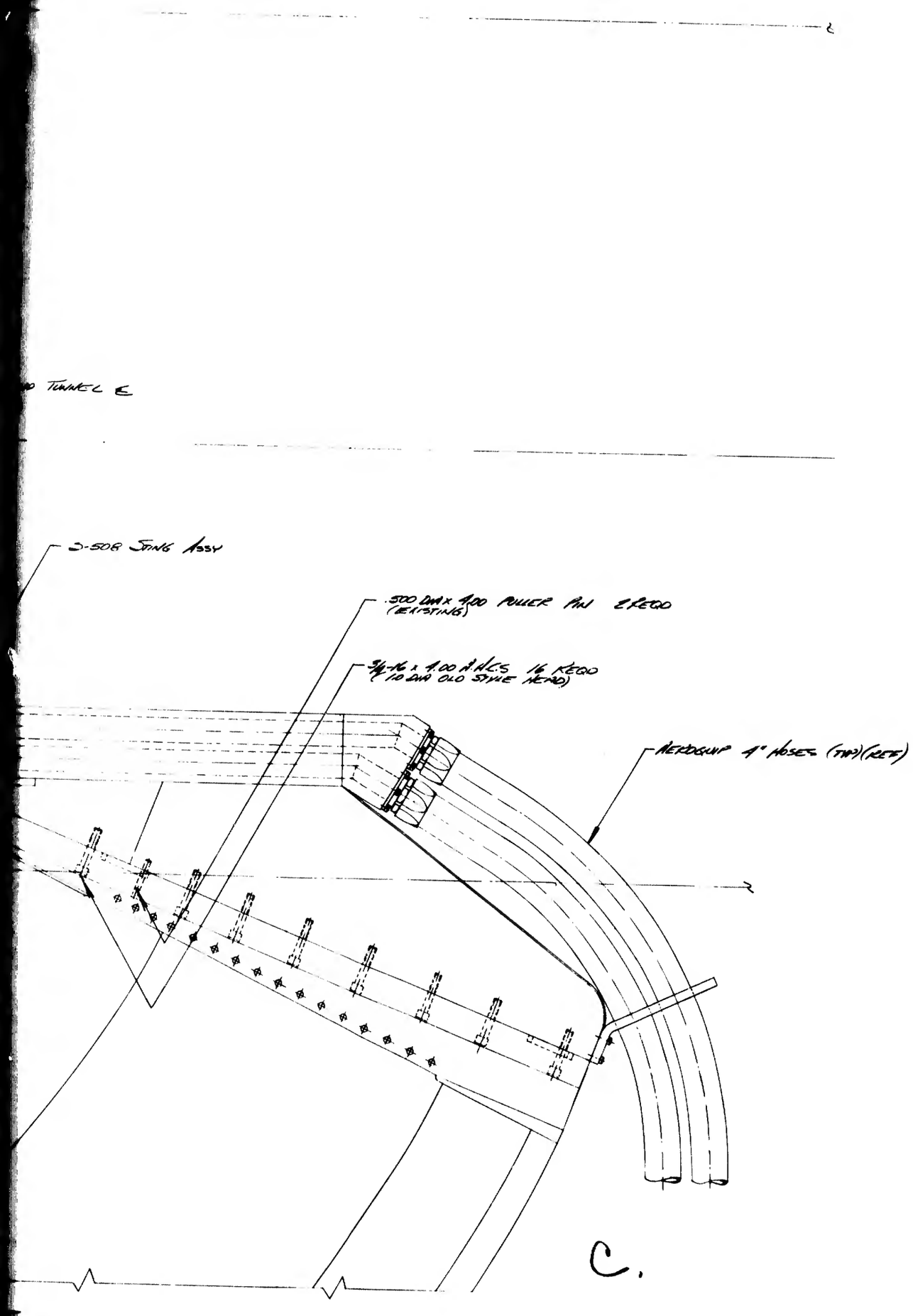
D-508 SWING ASSY
.500 DIA x 4.00 ROLLER PIN EREQD (EXISTING)
9/16-16 x 4.00 H.C.S. 16 REQD (1.10 DIA OLD STYLE METRO)
AEROQUIP 4" HOSES (TYP) (REF)

C.

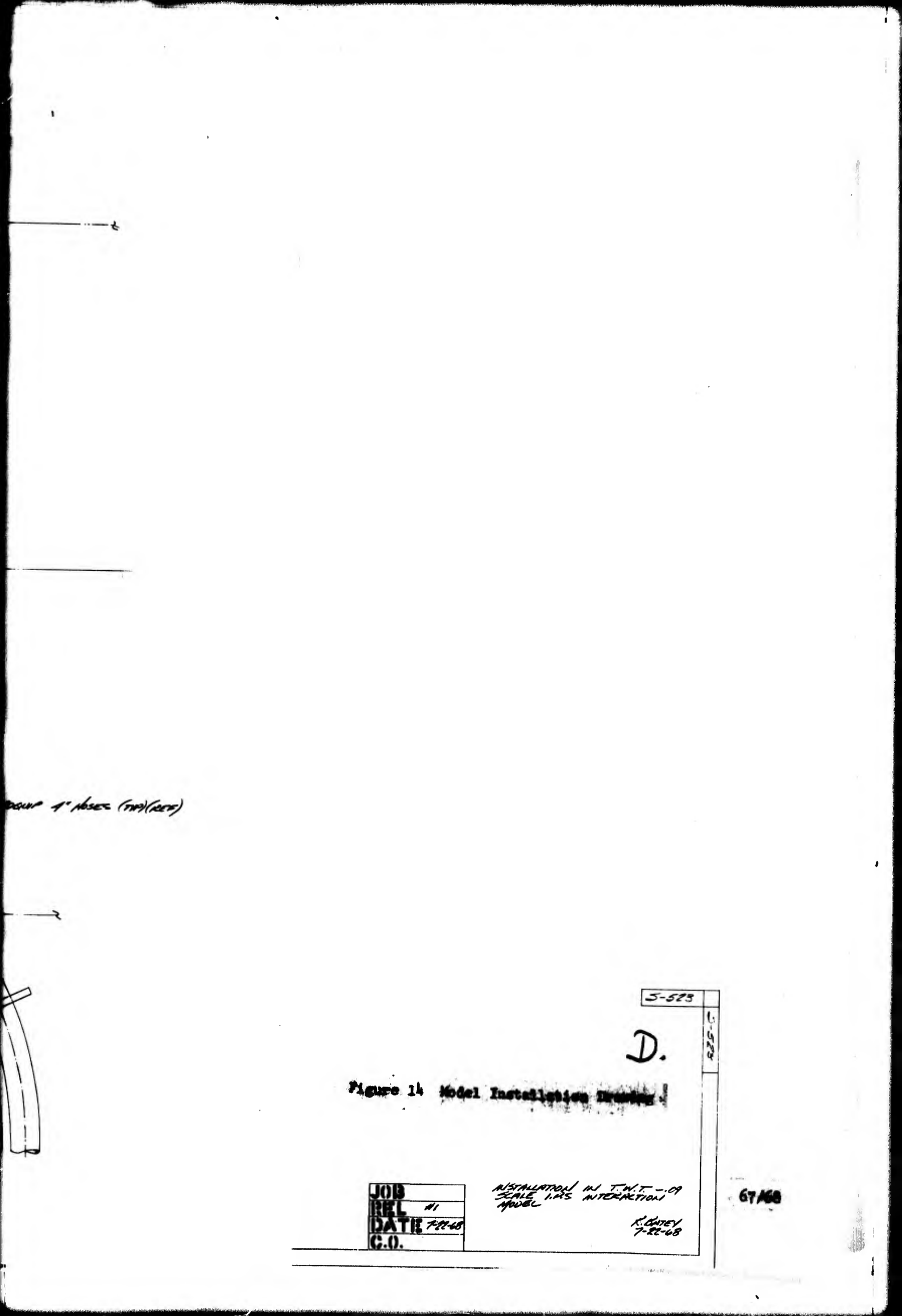

Figure 14 Model Installation Drawing

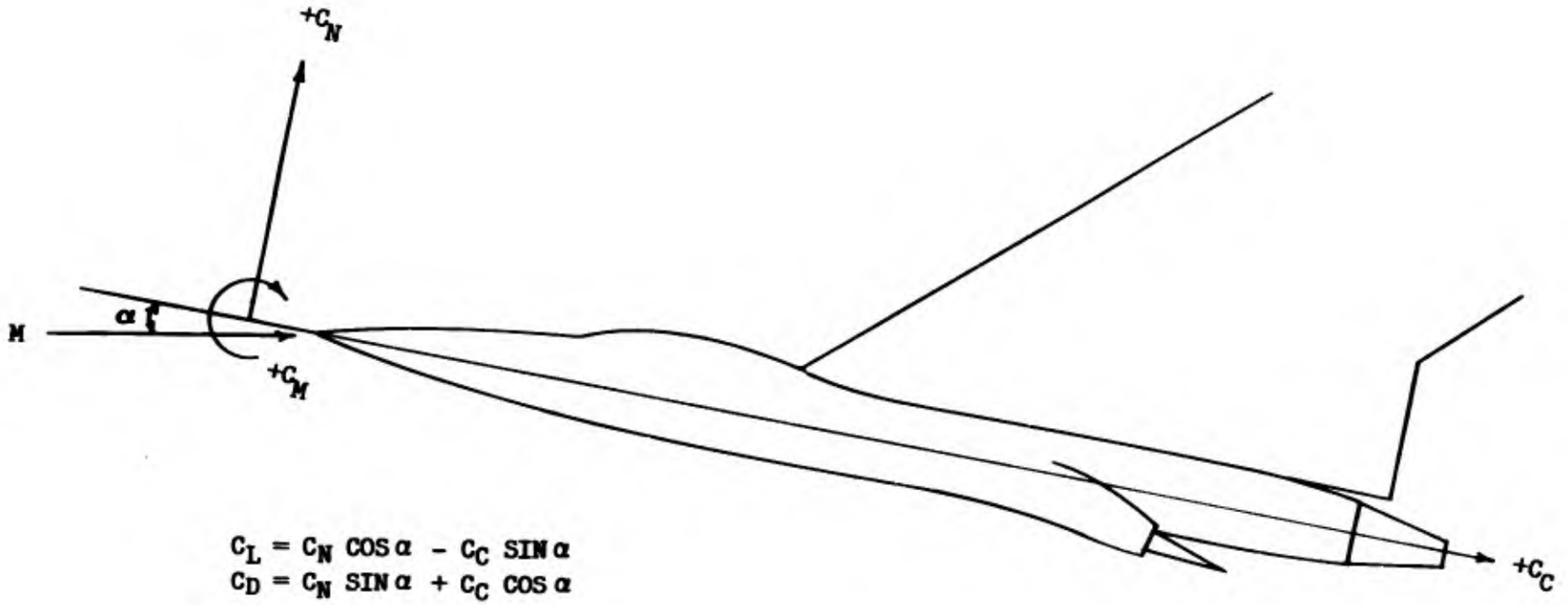

$$C_L = C_N \cos\alpha - C_C \sin\alpha$$
$$C_D = C_N \sin\alpha + C_C \cos\alpha$$

Figure 15. Model Forces Sign Convention

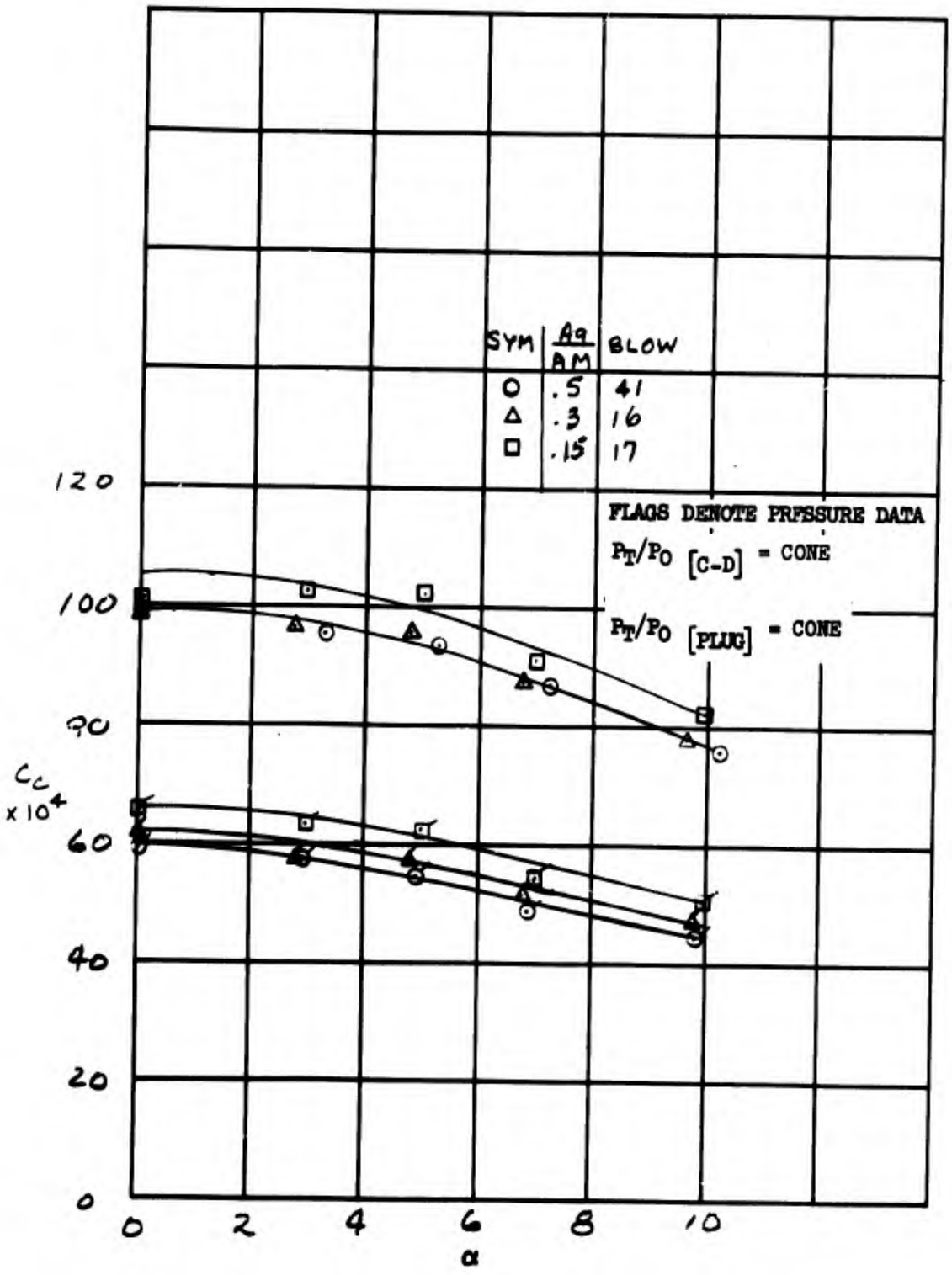

Figure 16. Effect of C-D Configuration on Chord Force - M=.614

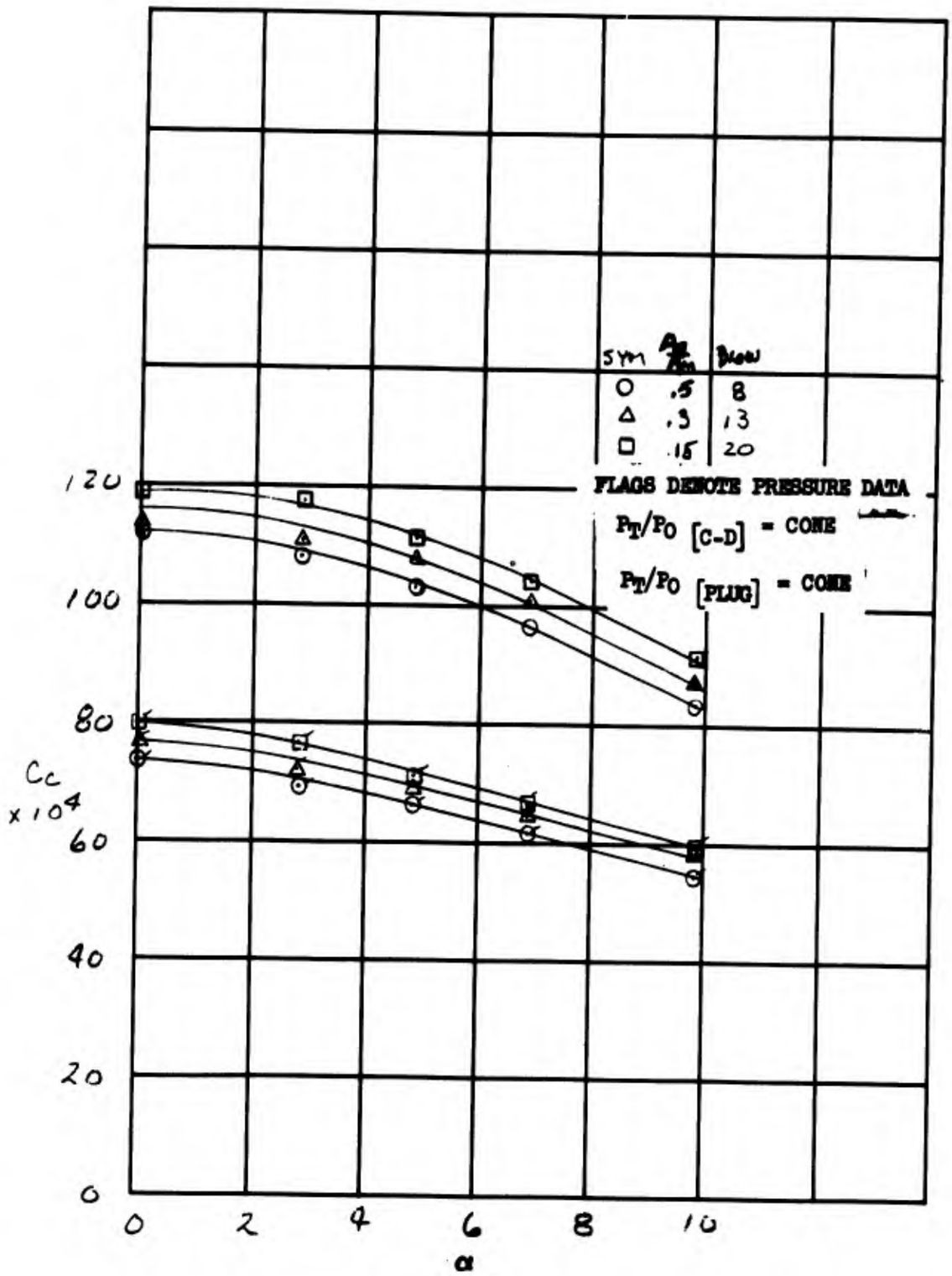

Figure 17. Effect of C-D Configuration on Chord Force - M=.85

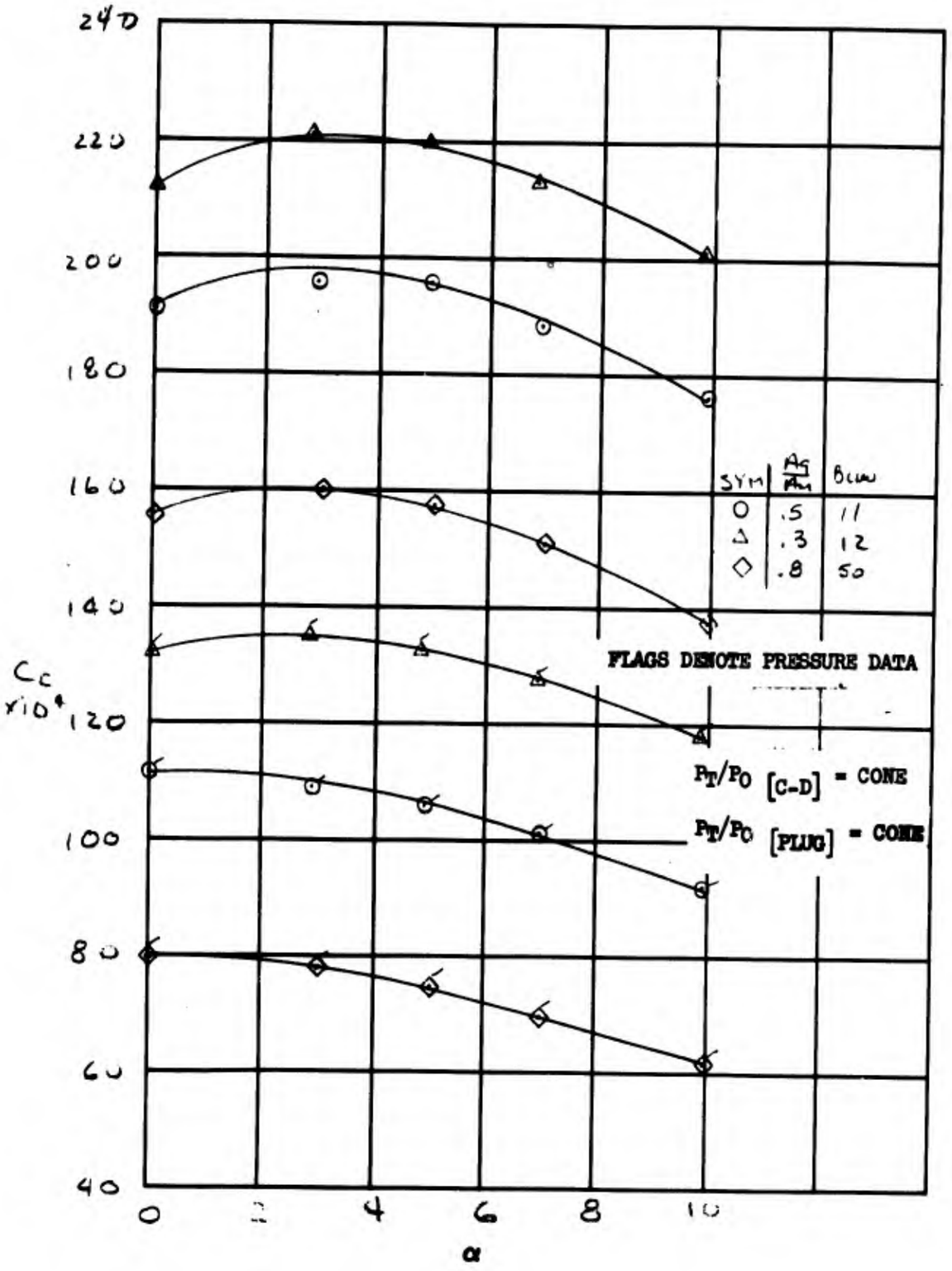

Figure 18. Effect of C-D Configuration on Chord Force - M=1.27

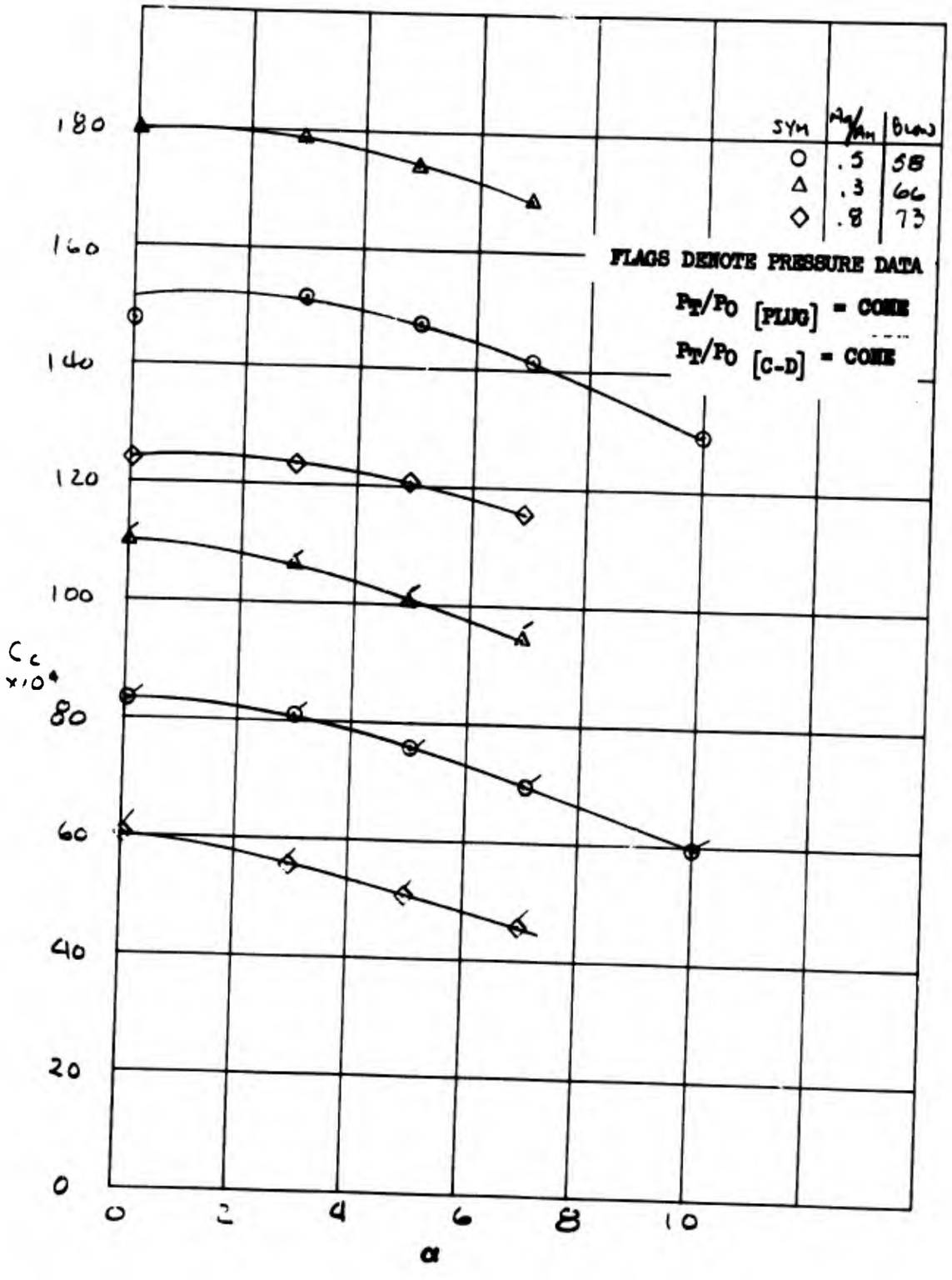

Figure 19. Effect of C-D Configuration on Chord Force - M=1.7

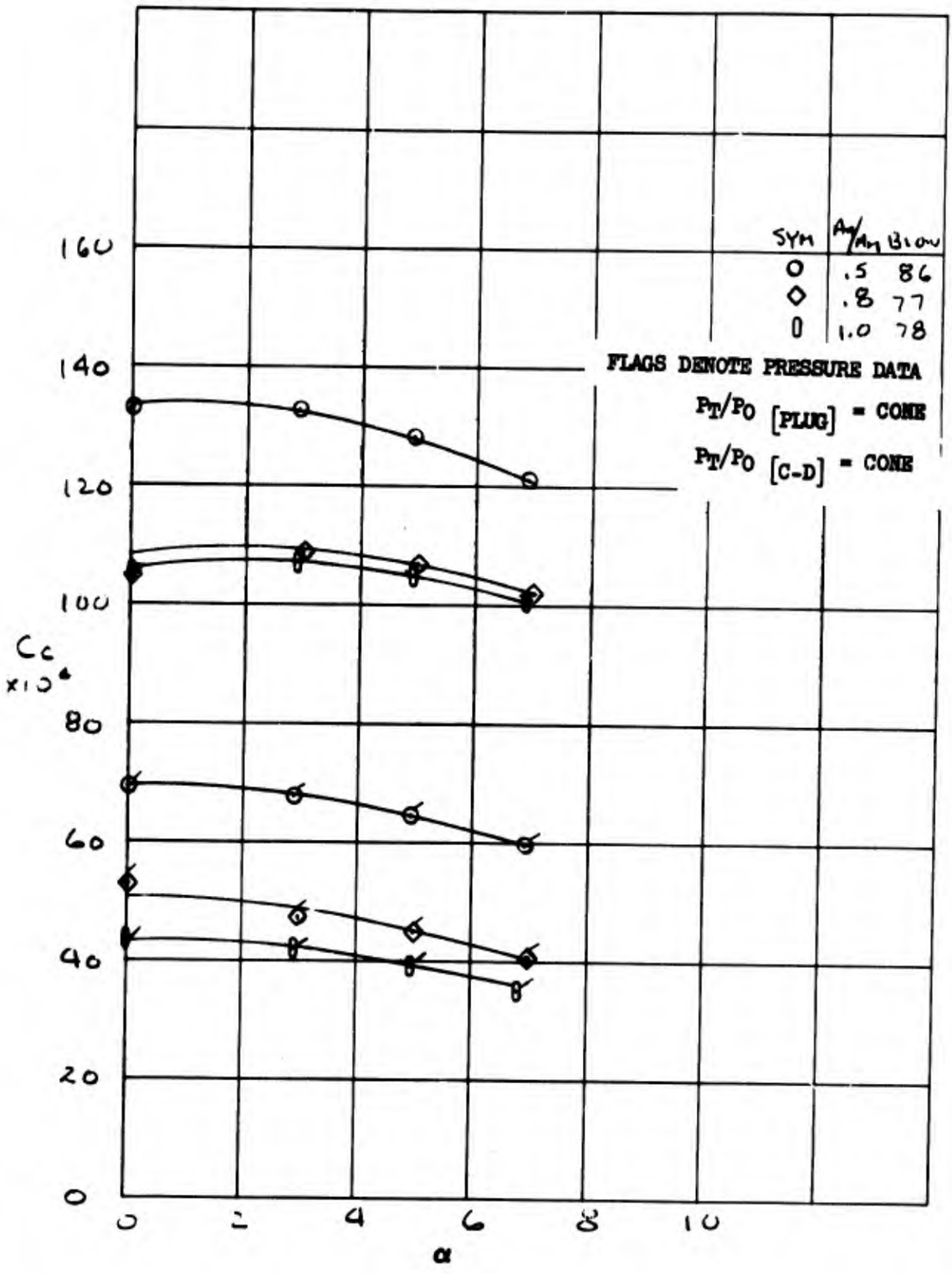

Figure 20. Effect of C-D Configuration on Chord Force - M=2.0

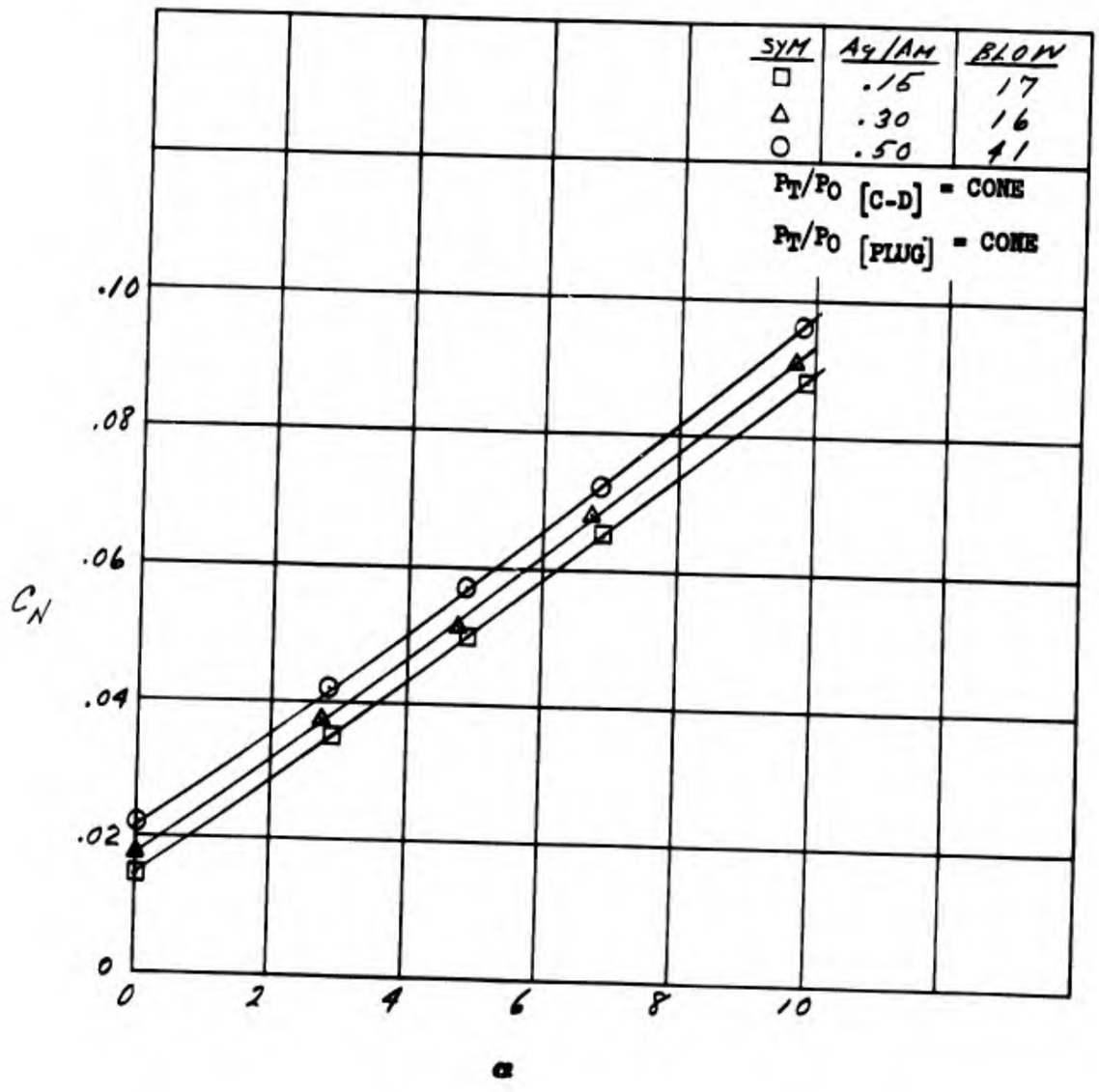

Figure 21. Effect of C-D Configuration On Normal Force - M = .614

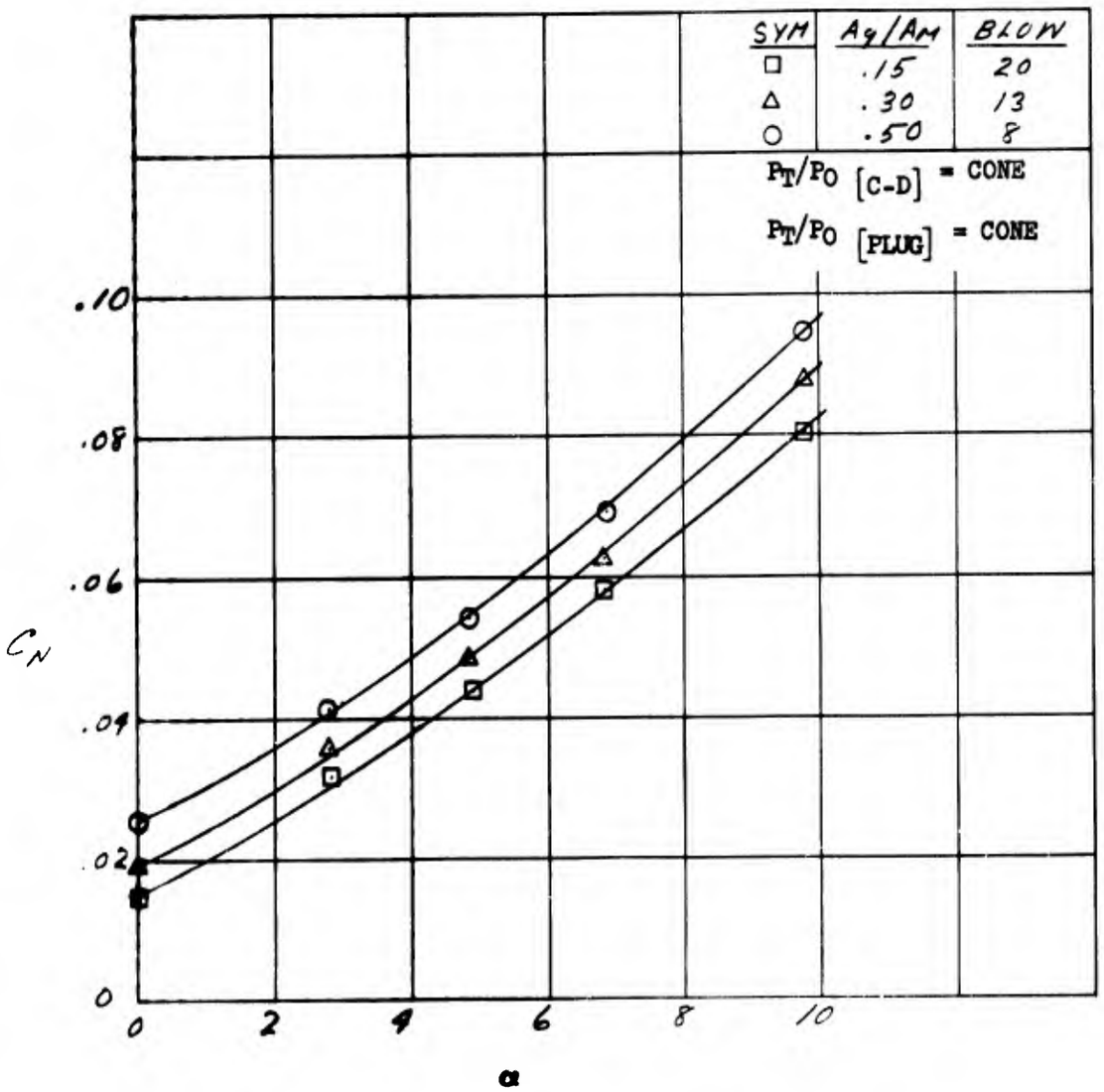

Figure 22. Effect of C-D Configuration On Normal Force - M = .85

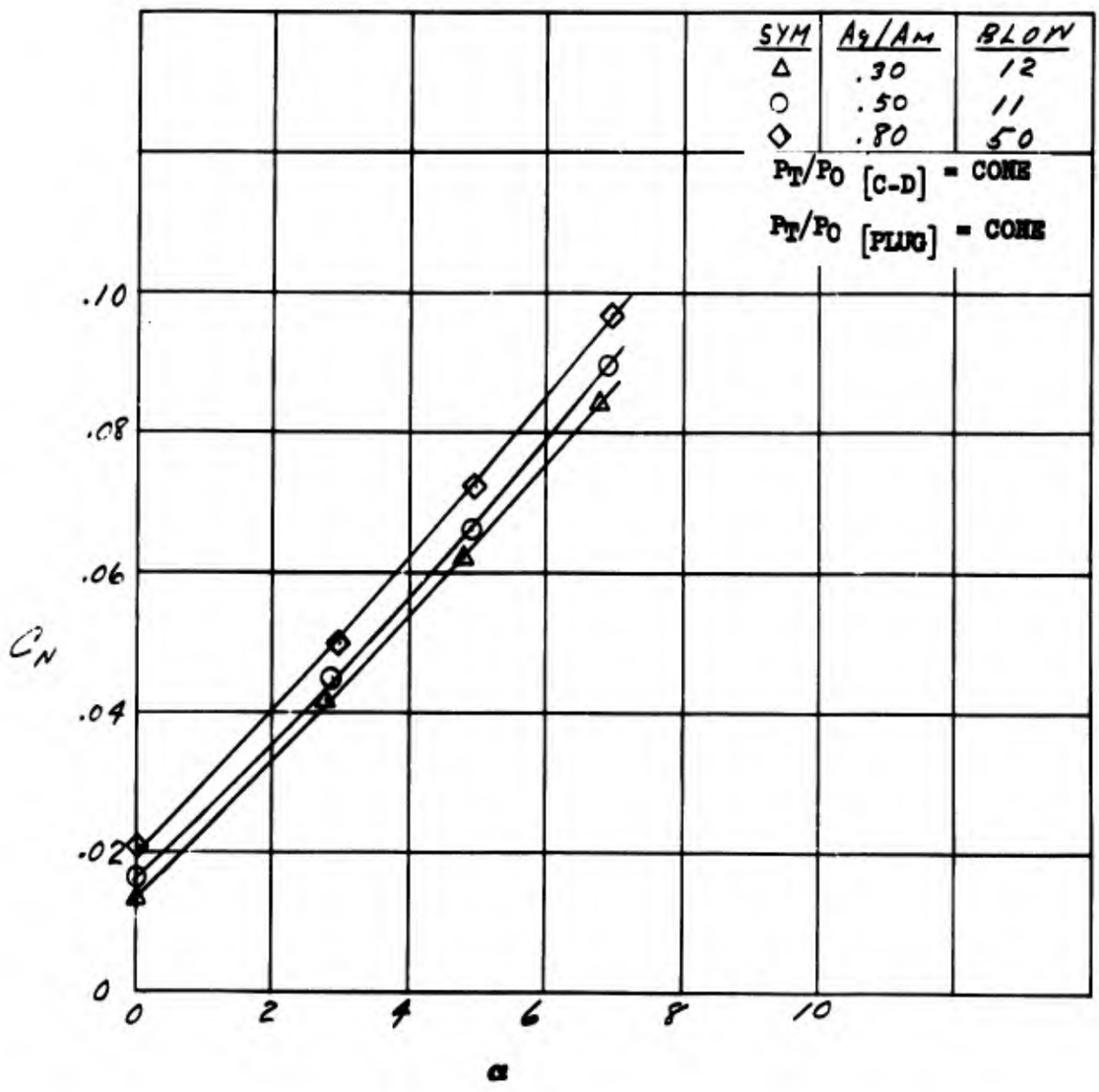

Figure 23. Effect of C-D Configuration On Normal Force - M = 1.27

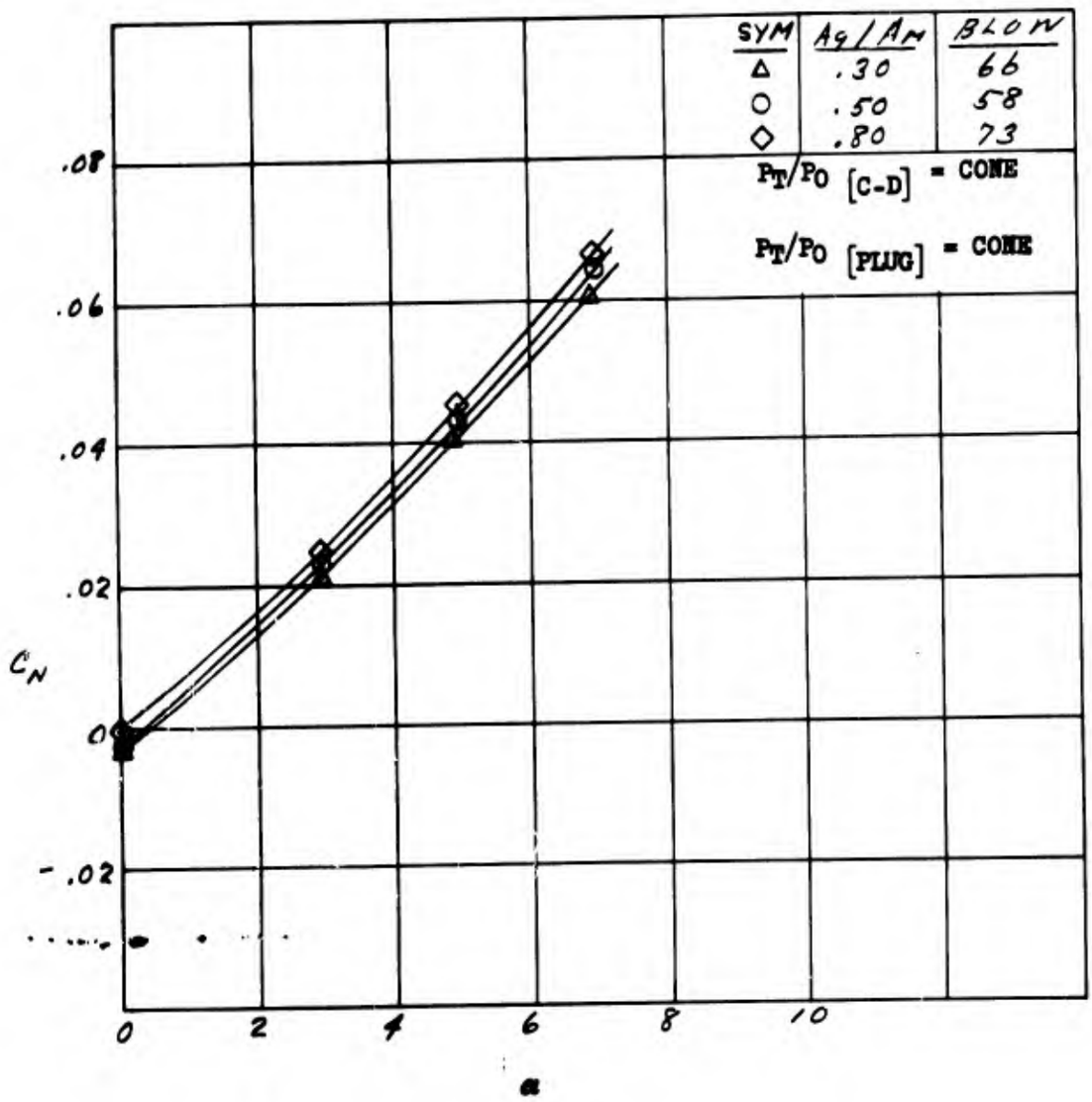

Figure 24. Effect of C-D Configuration On Normal Force - M = 1.7

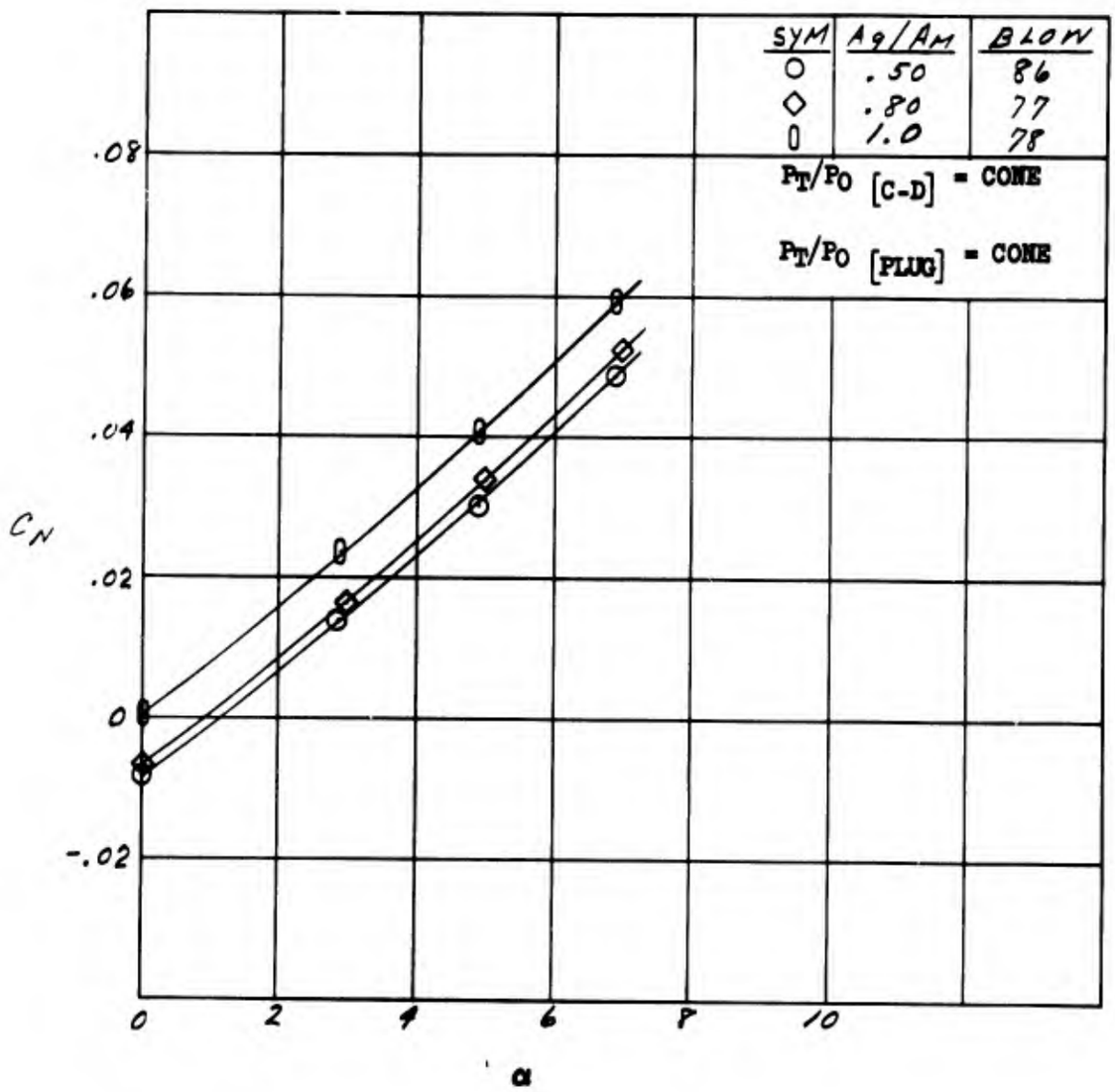

Figure 25. Effect of C-D Configuration On Normal Force - M = 2.0

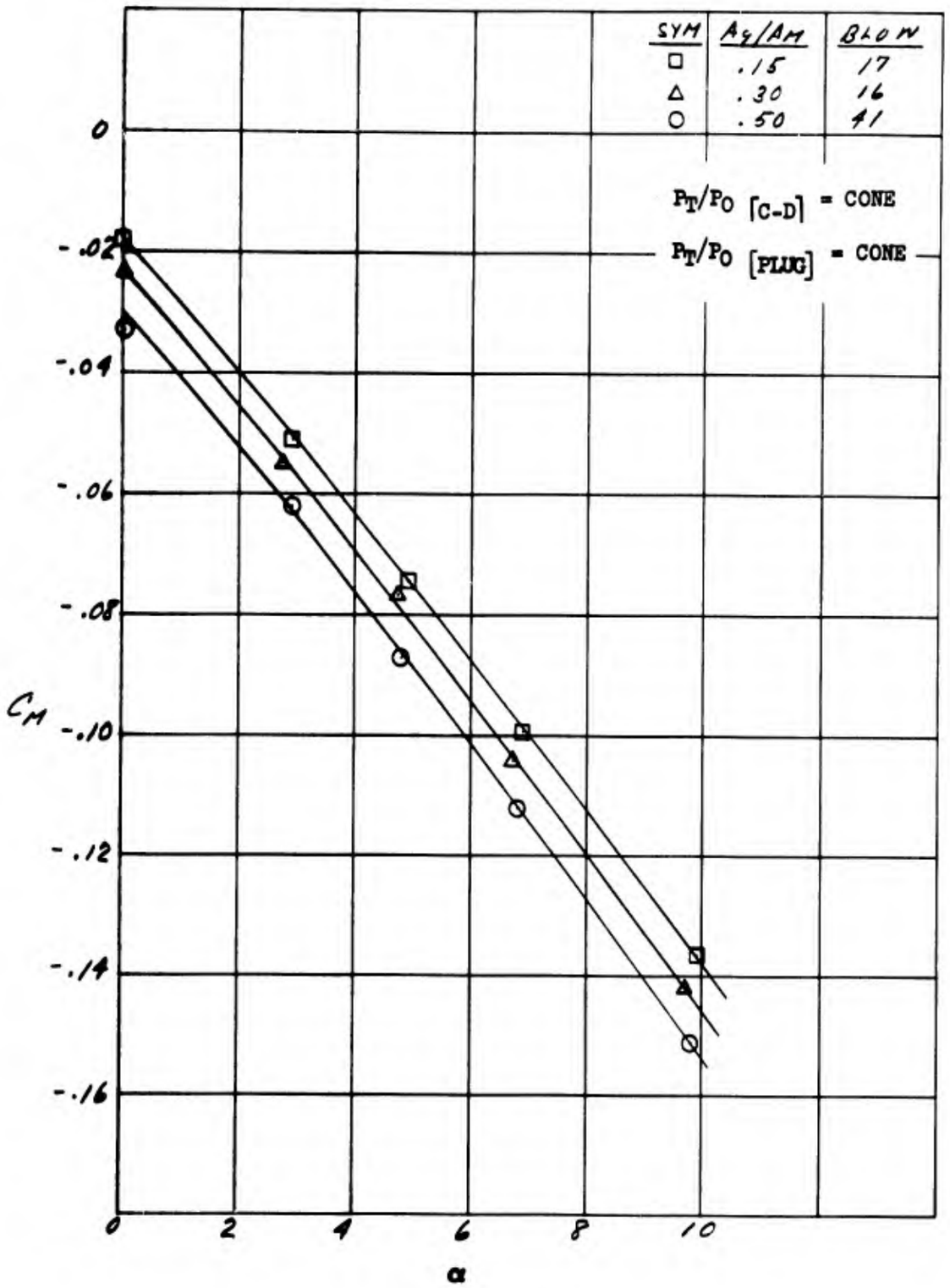

Figure 26. Effect of C-D Configuration On Pitching Moment - M = .614

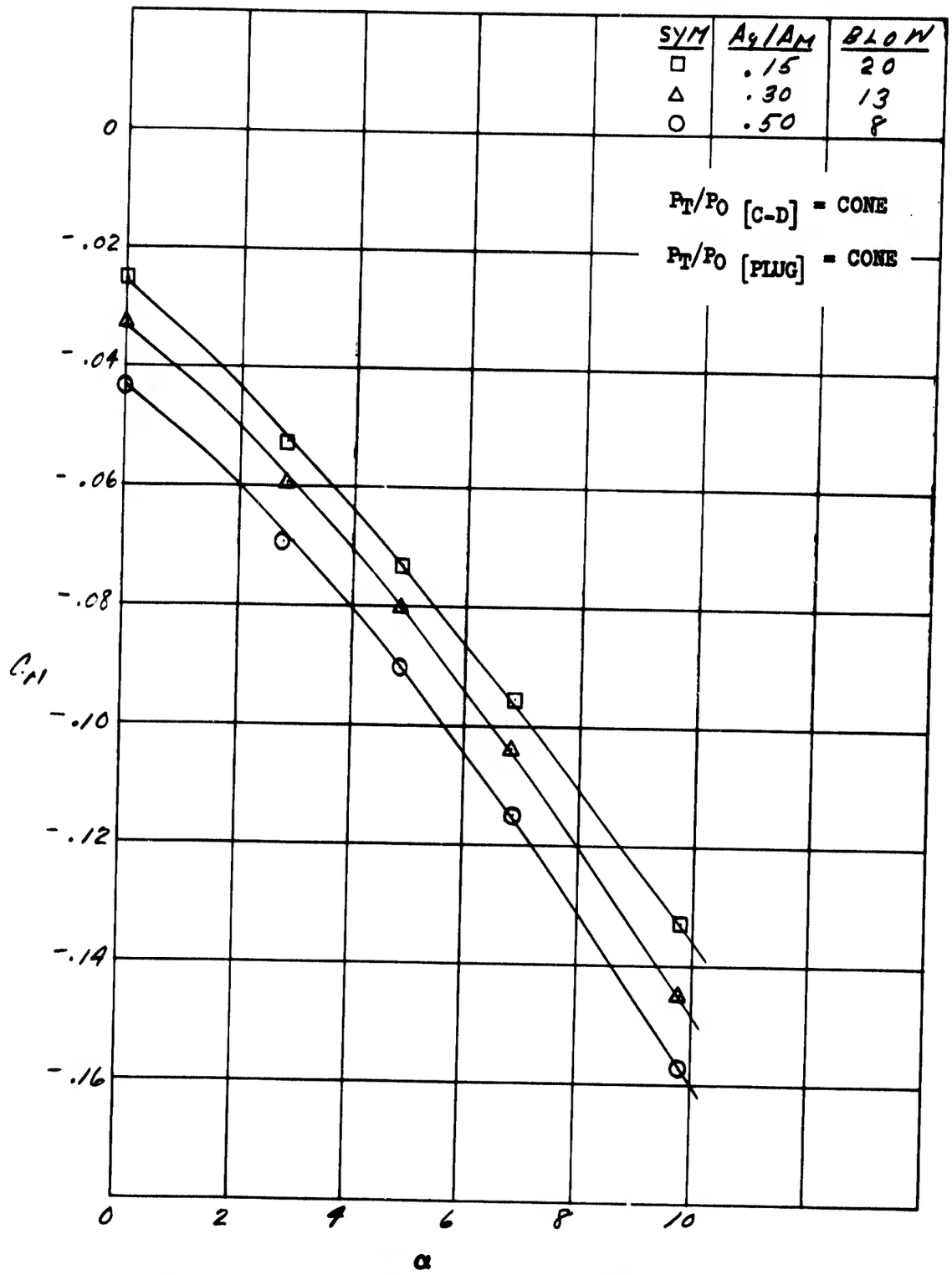

Figure 27. Effect of C-D Configuration On Pitching Moment - M = .85

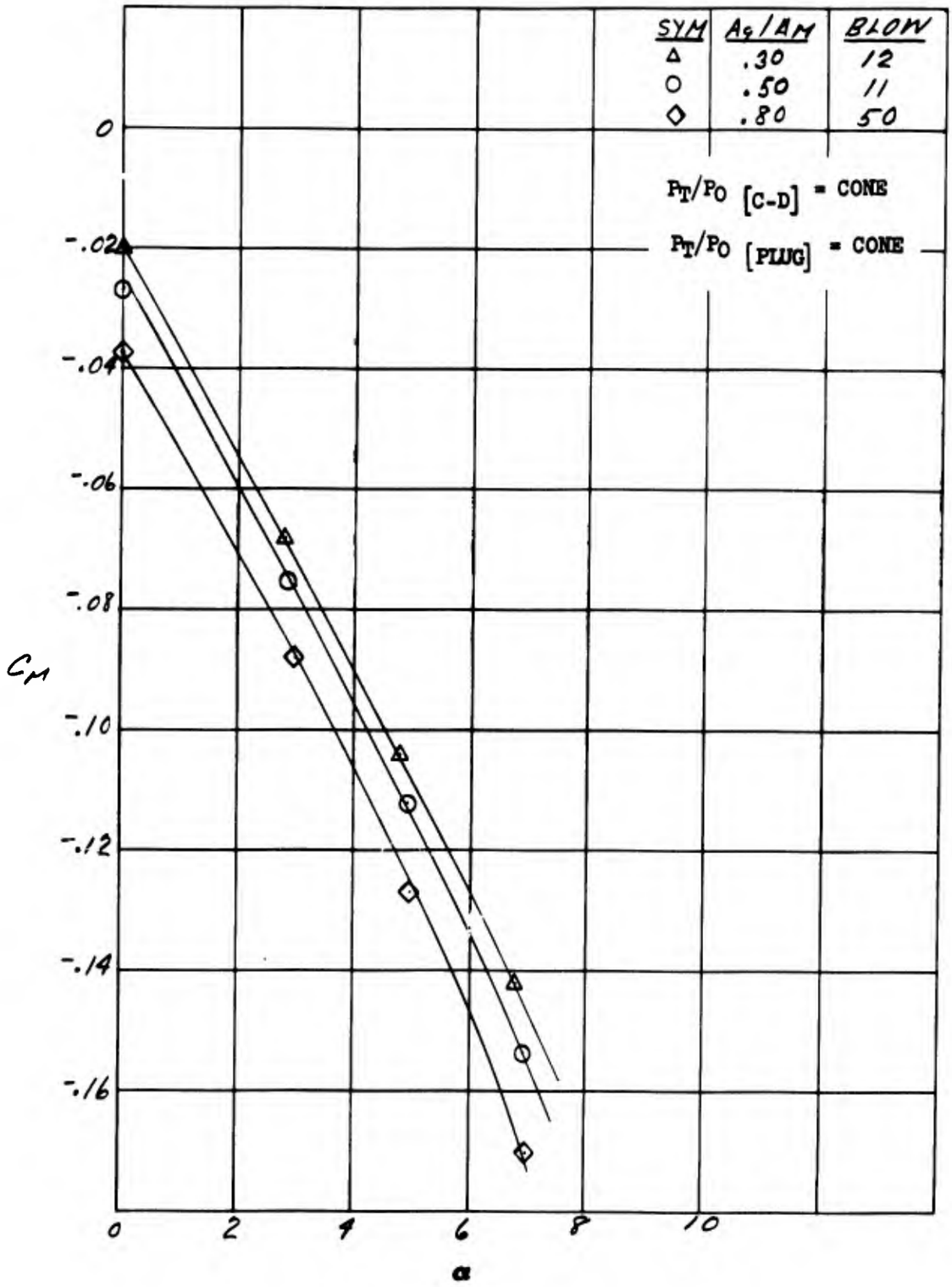

Figure 28. **Effect of C-D Configuration On Pitching Moment -** M = 1.27

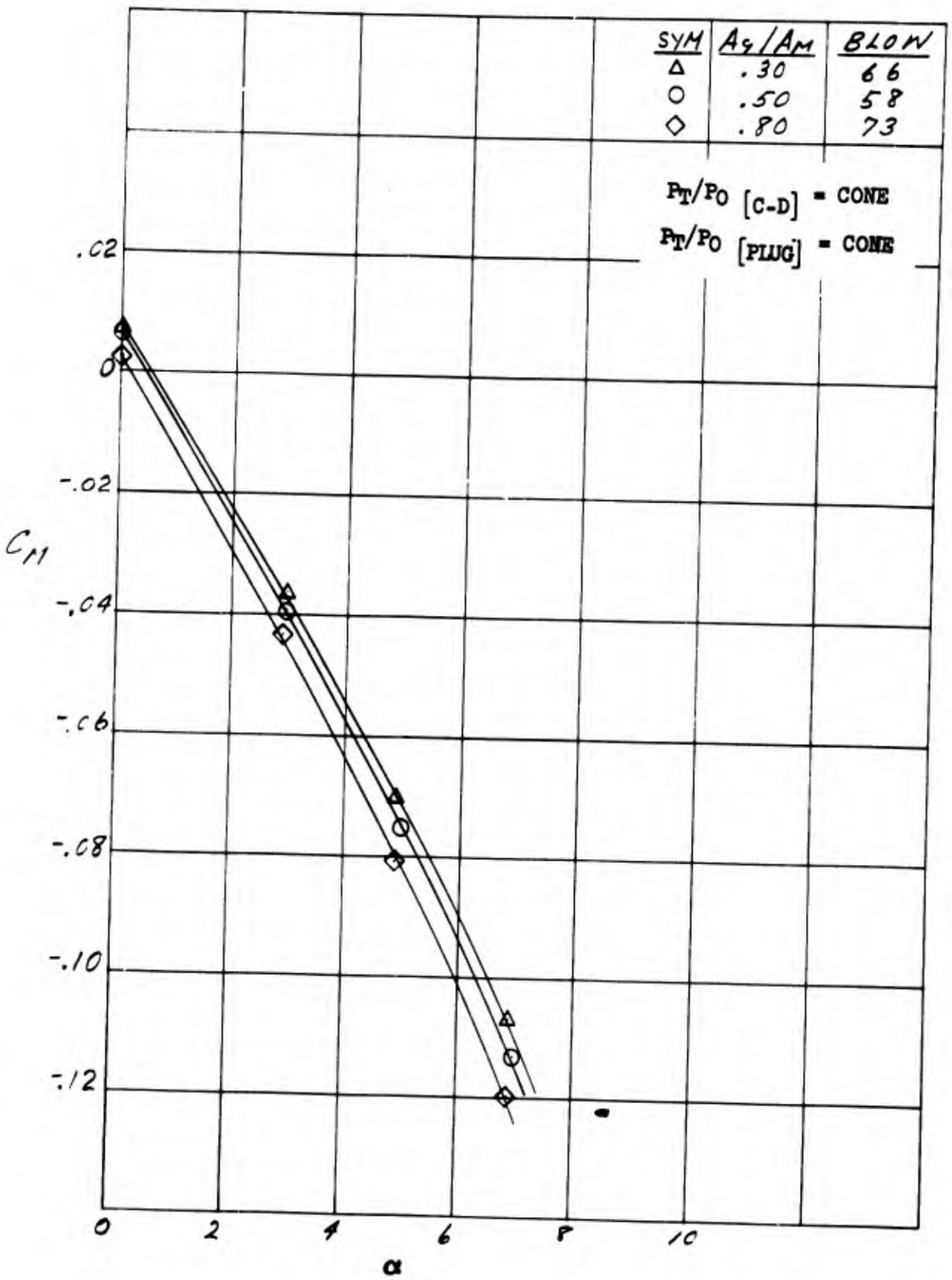

Figure 29. Effect of C-D Configuration On Pitching Moment - M = 1.7

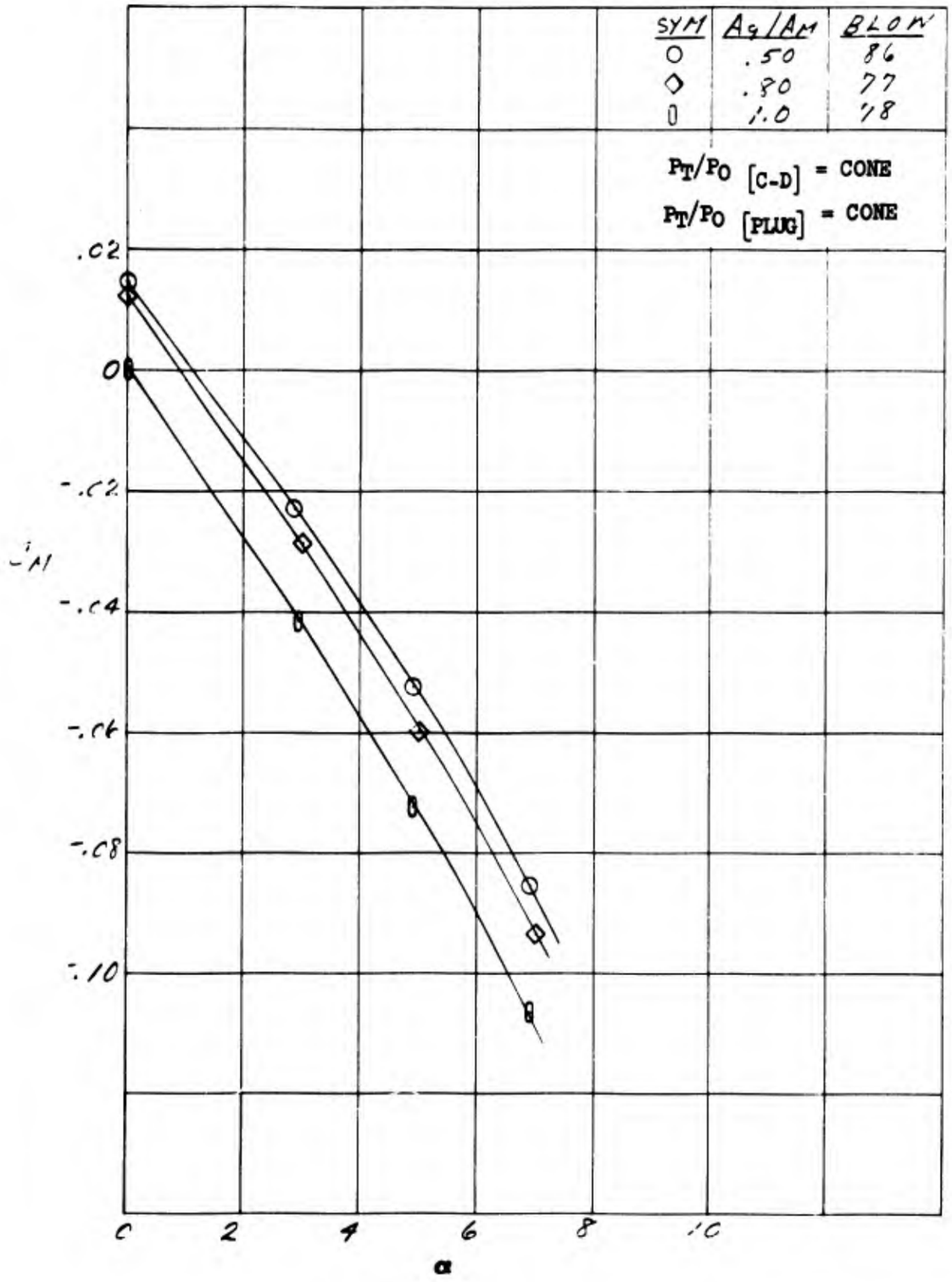

Figure 30. Effect of C-D Configuration On Pitching Moment - M = 2.0

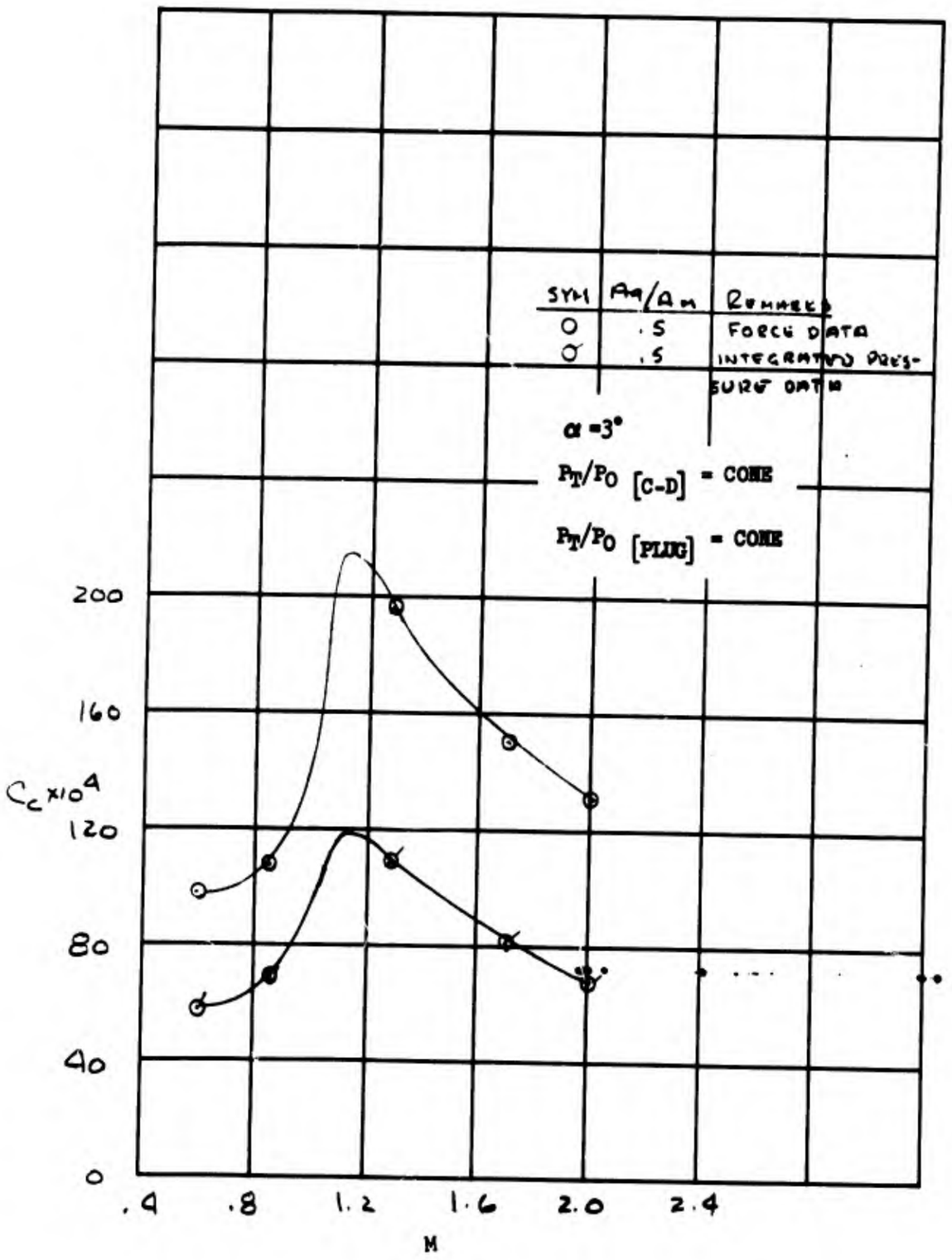

Figure 31. Base Line Configuration Chord Force

$\alpha = 3°$
Jets Off
$A_9/A_M = .50$

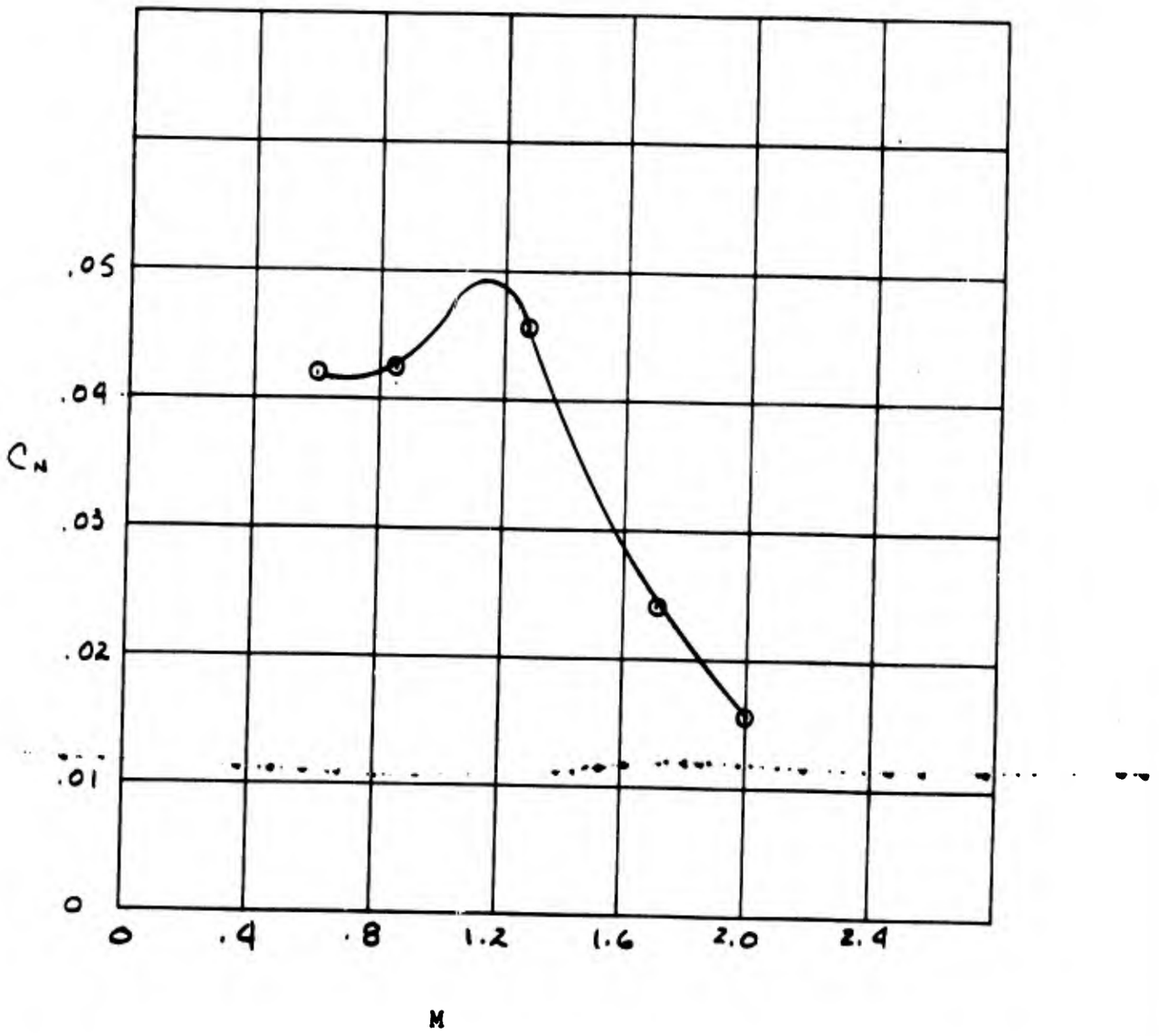

Figure 32. Base Line Configuration Normal Force

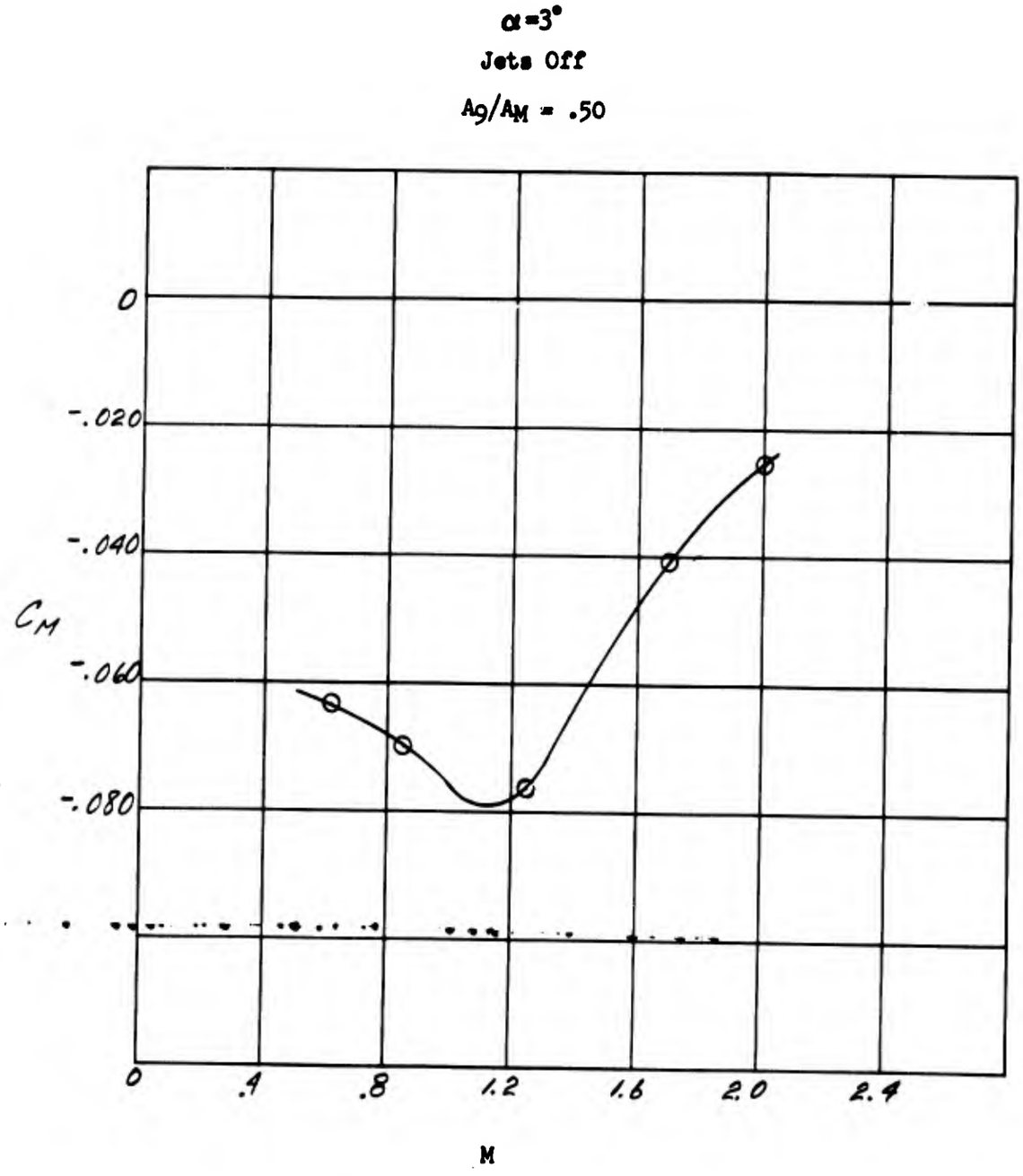

Figure 33. Base Line Configuration Pitching Moment

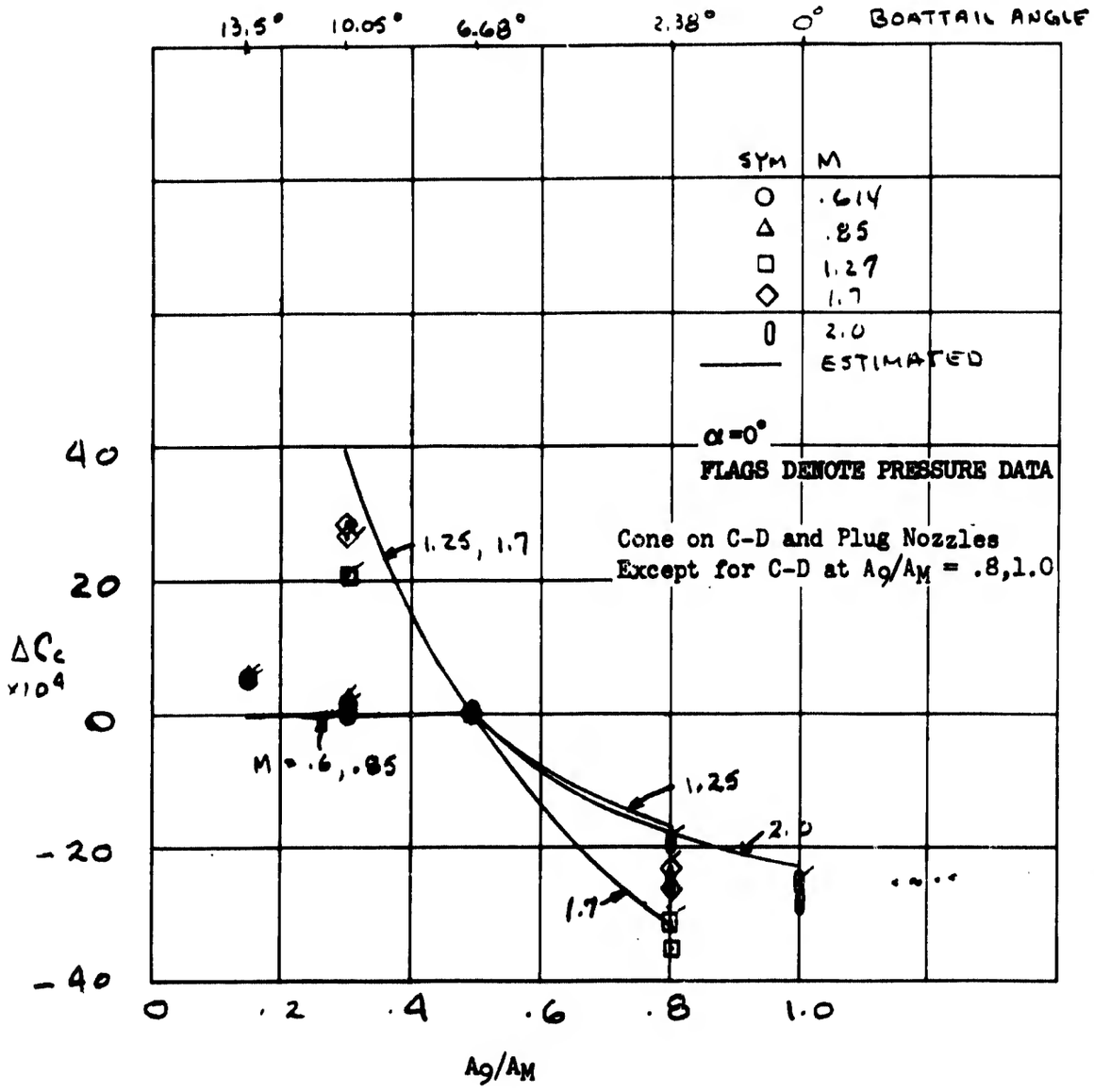

Figure 34. Afterbody Configuration Effects on Chord Force Increments - Comparison with Estimates

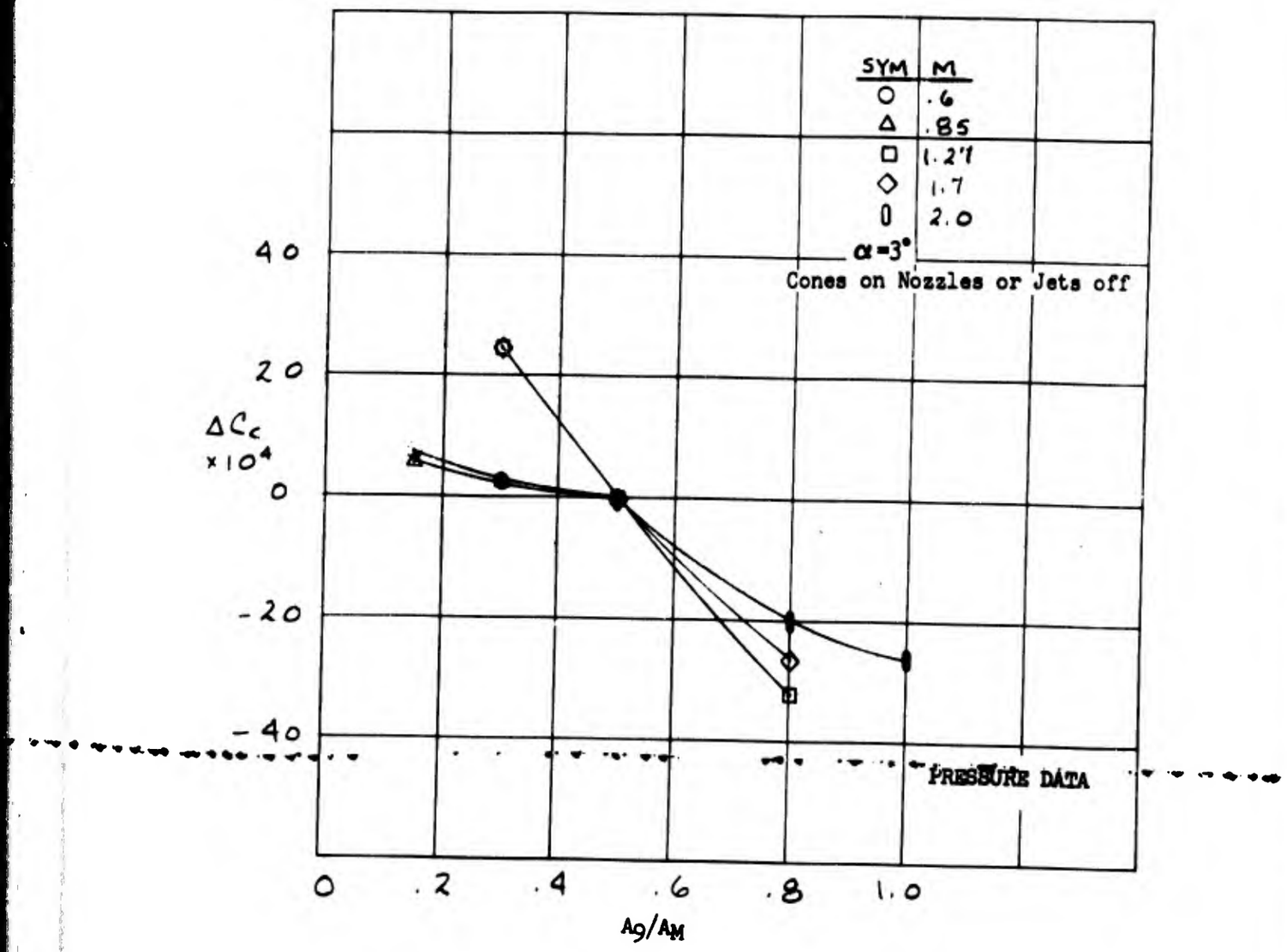

Figure 35. Afterbody Configuration Effects on Chord Force Increment - Summary.

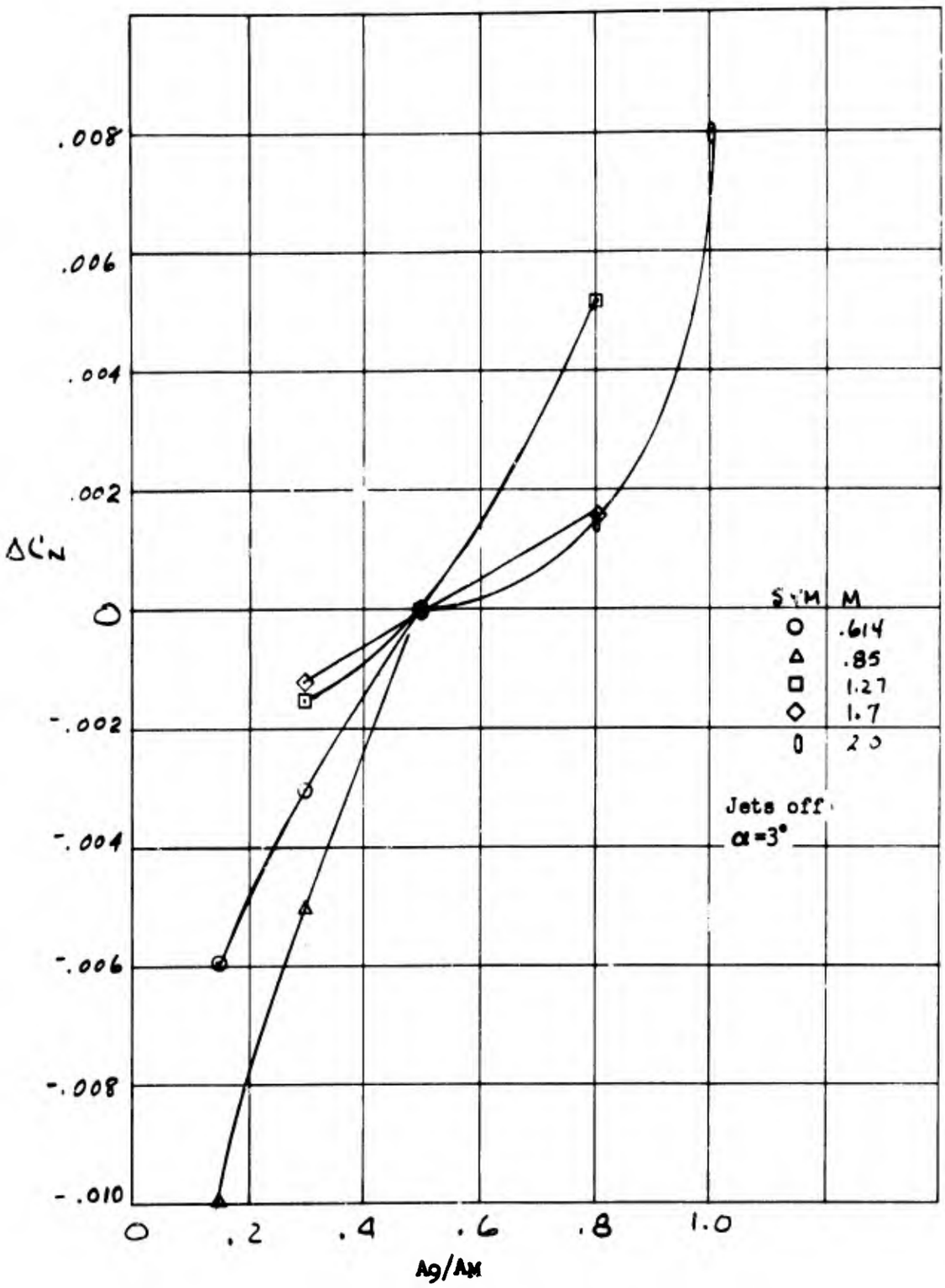

Figure 36. Afterbody Configuration Effects on Normal Force Increment - Summary

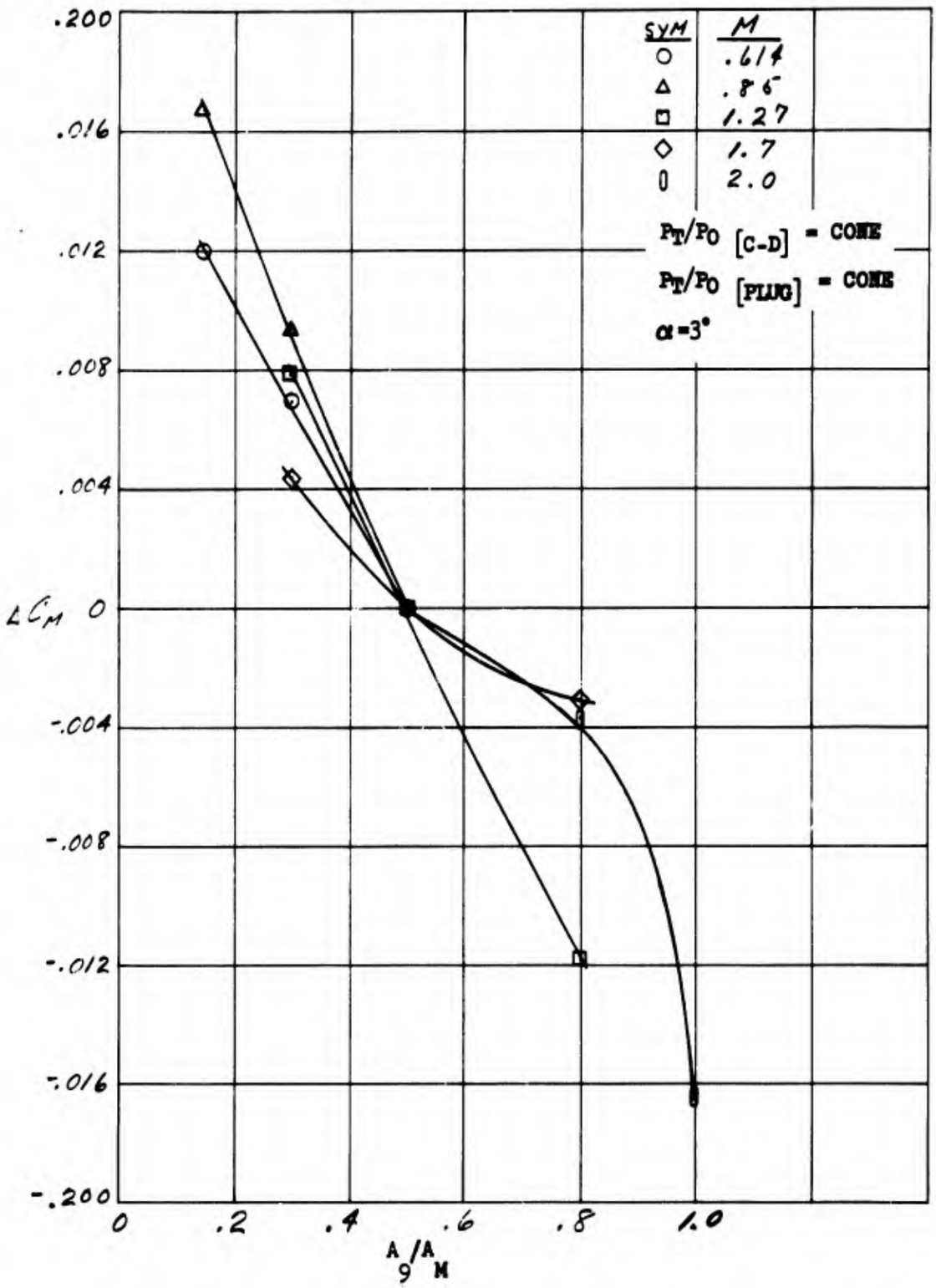

Figure 37. Afterbody Configuration Effects on Pitching Moment Increment -Summary

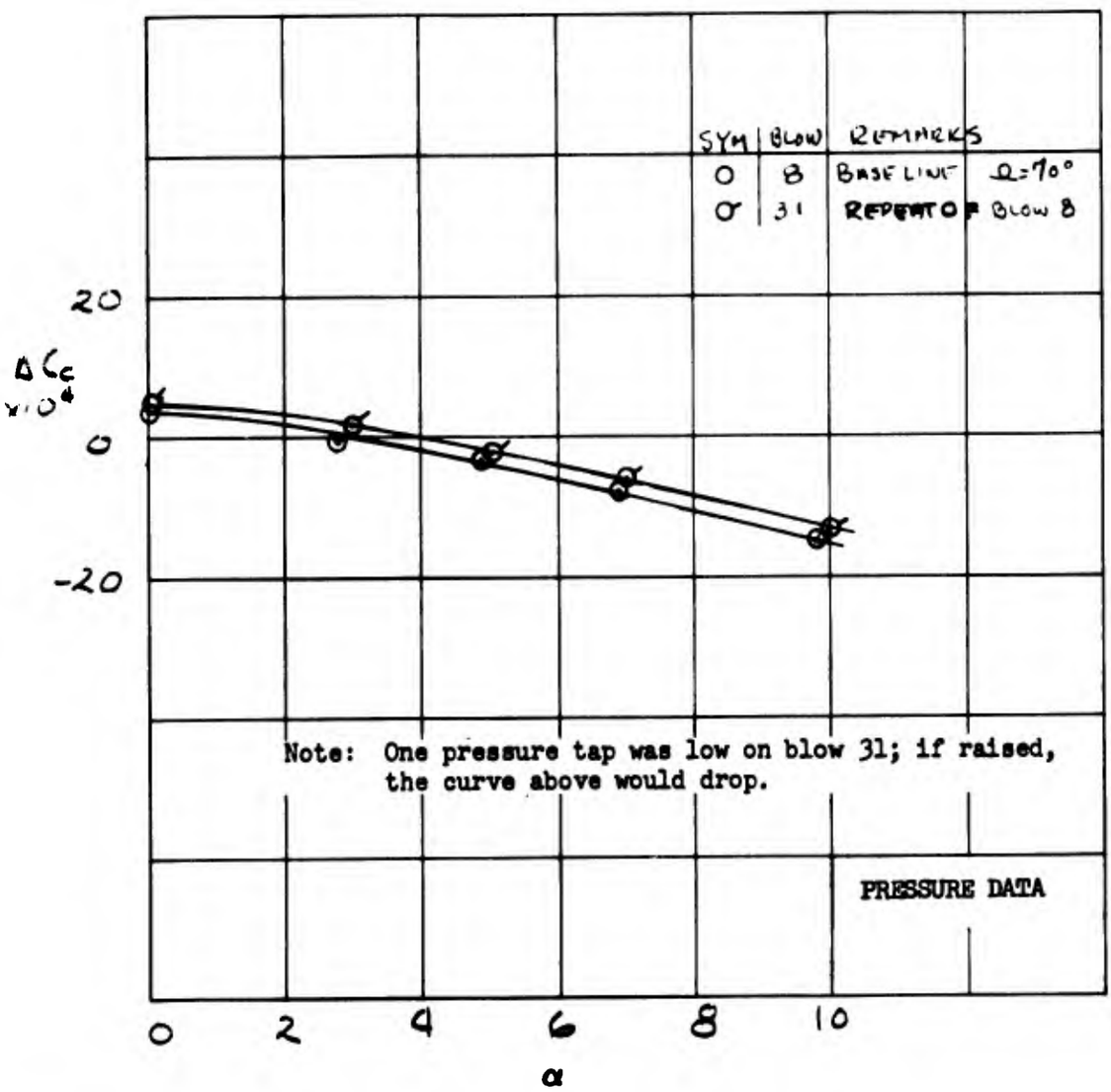

Figure 38. Chord Force Repeatability- M=.85

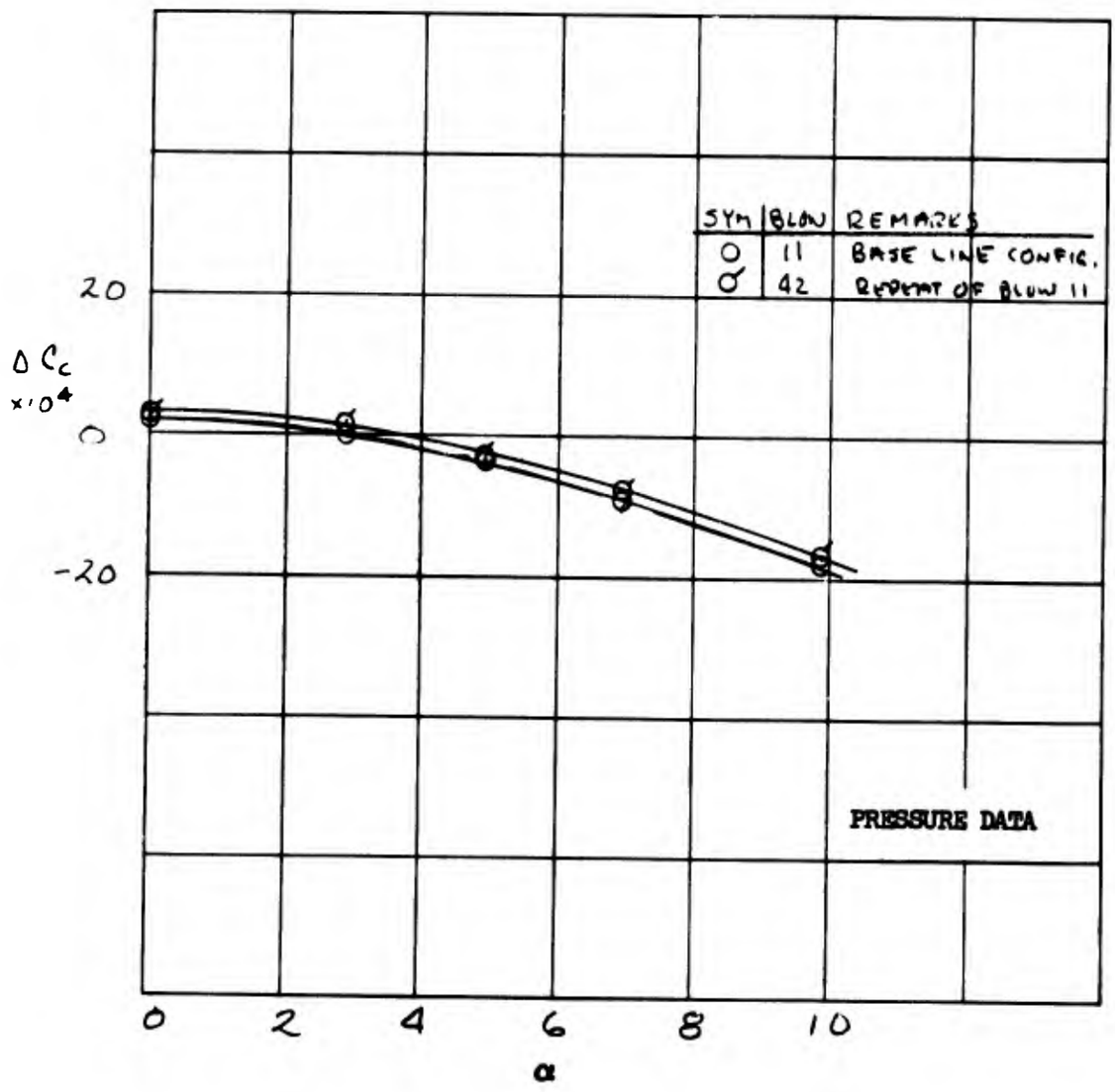

Figure 39. Chord Force Repeatability- M=1.27

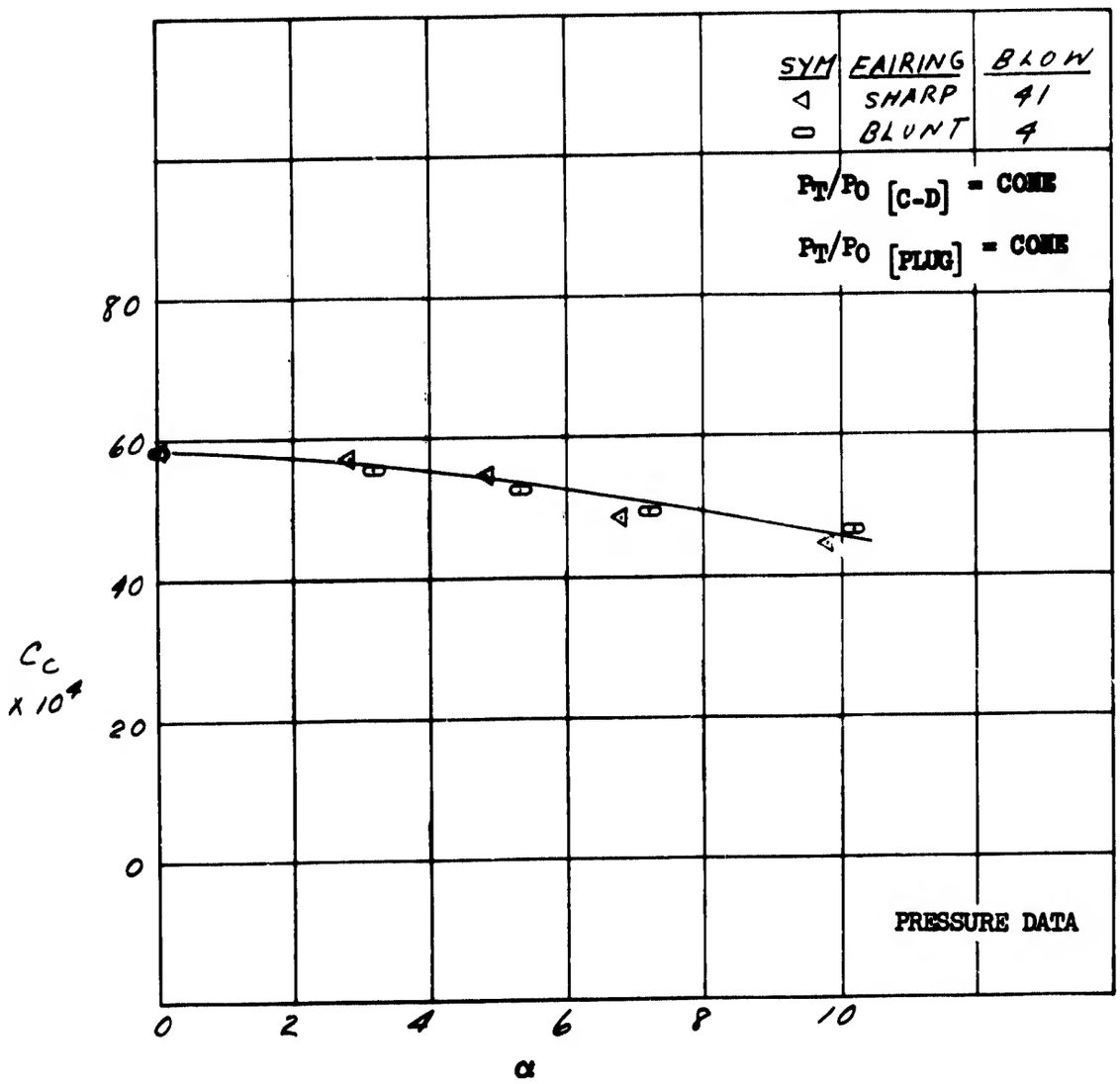

Figure 40. Effect of Blunt Inlet Fairing On Chord Force - M = .614

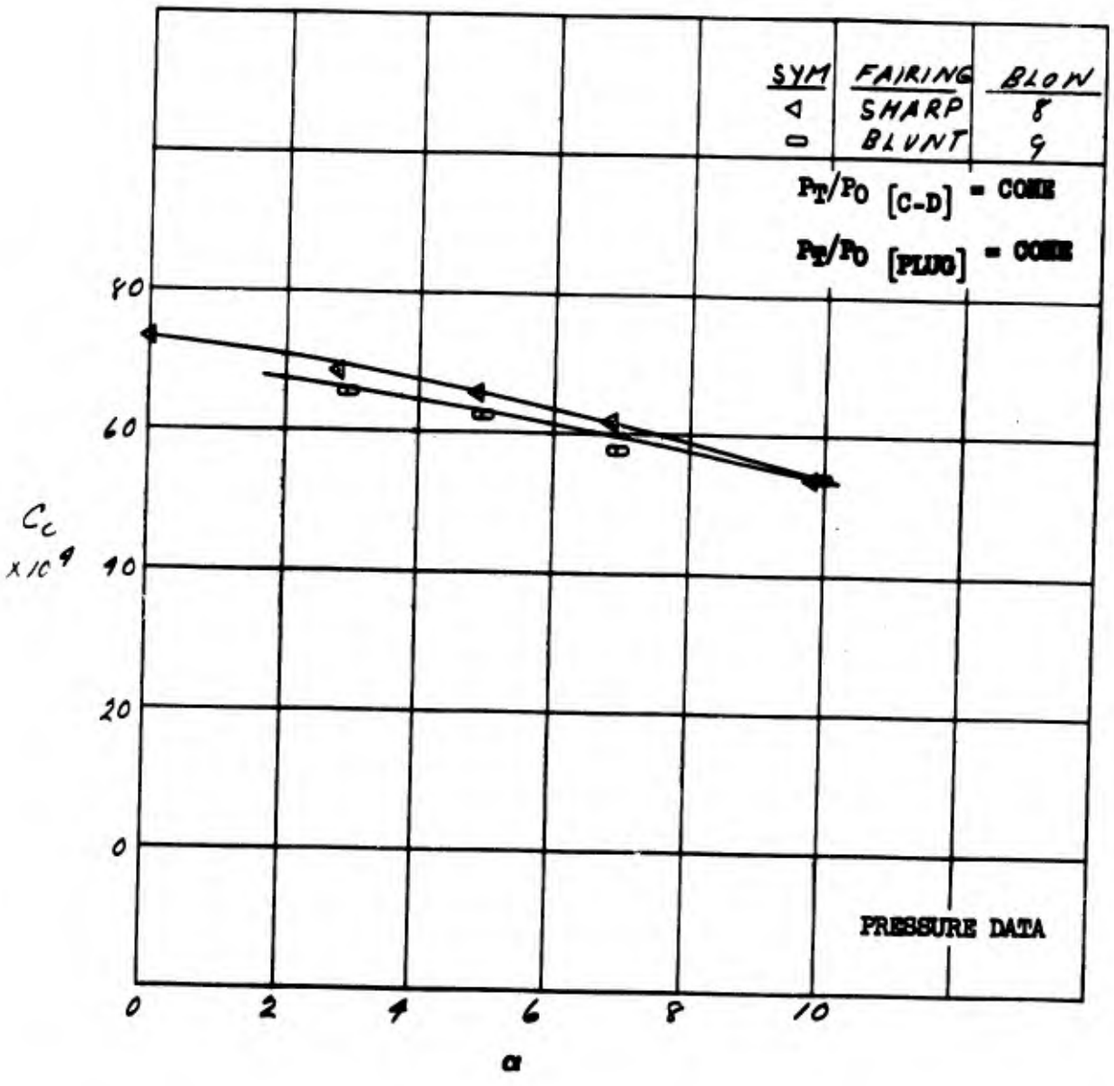

Figure 41. Effect of Blunt Inlet Fairing on Chord Force - M=.85

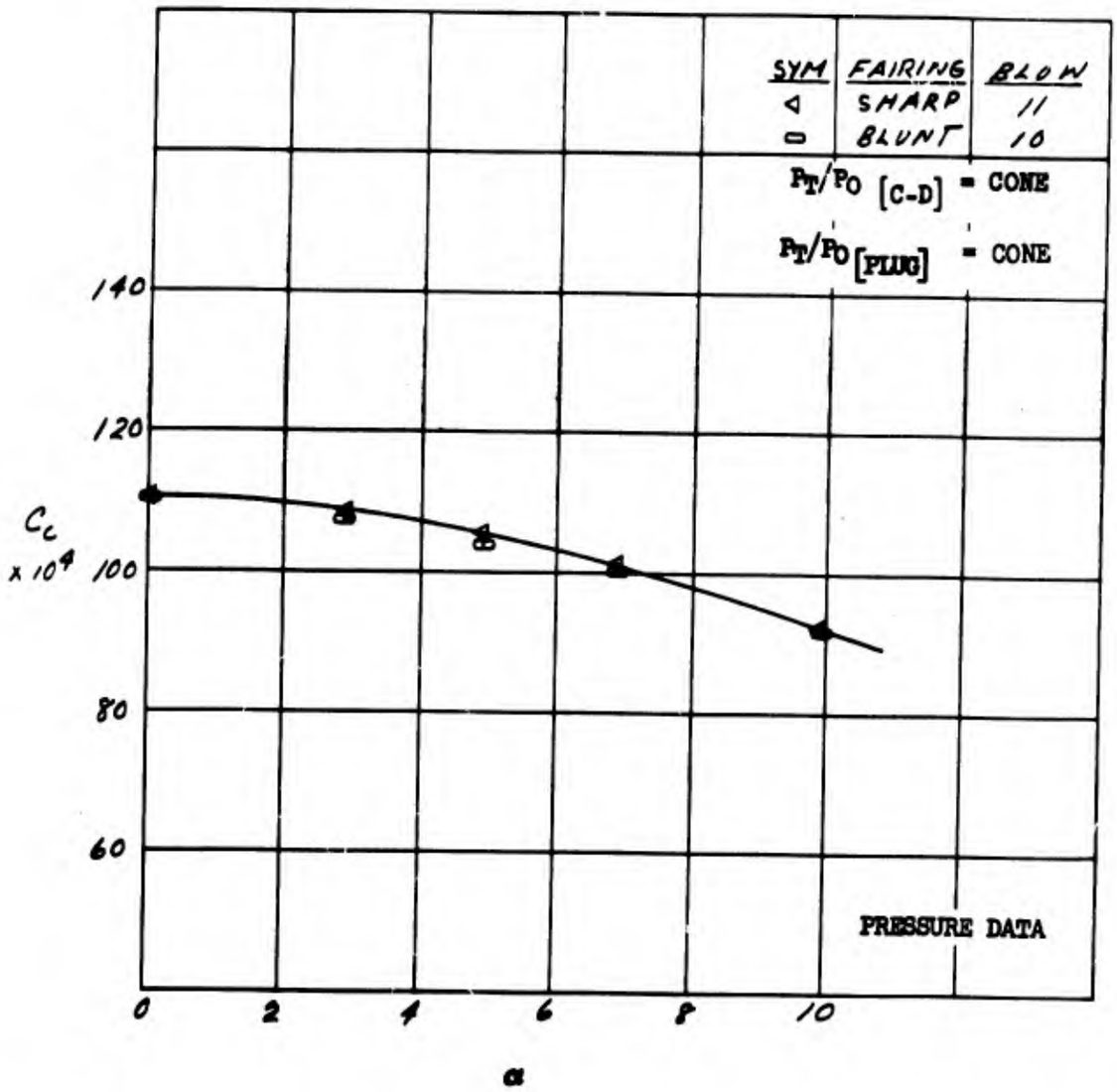

Figure 42. Effect of Blunt Inlet Fairing on Chord Force - M=1.27

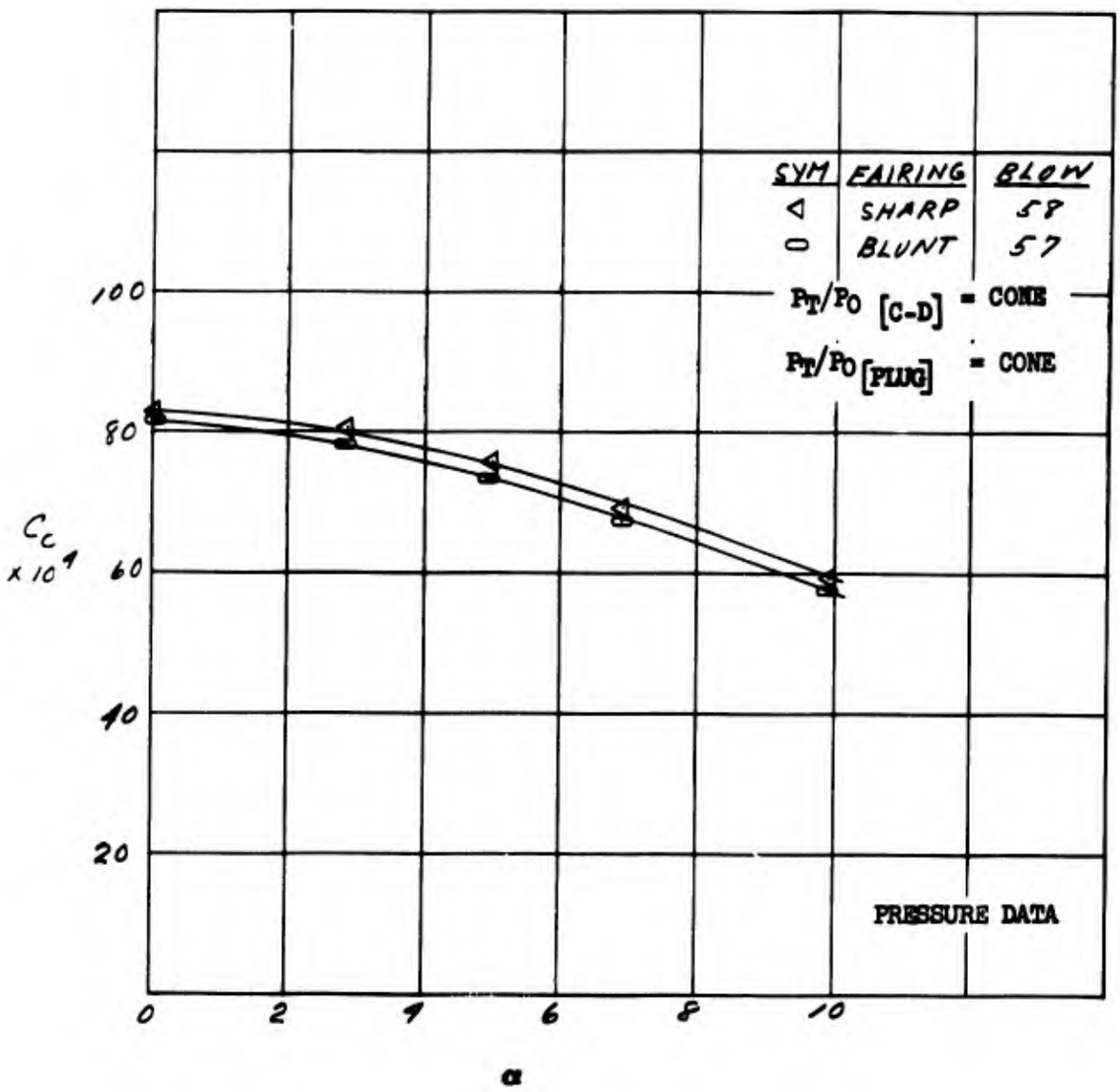

Figure 43. Effect of Blunt Inlet Fairing On Chord Force - M = 1.7

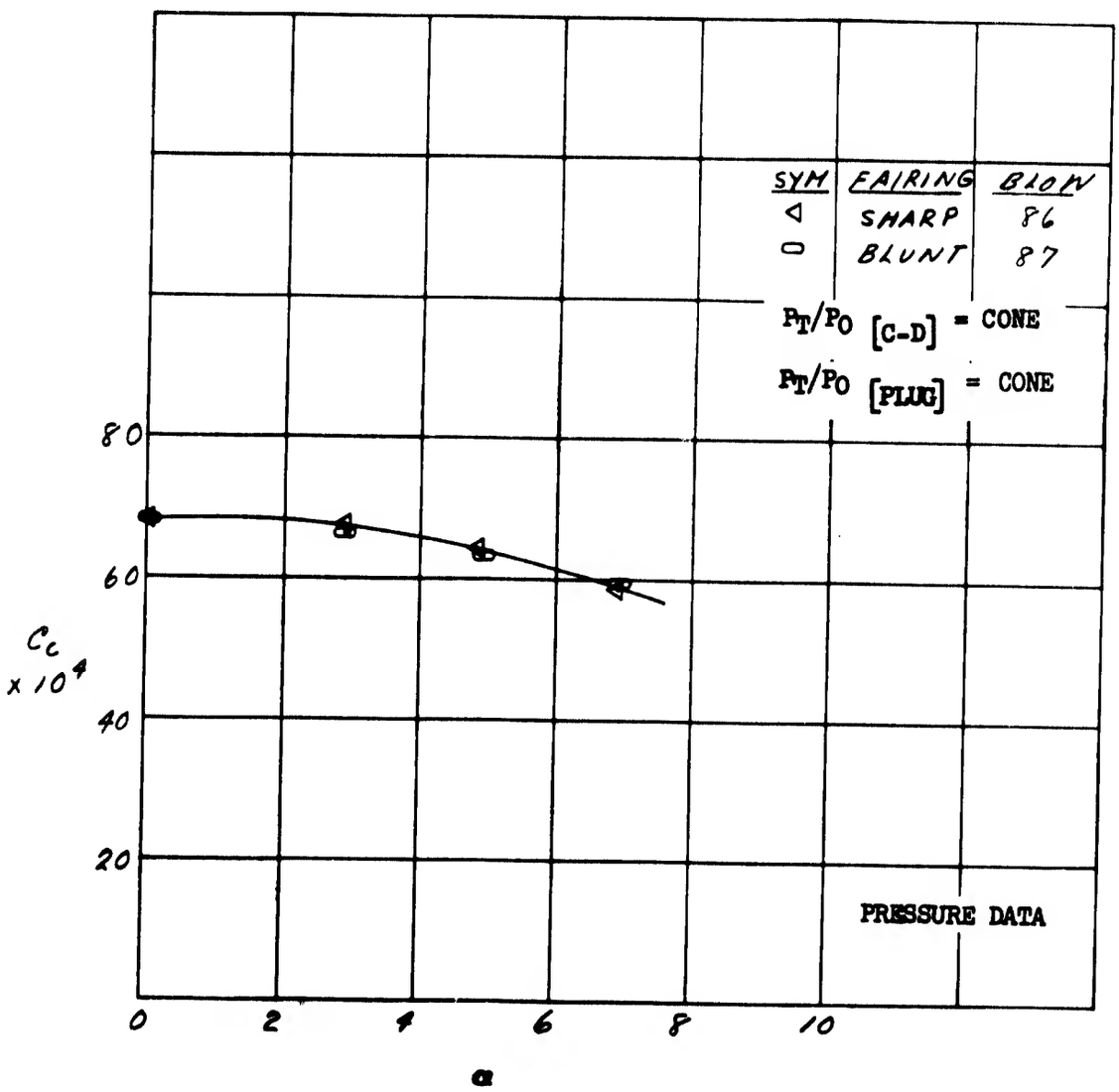

Figure 44. Effect of Blunt Inlet Fairing on Chord Force - M=2.0

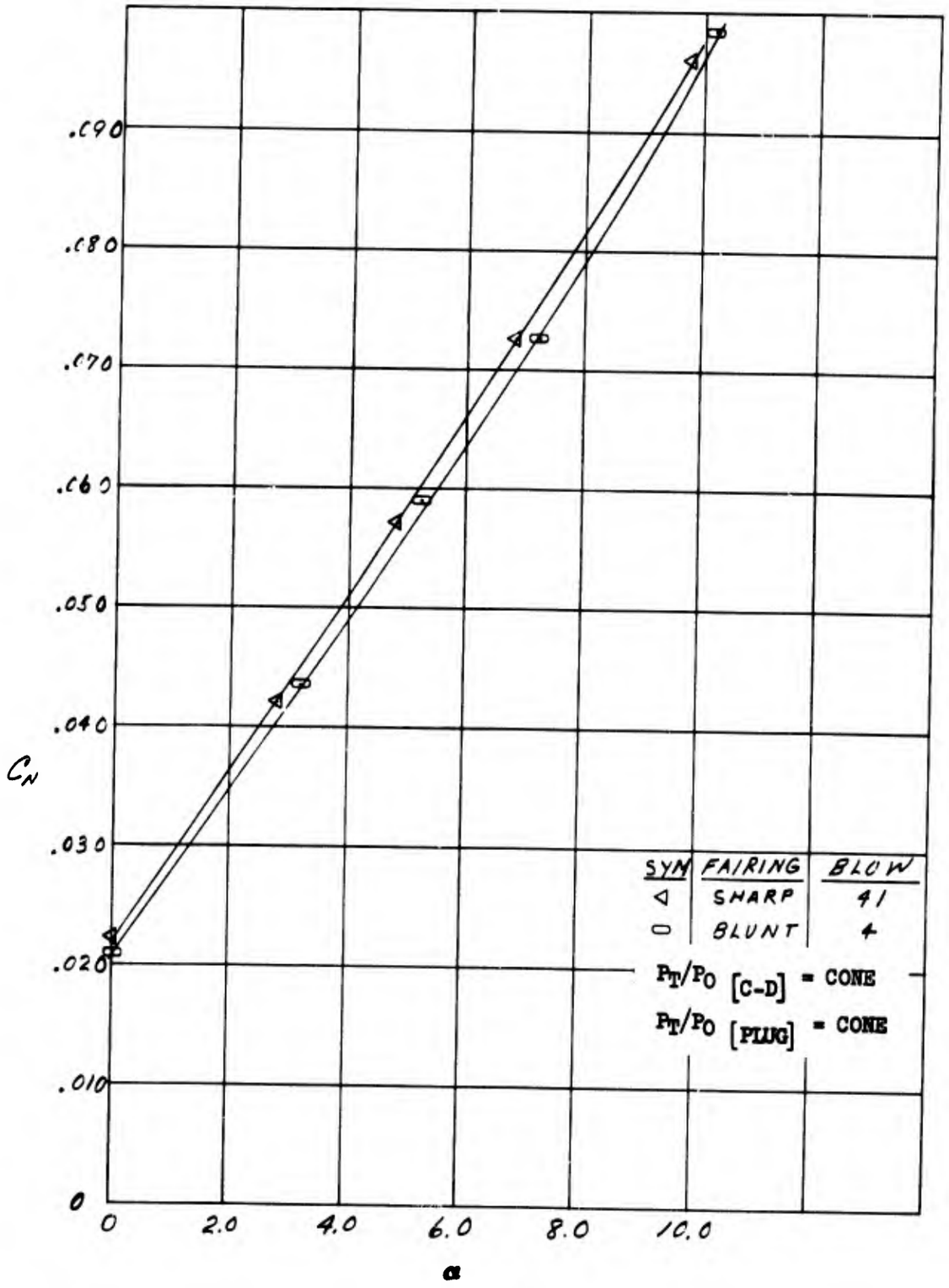

Figure 45. Effect of Blunt Inlet Fairing On Normal Force - M = .614

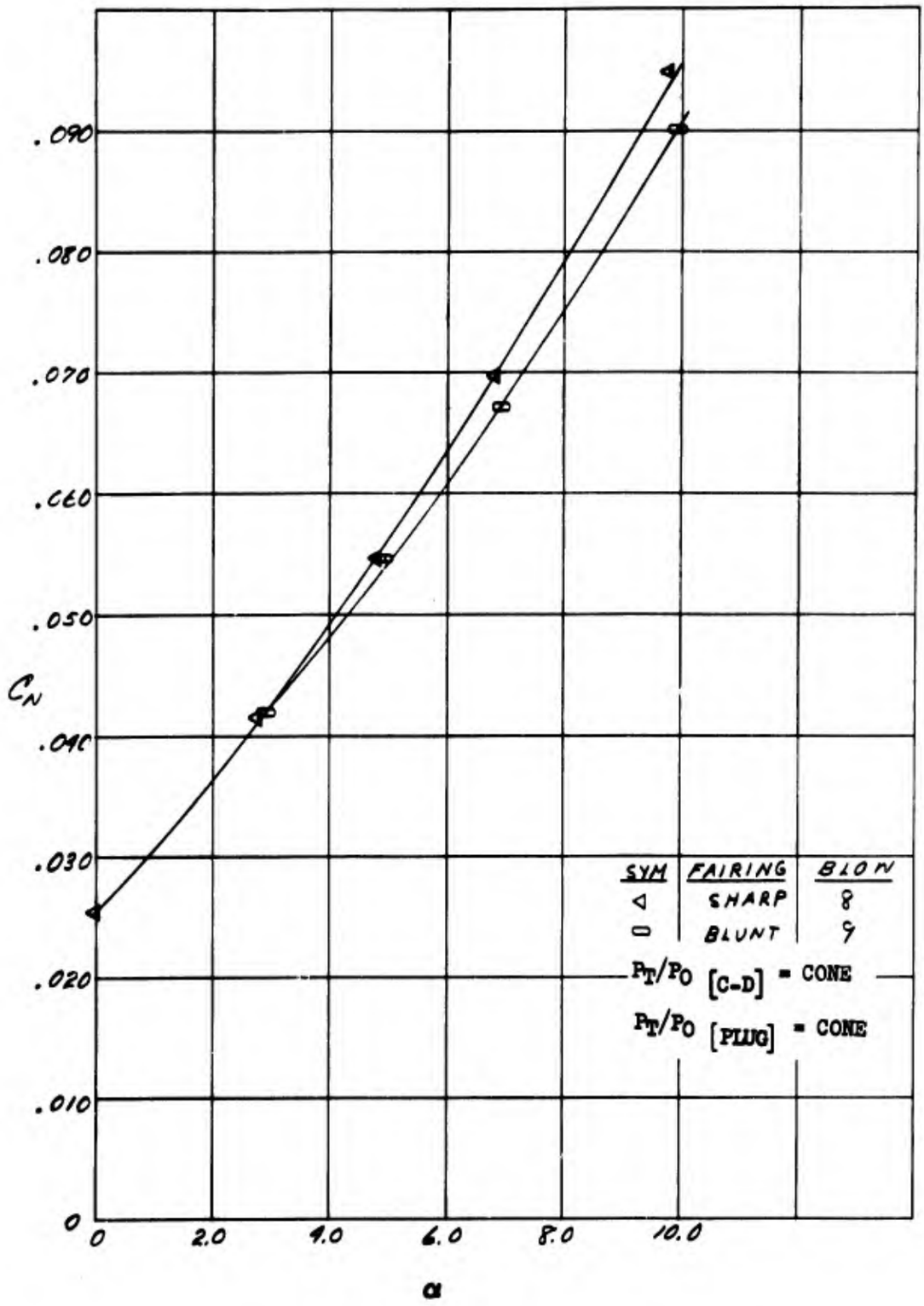

Figure 46. Effect of Blunt Inlet Fairing on Normal Force - M=.85

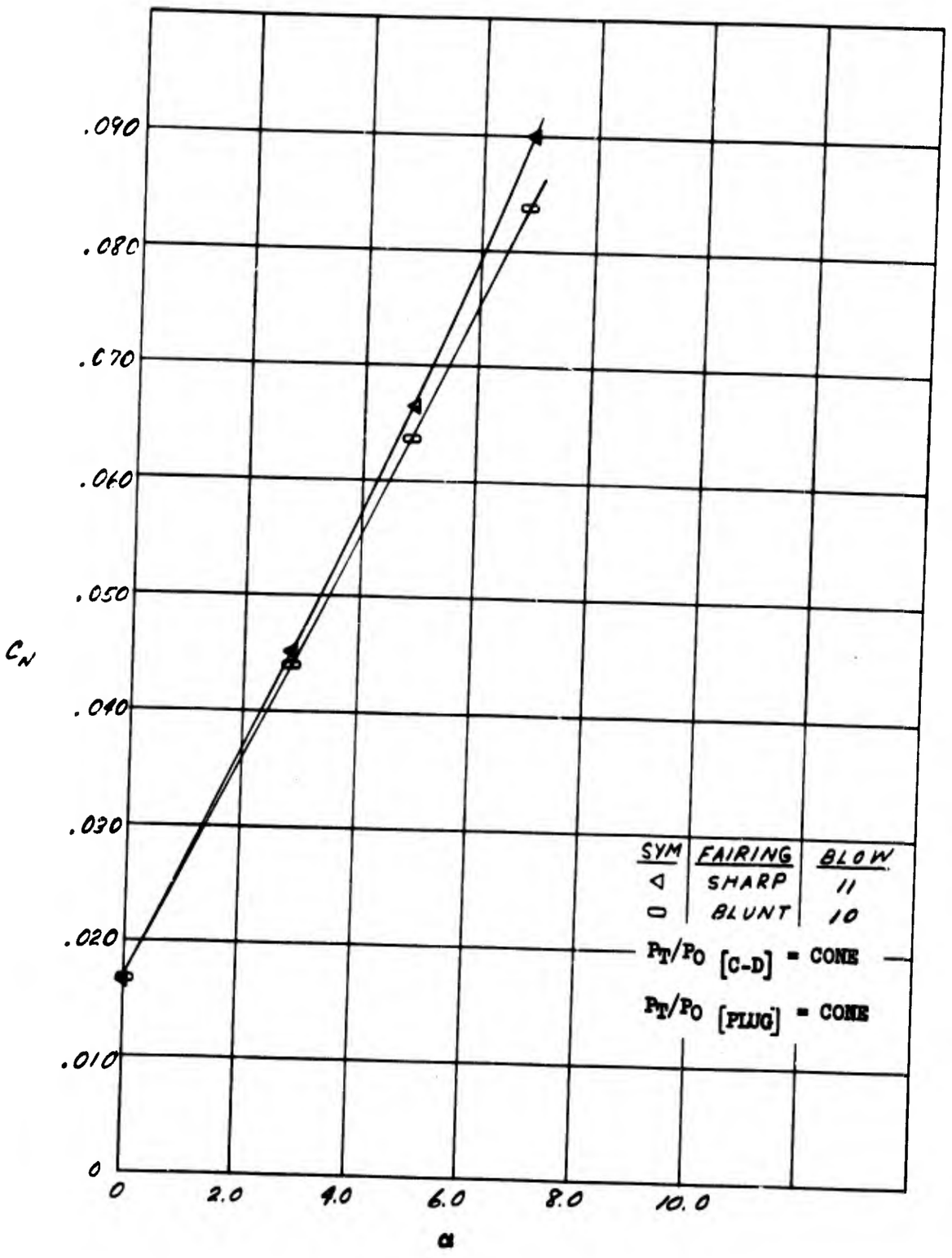

Figure 47. Effect of Blunt Inlet Fairing on Normal Force - M=1.27

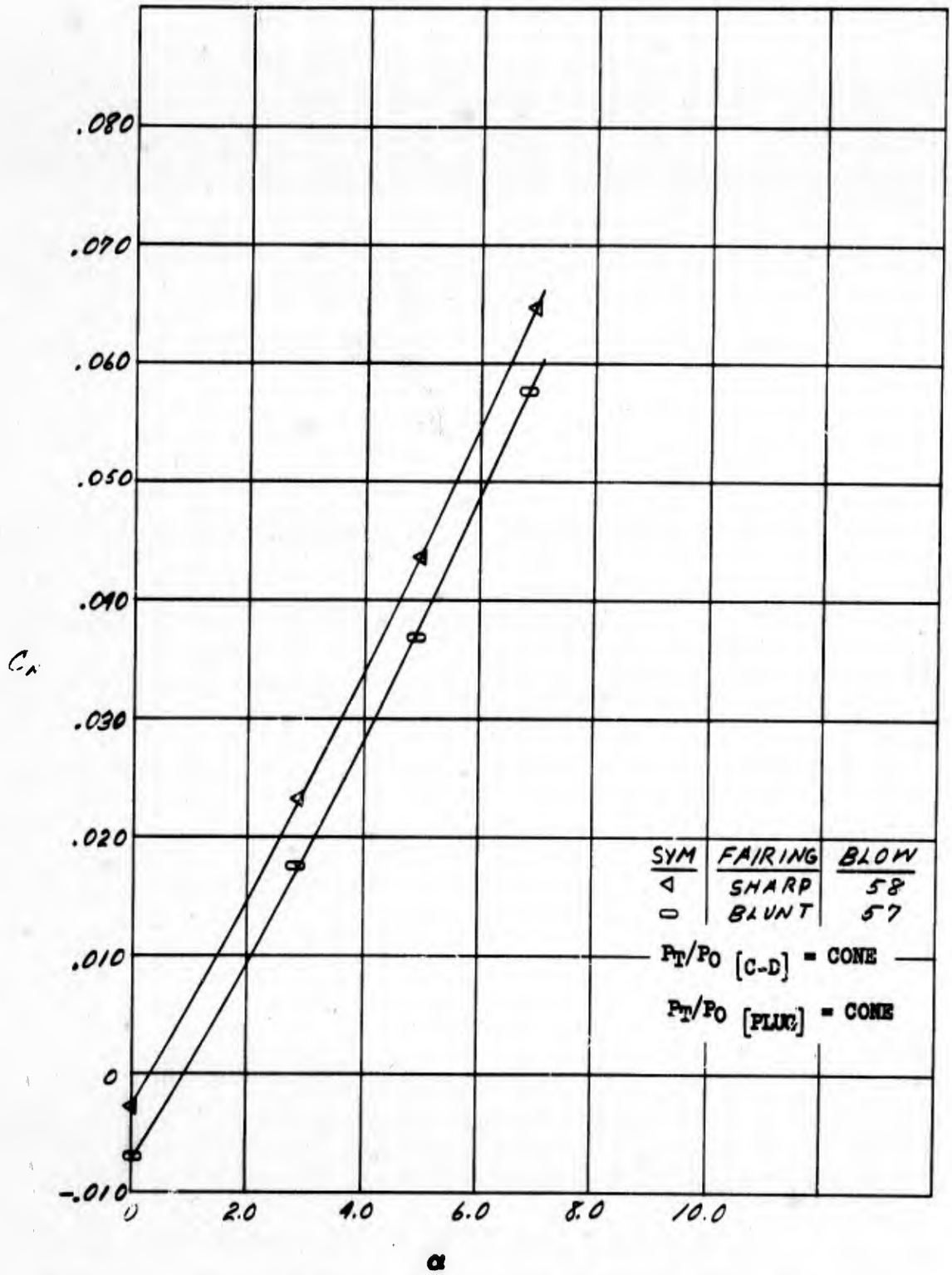

Figure 48. Effect of Blunt Inlet Fairing On Normal Force - M = 1.7

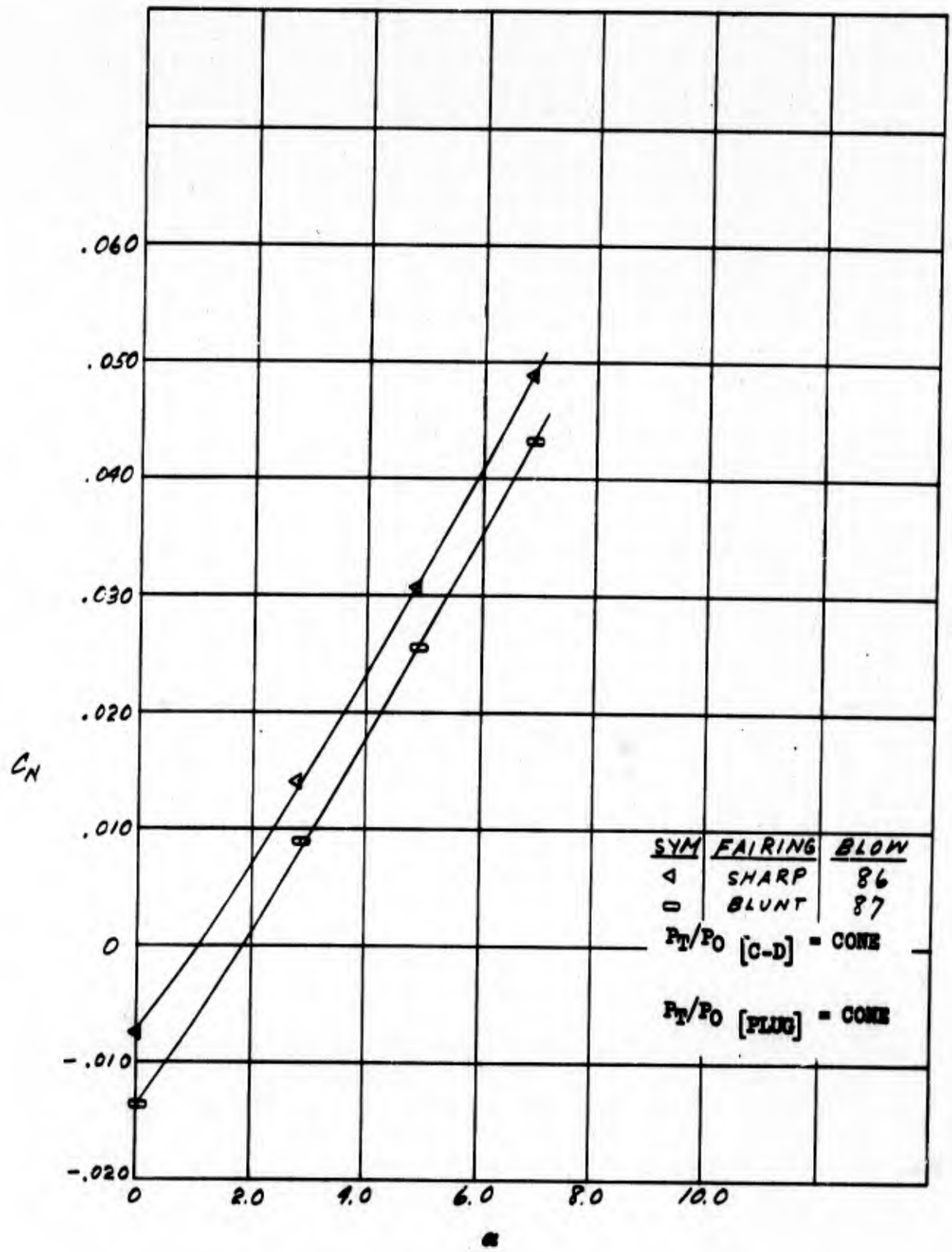

Figure 49. Effect of Blunt Inlet Fairing on Normal Force - M=2.0

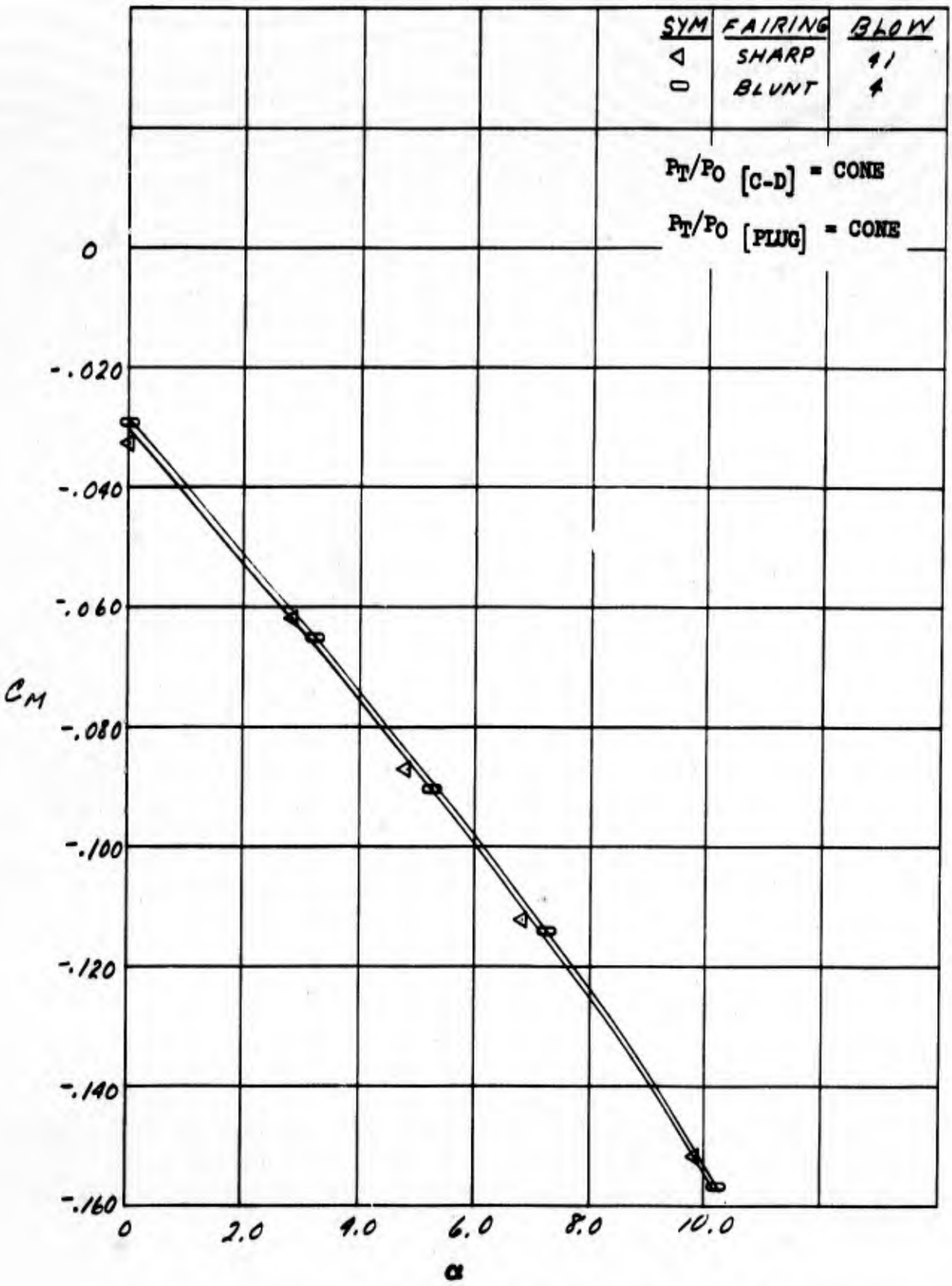

Figure 50. Effect of Blunt Inlet Fairing On Pitching Moment - M = .614

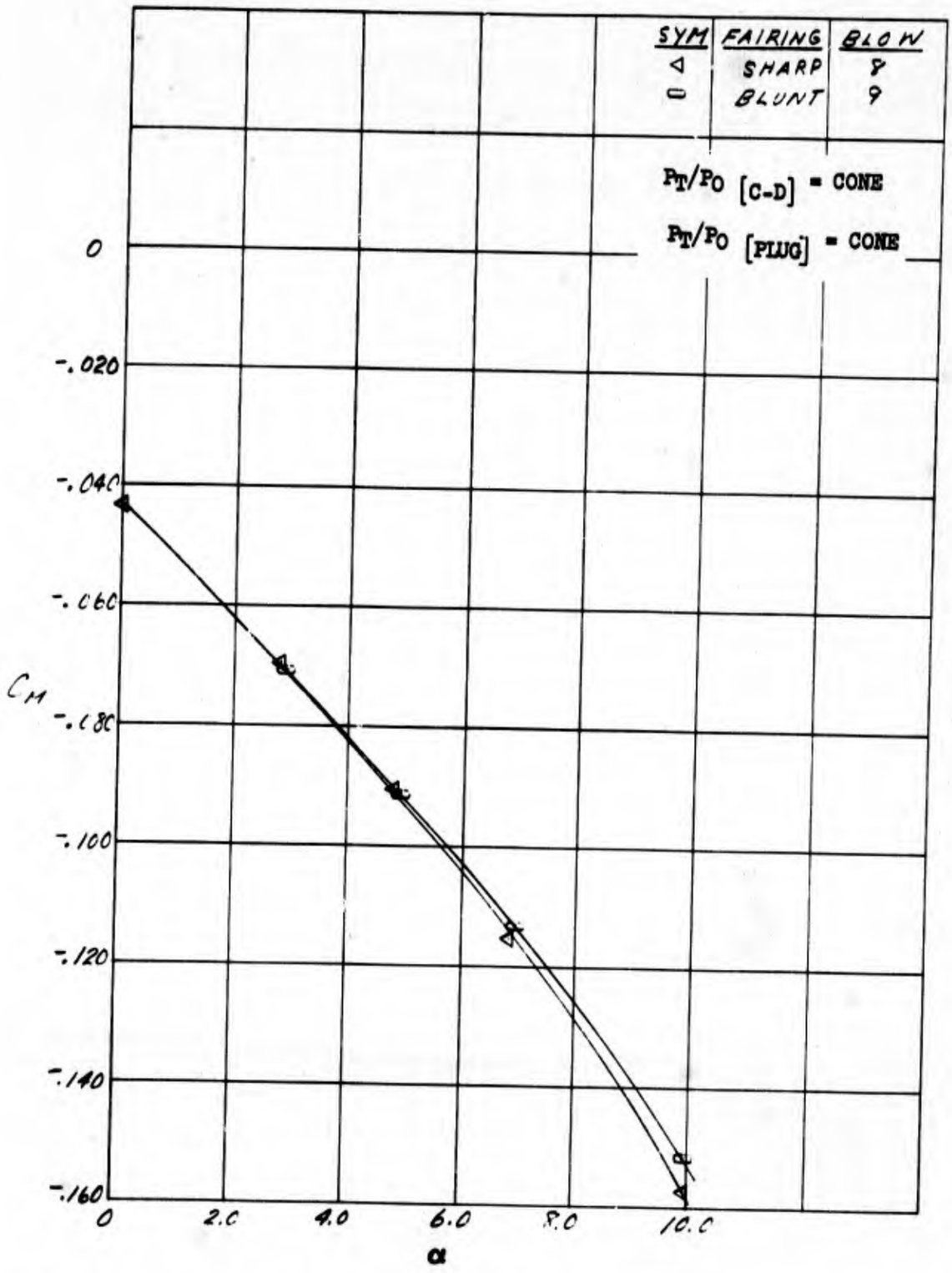

Figure 51. Effect of Blunt Inlet Fairing On Pitching Moment - M = .85

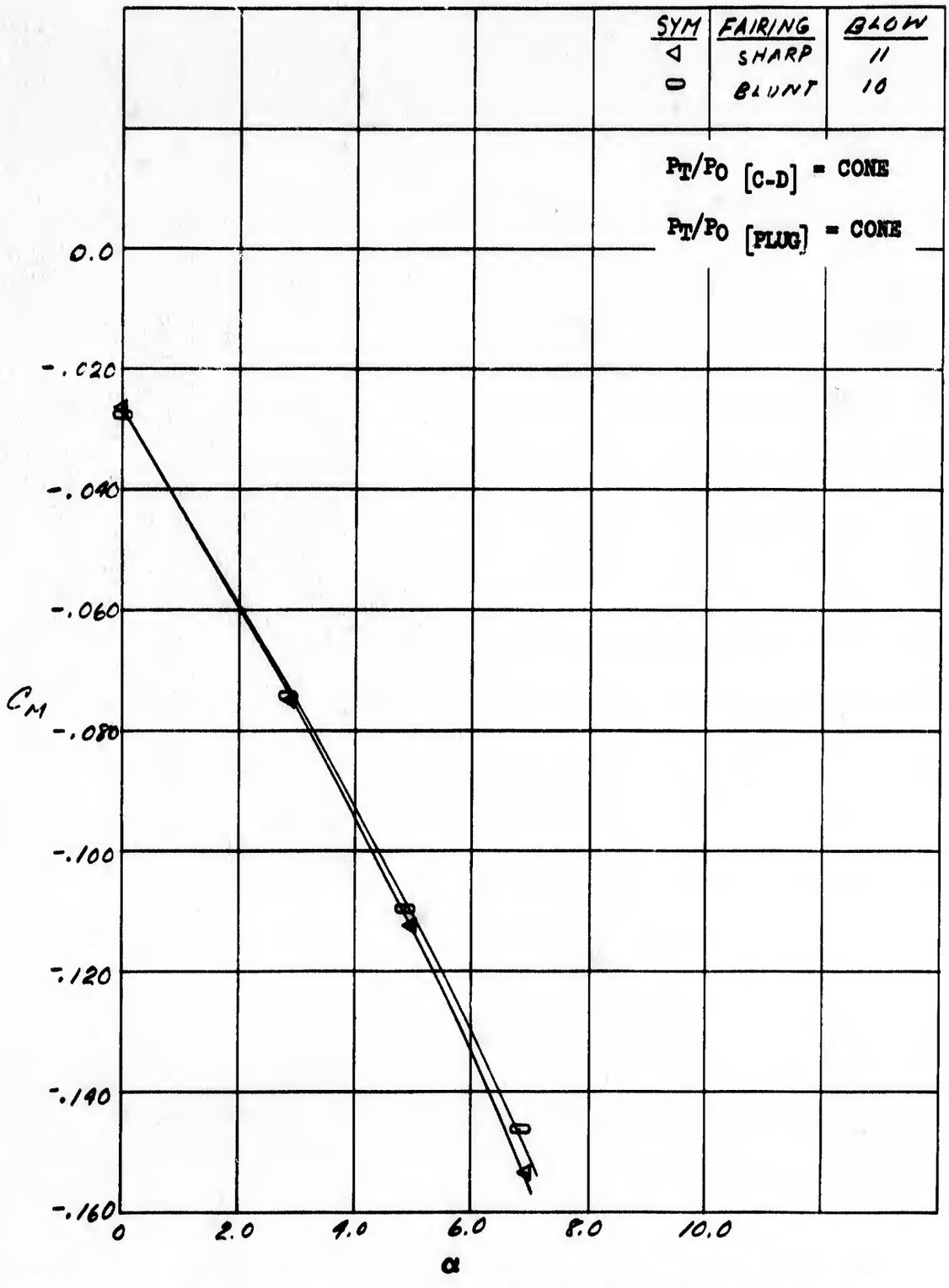

Figure 52. Effect of Blunt Inlet Fairing On Pitching Moment - M = 1.27

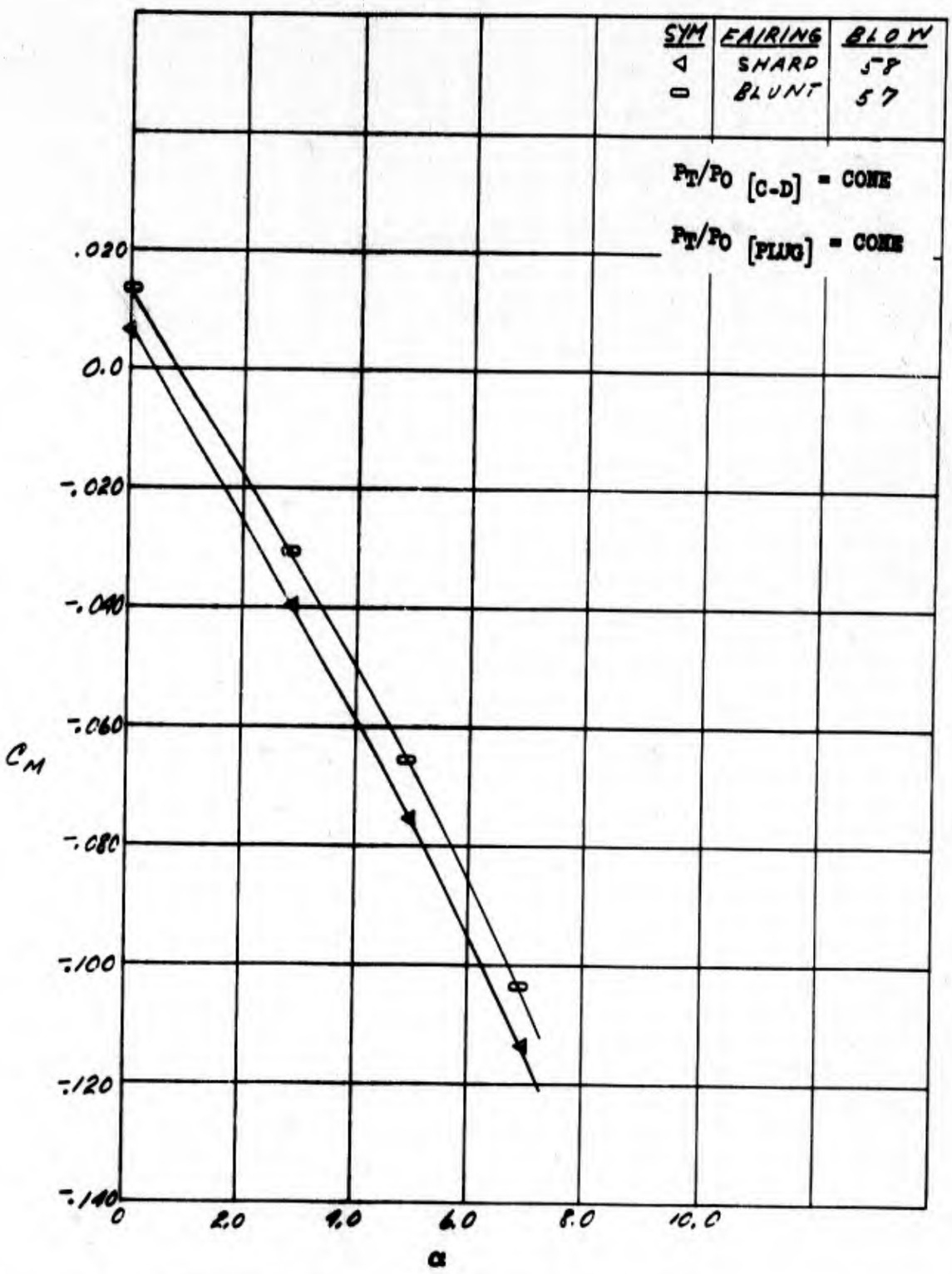

Figure 53. Effect of Blunt Inlet Fairing On Pitching Moment - M = 1.7

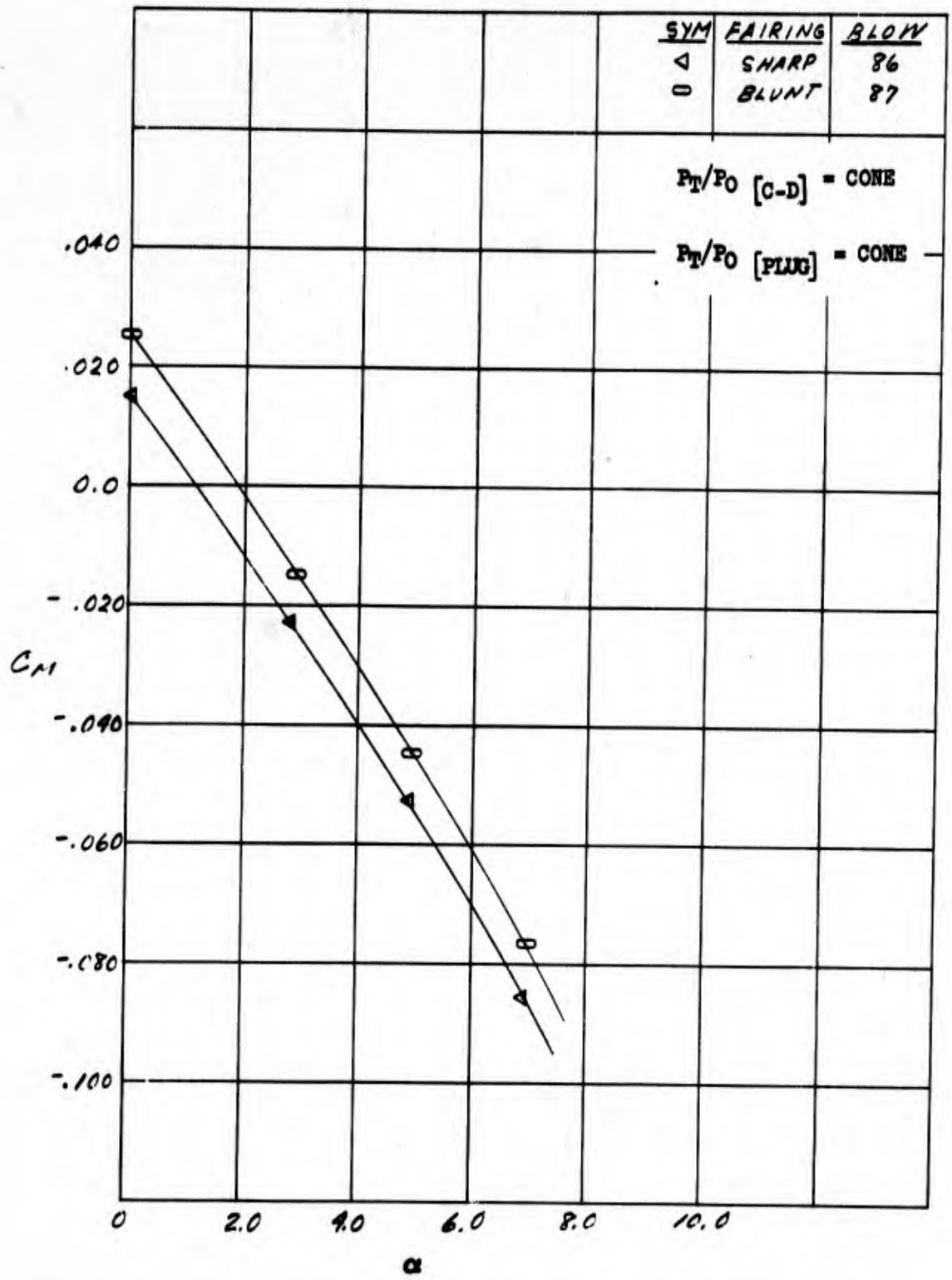

Figure 54. Effect of Blunt Inlet Fairing On Pitching Moment - M = 2.0

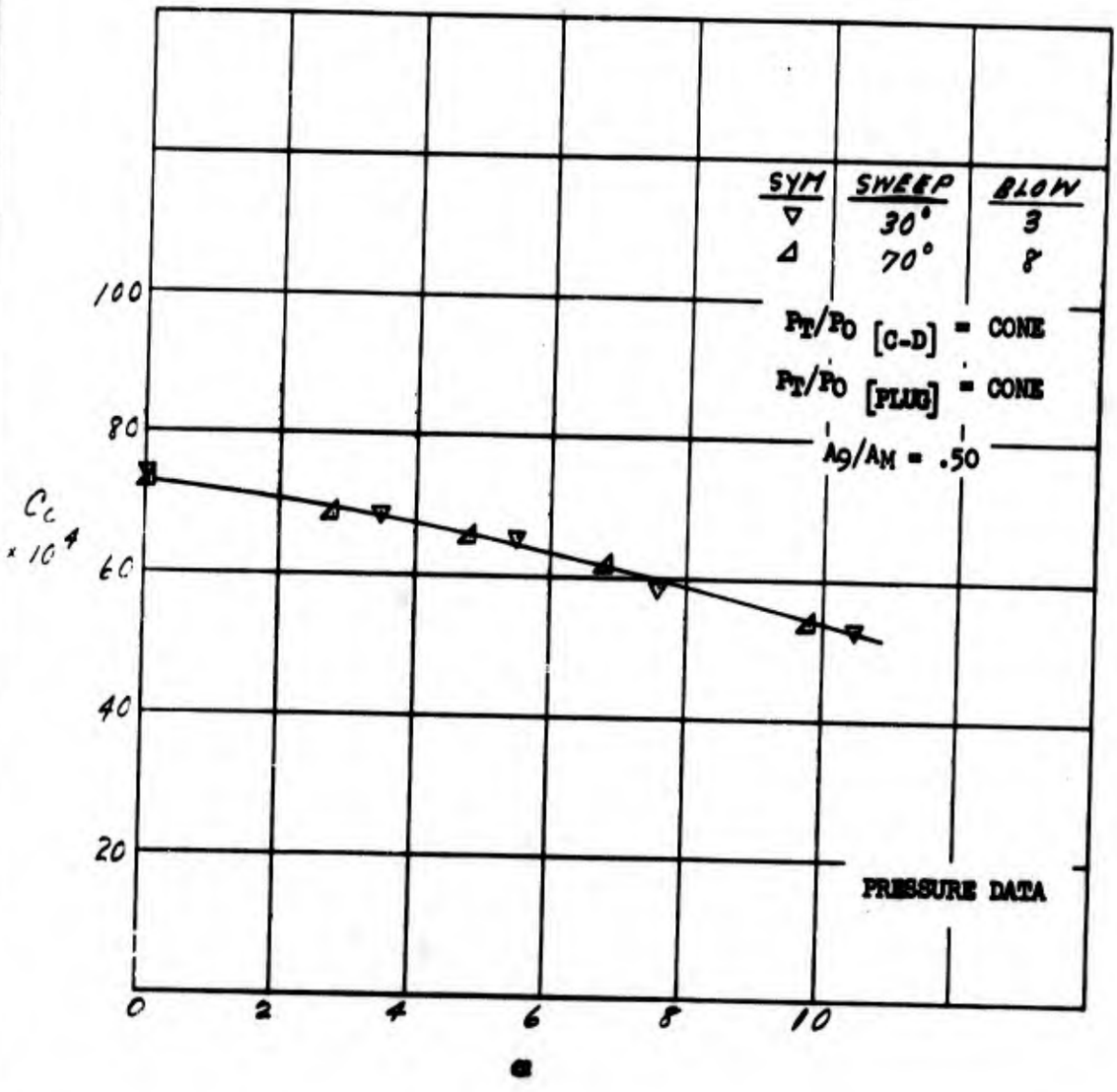

Figure 55. Wing Sweep Effects on Chord Force - M = .85

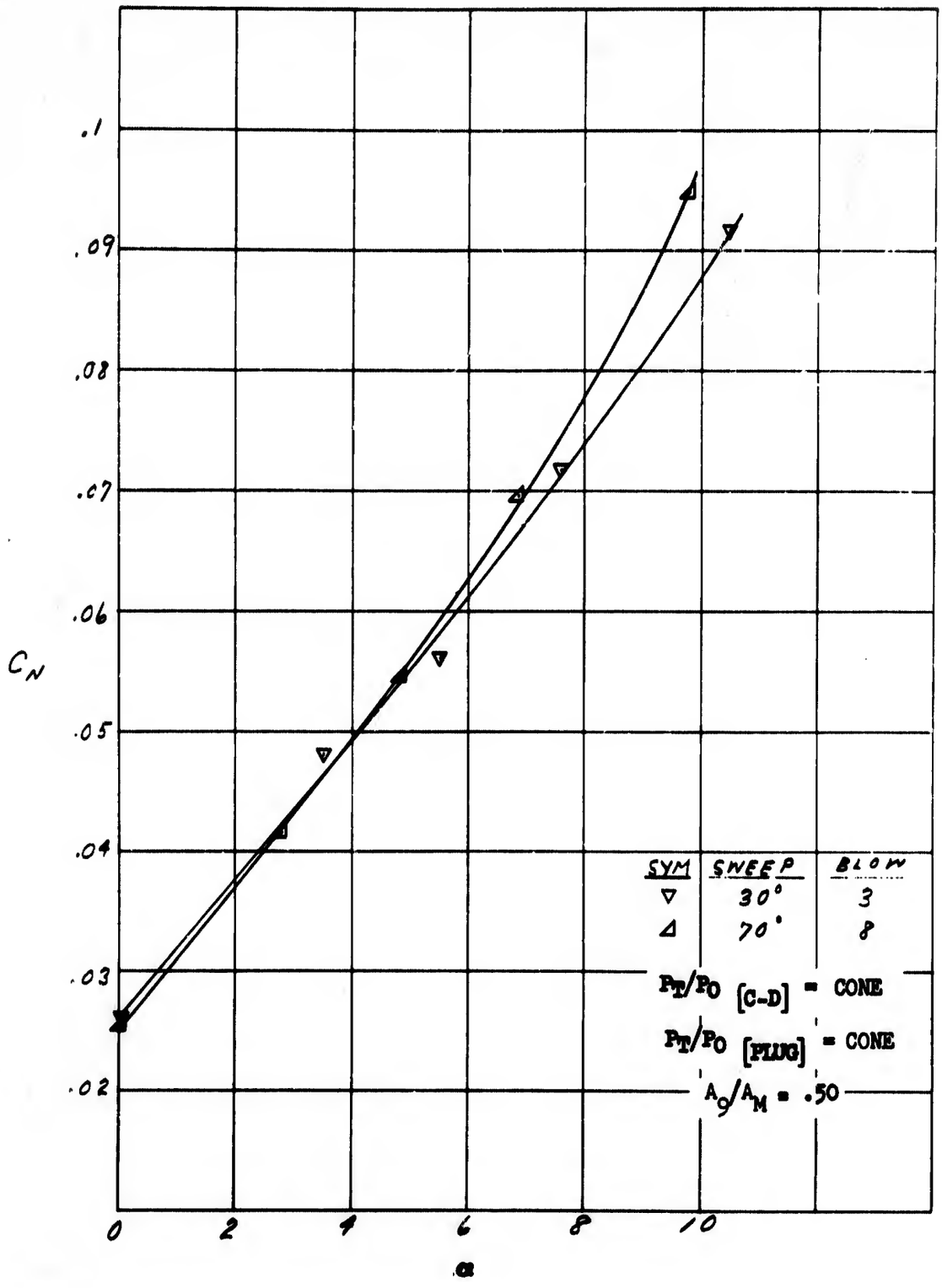

Figure 56. Wing Sweep Effects on Normal Force - M = .85.

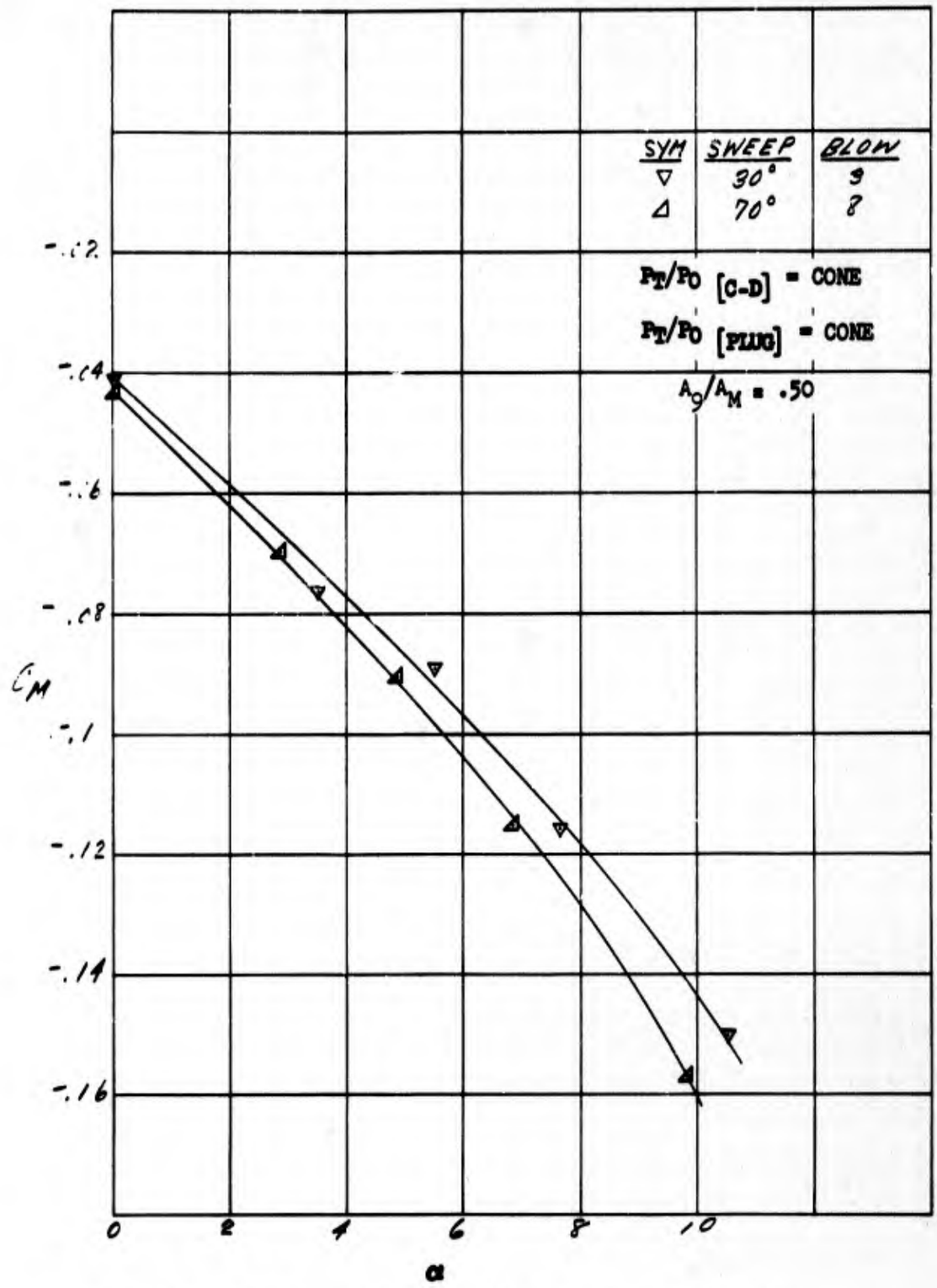

Figure 57. Wing Sweep Effects on Pitching Moment - M = .85

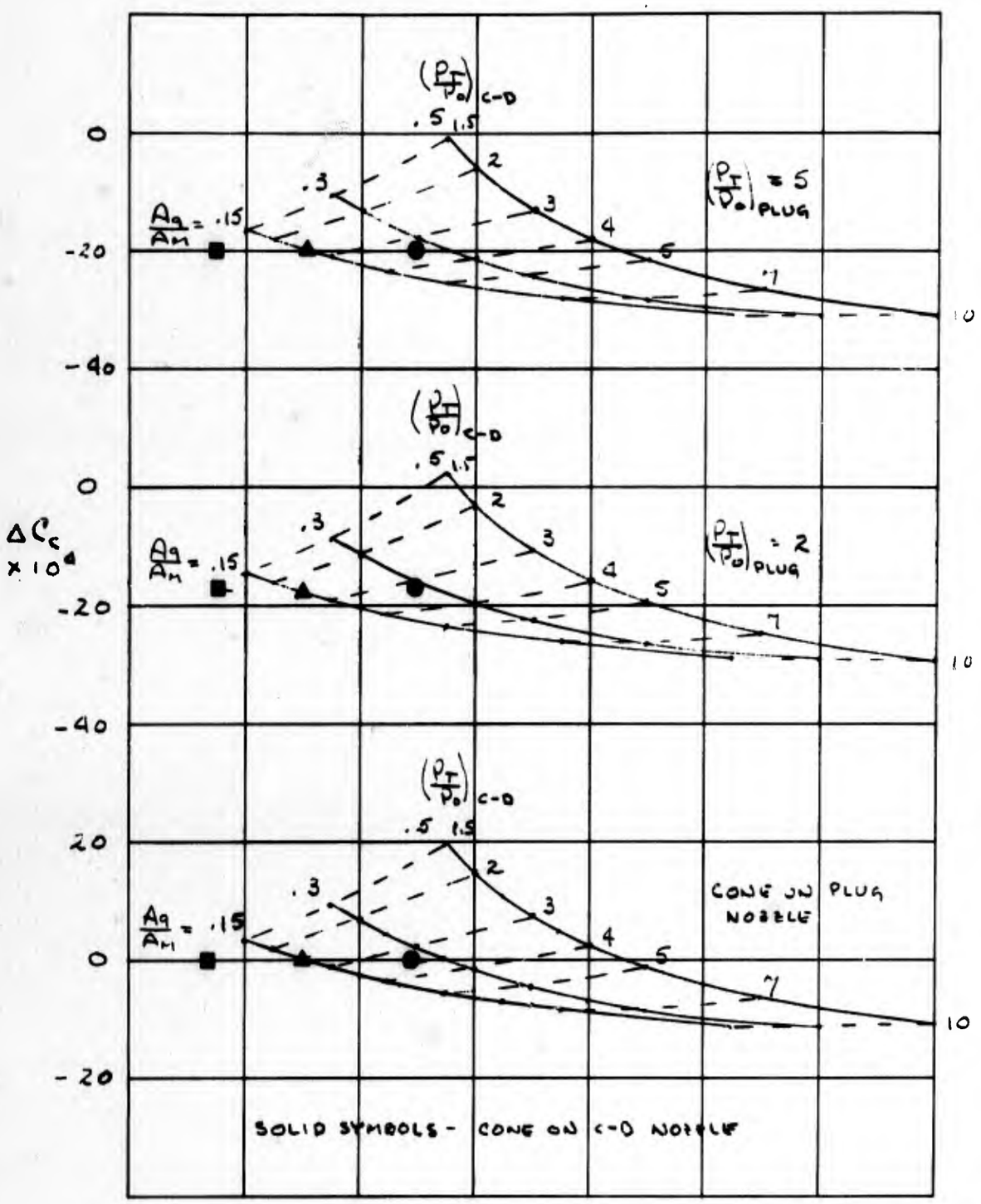

Figure 58. Estimated Total Chord Force Increment - M=.60

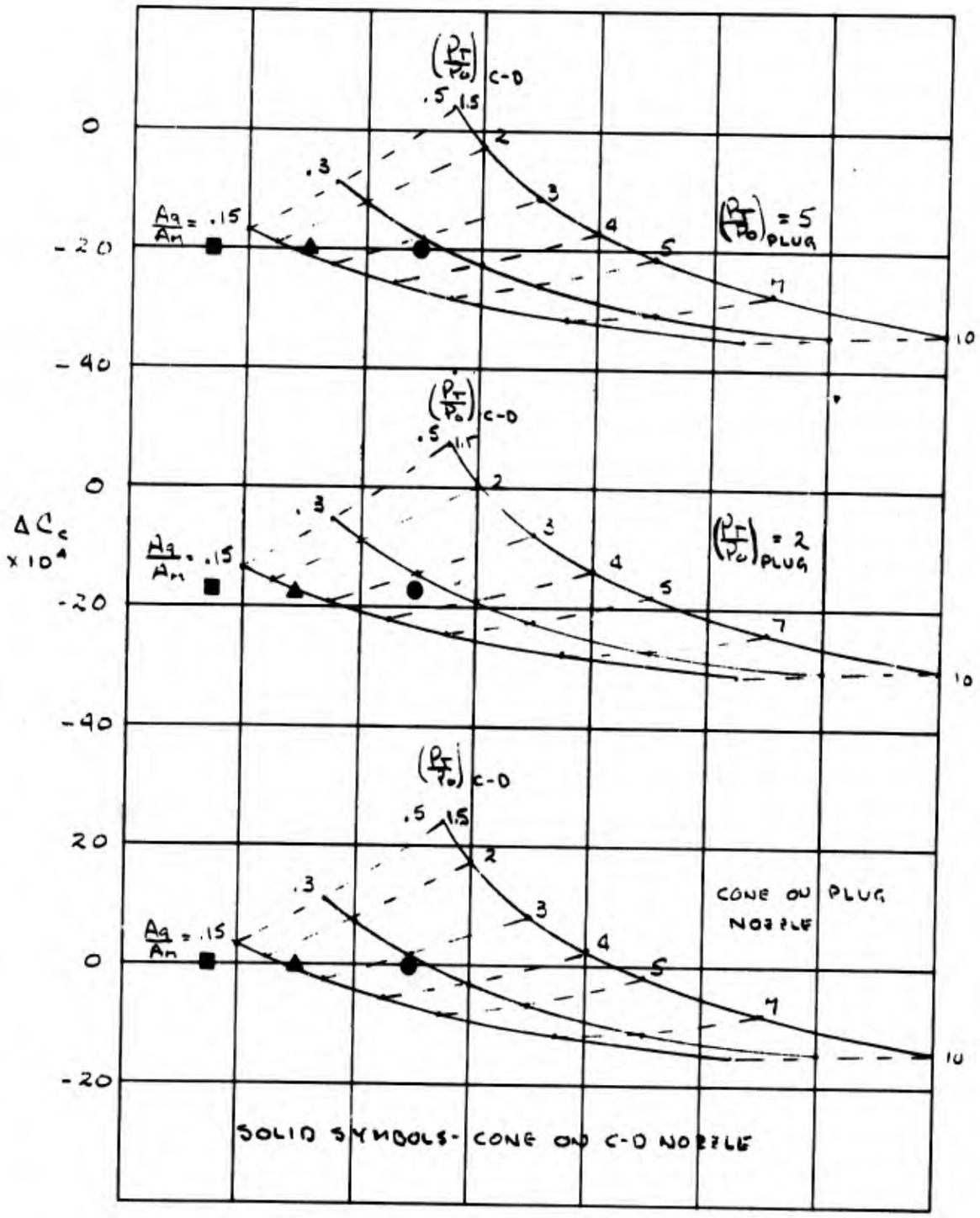

Figure 59. Estimated Total Chord Force Increment - M=.85

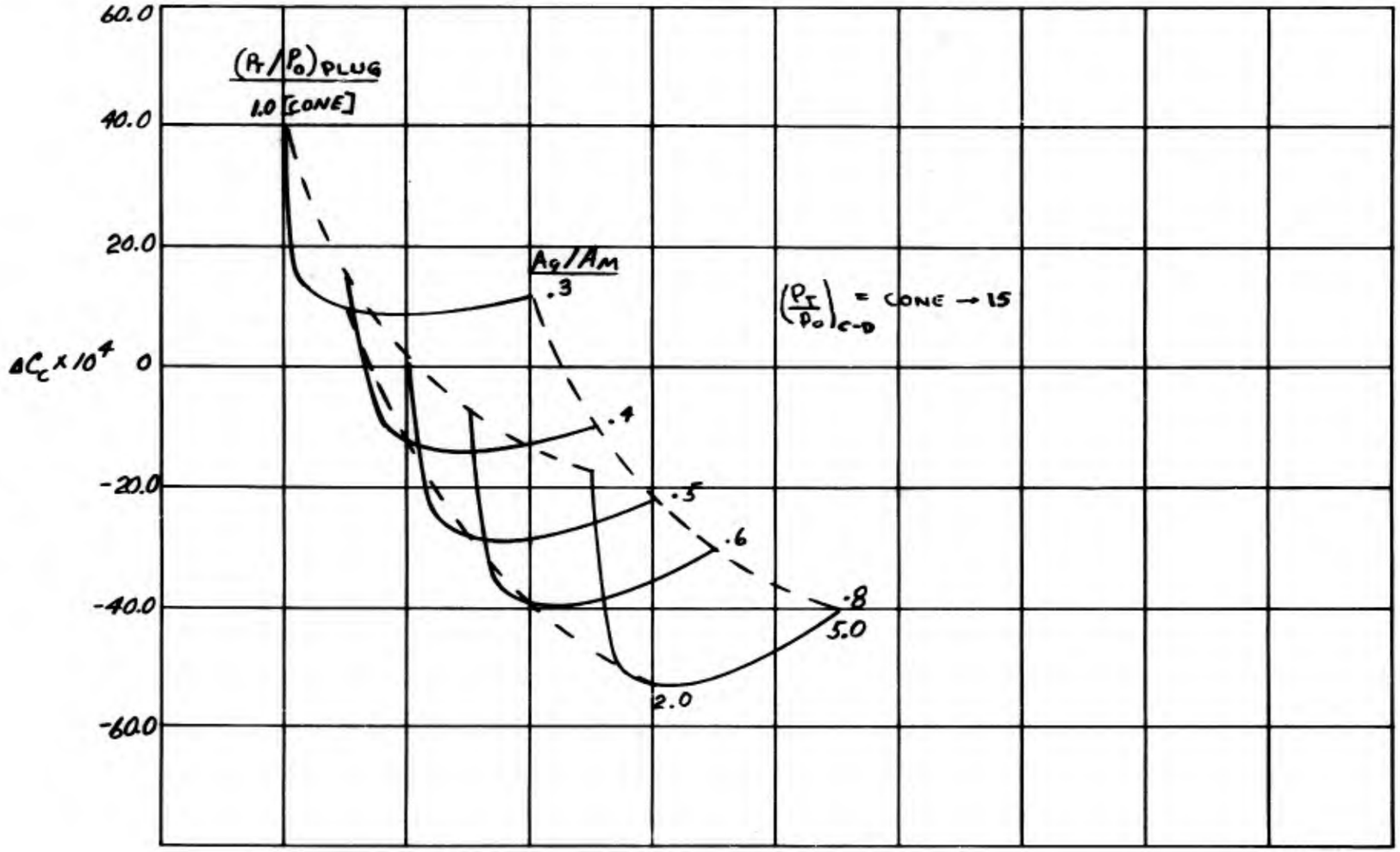

Figure 60. Estimated Total Chord Force Increment - M=1.25

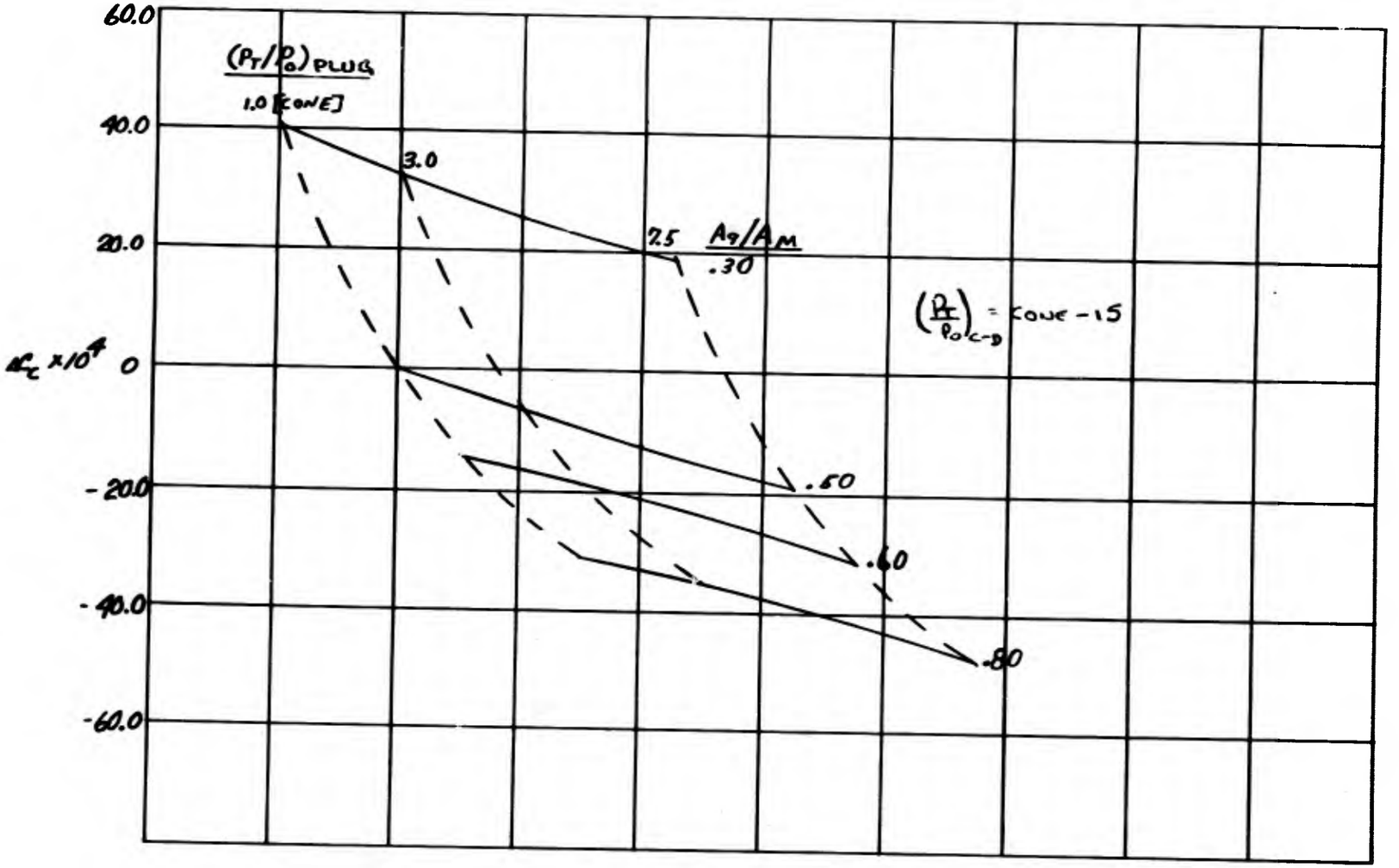

Figure 61. Estimated Total Chord Force Increment - M=1.7

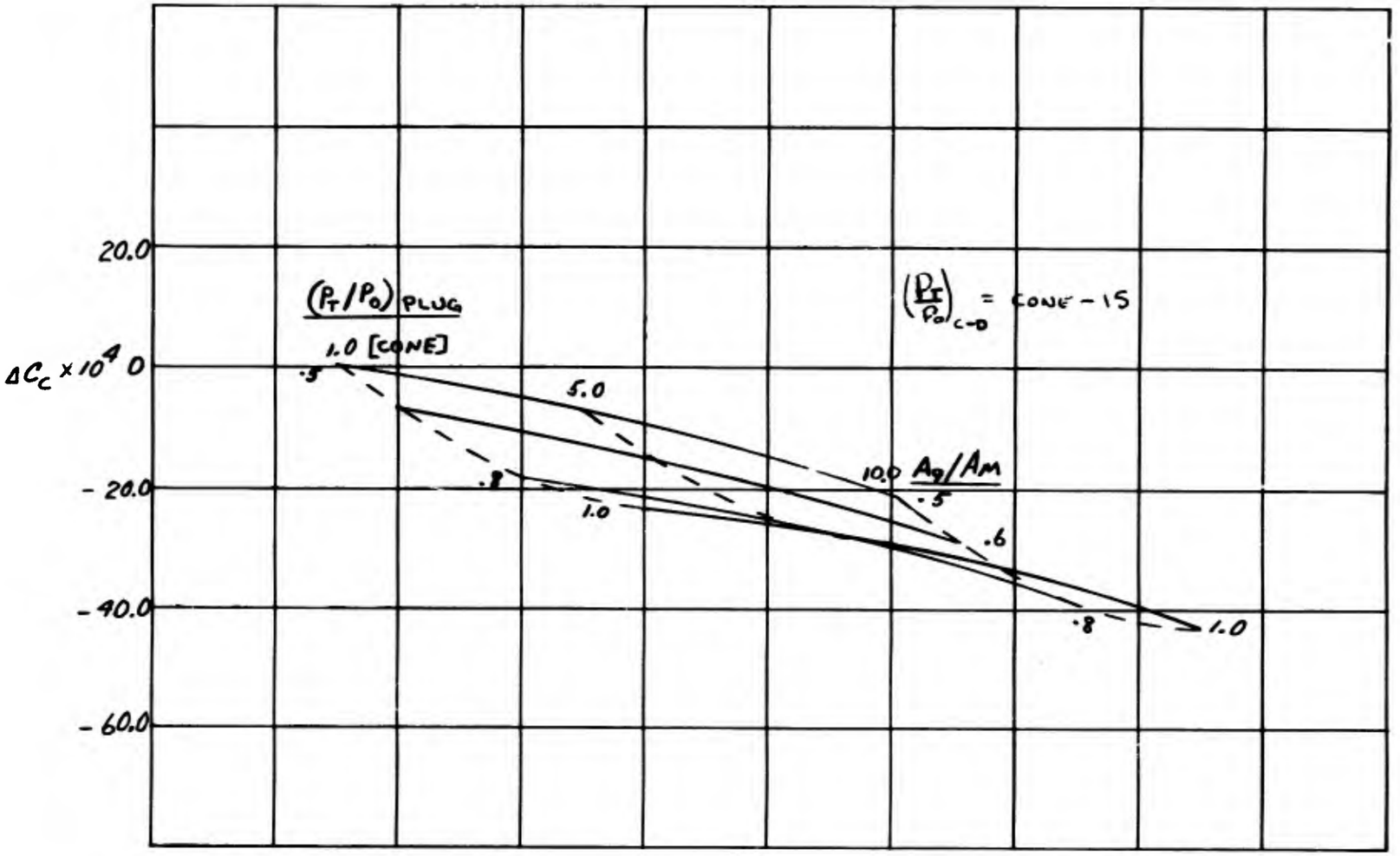

Figure 62. Estimated Total Chord Force Increment - M=2.0

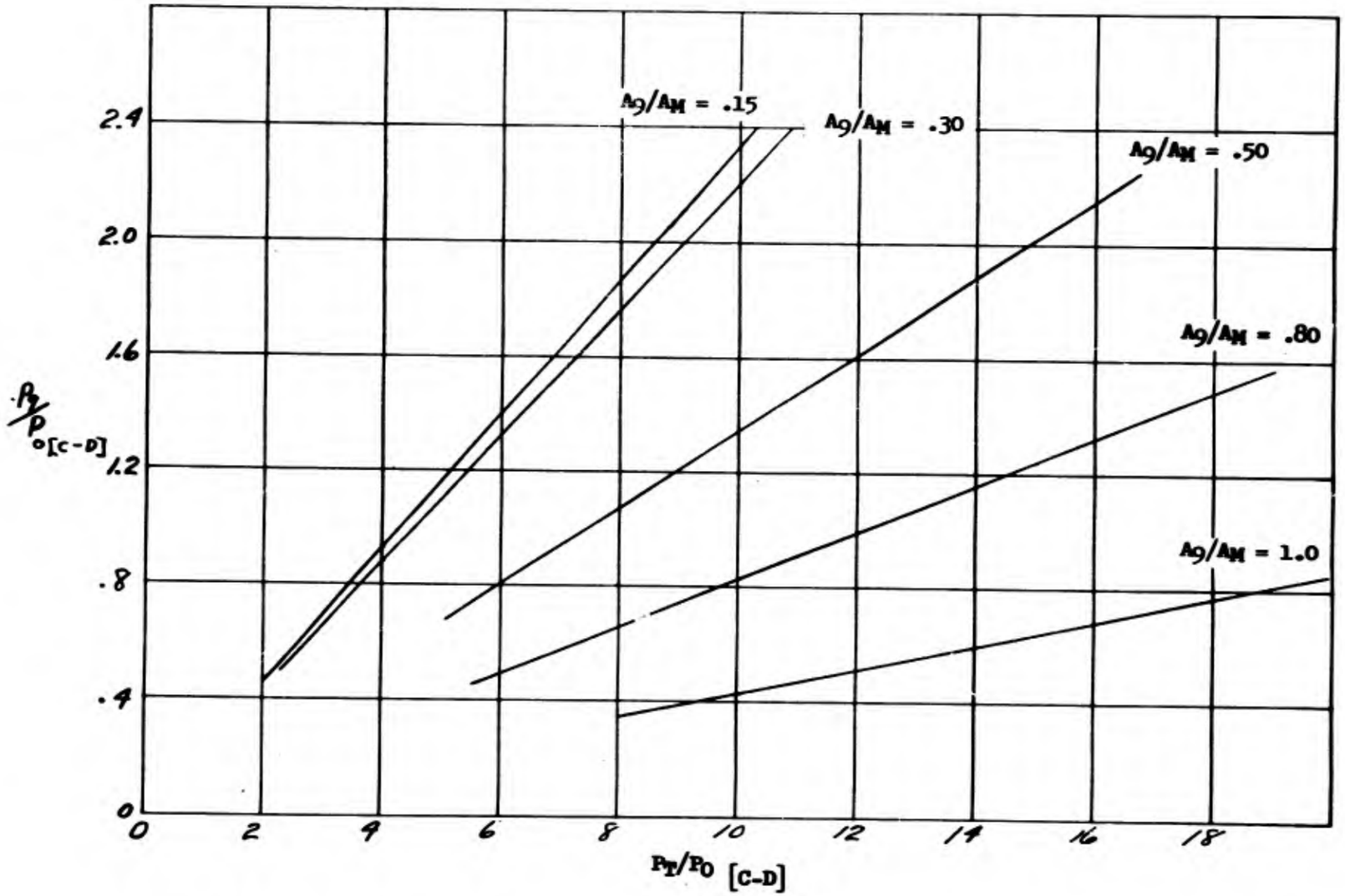

Figure 63. Relationship Between C-D Nozzle Total and Exit Static Pressure Ratios.

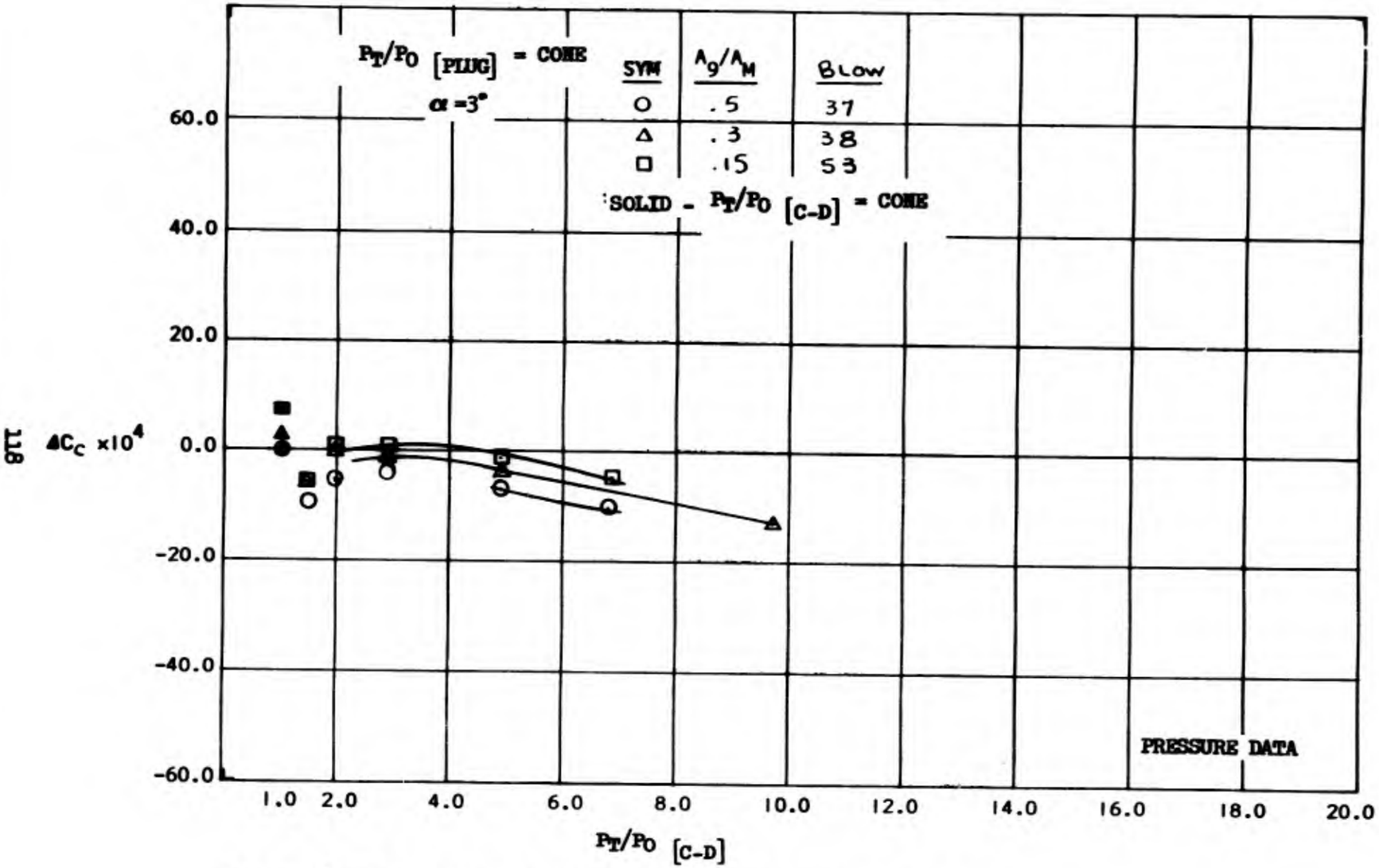

Figure 64. C-D Nozzle Jet Effects on Chord Force Increment - M=.614

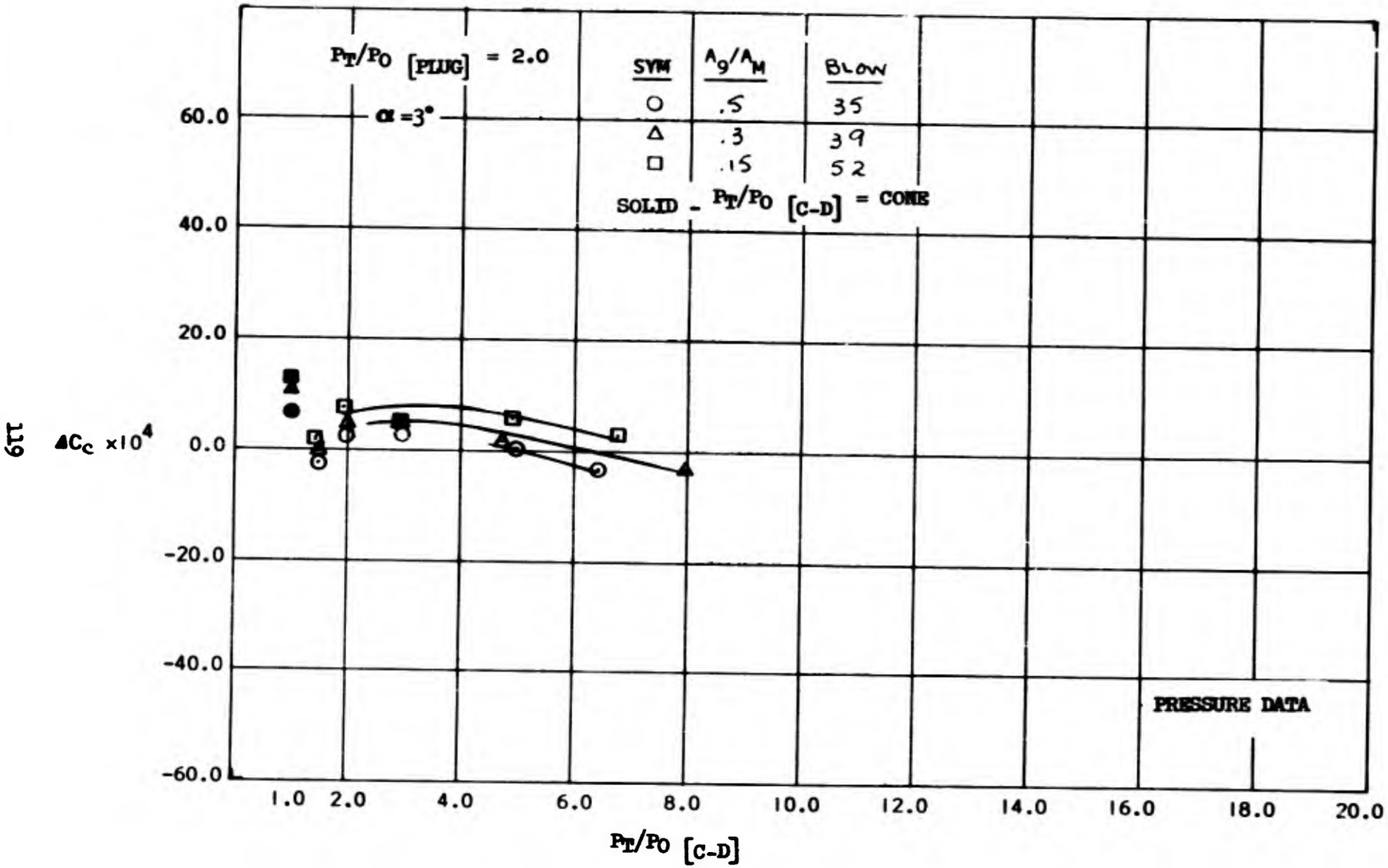

Figure 65. C-D Nozzle Jet Effects on Chord Force Increment - M=.614

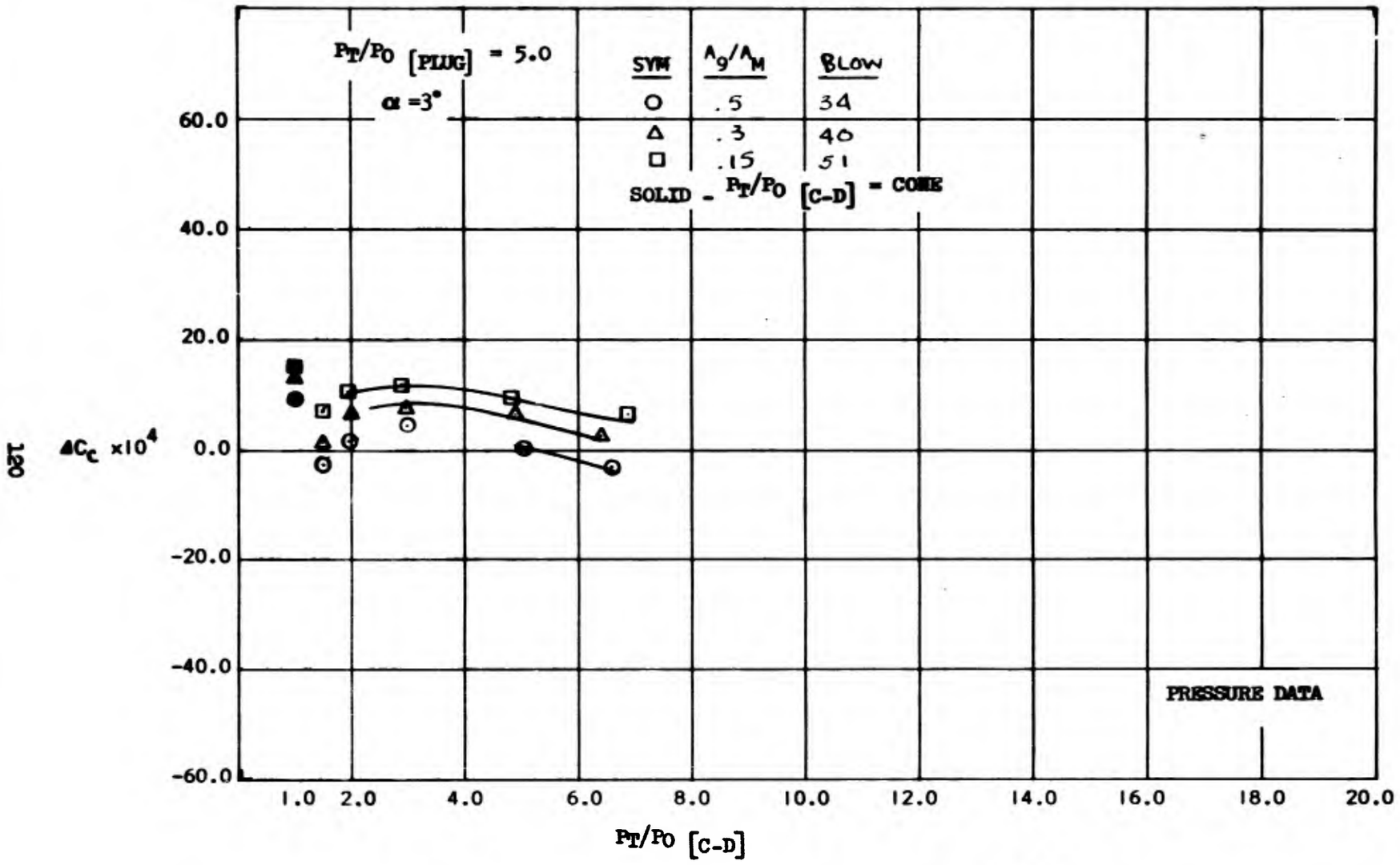

Figure 66. C-D Nozzle Jet Effects on Chord Force Increment - M=.614

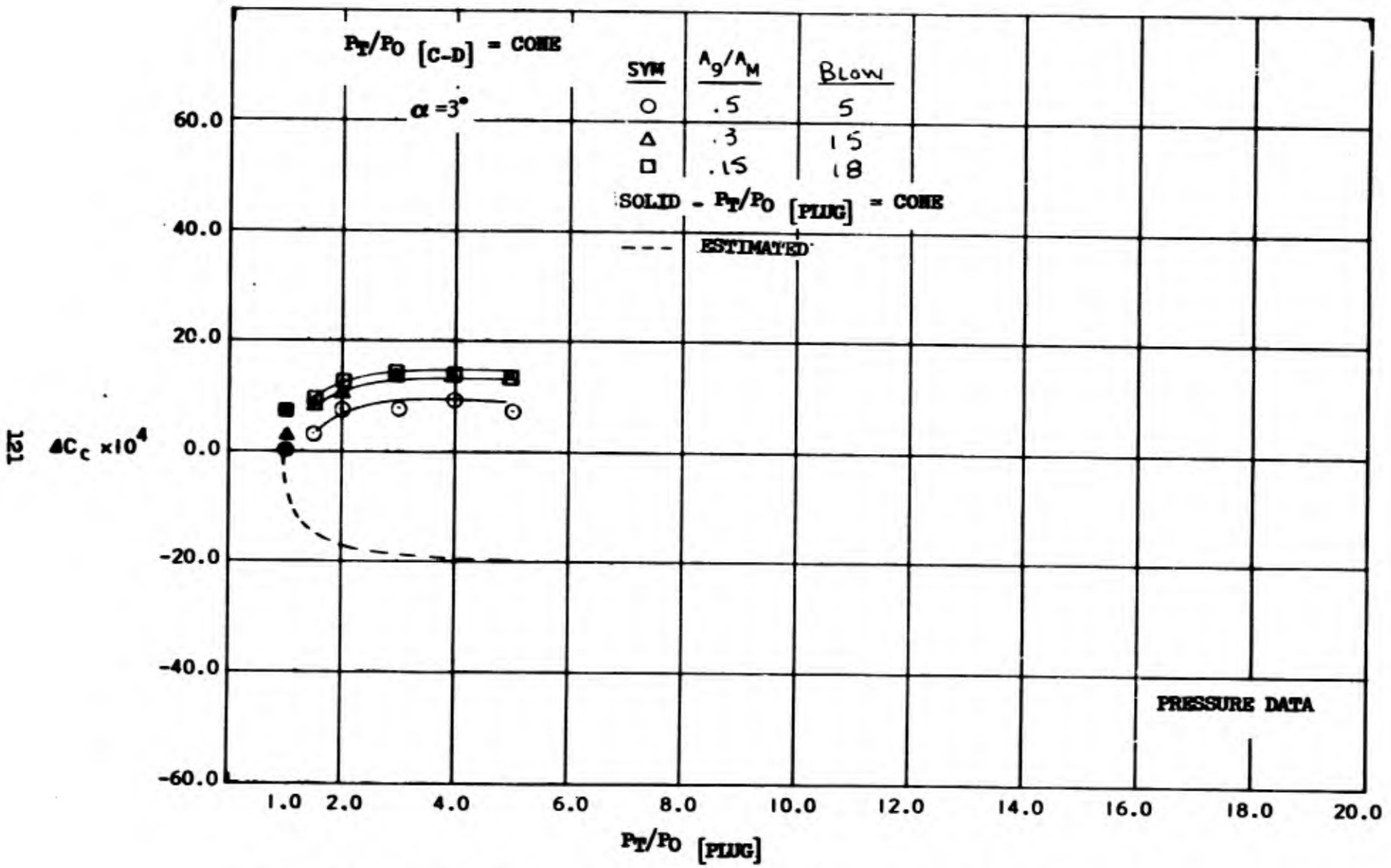

Figure 67. Plug Nozzle Jet Effects on Chord Force Increment - M=.614

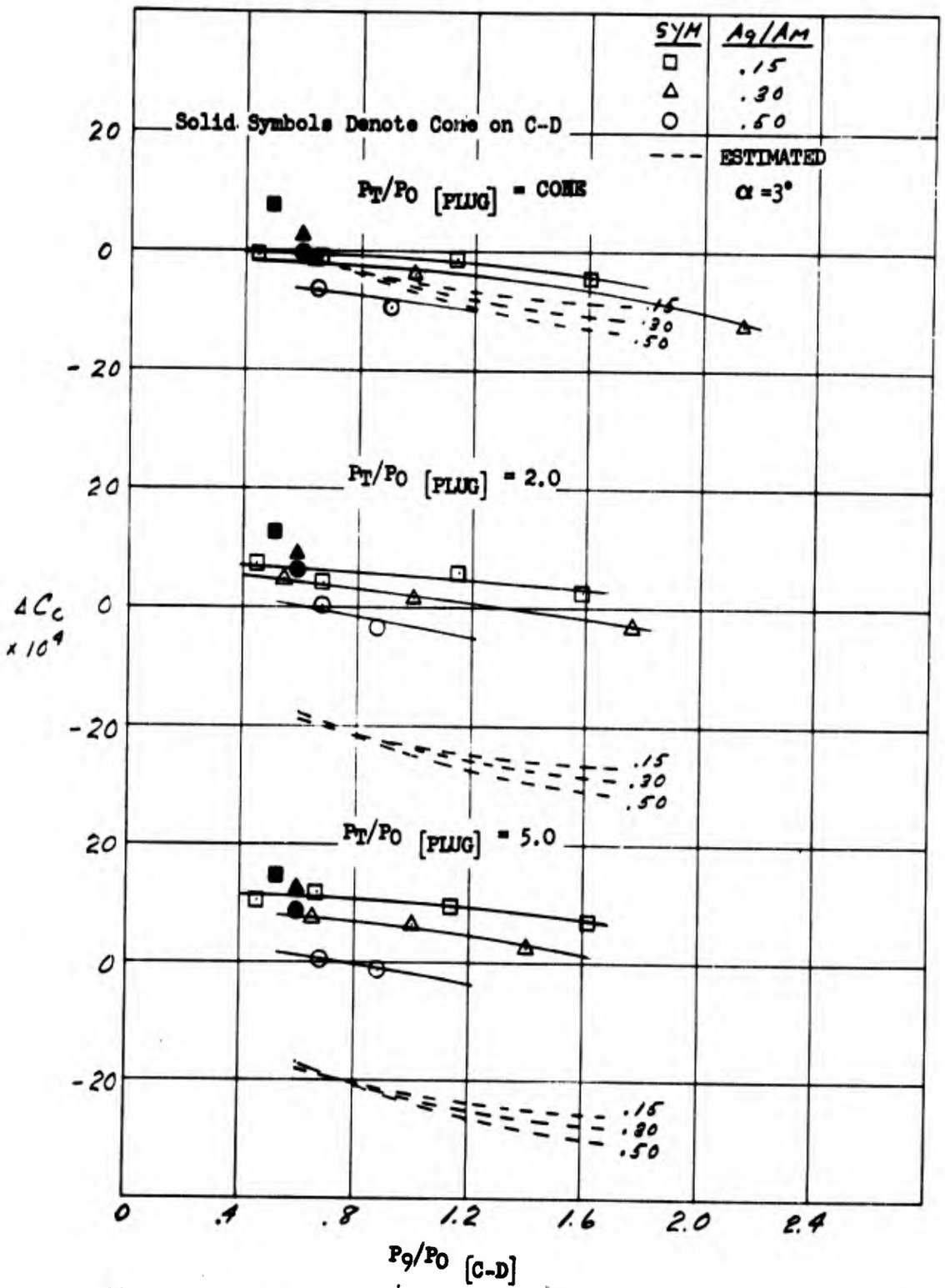

Figure 68. C-D Nozzle Static Pressure Ratio Effect on Chord Force Increment - M = .614.

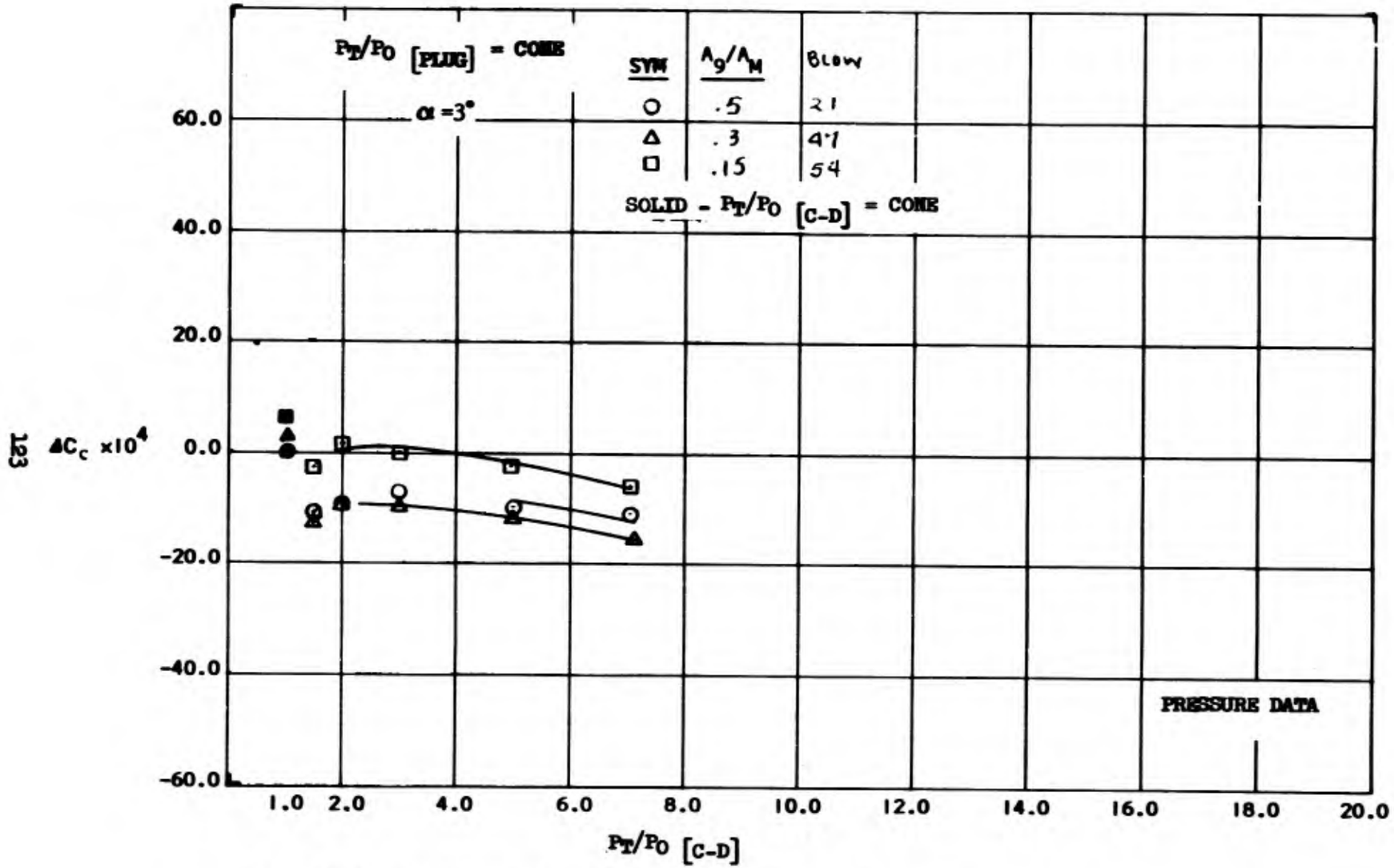

Figure 69 C-D Nozzle Jet Effects on Chord Force Increment - M=.85

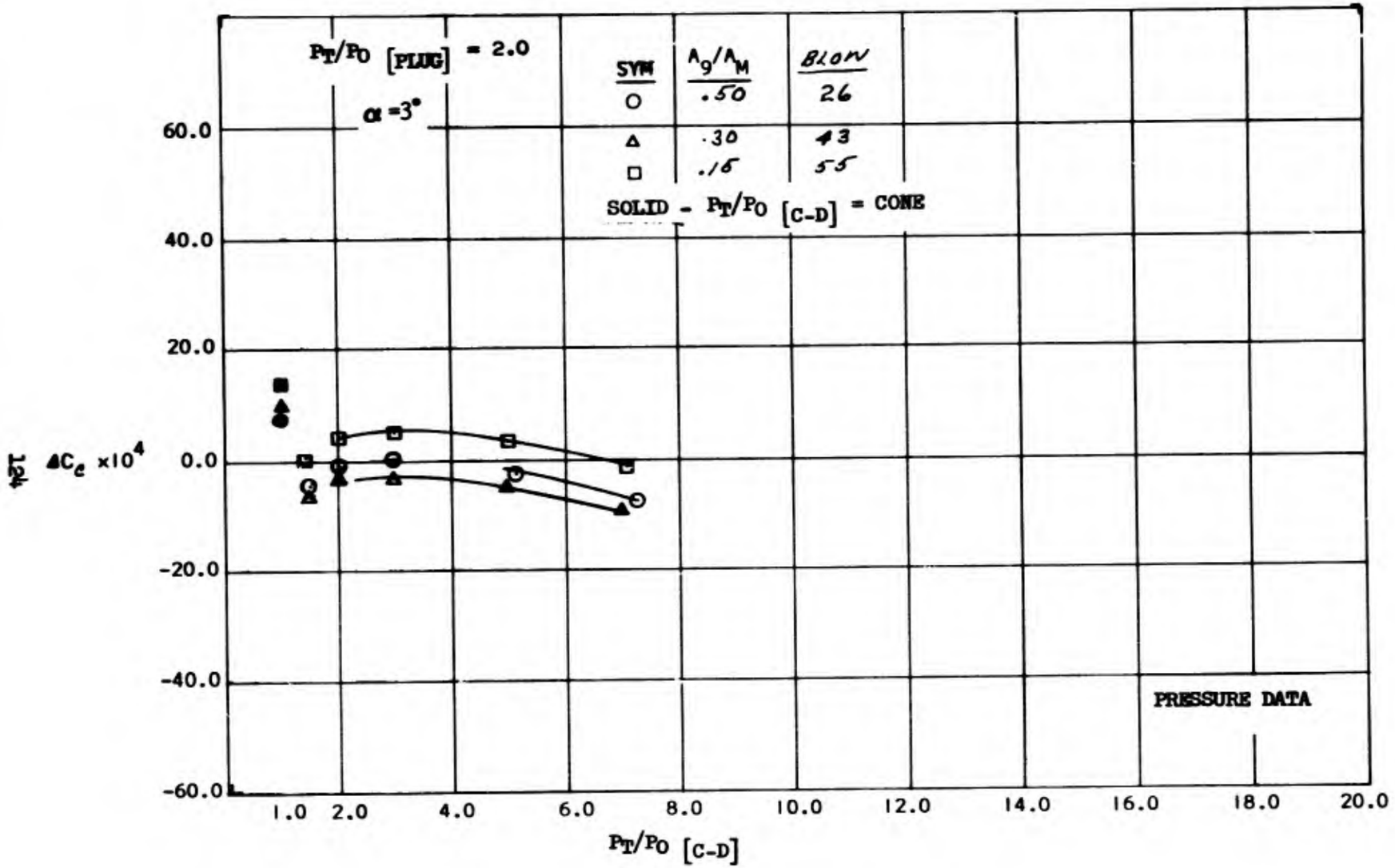

Figure 70. C-D Nozzle Jet Effects on Chord Force Increment - M=.85

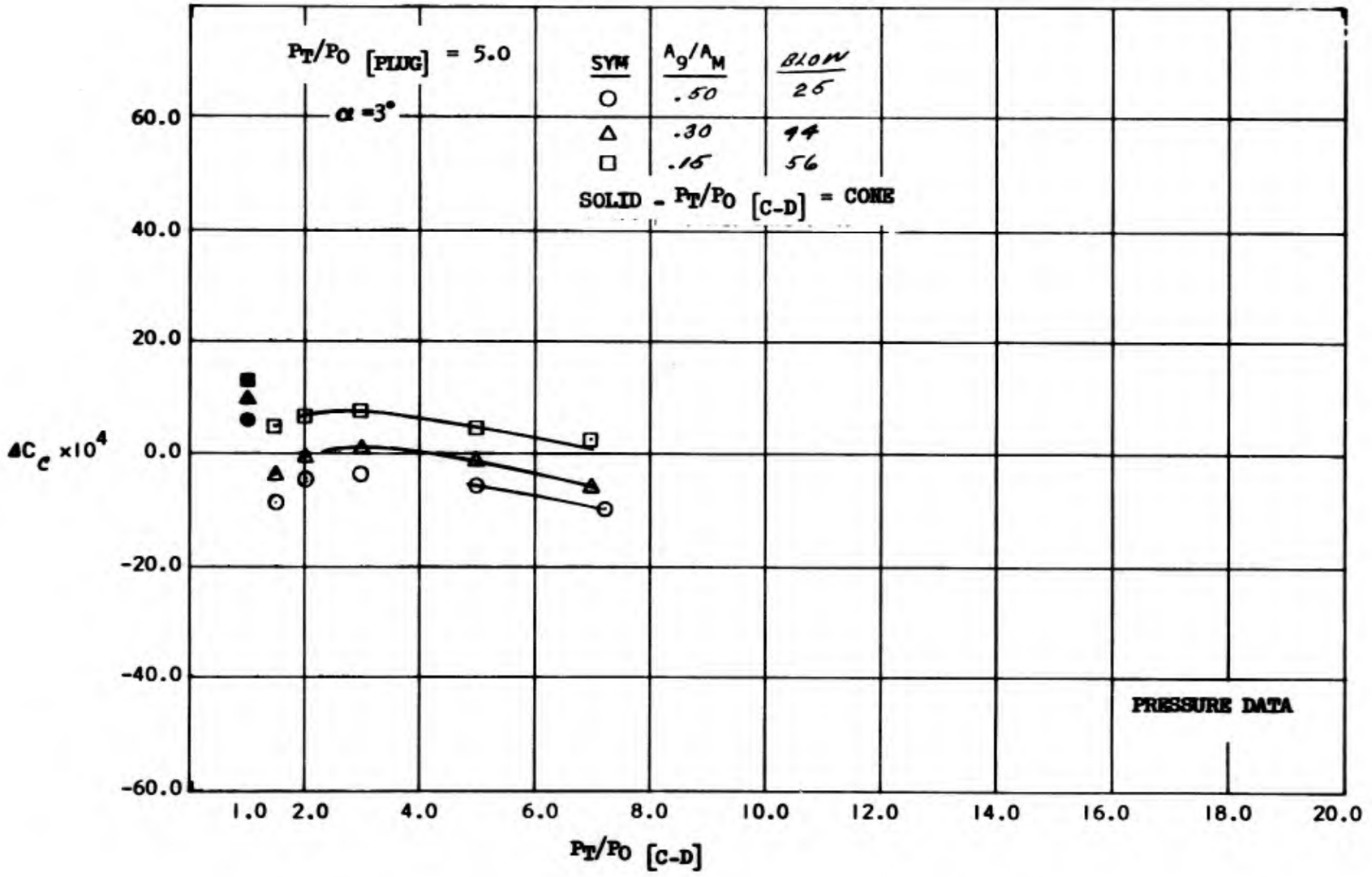

Figure 71. C-D Nozzle Jet Effects on Chord Force Increment - M=.85

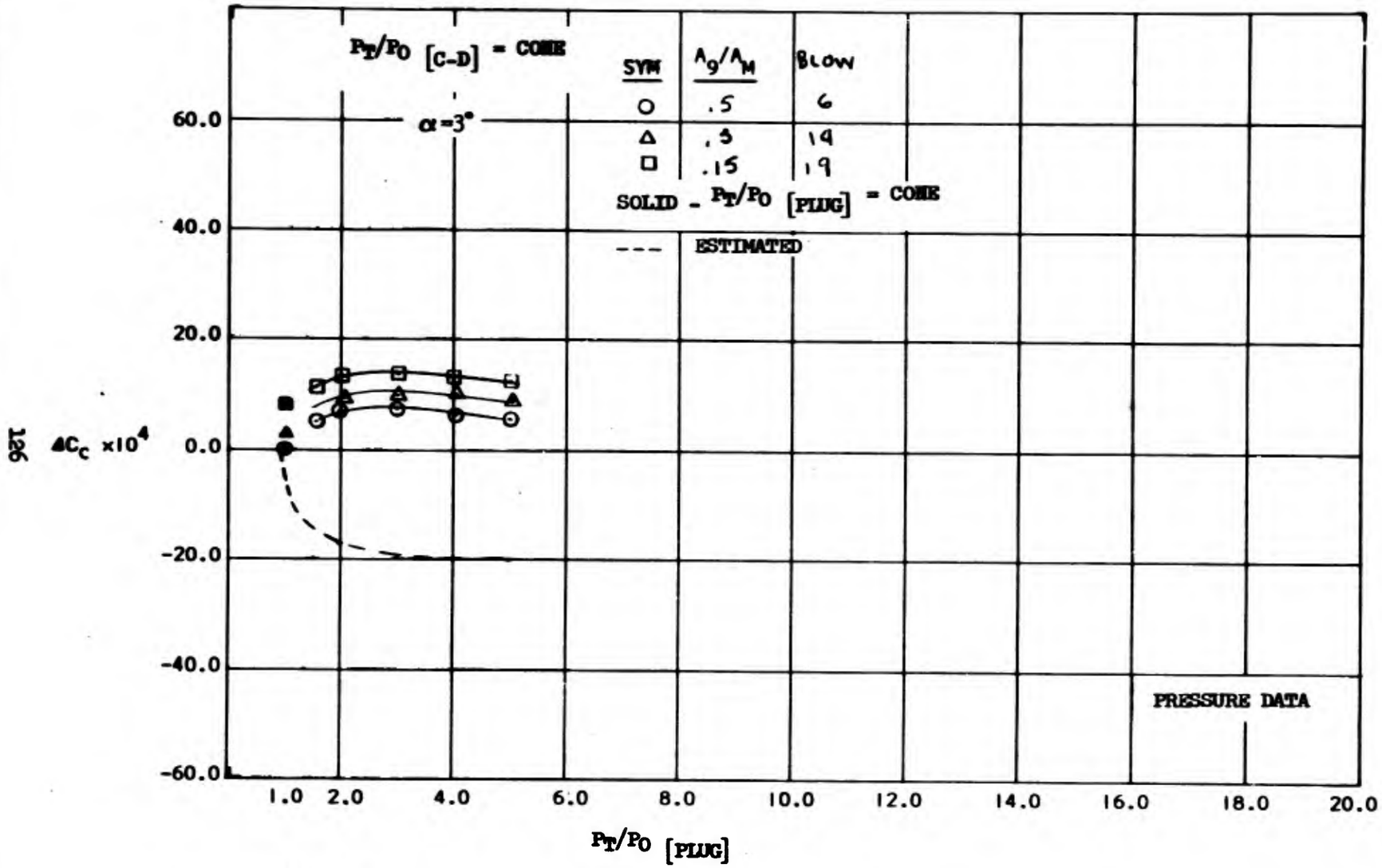

Figure 72. Plug Nozzle Jet Effects on Chord Force Increment - M=.85

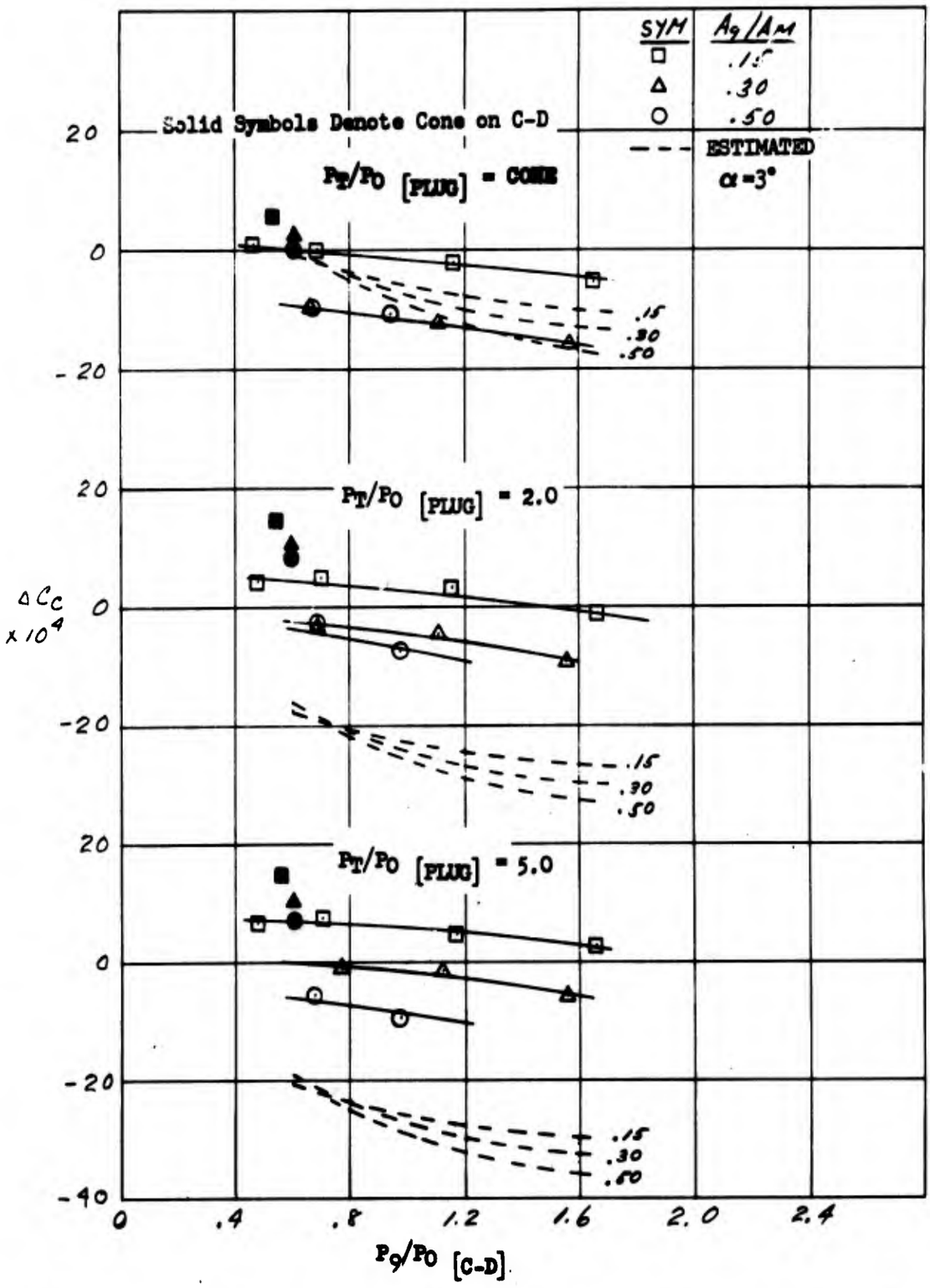

Figure 73. C-D Nozzle Static Pressure Ratio Effect on Chord Force Increment - M = .85

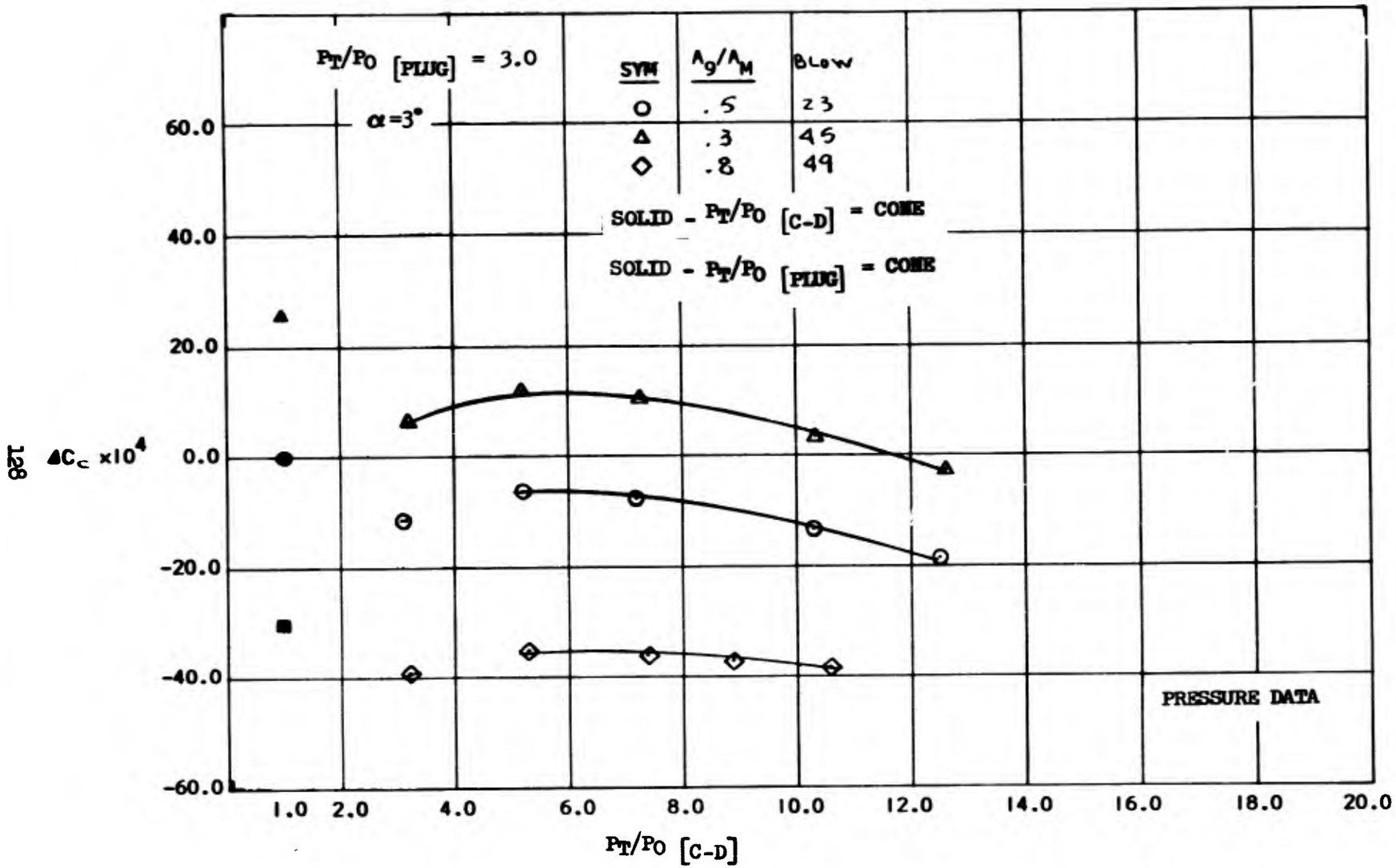

Figure 74. C-D Nozzle Jet Effects on Chord Force Increment - M=1.27

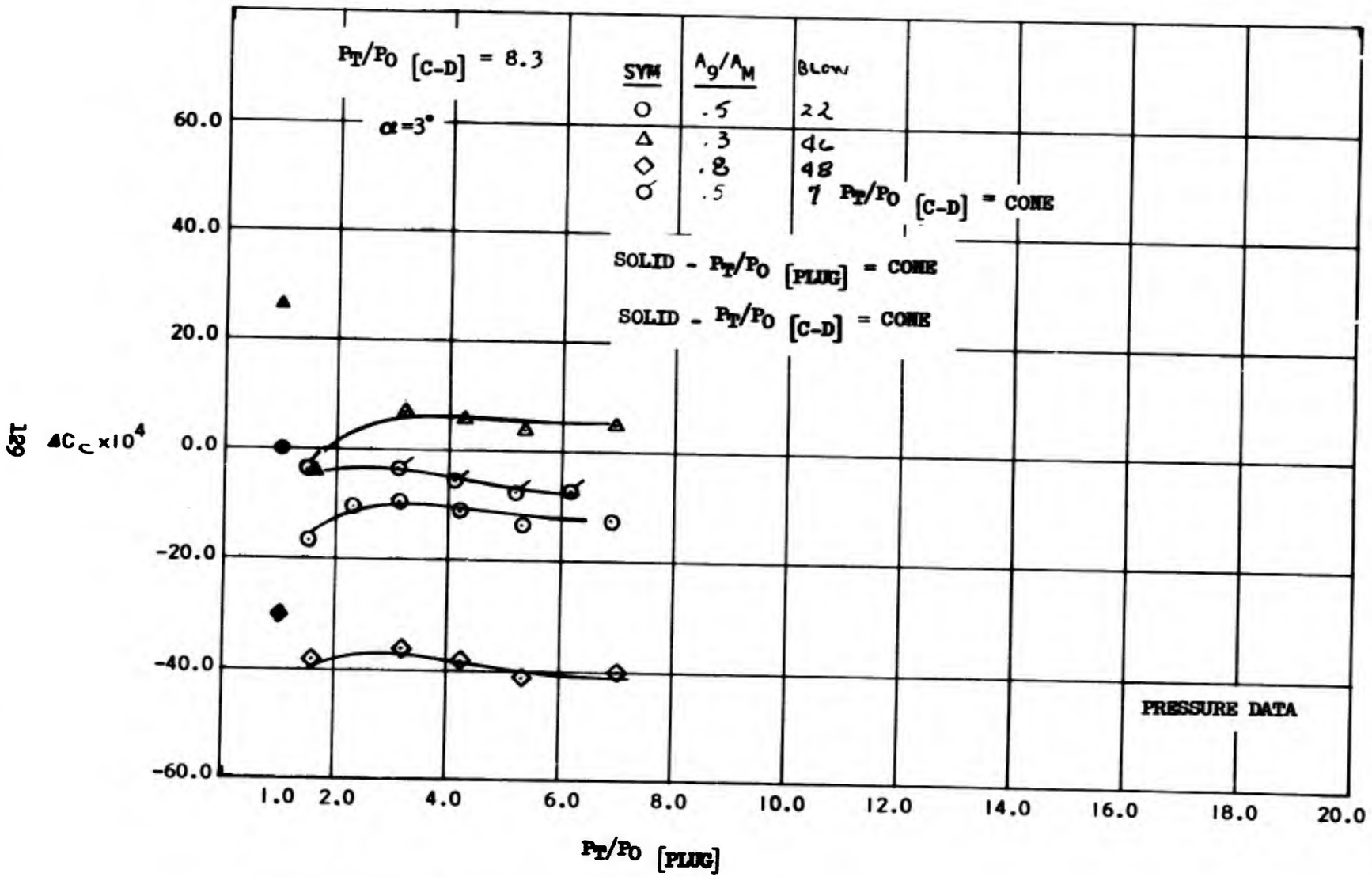

Figure 75. Plug Nozzle Jet Effects on Chord Force Increment - M=1.27

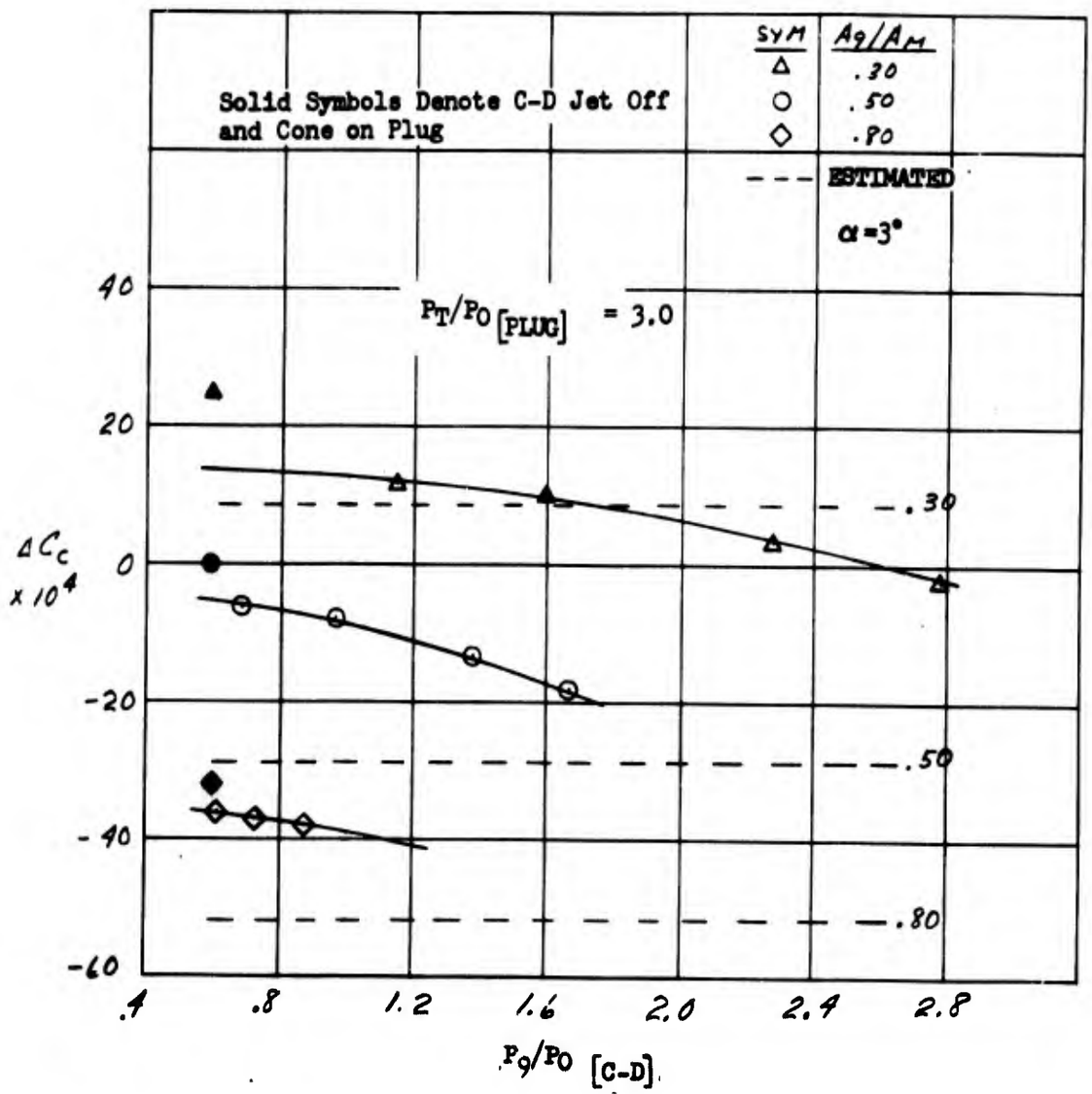

Figure 76. C-D Nozzle Static Pressure Ratio Effect on Chord Force Increment - M = 1.27.

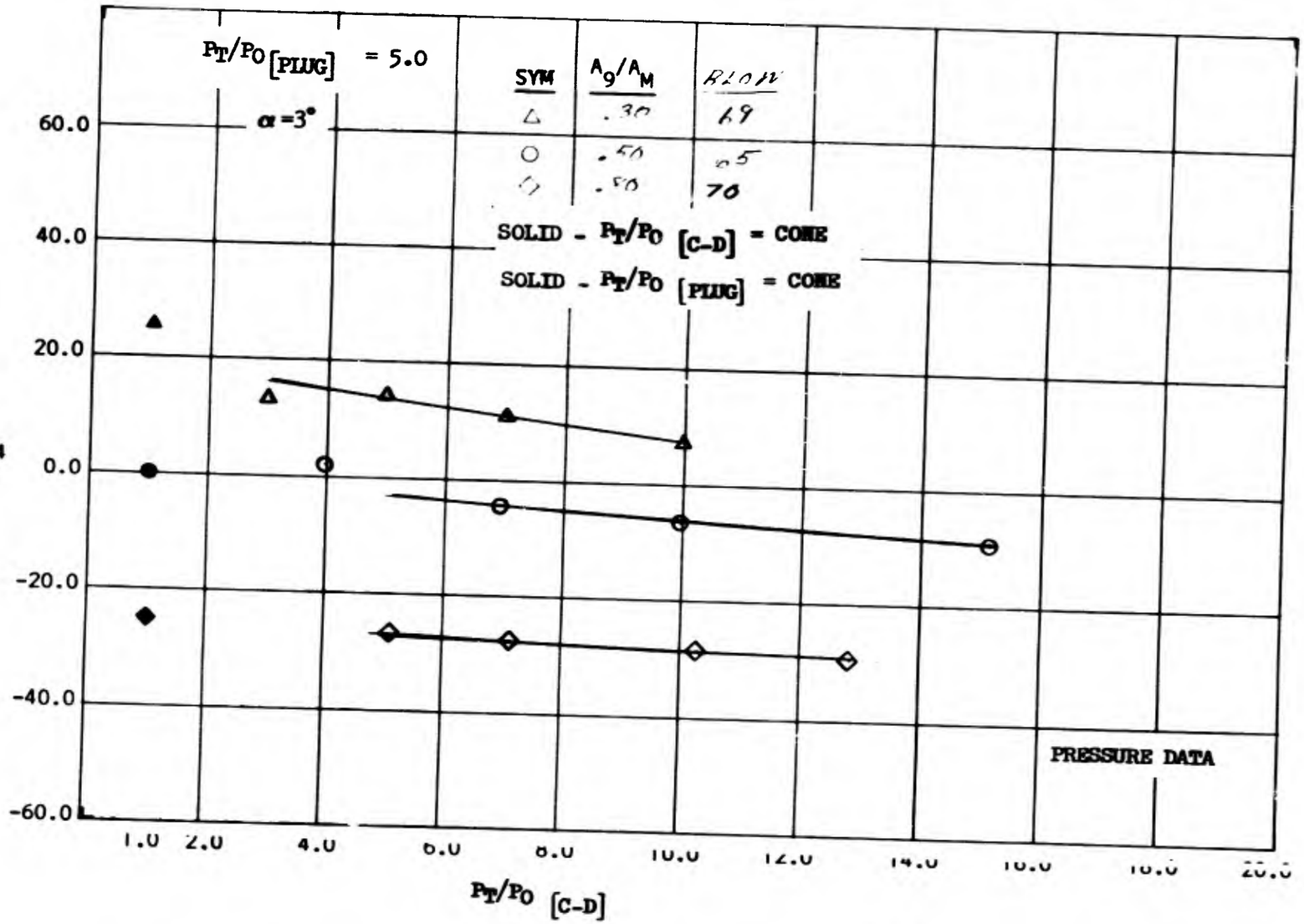

Figure 77. C-D Nozzle Jet Effects on Chord Force Increment - M=1.7

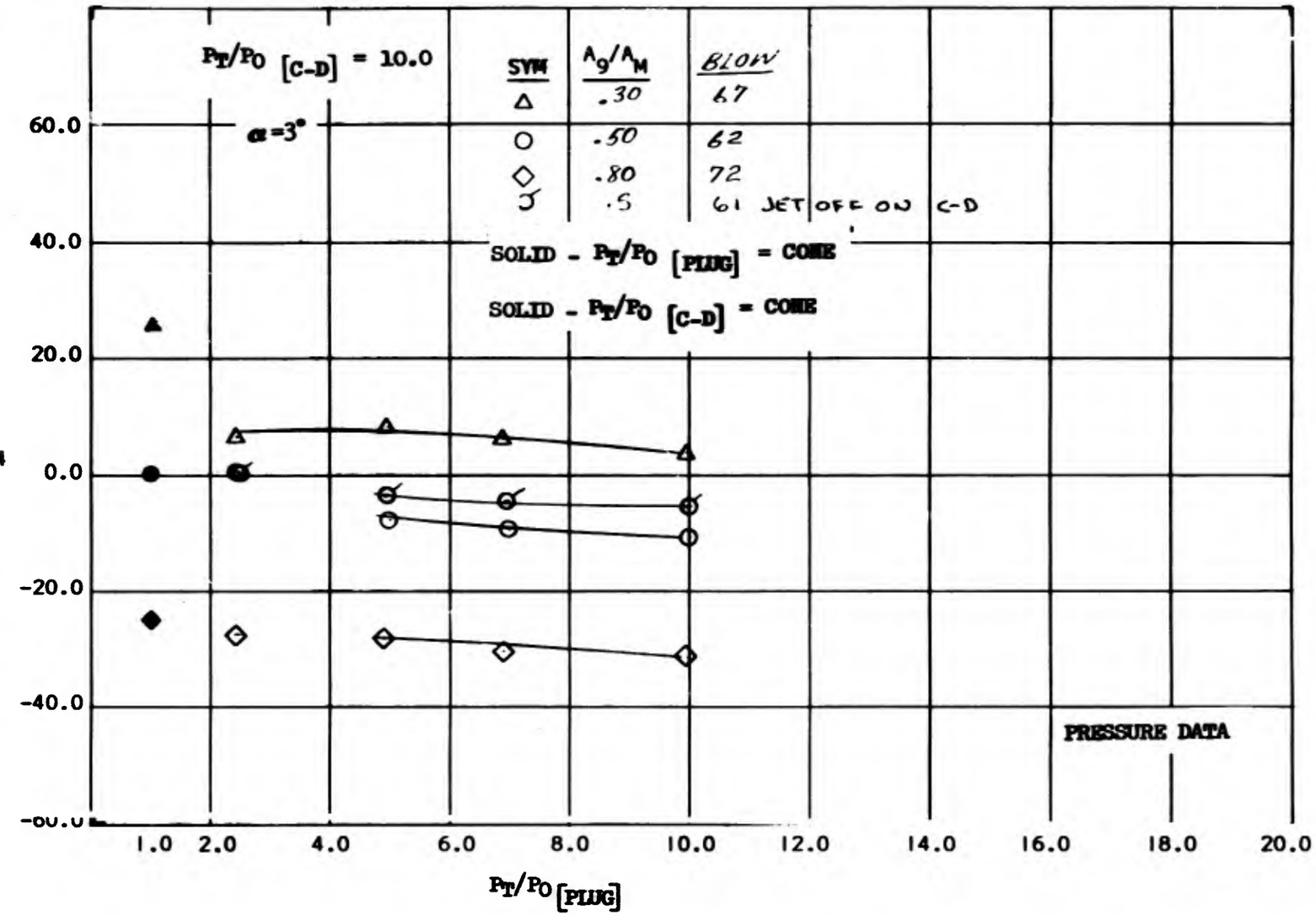

Figure 78. Plug Nozzle Jet Effects on Chord Force Increment - M=1.7

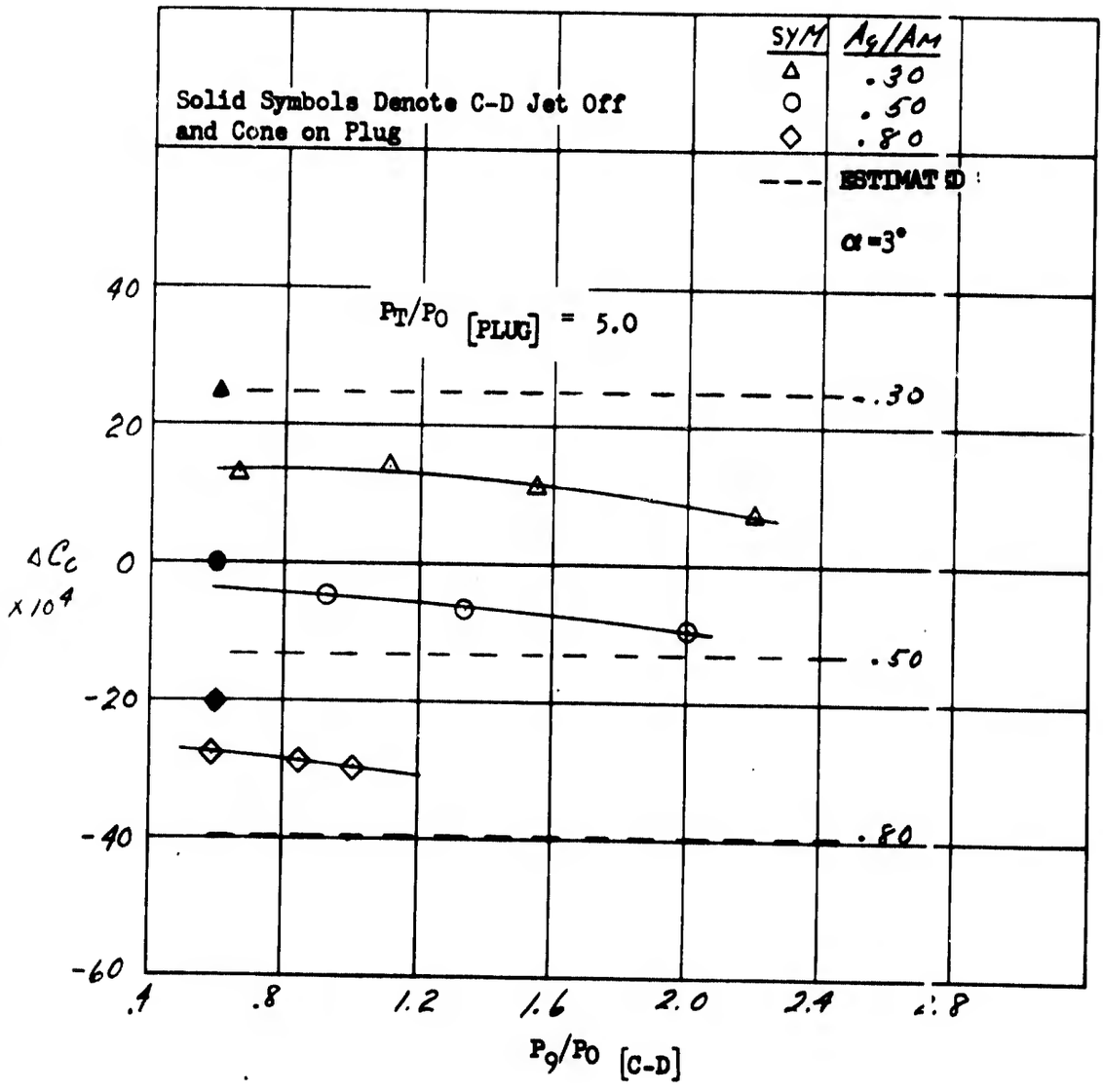

Figure 79. C-D Nozzle Static Pressure Ratio Effect on Chord Force Increment - M = 1.7.

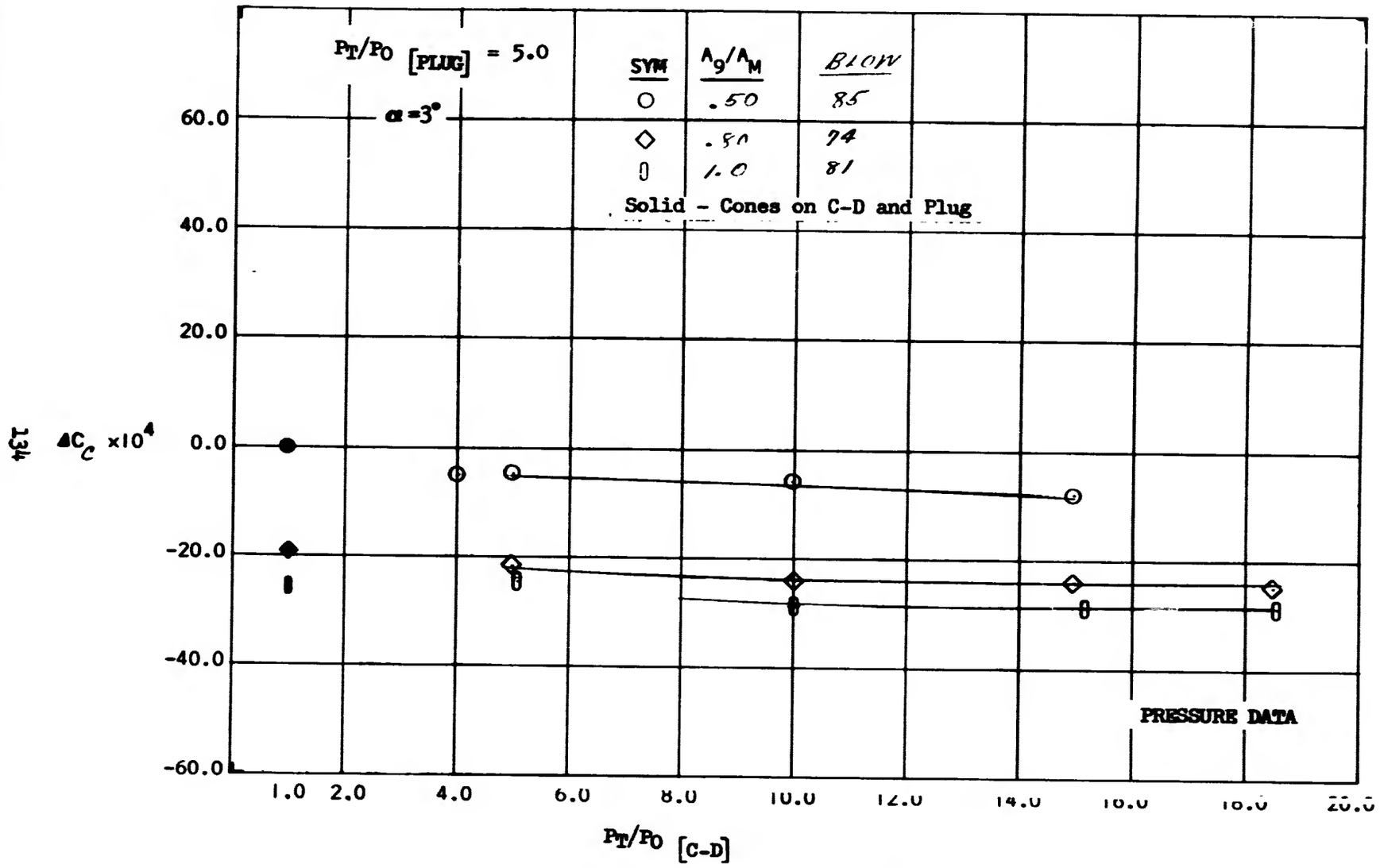

Figure 80. C-D Nozzle Jet Effects on Chord Force Increment - M=2.0

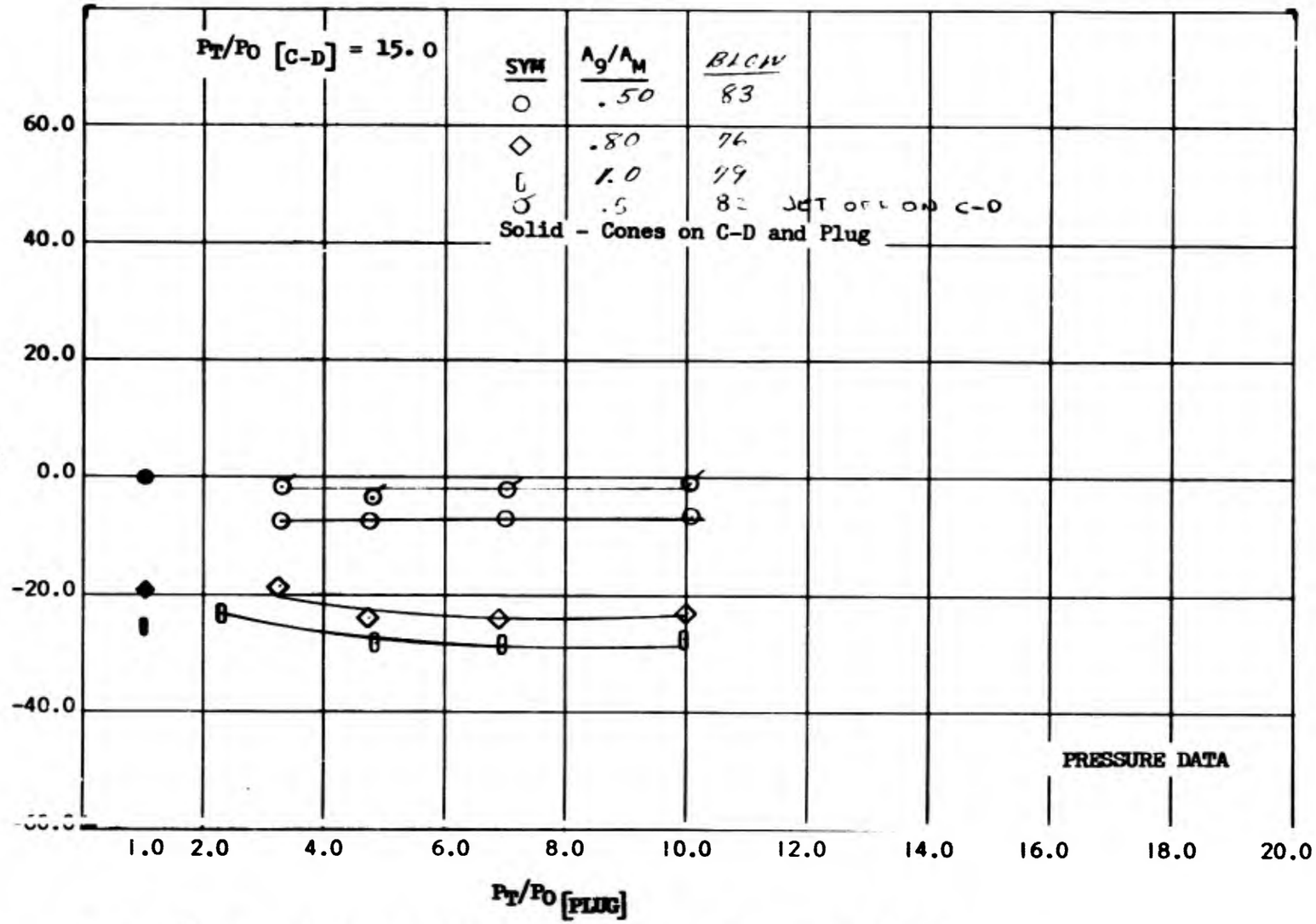

Figure 81. Plug Nozzle Jet Effects on Chord Force Increment - M=2.0

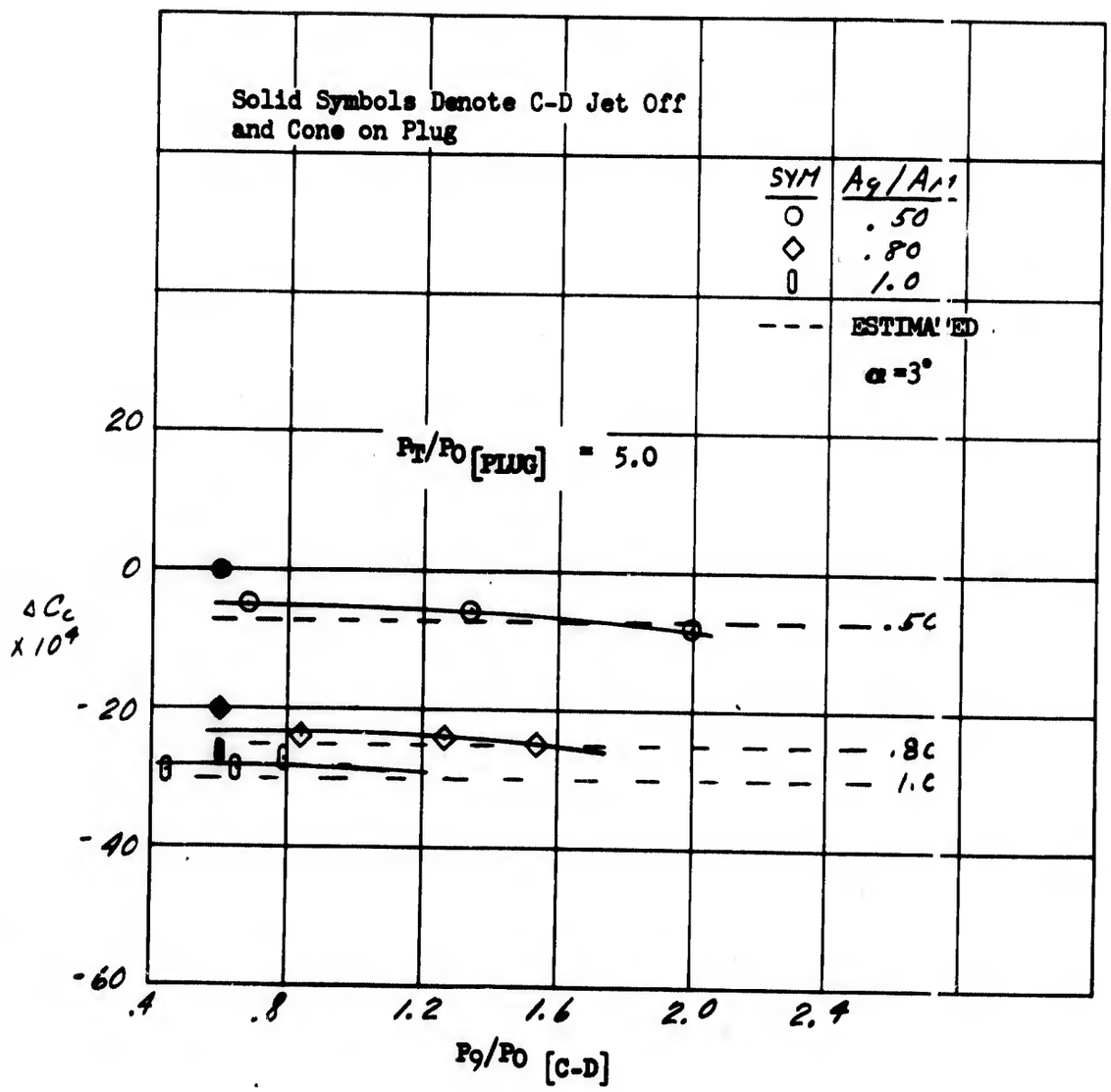

Figure 82. C-D Nozzle Static Pressure Ratio Effect on Chord Force Increment - M = 2.0.

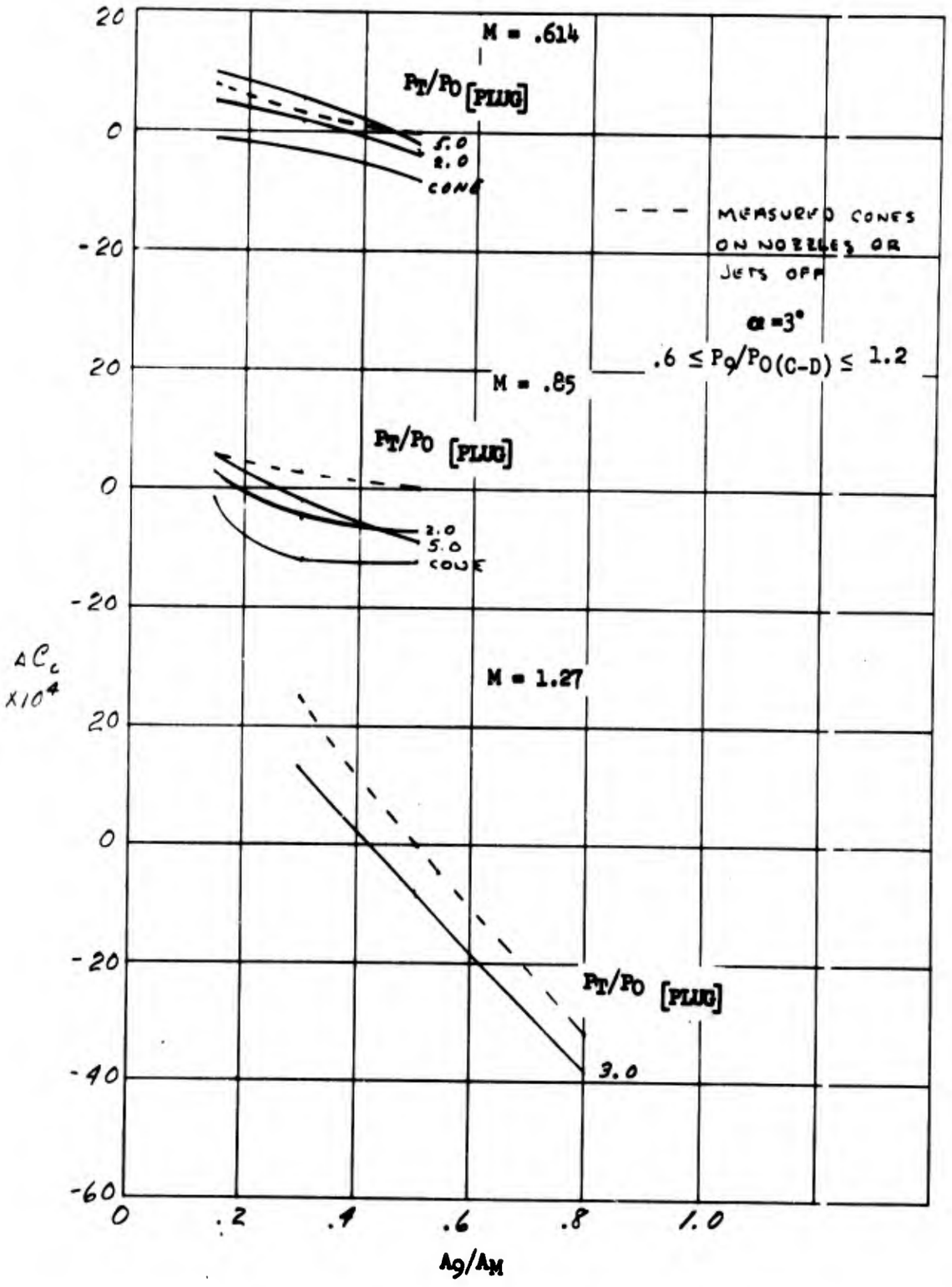

Figure 83. Summary of Configuration and Jet Effects on Chord Force Increment - M = .6, .85, and 1.27.

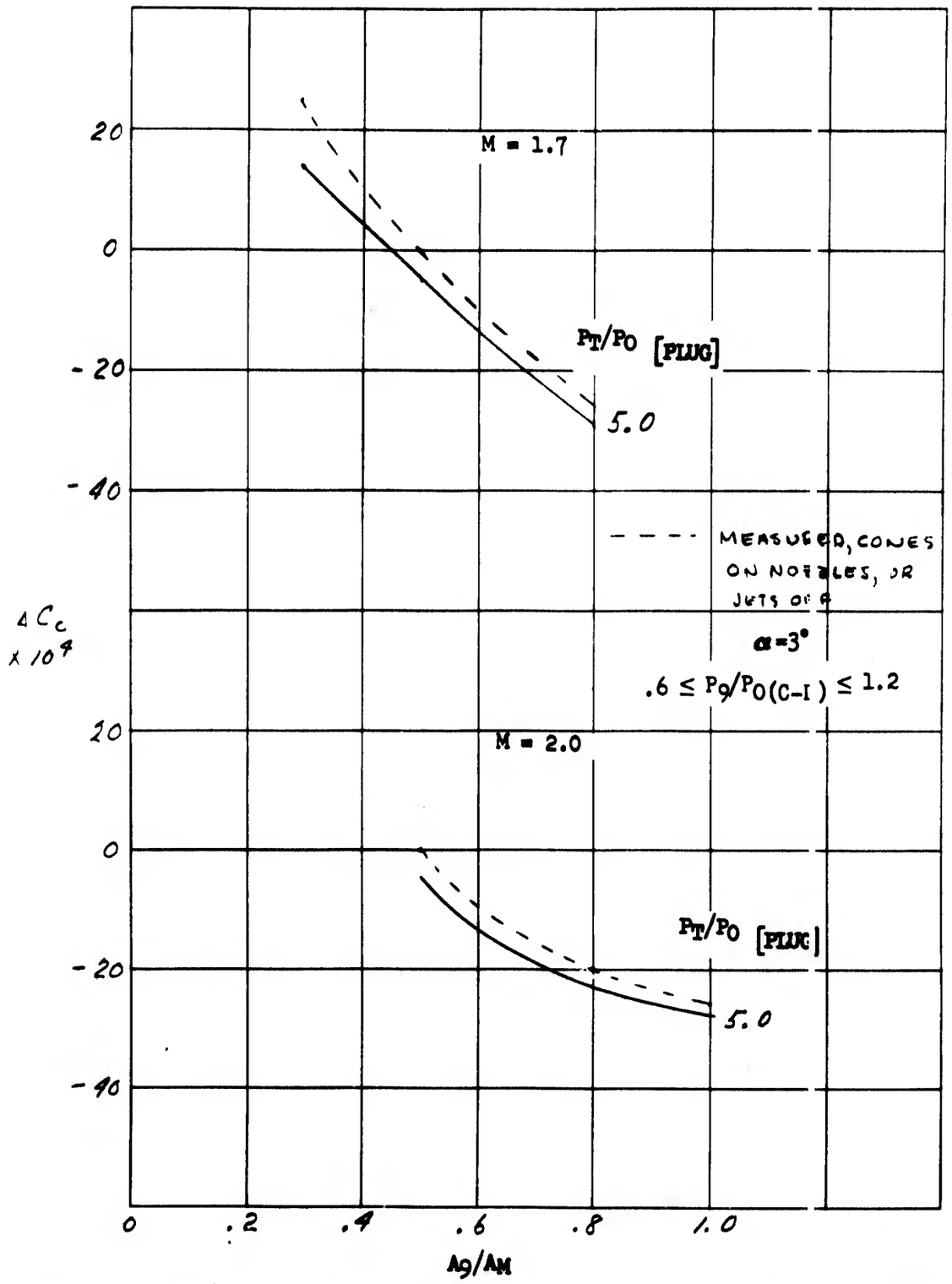

Figure 84. Summary of Configuration and Jet Effects on Chord Force Increment - M ≐ 1.7 and 2.0.

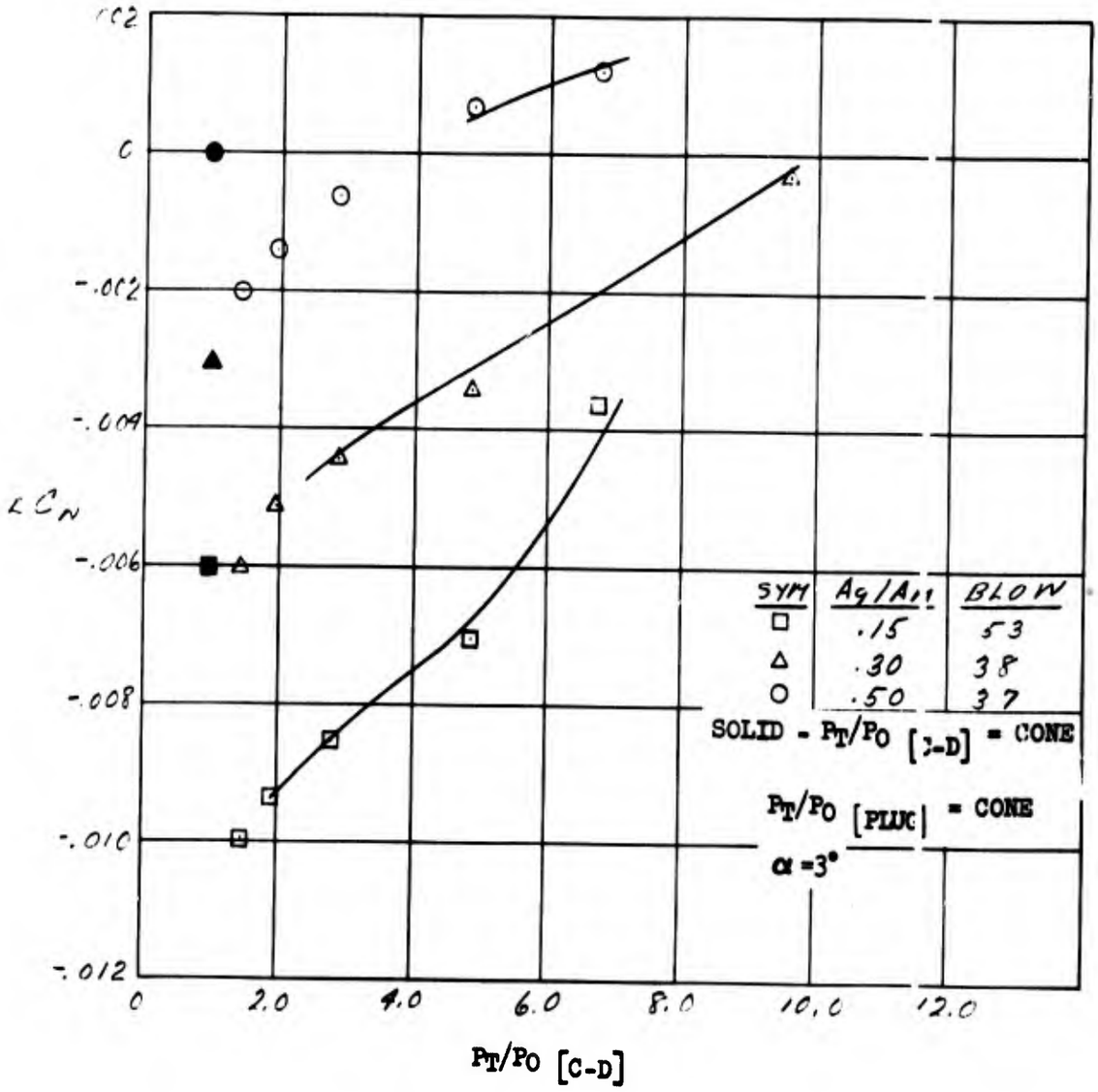

Figure 85. C-D Nozzle Jet Effects On Normal Force Increment - M = .614

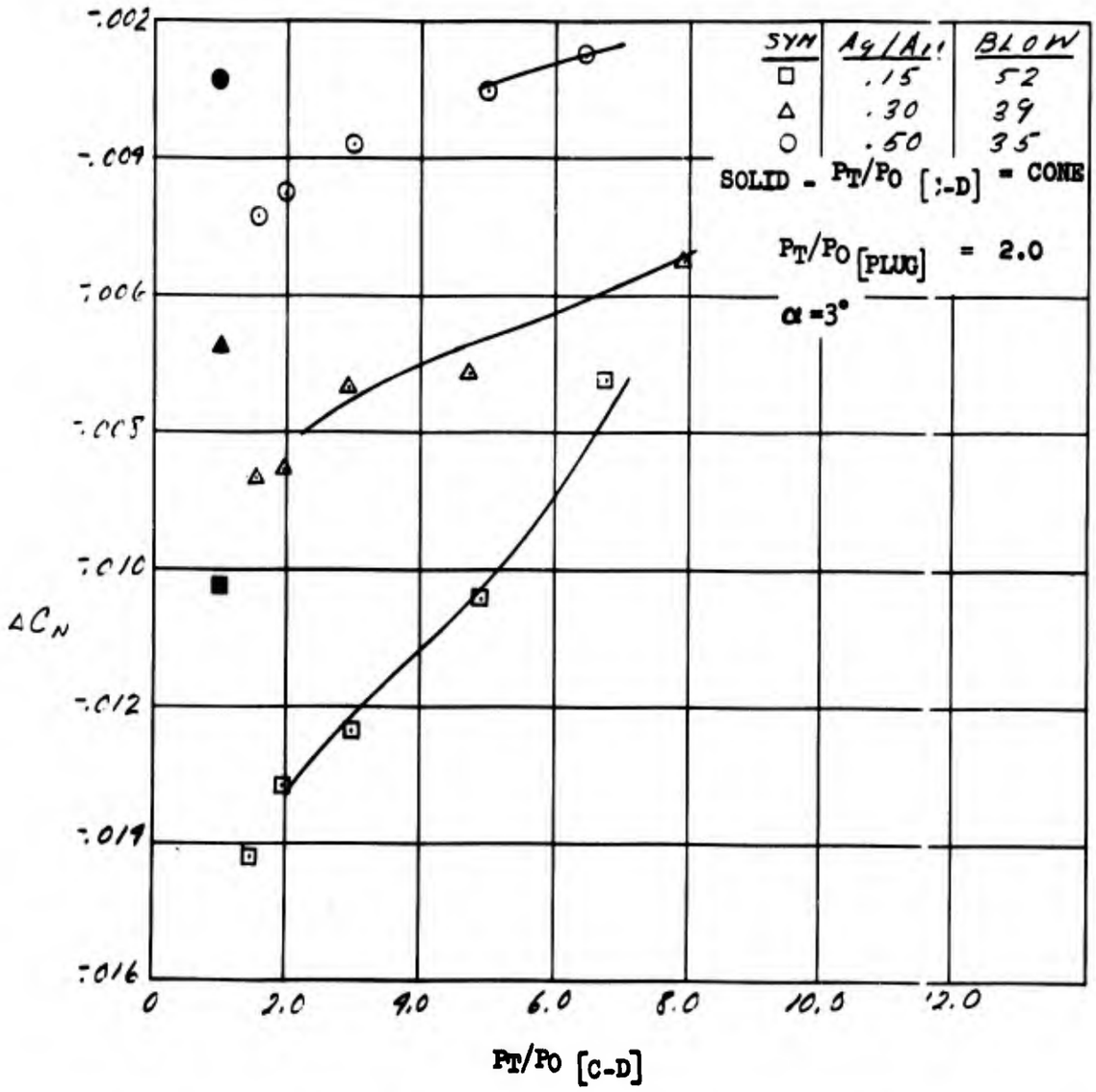

Figure 86. C-D Nozzle Jet Effects On Normal Force Increment - M = .614

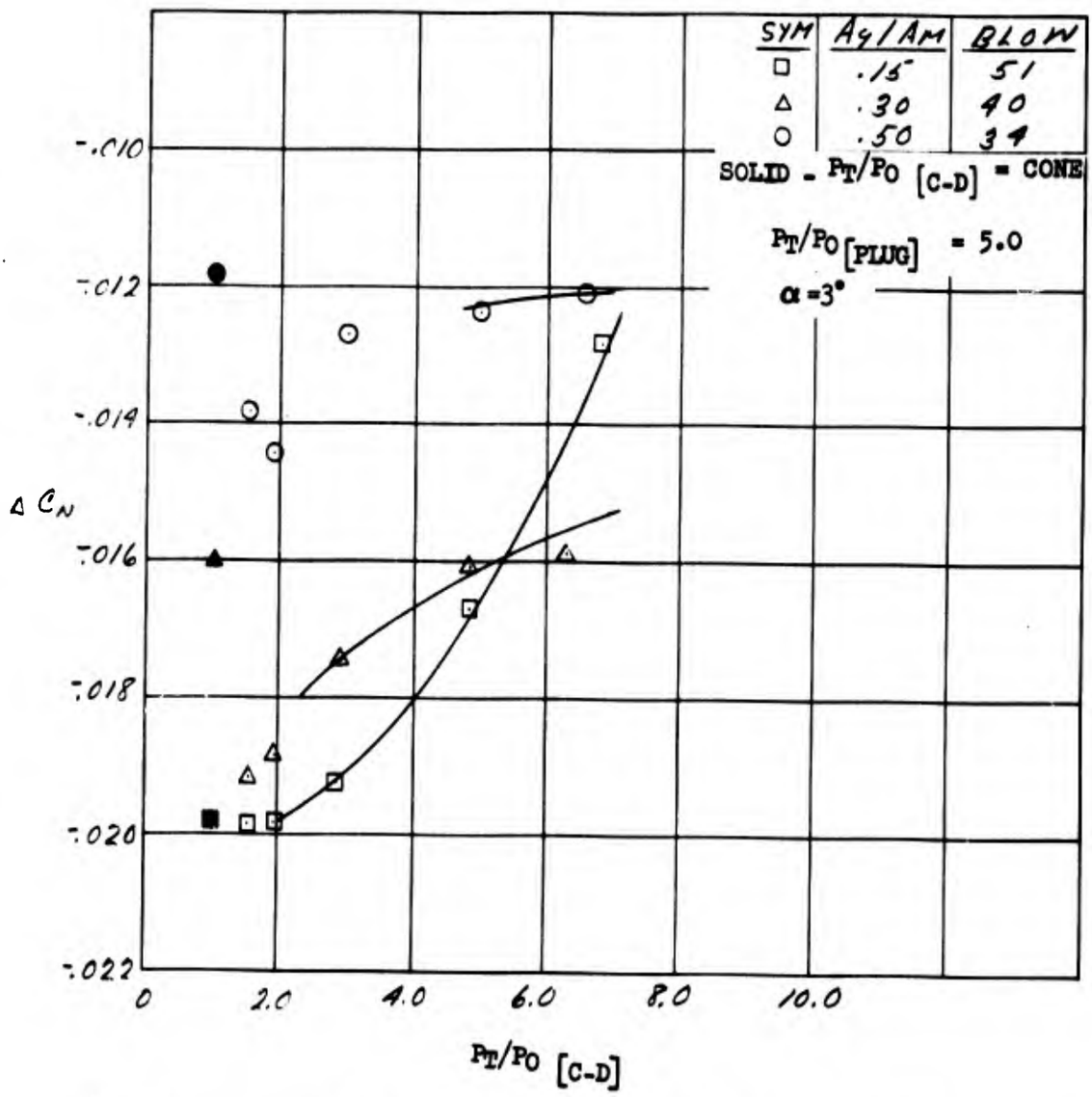

Figure 87. C-D Nozzle Jet Effects On Normal Force Increment - M = .614

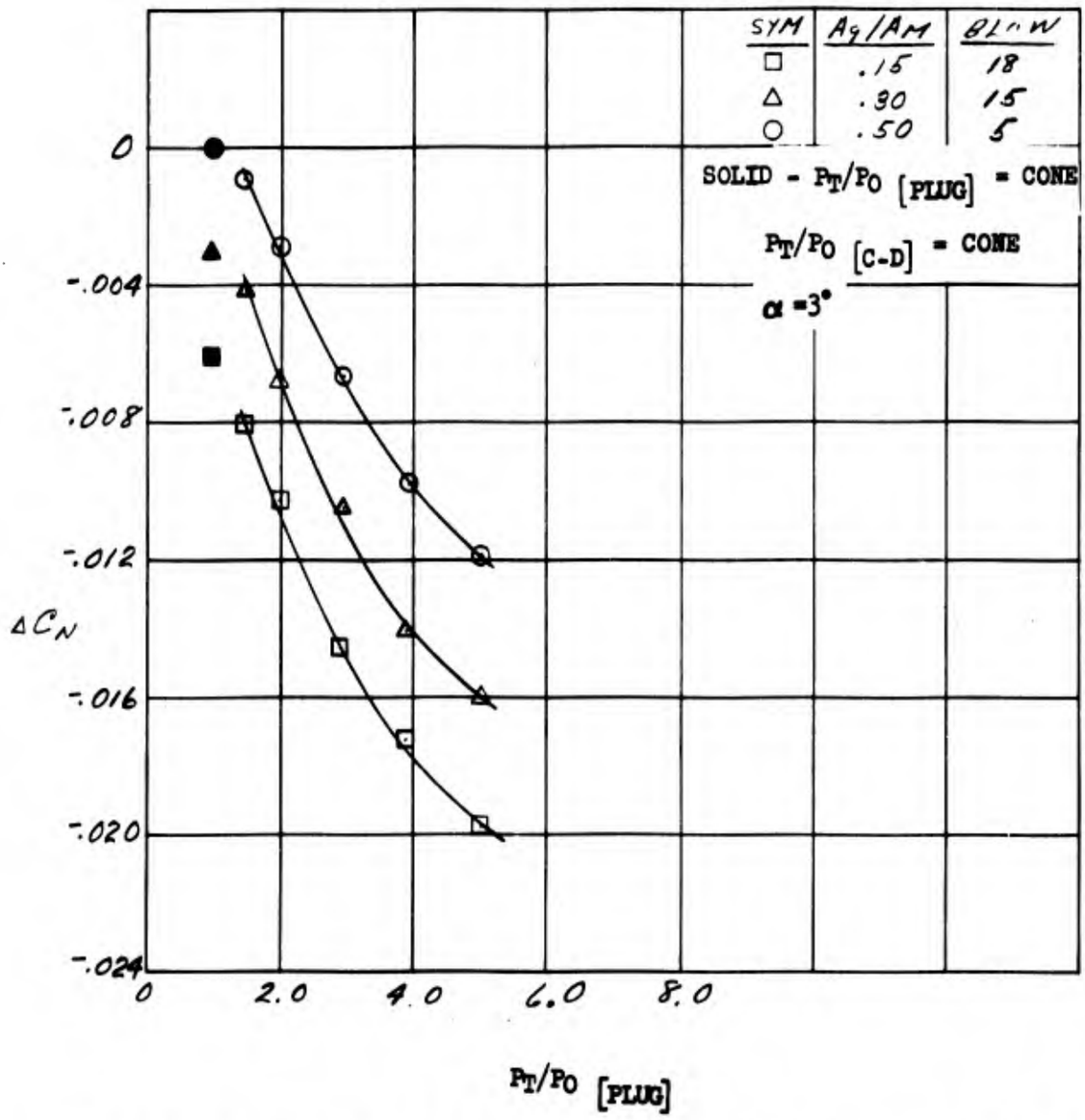

Figure 88. Plug Nozzle Jet Effects On Normal Force Increment - M = .614

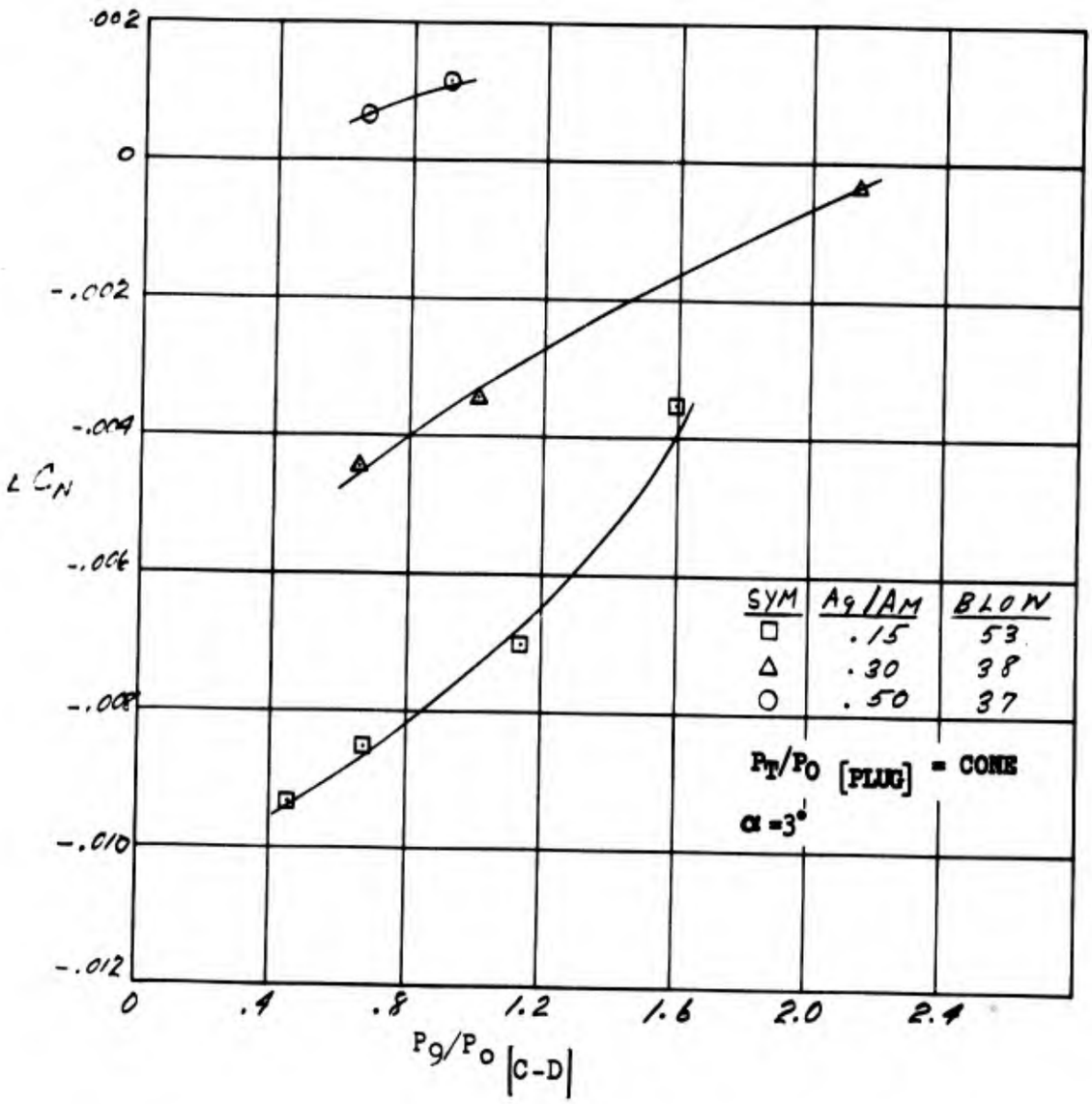

Figure 89. C-D Nozzle Static Pressure Ratio Effect On Normal Force Increment - M =.614

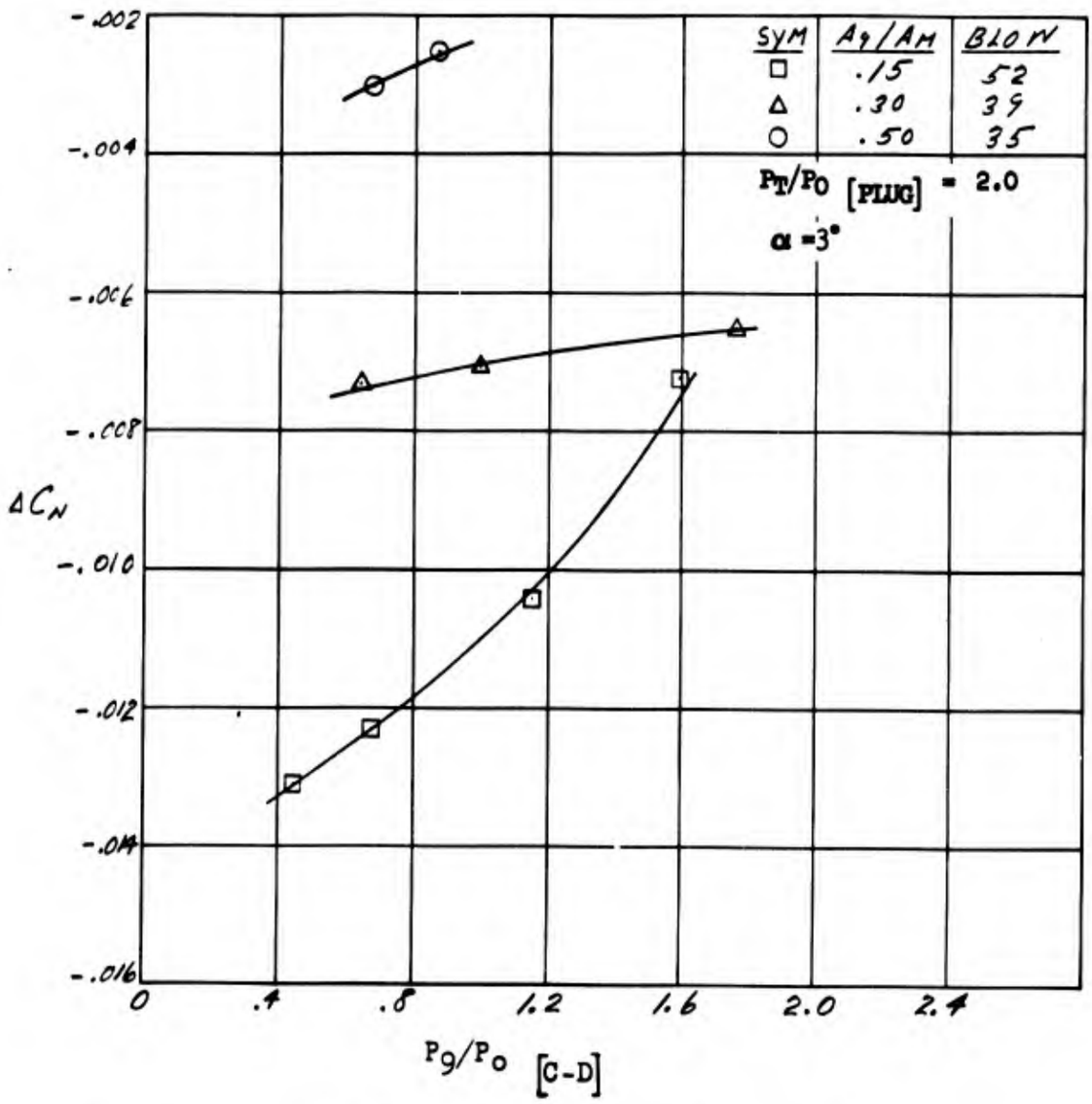

Figure 90. C-D Nozzle Static Pressure Ratio Effect On Normal Force Increment - M=.6

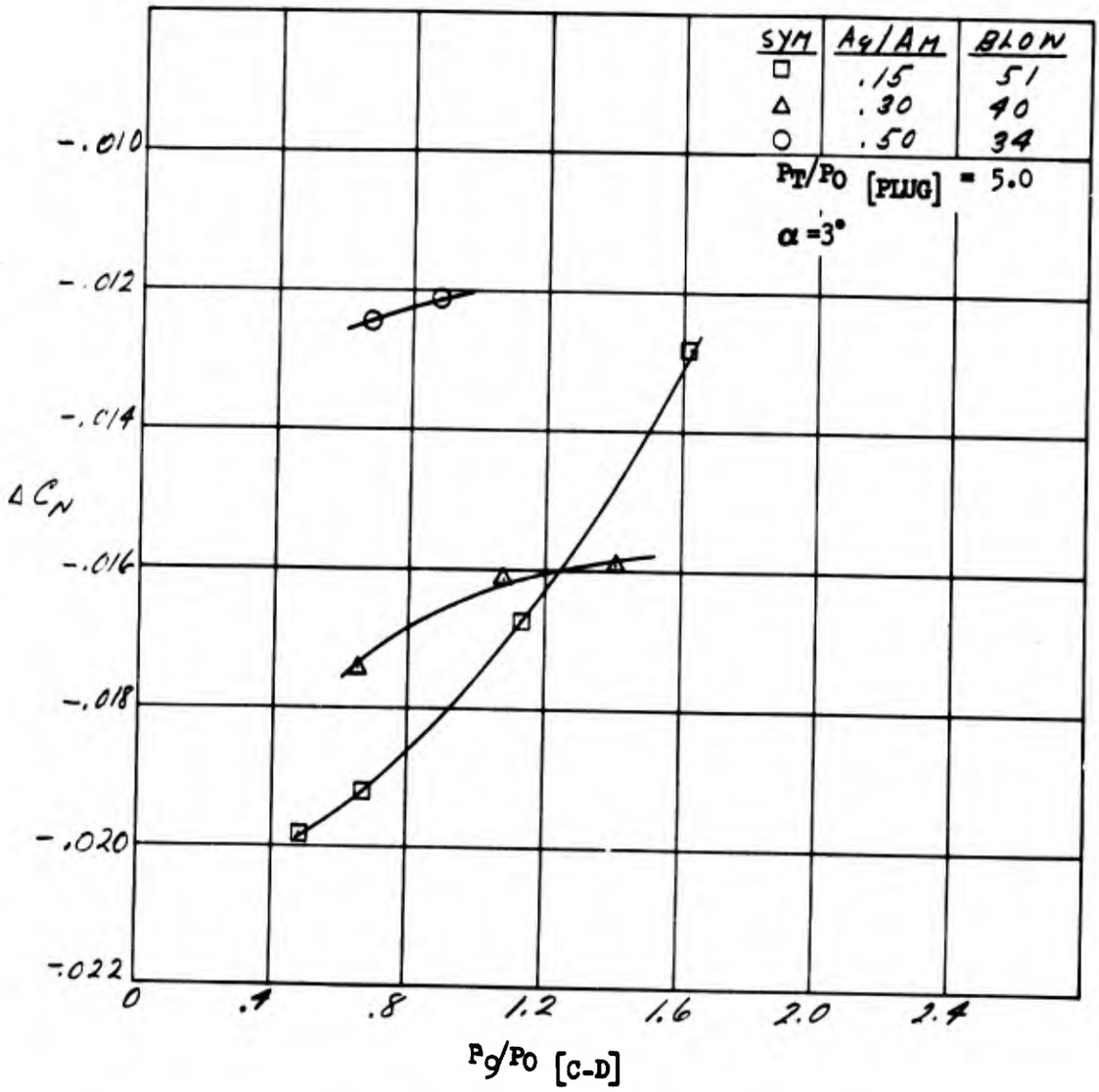

Figure 91. C-D Nozzle Static Pressure Ratio Effect On Normal Force Increment -M=.61

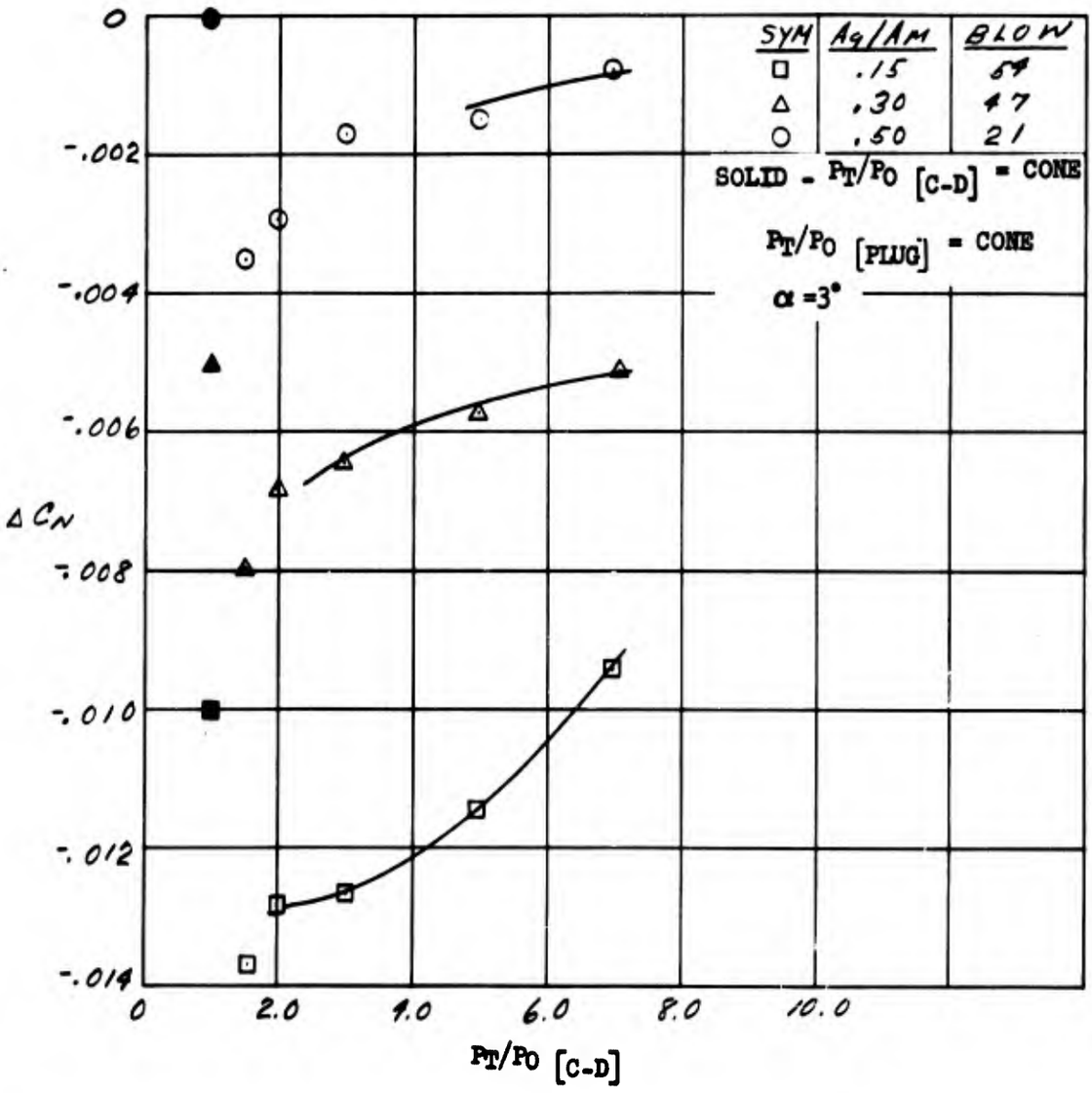

Figure 92. C-D Nozzle Jet Effects On Normal Force Increment - M = .85

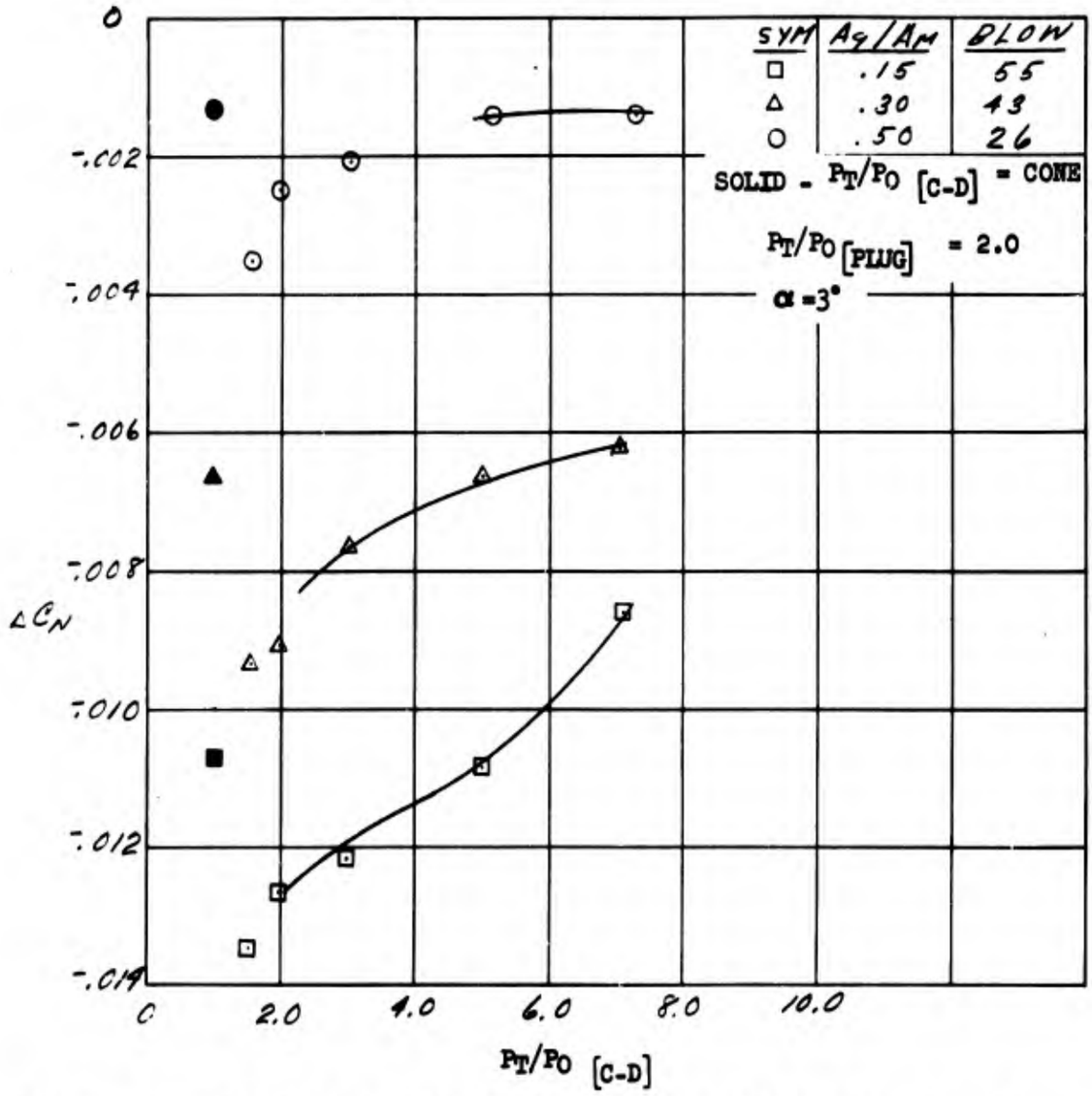

Figure 93. C-D Nozzle Jet Effects On Normal Force Increment - M = .85

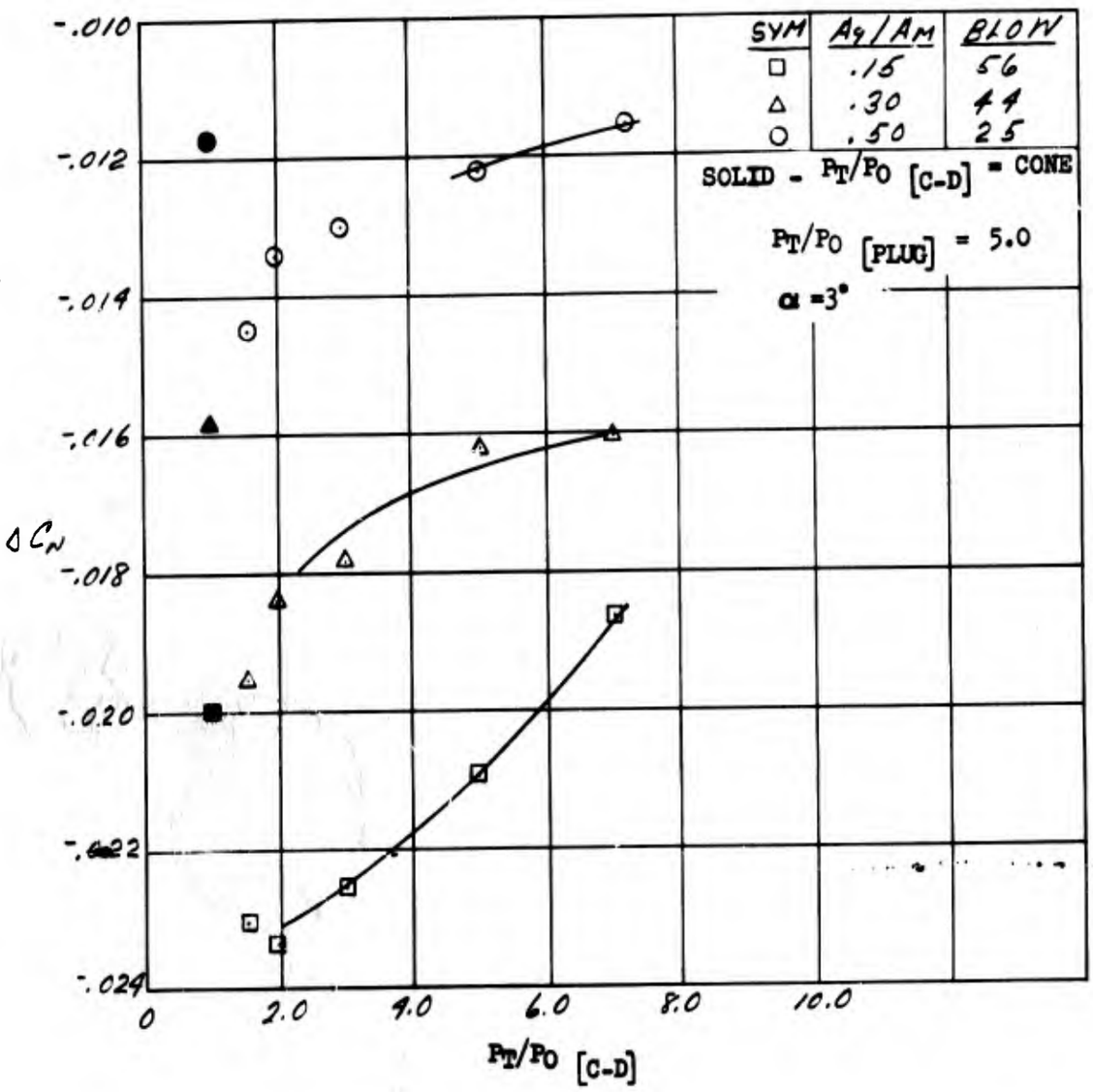

Figure 94. C-D Nozzle Jet Effects On Normal Force Increment - M = .85

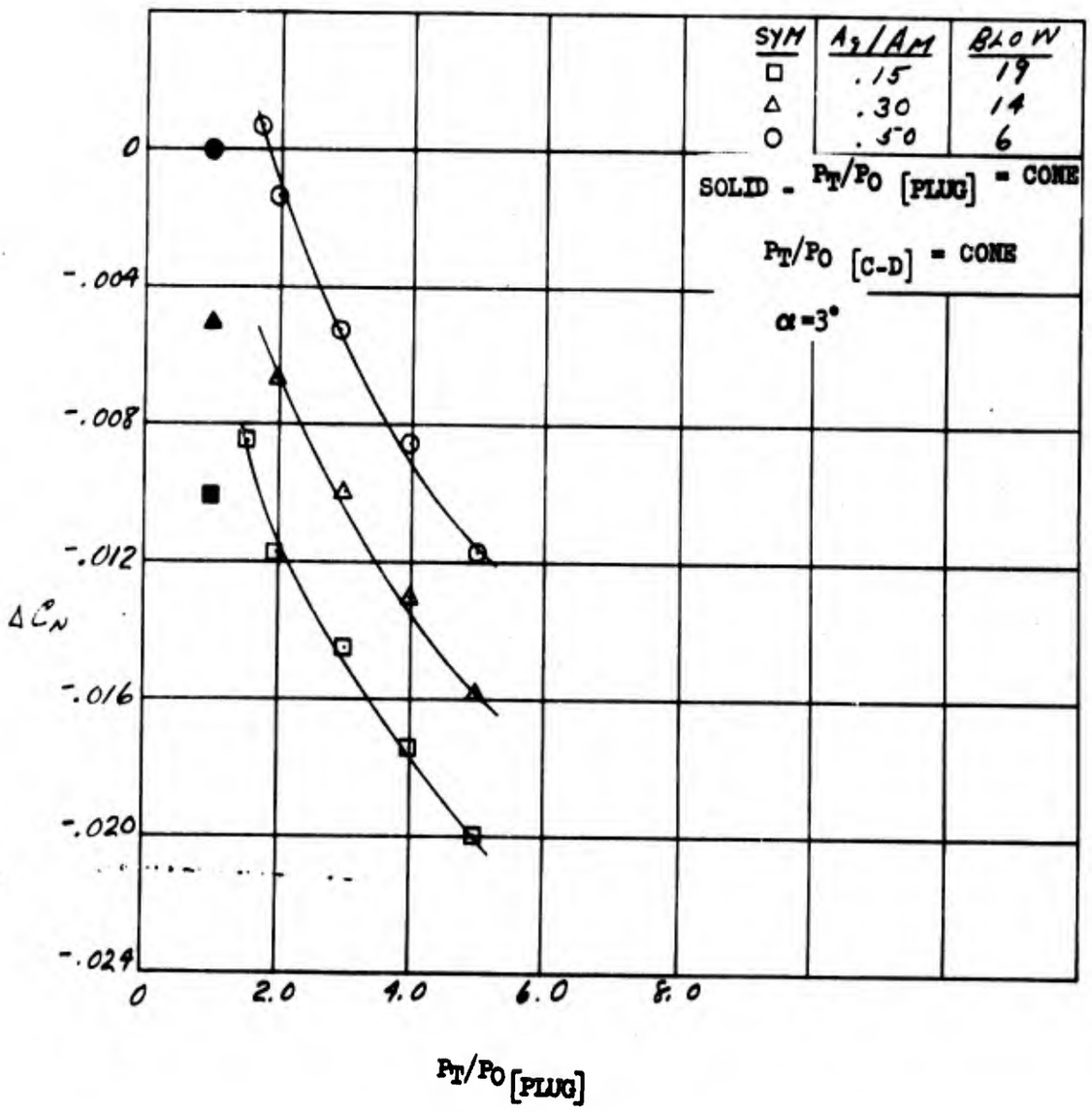

Figure 95. Plug Nozzle Jet Effects on Normal Force Increment - M = .85.

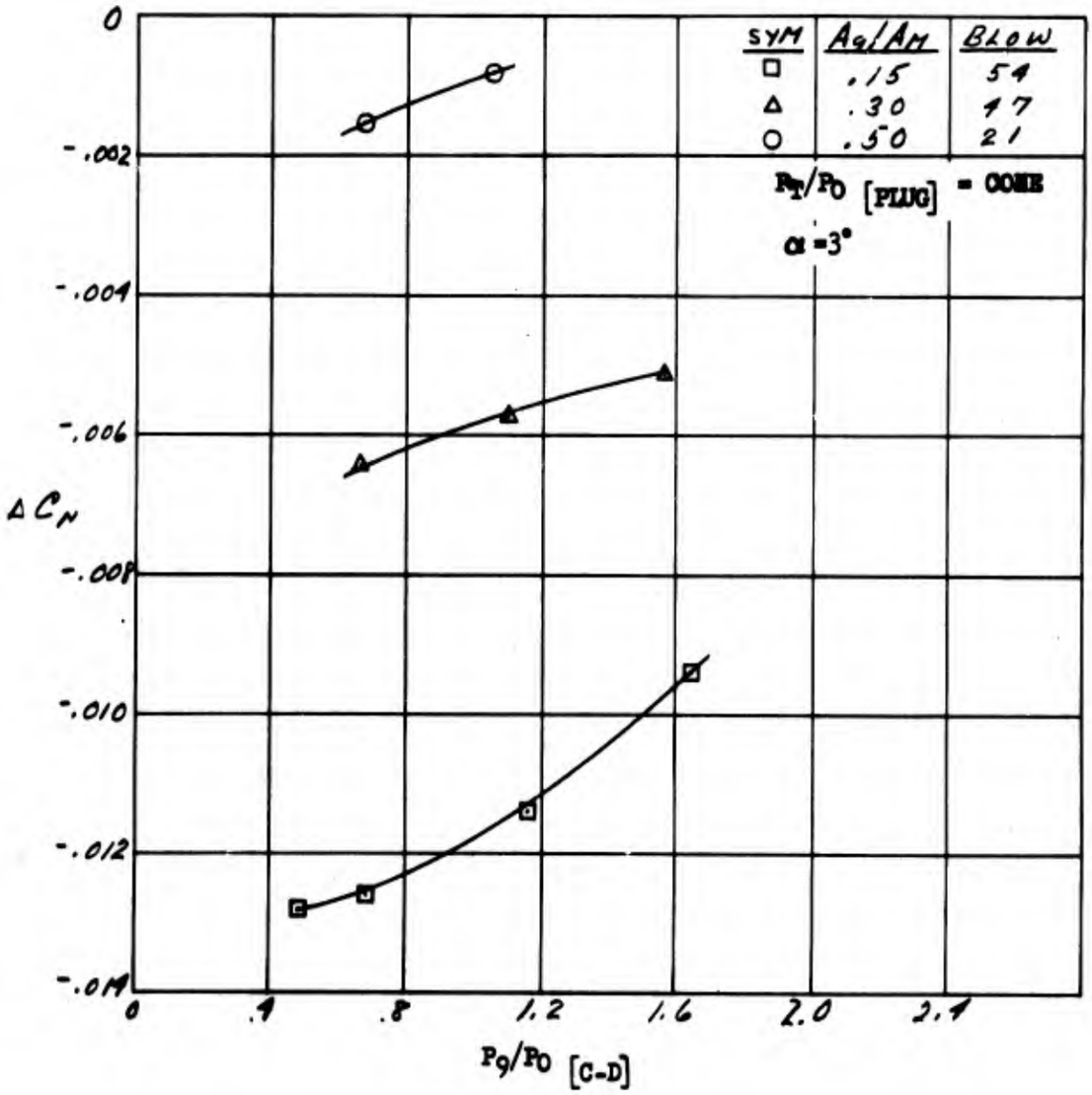

Figure 96. C-D Nozzle Static Pressure Ratio Effects on Normal Force Increment - M = .85.

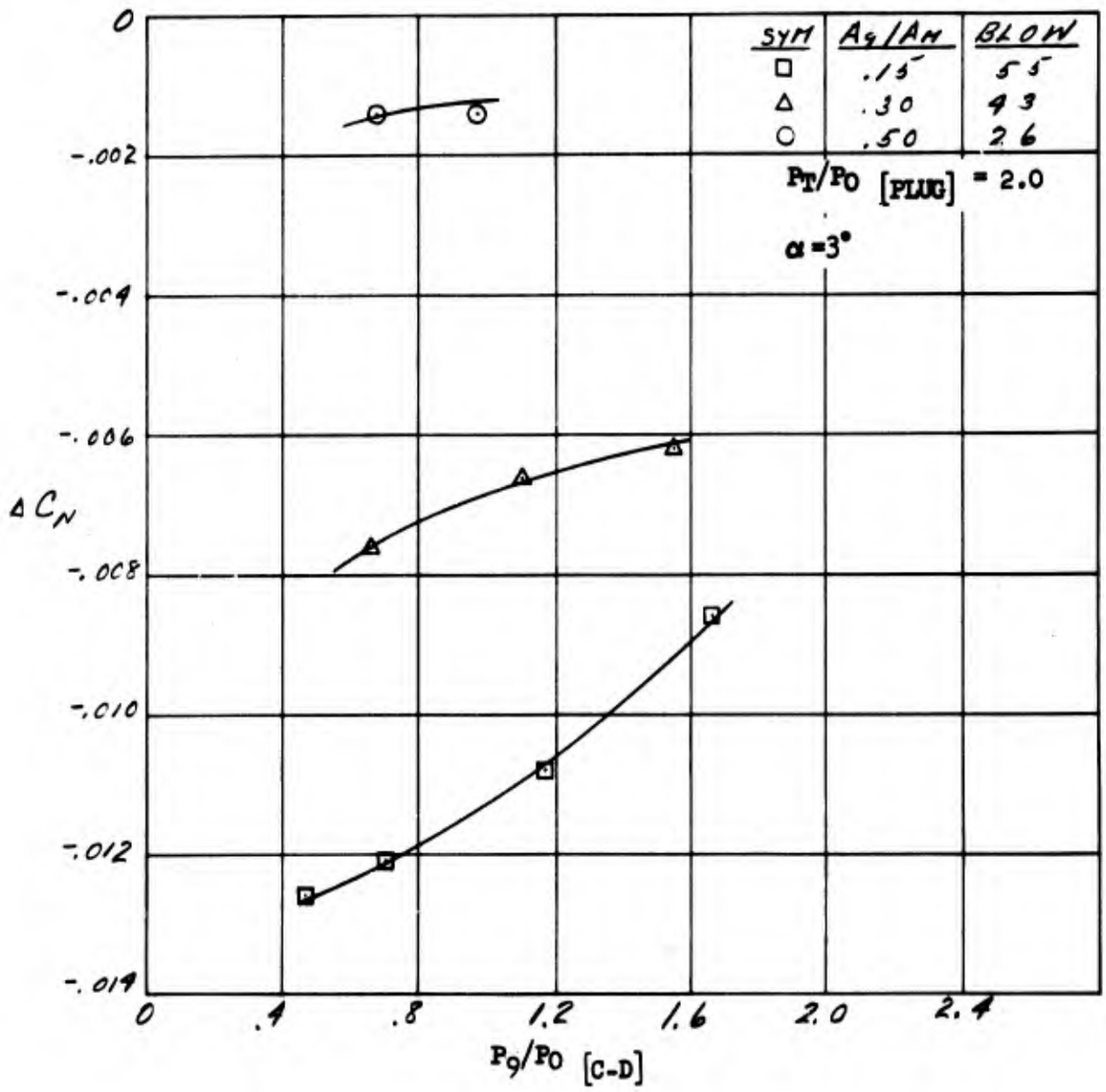

Figure 97. C-D Nozzle Static Pressure Ratio Effects on Normal Force Increment - M = .85

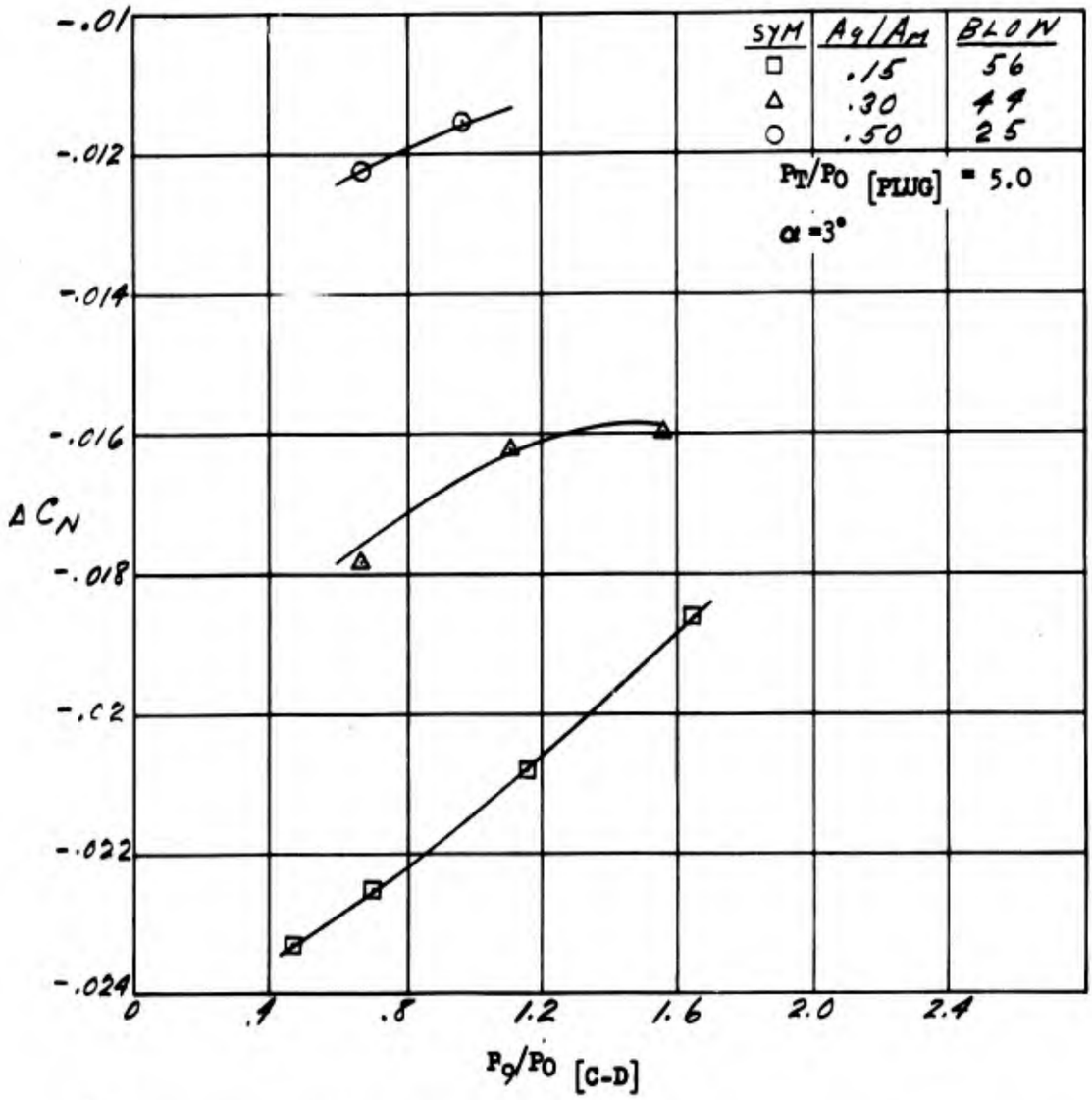

Figure 98. C-D Nozzle Static Pressure Ratio Effects on Normal Force Increment - M = .85

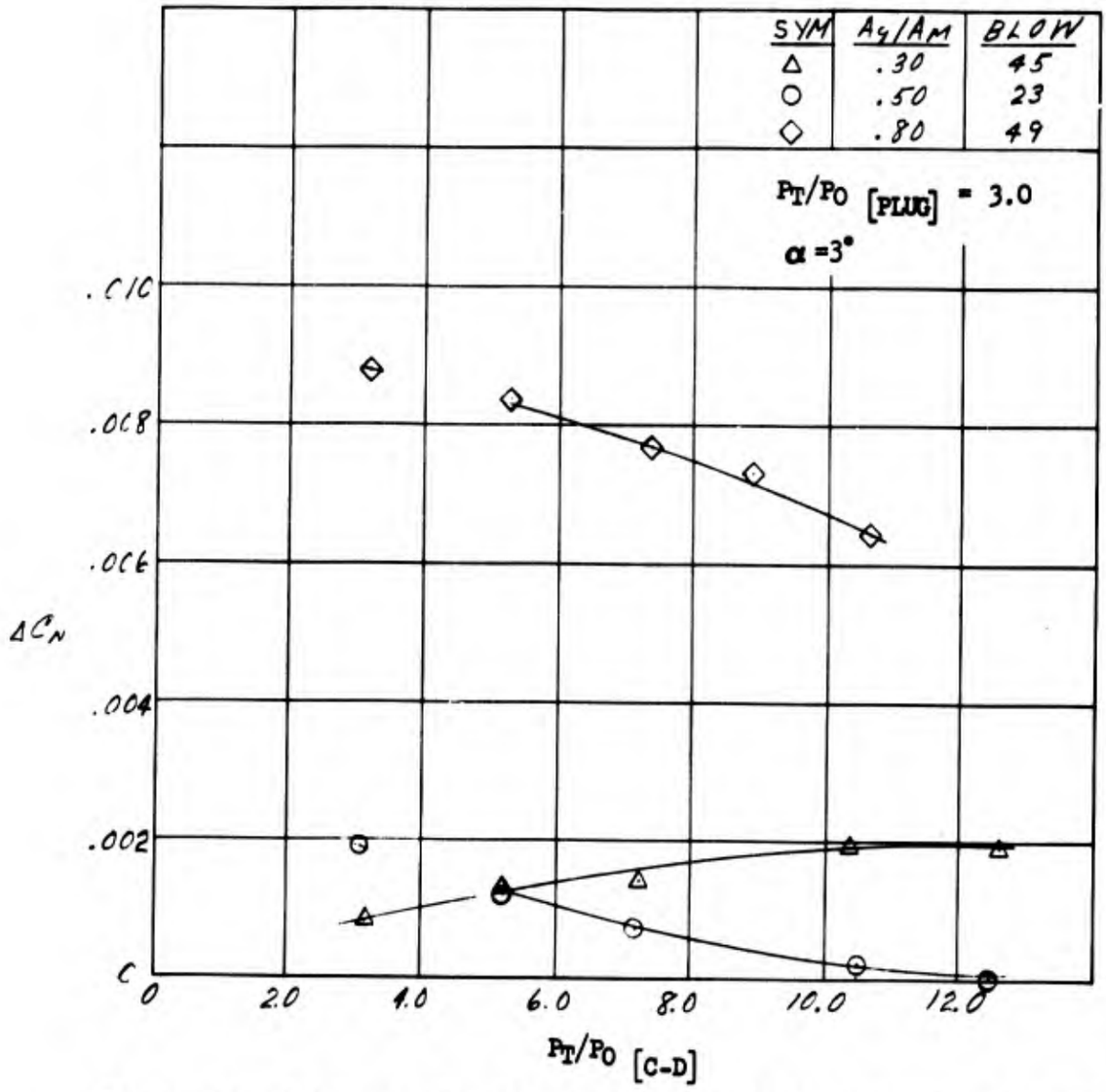

Figure 99. C-D Nozzle Jet Effects On Normal Force Increment - M = 1.27

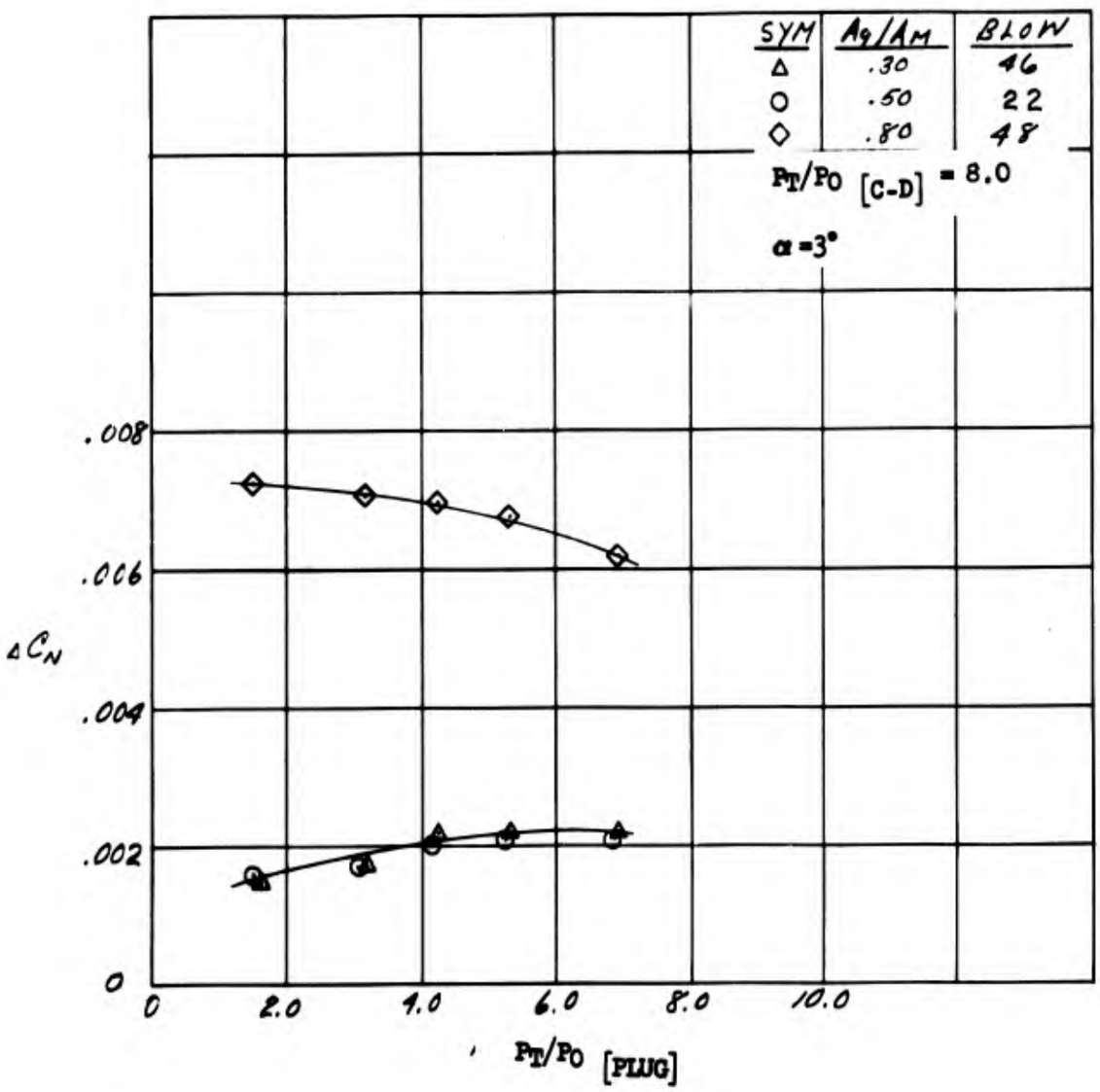

Figure 100. Plug Nozzle Jet Effects On Normal Force Increment - M = 1.27

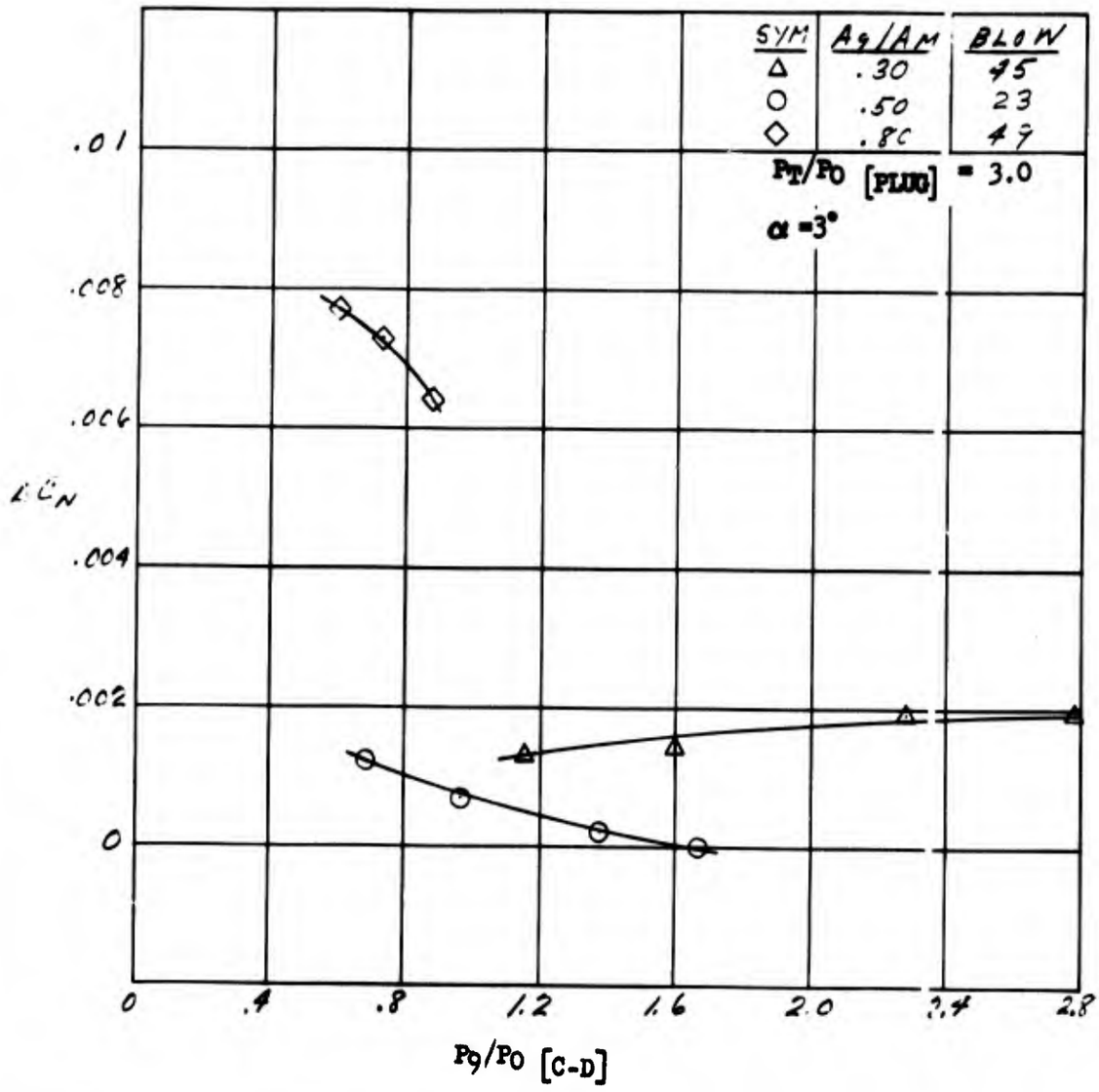

Figure 101. C-D Nozzle Static Pressure Ratio Effects on Normal Force Increment - M = 1.27

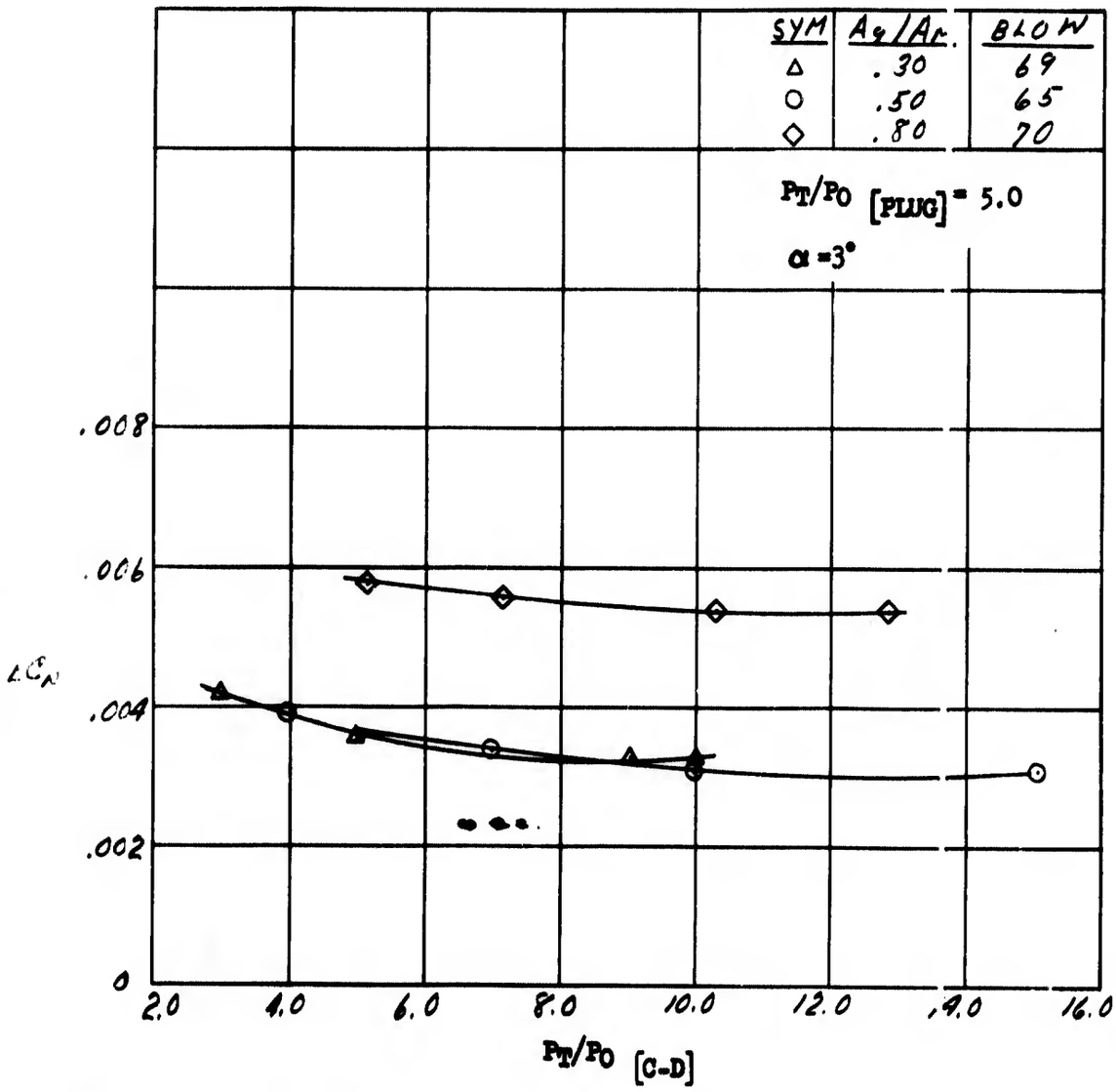

Figure 102. C-D Nozzle Jet Effects On Normal Force Increment - M = 1.7

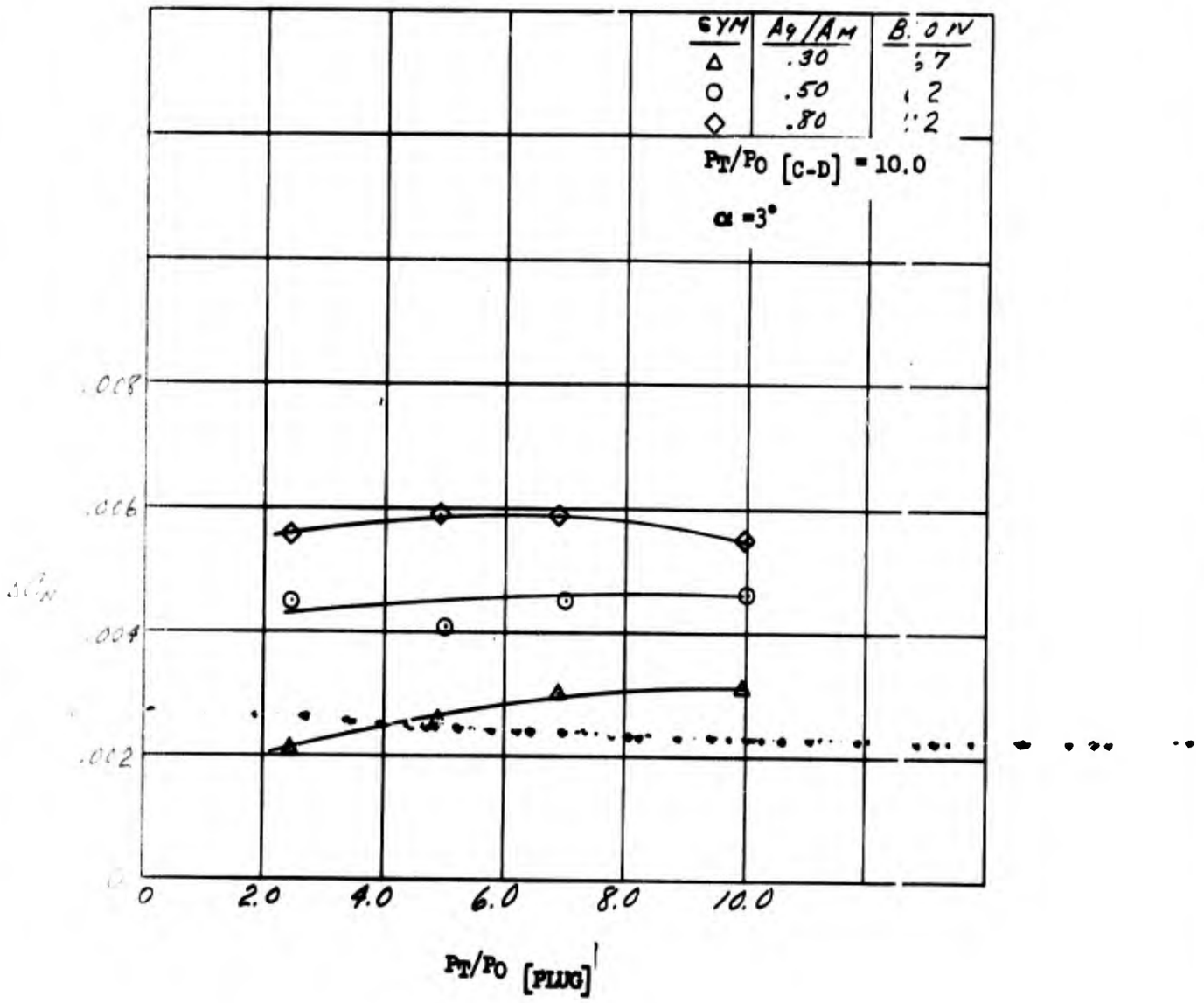

Figure 103. Plug Nozzle Jet Effects on Normal Force Increments - M = 1.7.

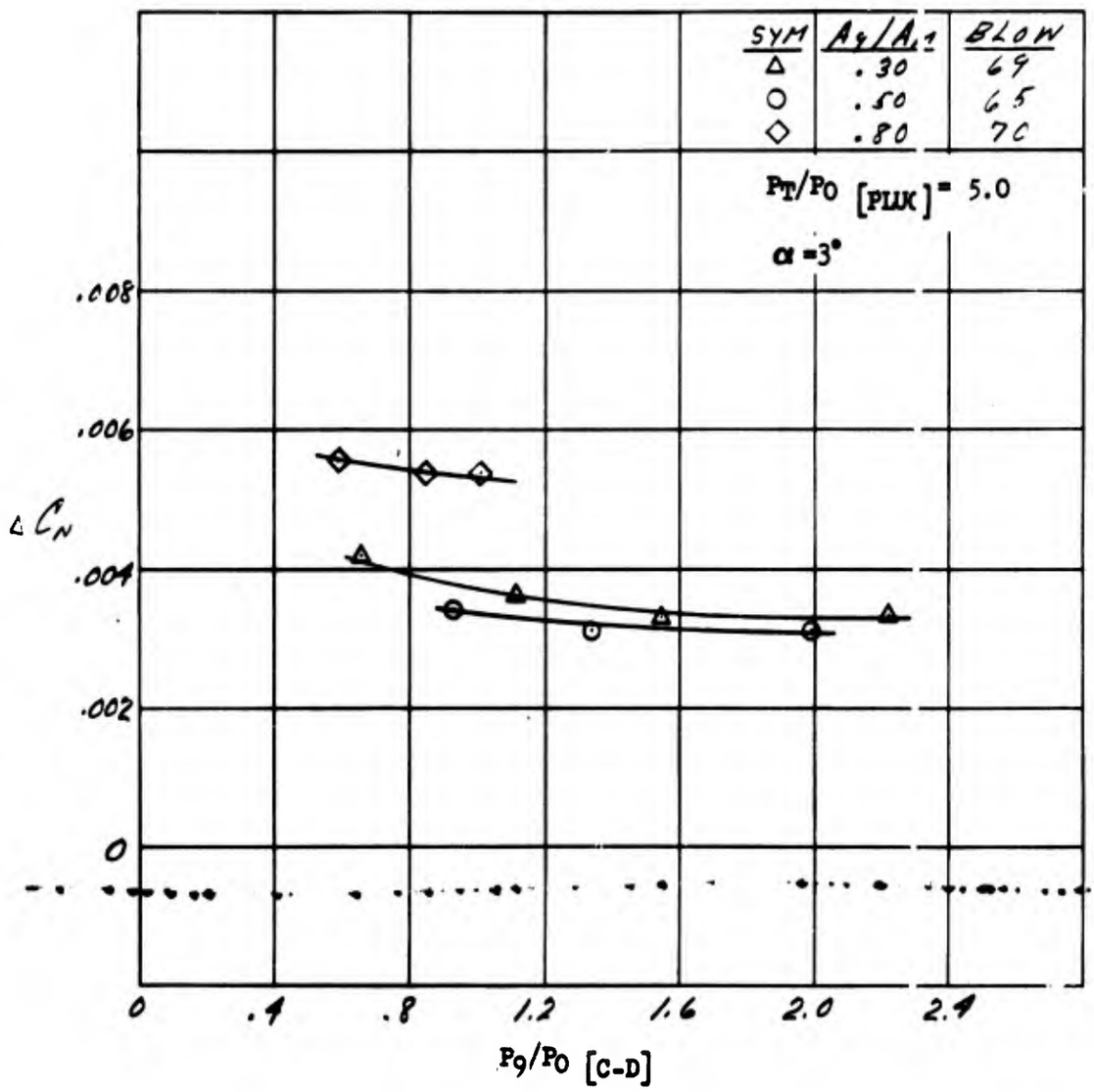

Figure 104. C-D Nozzle Static Pressure Ratio Effects on Normal Force Increment - M = 1.7.

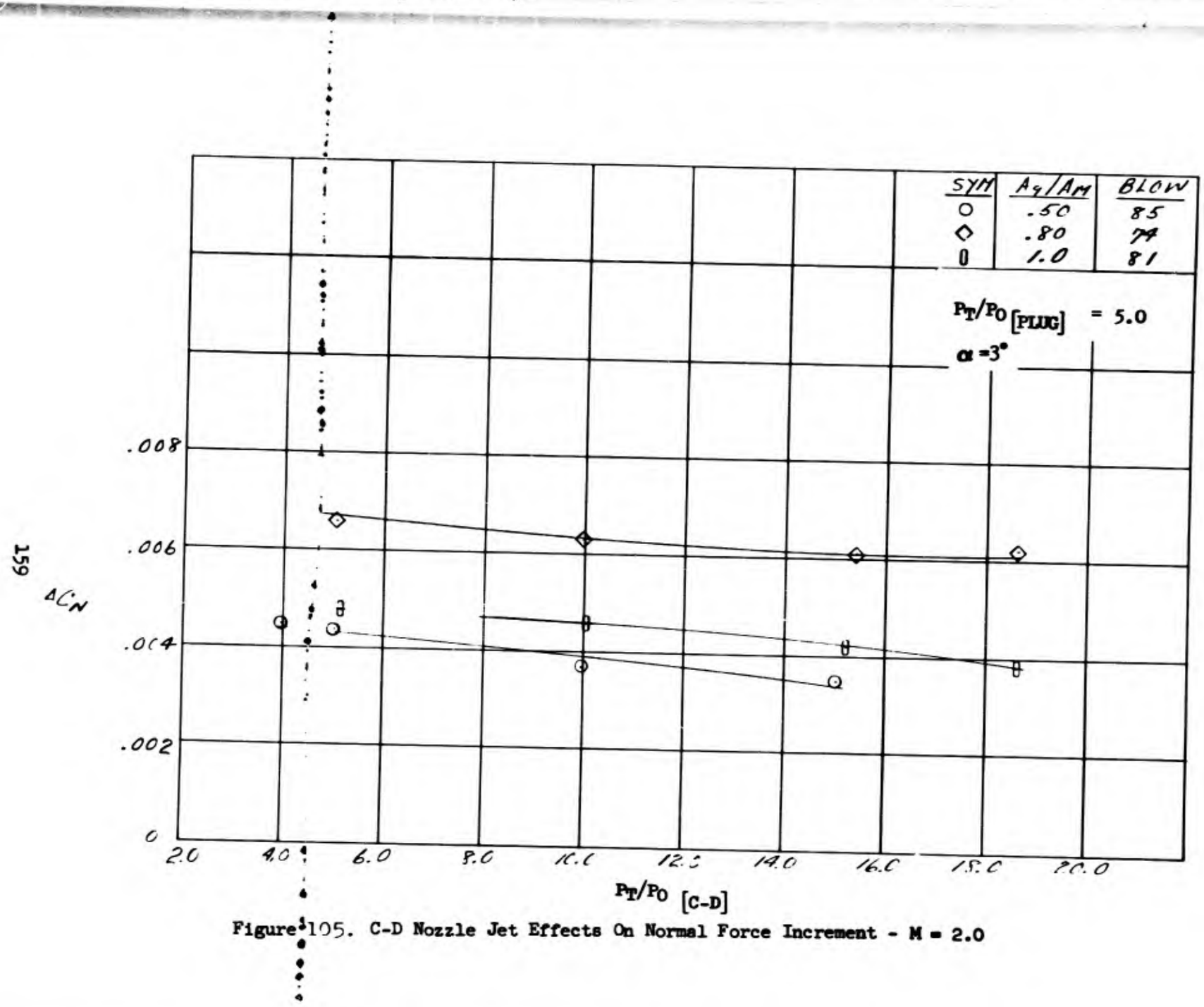

Figure 105. C-D Nozzle Jet Effects On Normal Force Increment - M = 2.0

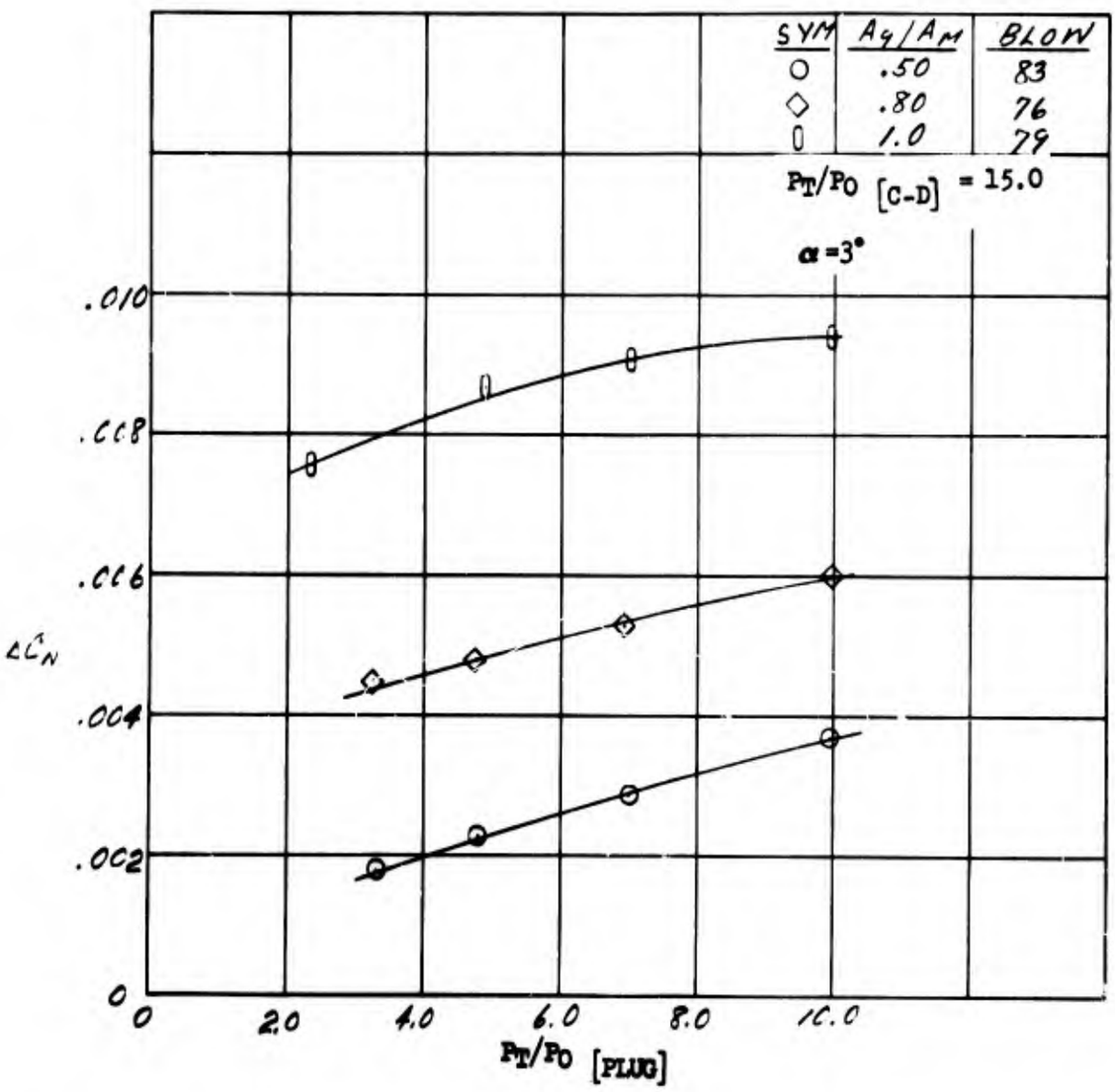

Figure 106. Plug Nozzle Jet Effects On Normal Force Increment - M = 2.0

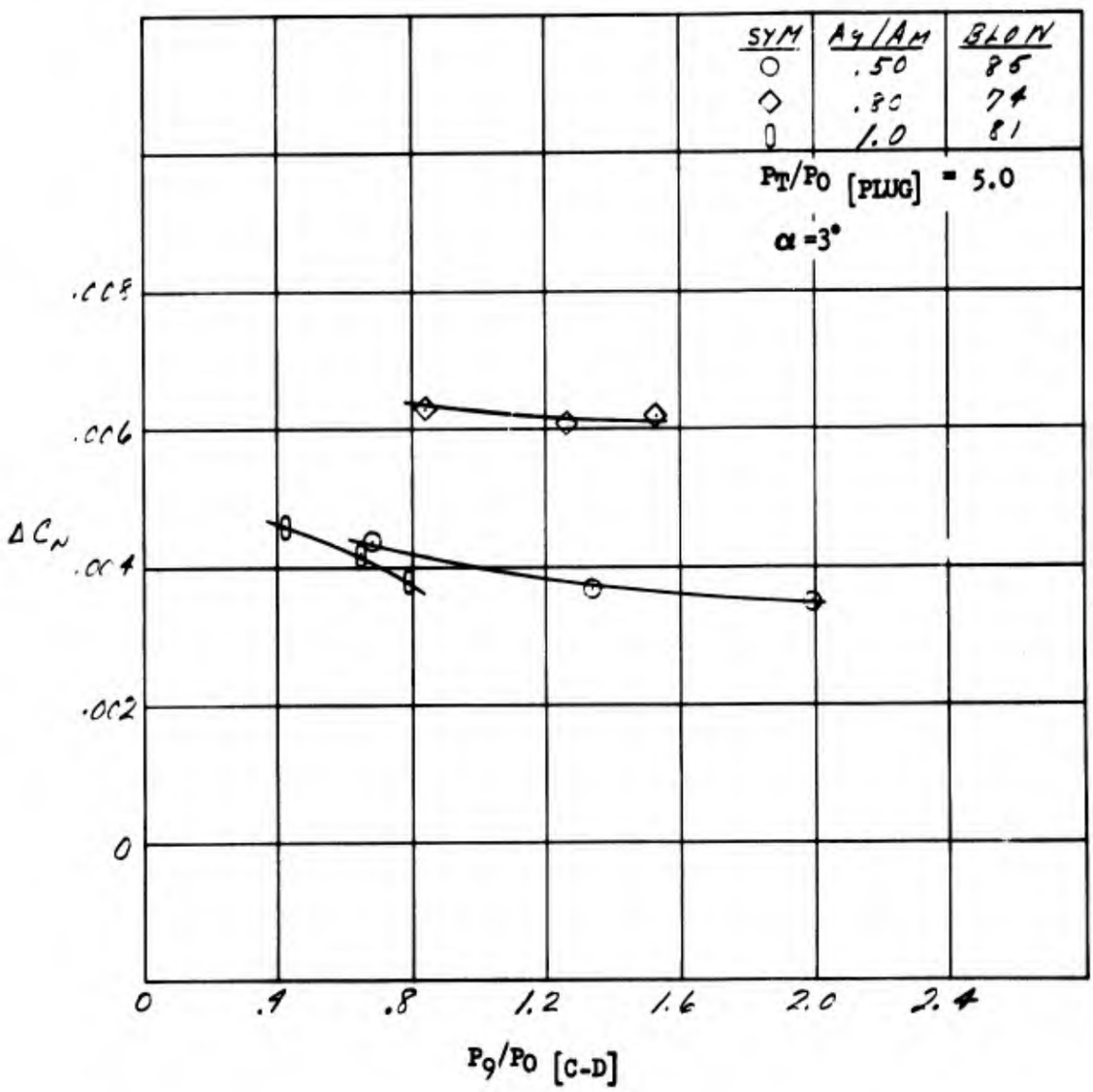

Figure 107. C-D Nozzle Static Pressure Ratio Effects on Normal Force Increment - M = 2.0

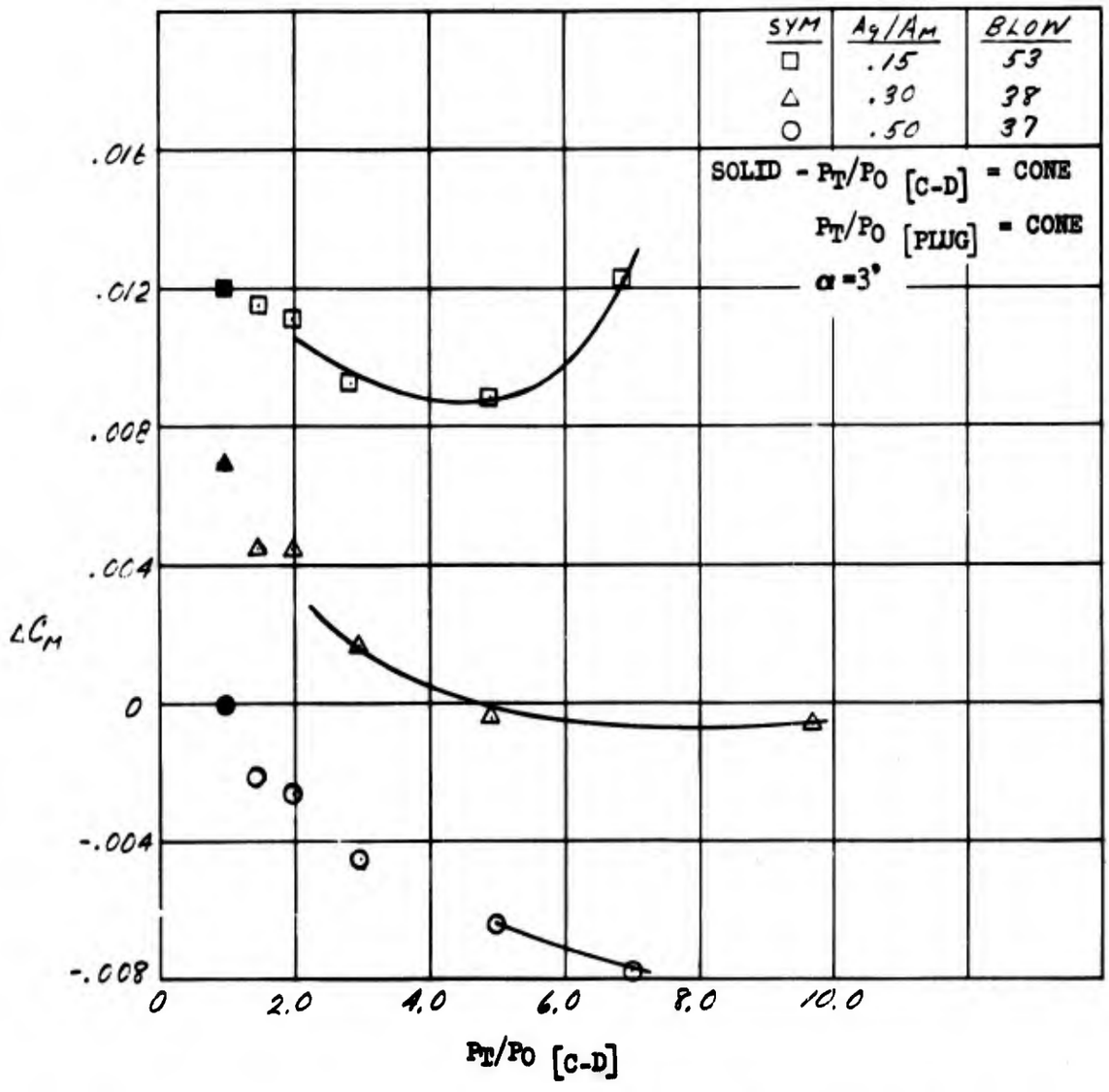

Figure 108. C-D Nozzle Jet Effects On Pitching Moment Increment - M = .614

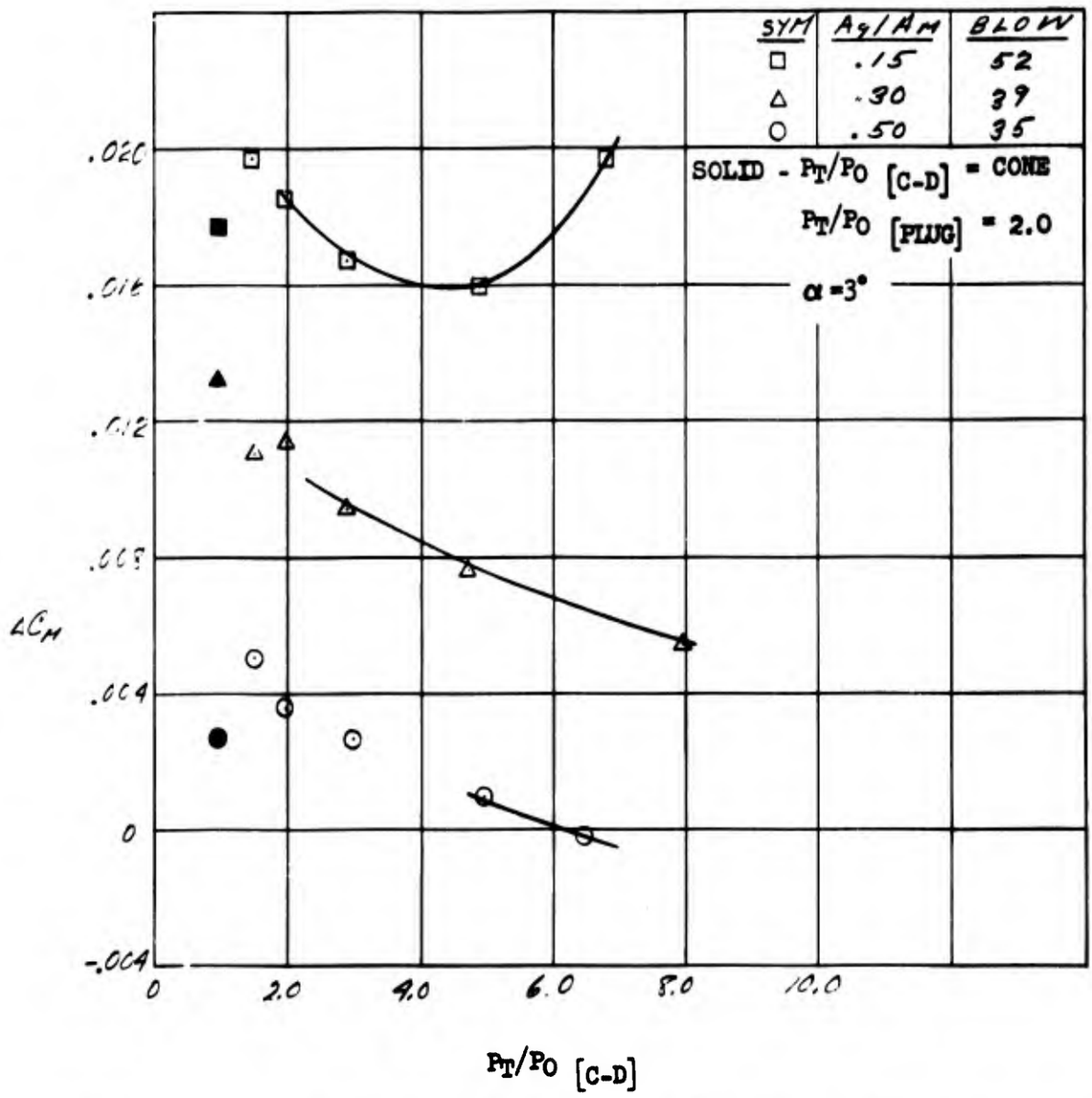

Figure 109. C-D Nozzle Jet Effects On Pitching Moment Increment - M = .614

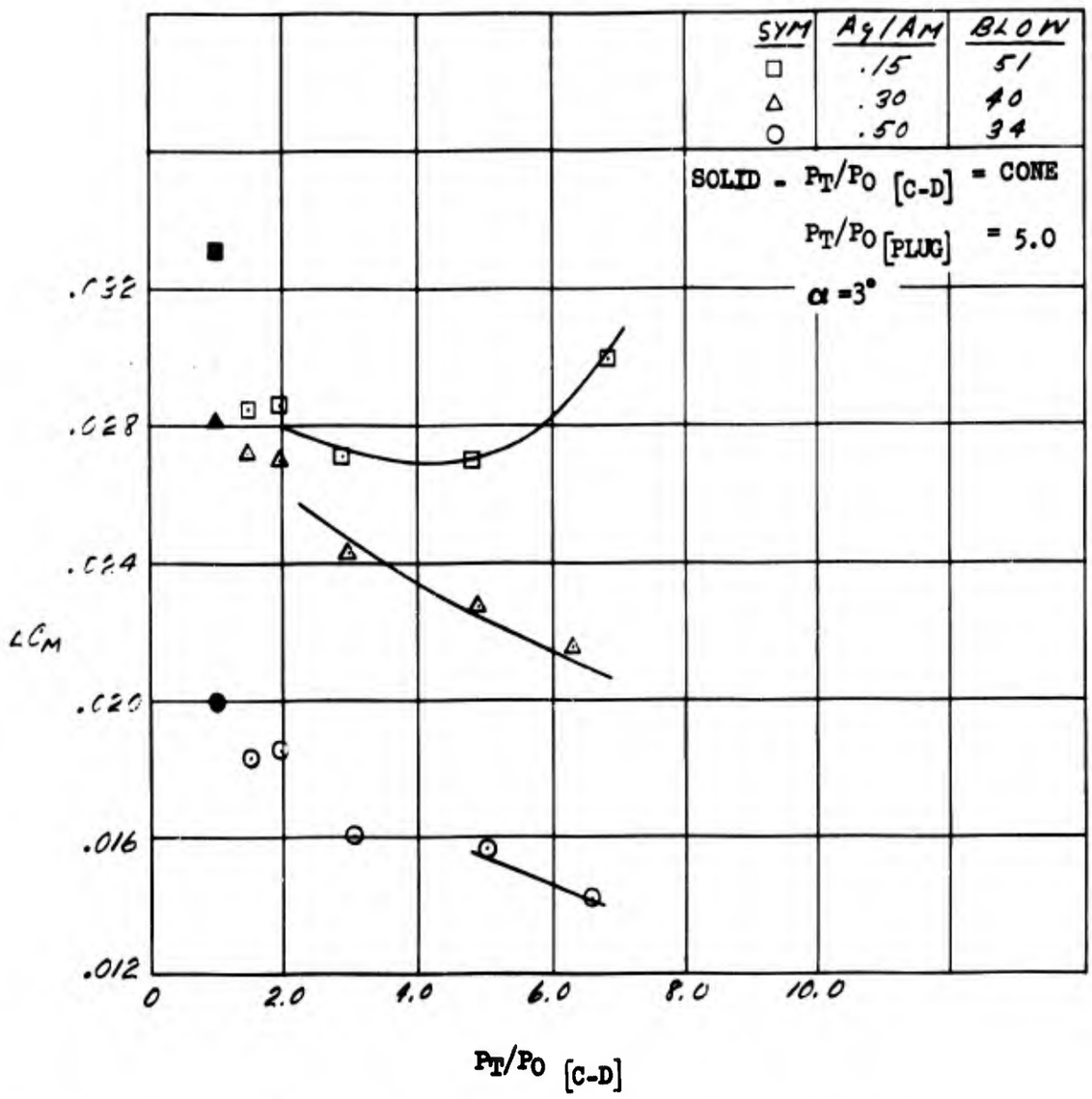

Figure 110. C-D Nozzle Jet Effects On Pitching Moment Increment - M = .614

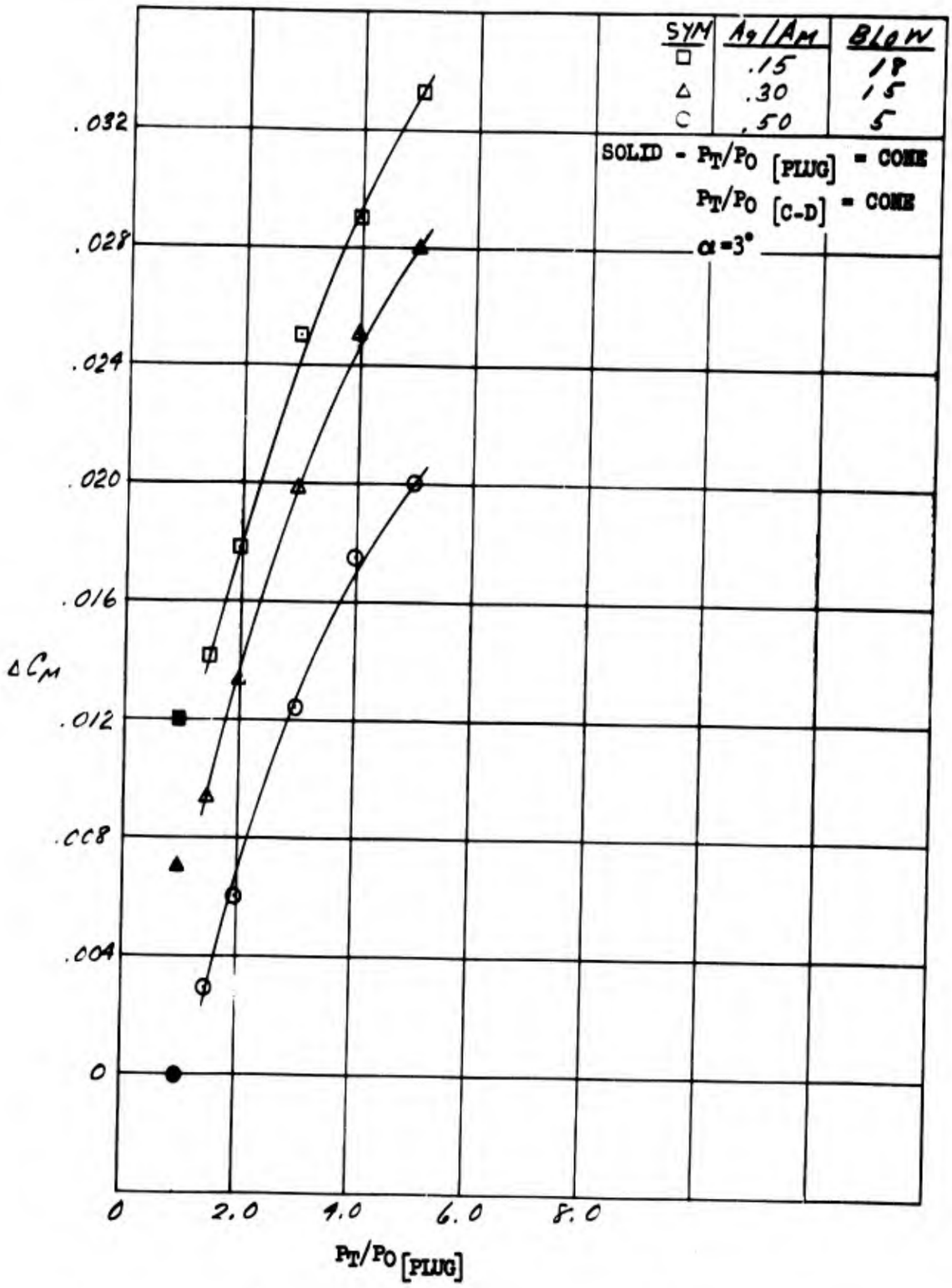

Figure 111. Plug Nozzle Jet Effects On Pitching Moment Increment - M = .614

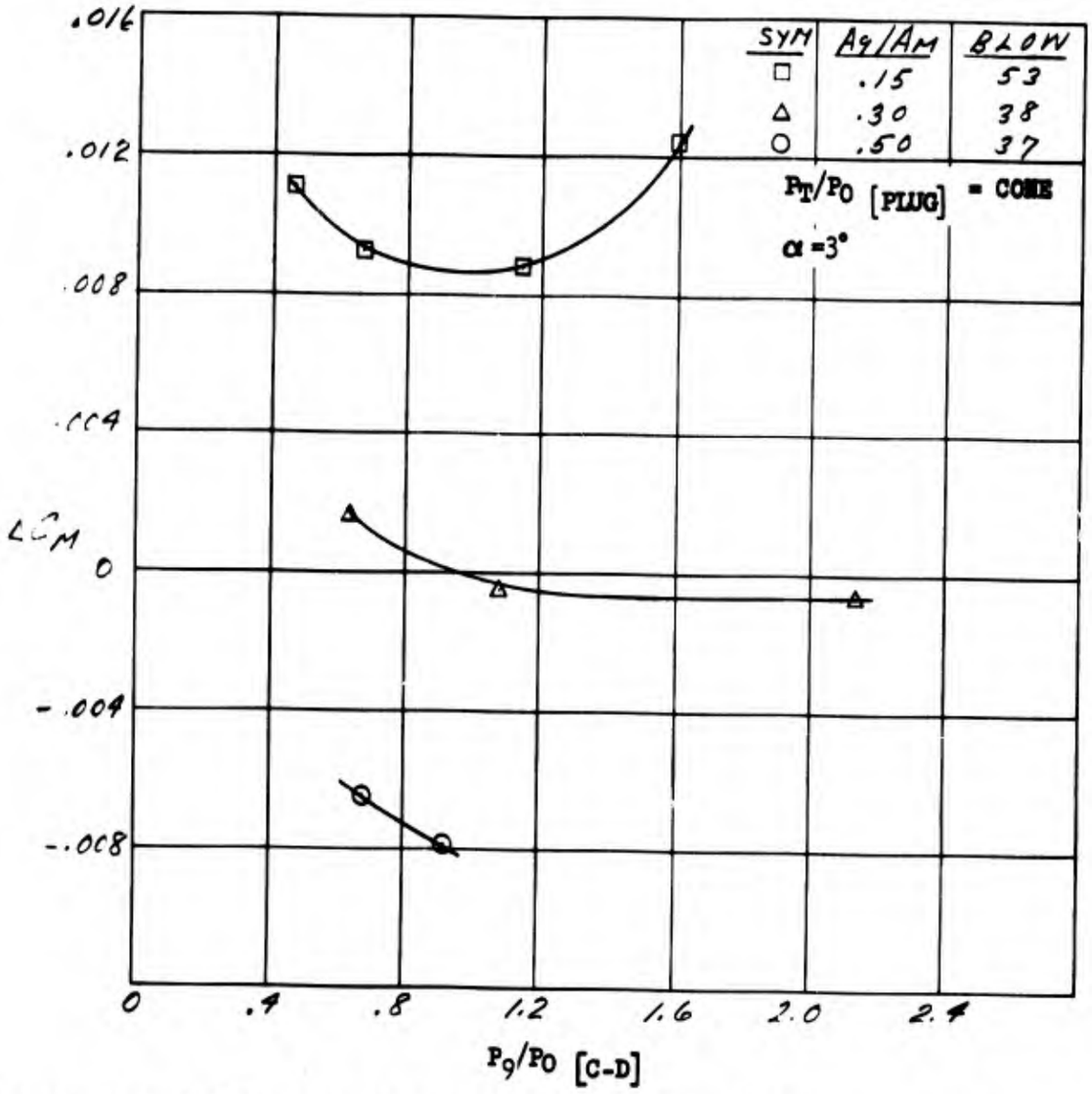

Figure 112. C-D Nozzle Static Pressure Ratio Effects on Pitching Moment Increment - M = .614

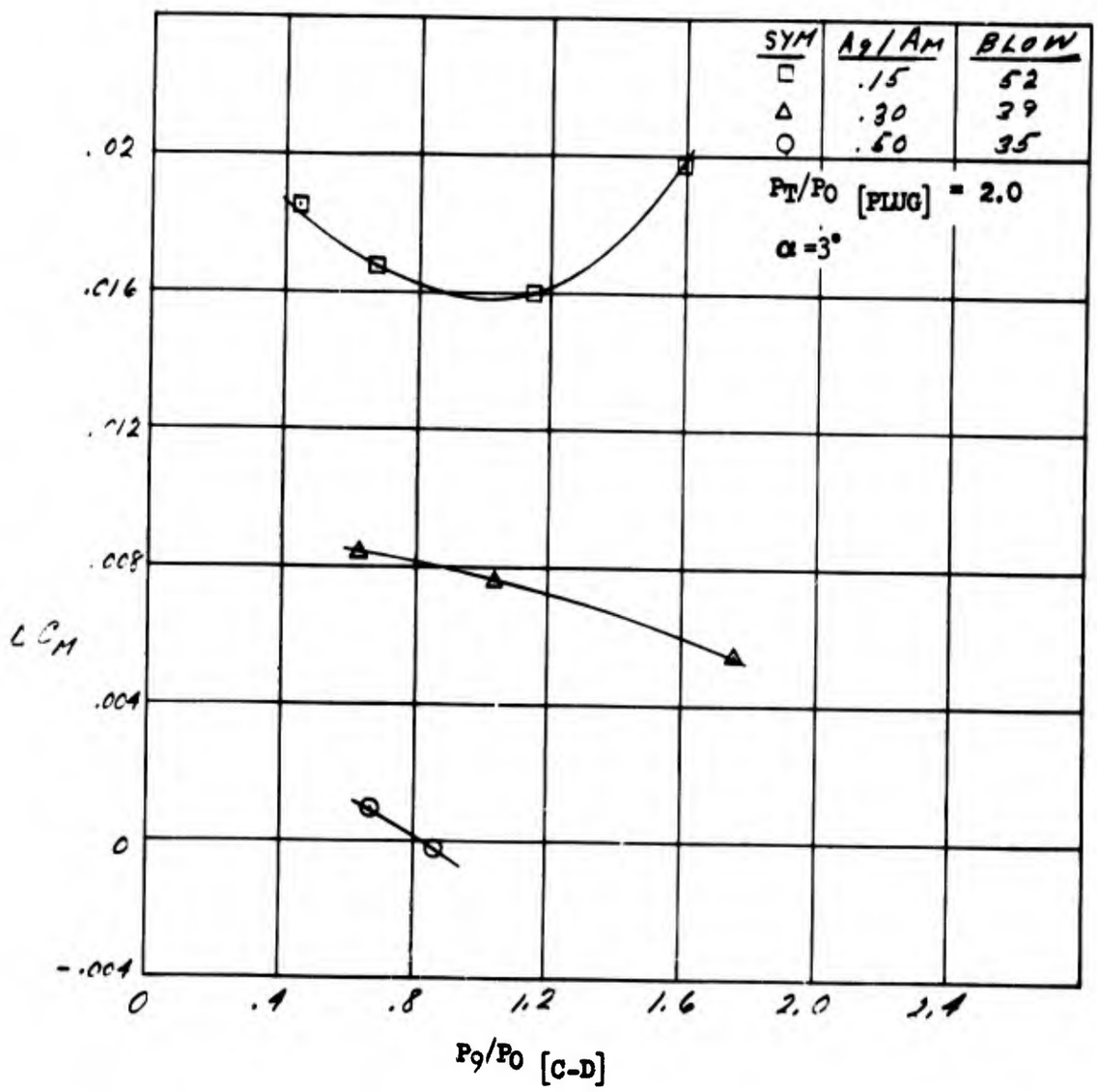

Figure 113. C-D Nozzle Static Pressure Ratio Effects on Pitching Moment Increment - M = .614

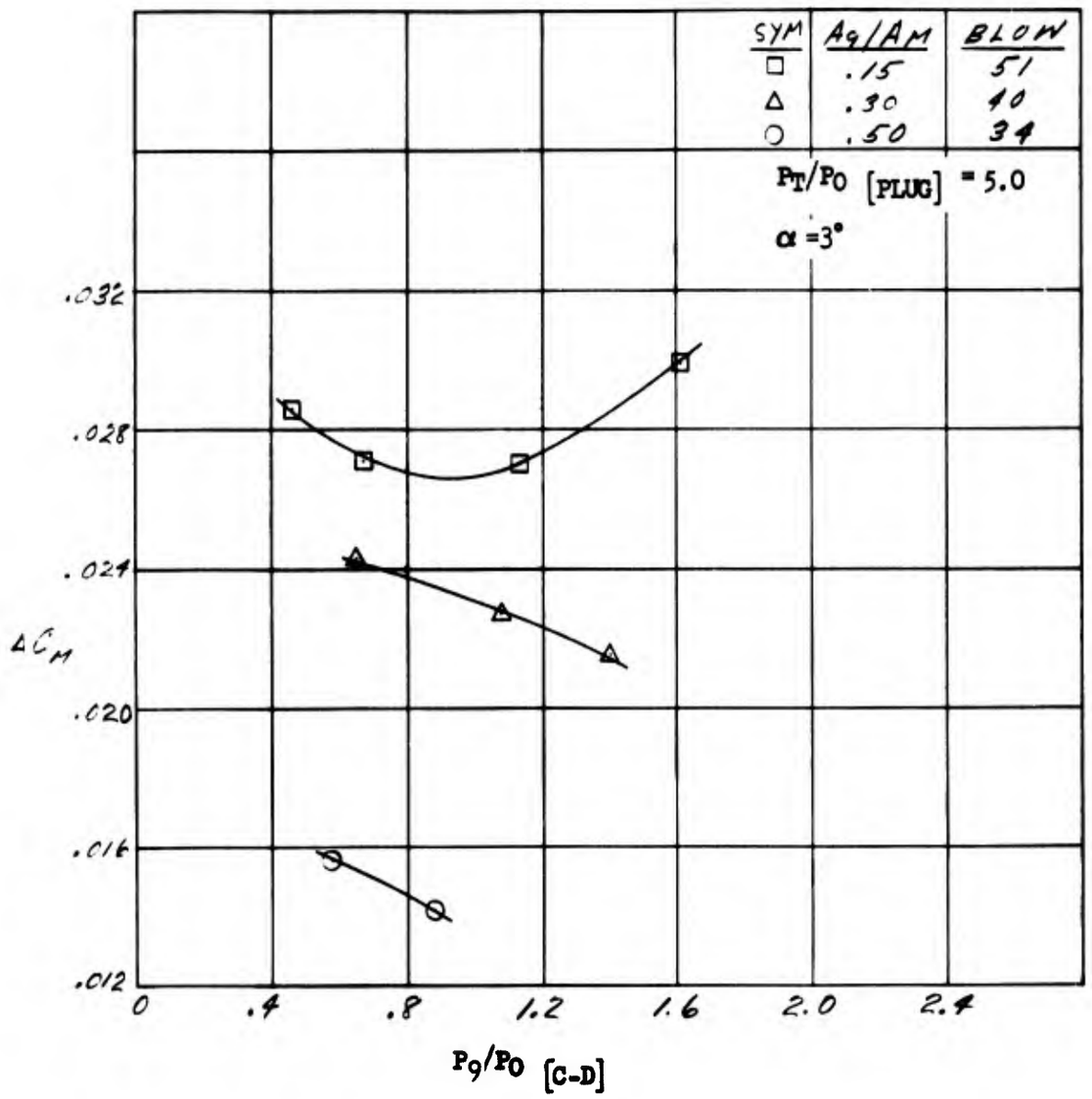

Figure 114. C-D Nozzle Static Pressure Ratio Effects on Pitching Moment Increment - M = .614

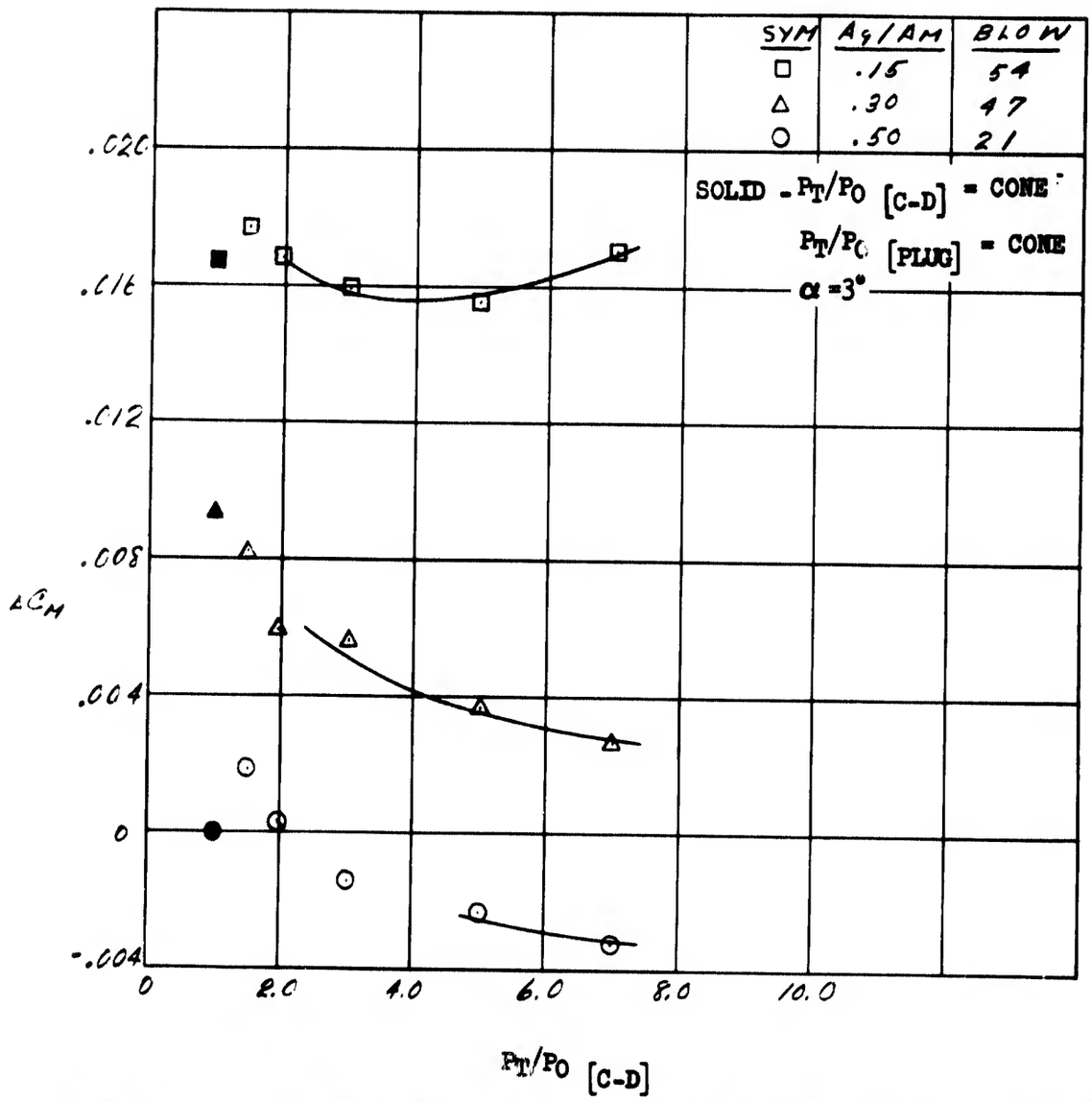

Figure 115. C-D Nozzle Jet Effects On Pitching Moment Increment - M = .85

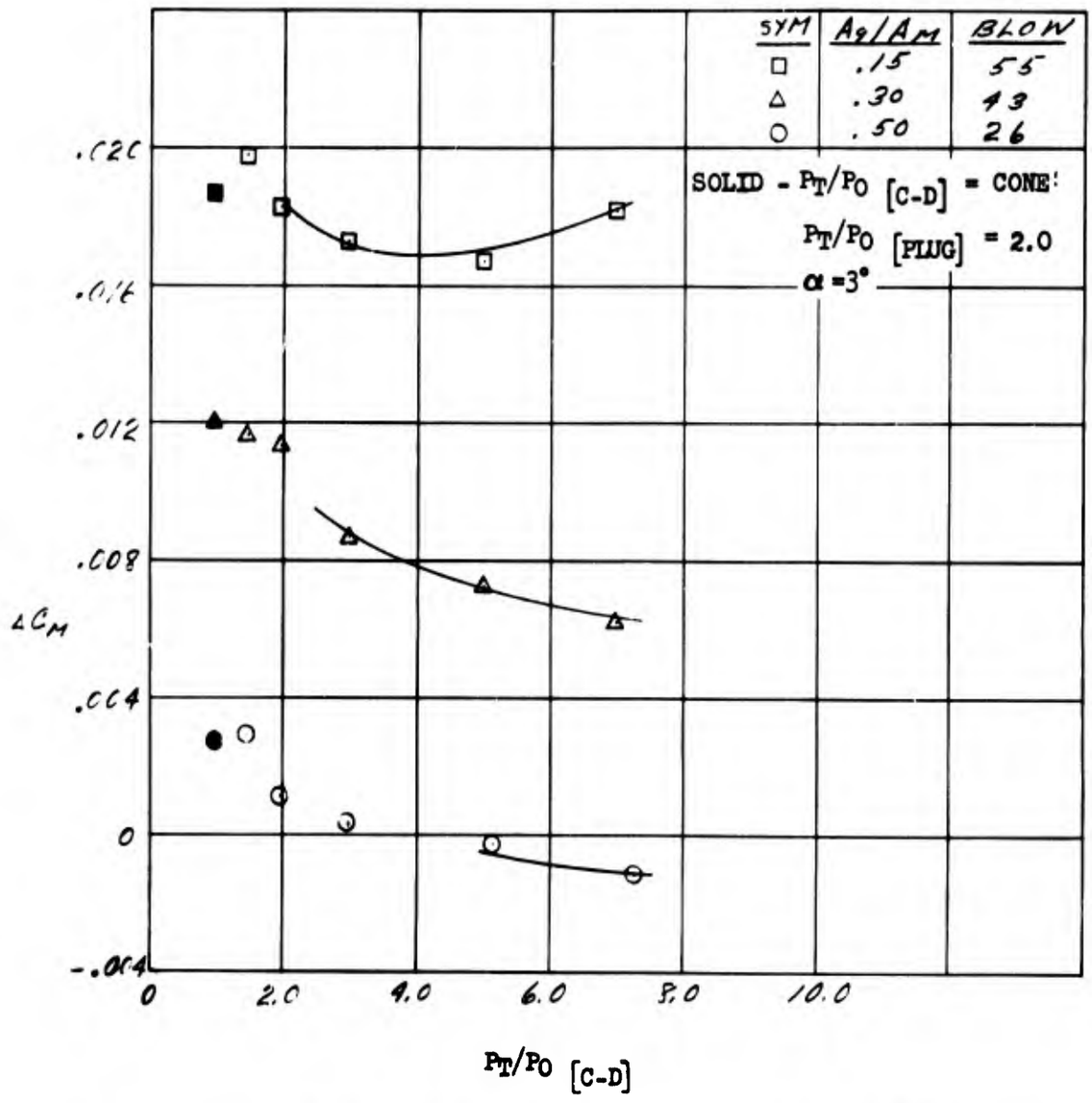

Figure 116. C-D Nozzle Jet Effects On Pitching Moment Increment - M = .85

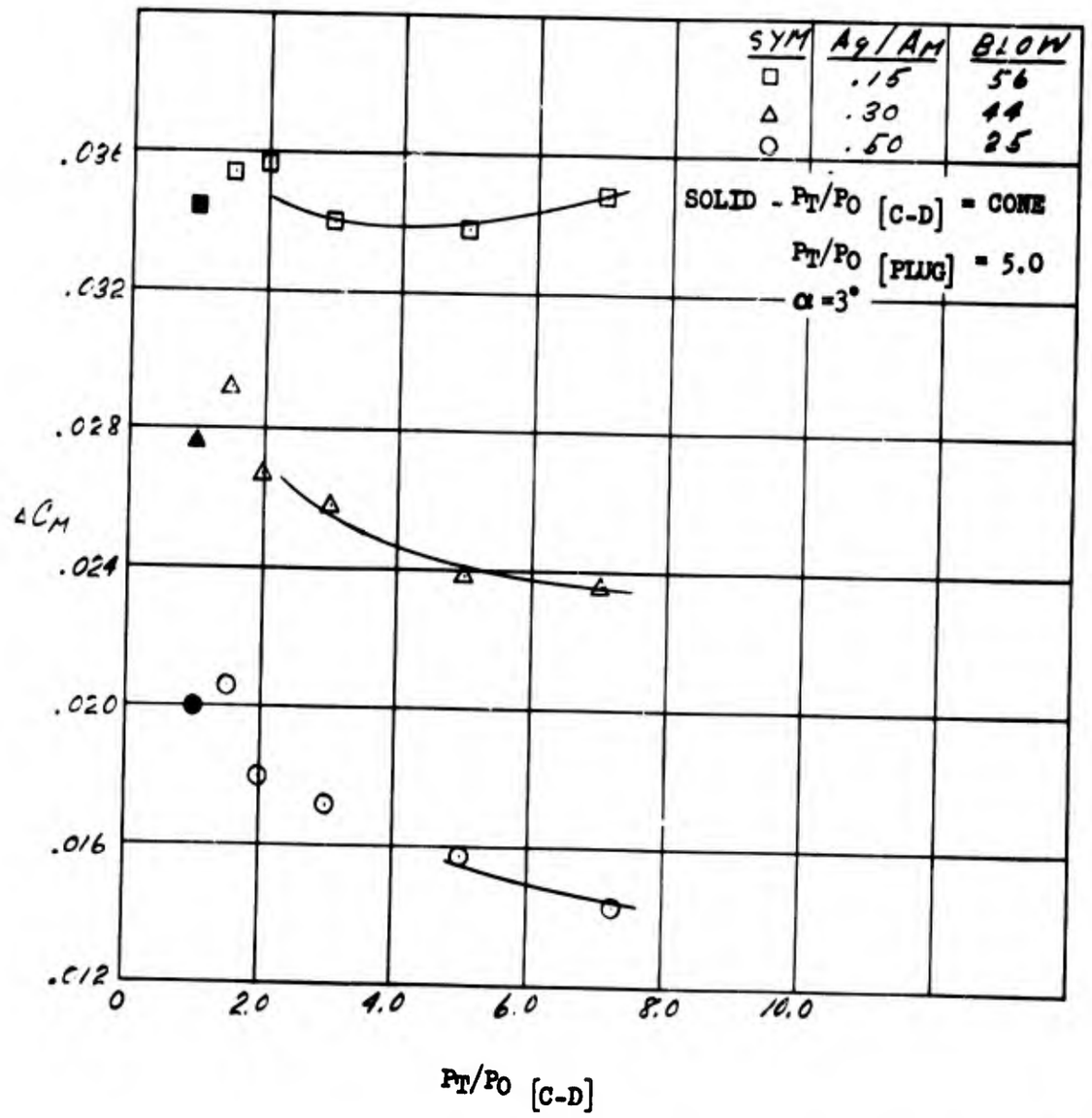

Figure 117. C-D Nozzle Jet Effects On Pitching Moment Increment - M = .85

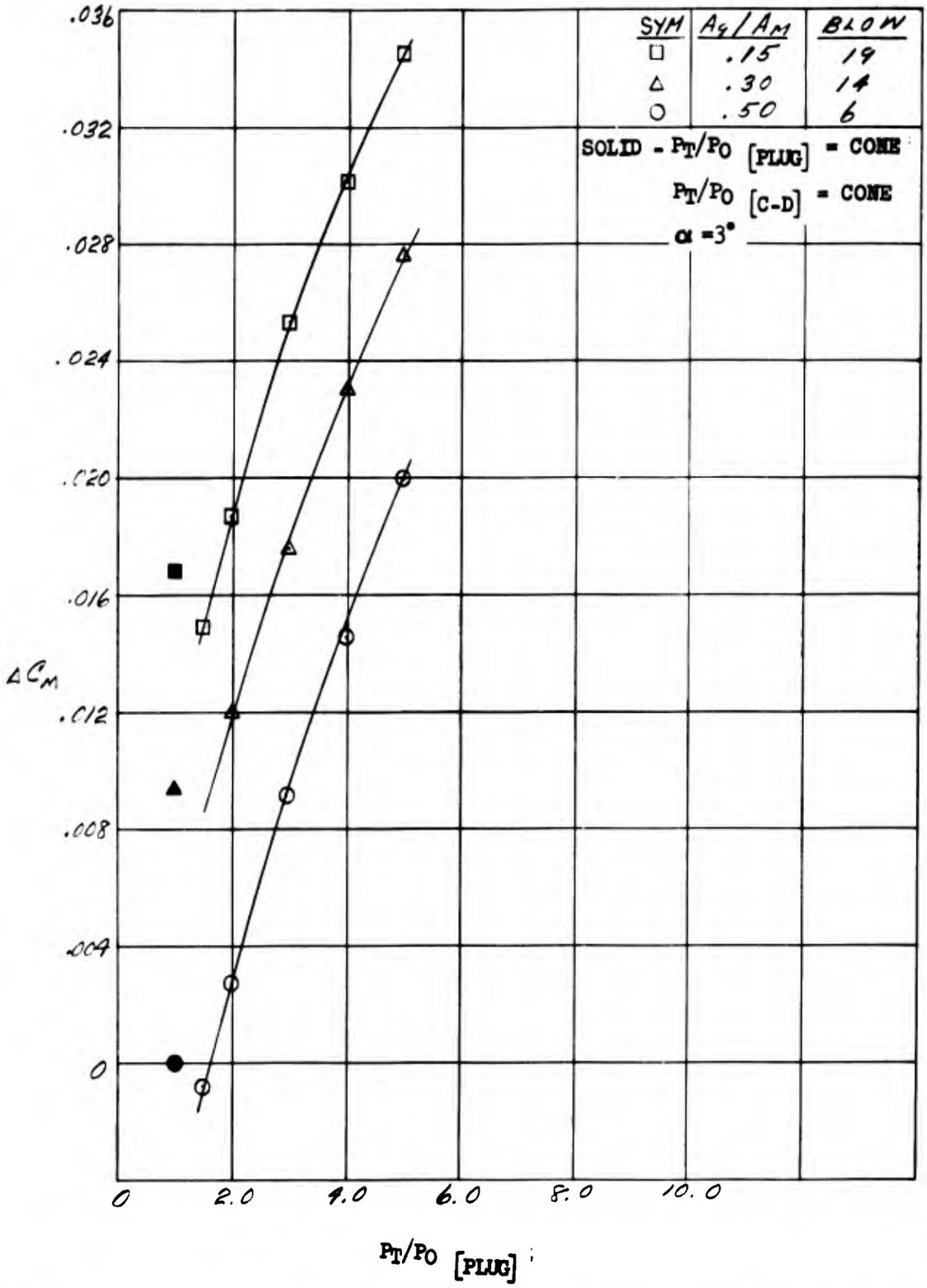

Figure 118. Plug Nozzle Jet Effects On Pitching Moment Increment - M = .85

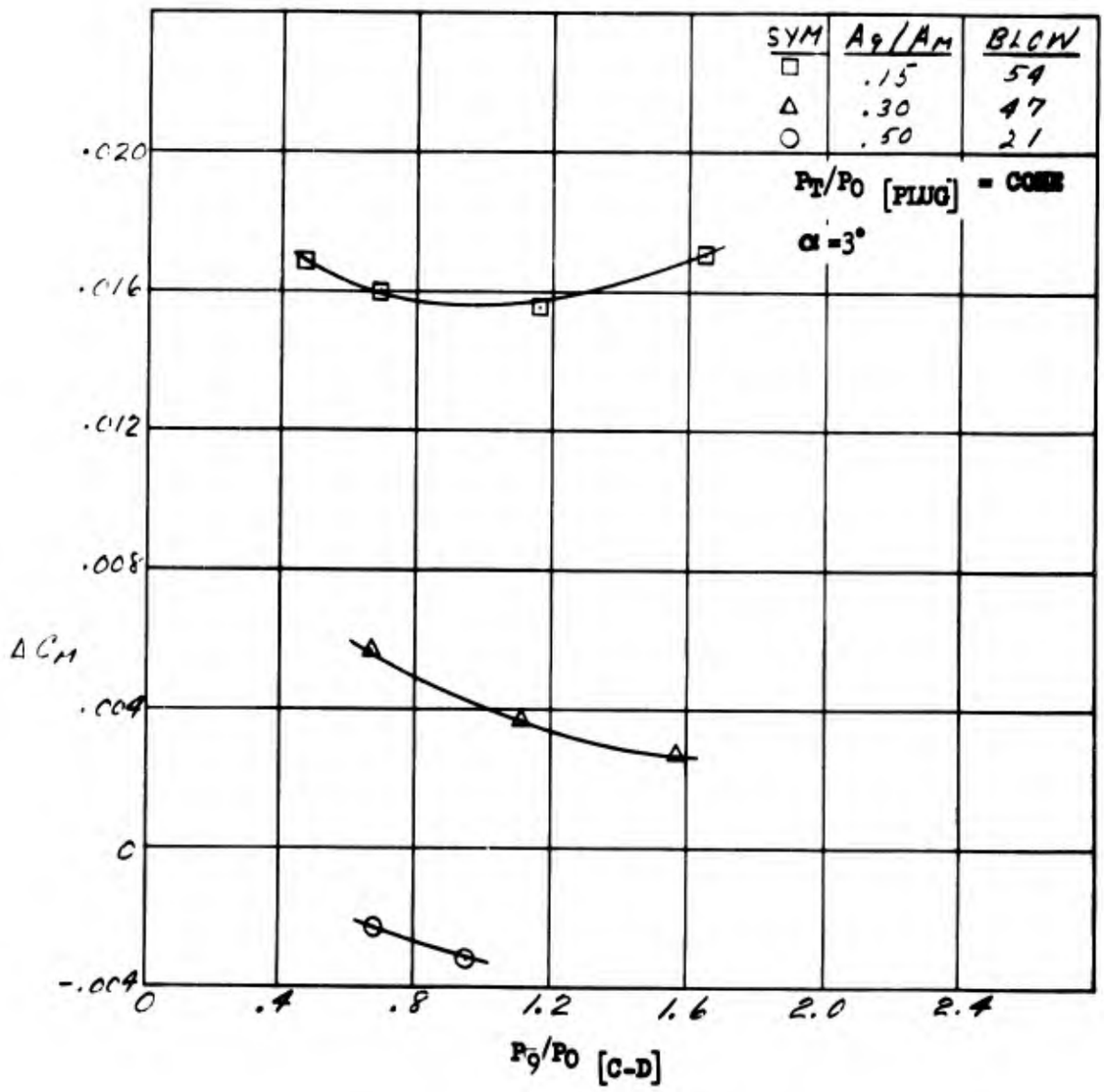

Figure 119. C-D Nozzle Static Pressure Ratio Effects on Pitching Moment Increment - M = .85

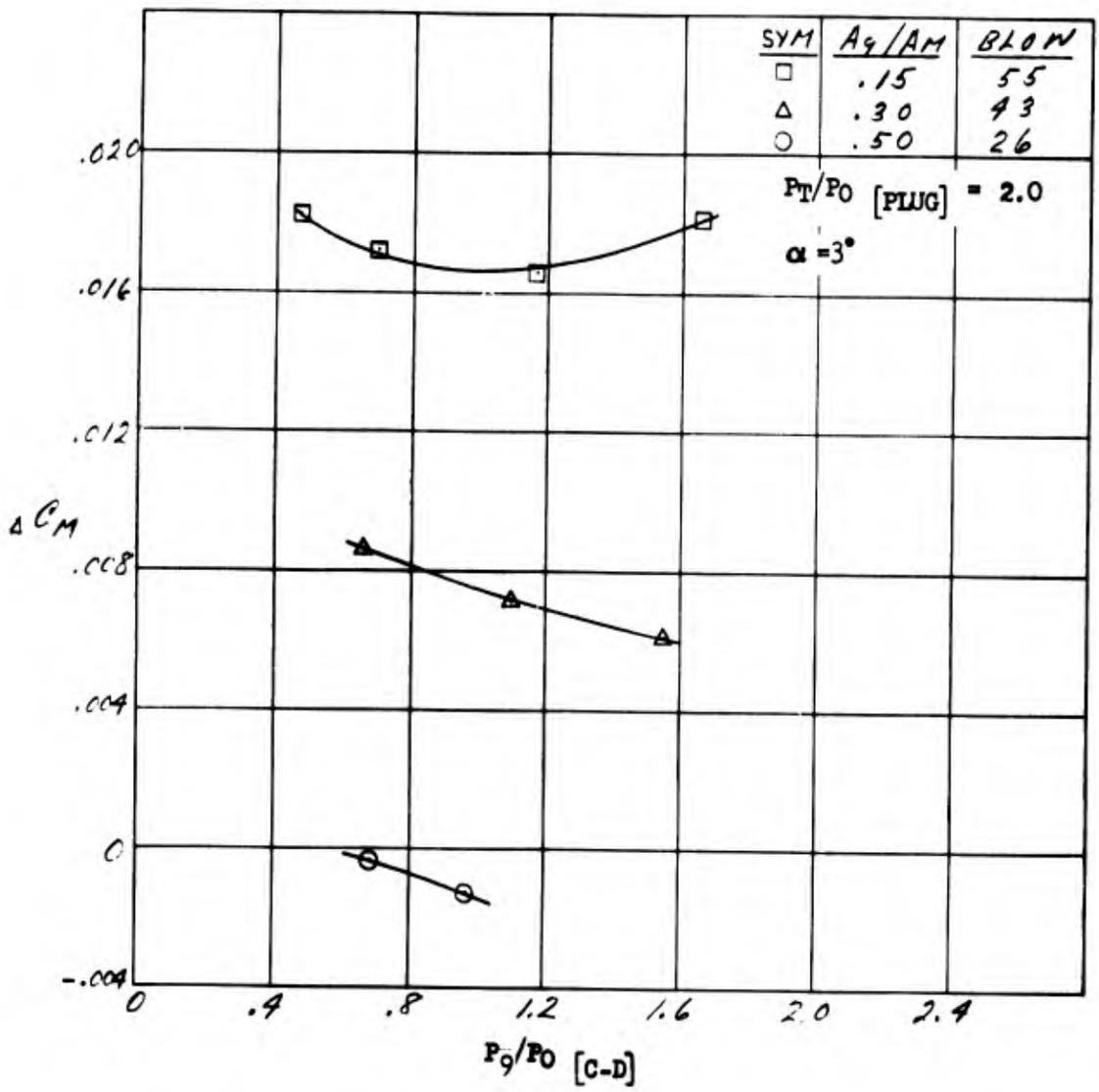

Figure 120. C-D Nozzle Static Pressure Ratio Effects on Pitching Moment Increment - M = .85

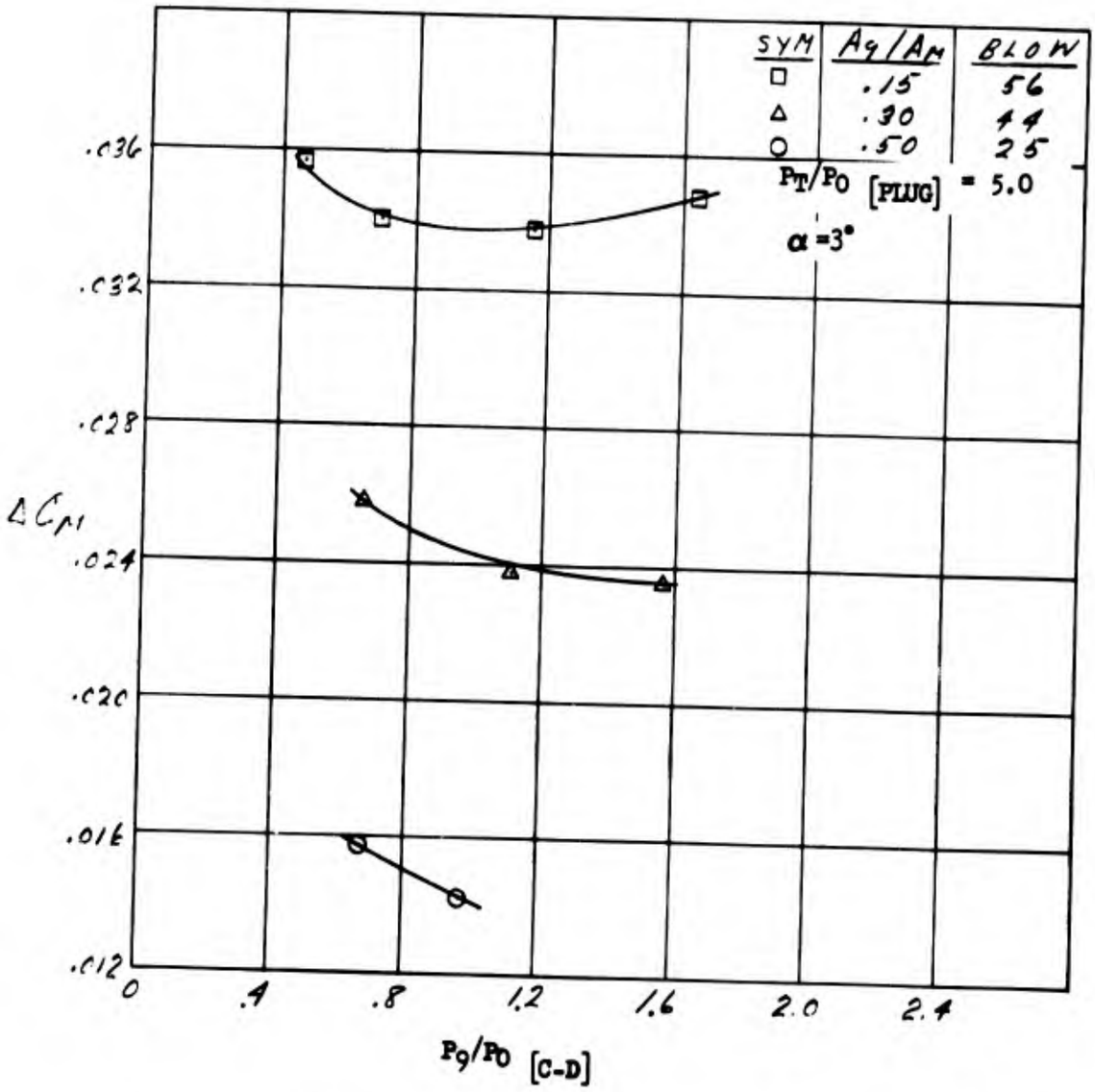

Figure 121. C-D Nozzle Static Pressure Ratio Effects on Pitching Moment Increment - M = .85

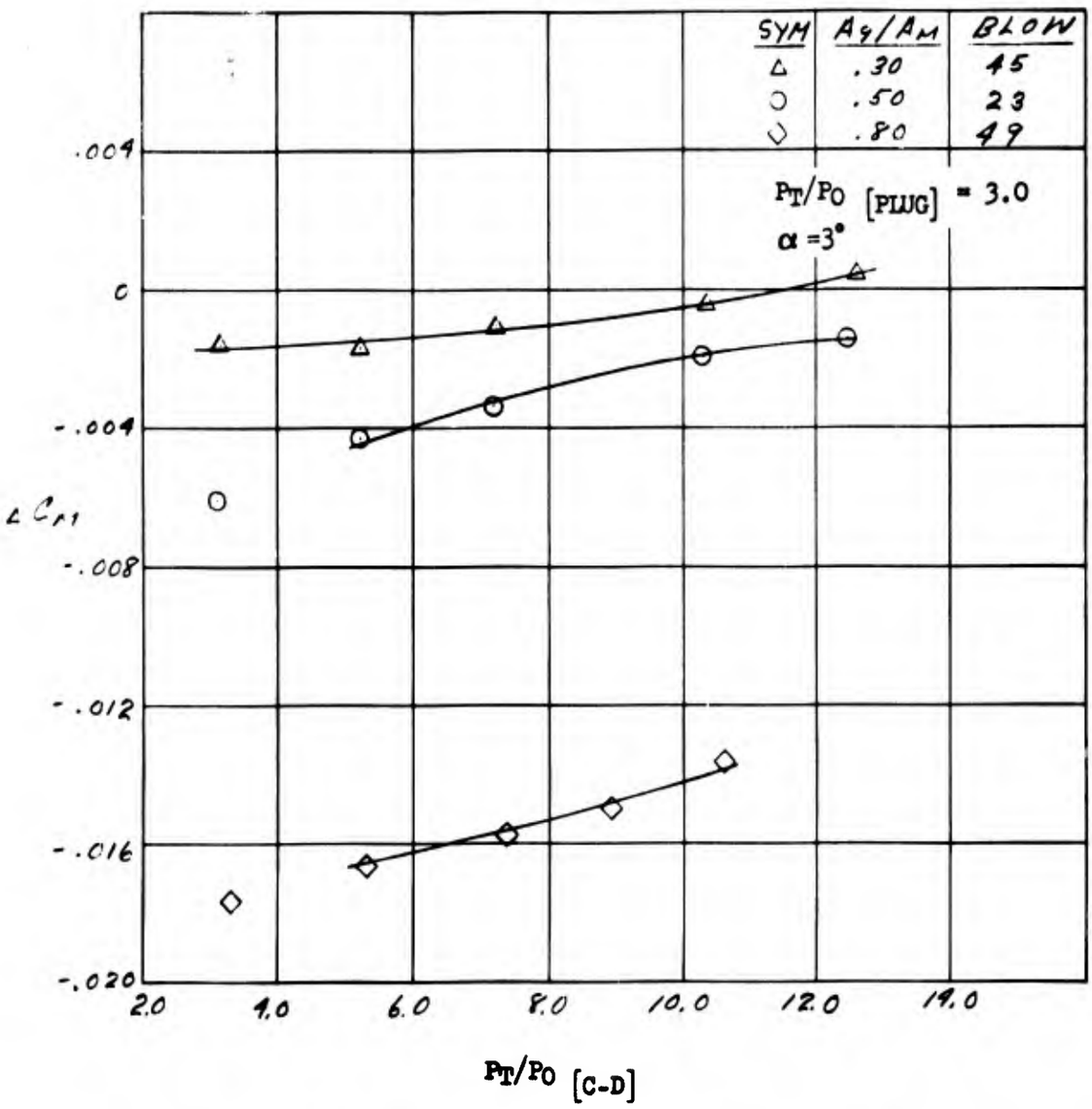

Figure 122. C-D Nozzle Jet Effects On Pitching Moment Increment - M = 1.27

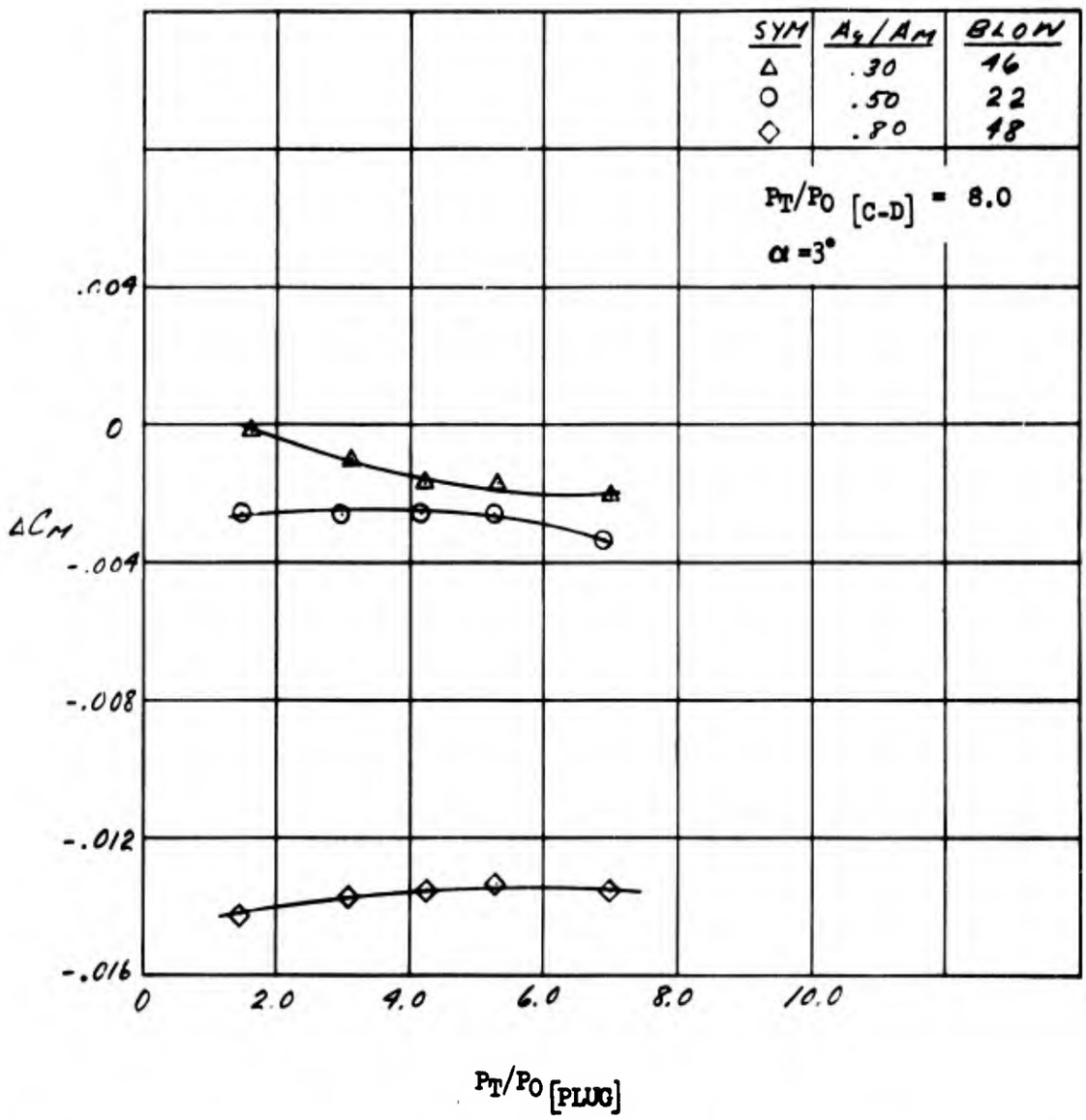

Figure 123. Plug Nozzle Jet Effects On Pitching Moment Increment - M = 1.27

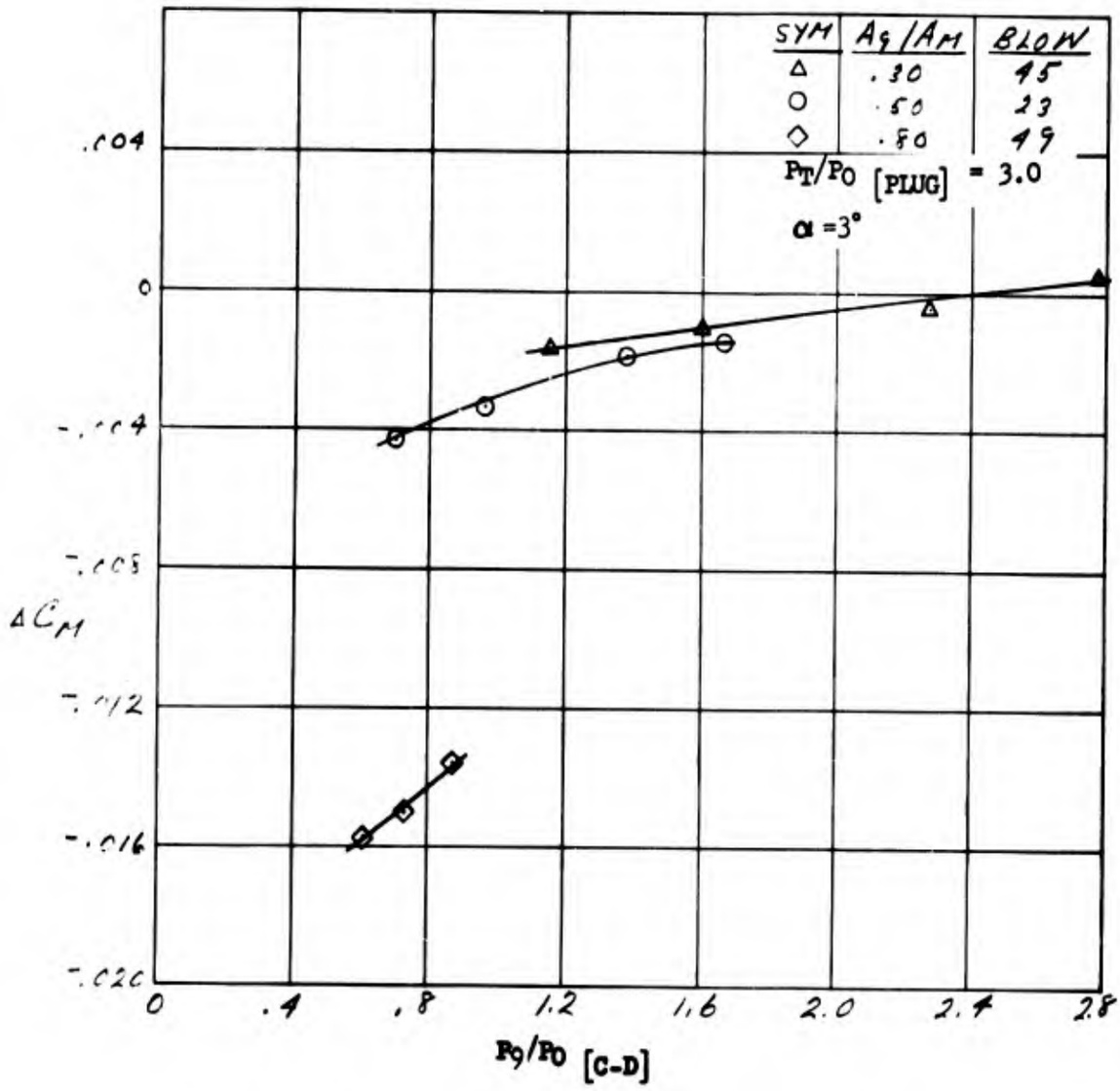

Figure 124. C-D Nozzle Static Pressure Ratio Effects on Pitching Moment Increment - M = 1.27

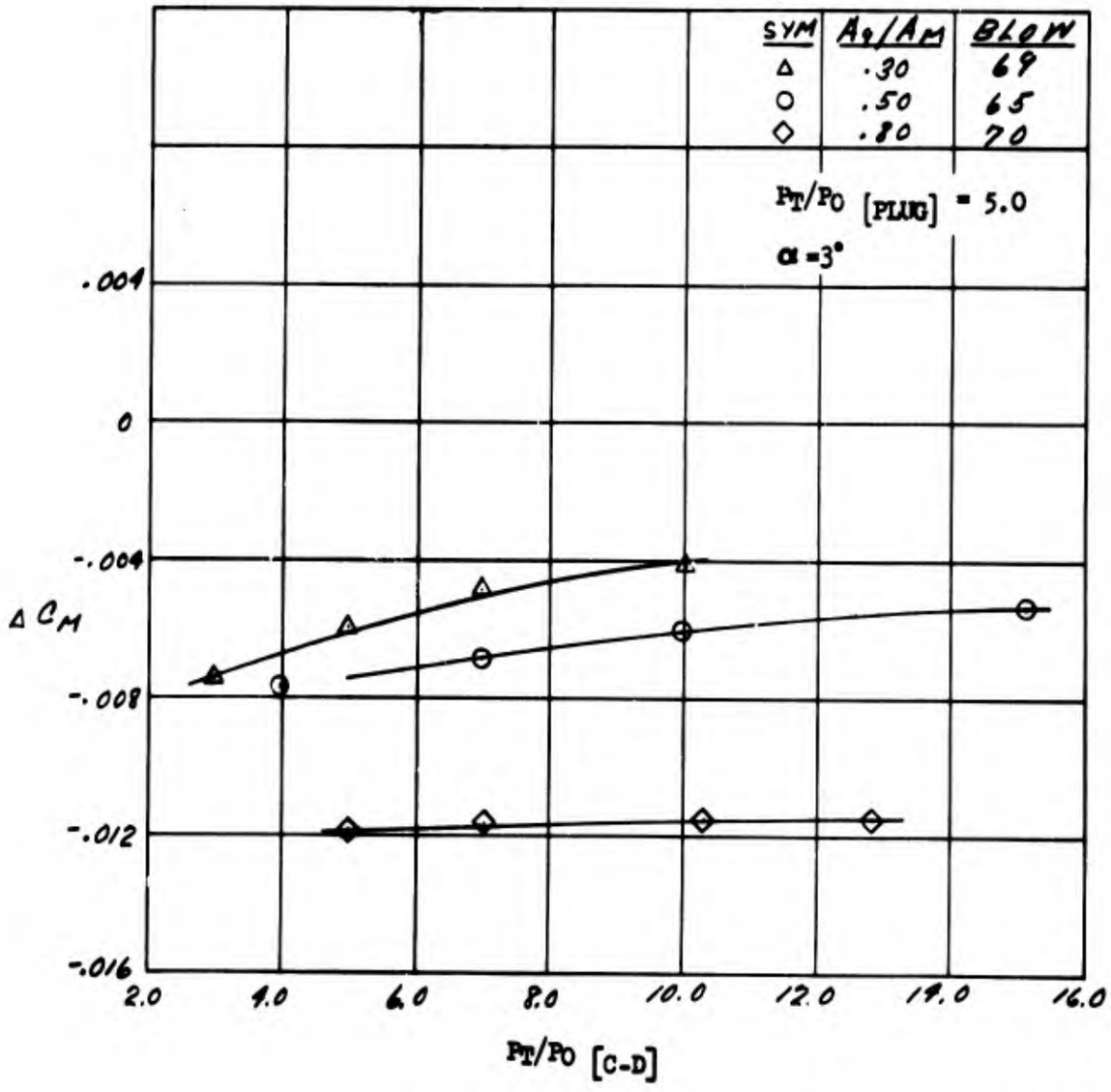

Figure 125. C-D Nozzle Jet Effects On Pitching Moment Increment - M = 1.7

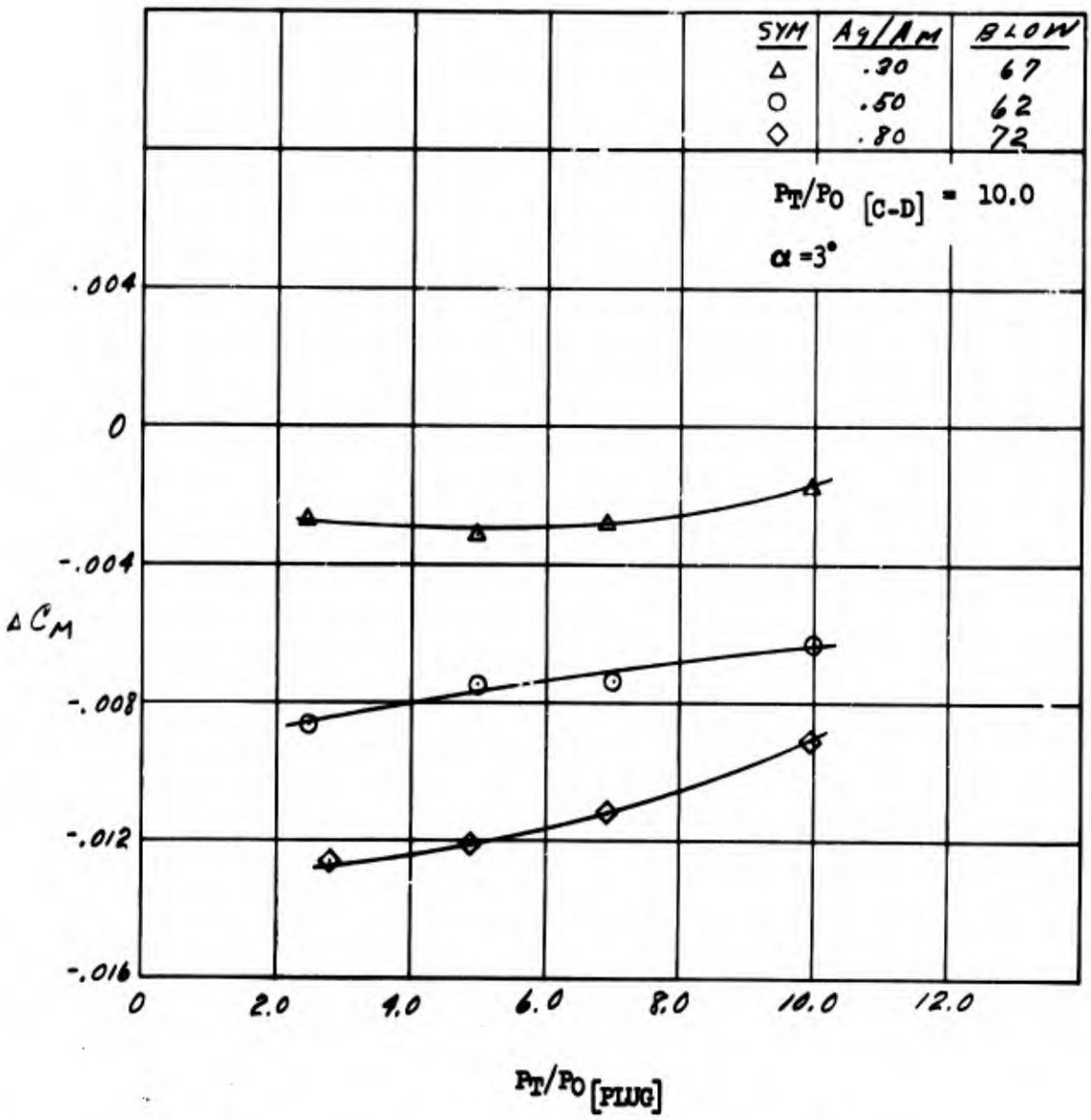

Figure 126. Plug Nozzle Jet Effects On Pitching Moment Increment - M = 1.7

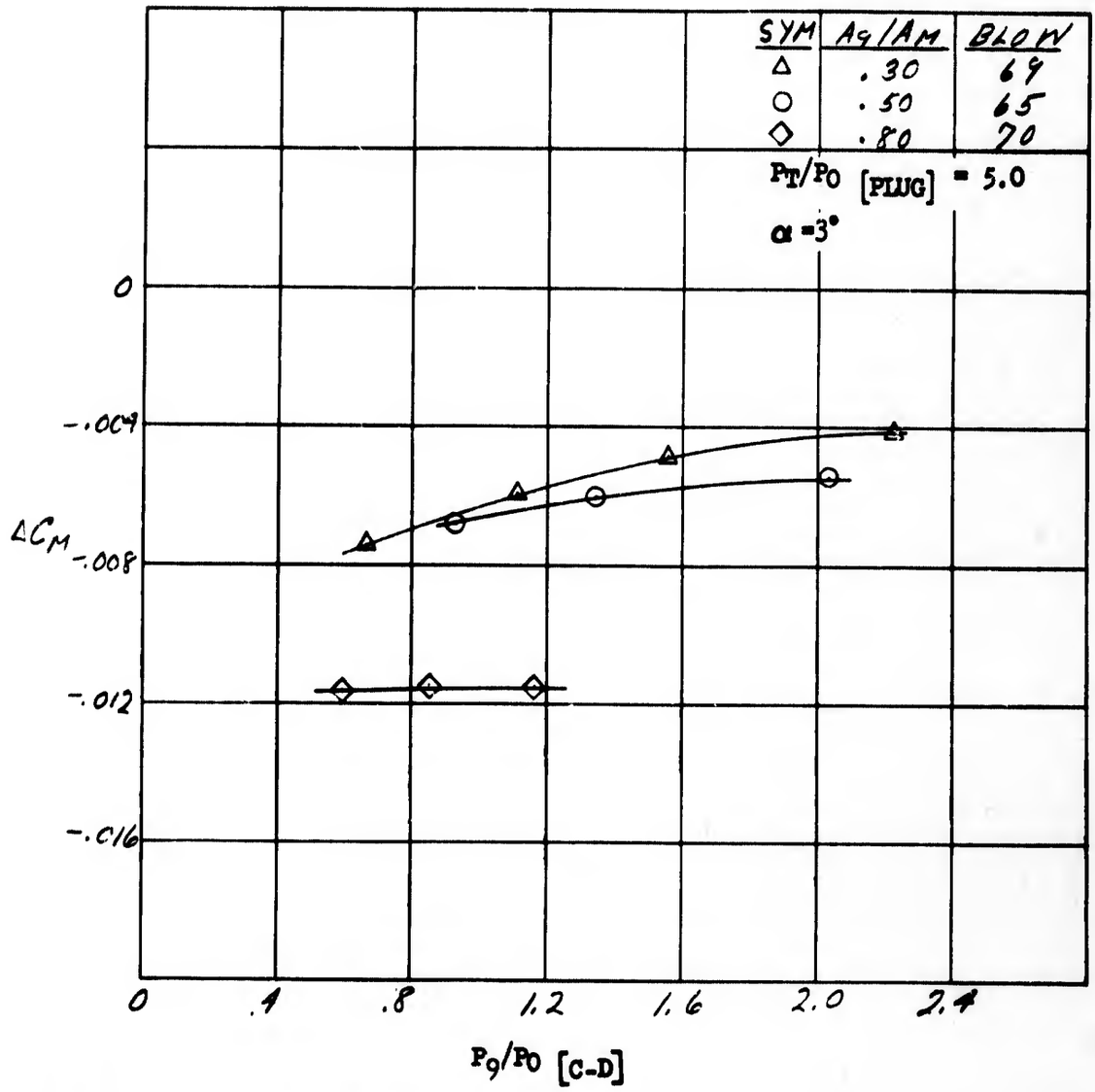

Figure 127. C-D Nozzle Static Pressure Ratio Effects on Pitching Moment Increment - M = 1.7

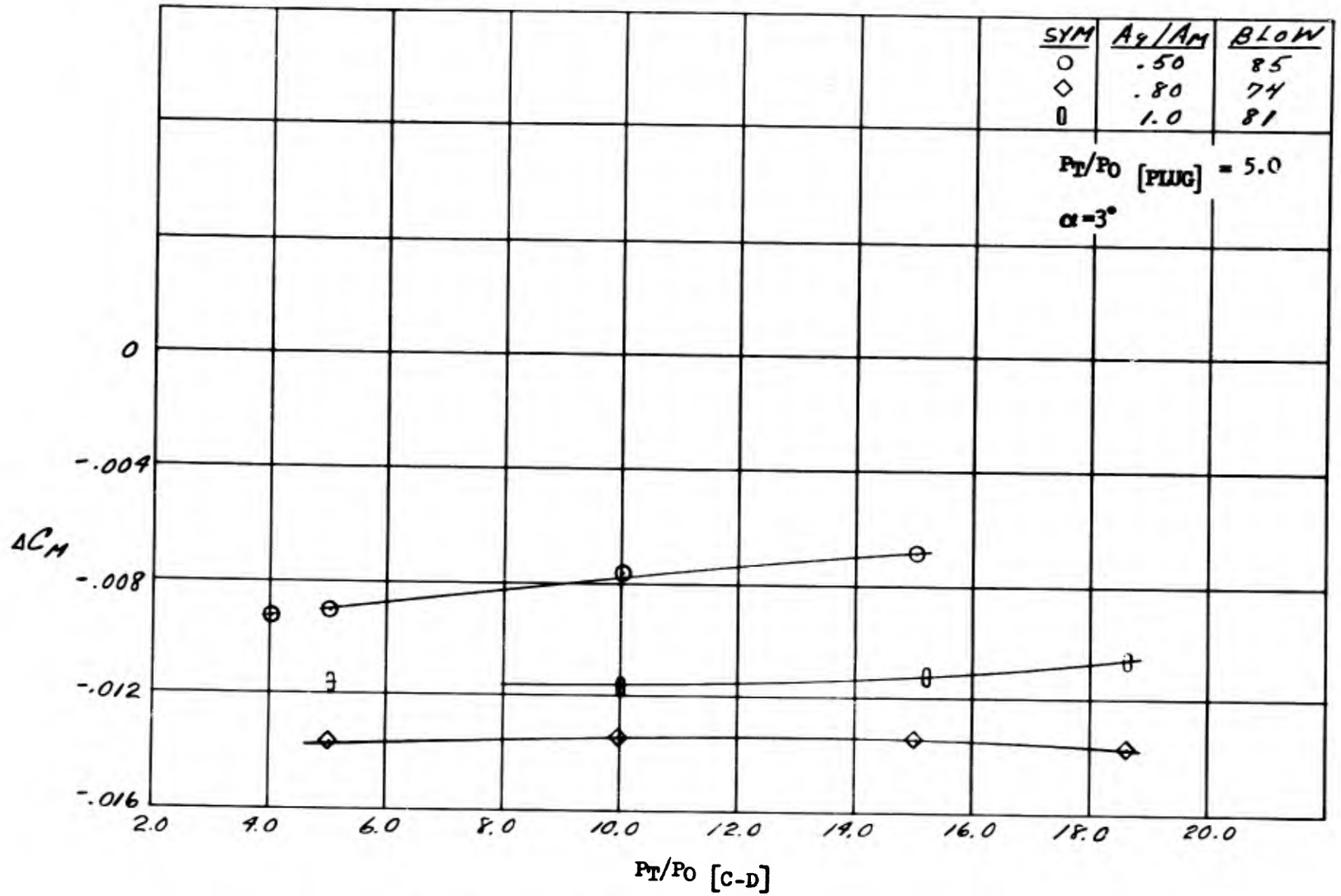

Figure 128. C-D Nozzle Jet Effects On Pitching Moment Increment - M = 2.0

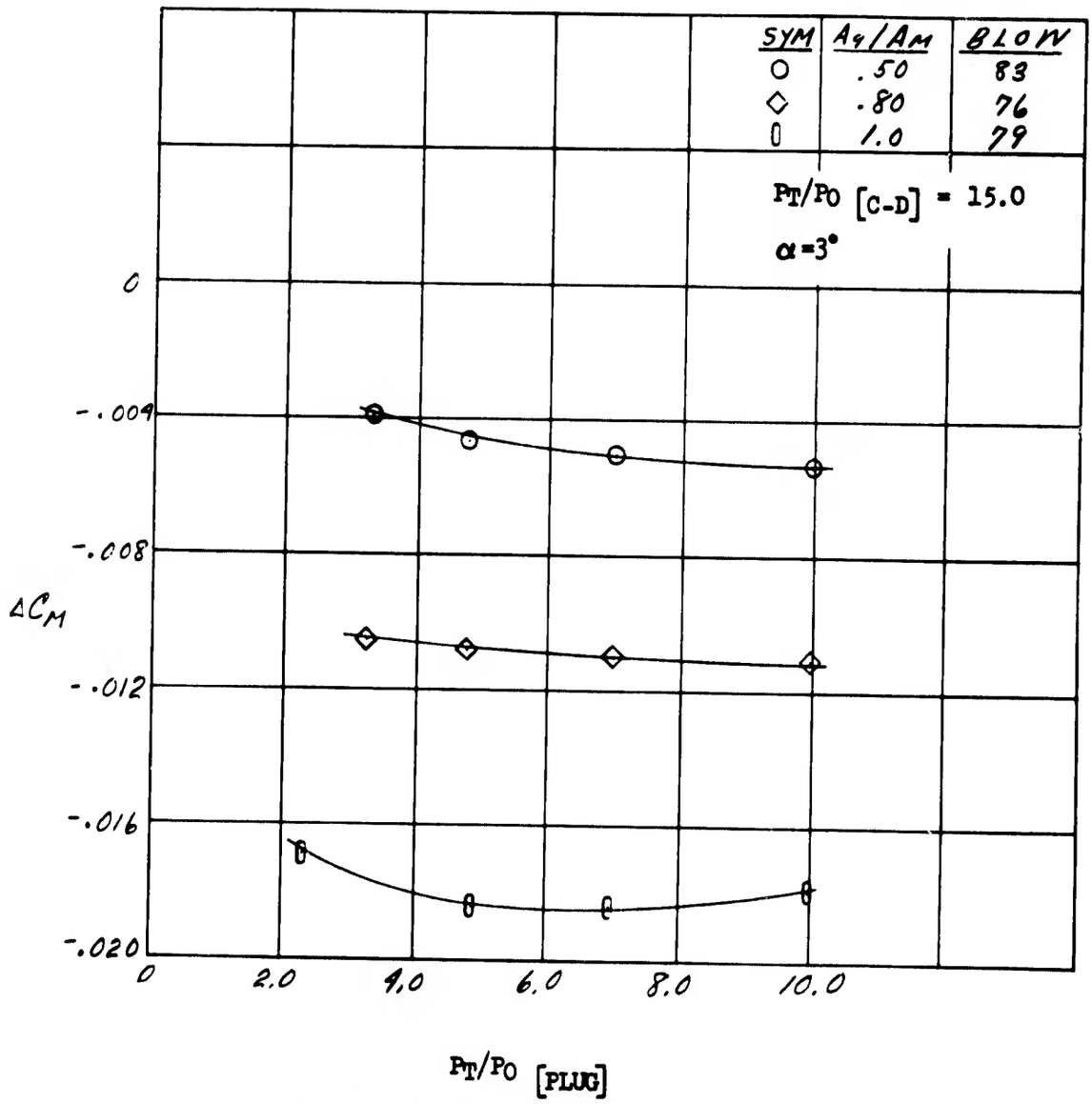

Figure 129. Plug Nozzle Jet Effects On Pitching Moment Increment - M = 2.0

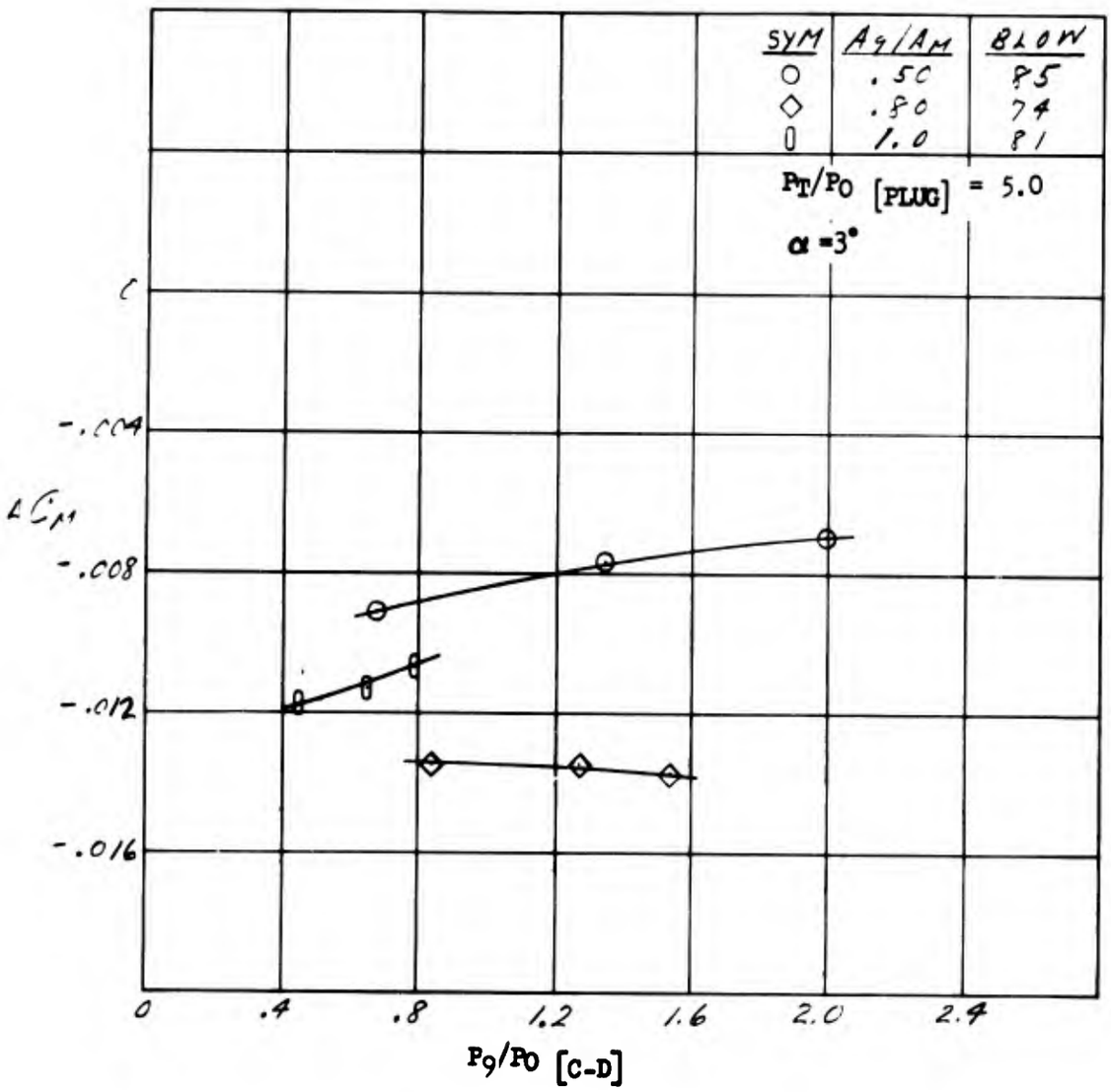

Figure 130. C-D Nozzle Static Pressure Ratio Effects on Pitching Moment Increment - M = 2.0

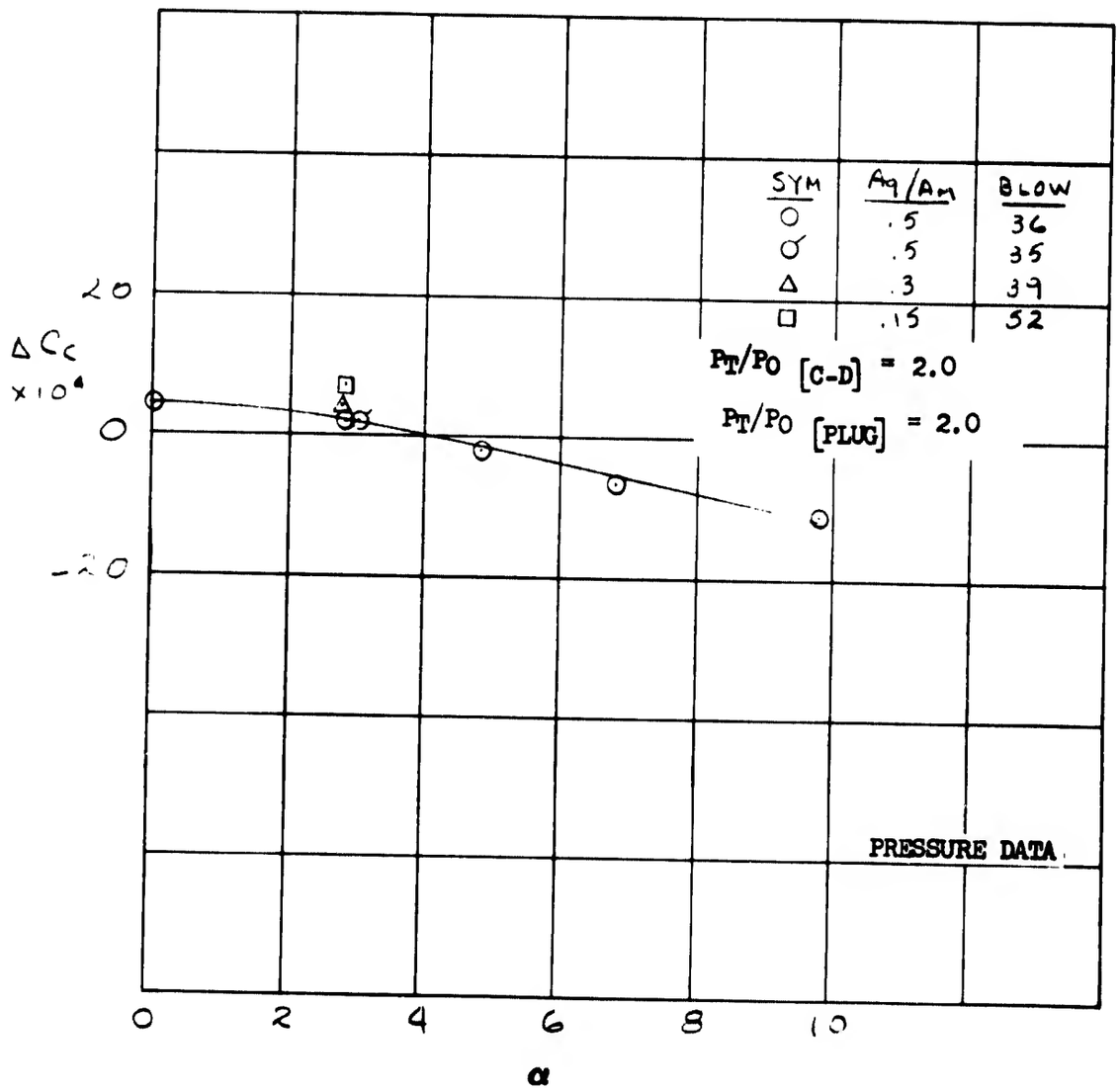

Figure 131. Angle of Attack Effects - M=.614

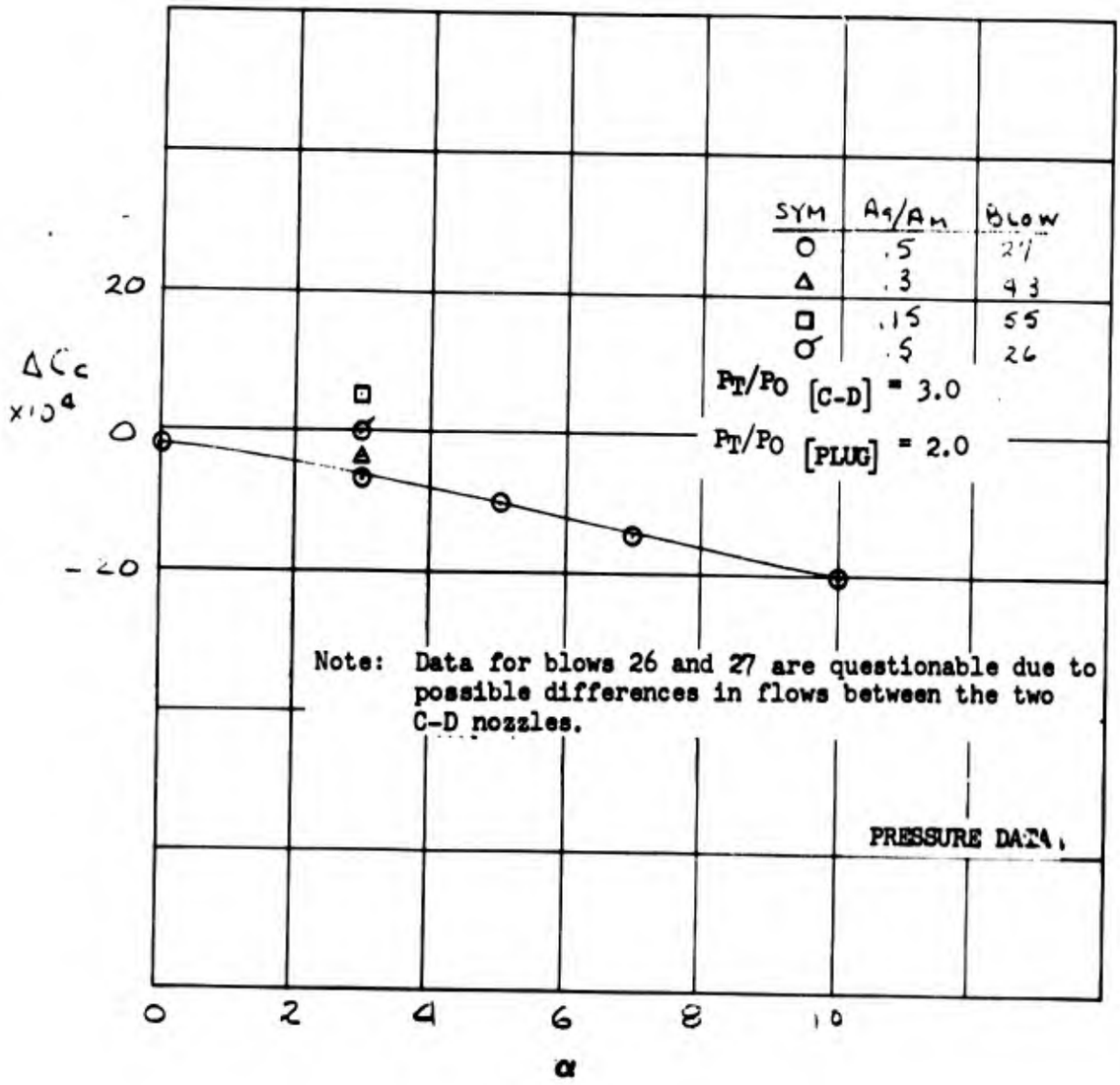

Figure 132. Angle of Attack Effects - M=.85

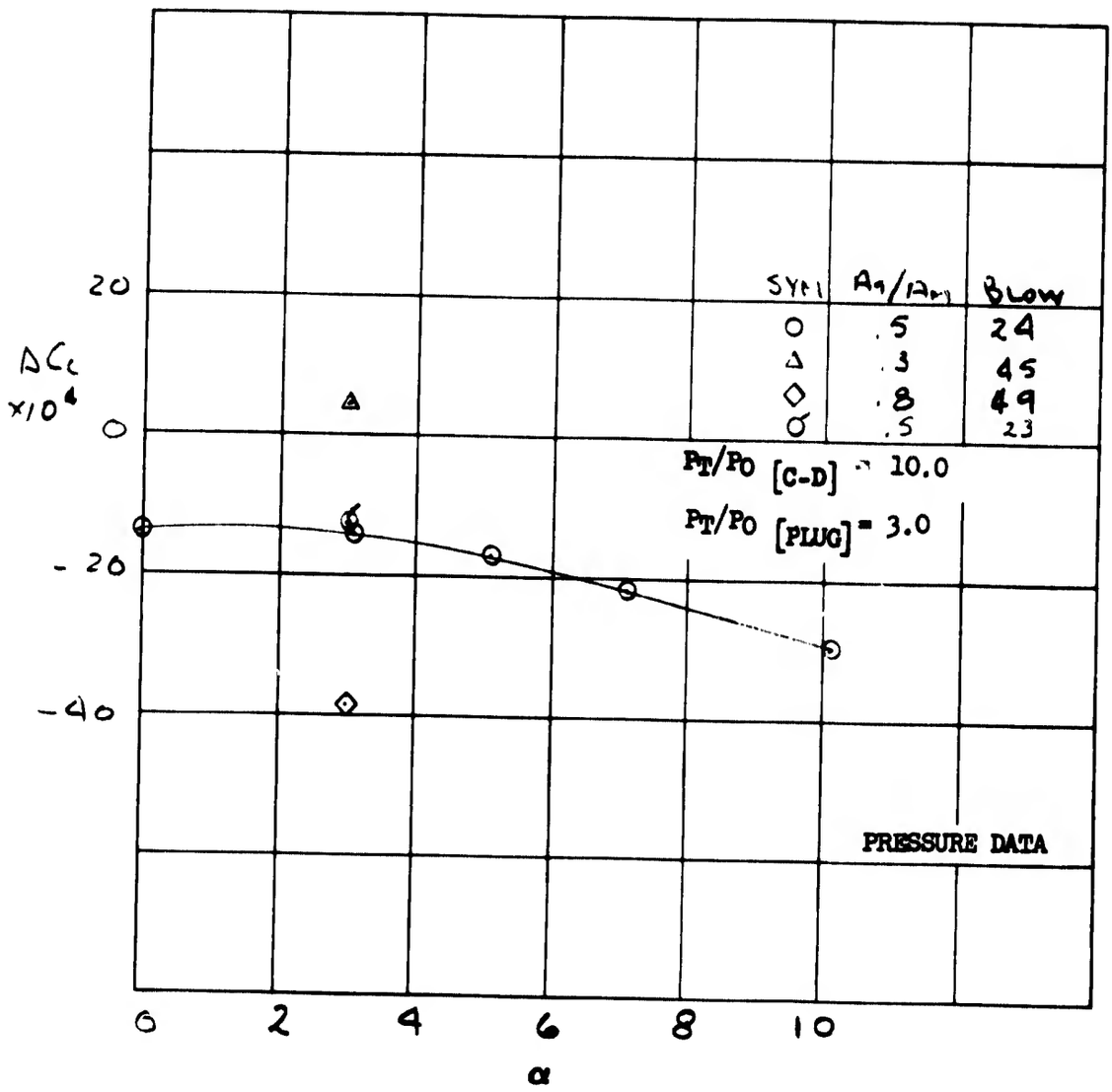

Figure 133. Angle of Attack Effects - M=1.27

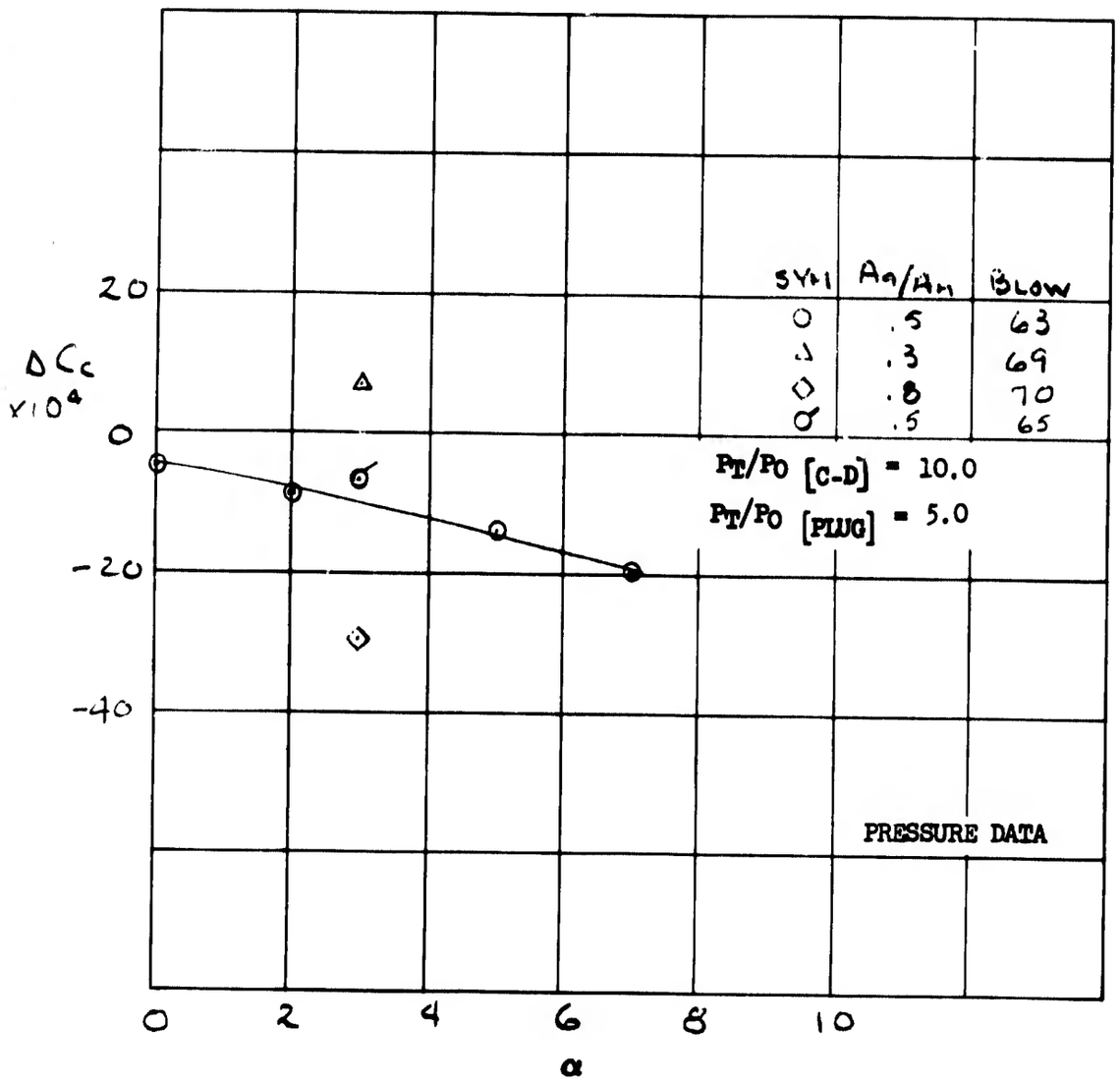

Figure 134. Angle of Attack Effects - M=1.7

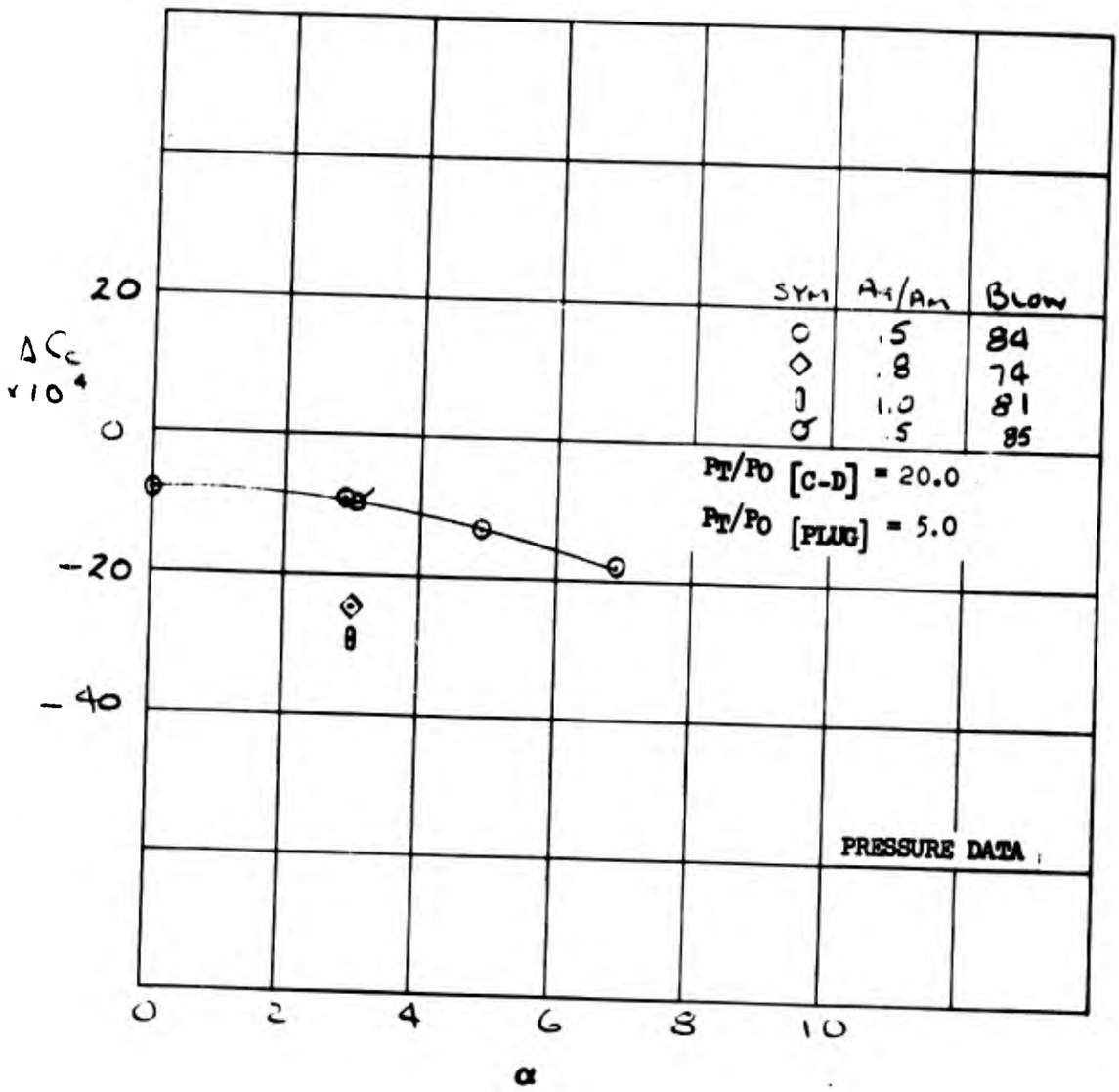

Figure 135. Angle of Attack Effects - M=2.0

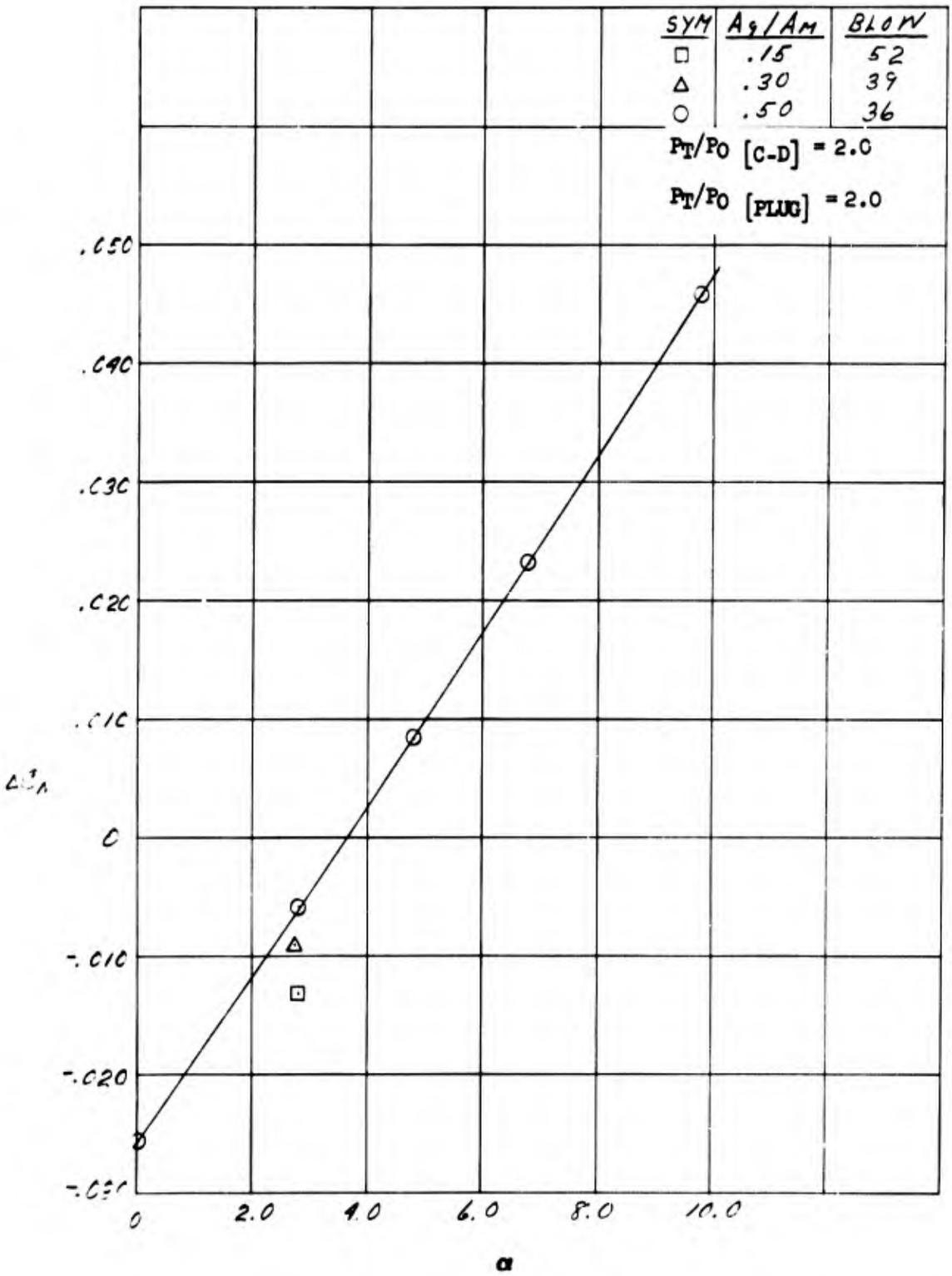

Figure 136. Angle of Attack Effects On Normal Force Increment - M = .614

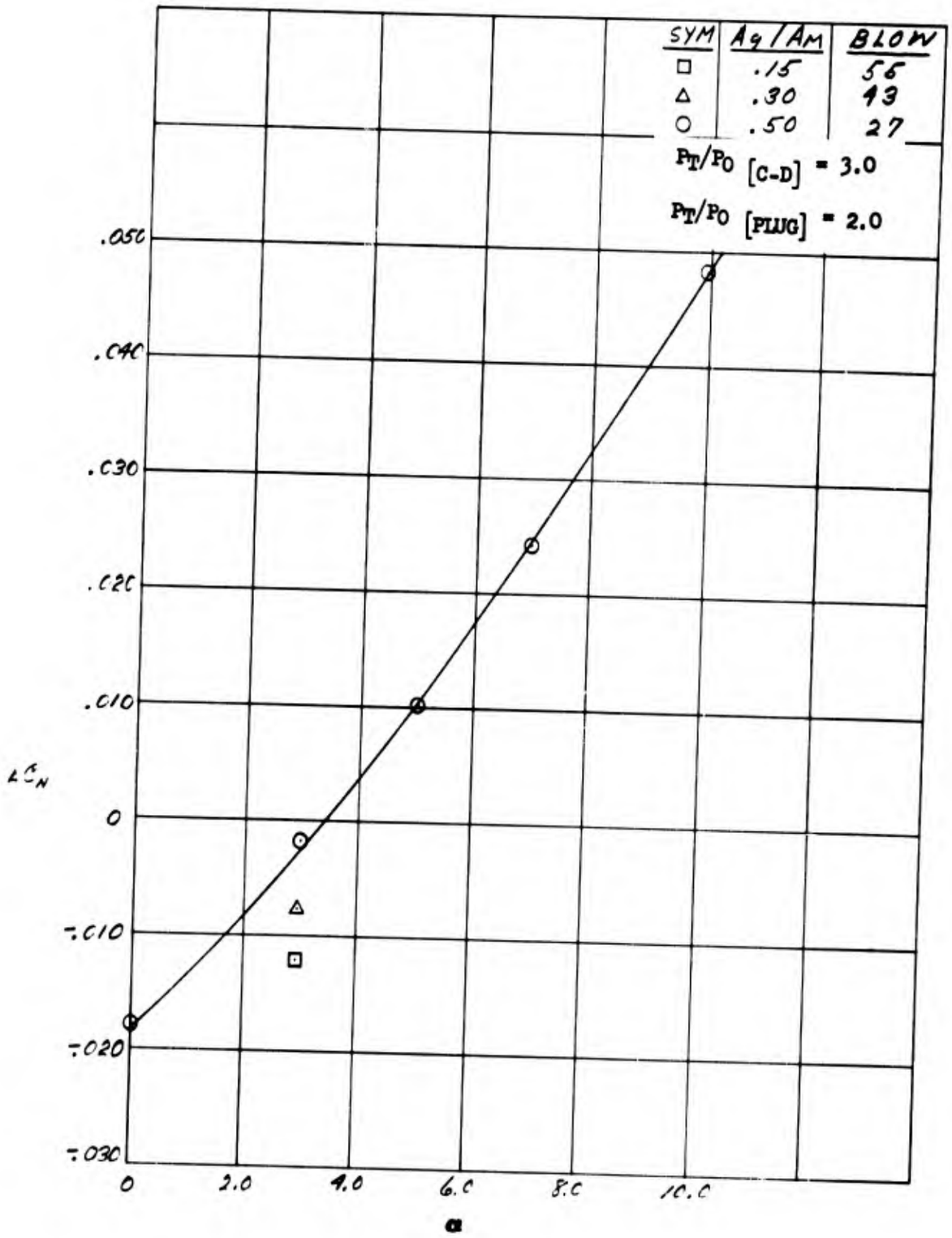

Figure 137. Angle of Attack Effects On Normal Force Increment - M = .85

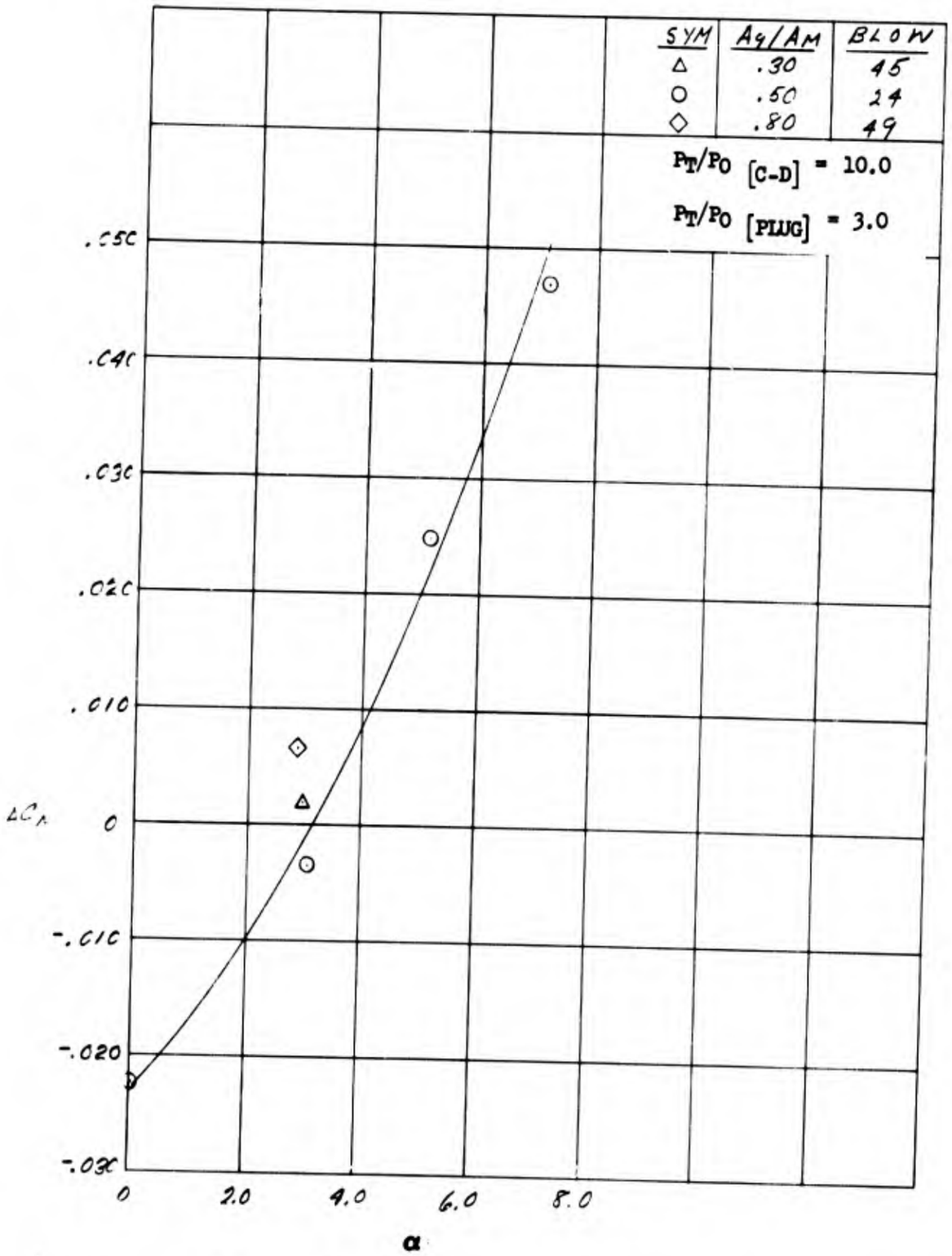

Figure 138. Angle of Attack Effects On Normal Force Increment - M = 1.27

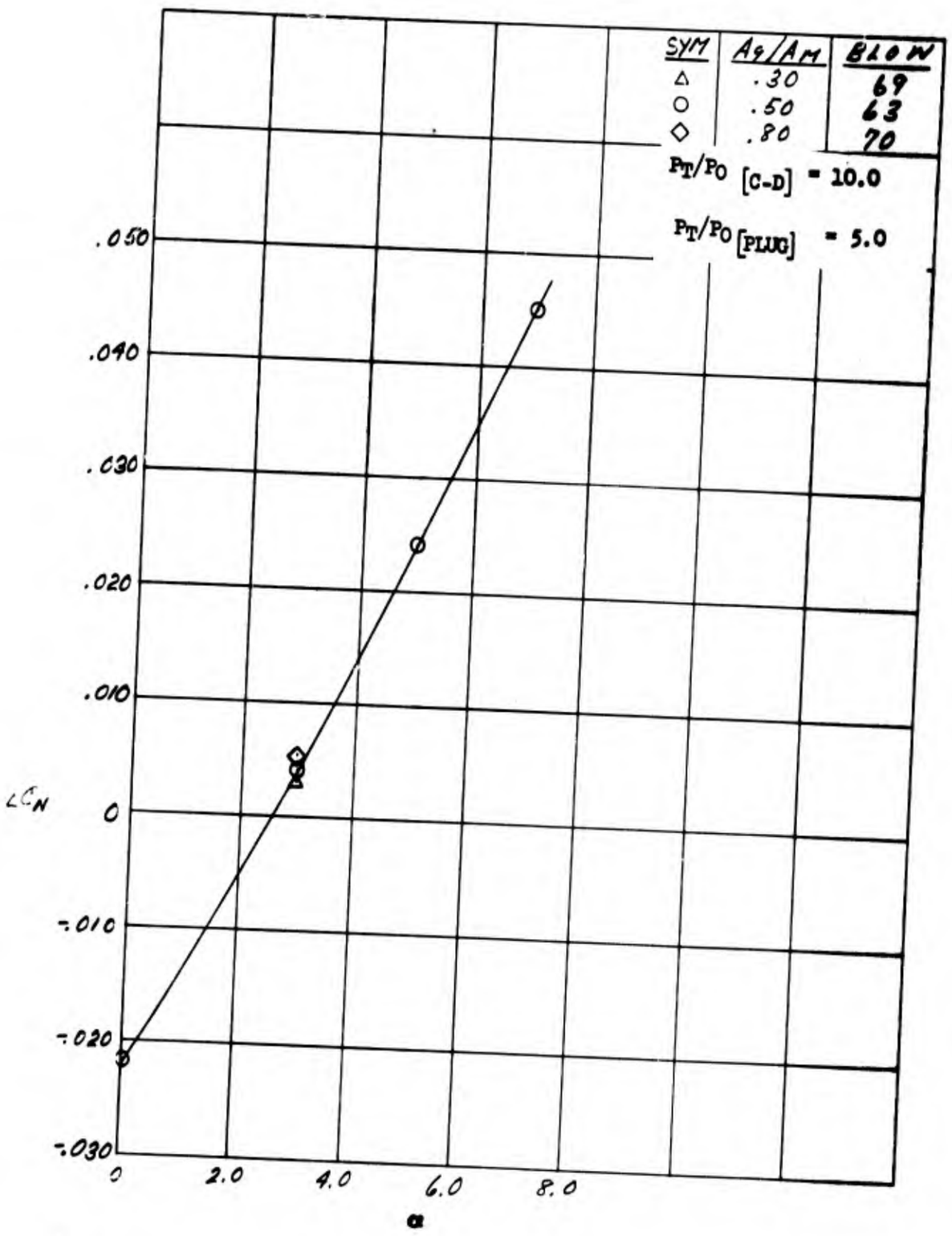

Figure 139. Angle of Attack Effects On Normal Force Increment - M = 1.7

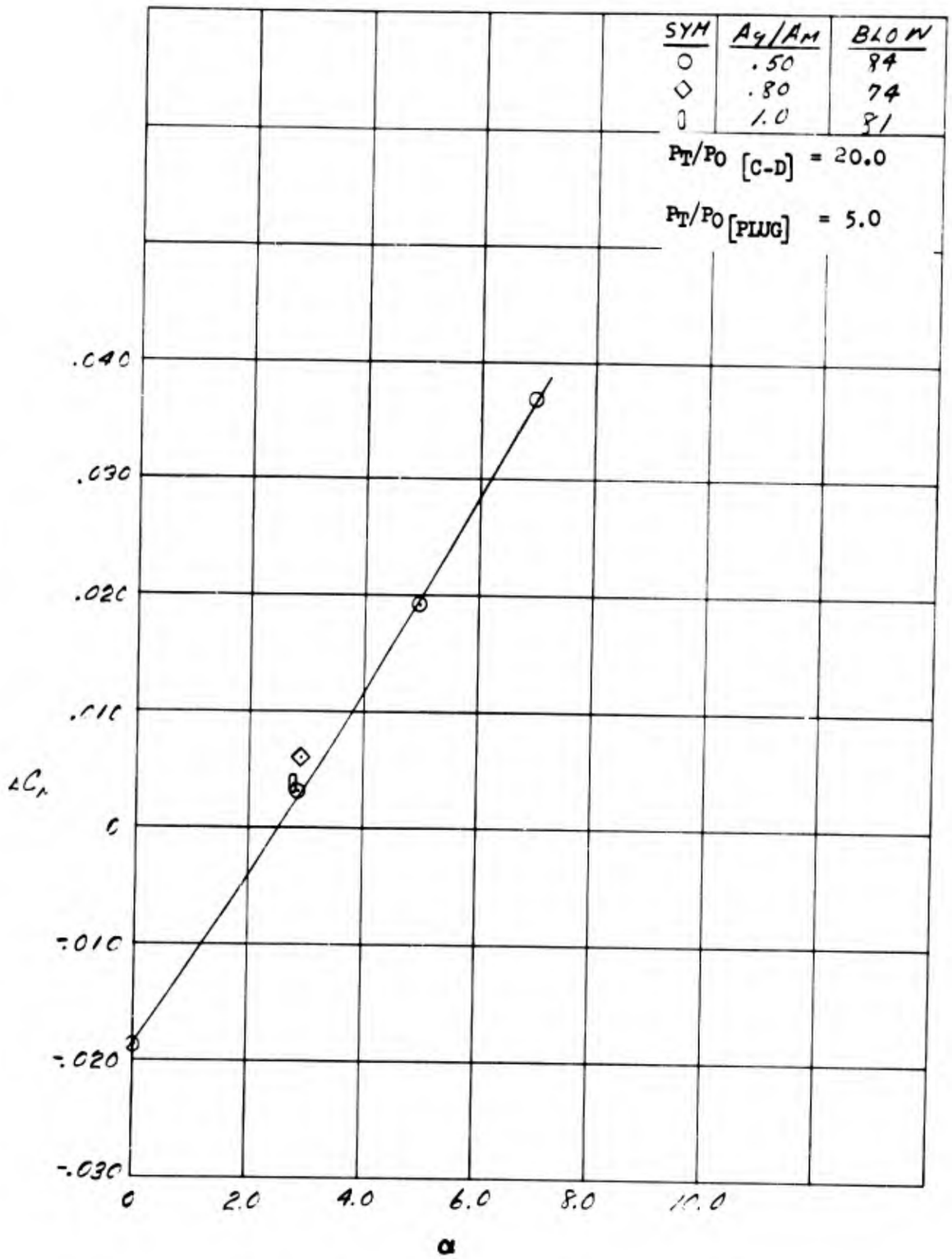

Figure 140. Angle of Attack Effects On Normal Force Increment - M = 2.0

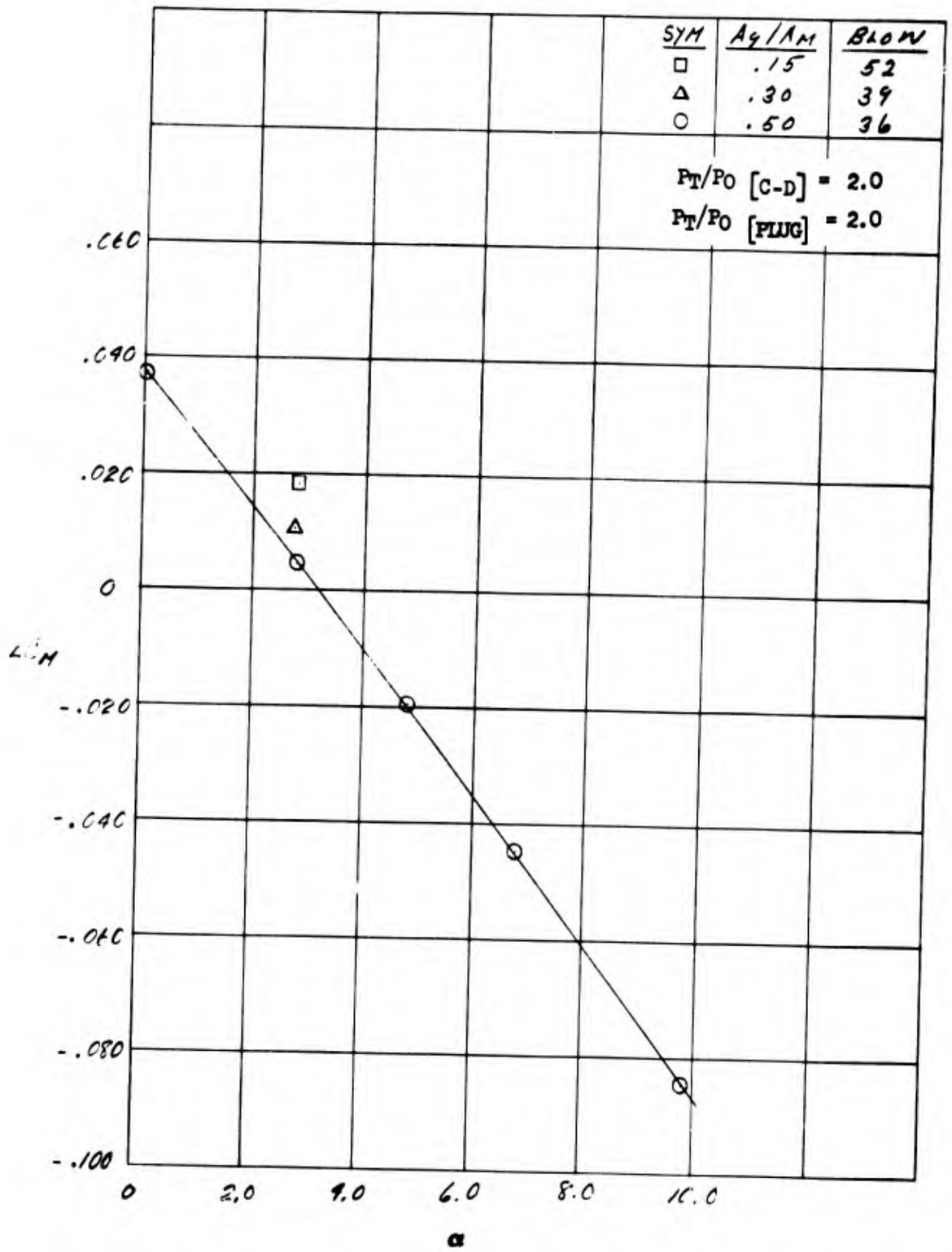

Figure 141. Angle of Attack Effects On Pitching Moment Increment - M = .614

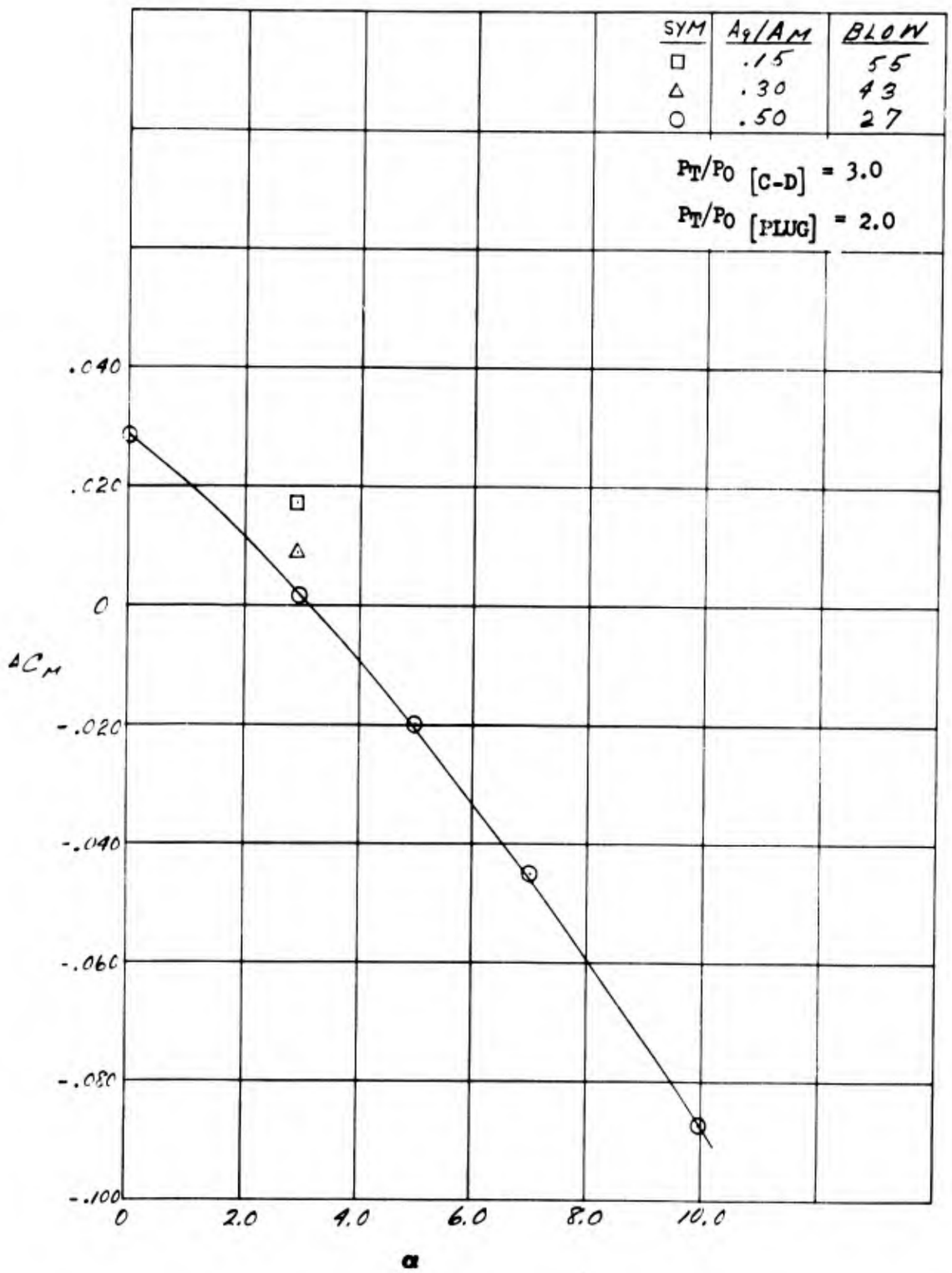

Figure 142. Angle of Attack Effects On Pitching Moment Increment - M = .85

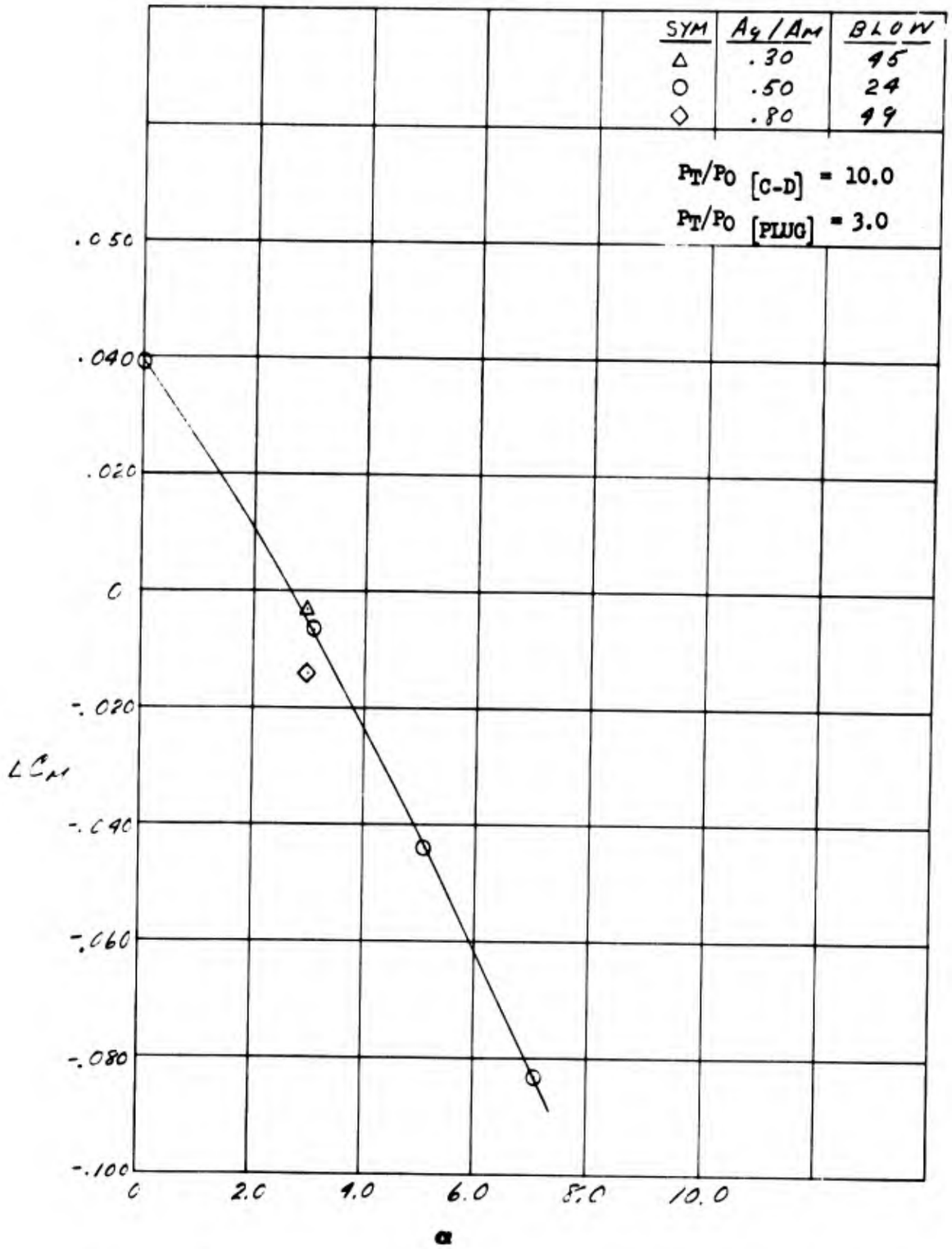

Figure 143. Angle of Attack Effects On Pitching Moment Increment - M = 1.27

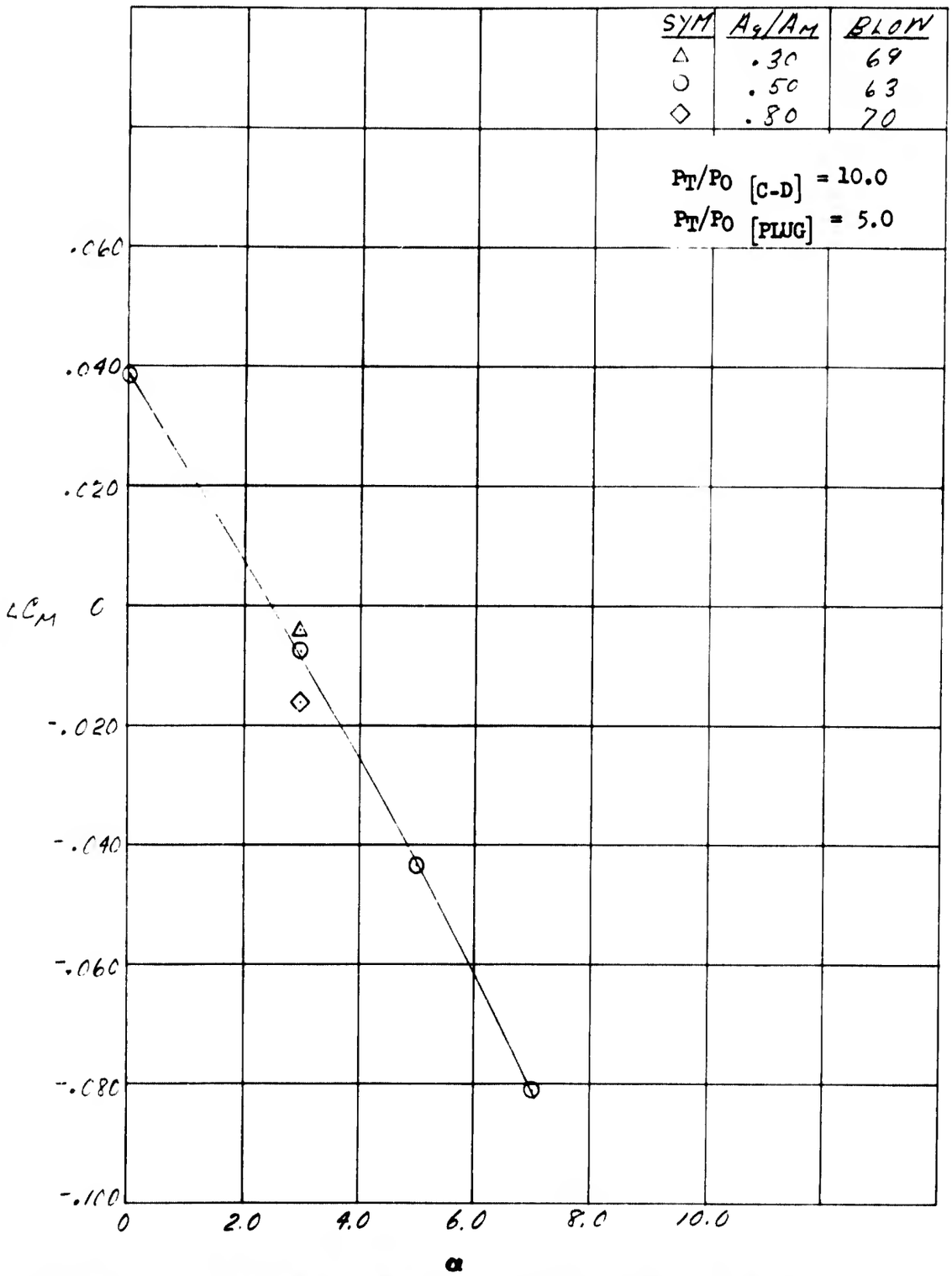

Figure 144. Angle of Attack Effects On Pitching Moment Increment - M = 1.7

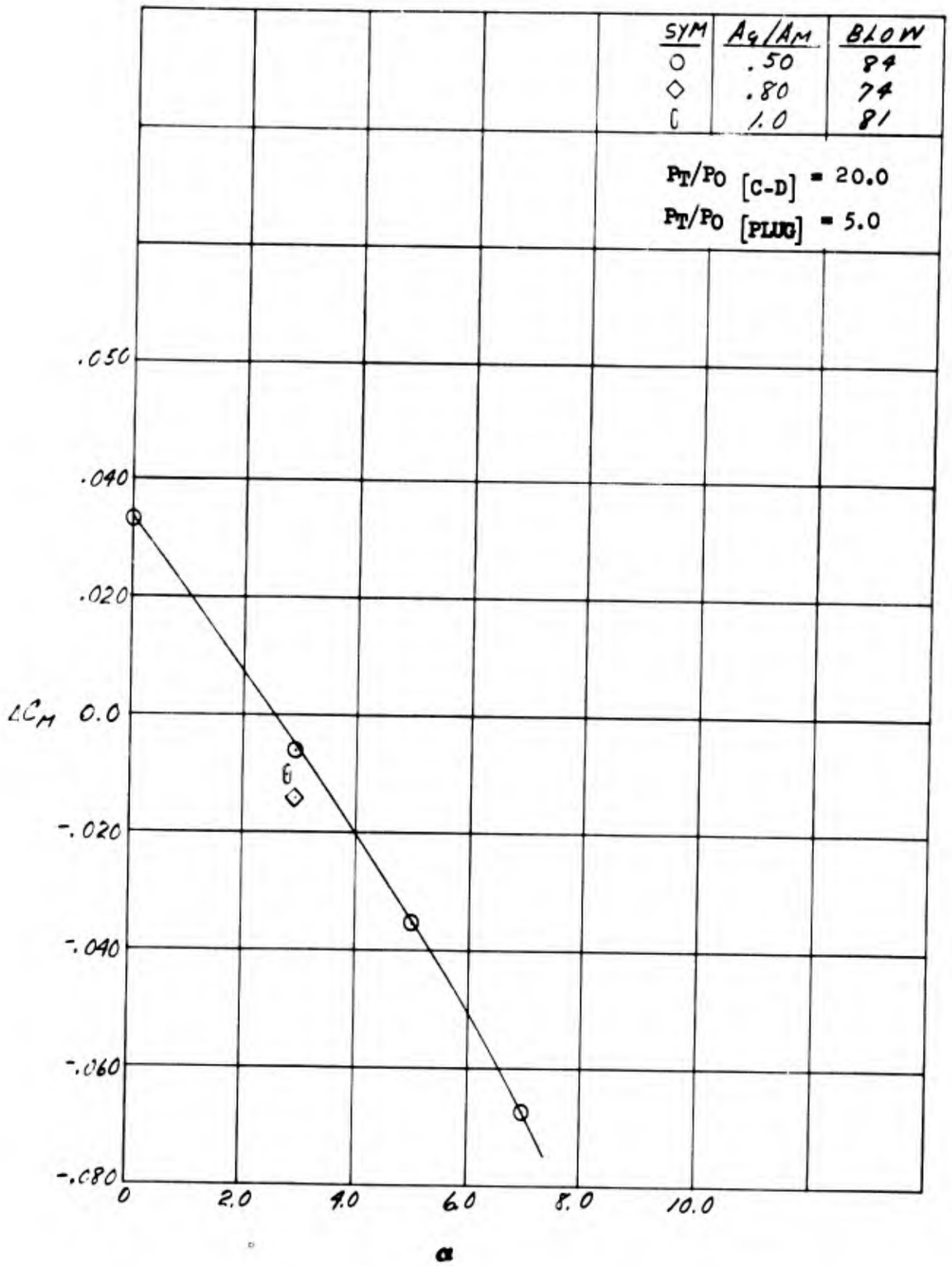

Figure 145. Angle of Attack Effects On Pitching Moment Increment - M = 2.0

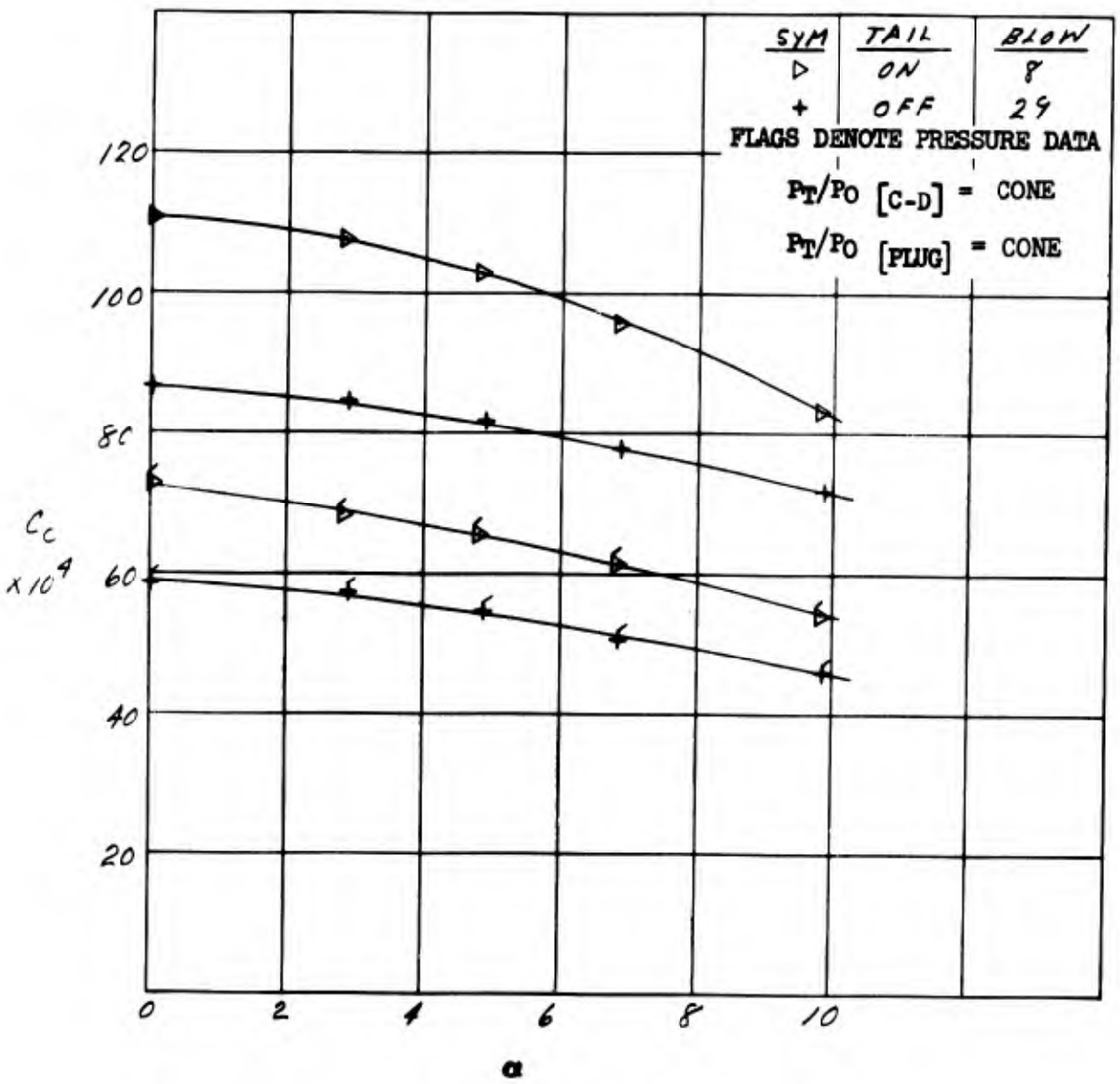

Figure 146. Effect of Horizontal Tail On Chord Force - M = .85

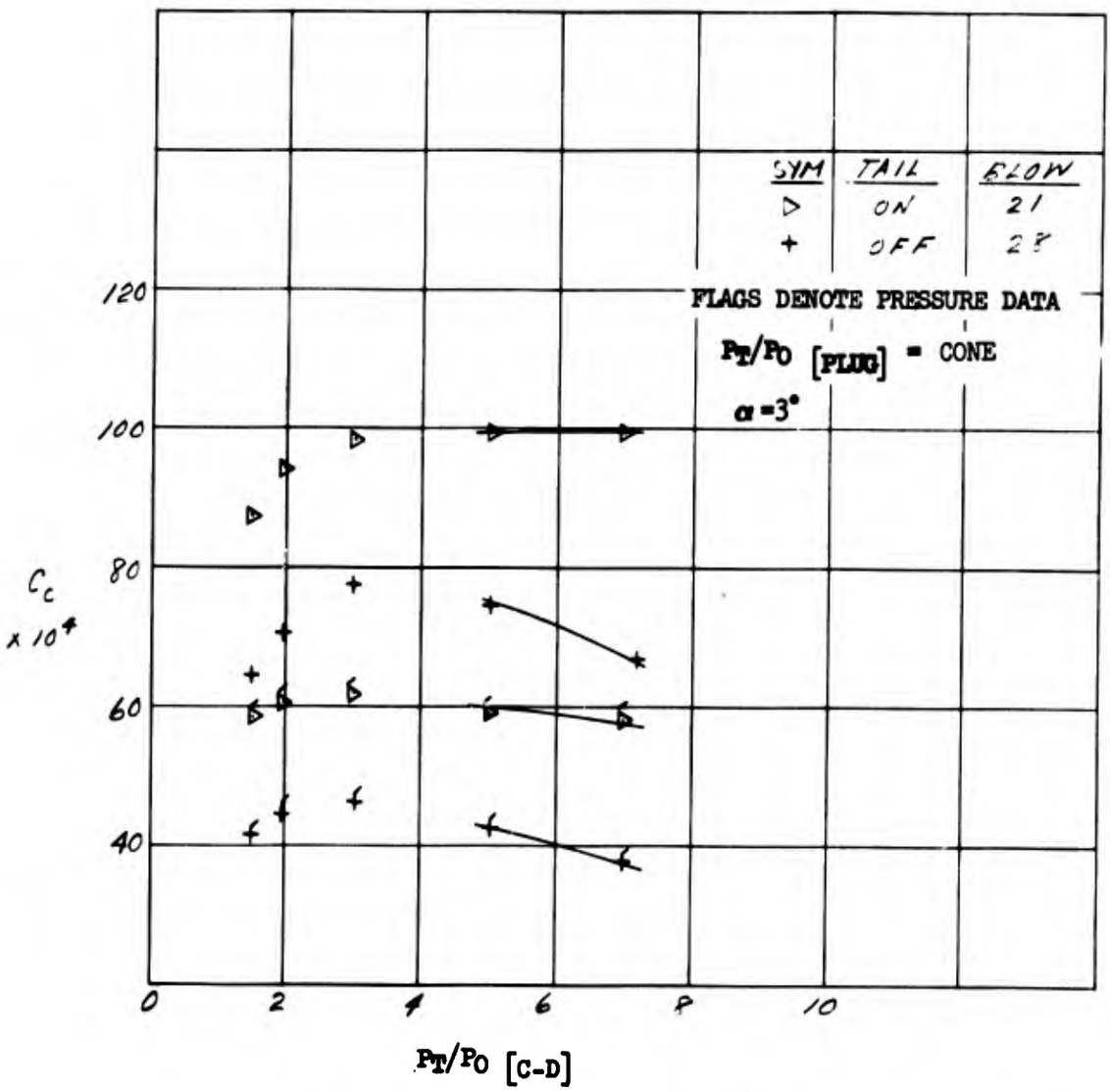

Figure 147. Effect of Horizontal Tail On Chord Force - M = .85

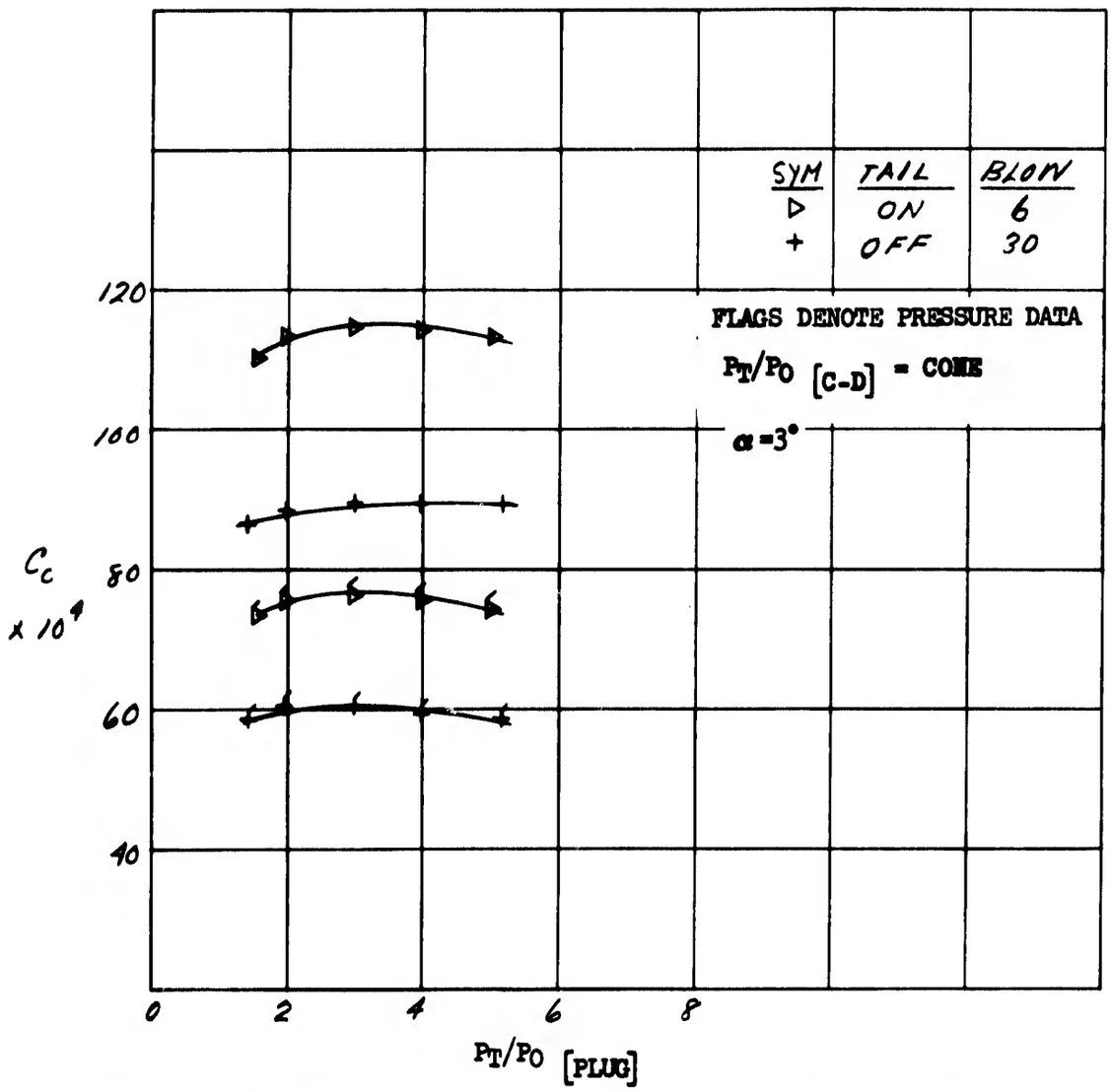

Figure 148. Effect of Horizontal Tail On Chord Force - M = .85

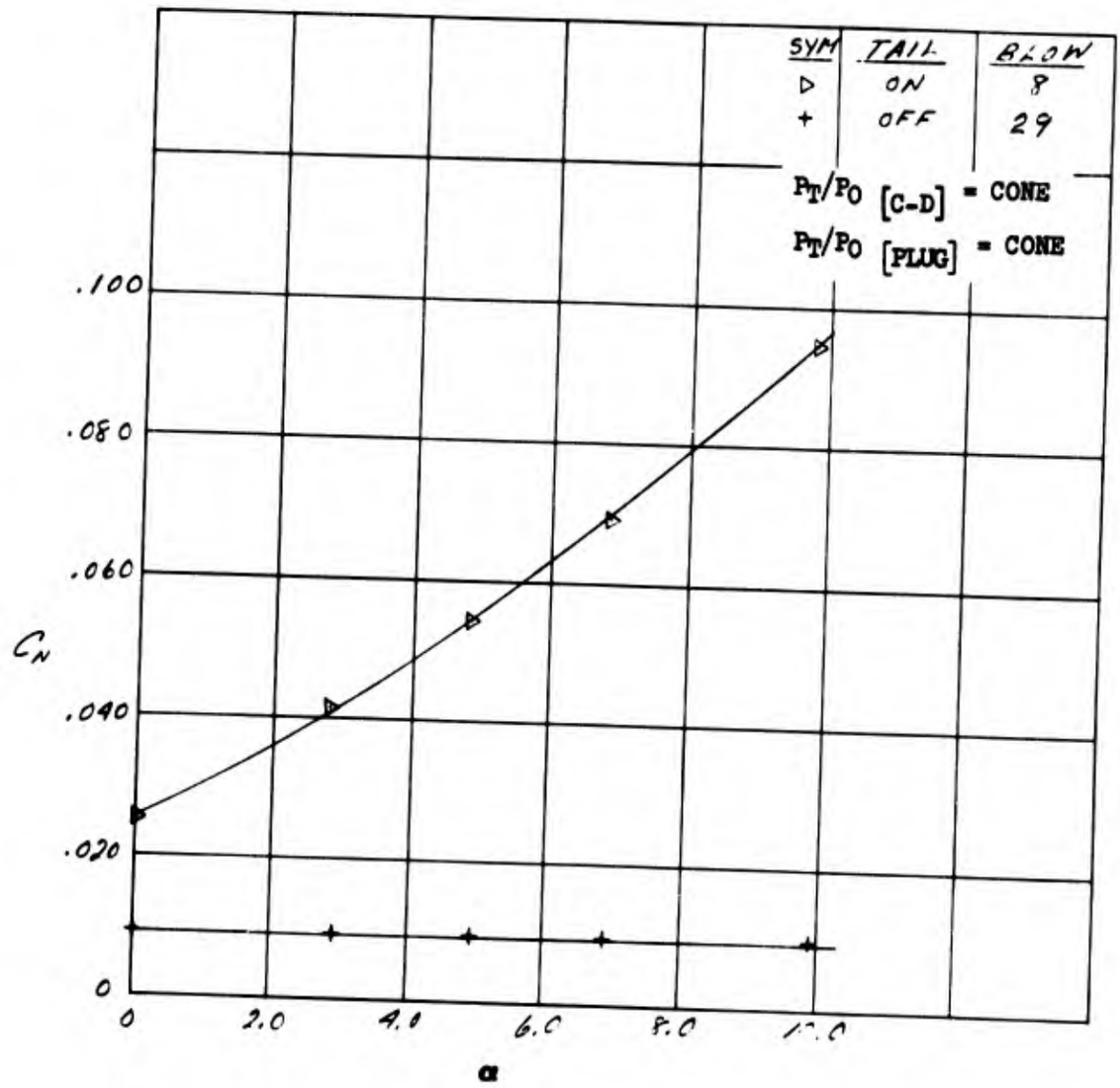

Figure 149. Effect of Horizontal Tail On Normal Force - M = .85

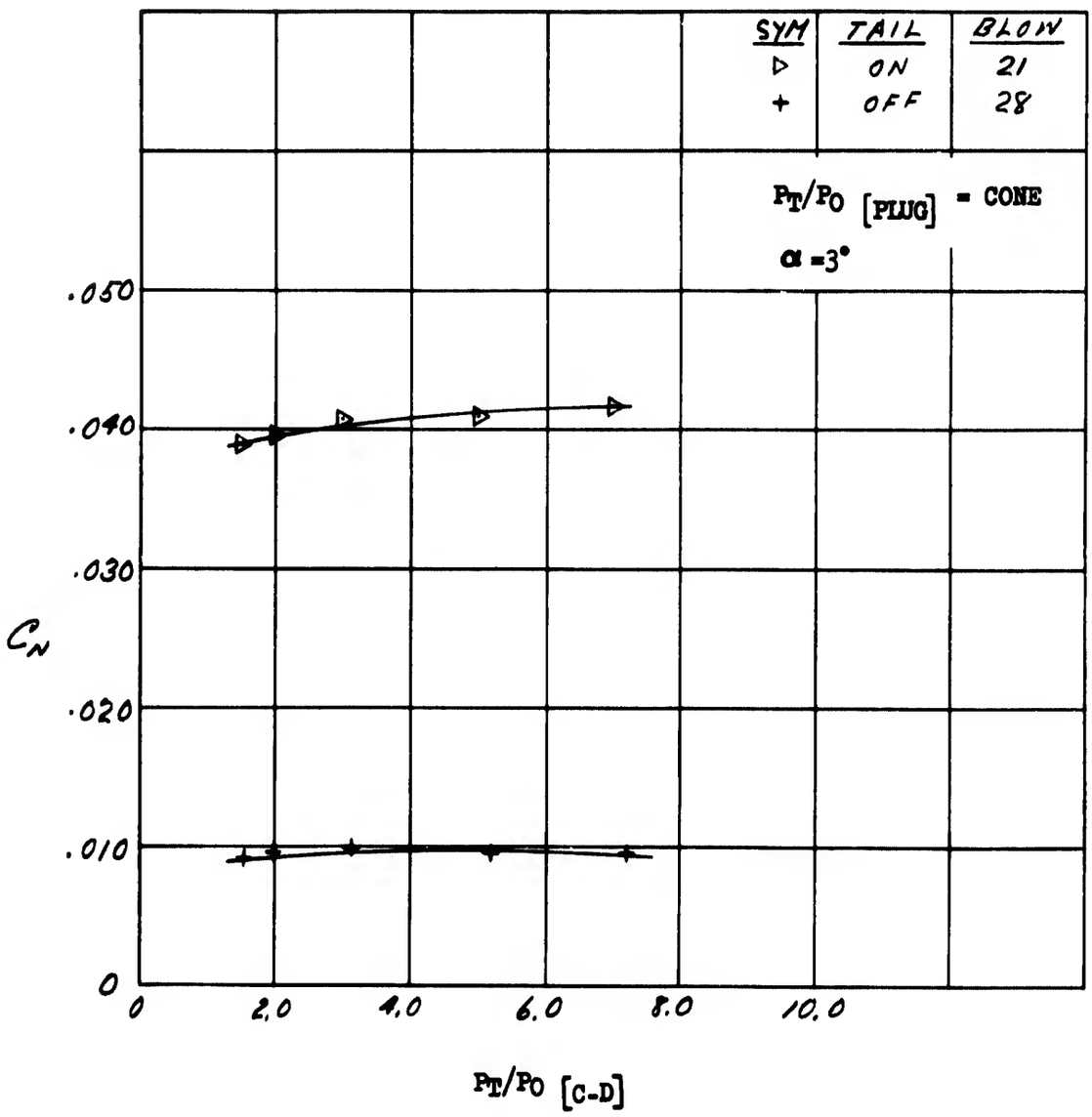

Figure 150. Effect of Horizontal Tail on Normal Force - M = .85.

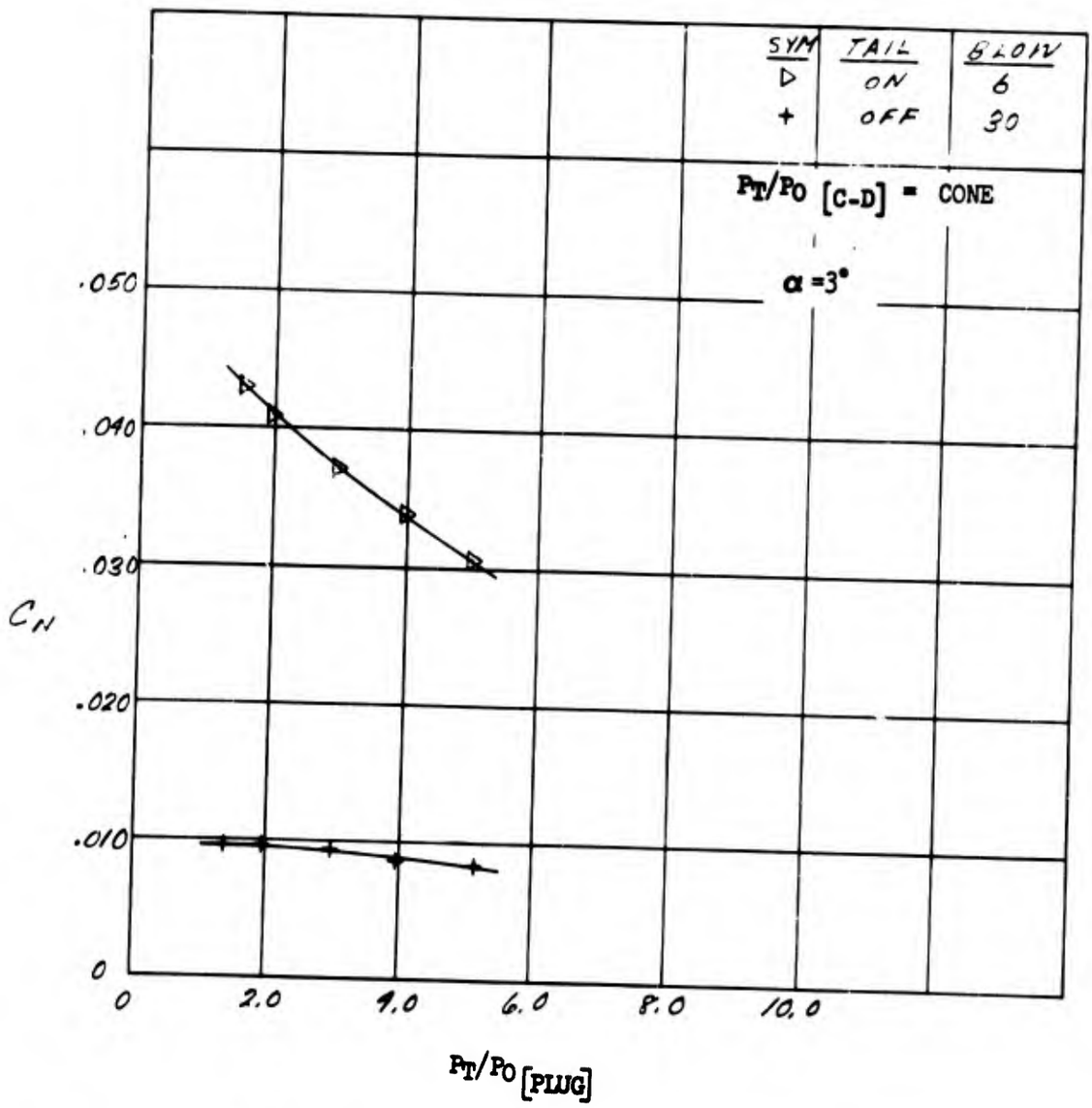

Figure 151. Effect of Horizontal Tail On Normal Force - M = .85

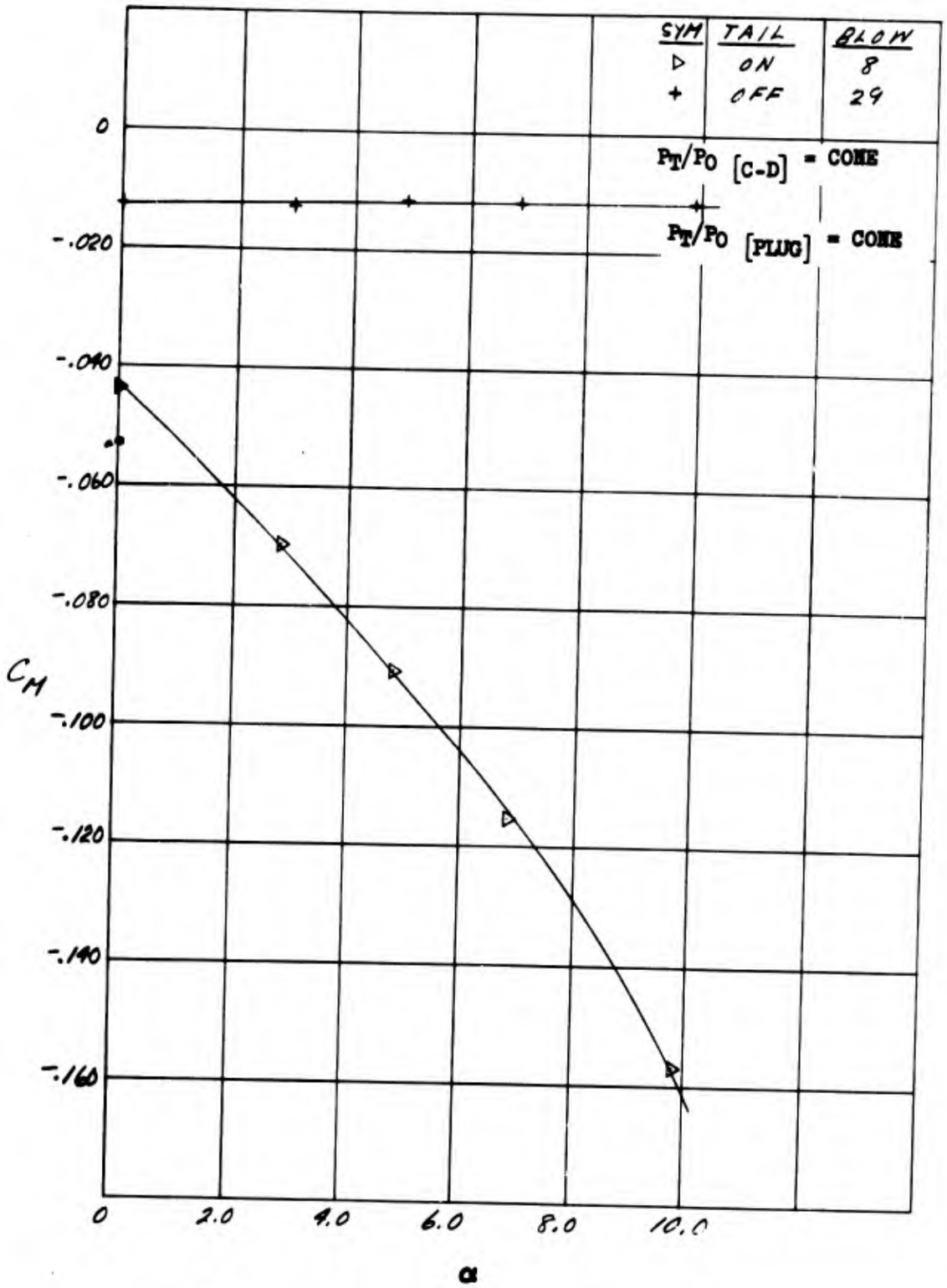

Figure 152. Effect of Horizontal Tail On Pitching Moment - M = .85

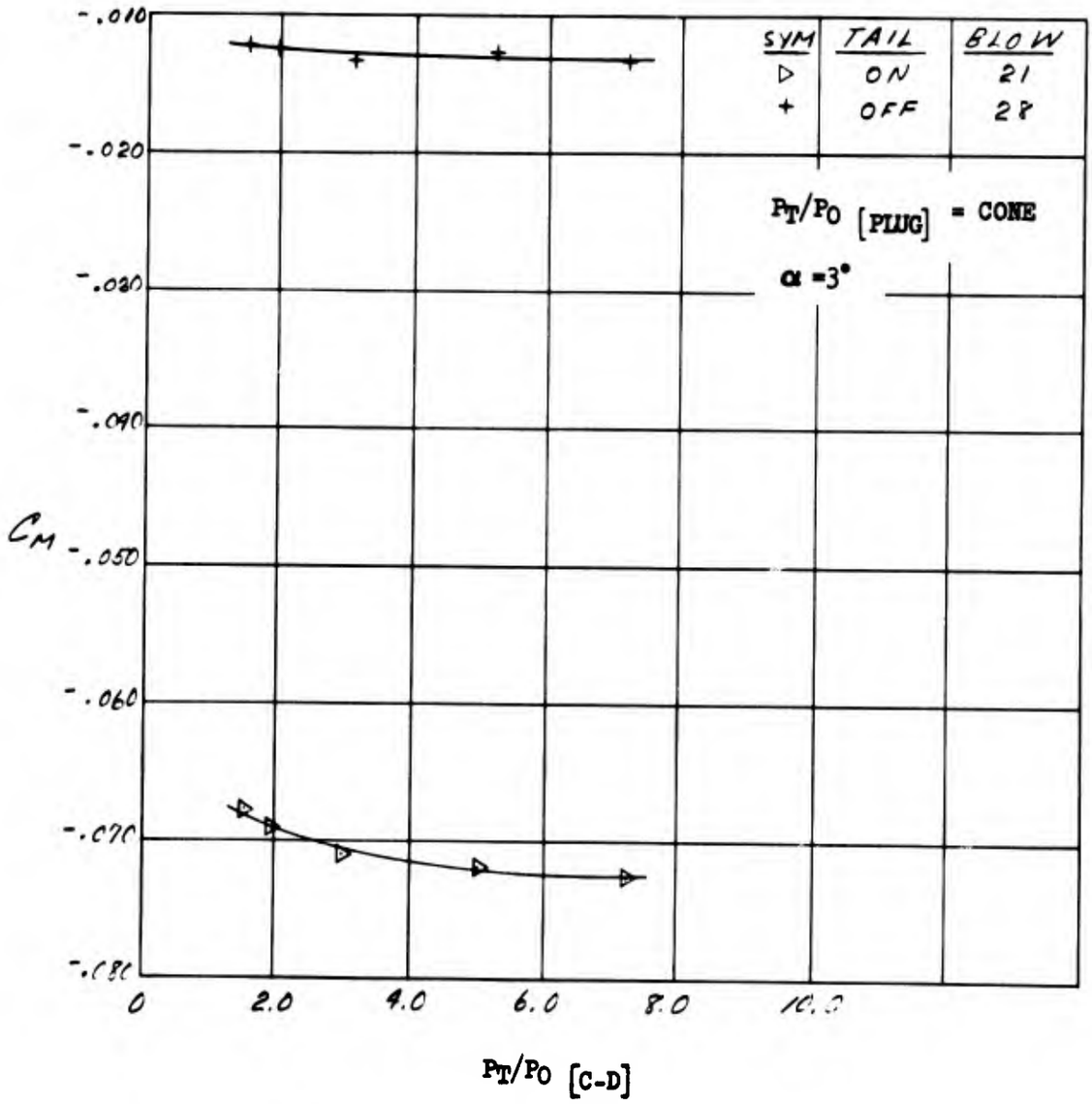

Figure 153. Effect of Horizontal Tail On Pitching Moment - M = .85

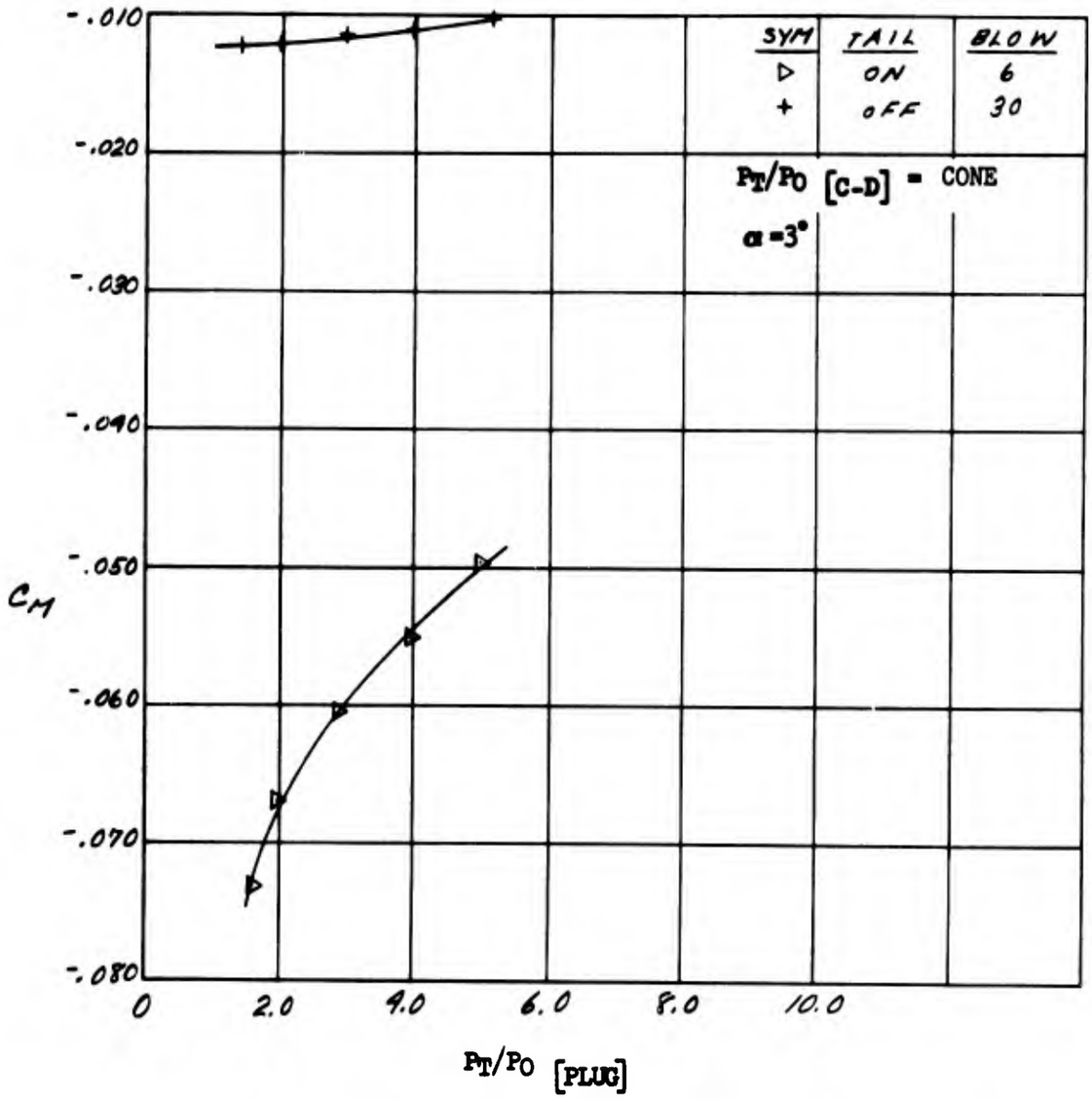

Figure 154. Effect of Horizontal Tail On Pitching Moment - M = .85

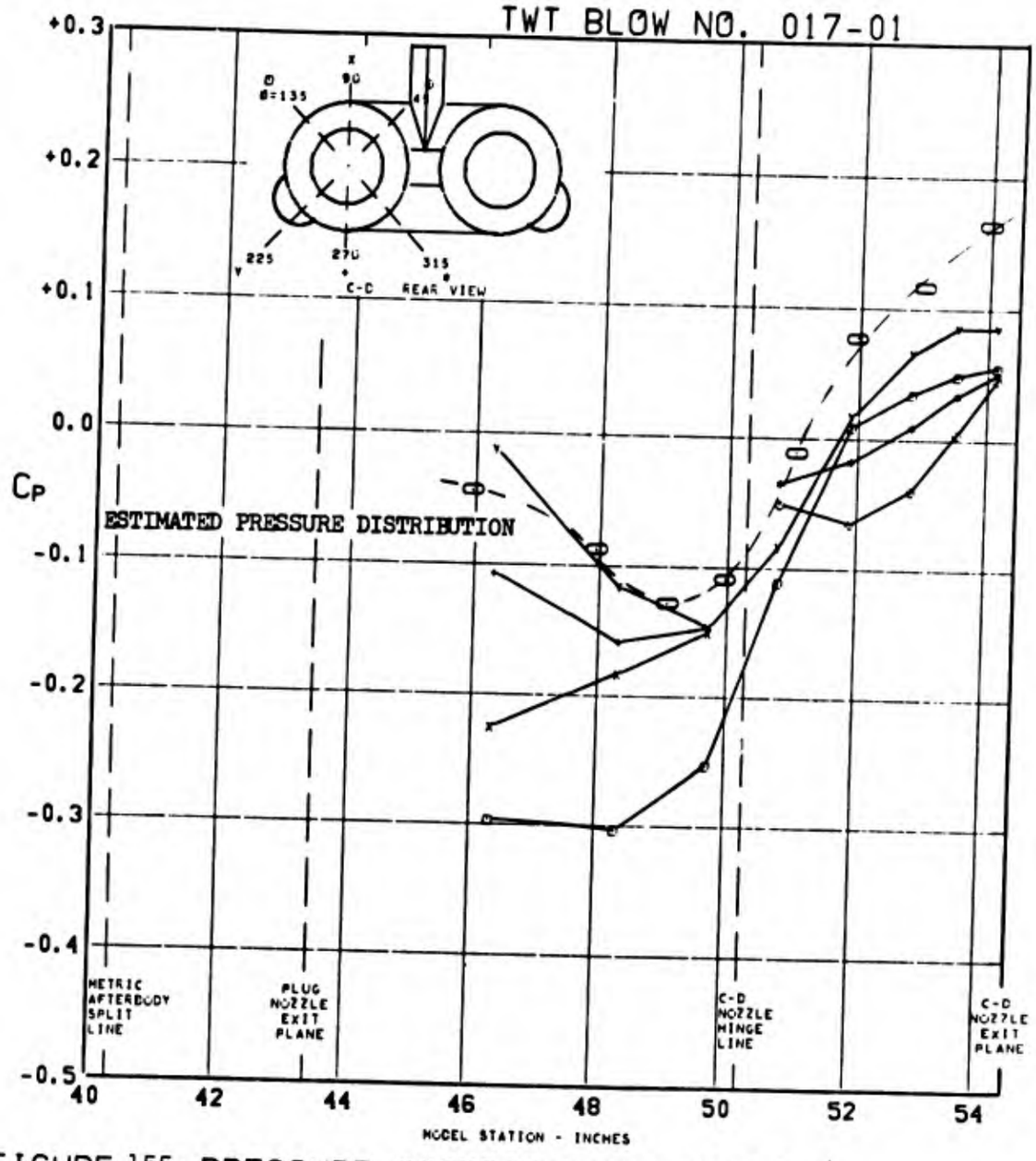

FIGURE 155. PRESSURE COEFFICIENTS ON C-D AFTERBODY $A_9/A_M = .15$ $\Lambda_{LE} = 30°$ AT 0.614 M_0, $(P_T/P_0)_{C-D}$=CONE, $(P_T/P_0)_{PLUG}$=CONE, α= 0.0

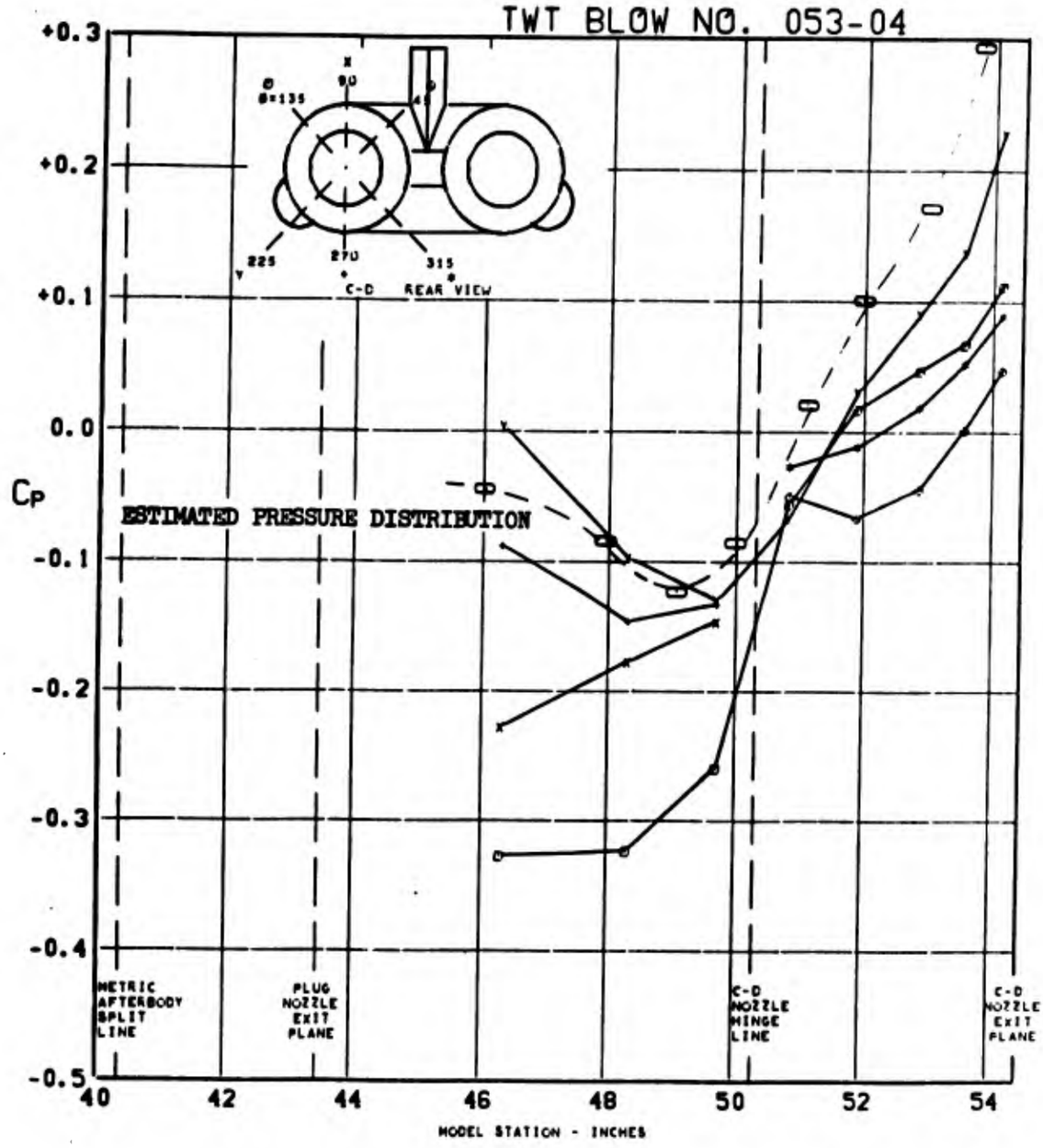

FIGURE 156. PRESSURE COEFFICIENTS ON C-D AFTERBODY $A_9/A_M = .15$ $\Lambda_{LE} = 30°$ AT 0.612 M_0, $(P_T/P_0)_{C-D} = 4.900$, $(P_T/P_0)_{PLUG} = CONE$, $\alpha = 2.7$

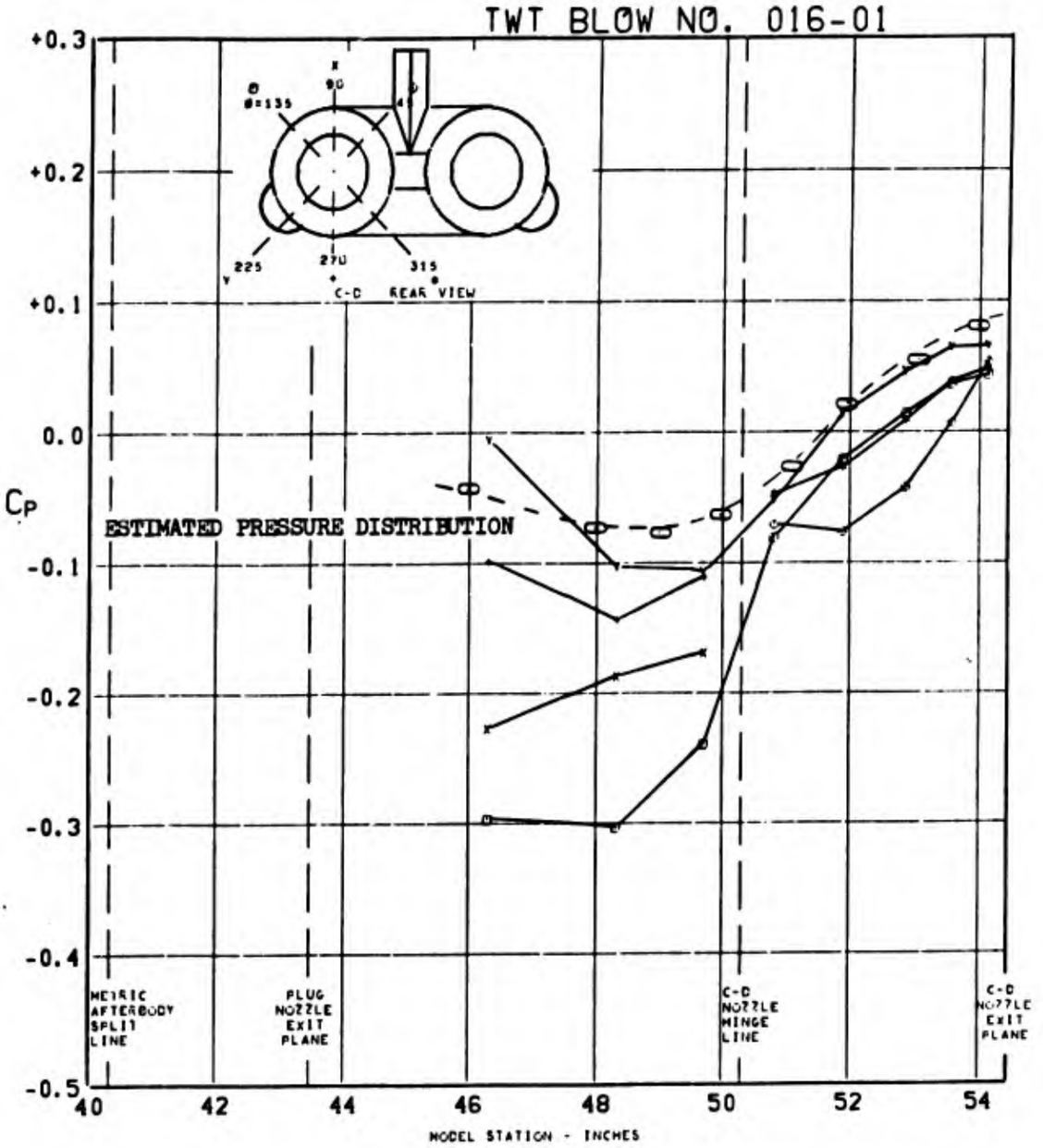

FIGURE 157. PRESSURE COEFFICIENTS ON C-D AFTERBODY $A_9/A_M = .3$ $\Lambda_{LE} = 30°$ AT 0.613 M_0, $(P_T/P_0)_{C-D}$=CONE, $(P_T/P_0)_{PLUG}$=CONE, α= 0.0

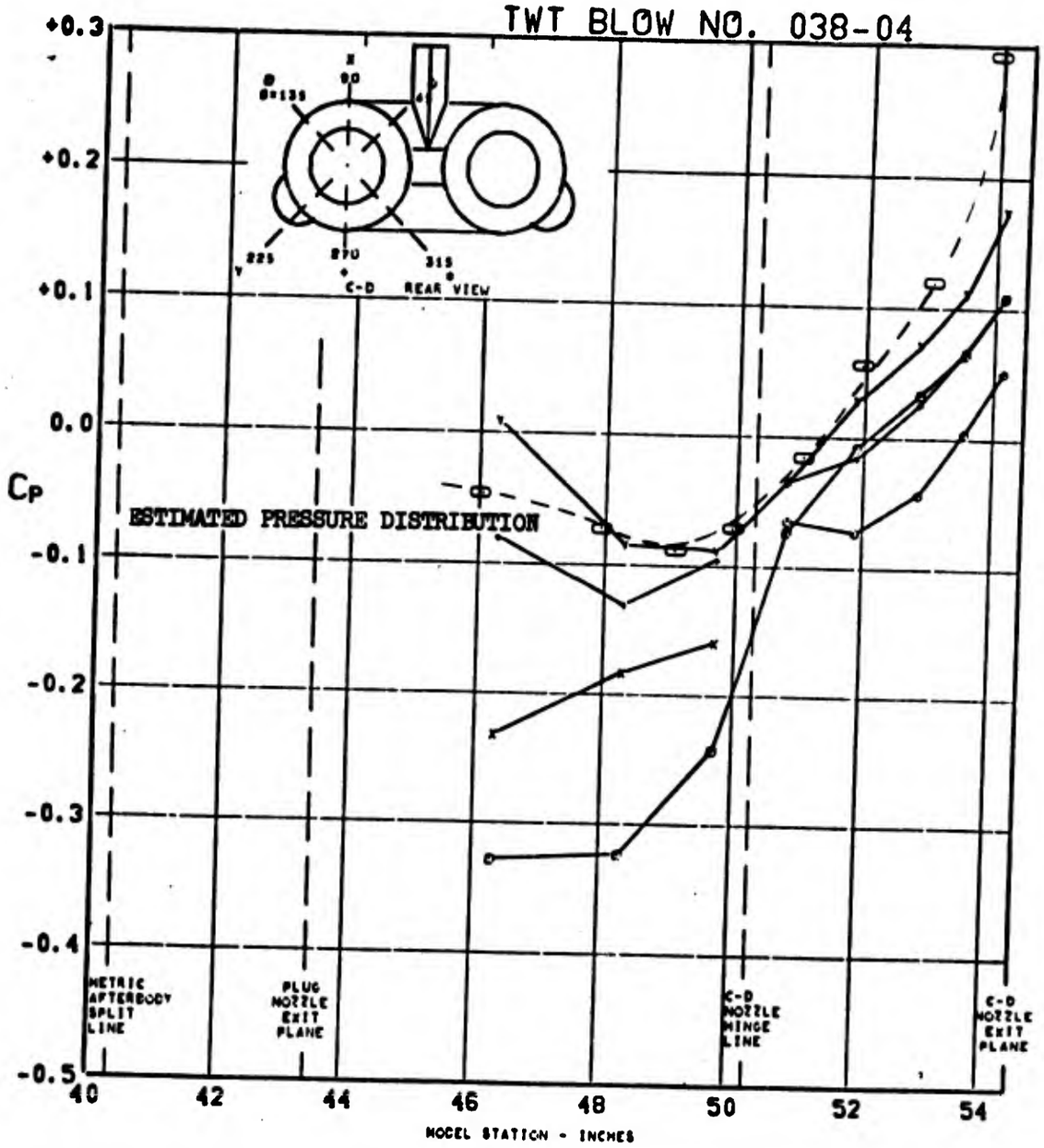

FIGURE 158. PRESSURE COEFFICIENTS ON C-D AFTERBODY $A_9/A_M = .3$ $\Lambda_{LE}=30°$ AT 0.612 M_0, $(P_T/P_0)_{C-D}=4.897$, $(P_T/P_0)_{PLUG}$ =CONE , $\alpha=$ 2.7

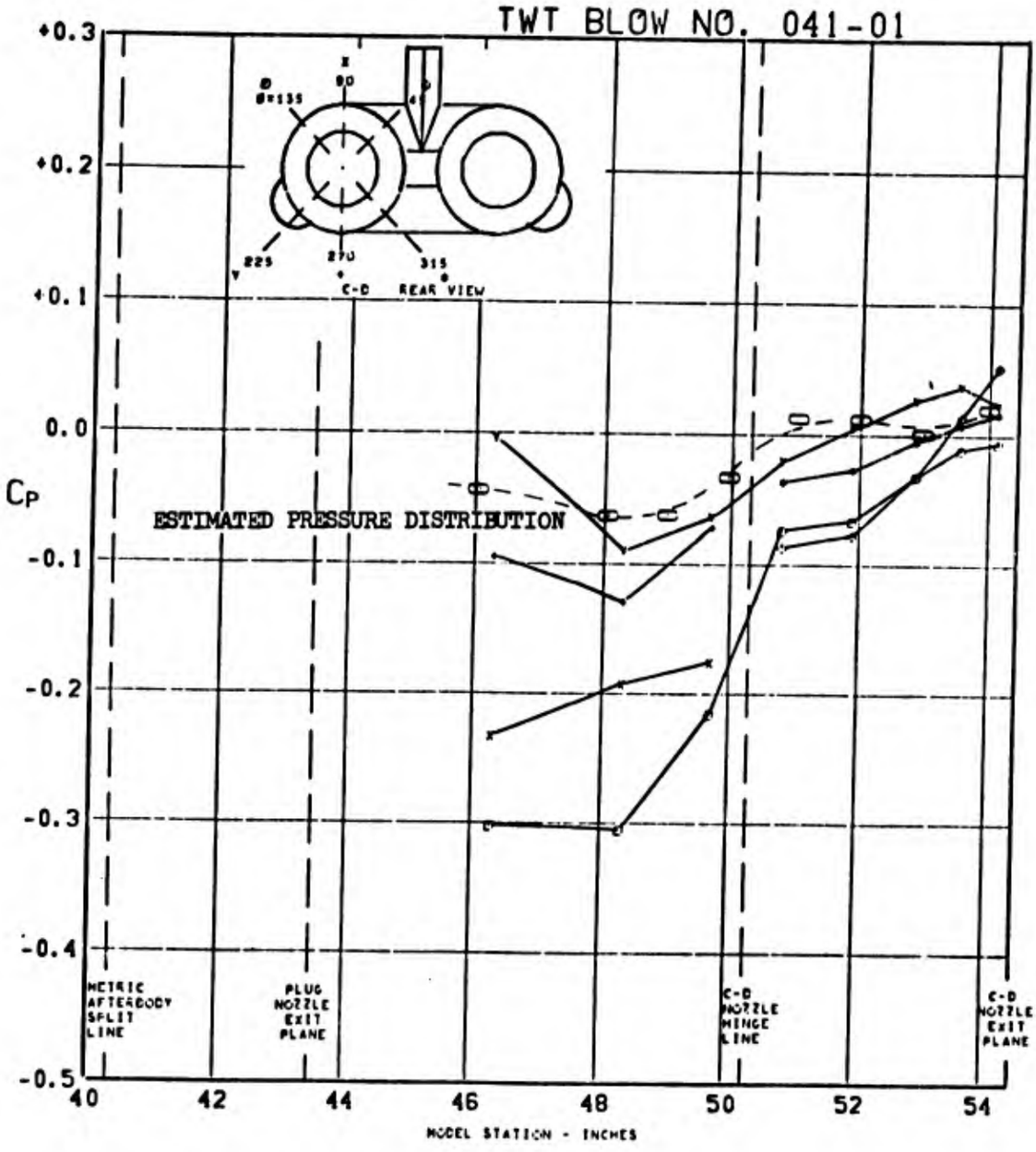

FIGURE 159. PRESSURE COEFFICIENTS ON C-D AFTERBODY $A_9/A_M = .50$ $\Lambda_{LE} = 30°$ AT 0.613 M_0, $(P_T/P_0)_{C-D}$=CONE, $(P_T/P_0)_{PLUG}$=CONE, α= 0.0

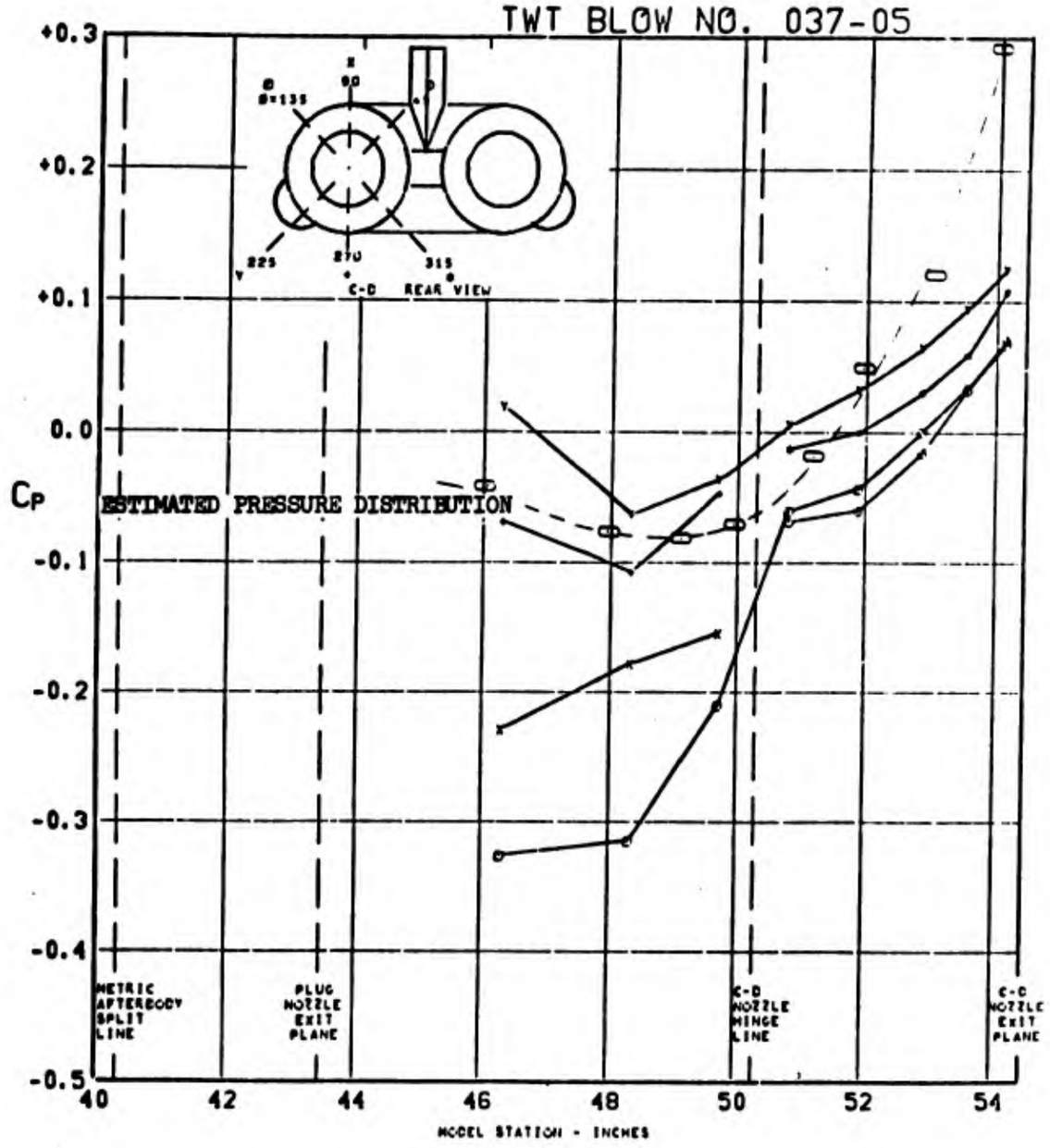

FIGURE 160. PRESSURE COEFFICIENTS ON C-D AFTERBODY $A_9/A_M = .5$ $\Lambda_{LE} = 30°$ AT 0.611 M_0, $(P_T/P_0)_{C-D} = 6.836$, $(P_T/P_0)_{PLUG}$ = CONE, $\alpha = 2.8$

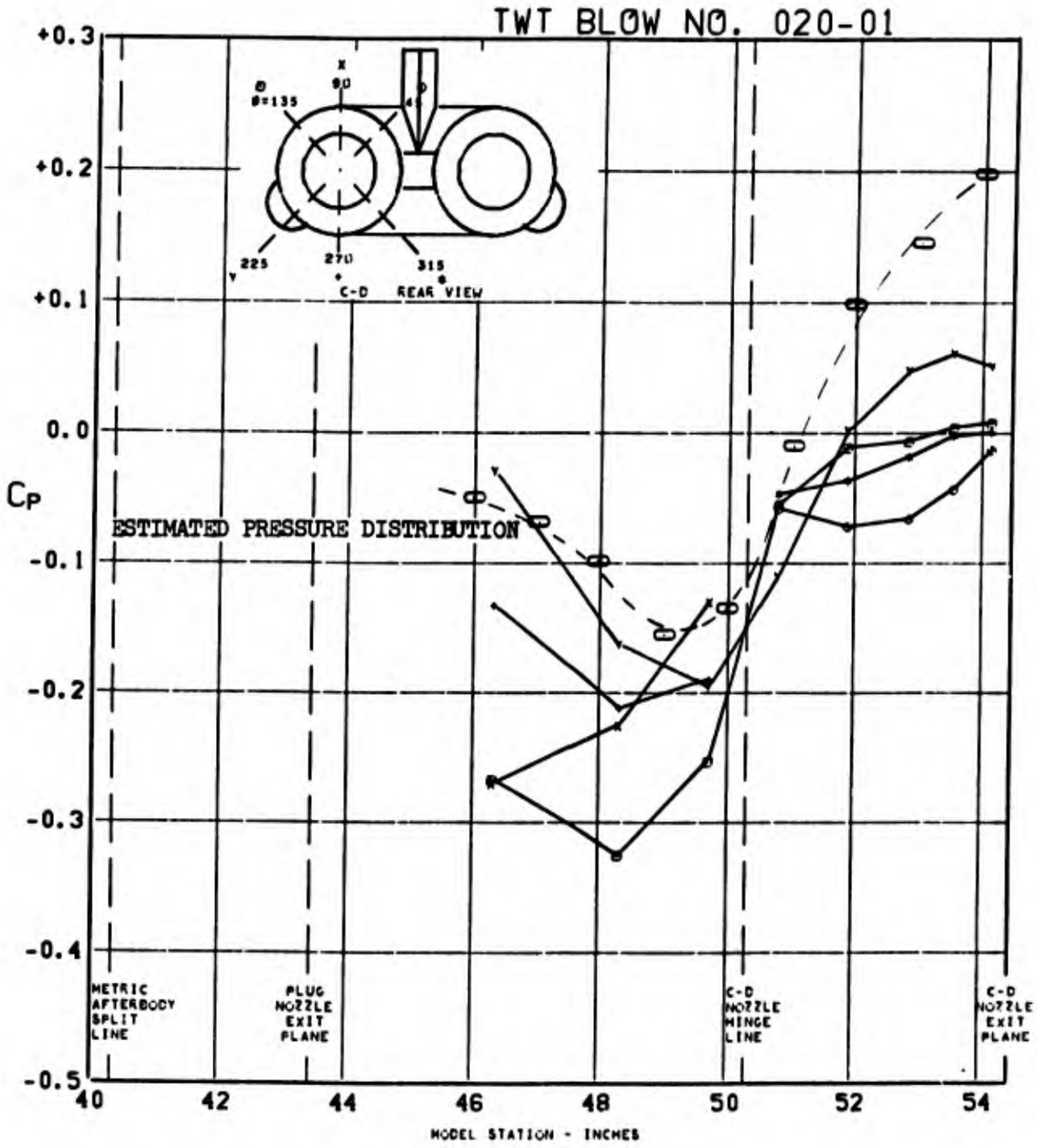

FIGURE 161. PRESSURE COEFFICIENTS ON C-D AFTERBODY $A_9/A_M = .15$, $\Lambda_{LE} = 70°$ AT 0.848 M_0, $(P_T/P_0)_{C-D}$=CONE, $(P_T/P_0)_{PLUG}$=CONE, α= 0.0

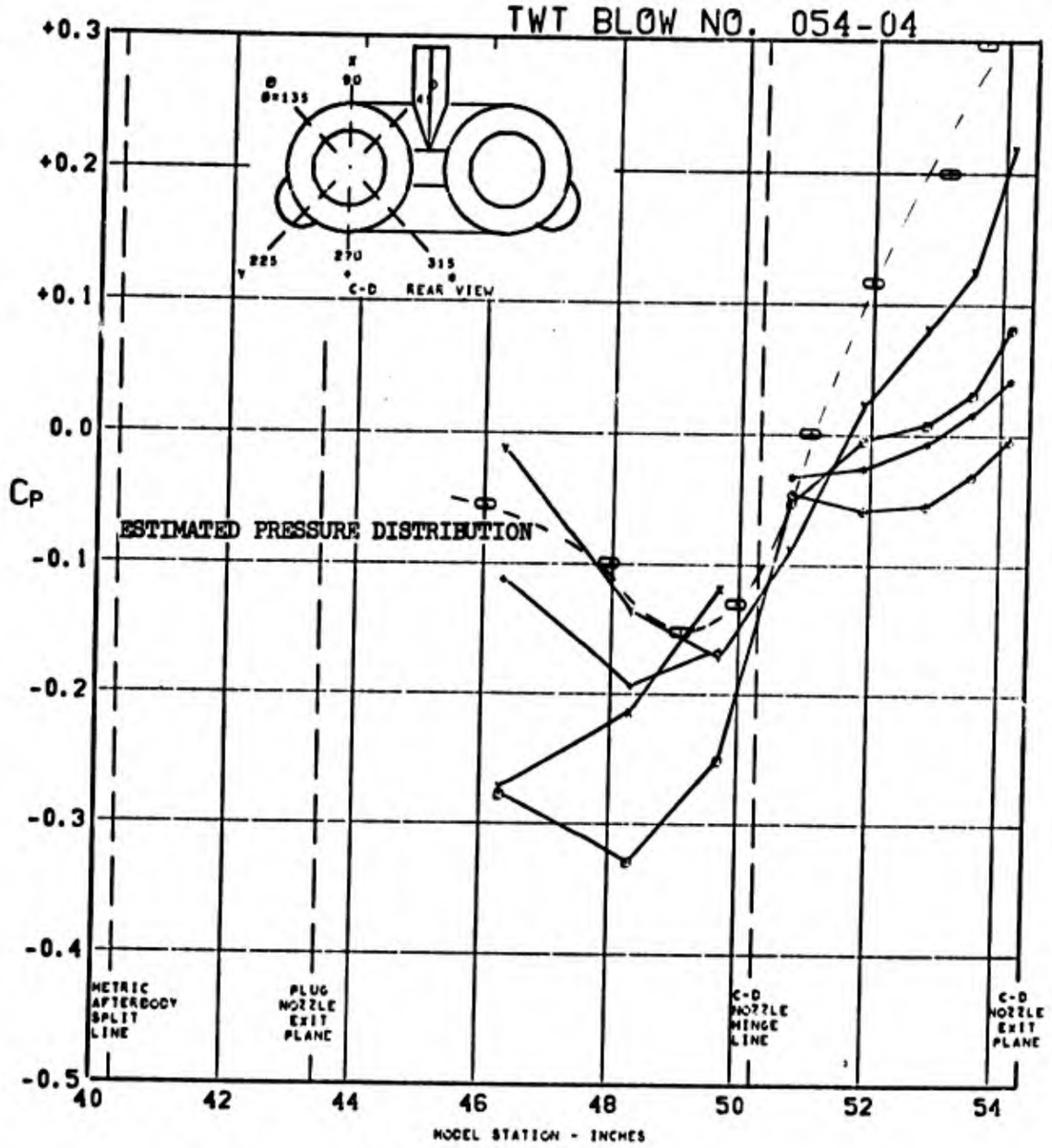

FIGURE 162. PRESSURE COEFFICIENTS ON C-D AFTERBODY A_9/A_M = .15 Λ_{LE} = 70° AT 0.849 M_0, $(P_T/P_0)_{C-D}$ = 4.960, $(P_T/P_0)_{PLUG}$ = CONE, α = 2.6

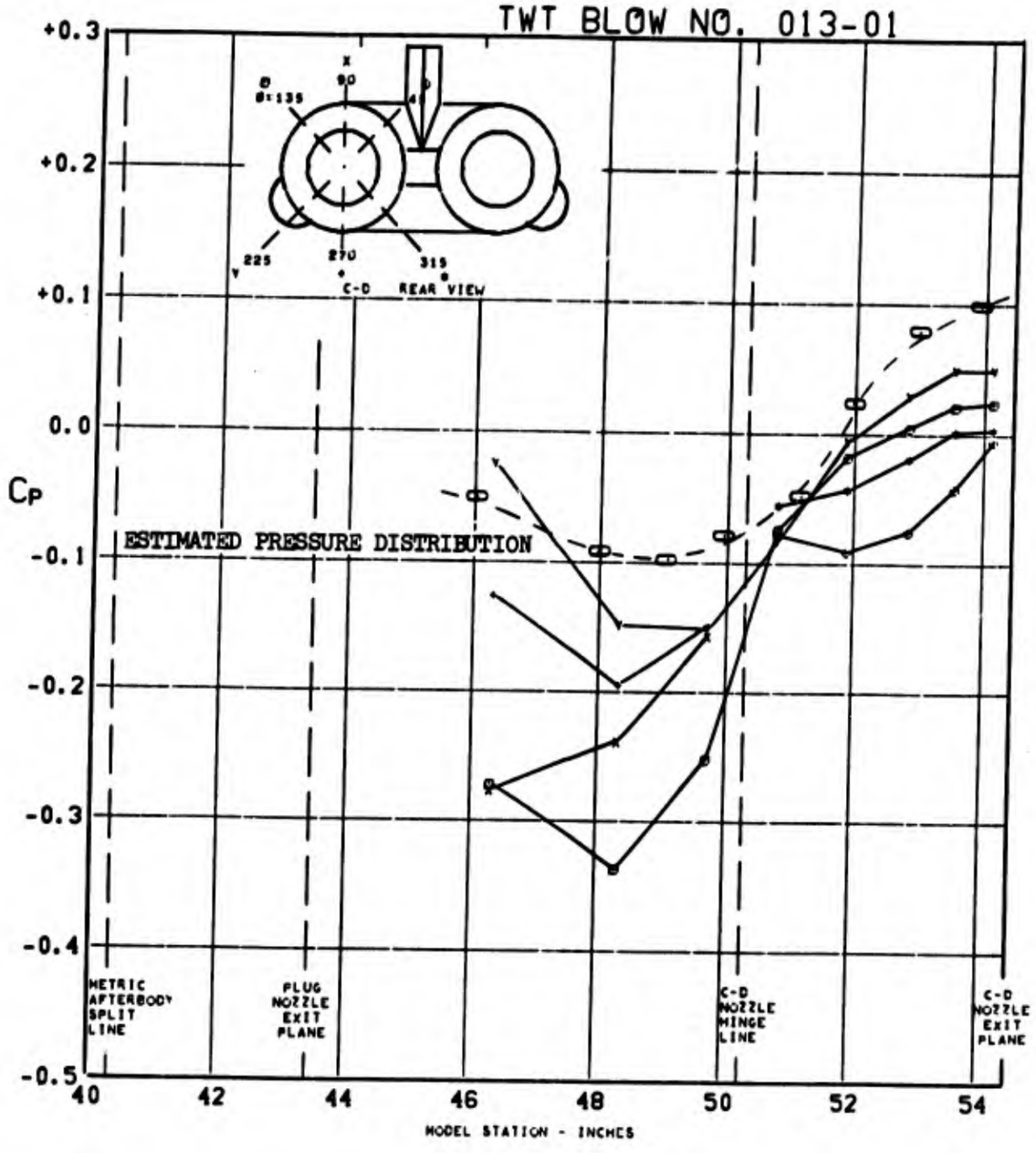

FIGURE 163. PRESSURE COEFFICIENTS ON C-D AFTERBODY $A_9/A_M = .30$ $\Lambda_{LE} = 70°$ AT 0.851 M_0, $(P_T/P_0)_{C-D}$=CONE, $(P_T/P_0)_{PLUG}$=CONE, α= 0.0

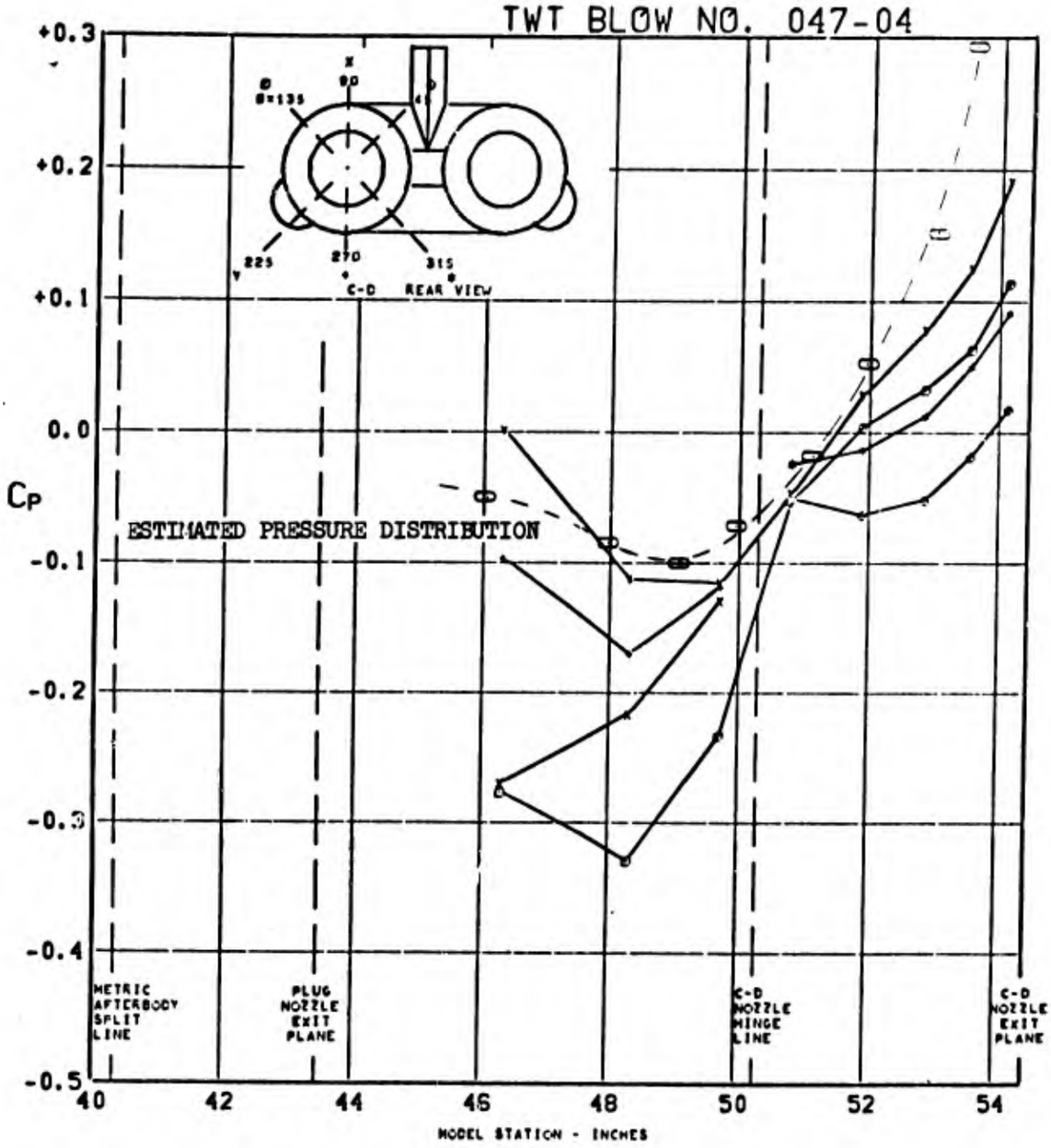

FIGURE 164. PRESSURE COEFFICIENTS ON C-D AFTERBODY $A_g/A_M = .30$ $\Lambda_{LE}=70°$ AT 0.847 M_0, $(P_T/P_0)_{C-D}=5.028$, $(P_T/P_0)_{PLUG}$ =CONE , $\alpha=$ 2.9

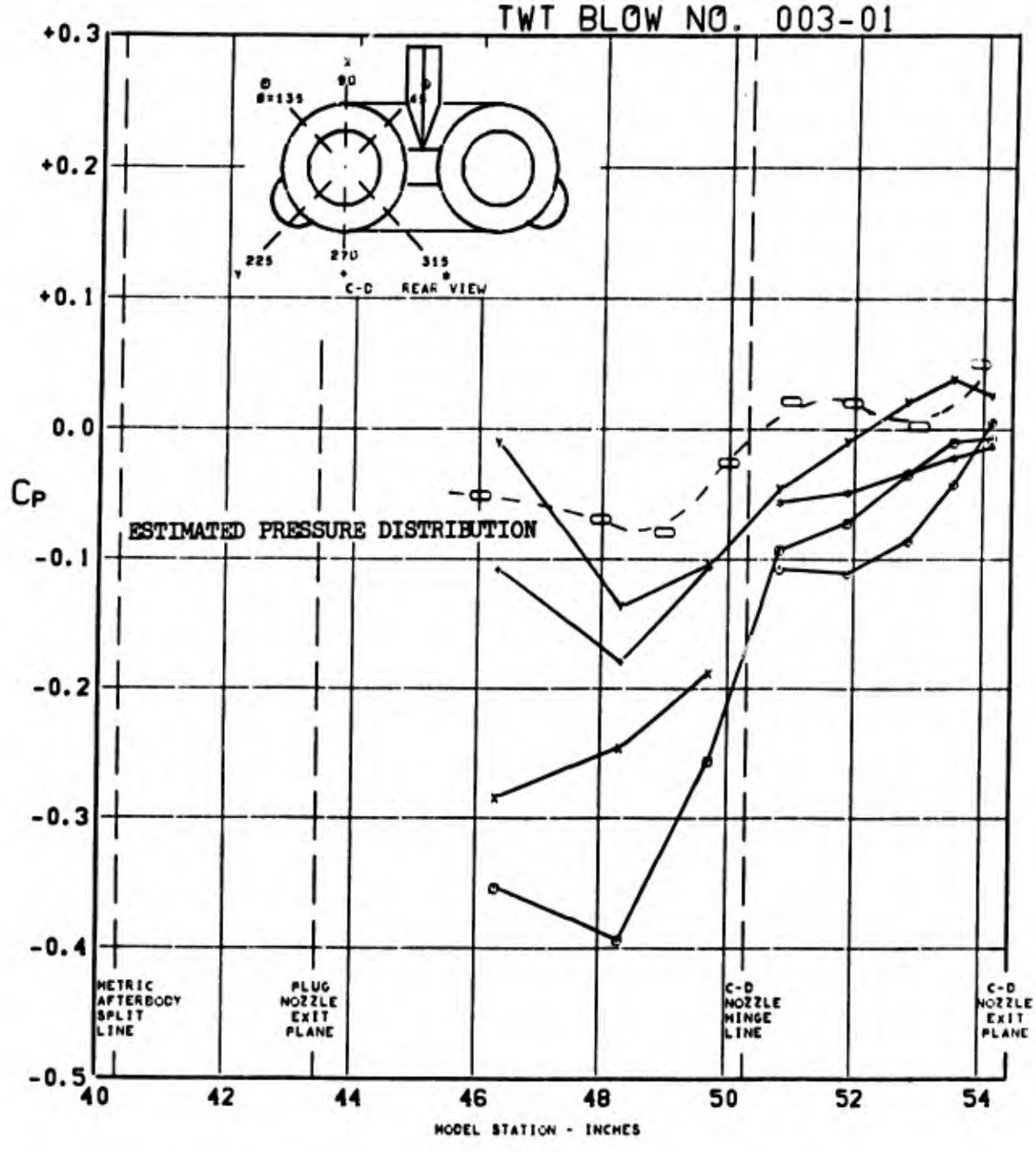

FIGURE 165. PRESSURE COEFFICIENTS ON C-D AFTERBODY $A_9/A_M = .50$ $\Lambda_{LE}=30°$ AT 0.850 M_0, $(P_T/P_0)_{C-D}$=CONE, $(P_T/P_0)_{PLUG}$=CONE, α= 0.0

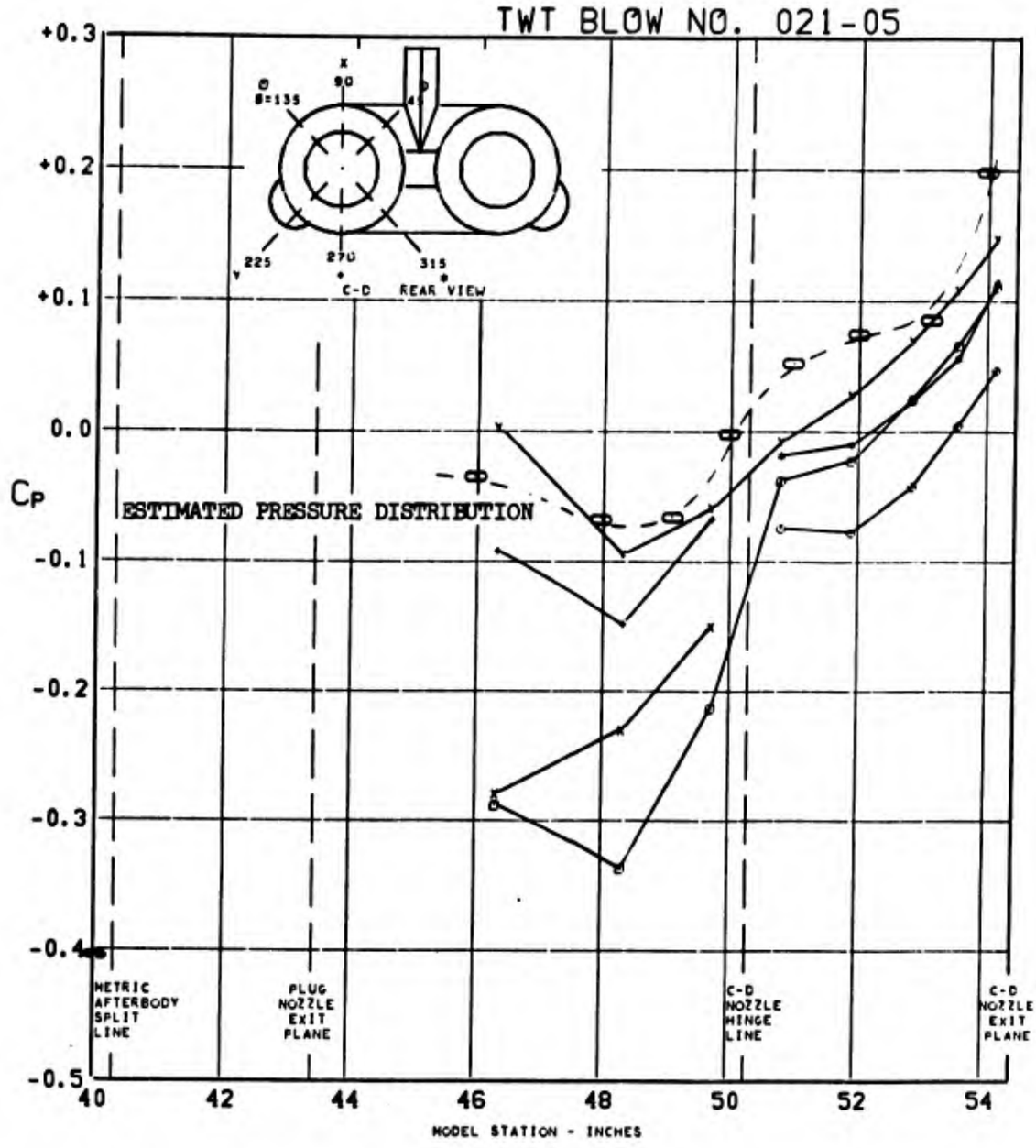

FIGURE 166. PRESSURE COEFFICIENTS ON C-D AFTERBODY $A_9/A_M = .50$ $\Lambda_{LE} = 70°$ AT 0.843 M_0, $(P_T/P_0)_{C-D} = 7.088$, $(P_T/P_0)_{PLUG}$ = CONE, $\alpha = 2.9$

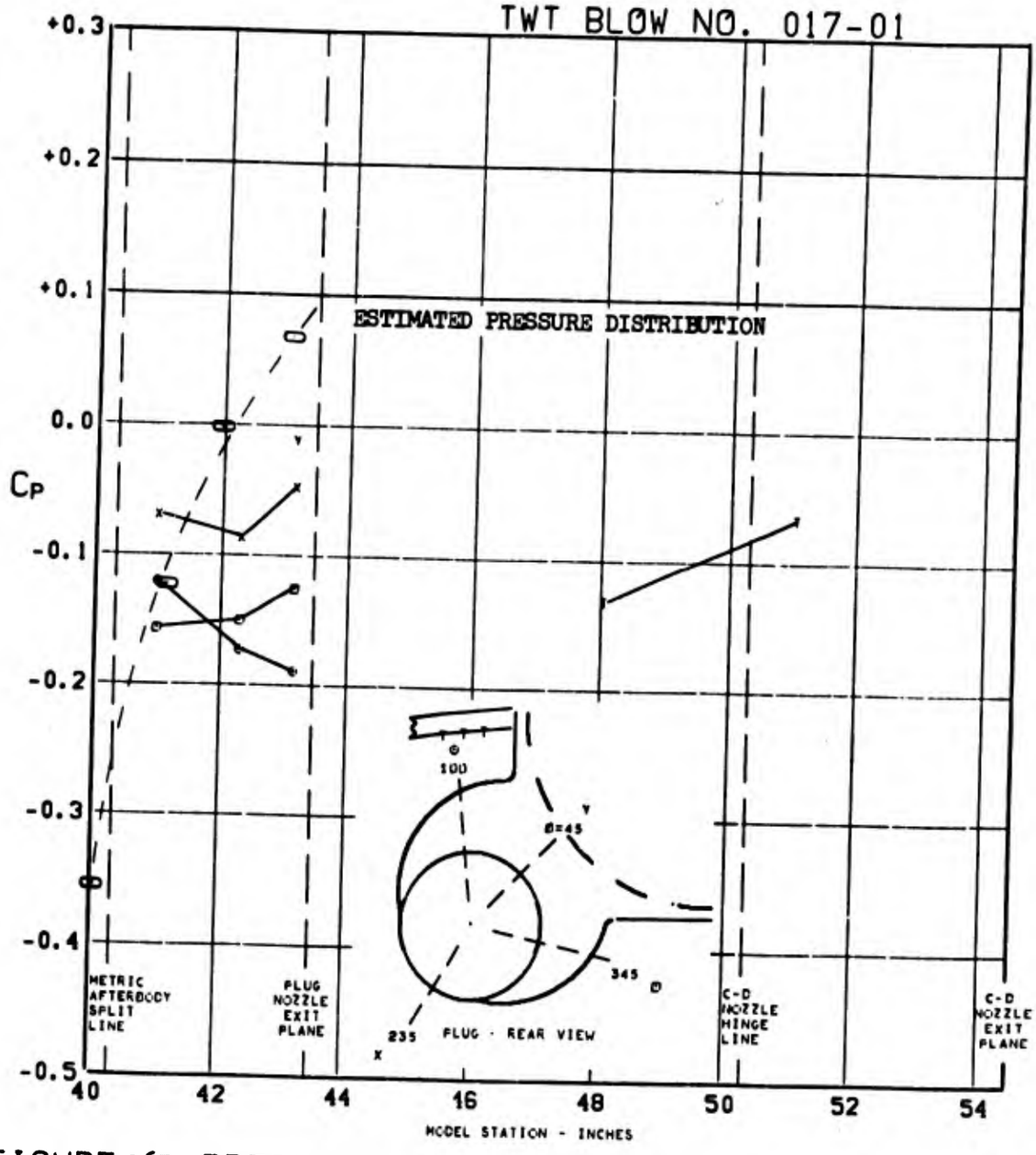

FIGURE 167. PRESSURE COEFFICIENTS ON TAIL & PLUG AFTERBODY (W1B1K1N1 P03 H1V1) Λ_{LE}=30° AT 0.614 M_0, $(P_T/P_0)_{C-D}$=CONE, $(P_T/P_0)_{PLUG}$=CONE, α= 0.0

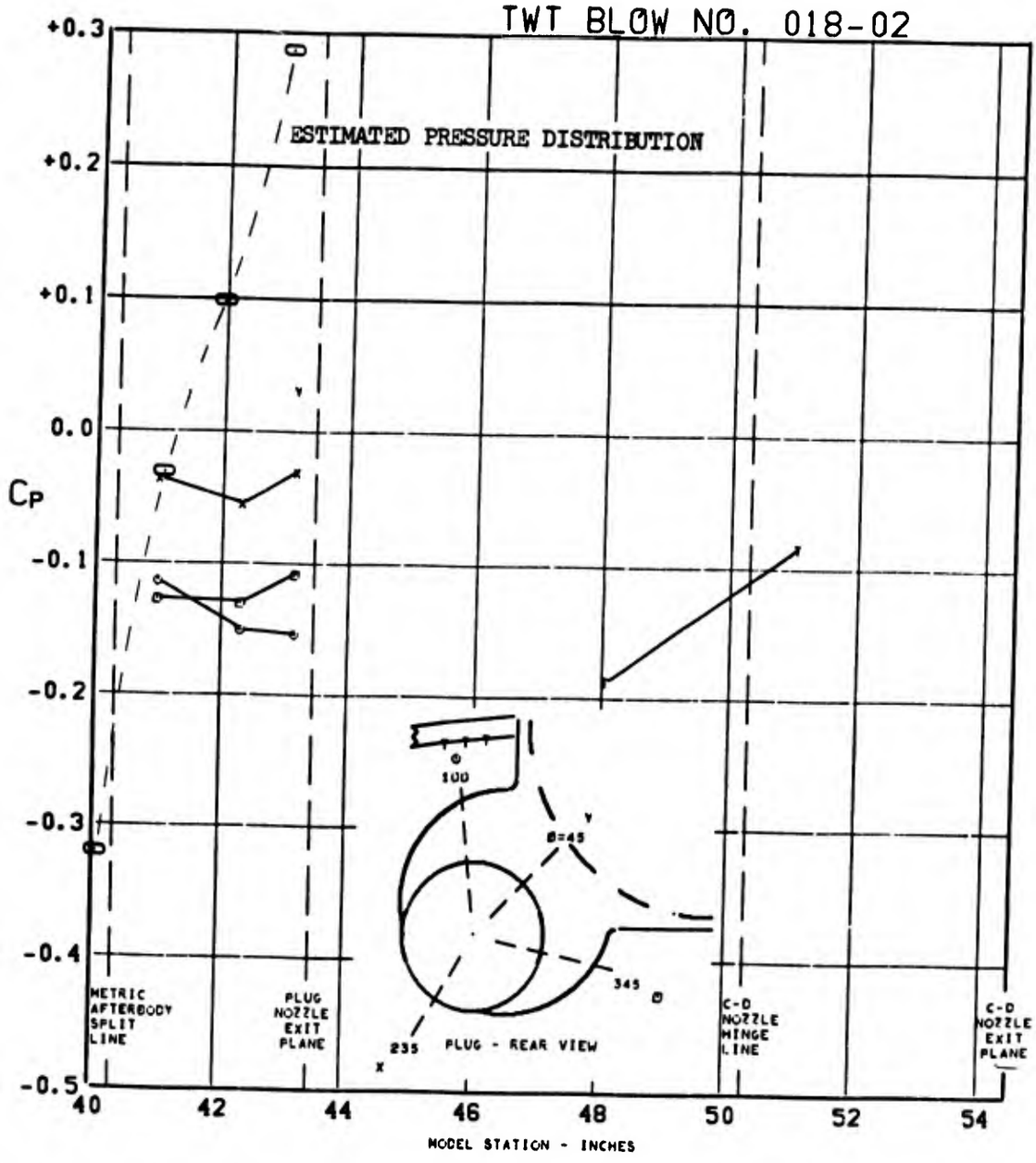

FIGURE 168. PRESSURE COEFFICIENTS ON TAIL & PLUG AFTERBODY (W1B1K1N1 P06 H1V1) $\Lambda_{LE}=30°$ AT 0.612 M_0, $(P_T/P_0)_{C-D}$=CONE, $(P_T/P_0)_{PLUG}=1.978$, $\alpha=2.9$

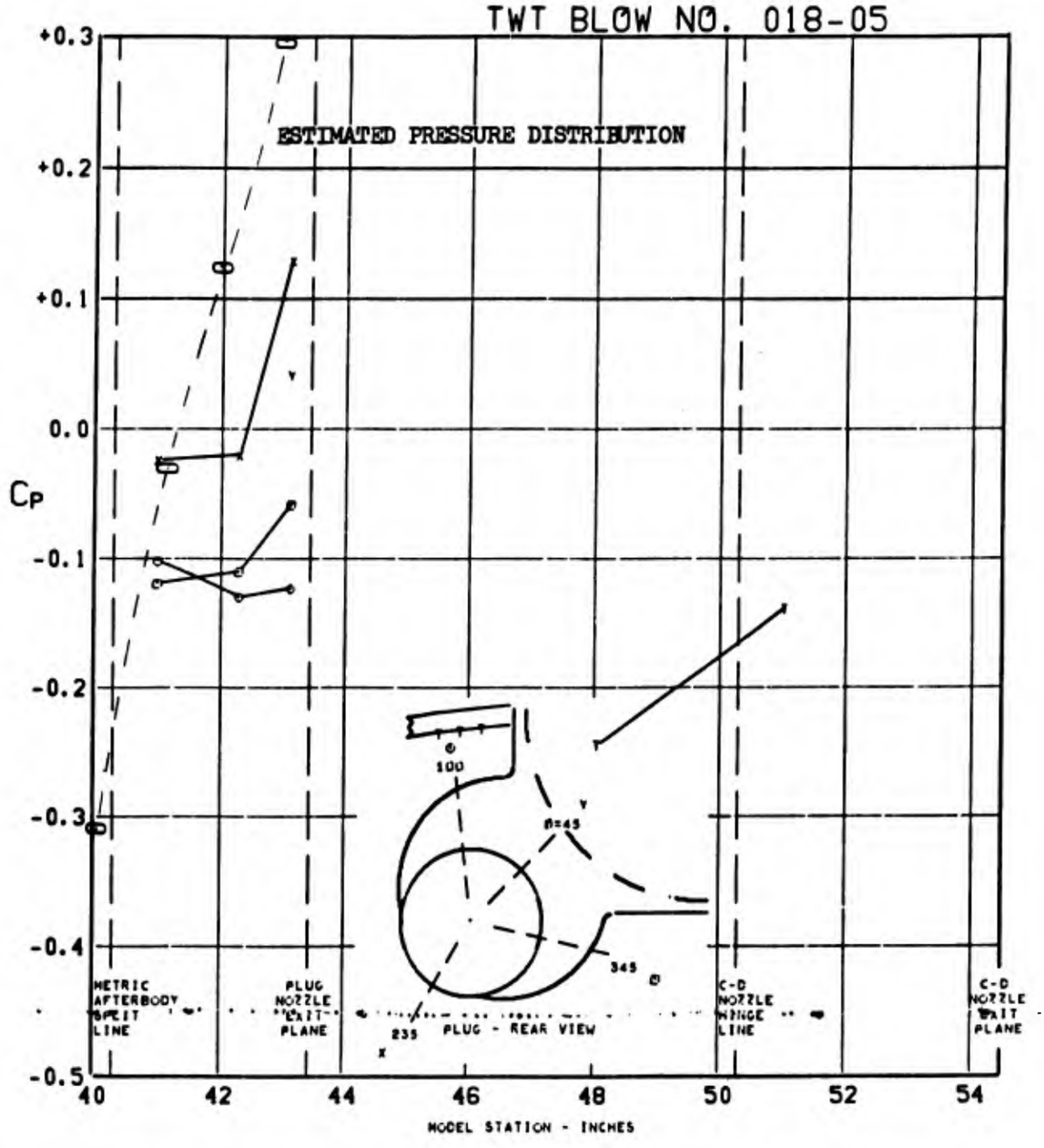

FIGURE 169. PRESSURE COEFFICIENTS ON TAIL & PLUG AFTERBODY (W1B1K1N1 P06 H1V1) Λ_{LE}=30° AT .0.612 M_0, $(P_T/P_0)_{C-D}$=CONE , $(P_T/P_0)_{PLUG}$=5.060, α= 2.9

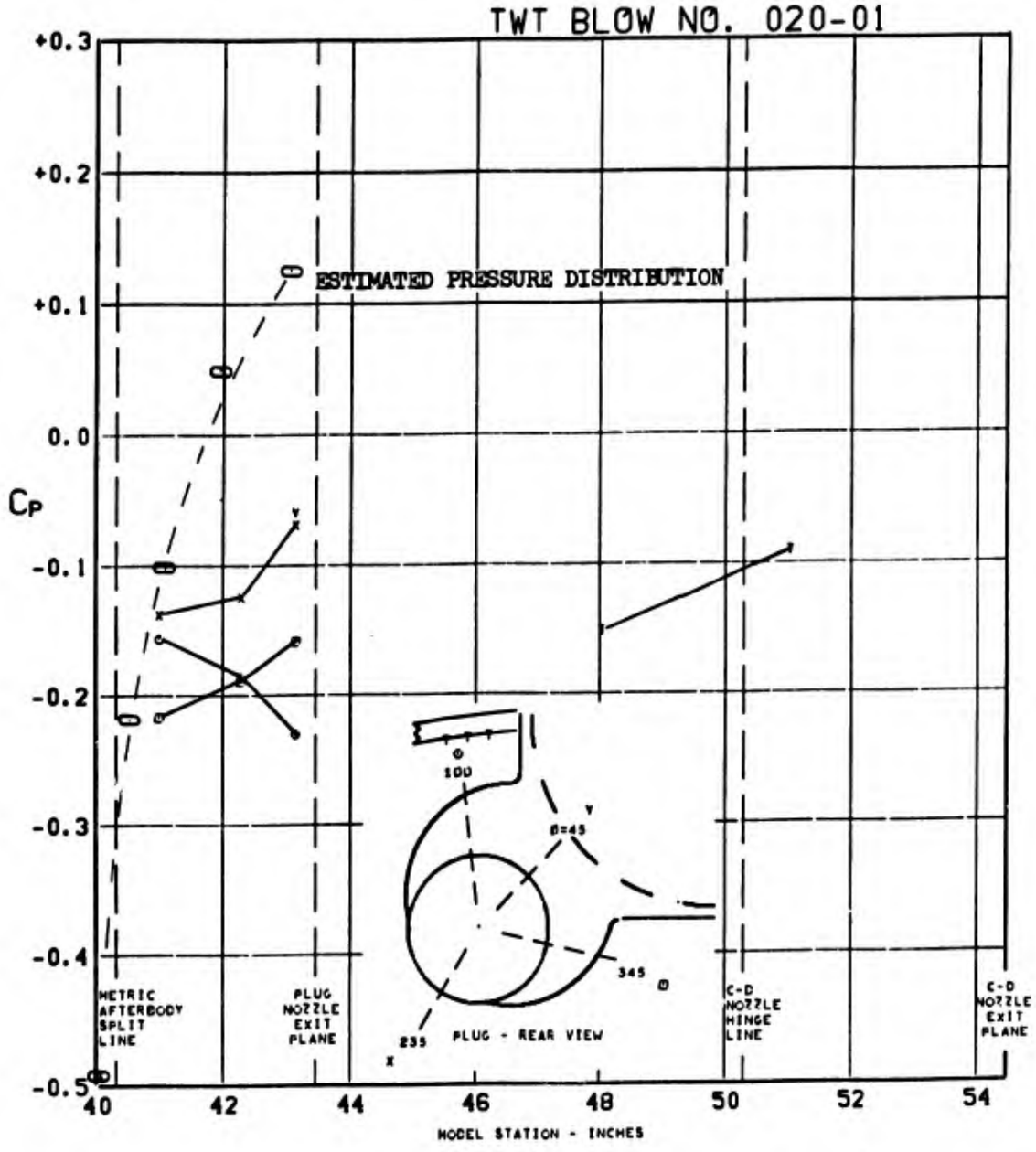

FIGURE 170. PRESSURE COEFFICIENTS ON TAIL & PLUG AFTERBODY (W1B1K1N1 P03 H1V1) Λ_{LE}=70° AT 0.848 M_0, $(P_T/P_0)_{C-D}$=CONE, $(P_T/P_0)_{PLUG}$=CONE, α= 0.0

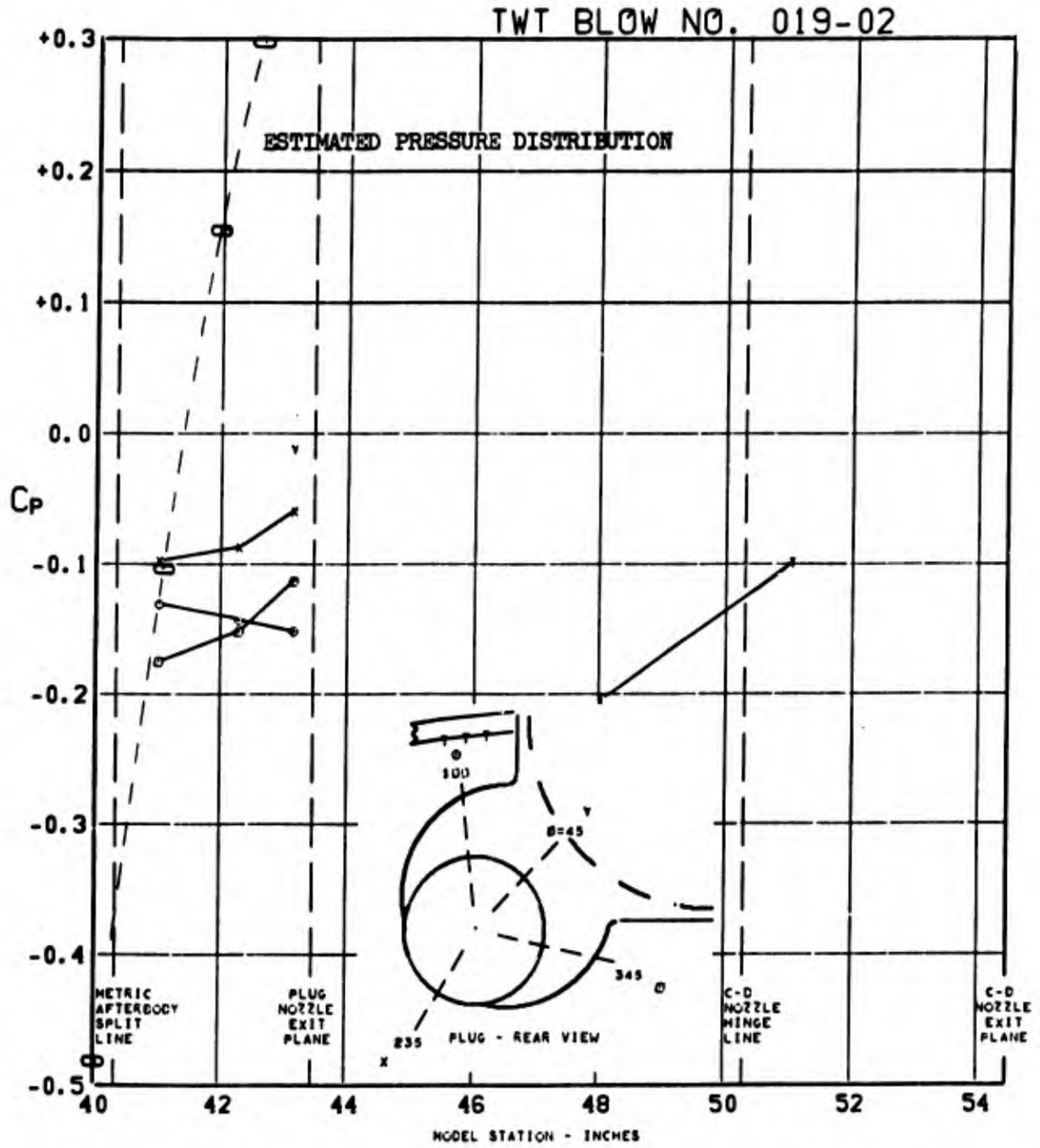

FIGURE 171. PRESSURE COEFFICIENTS ON TAIL & PLUG AFTERBODY (W1B1K1N1 P06 H1V1) $\Lambda_{LE}=70°$ AT 0.847 M_0, $(P_T/P_0)_{C-D}$=CONE, $(P_T/P_0)_{PLUG}$=2.005, α= 2.9

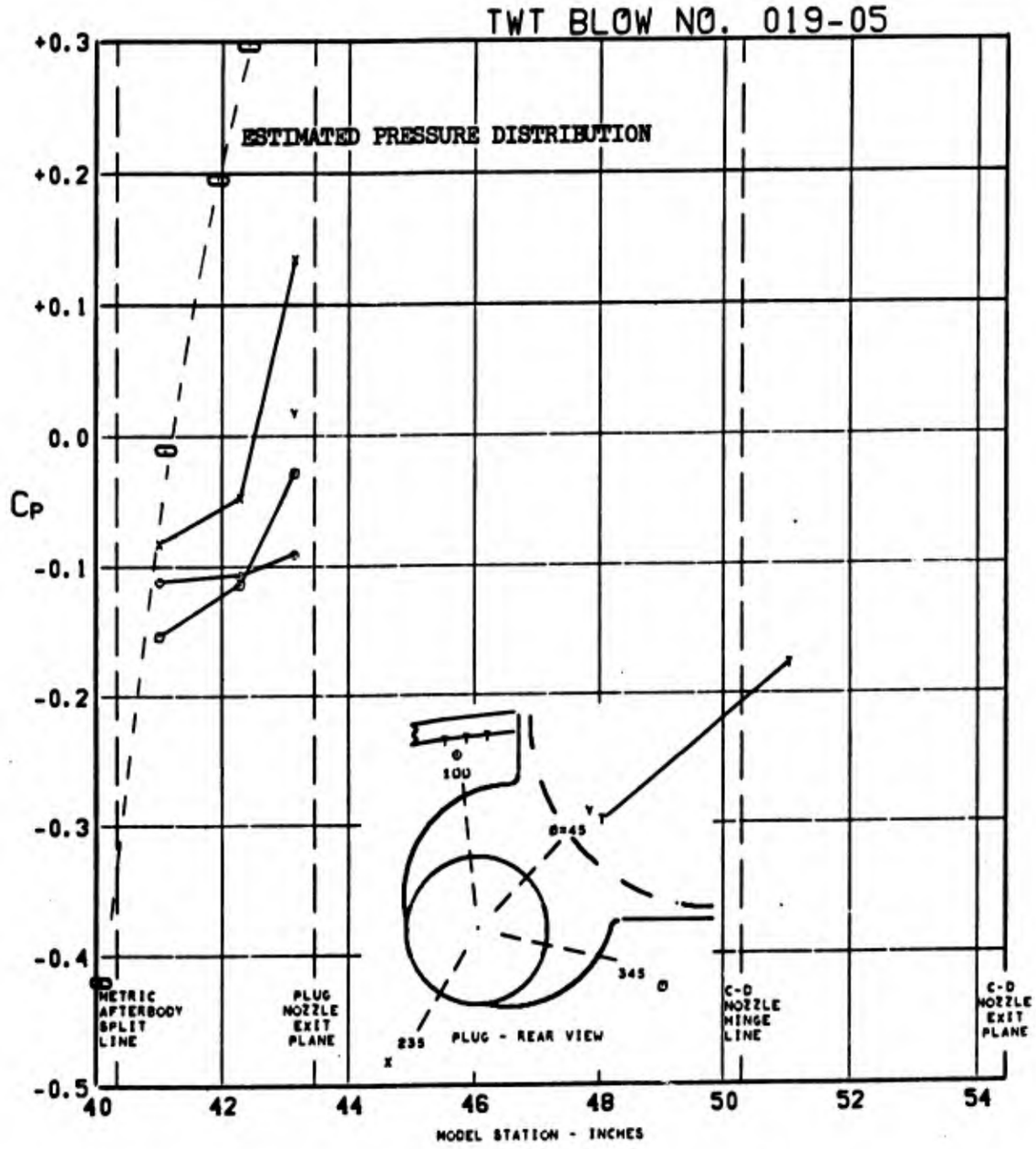

FIGURE 172. PRESSURE COEFFICIENTS ON TAIL & PLUG AFTERBODY (W1B1K1N1 P06 H1V1) Λ_{LE}=70° AT 0.846 M_0, $(P_T/P_0)_{C-D}$=CONE, $(P_T/P_0)_{PLUG}$=5.018, α= 2.9

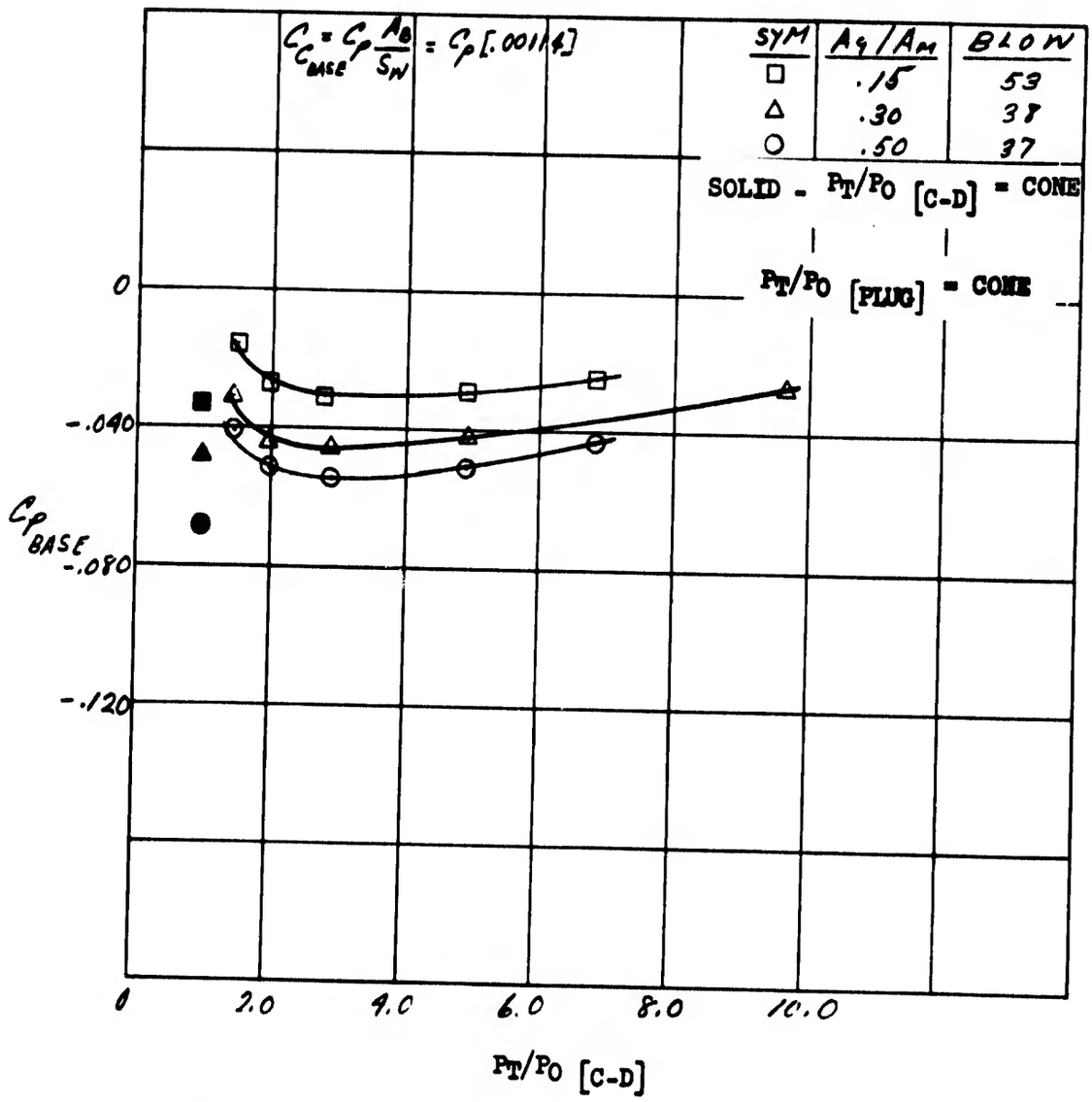

Figure 173. C-D Nozzle Jet Effects on Base Pressure - M = .614

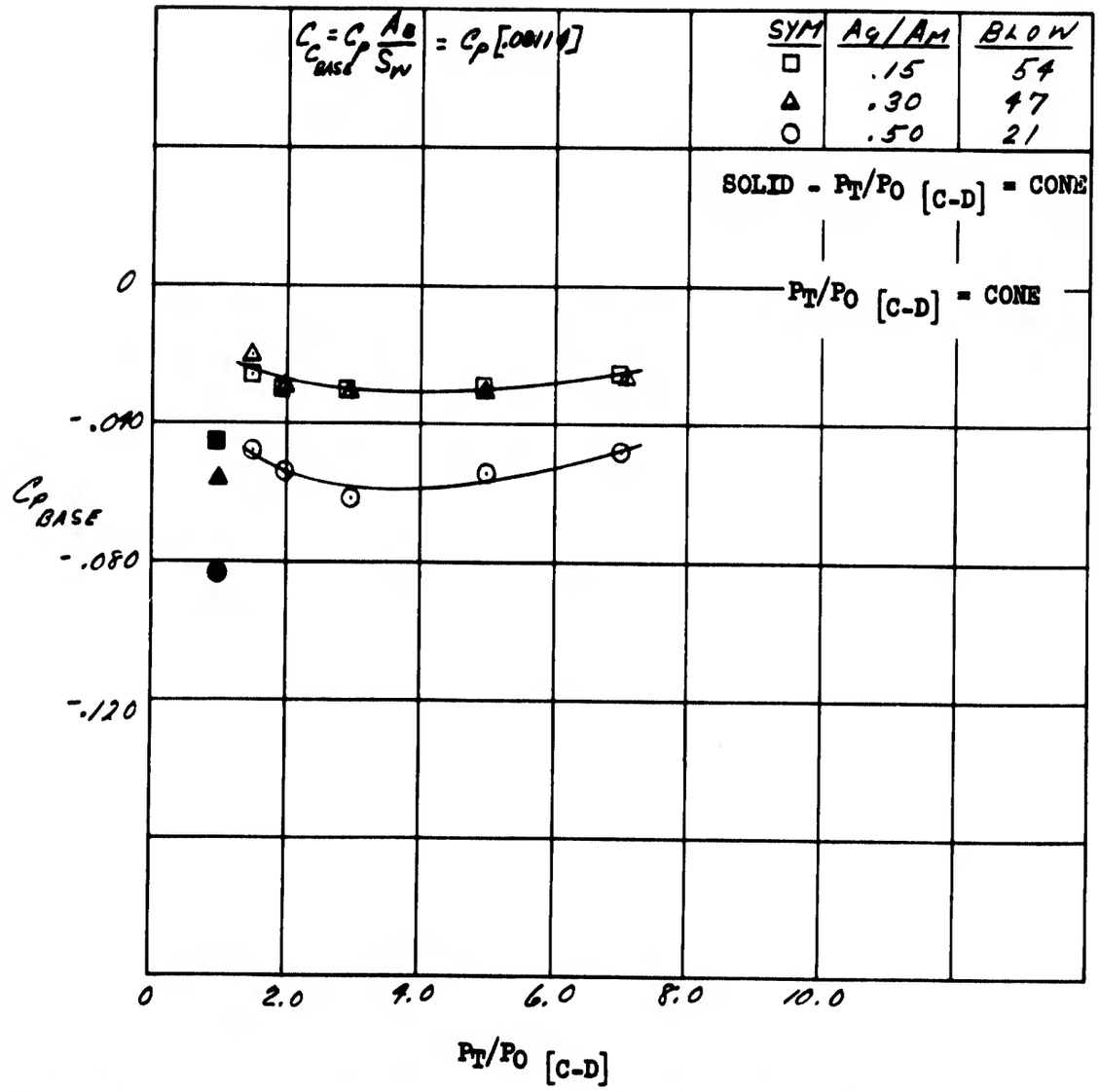

Figure 174. C-D Nozzle Jet Effects on Base Pressure-M = .85

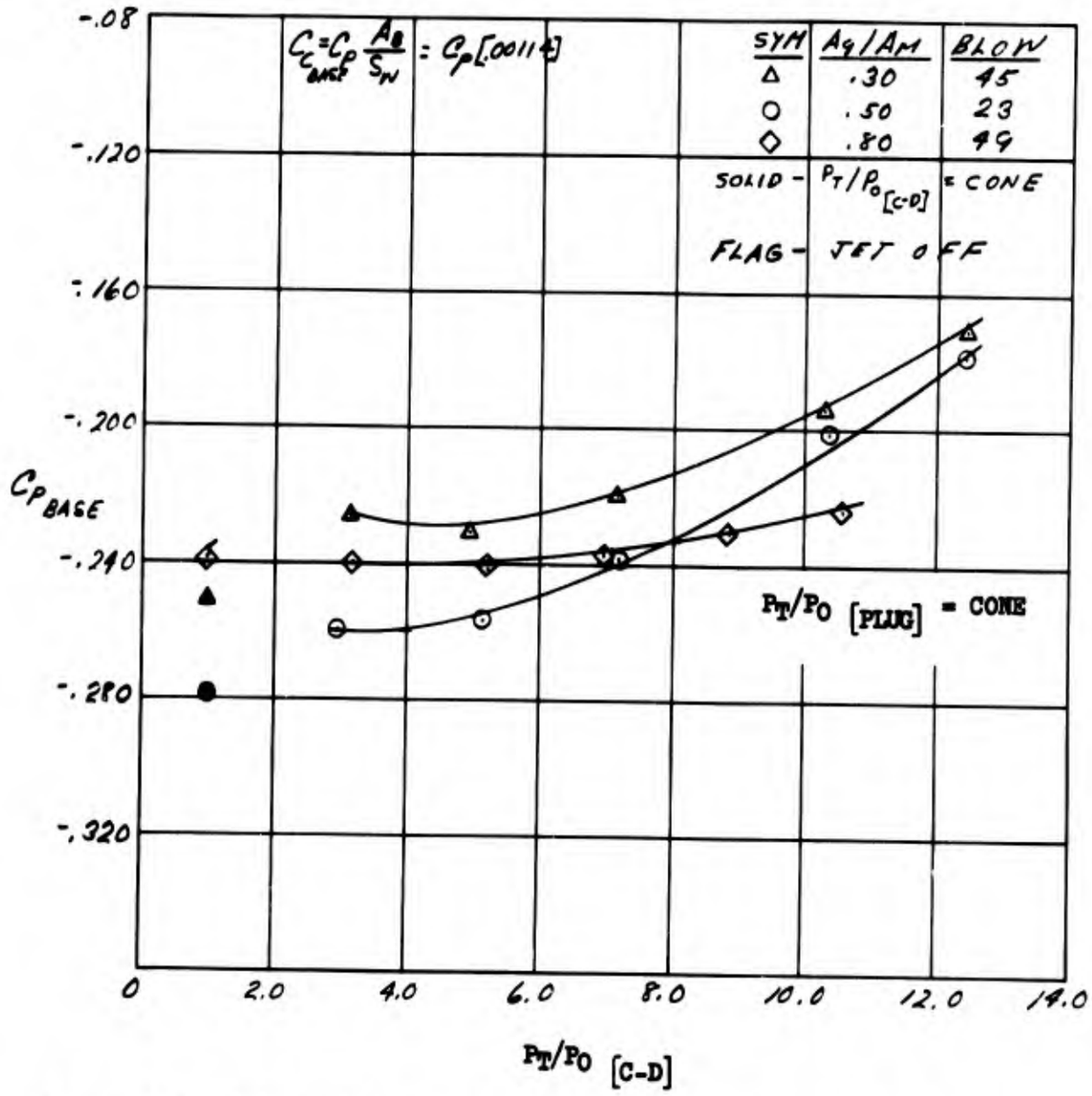

Figure 175. C-D Nozzle Jet Effects on Base Pressure - M = 1.27

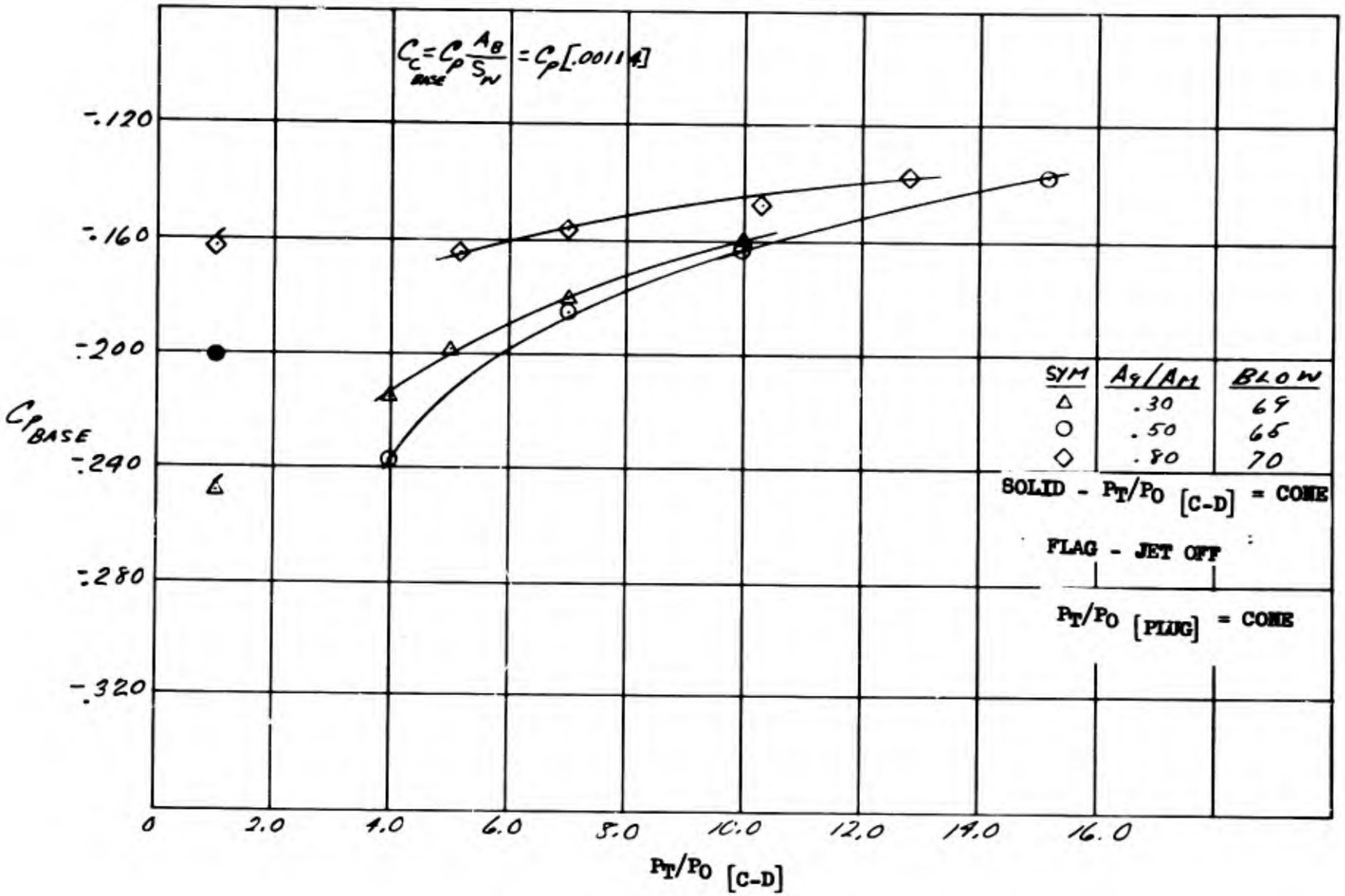

Figure 176. C-D Nozzle Jet Effects on Base Pressure - M = 1.7

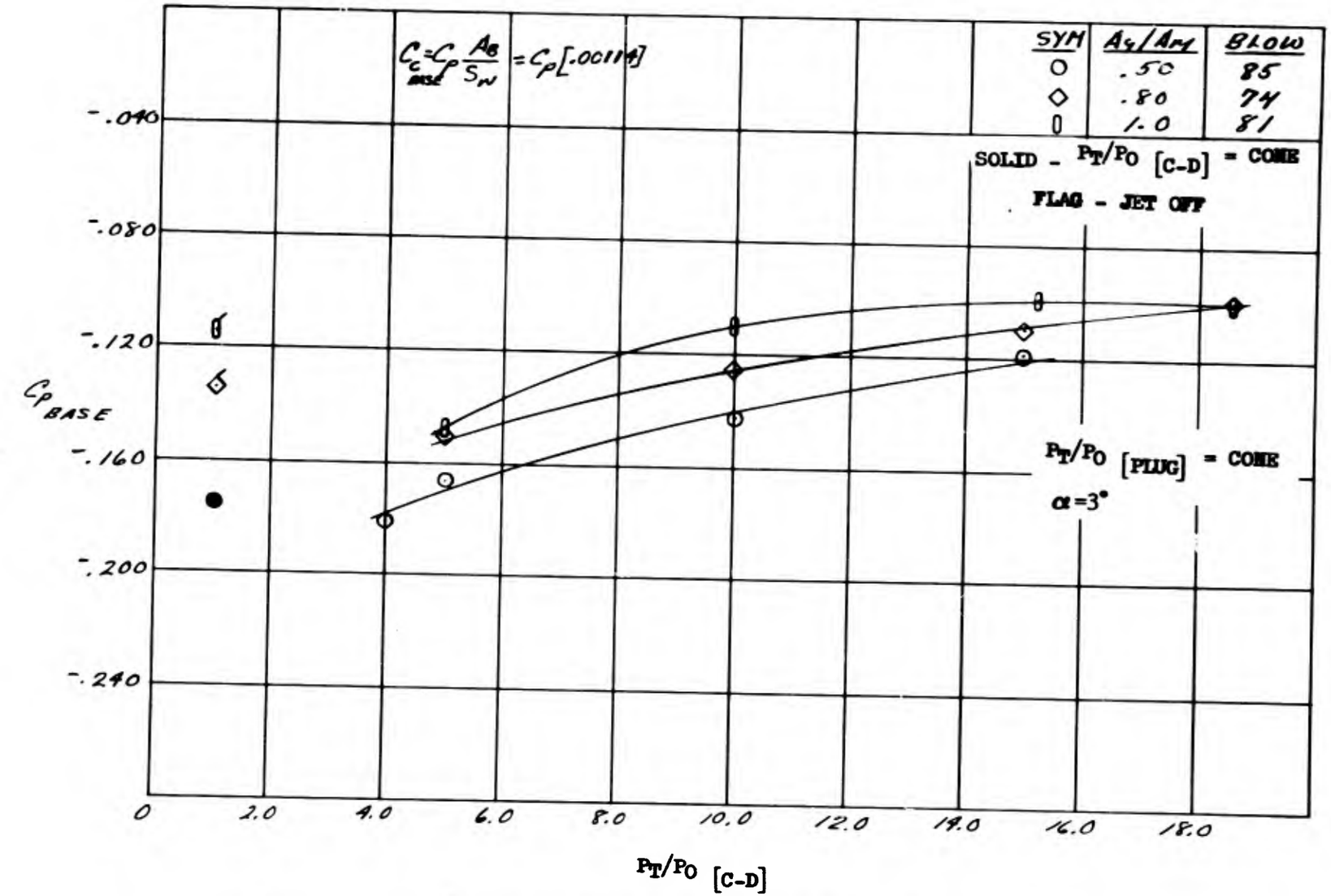

Figure 177. C-D Nozzle Jet Effects on Base Pressure - M = 2.0

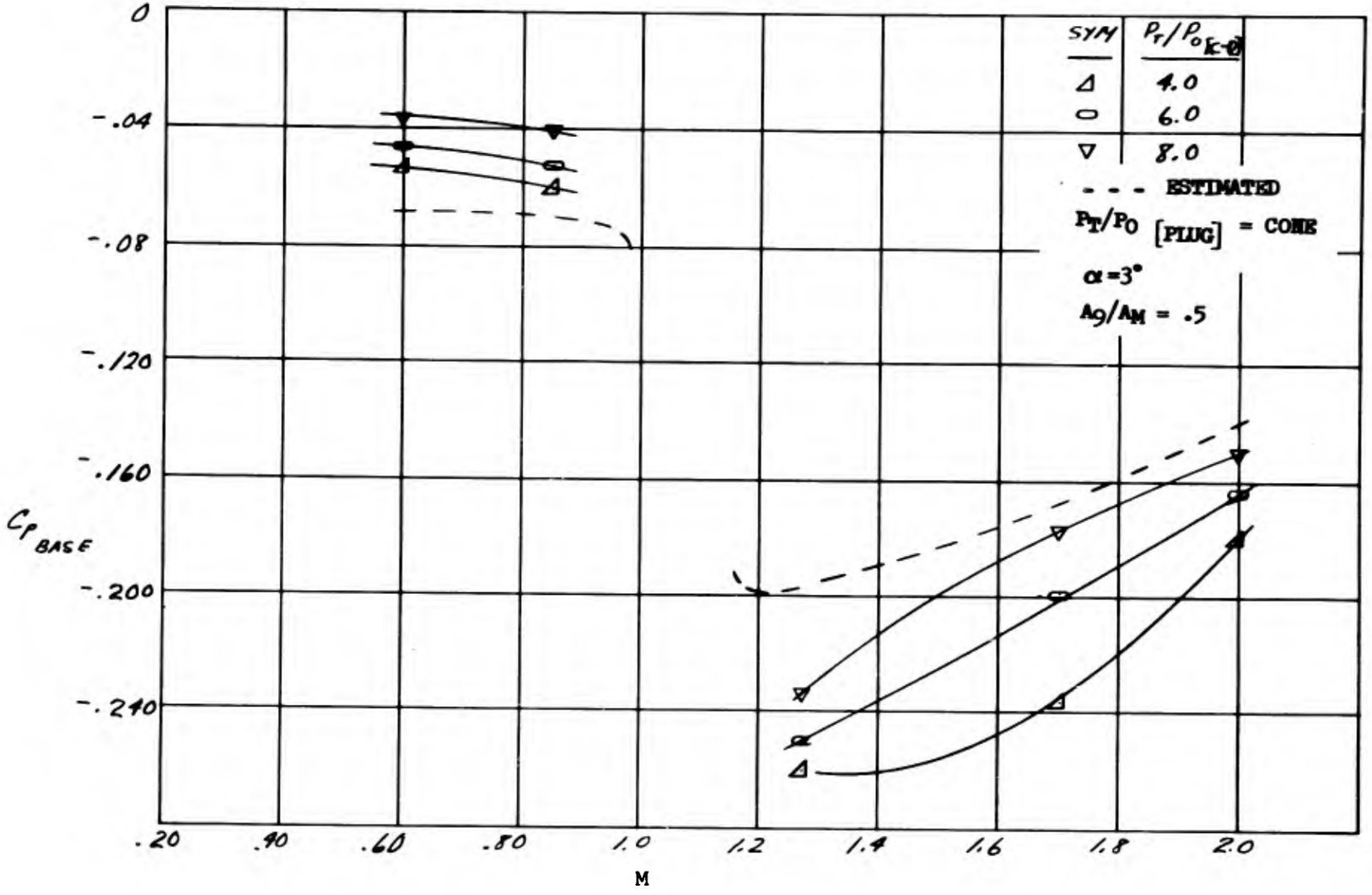

Figure 178. Comparison of Estimated and Measured Base Pressure Coefficients

$$\frac{\delta^*}{x^{.8}} = \frac{.0475(1+.35M^2)}{(1+.88\frac{k-1}{2}M^2)^{.44}(R_{\theta/l+})^{.2}}$$

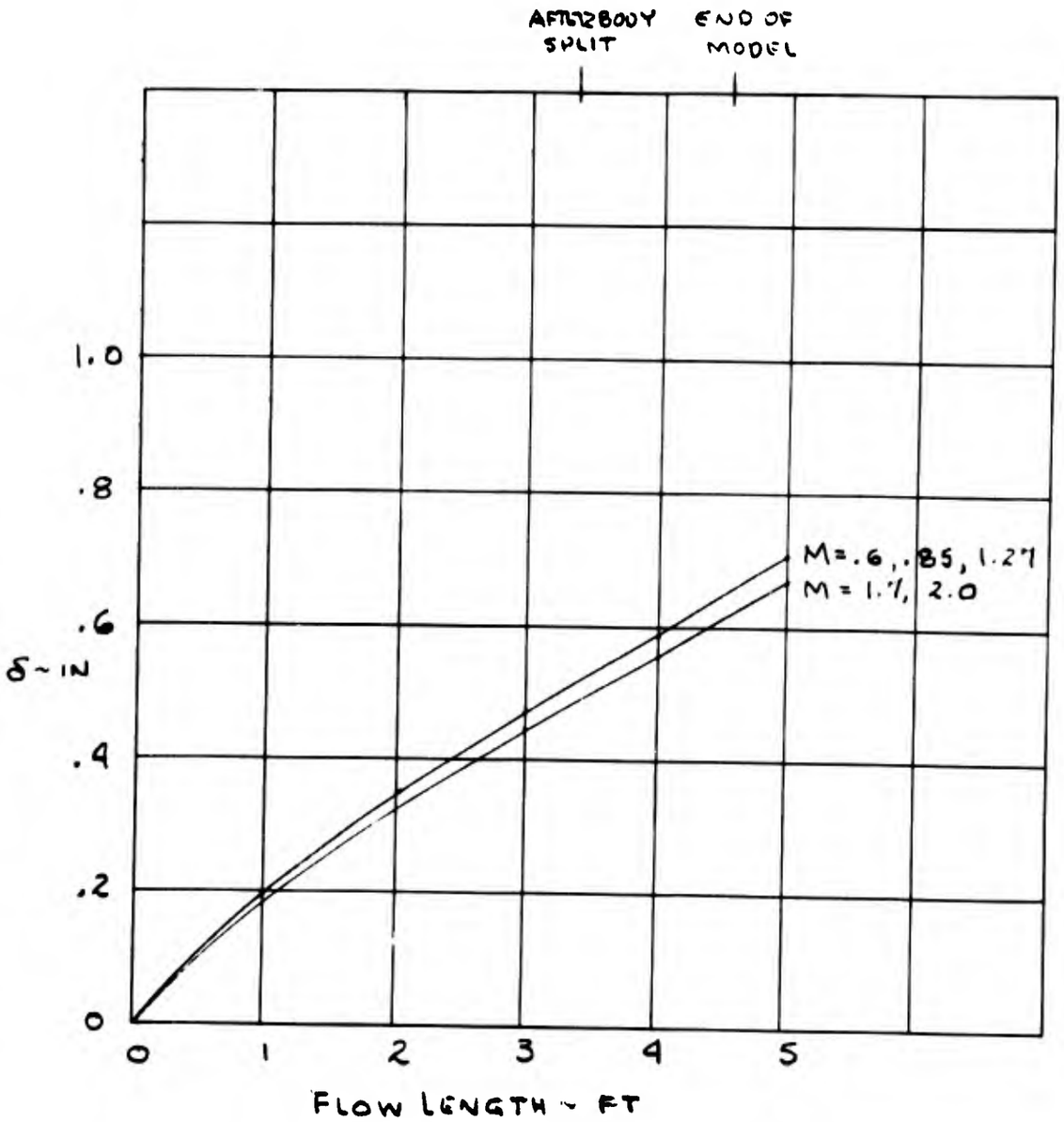

Figure 179. Estimated Turbulent Boundary Layer Thickness on Model

(The reverse of this page is blank)

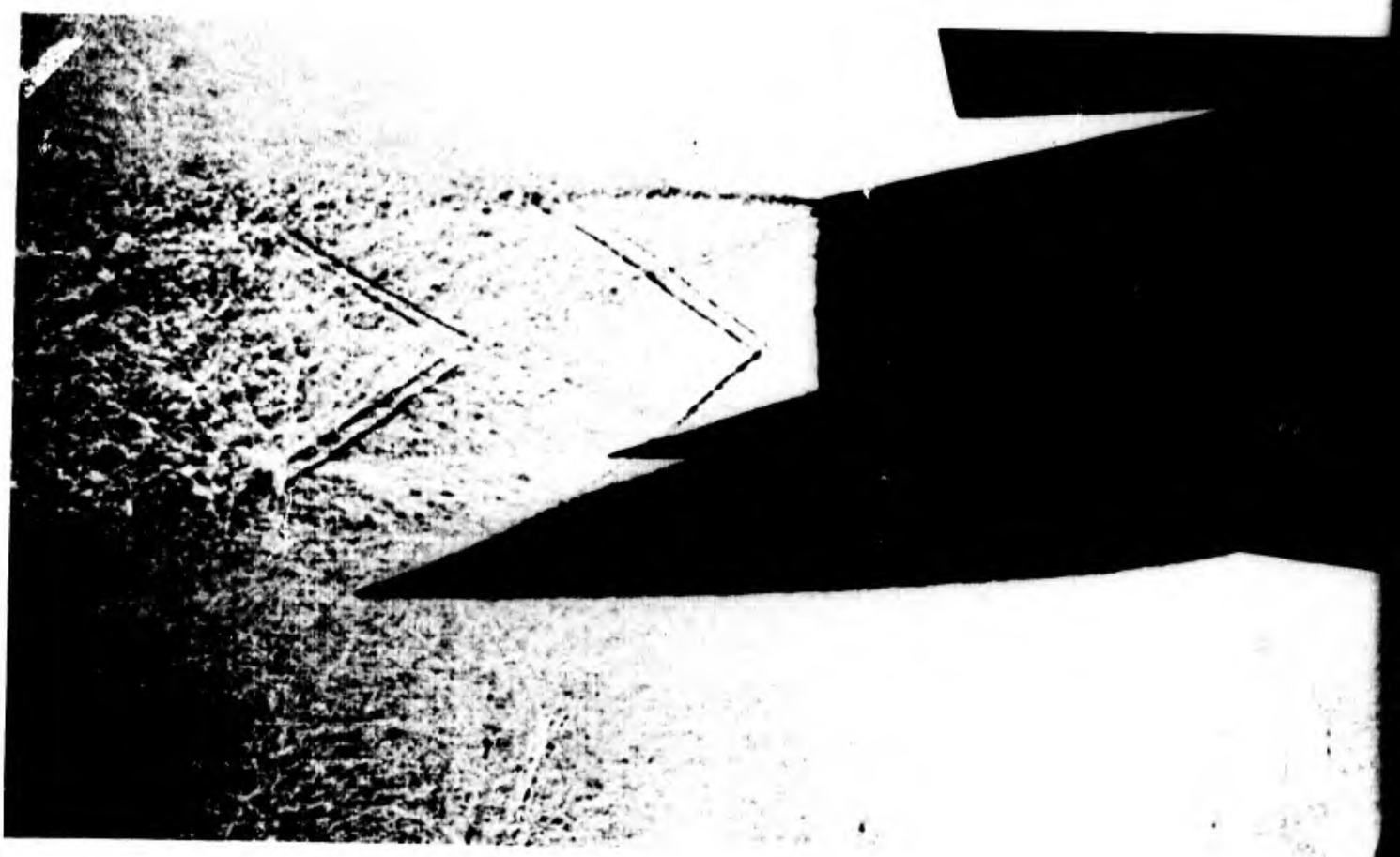

A.

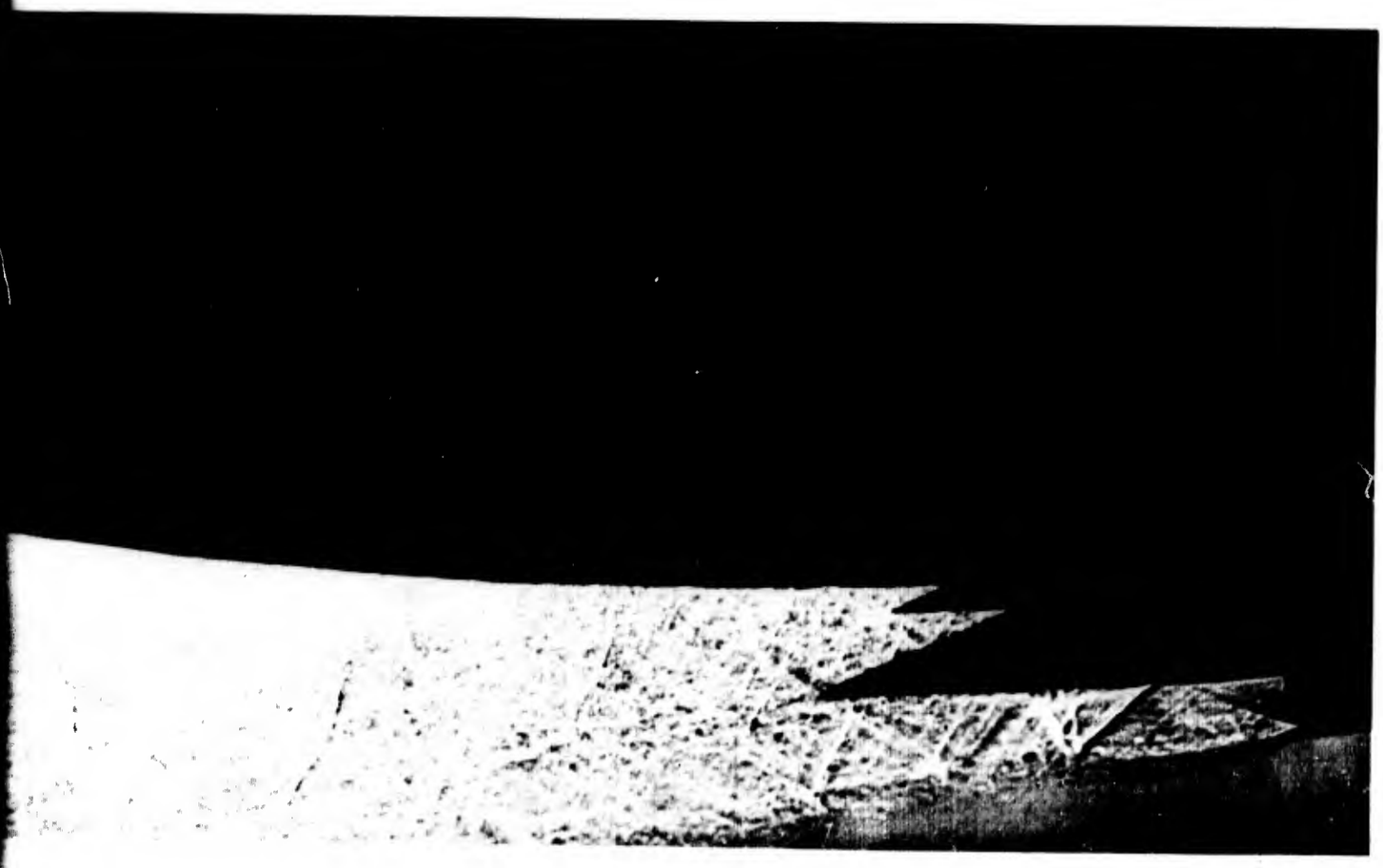

Figure 180. Composite Shadowgraph of C-D and Plug Nozzles

B.

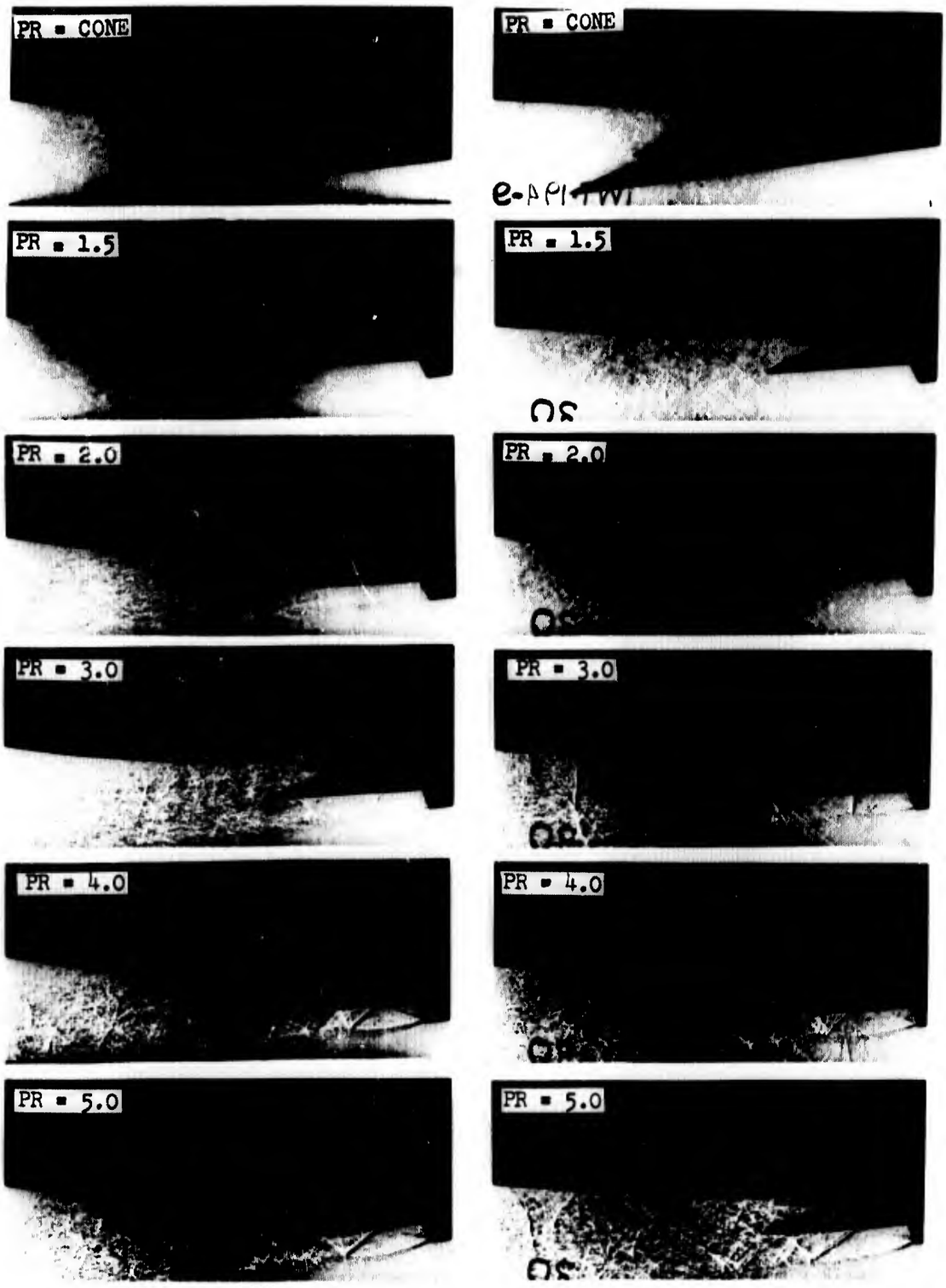

Figure 181. Shadowgraph of Plug Nozzle Exhaust Plume

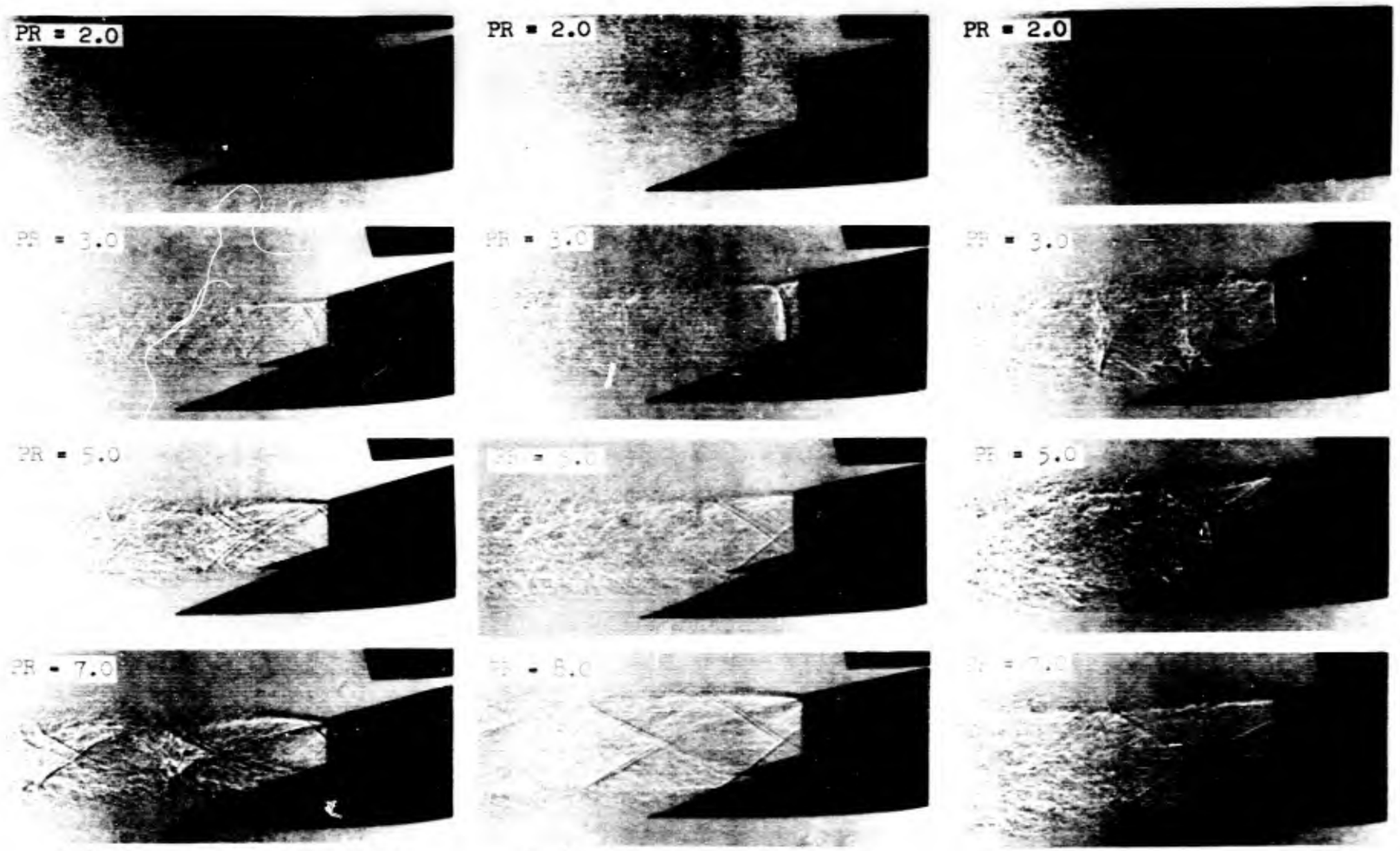

Figure 182. Shadowgraph of C-D Nozzle Exhaust Plume - M= .614

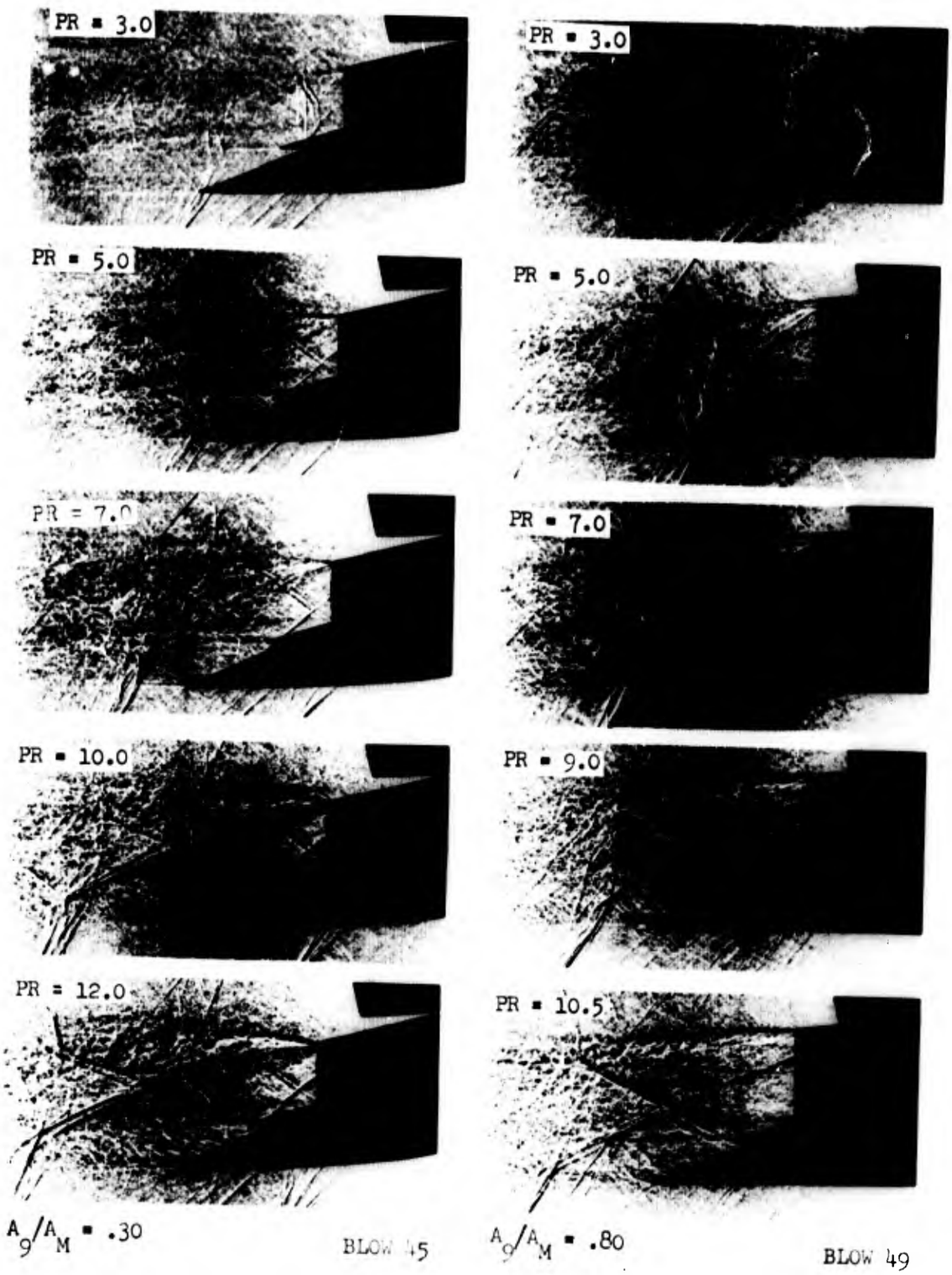

α =3°

Figure 183. Shadowgraph of C-D Nozzle Exhaust Plume-M = 1.27

A_9/A_M = .50 $P_T/P_{O\,[C-D]}$ = 1.0 $P_T/P_{O\,[PLUG]}$ = 10.0 α=3°

Figure 184. Schlieren Photograph of Complete Model - M = 1.70

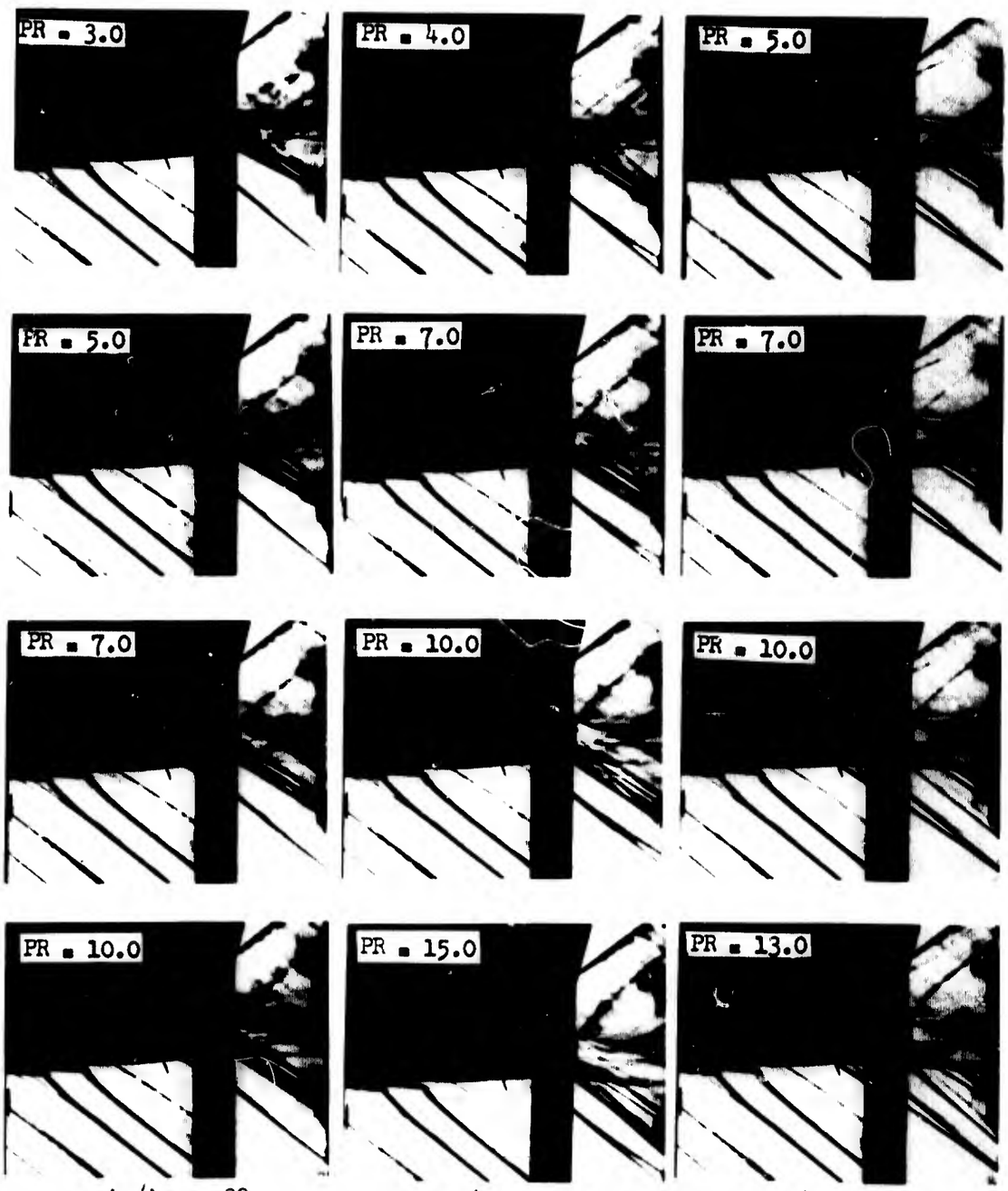

Figure 185. Exhaust Plume for Varying C-D Nozzle Pressure Ratio - M = 1.7

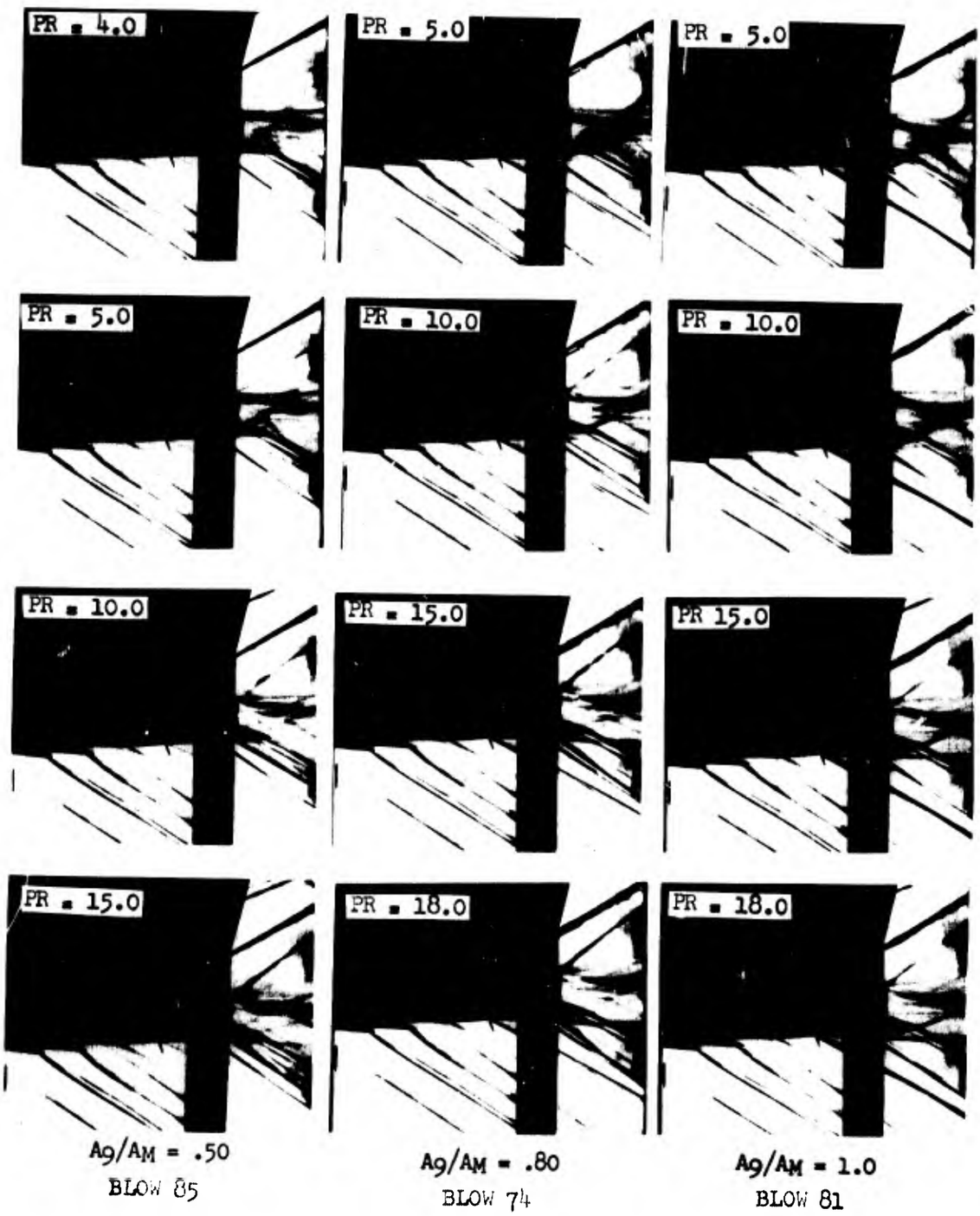

α =3° $P_T/P_{O\,[PLUG]}$ = 5.0

Figure 186. Exhaust Plume for Varying C-D Nozzle Pressure Ratio -M = 2.0

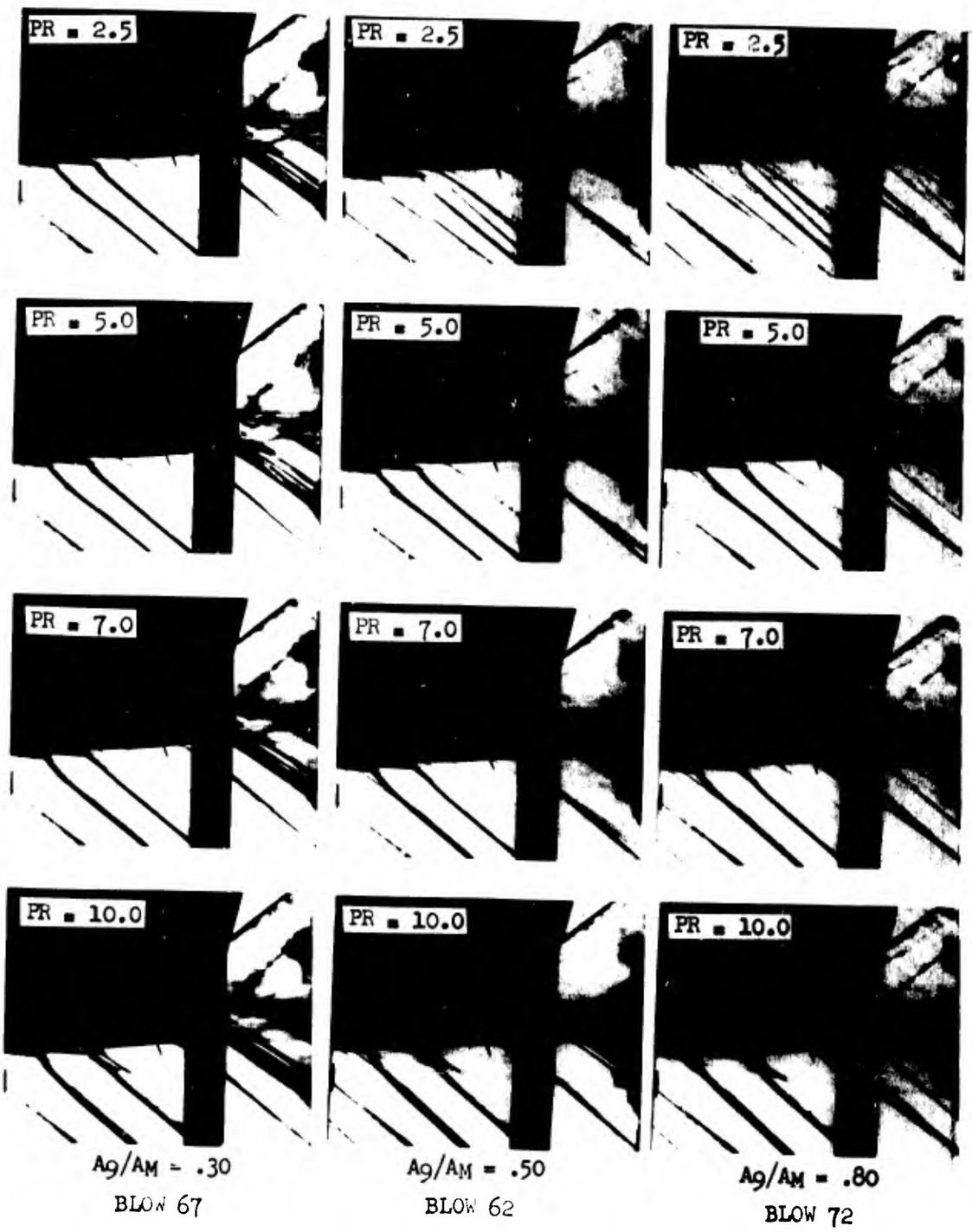

$\alpha = 3°$ P_T/P_0 [C-D] = 10.0

Figure 187. Exhaust Plume for Varying Plug Nozzle Pressure Ratio

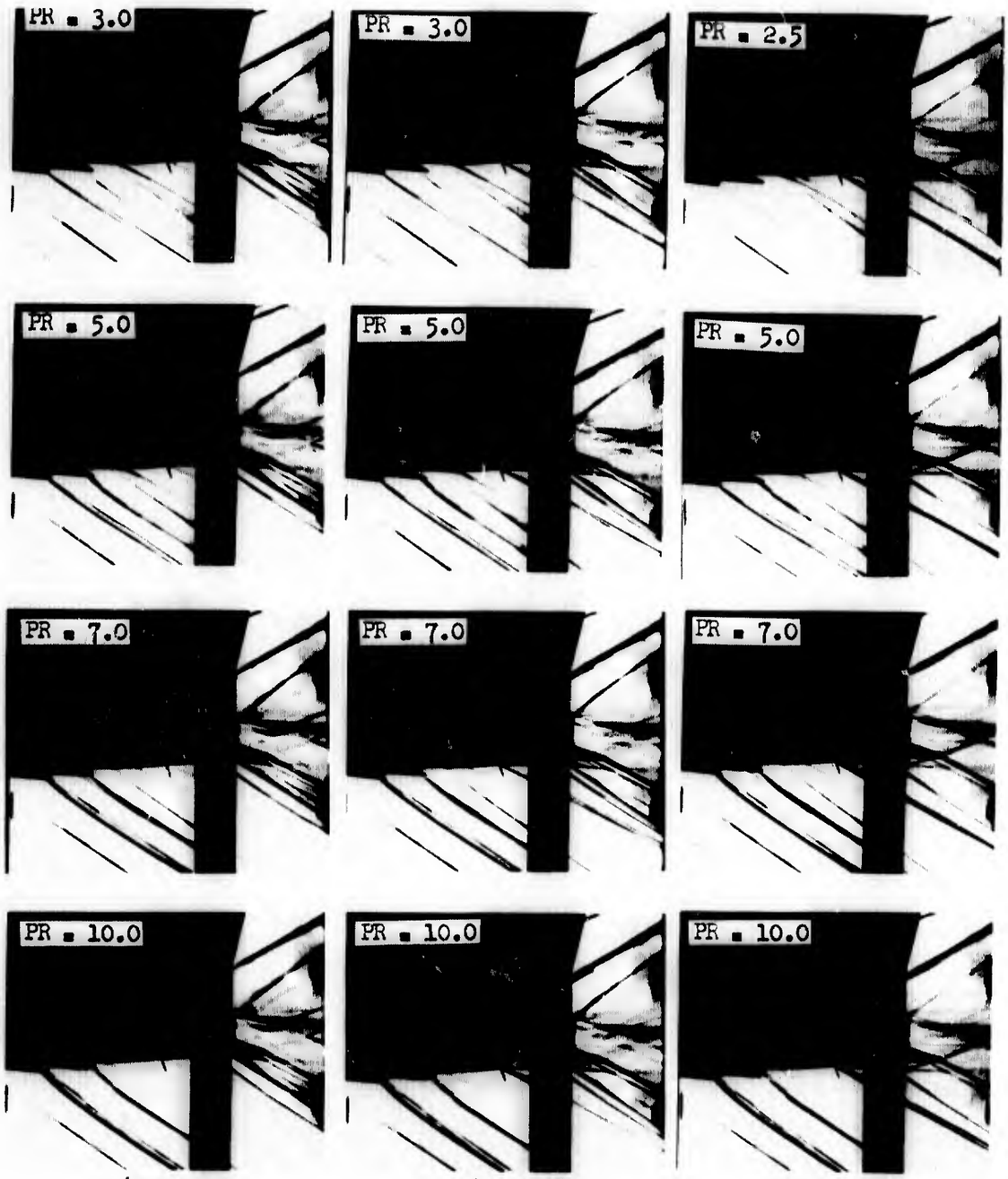

Figure 188. Exhaust Plume for Varying Plug Nozzle Pressure Ratio- M = 2.0

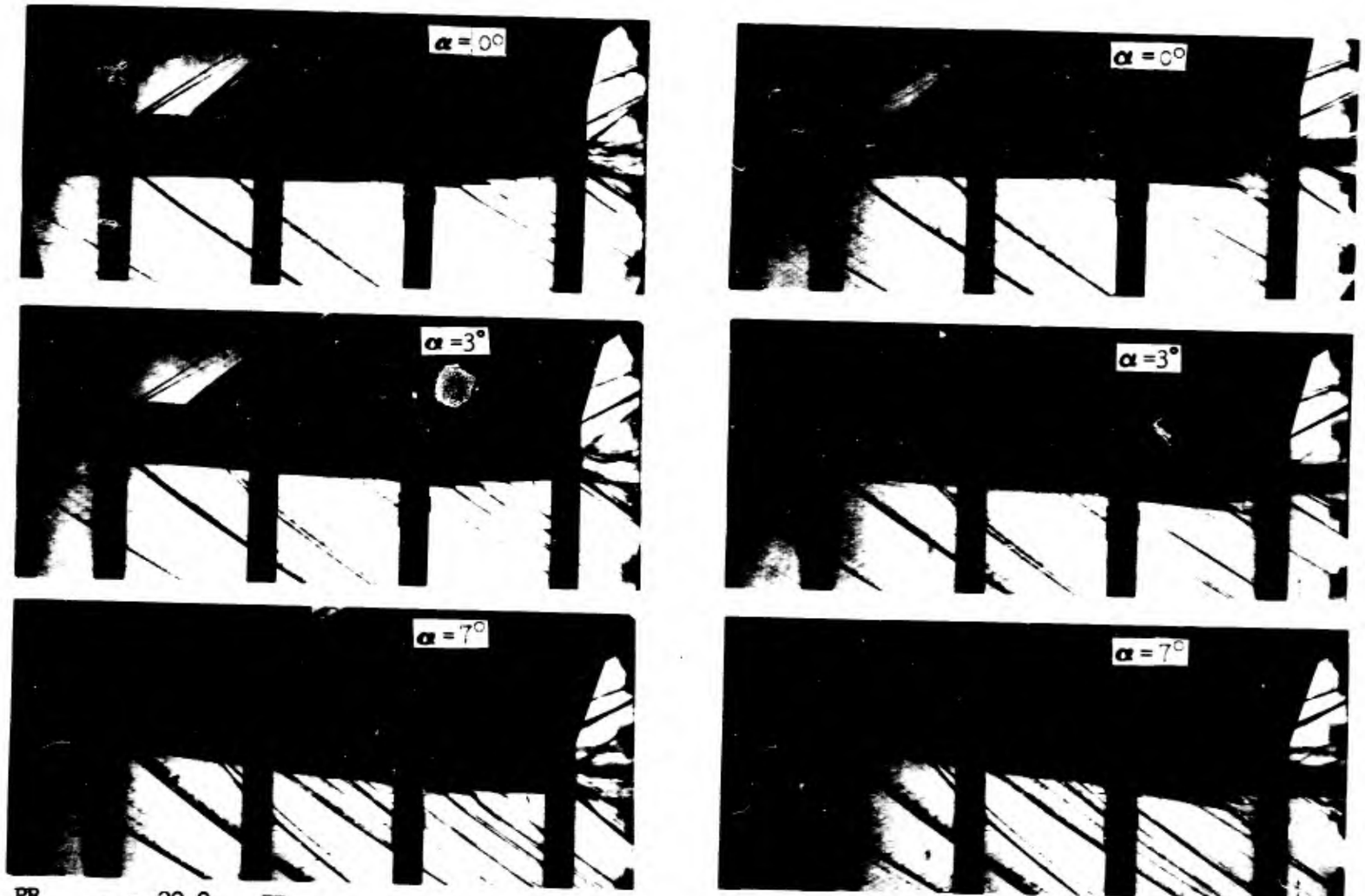

Figure 189. Angle of Attack Variation

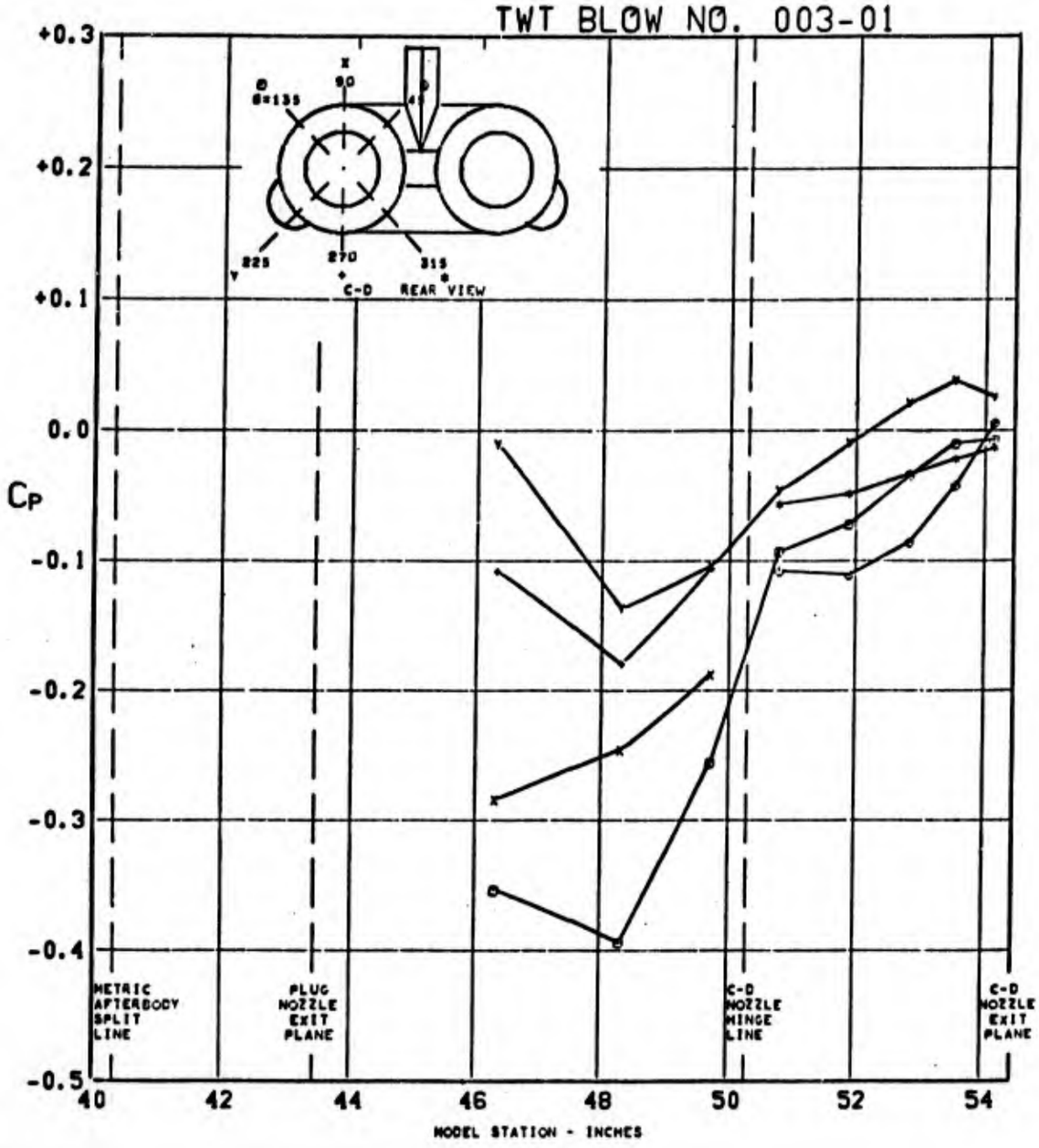

FIGURE 190. PRESSURE COEFFICIENTS ON C-D AFTERBODY (W1B1K1N1 P01 H1V1) Λ_{LE}=30° AT 0.850 M_0, $(P_T/P_0)_{C-D}$=CONE, $(P_T/P_0)_{PLUG}$=CONE, α= 0.0

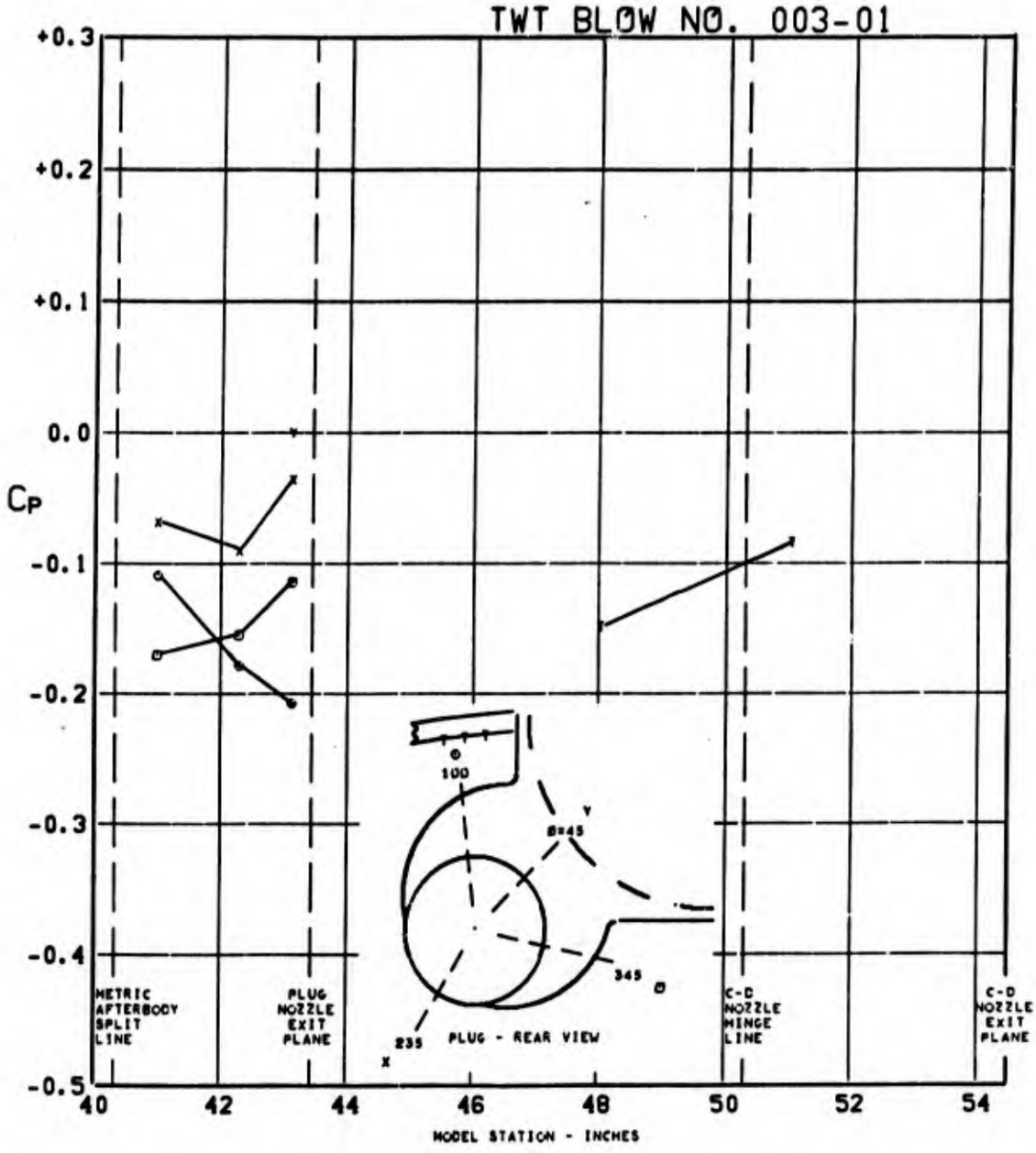

FIGURE 191. PRESSURE COEFFICIENTS ON TAIL & PLUG AFTERBODY (W1B1K1N1 P01 H1V1) Λ_{LE}=30° AT 0.850 M_0, $(P_T/P_0)_{C-D}$=CONE, $(P_T/P_0)_{PLUG}$=CONE, α= 0.0

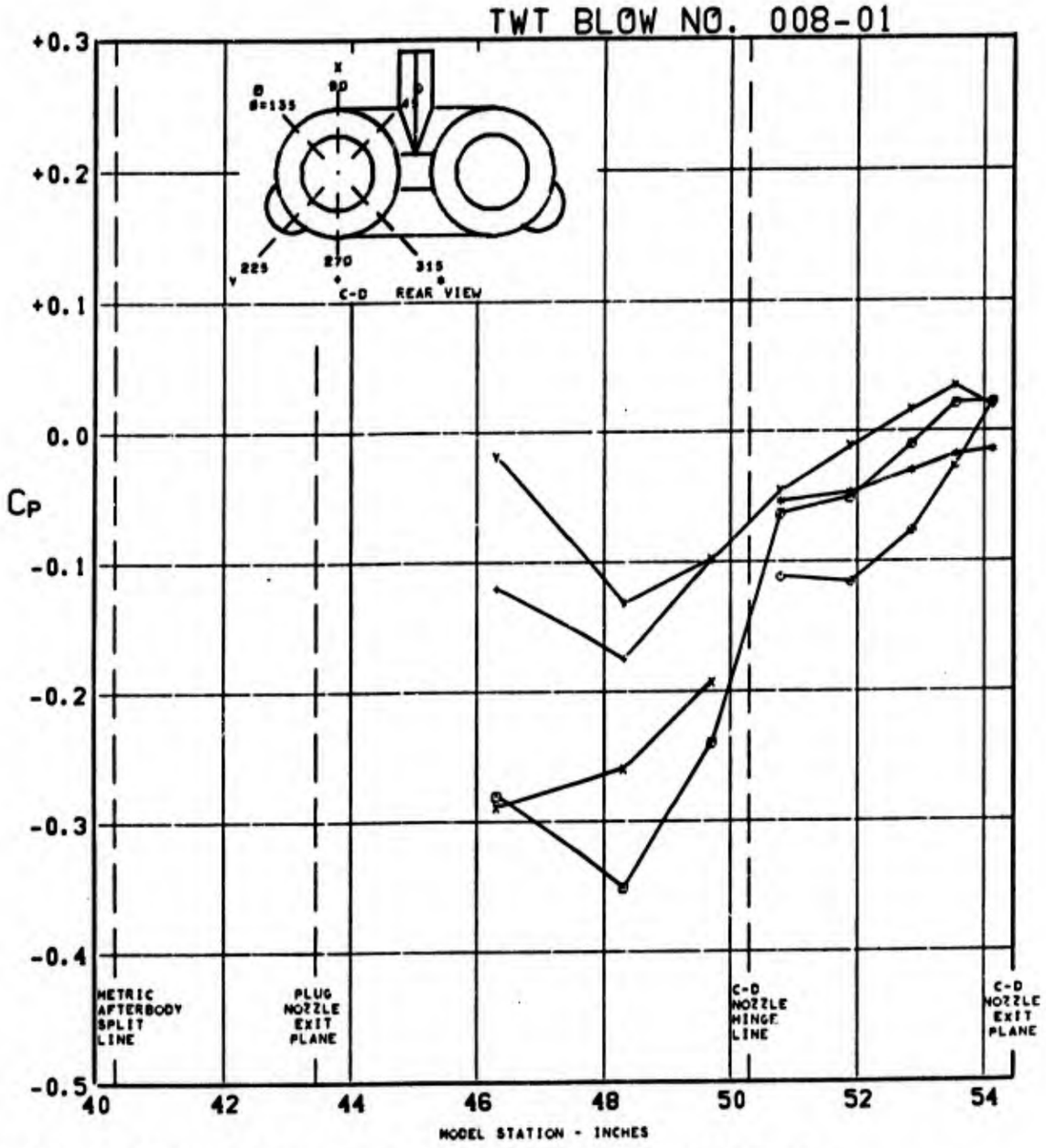

FIGURE 192. PRESSURE COEFFICIENTS ON C-D AFTERBODY (W1B1K1N1 P01 H1V1) Λ_{LE}=70° AT . 0.852 M_0 , $(P_T/P_0)_{C-D}$=CONE , $(P_T/P_0)_{PLUG}$ =CONE , α= 0.0

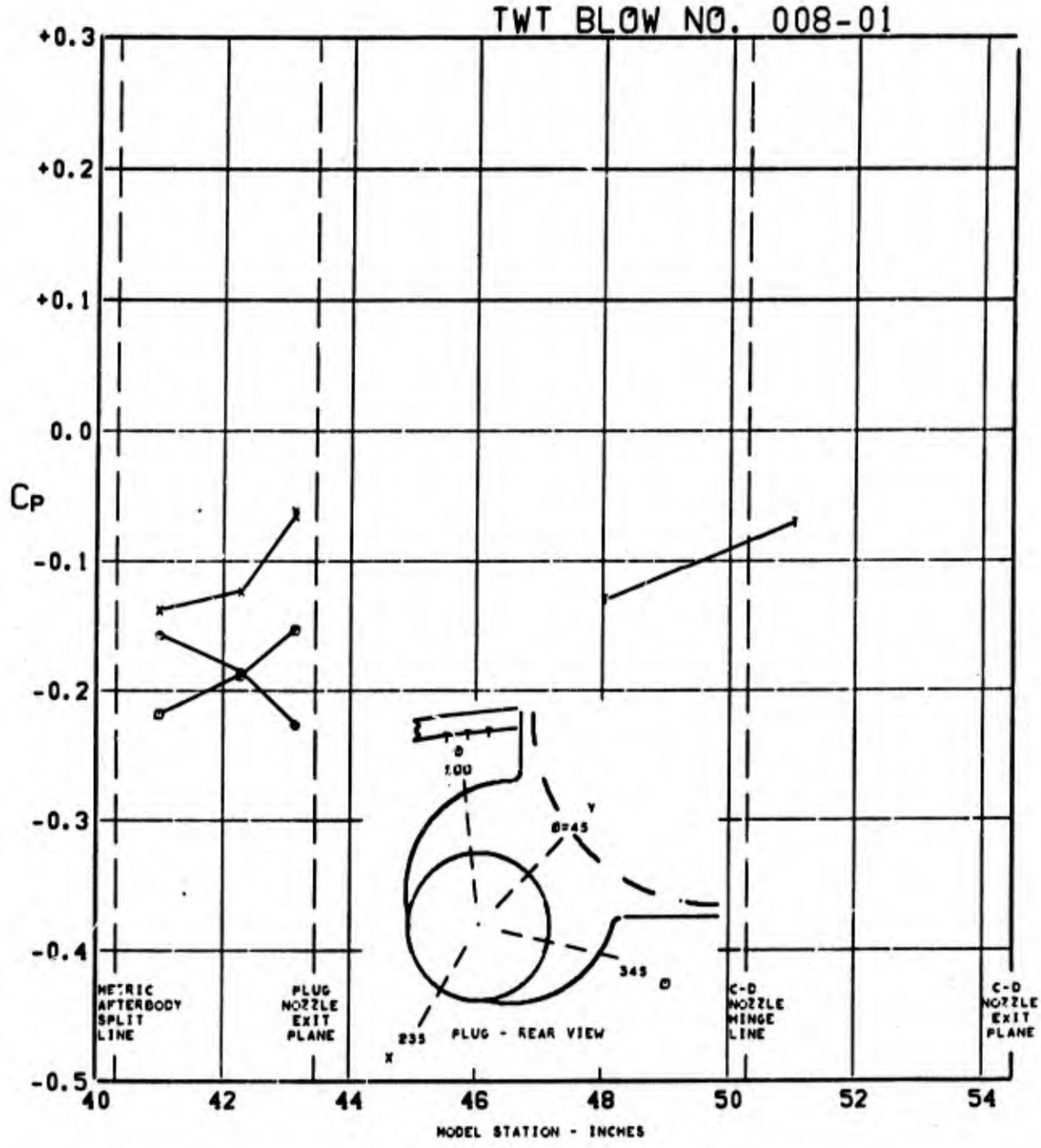

FIGURE 193. PRESSURE COEFFICIENTS ON TAIL & PLUG AFTERBODY (W1B1K1N1 P01 H1V1) Λ_{LE}=70° AT 0.852 M_0, $(P_T/P_0)_{C-D}$=CONE, $(P_T/P_0)_{PLUG}$=CONE, α= 0.0

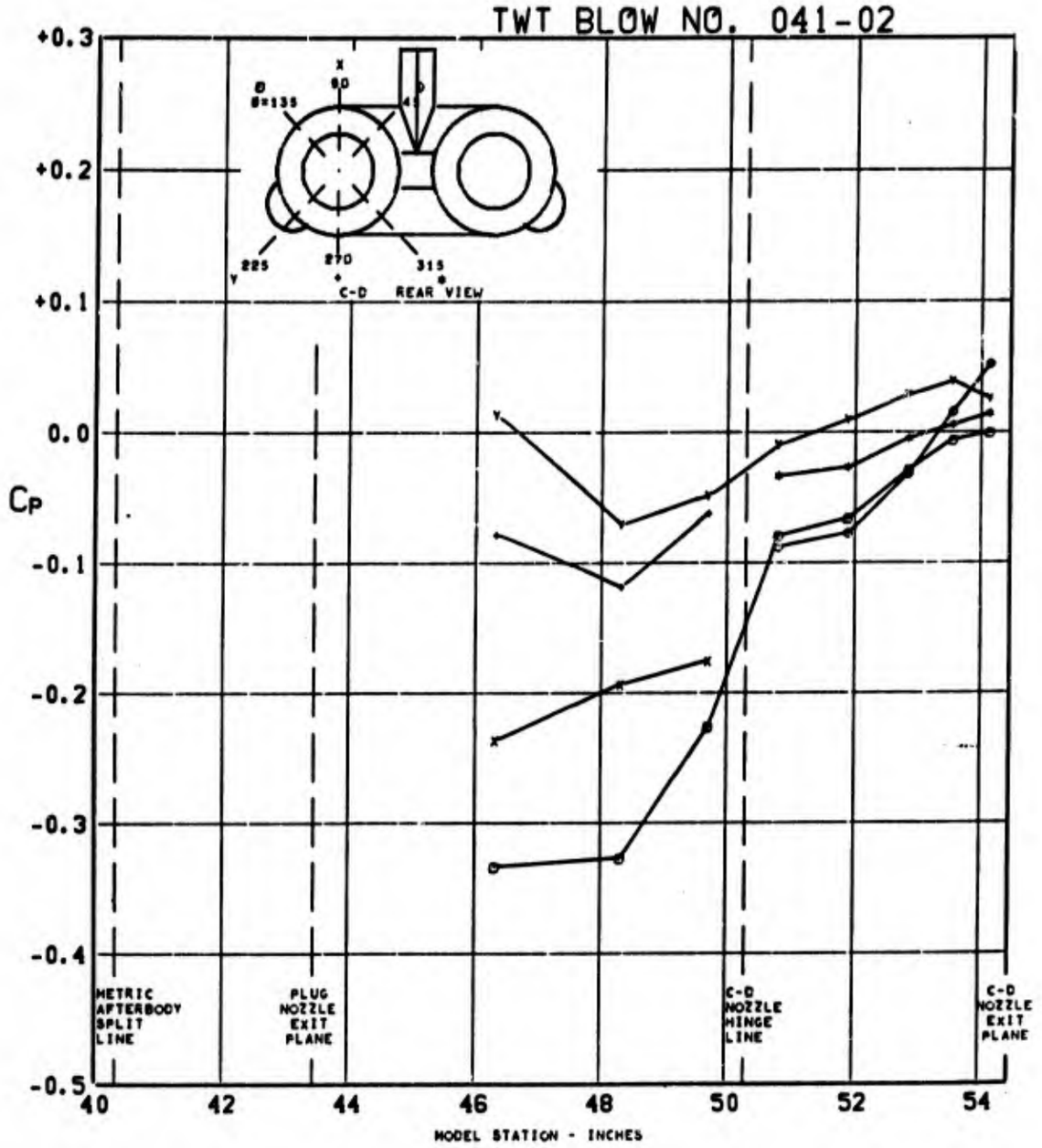

FIGURE 194. PRESSURE COEFFICIENTS ON C-D AFTERBODY (W1B1K1N1 P01 H1V1) Λ_{LE}=30° AT 0.613 M_0, $(P_T/P_0)_{C-D}$=CONE, $(P_T/P_0)_{PLUG}$=CONE, α= 2.8

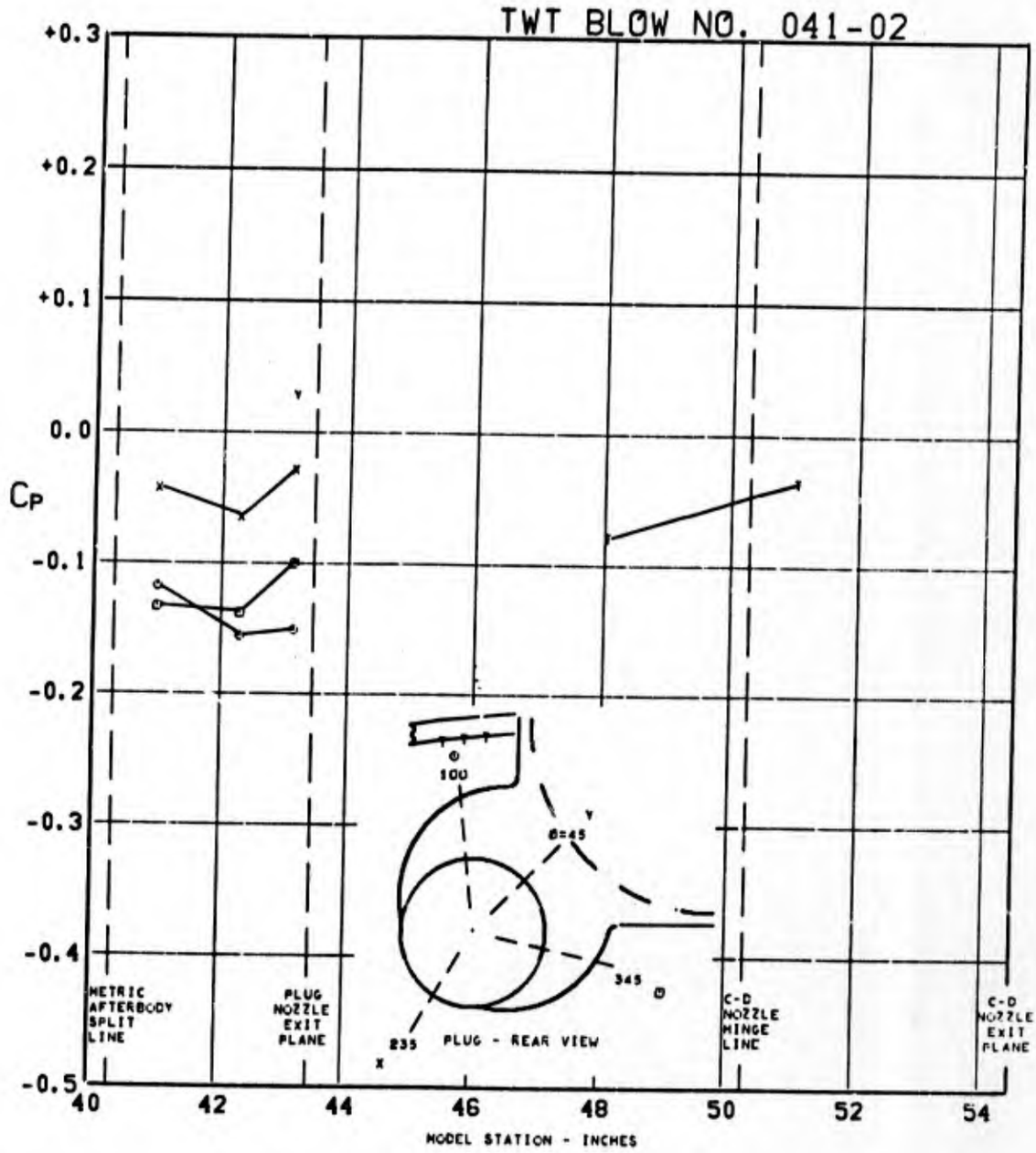

FIGURE 195. PRESSURE COEFFICIENTS ON TAIL & PLUG AFTERBODY (W1B1K1N1 P01 H1V1) $\Lambda_{LE}=30°$ AT 0.613 M_0, $(P_T/P_0)_{C-D}$=CONE, $(P_T/P_0)_{PLUG}$=CONE, α= 2.8

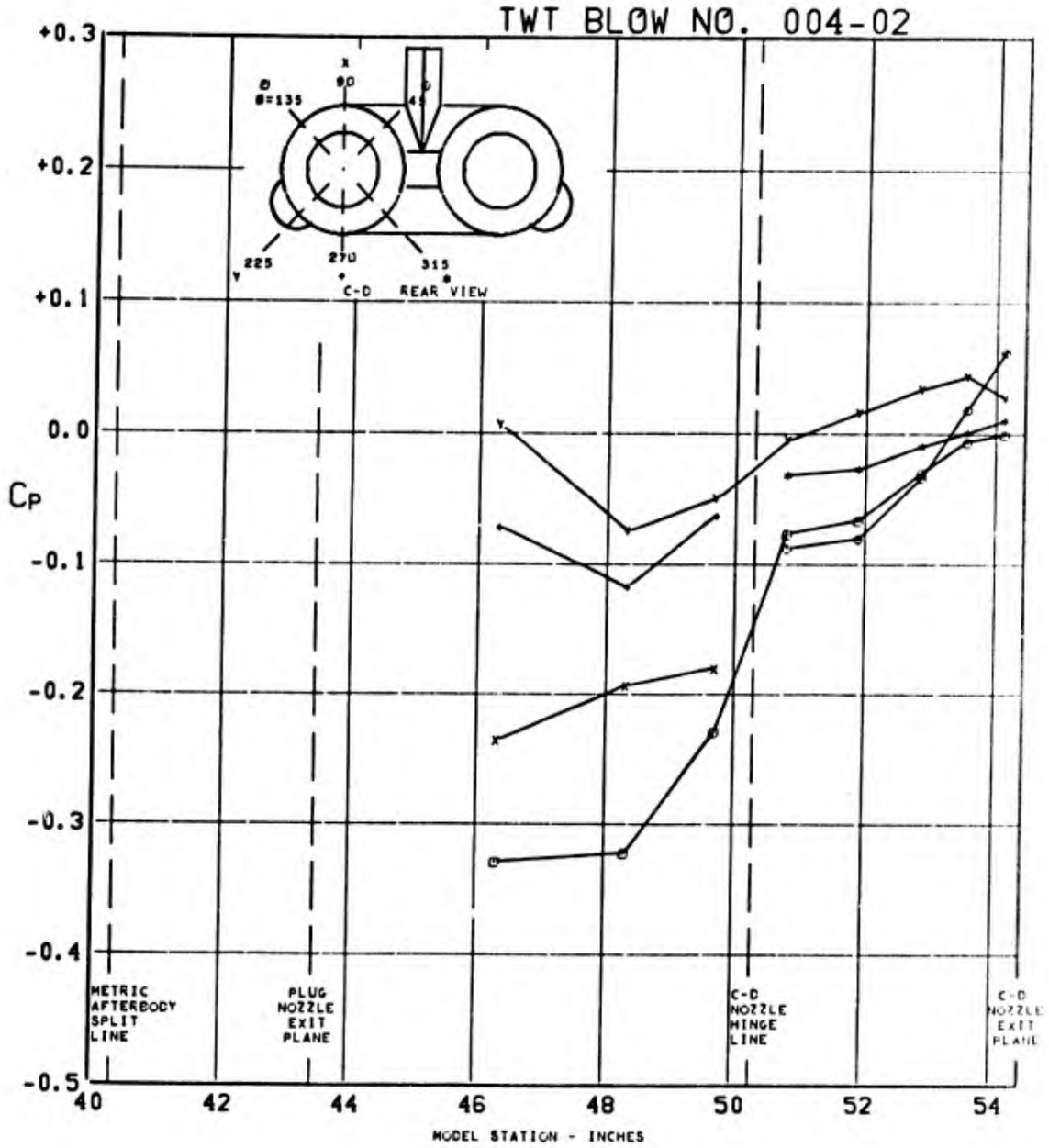

FIGURE 196. PRESSURE COEFFICIENTS ON C-D AFTERBODY (W1B1K1N2 P01 H1V1) $\Lambda_{LE}=30°$ AT 0.612 M_0, $(P_T/P_0)_{C-D}$=CONE, $(P_T/P_0)_{PLUG}$=CONE, α= 3.2

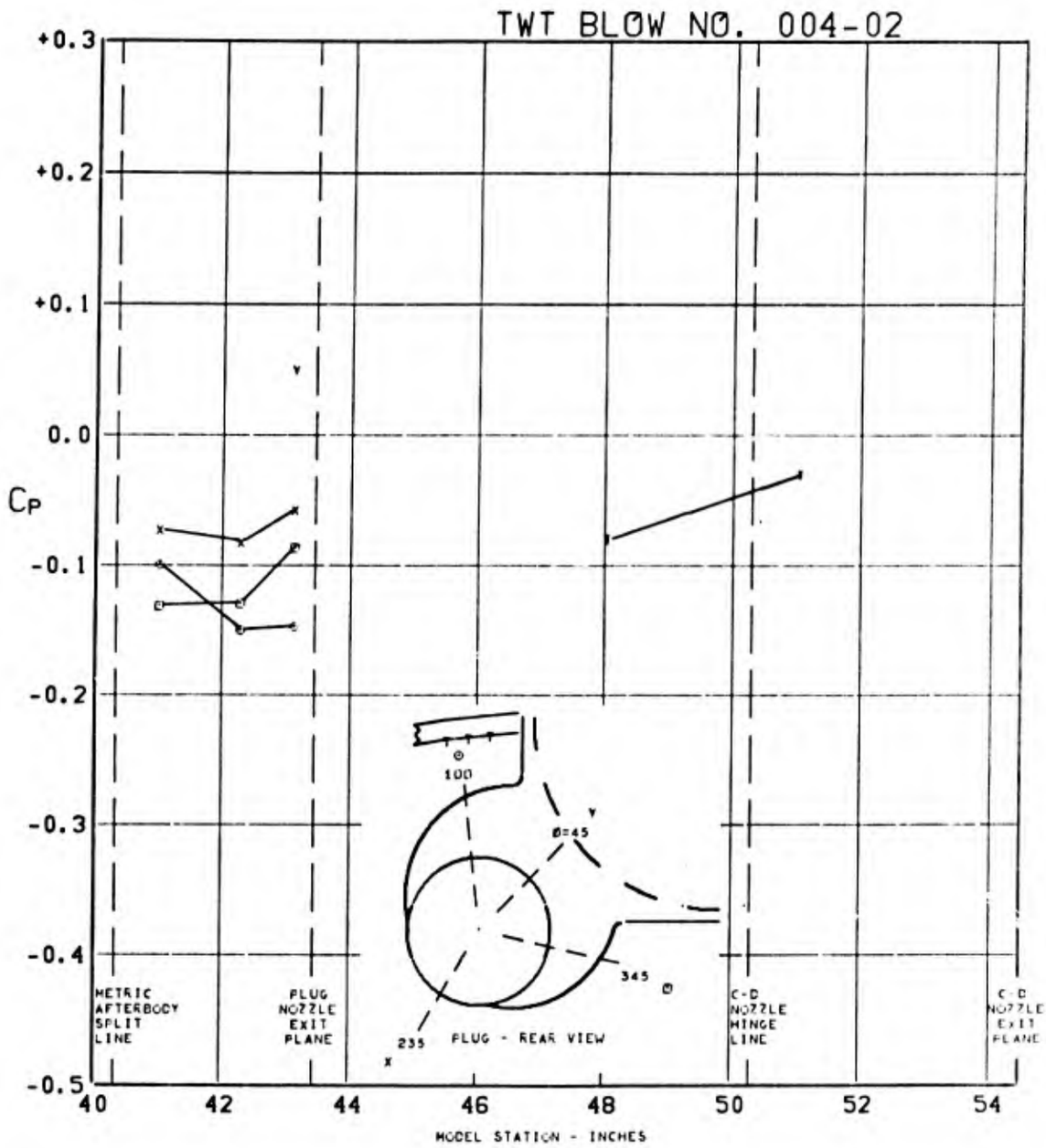

FIGURE 197. PRESSURE COEFFICIENTS ON TAIL & PLUG AFTERBODY (W1B1K1N2 P01 H1V1) Λ_{LE}=30° AT 0.612 M_0, $(P_T/P_0)_{C-D}$=CONE, $(P_T/P_0)_{PLUG}$=CONE, α= 3.2

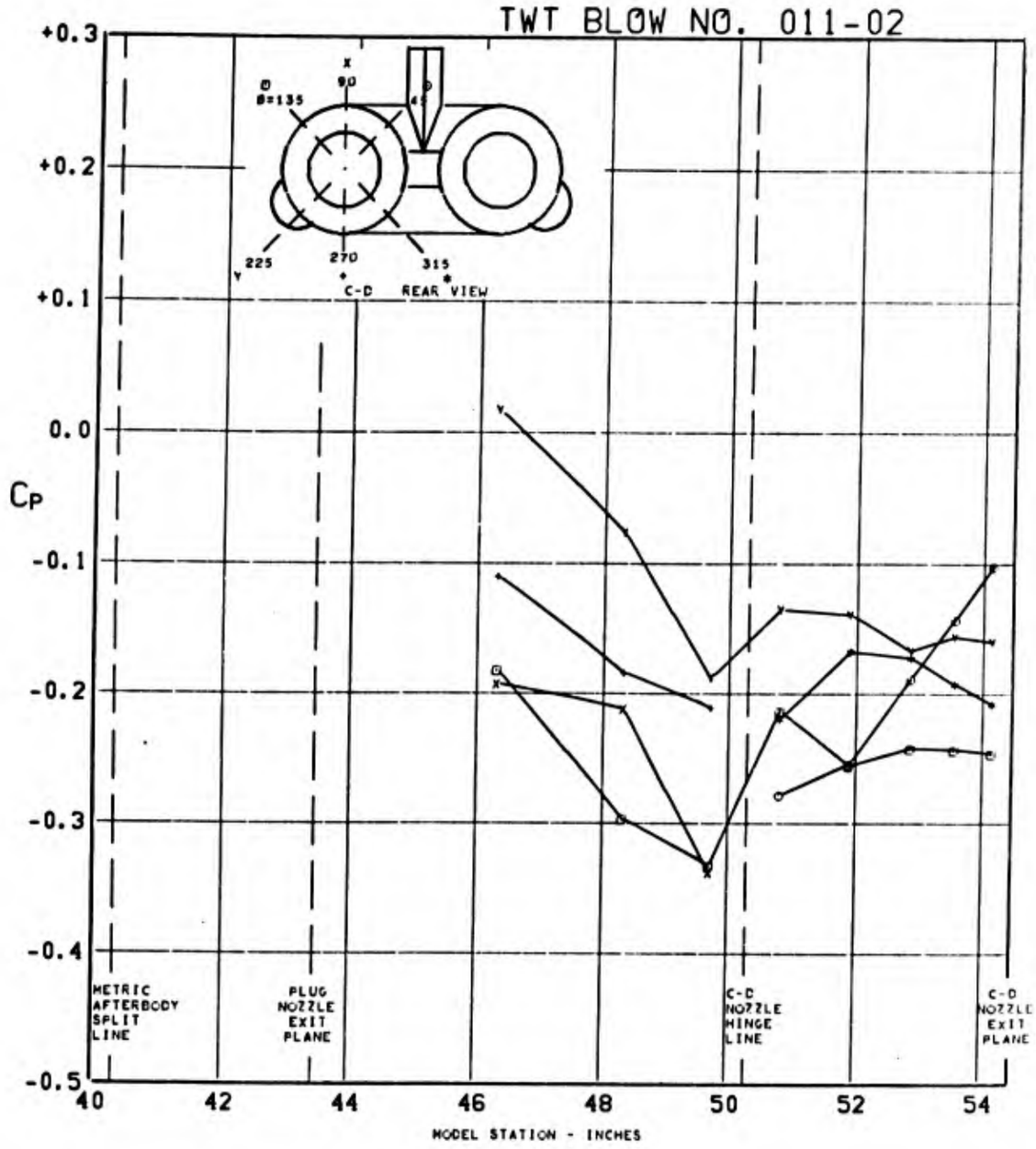

FIGURE 198. PRESSURE COEFFICIENTS ON C-D AFTERBODY (W1B1K1N1 P01 H1V1) Λ_{LE}=70° AT 1.271 M_0, $(P_T/P_0)_{C-D}$=CONE, $(P_T/P_0)_{PLUG}$=CONE, α= 2.8

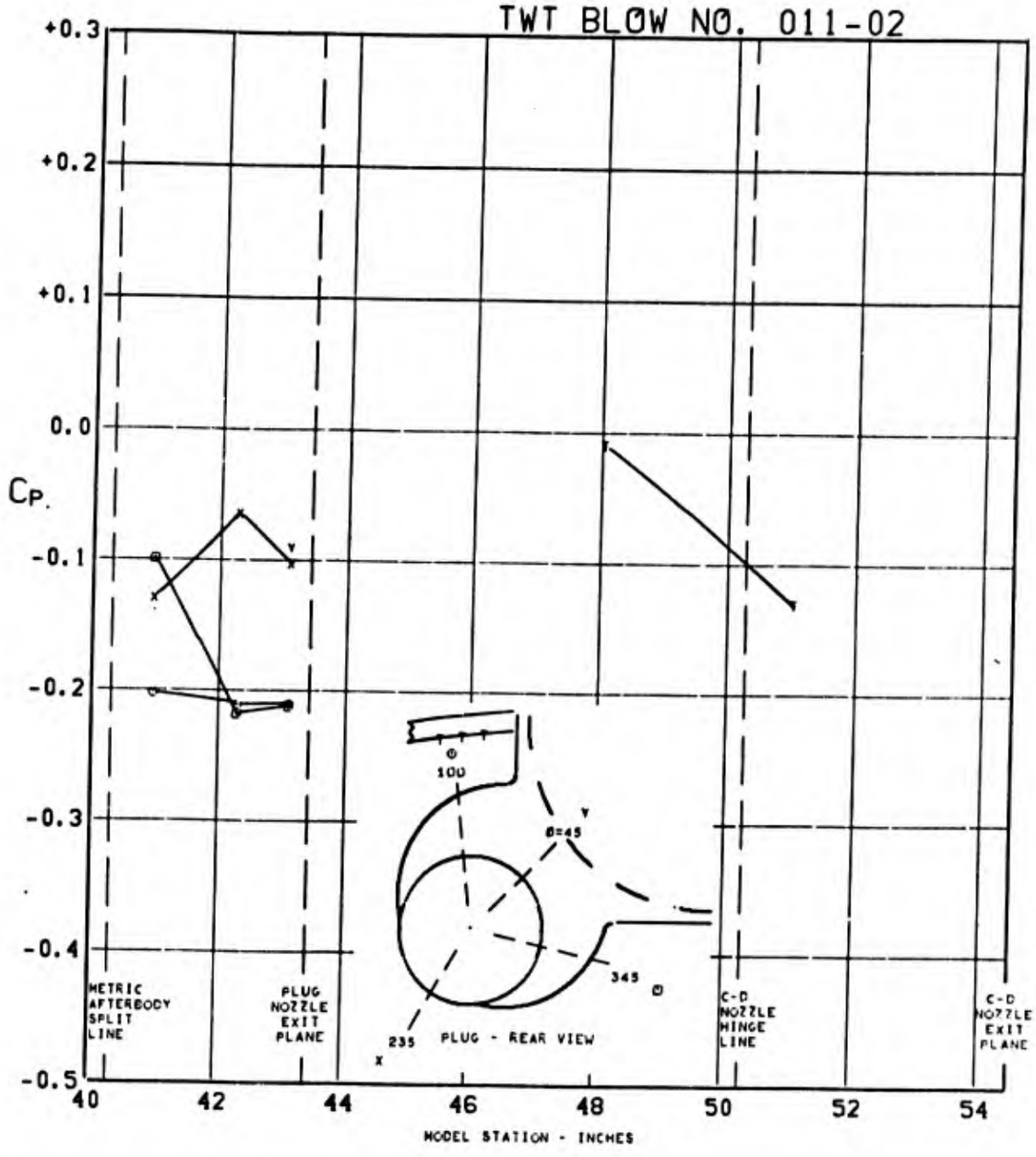

FIGURE 199. PRESSURE COEFFICIENTS ON TAIL & PLUG AFTERBODY (W1B1K1N1 P01 H1V1) $\Lambda_{LE}=70°$ AT 1.271 M_0, $(P_T/P_0)_{C-D}$=CONE, $(P_T/P_0)_{PLUG}$=CONE, α= 2.8

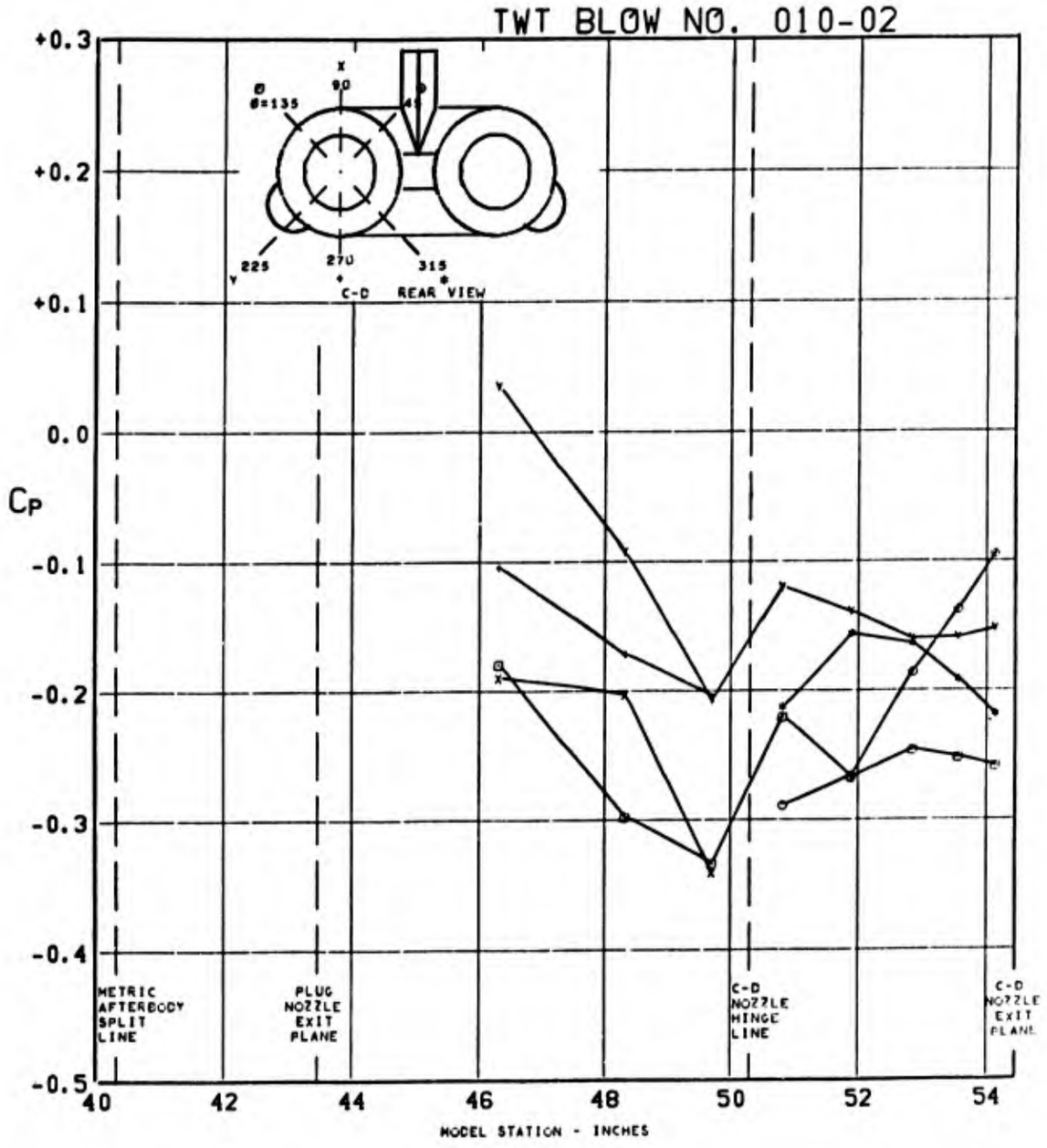

FIGURE 200. PRESSURE COEFFICIENTS ON C-D AFTERBODY (W1B1K1N2 P01 H1V1) $\Lambda_{LE}=70°$ AT 1.269 M_0, $(P_T/P_0)_{C-D}$=CONE, $(P_T/P_0)_{PLUG}$=CONE, α= 2.8

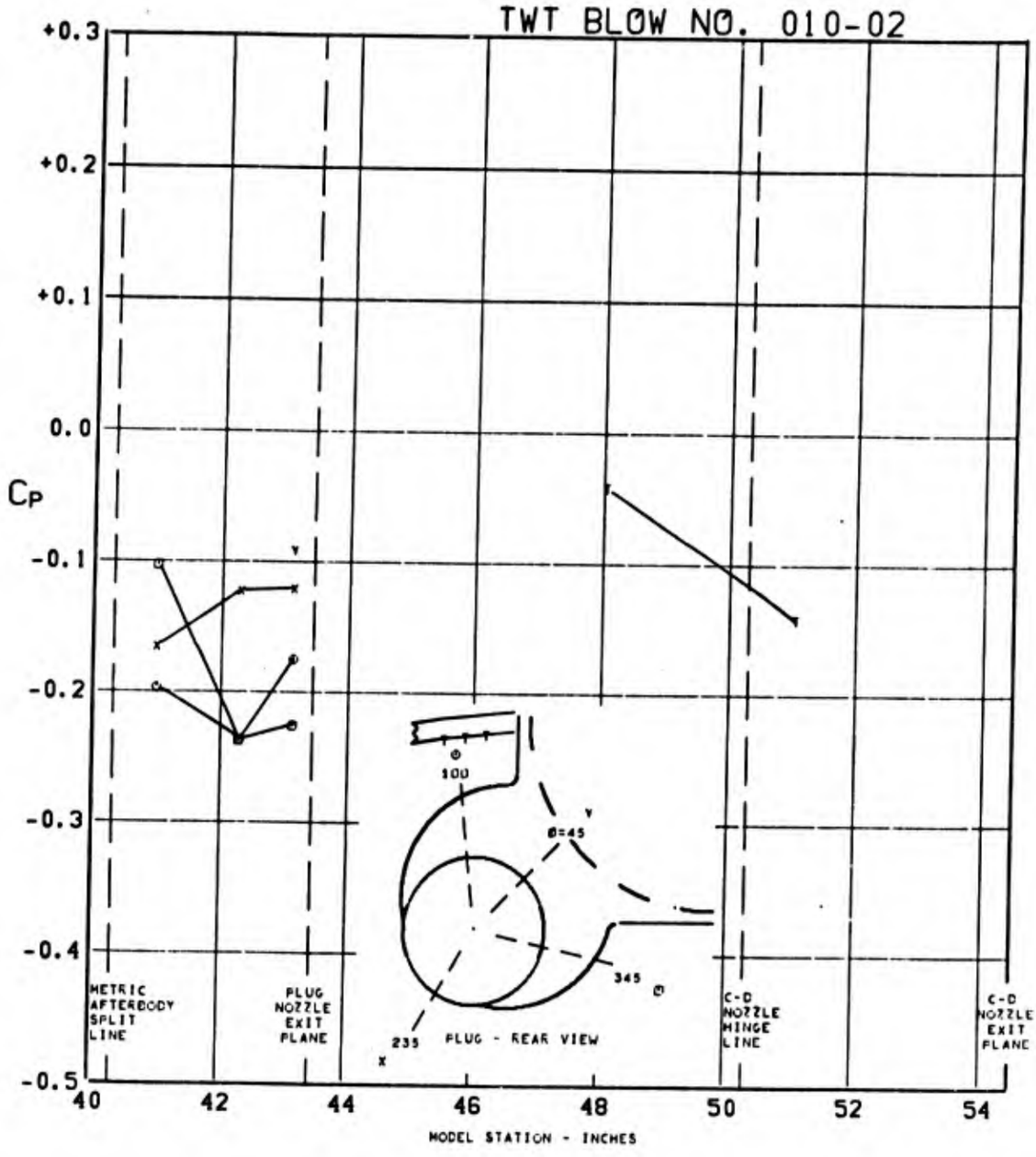

FIGURE 201. PRESSURE COEFFICIENTS ON TAIL & PLUG AFTERBODY (W1B1K1N2 P01 H1V1) $\Lambda_{LE}=70°$ AT 1.269 M_0, $(P_T/P_0)_{C-D}$=CONE, $(P_T/P_0)_{PLUG}$=CONE, α= 2.8

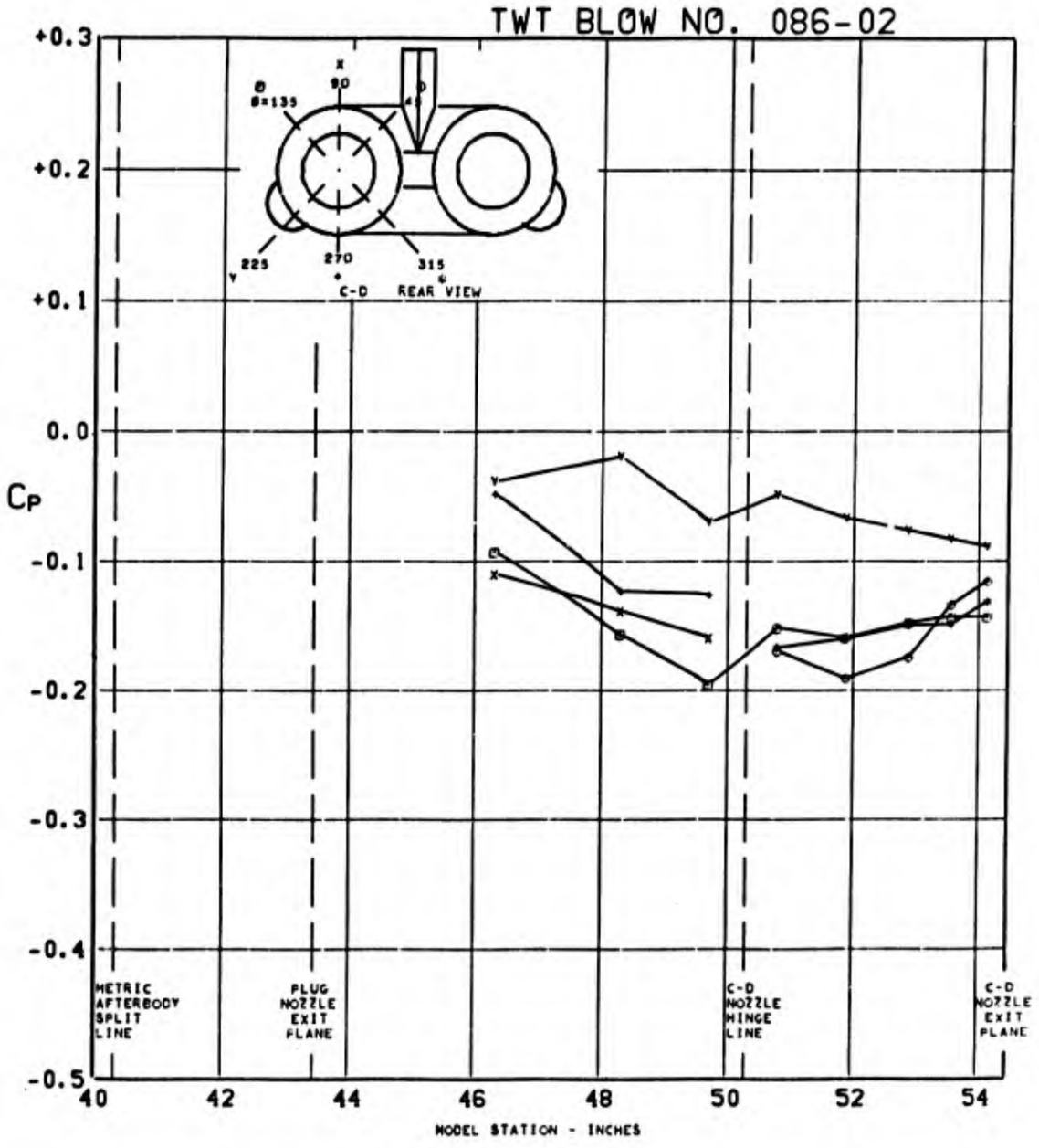

FIGURE 202. PRESSURE COEFFICIENTS ON C-D AFTERBODY (W1B1K1N1 P01 H1V1) Λ_{LE}=70° AT 1.998 M_0, $(P_T/P_0)_{C-D}$=CONE, $(P_T/P_0)_{PLUG}$=CONE, α= 2.8

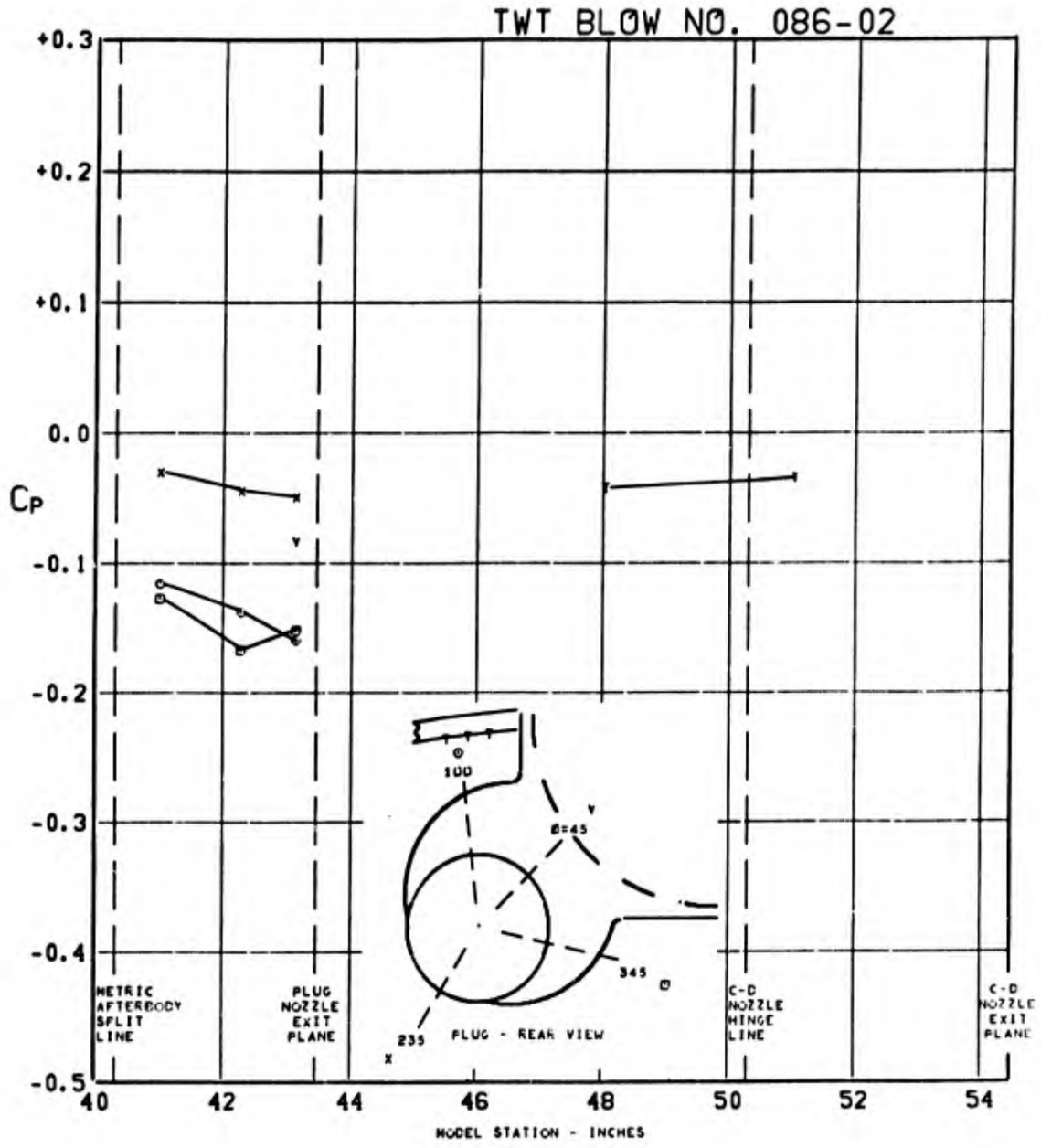

FIGURE 203. PRESSURE COEFFICIENTS ON TAIL & PLUG AFTERBODY (W1B1K1N1 P01 H1V1) Λ_{LE}=70° AT 1.998 M_0, $(P_T/P_0)_{C-D}$=CONE, $(P_T/P_0)_{PLUG}$=CONE, α= 2.8

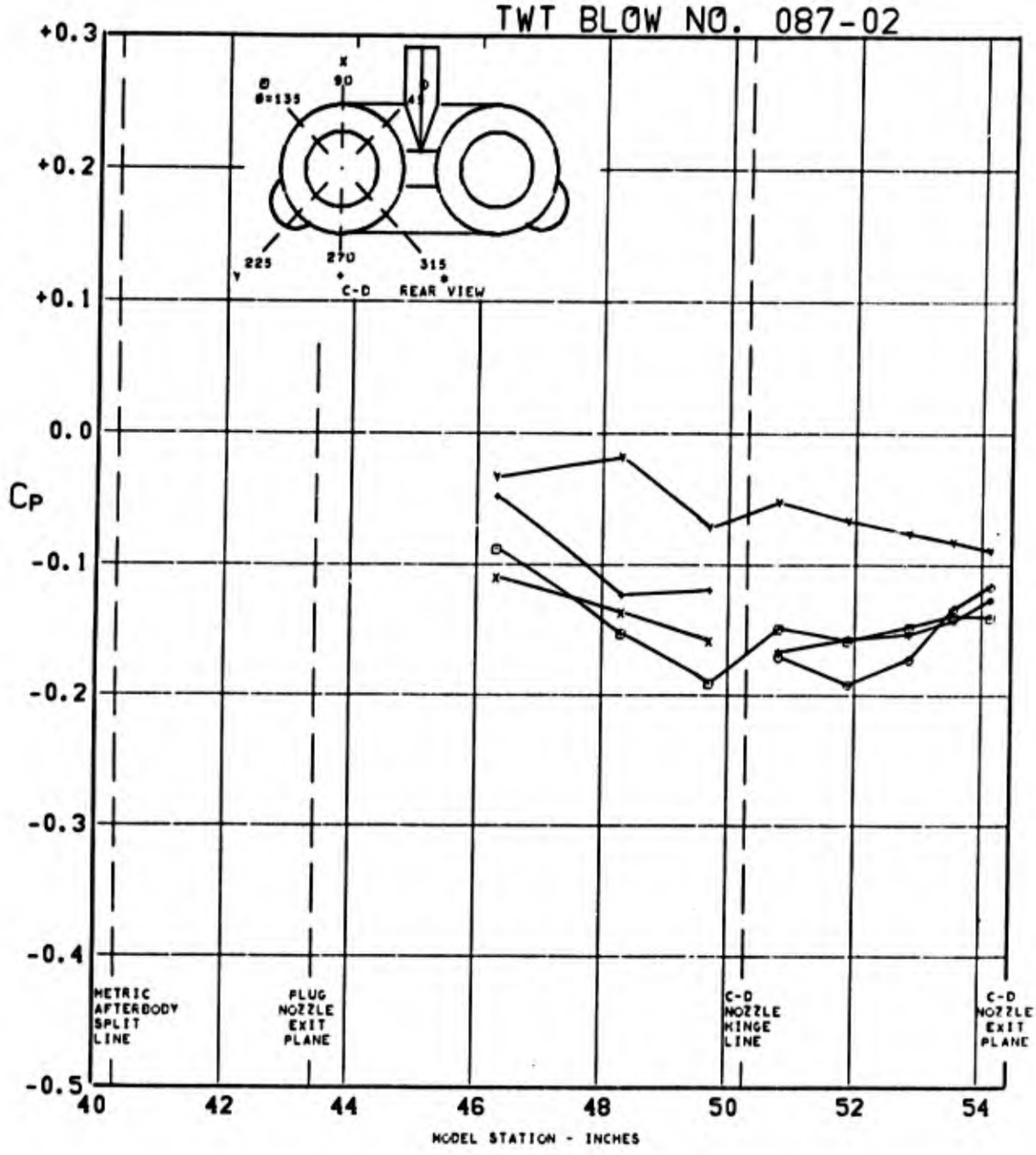

FIGURE 204. PRESSURE COEFFICIENTS ON C-D AFTERBODY (W1B1K1N2 P01 H1V1) Λ_{LE}=70° AT 1.998 M_0, $(P_T/P_0)_{C-D}$=CONE, $(P_T/P_0)_{PLUG}$=CONE, α= 2.9

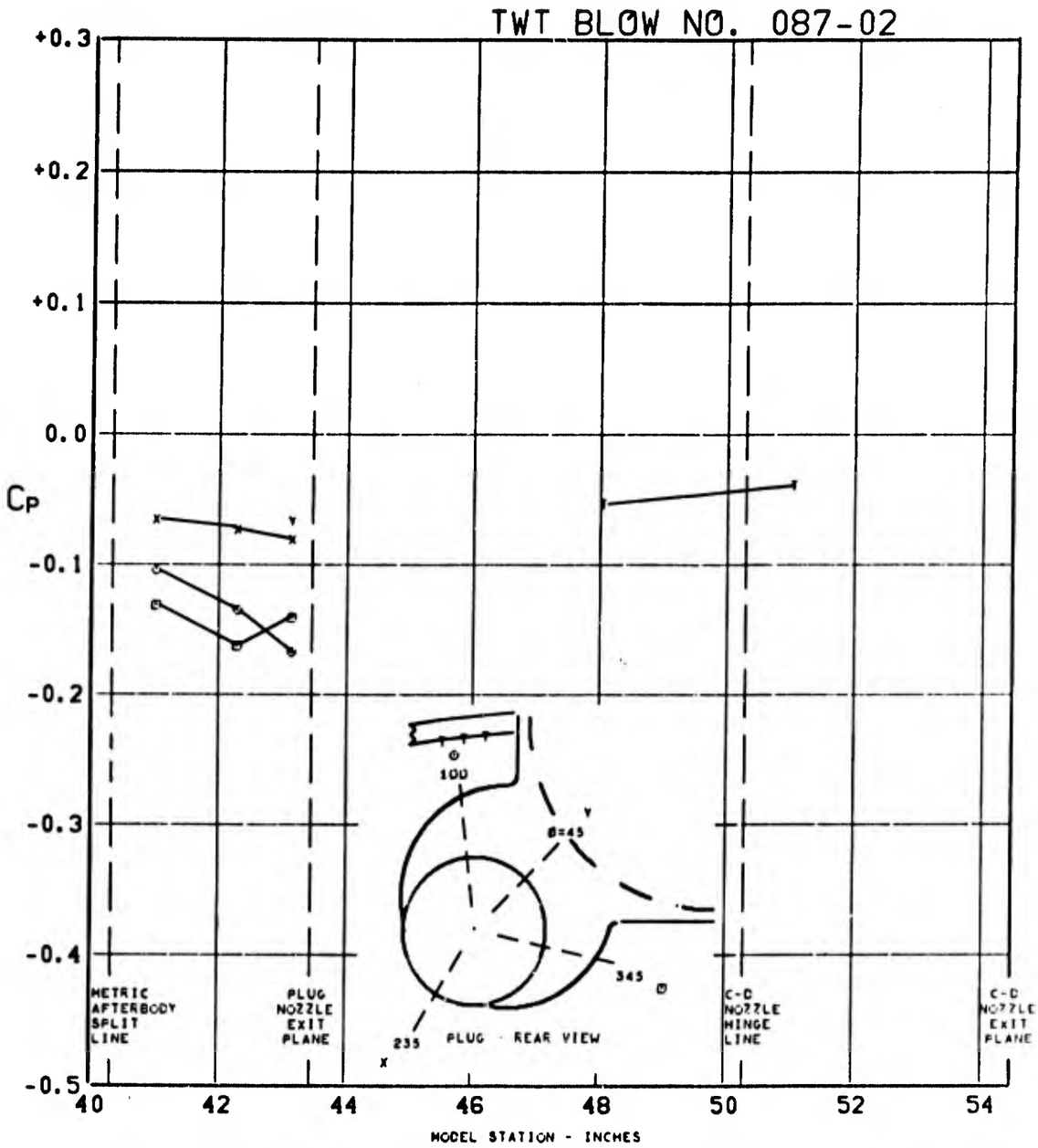

FIGURE 205. PRESSURE COEFFICIENTS ON TAIL & PLUG AFTERBODY (W1B1K1N2 P01 H1V1) Λ_{LE}=70° AT 1.998 M_0, $(P_T/P_0)_{C-D}$=CONE, $(P_T/P_0)_{PLUG}$=CONE, α= 2.9

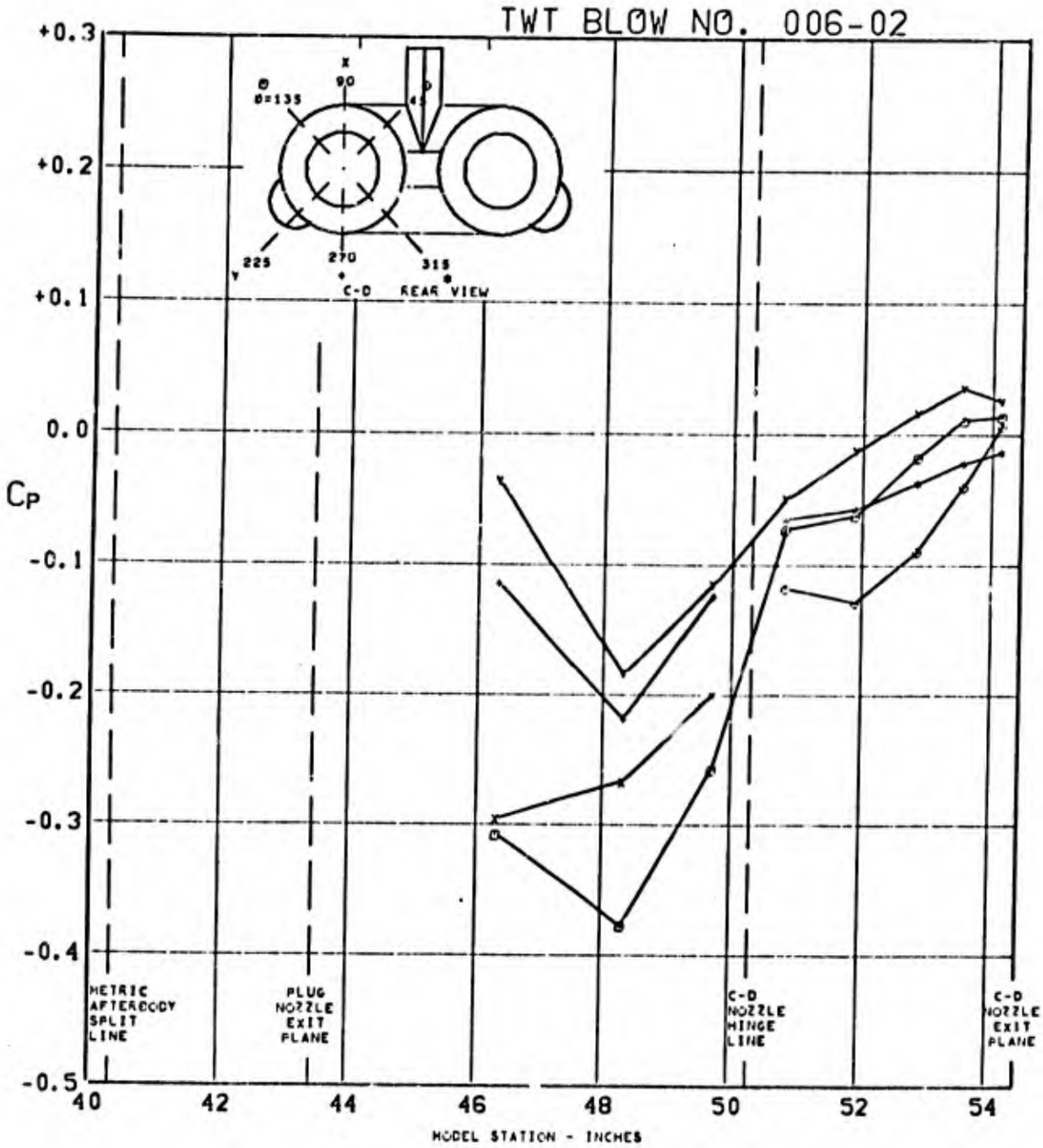

FIGURE 206. PRESSURE COEFFICIENTS ON C-D AFTERBODY (W1B1K1N1 P04 H1V1) $\Lambda_{LE}=70°$ AT 0.848 M_0, $(P_T/P_0)_{C-D}$=CONE, $(P_T/P_0)_{PLUG}=2.010$, $\alpha=2.8$

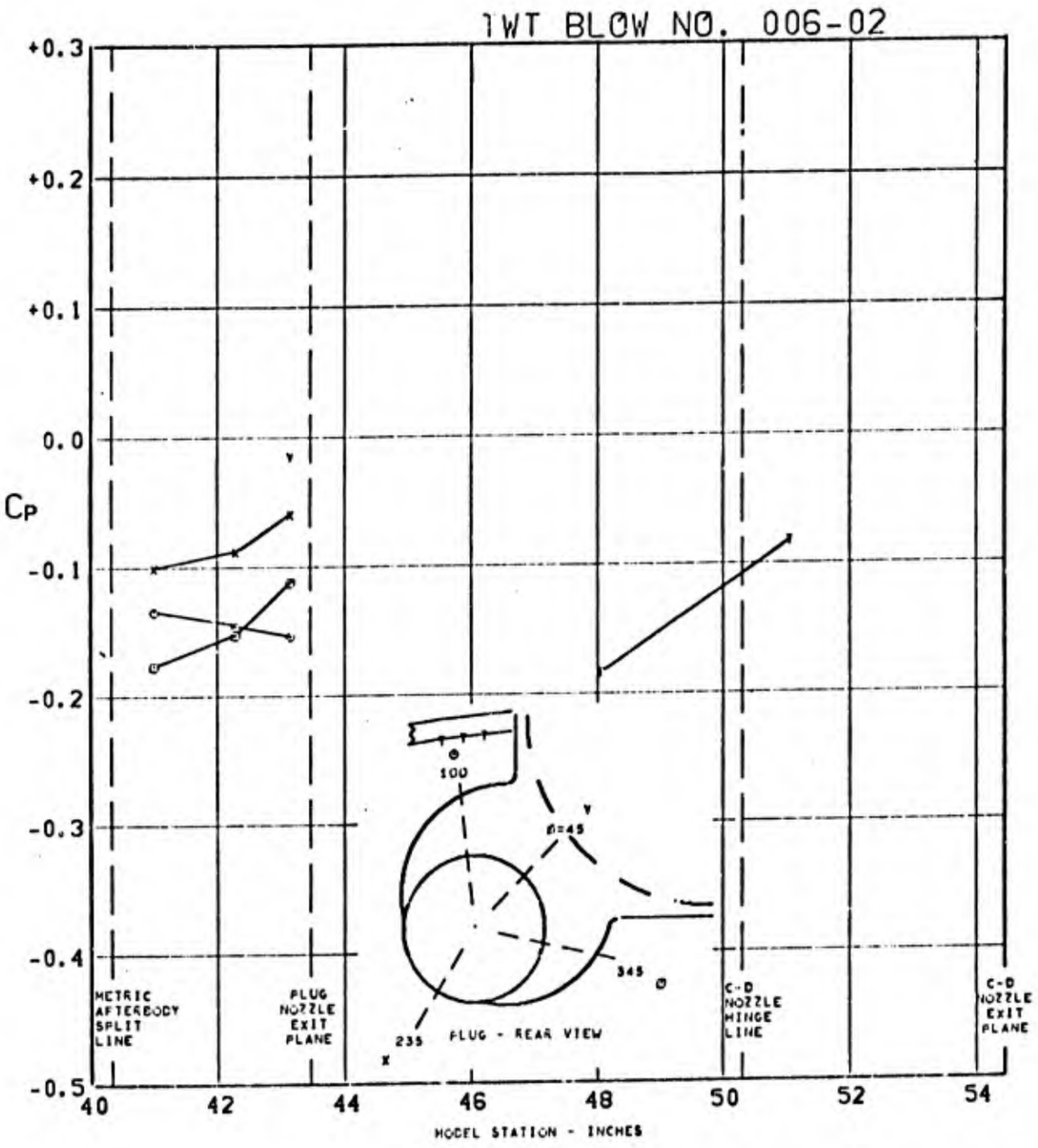

FIGURE 207. PRESSURE COEFFICIENTS ON TAIL & PLUG AFTERBODY (W1B1K1N1 P04 H1V1) $\Lambda_{LE}=70°$ AT 0.848 M_0, $(P_T/P_0)_{C-D}$=CONE , $(P_T/P_0)_{PLUG}=2.010$, $\alpha=2.8$

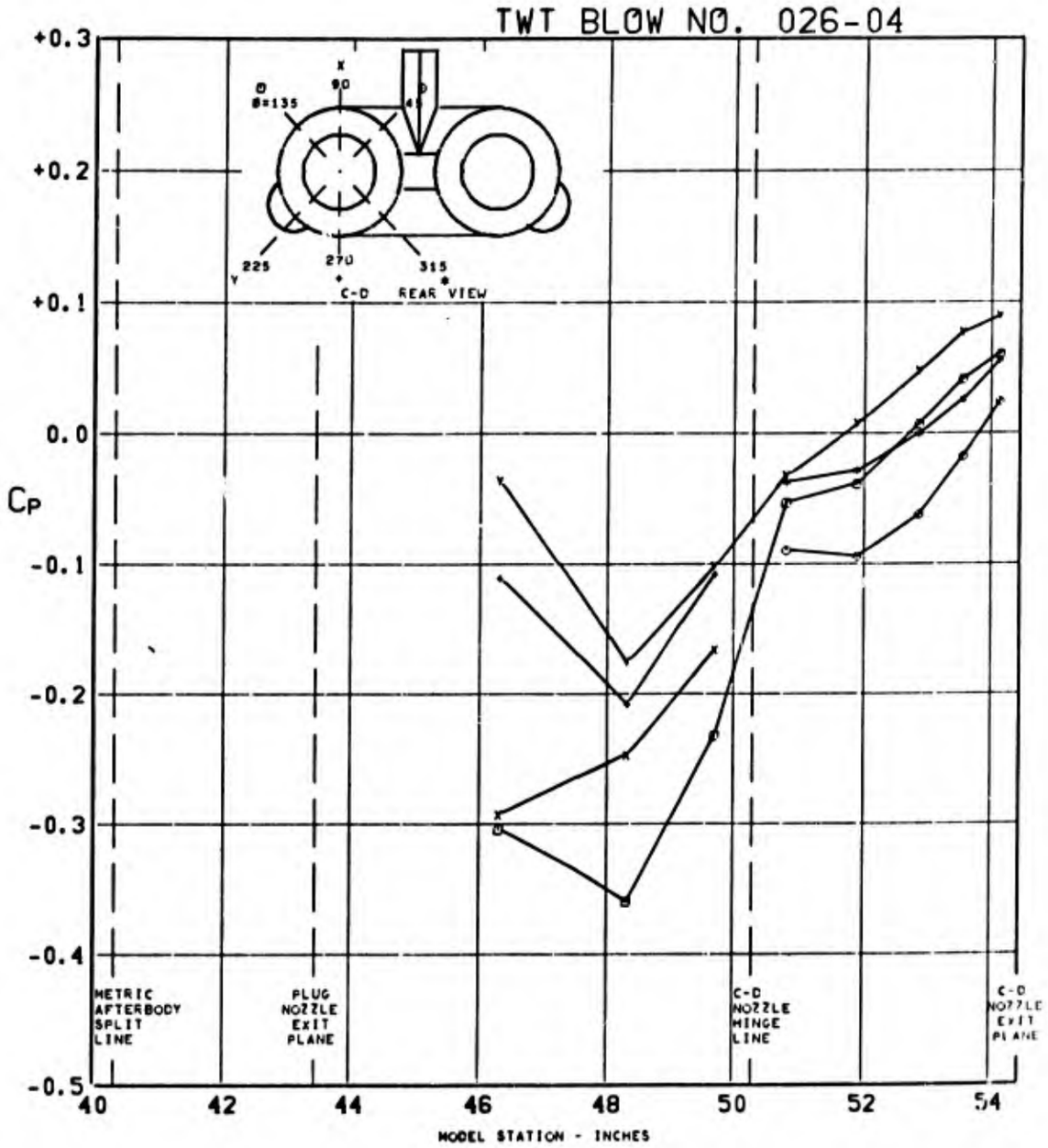

FIGURE 208. PRESSURE COEFFICIENTS ON C-D AFTERBODY (W1B1K1N1 P07 H1V1) $\Lambda_{LE}=70°$ AT 0.842 M_0, $(P_T/P_0)_{C-D}=5.153$, $(P_T/P_0)_{PLUG}=1.988$, $\alpha=2.9$

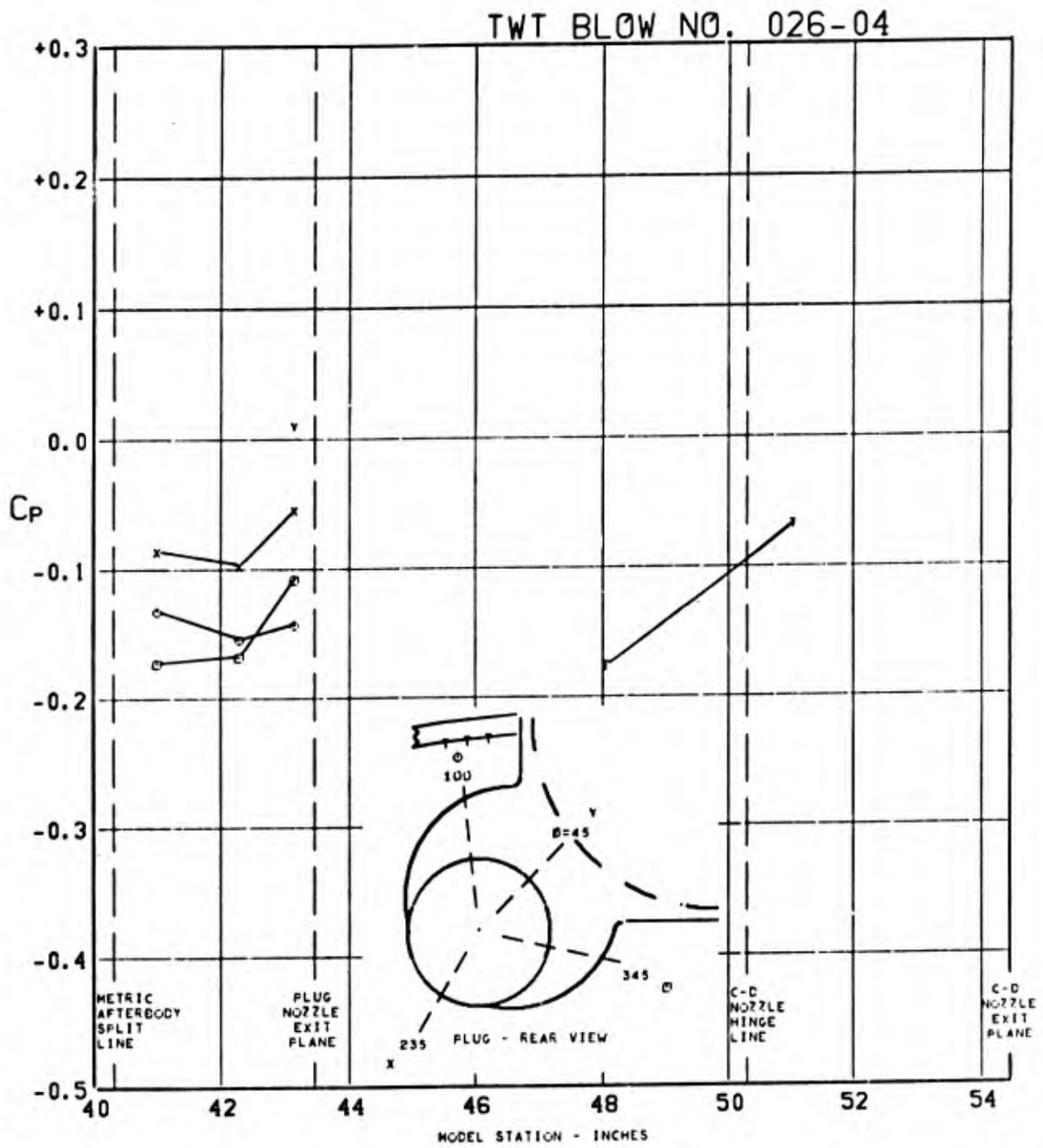

FIGURE 209. PRESSURE COEFFICIENTS ON TAIL & PLUG AFTERBODY (W1B1K1N1 P07 H1V1) $\Lambda_{LE}=70°$ AT 0.842 M_0, $(P_T/P_0)_{C-D}=5.153$, $(P_T/P_0)_{PLUG}=1.988$, $\alpha=2.9$

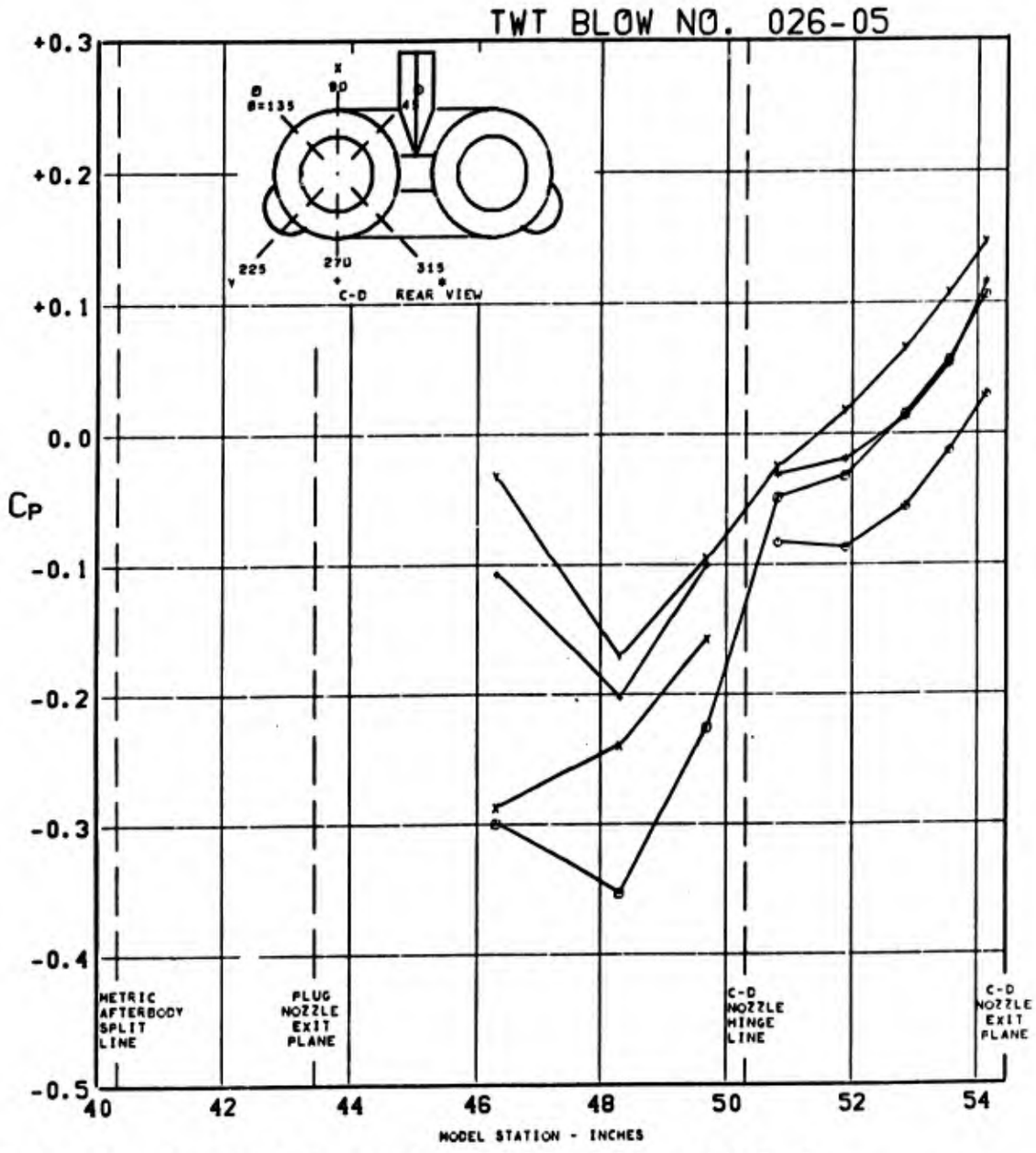

FIGURE 210. PRESSURE COEFFICIENTS ON C-D AFTERBODY (W1B1K1N1 P07 H1V1) $\Lambda_{LE}=70°$ AT 0.842 M_0, $(P_T/P_0)_{C-D}=7.294$, $(P_T/P_0)_{PLUG}=2.018$, $\alpha=2.9$

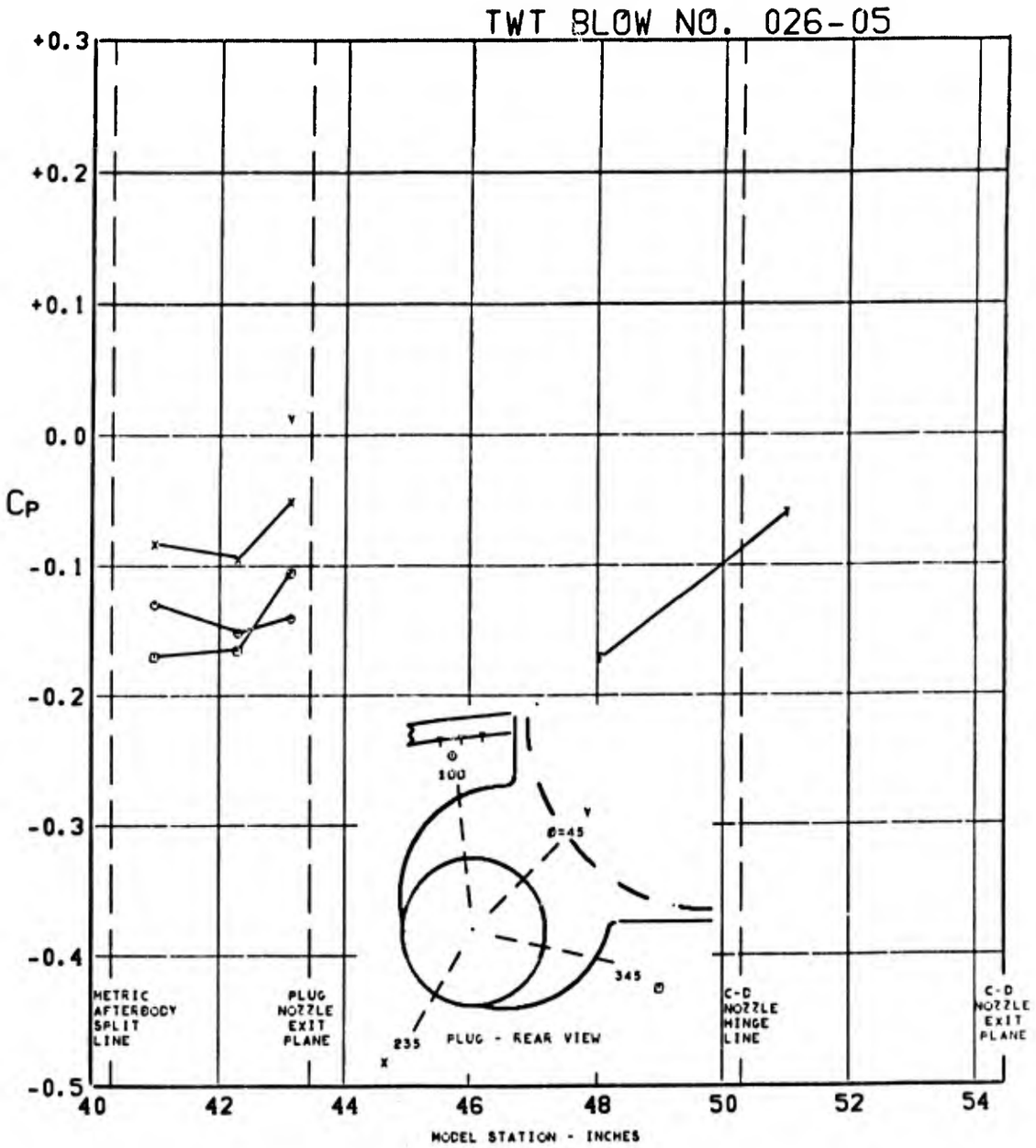

FIGURE 211. PRESSURE COEFFICIENTS ON TAIL & PLUG AFTERBODY (W1B1K1N1 P07 H1V1) Λ_{LE}=70° AT 0.842 M_0, $(P_T/P_0)_{C-D}$=7.294, $(P_T/P_0)_{PLUG}$=2.018, α= 2.9

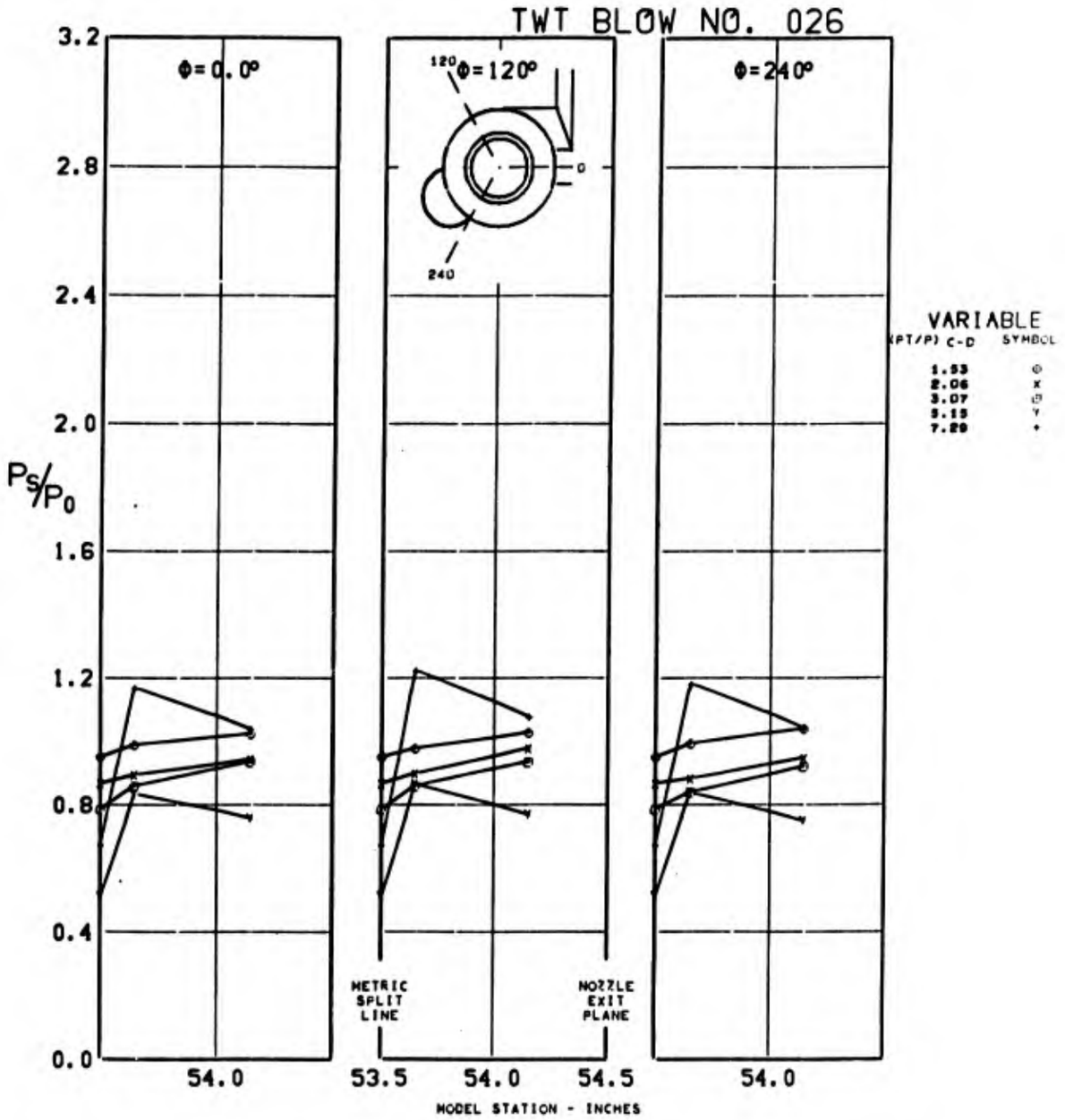

FIGURE 212. C-D NOZZLE EXIT STATIC PRESSURE CONFIGURATION (W1B1K1N1 P07 H1V1) $\Lambda_{LE}=70°$ AT 0.842 M_0, $(P_T/P_0)_{C-D}$=VARY, $(P_T/P_0)_{PLUG}=2.018$, $\alpha=2.9$

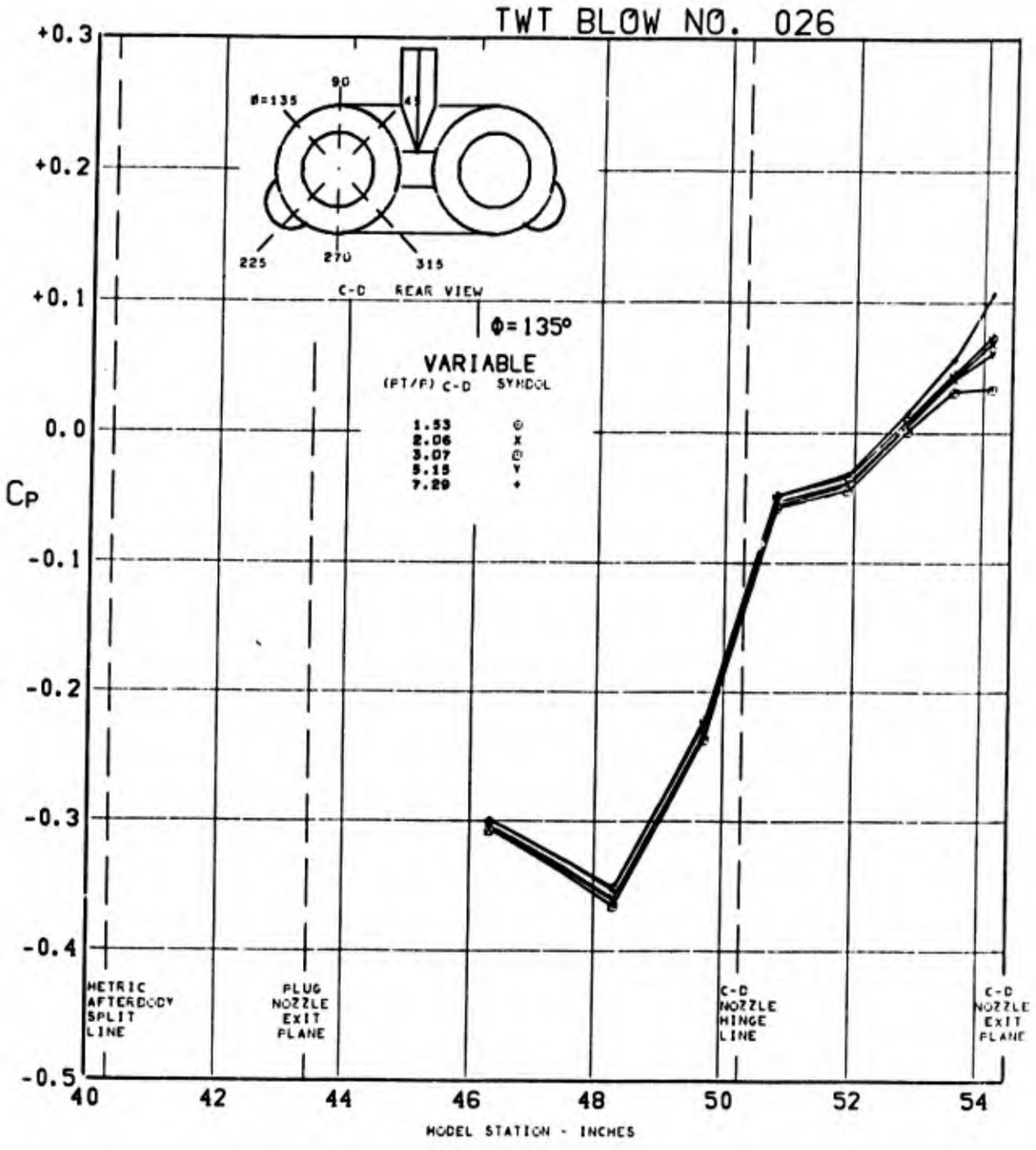

FIGURE 213. PRESSURE COEFFICIENTS ON C-D AFTERBODY (W1B1K1N1 P07 V1) $\Lambda_{LE}=70°$ AT 0.842 M_0, $(P_T/P_0)_{C-D}$=VARY, $(P_T/P_0)_{PLUG}=2.018$, $\alpha=2.9$

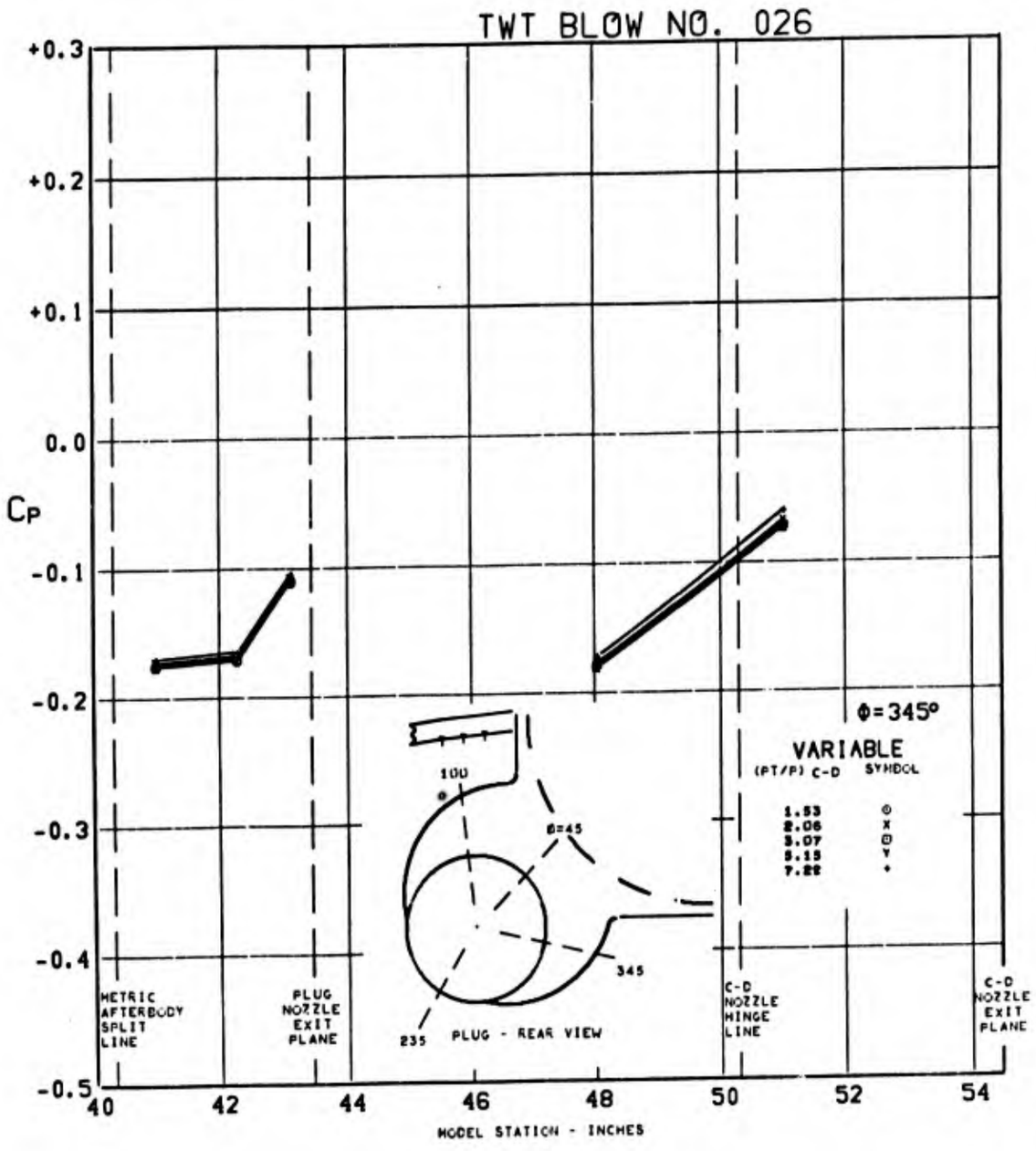

FIGURE 214. PRESSURE COEFFICIENTS ON TAIL & PLUG AFTERBODY (W1B1K1N1 P07 V1) Λ_{LE}=70° AT 0.842 M_0, $(P_T/P_0)_{C-D}$=VARY, $(P_T/P_0)_{PLUG}$=2.018, α= 2.9

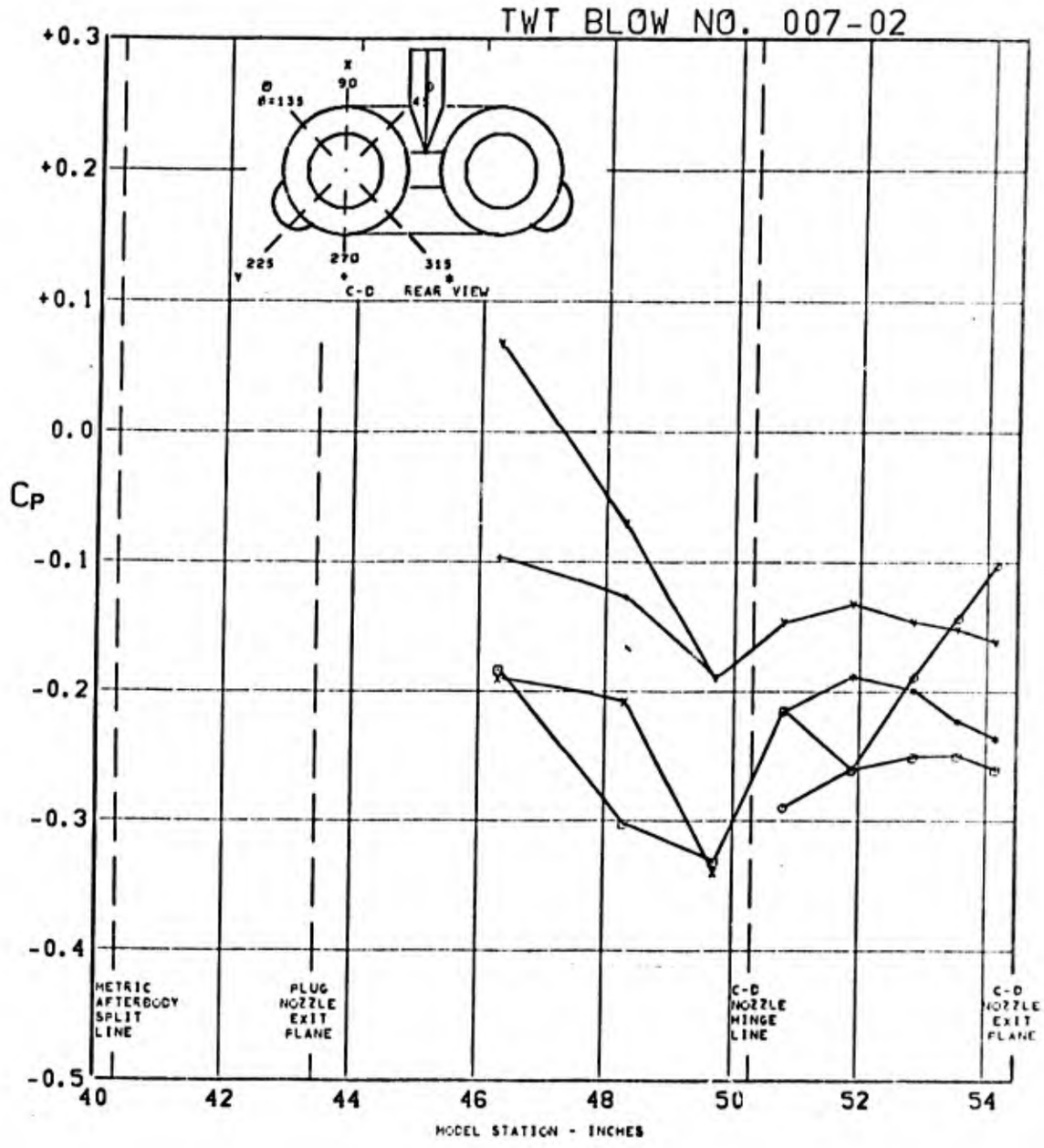

FIGURE 215. PRESSURE COEFFICIENTS ON C-D AFTERBODY (W1B1K1N1 P04 H1V1) Λ_{LE}=70° AT 1.270 M_0, $(P_T/P_0)_{C-D}$=CONE, $(P_T/P_0)_{PLUG}$=3.116, α= 2.9

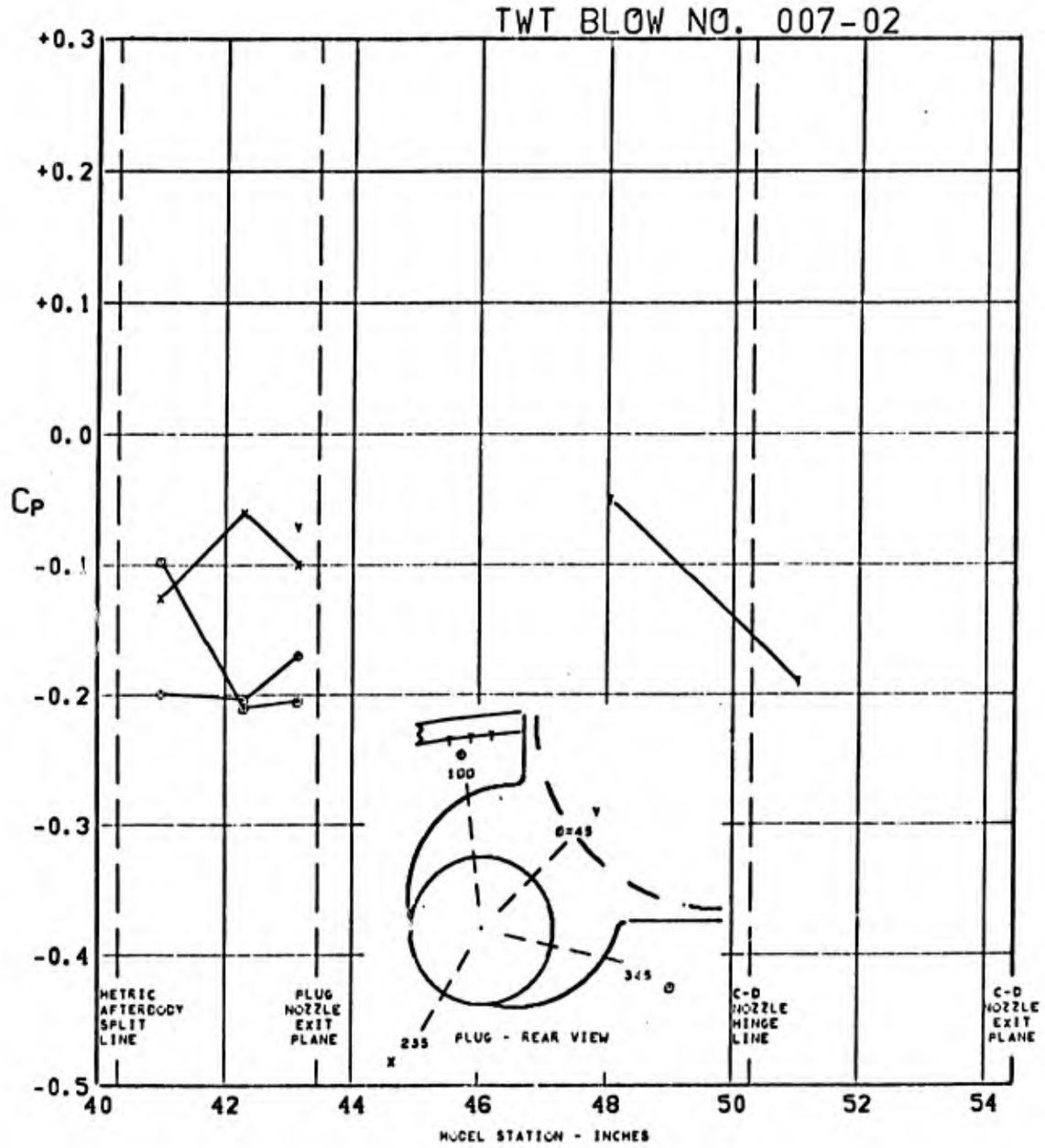

FIGURE 216. PRESSURE COEFFICIENTS ON TAIL & PLUG AFTERBODY (W1B1K1N1 P04 H1V1) Λ_{LE}=70° AT 1.270 M_0, $(P_T/P_0)_{C-D}$=CONE, $(P_T/P_0)_{PLUG}$=3.116, α= 2.9

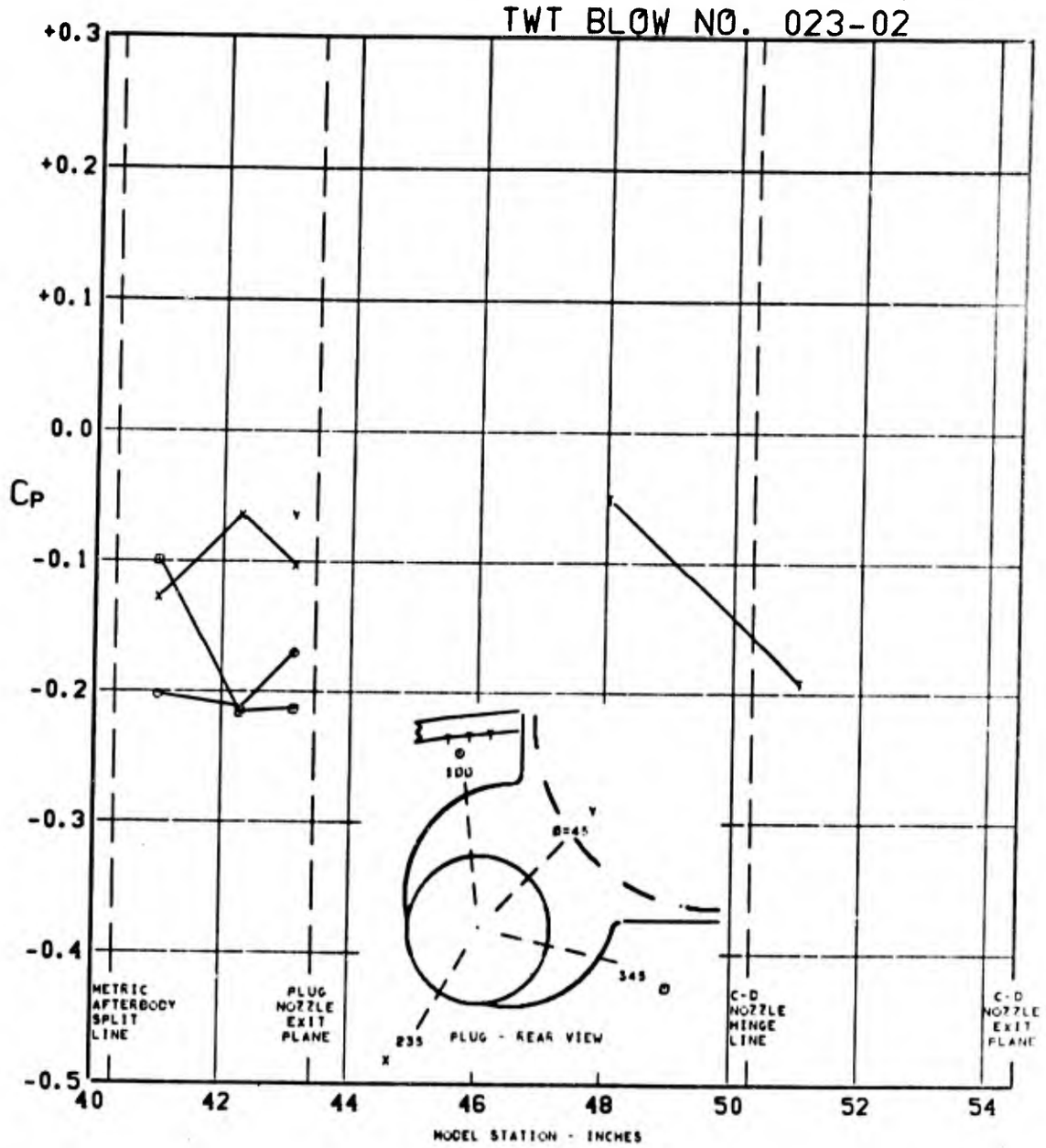

FIGURE 217. PRESSURE COEFFICIENTS ON TAIL & PLUG AFTERBODY (W1B1K1N1 P07 H1V1) $\Lambda_{LE}=70°$ AT 1.269 M_0, $(P_T/P_0)_{C-D}=5.218$, $(P_T/P_0)_{PLUG}=3.102$, $\alpha=$ 2.8

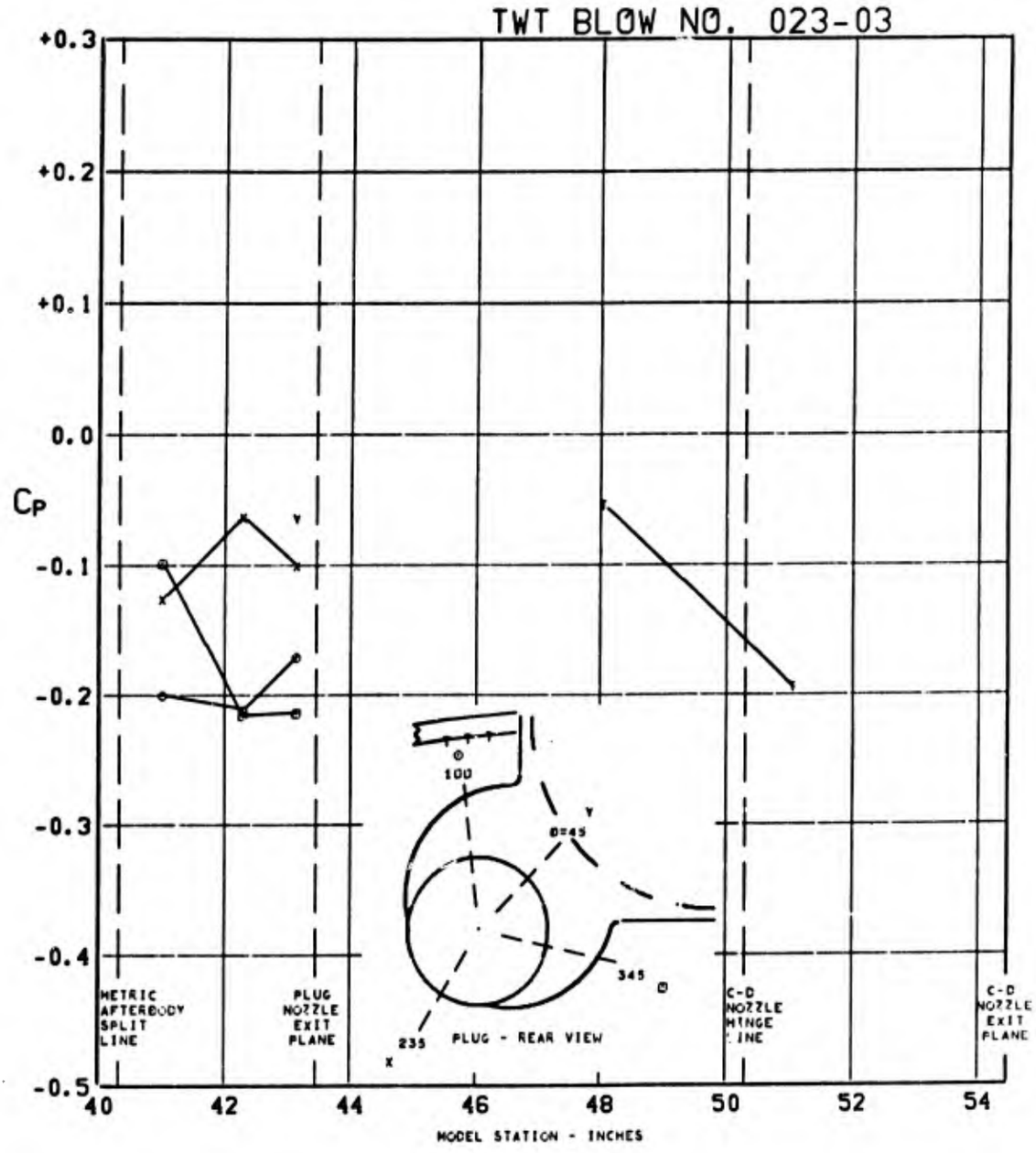

FIGURE 218. PRESSURE COEFFICIENTS ON TAIL & PLUG AFTERBODY (W1B1K1N1 P07 H1V1) Λ_{LE}=70° AT 1.269 M_0, $(P_T/P_0)_{C-D}$=7.205, $(P_T/P_0)_{PLUG}$=3.090, α= 2.8

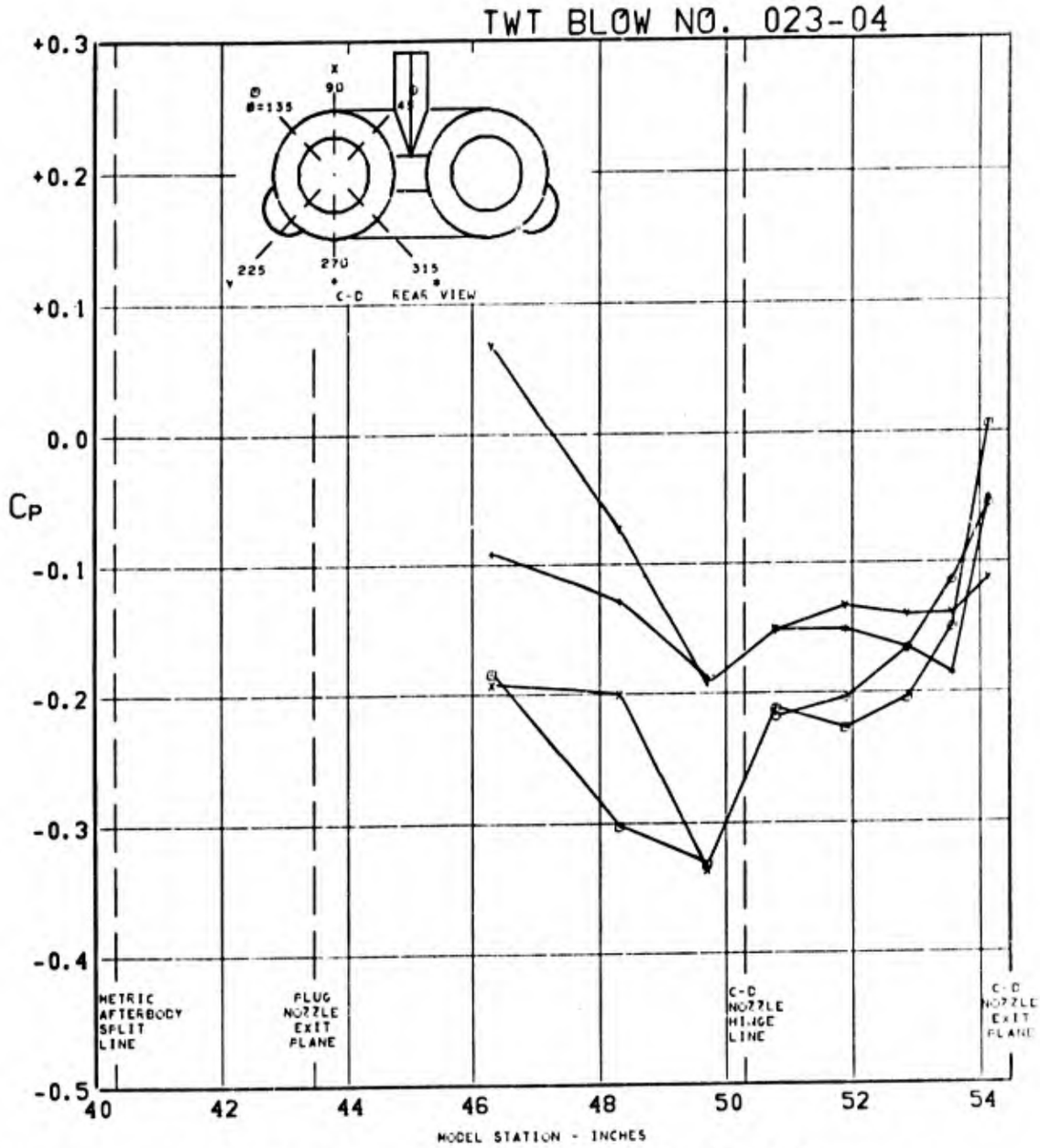

FIGURE 219. PRESSURE COEFFICIENTS ON C-D AFTERBODY (W1B1K1N1 P07 H1V1) $\Lambda_{LE}=70°$ AT $M_0 = 1.268$, $(P_T/P_0)_{C-D}=10.39$, $(P_T/P_0)_{PLUG}=3.075$, $\alpha = 2.8$

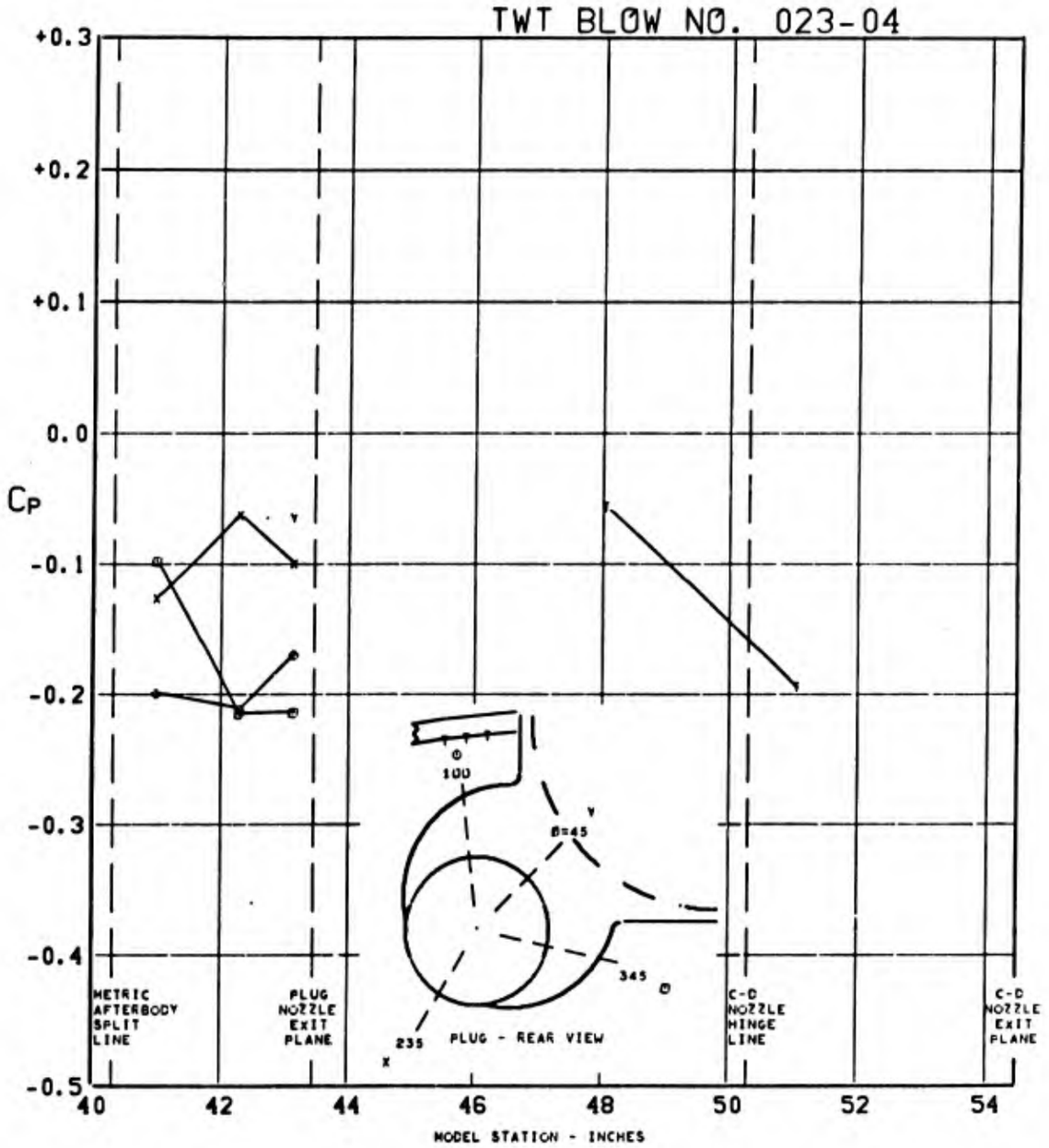

FIGURE 220. PRESSURE COEFFICIENTS ON TAIL & PLUG AFTERBODY (W1B1K1N1 P07 H1V1) $\Lambda_{LE}=70°$ AT 1.268 M_0, $(P_T/P_0)_{C-D}=10.39$, $(P_T/P_0)_{PLUG}=3.075$, $\alpha=2.8$

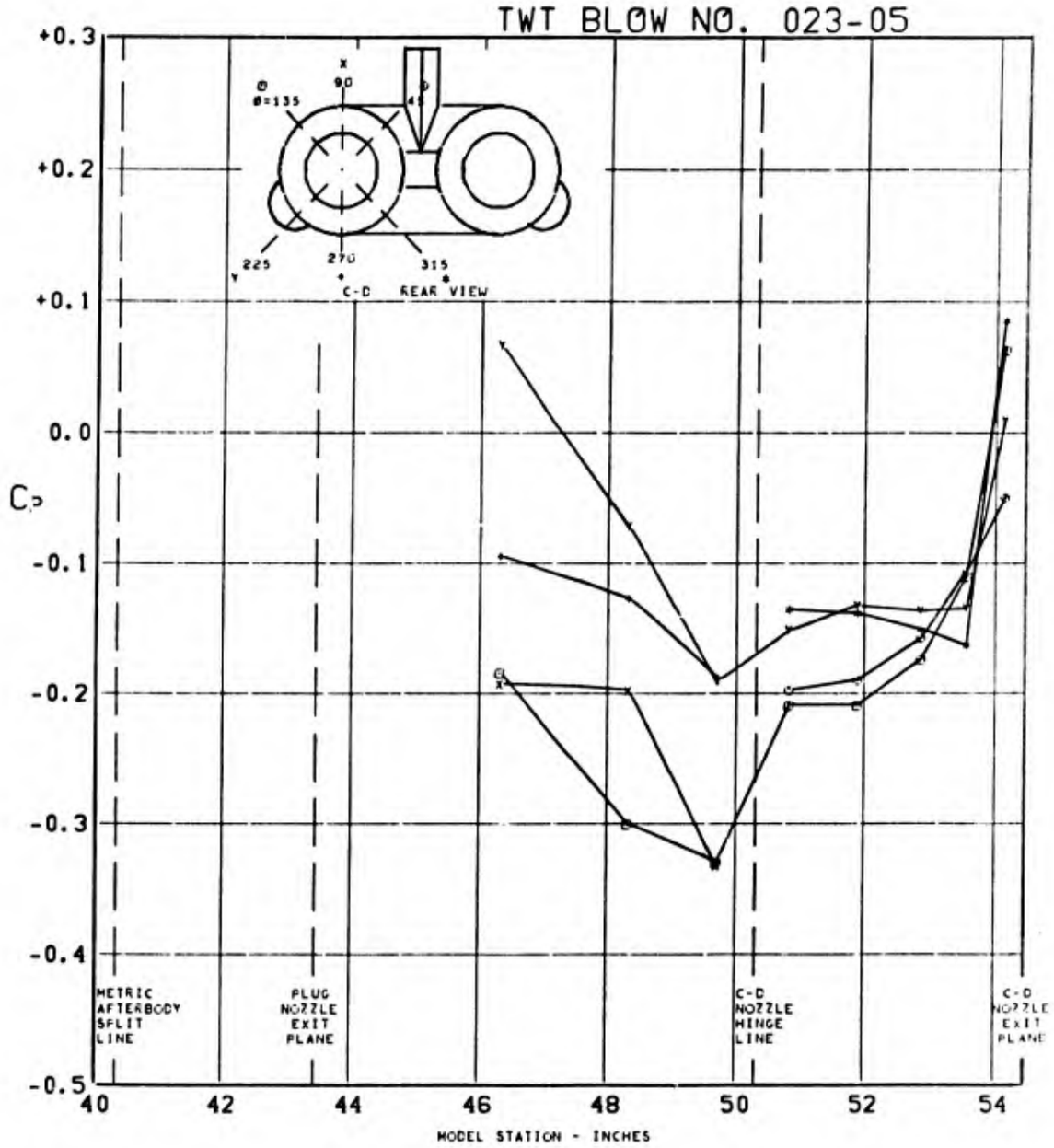

FIGURE 221. PRESSURE COEFFICIENTS ON C-D AFTERBODY (W1B1K1N1 P07 H1V1) Λ_{LE}=70° AT 1.268 M_0, $(P_T/P_0)_{C-D}$=12.47, $(P_T/P_0)_{PLUG}$=3.112, α= 2.8

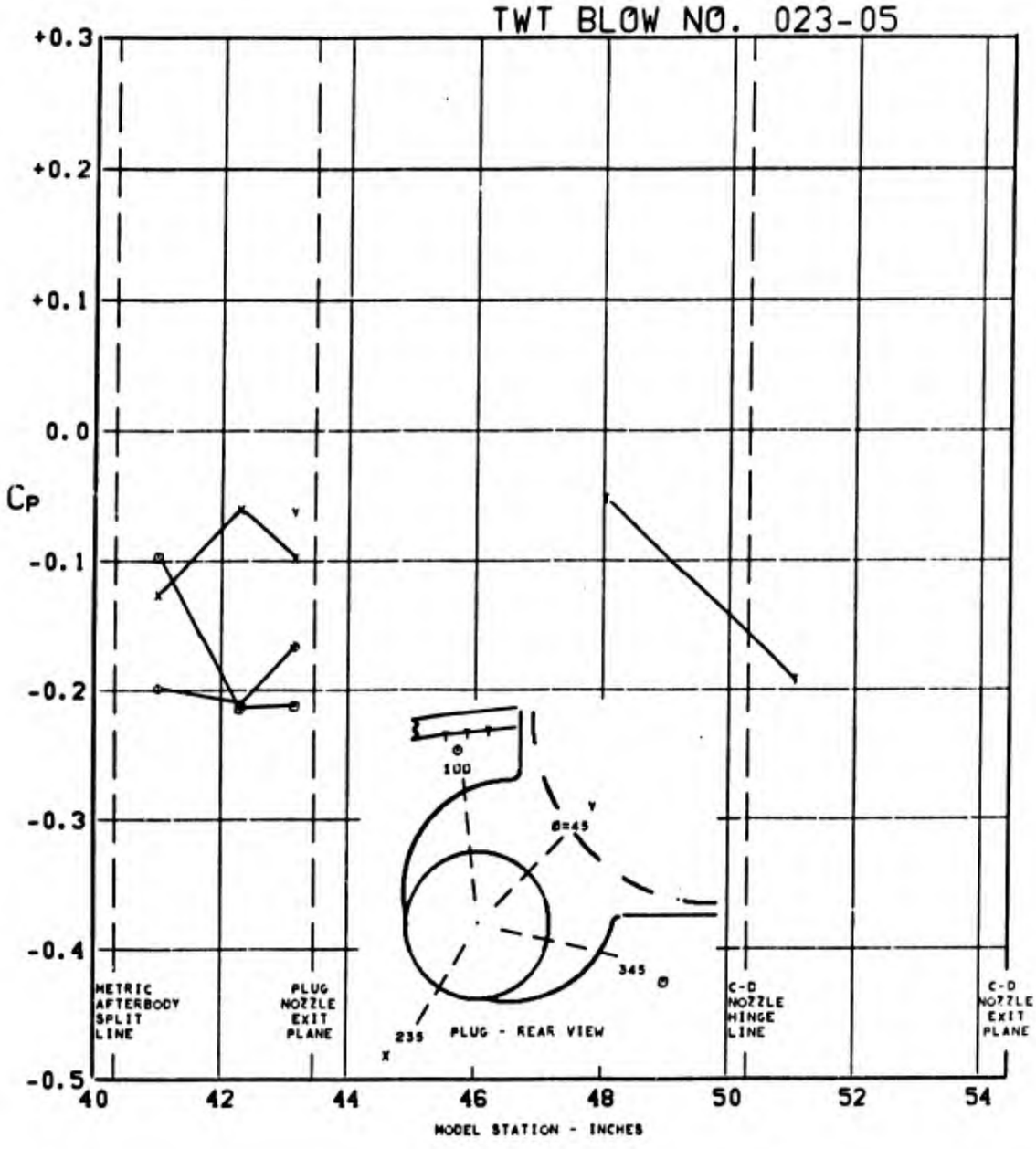

FIGURE 222. PRESSURE COEFFICIENTS ON TAIL & PLUG AFTERBODY (W1B1K1N1 P07 H1V1) $\Lambda_{LE}=70°$ AT 1.268 M_0, $(P_T/P_0)_{C-D}=12.47$, $(P_T/P_0)_{PLUG}=3.112$, $\alpha=2.8$

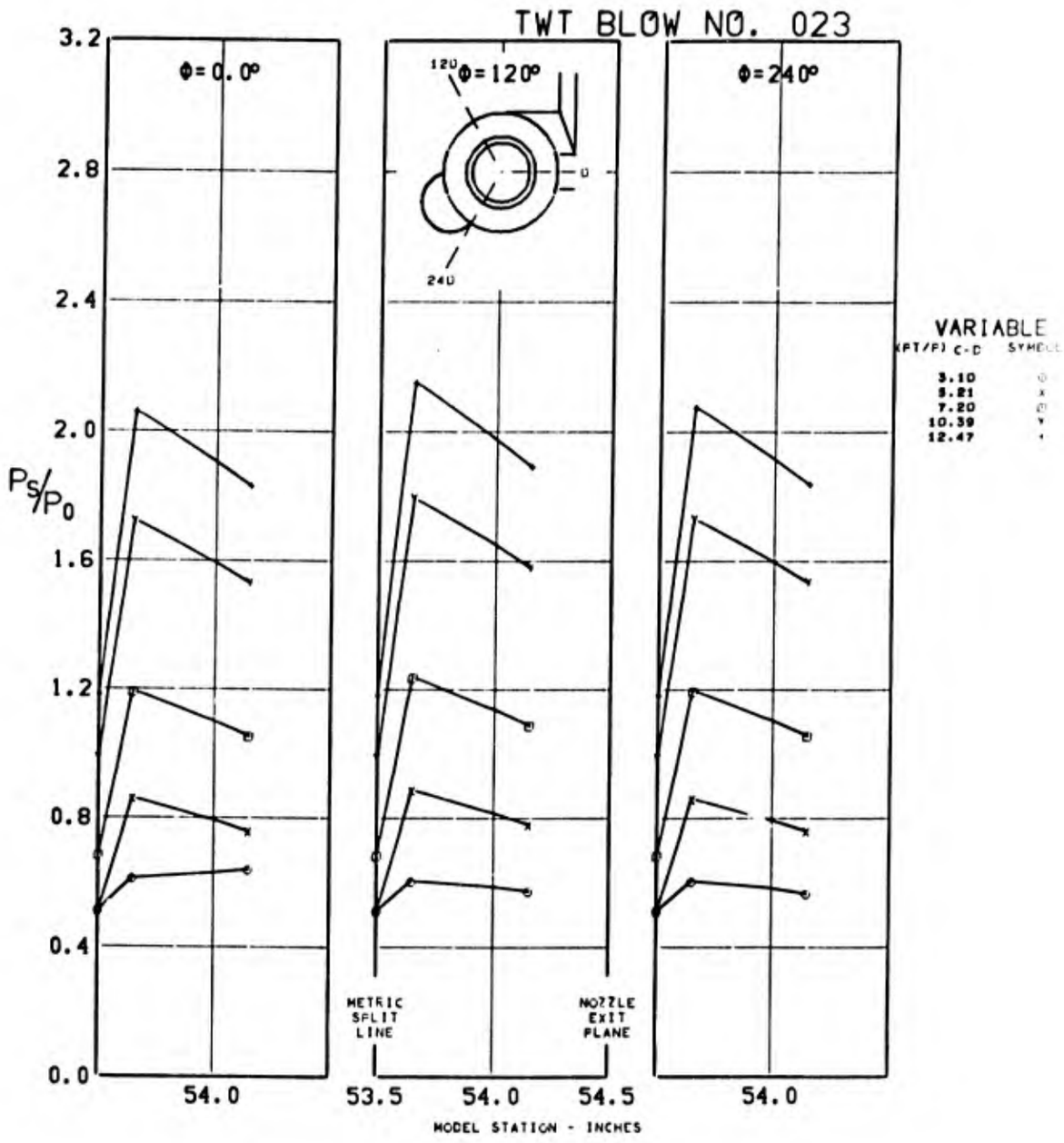

FIGURE 223. C-D NOZZLE EXIT STATIC PRESSURE CONFIGURATION (W1B1K1N1 P07 H1V1) Λ_{LE}=70° AT 1.268 M_0, $(P_T/P_0)_{C-D}$=VARY, $(P_T/P_0)_{PLUG}$=3.112, α= 2.8

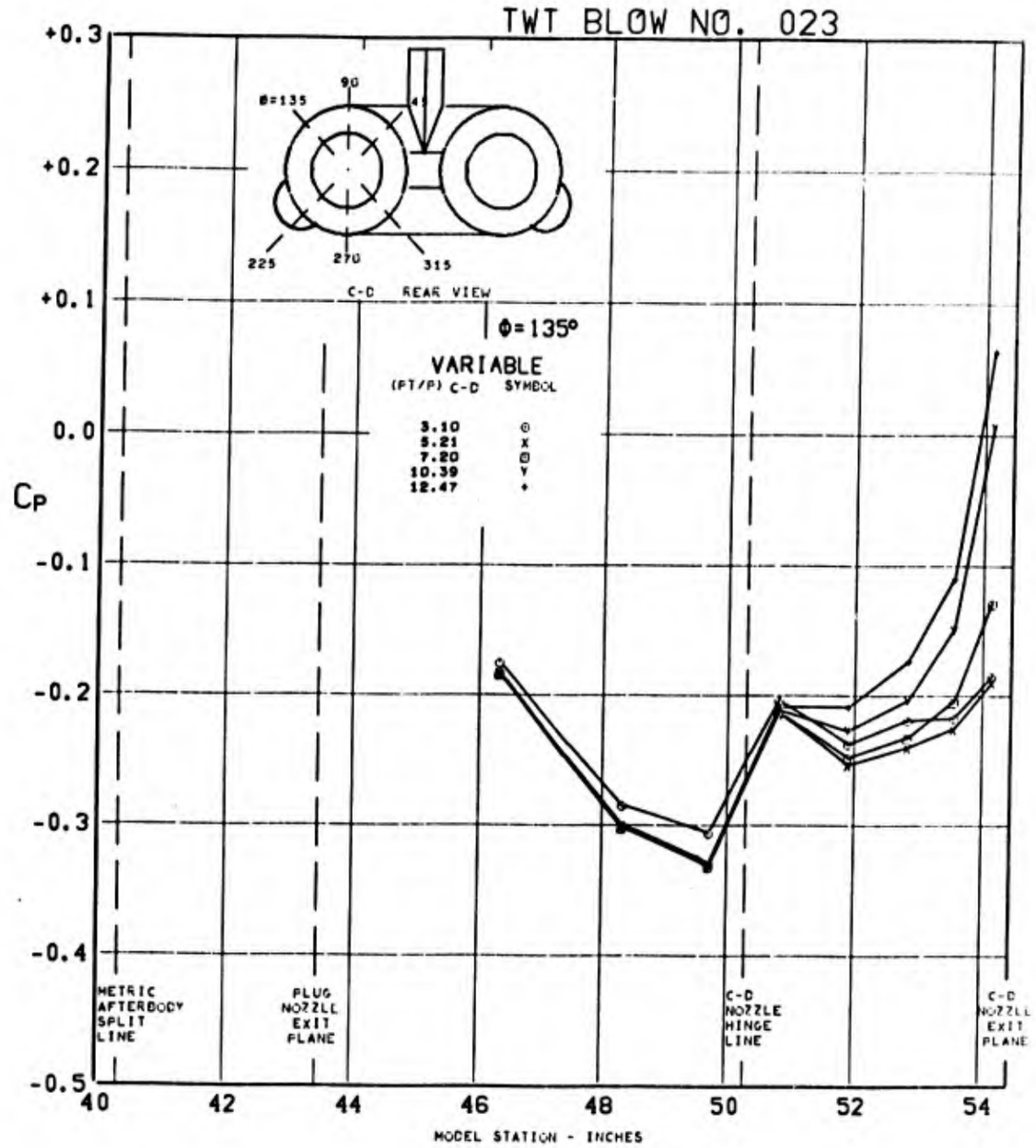

FIGURE 224. PRESSURE COEFFICIENTS ON C-D AFTERBODY (W1B1K1N1 P07 H1V1) $\Lambda_{LE}=70°$ AT 1.268 M_0, $(P_T/P_0)_{C-D}$=VARY, $(P_T/P_0)_{PLUG}=3.112$, $\alpha=2.8$

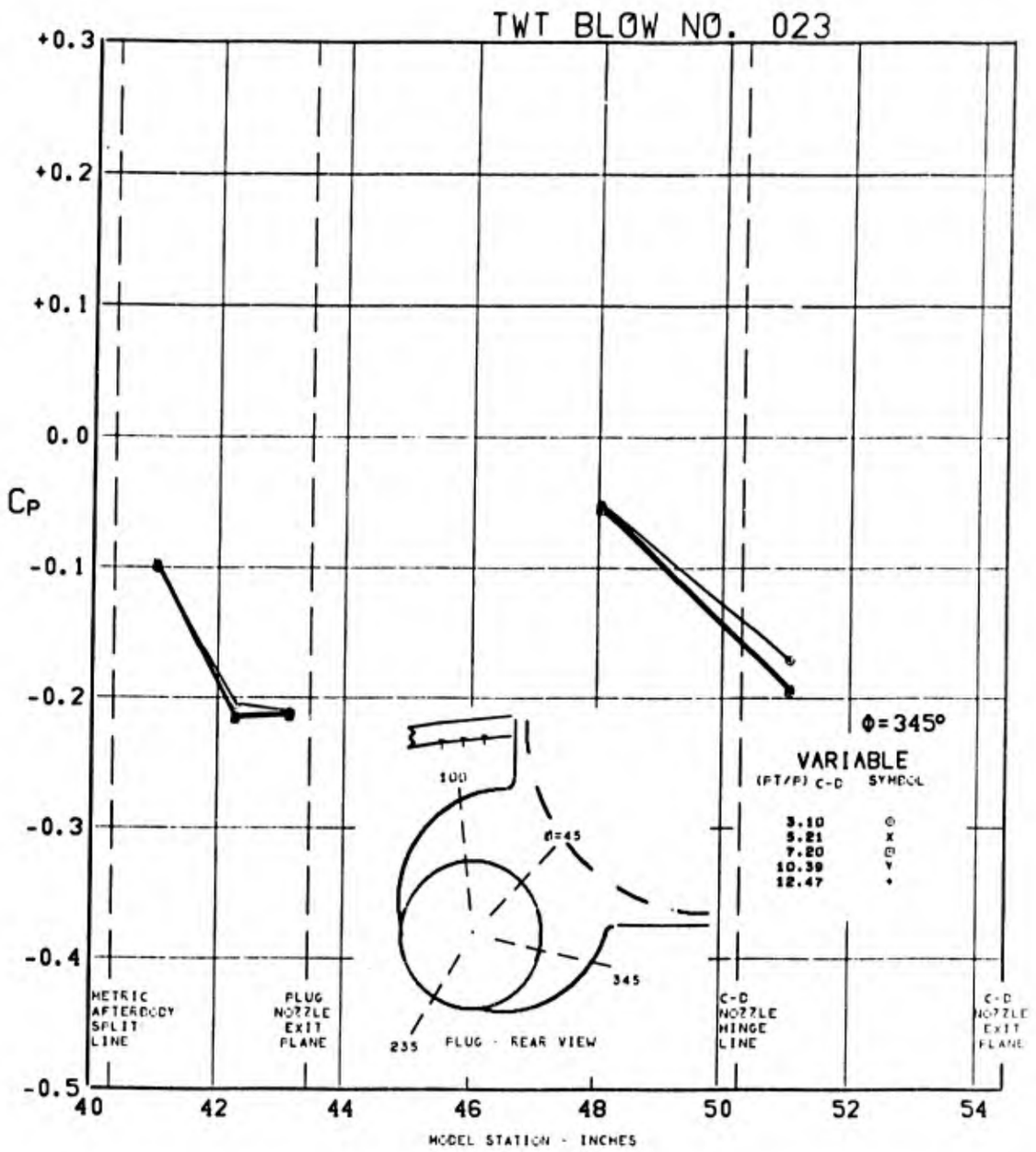

FIGURE 225. PRESSURE COEFFICIENTS ON TAIL & PLUG AFTERBODY (W1B1K1N1 P07 H1V1) $\Lambda_{LE}=70°$ AT 1.268 M_0, $(P_T/P_0)_{C-D}$=VARY, $(P_T/P_0)_{PLUG}=3.112$, $\alpha=2.8$

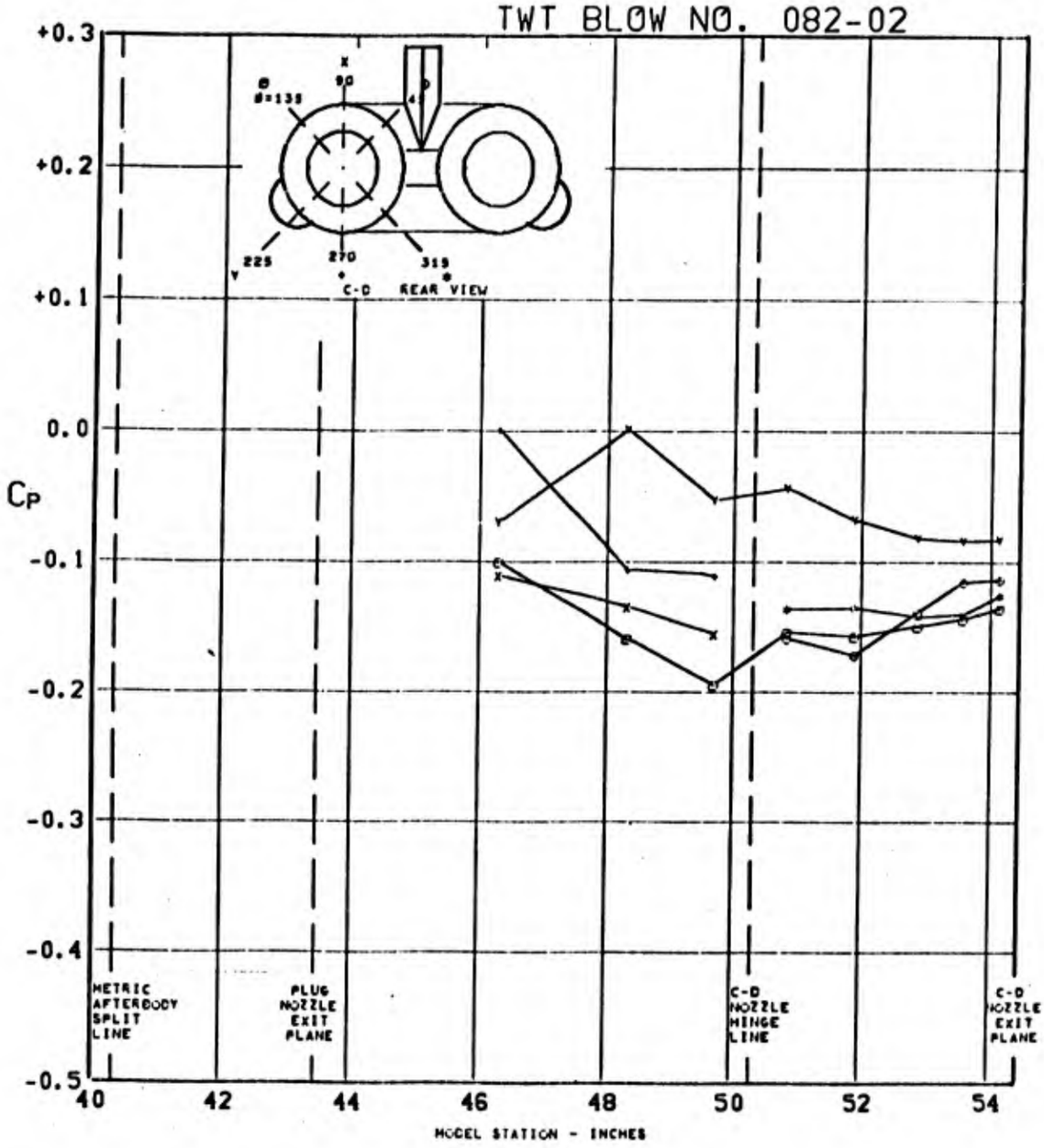

FIGURE 226. PRESSURE COEFFICIENTS ON C-D AFTERBODY (W1B1K1N1 P07 H1V1) $\Lambda_{LE}=70°$ AT 1.998 M_0, $(P_T/P_0)_{C-D}=0.741$, $(P_T/P_0)_{PLUG}=4.792$, $\alpha=2.9$

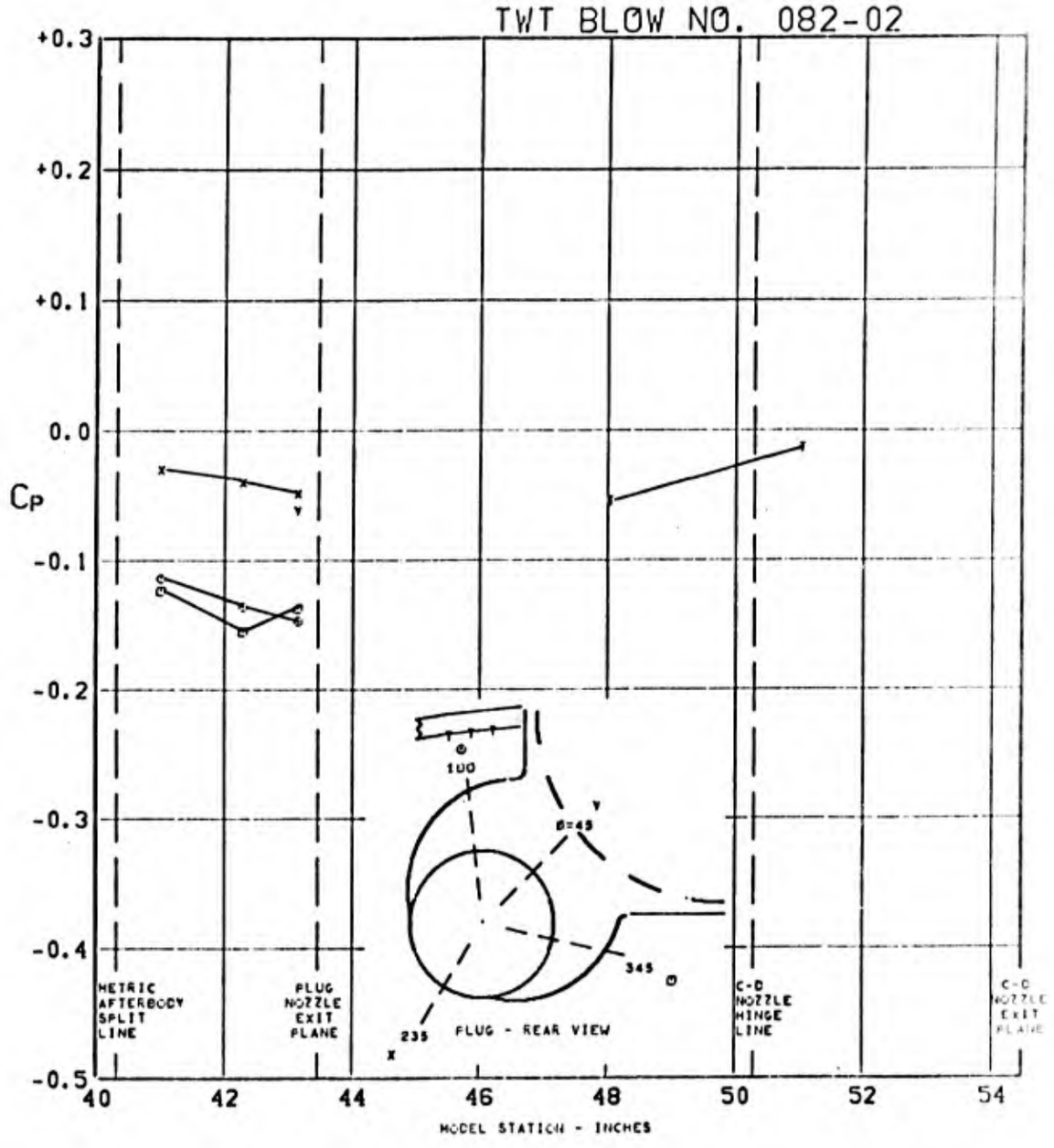

FIGURE 227. PRESSURE COEFFICIENTS ON TAIL & PLUG AFTERBODY (W1B1K1N1 P07 H1V1) $\Lambda_{LE}=70°$ AT 1.998 M_0, $(P_T/P_0)_{C-D}=0.741$, $(P_T/P_0)_{PLUG}=4.792$, $\alpha=$ 2.9

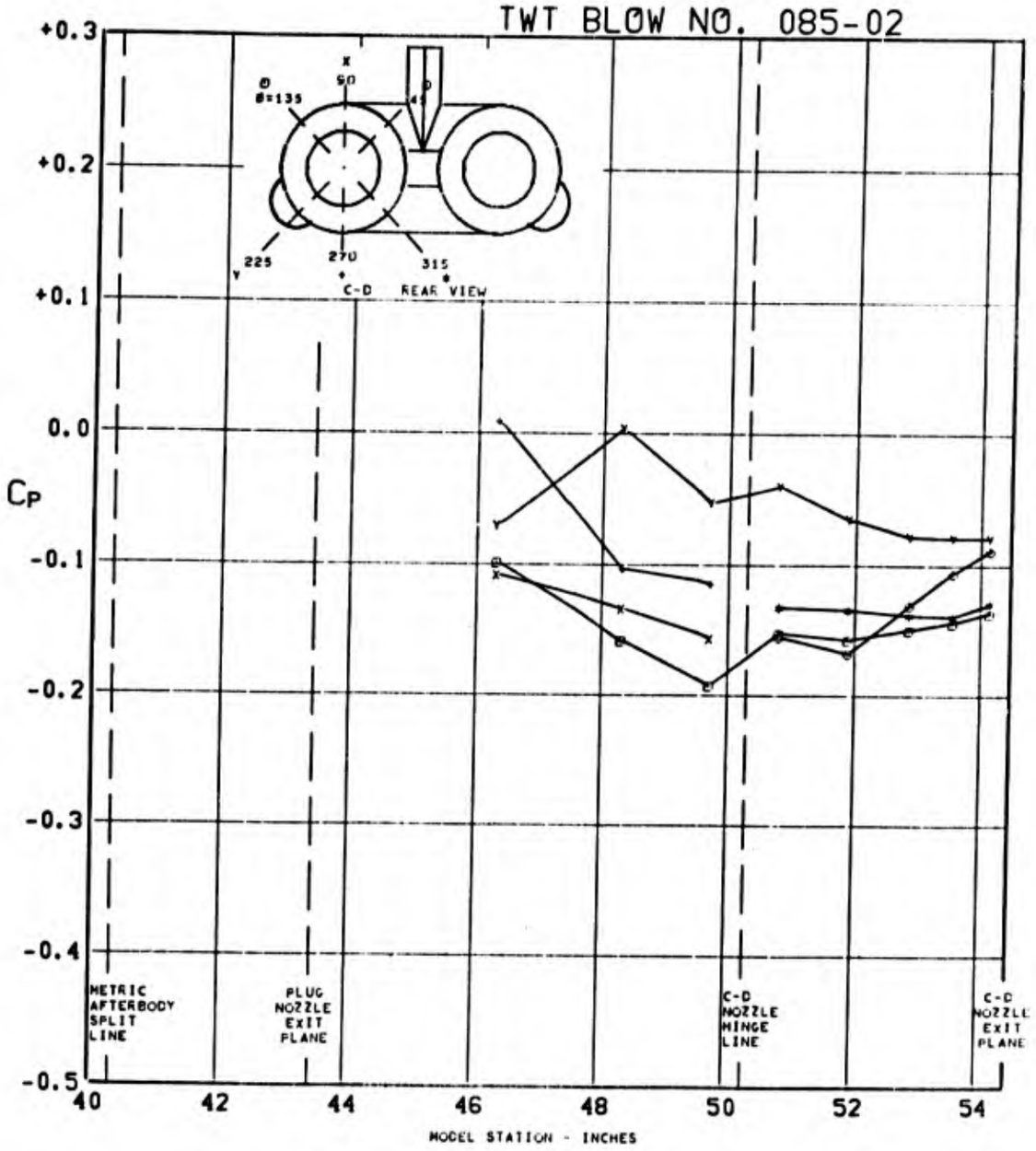

FIGURE 228. PRESSURE COEFFICIENTS ON C-D AFTERBODY (W1B1K1N1 P07 H1V1) $\Lambda_{LE}=70°$ AT 1.998 M_0, $(P_T/P_0)_{C-D}=5.068$, $(P_T/P_0)_{PLUG}=4.982$, $\alpha=2.9$

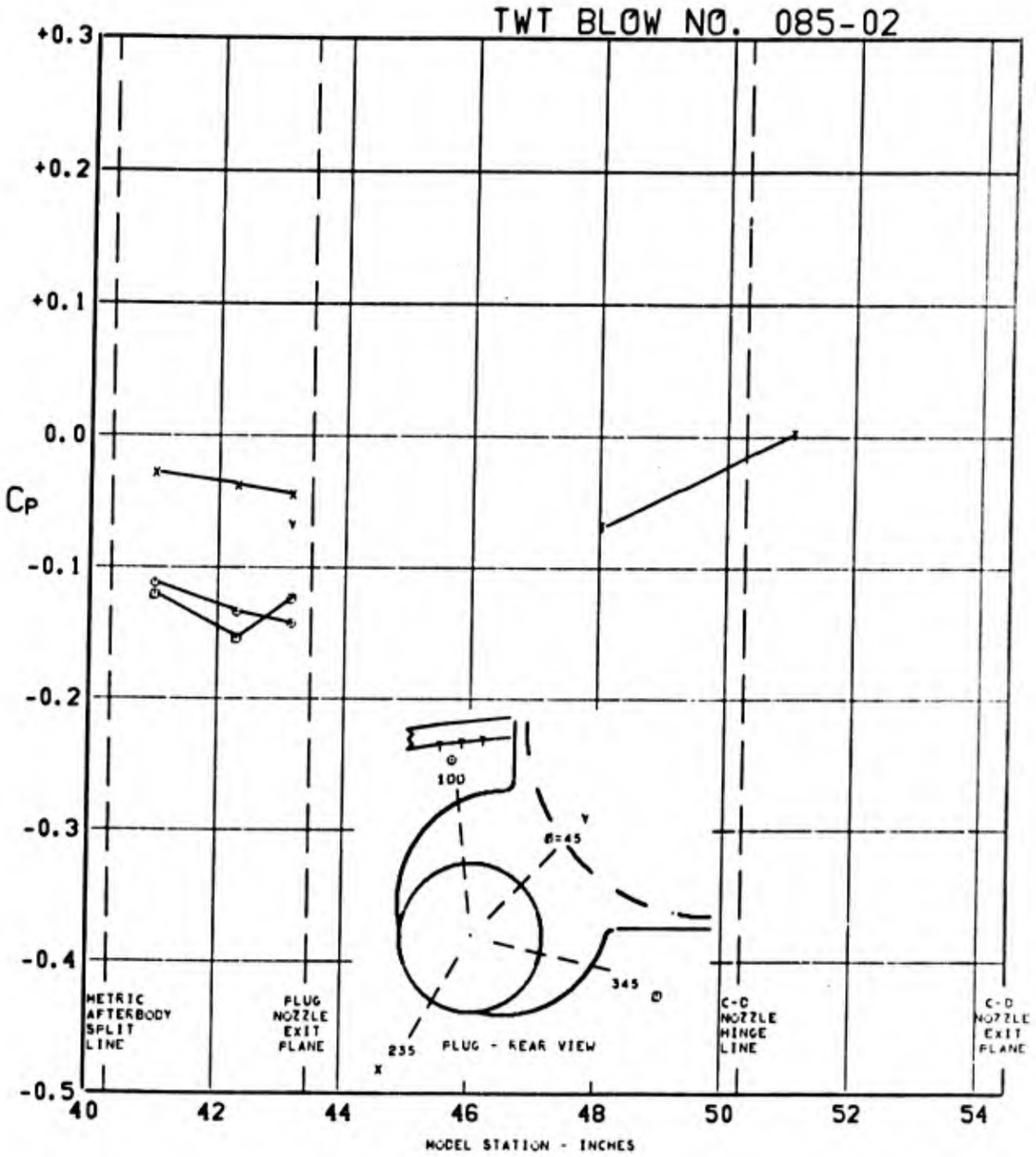

FIGURE 229. PRESSURE COEFFICIENTS ON TAIL & PLUG AFTERBODY (W1B1K1N1 P07 H1V1) Λ_{LE}=70° AT 1.998 M_0, $(P_T/P_0)_{C-D}$=5.068, $(P_T/P_0)_{PLUG}$=4.982, α= 2.9

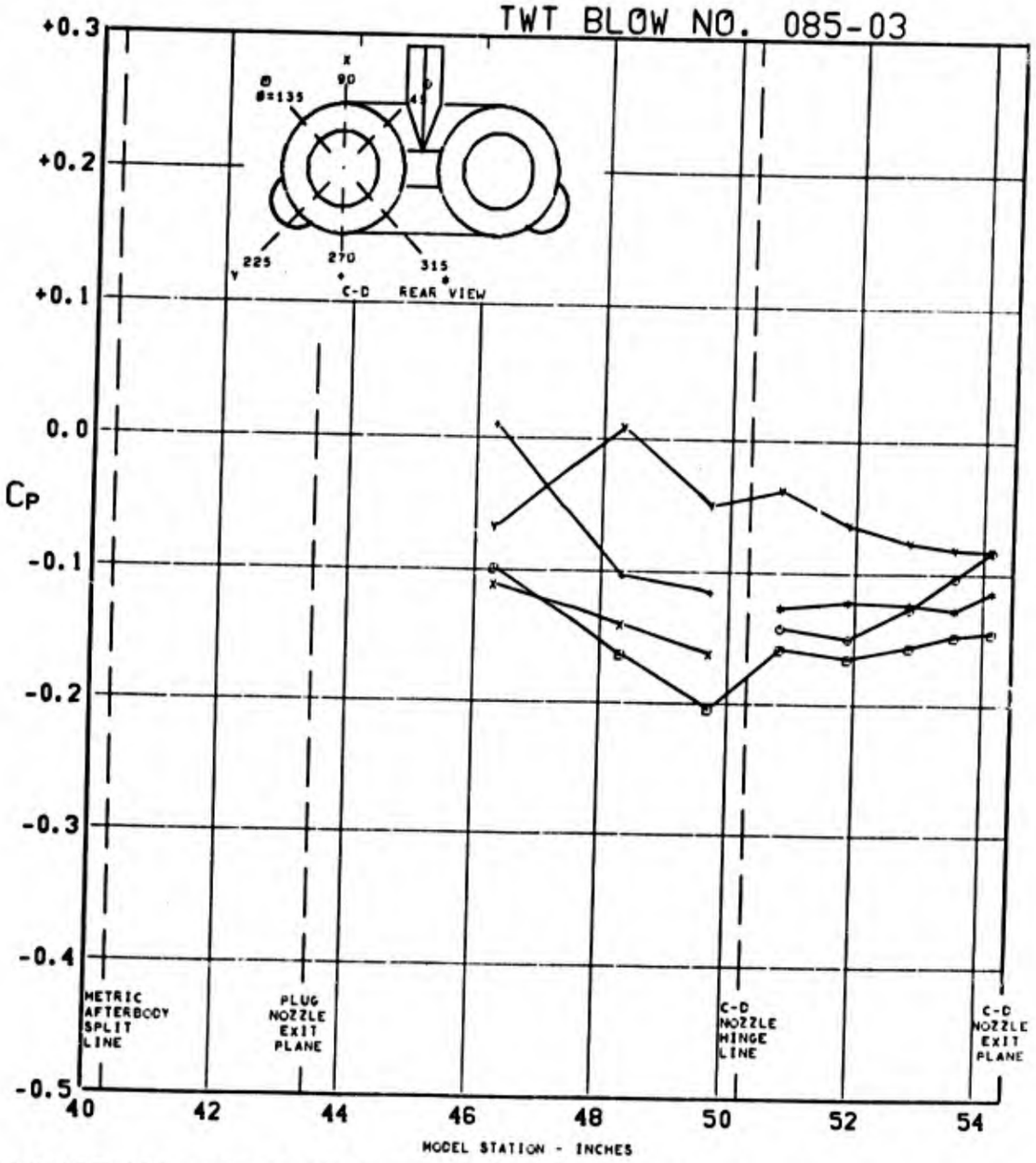

FIGURE 230. PRESSURE COEFFICIENTS ON C-D AFTERBODY (W1B1K1N1 P07 H1V1) $\Lambda_{LE}=70°$ AT 1.998 M_0, $(P_T/P_0)_{C-D}=10.02$, $(P_T/P_0)_{PLUG}=5.003$, $\alpha=2.9$

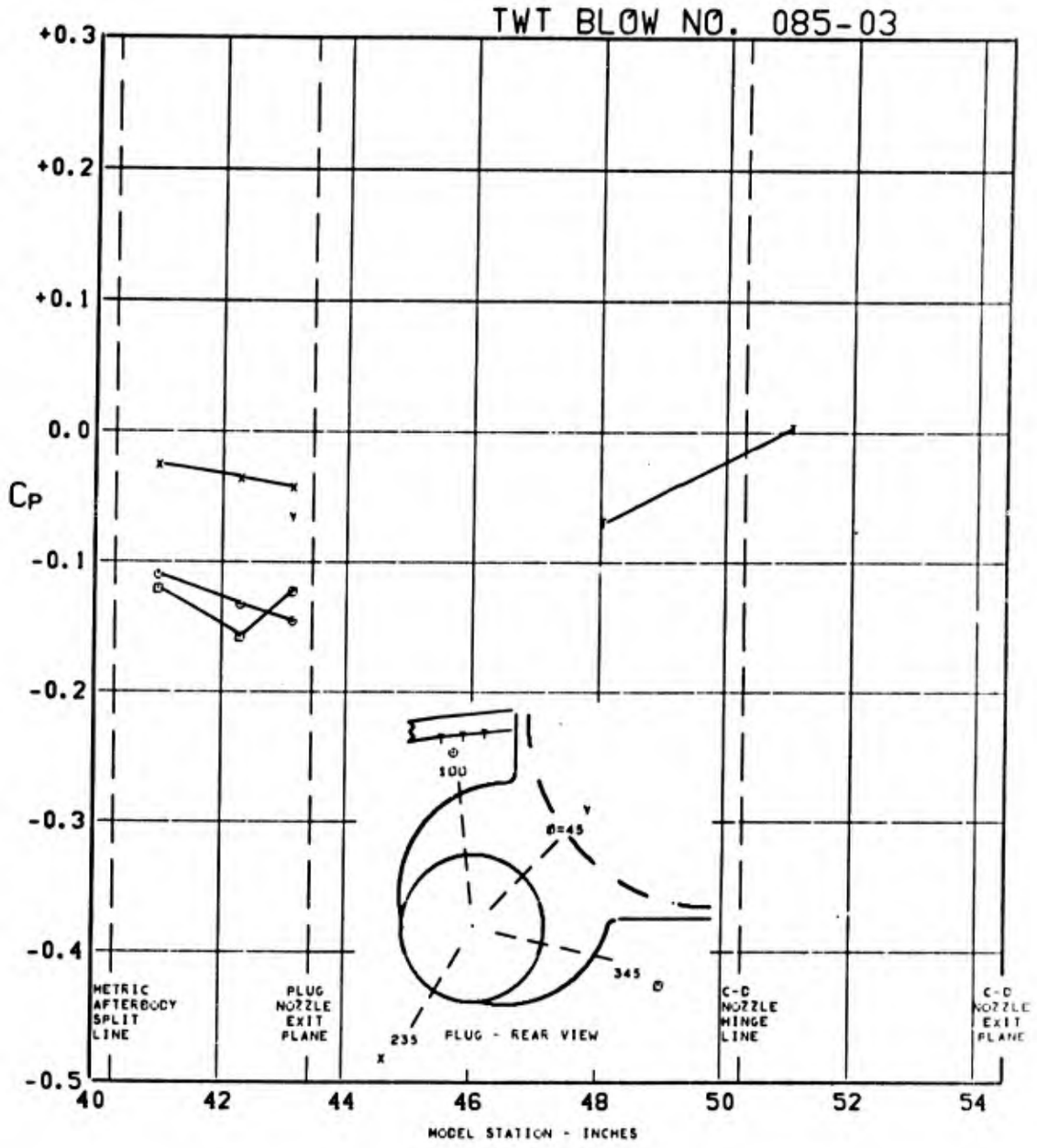

FIGURE 231. PRESSURE COEFFICIENTS ON TAIL & PLUG AFTERBODY (W1B1K1N1 P07 H1V1) $\Lambda_{LE}=70°$ AT 1.998 M_0, $(P_T/P_0)_{C-D}=10.02$, $(P_T/P_0)_{PLUG}=5.003$, $\alpha=2.9$

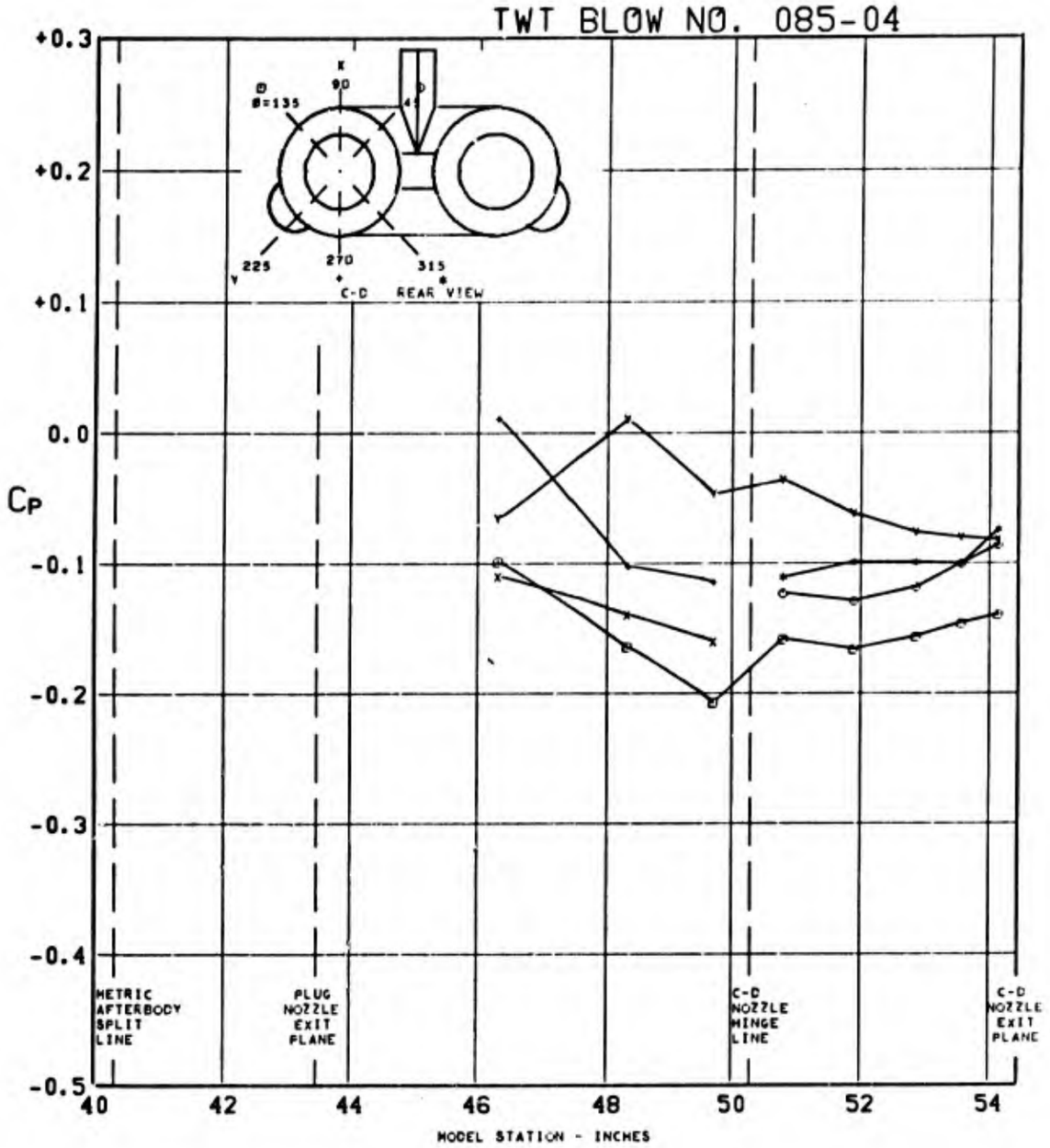

FIGURE 232. PRESSURE COEFFICIENTS ON C-D AFTERBODY (W1B1K1N1 P07 H1V1) Λ_{LE}=70° AT 1.998 M_0, $(P_T/P_0)_{C-D}$=14.90, $(P_T/P_0)_{PLUG}$=4.986, α= 2.9

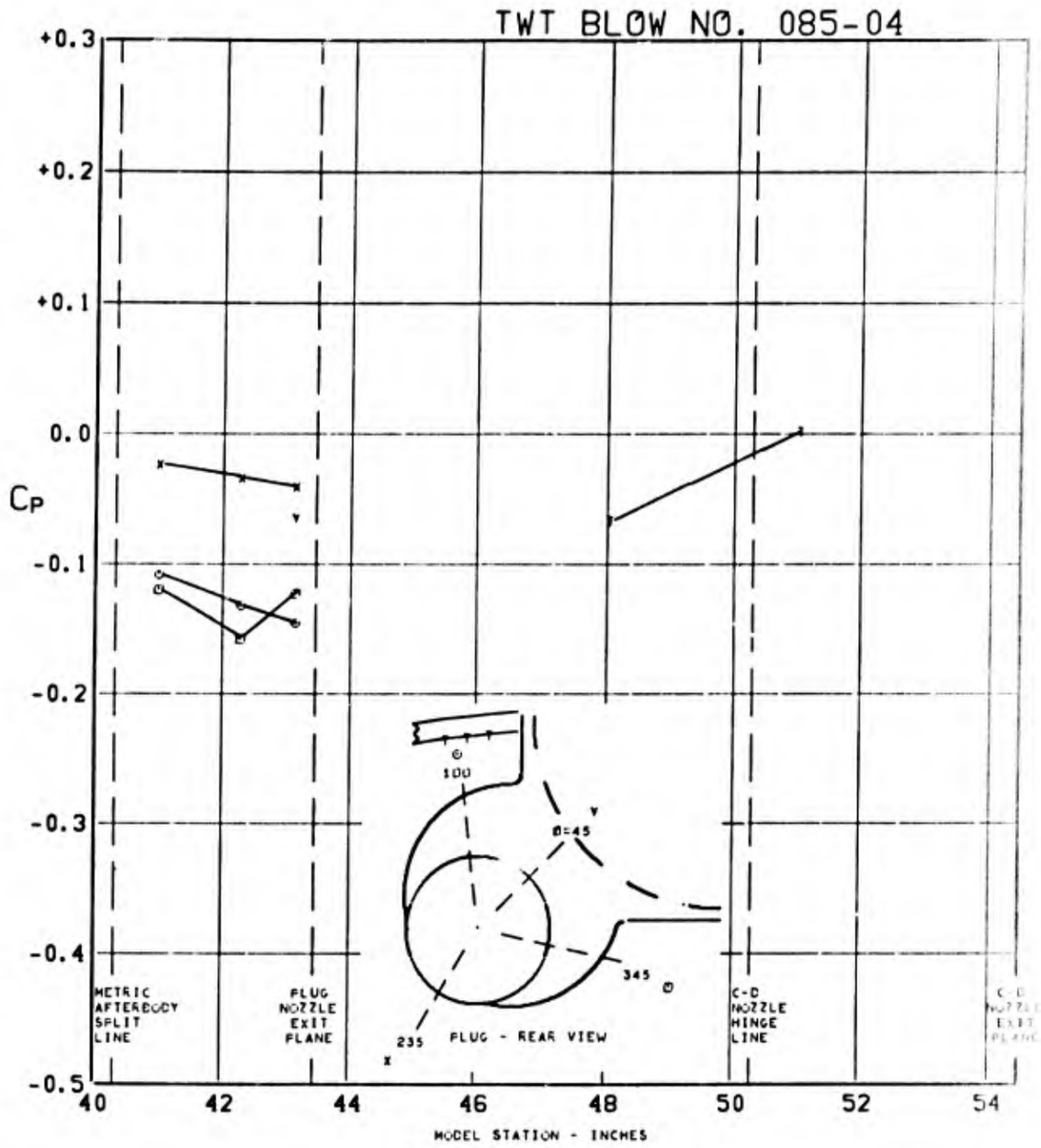

FIGURE 233. PRESSURE COEFFICIENTS ON TAIL & PLUG AFTERBODY (W1B1K1N1 P07 H1V1) Λ_{LE}=70° AT 1.998 M_0, $(P_T/P_0)_{C-D}$=14.90, $(P_T/P_0)_{PLUG}$=4.986, α= 2.9

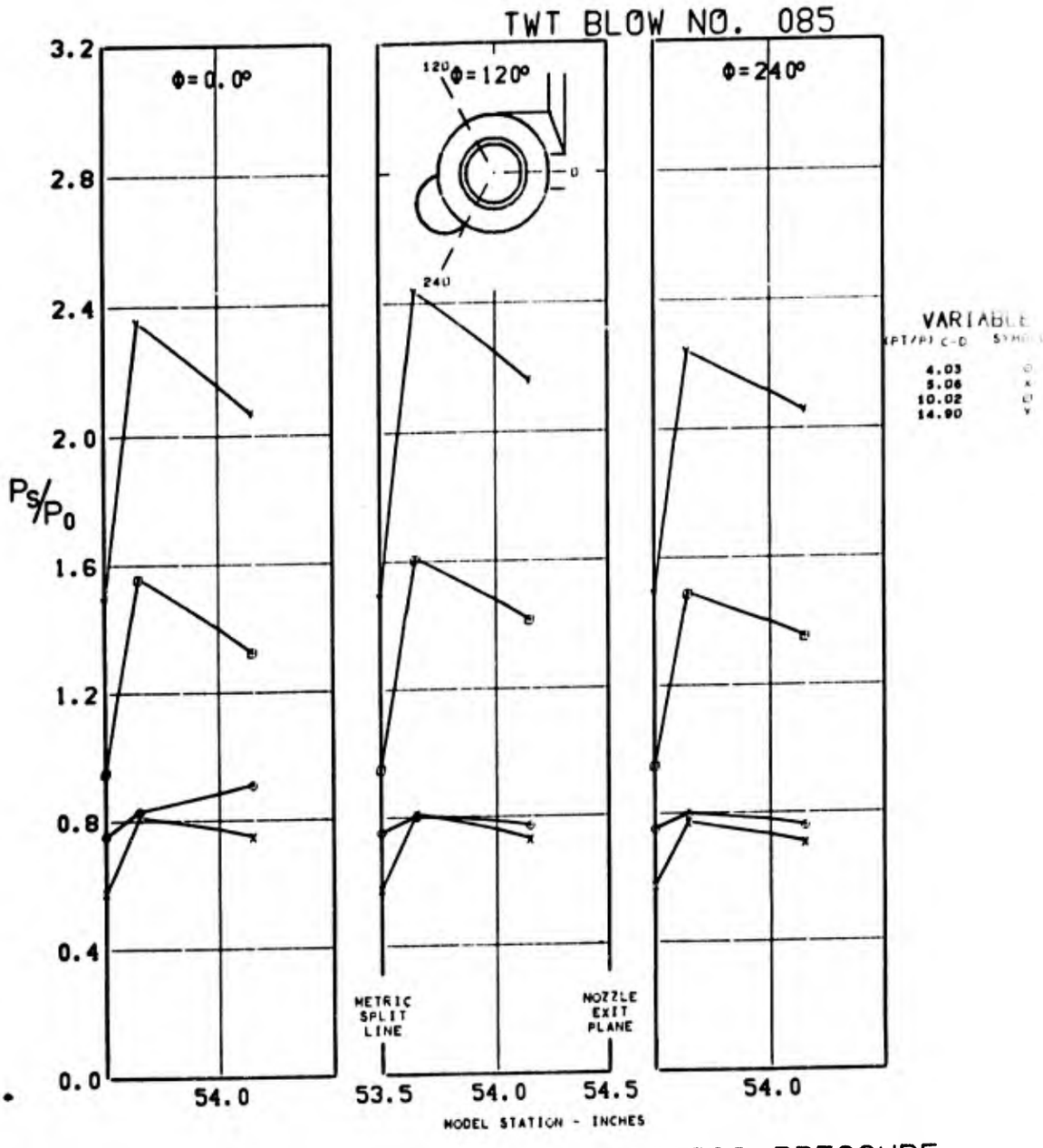

FIGURE 234. C-D NOZZLE EXIT STATIC PRESSURE CONFIGURATION (W1B1K1N1 P07 H1V1) Λ_{LE}=70° AT 1.998 M_0, $(P_T/P_0)_{C-D}$=VARY, $(P_T/P_0)_{PLUG}$=4.986, α= 2.9

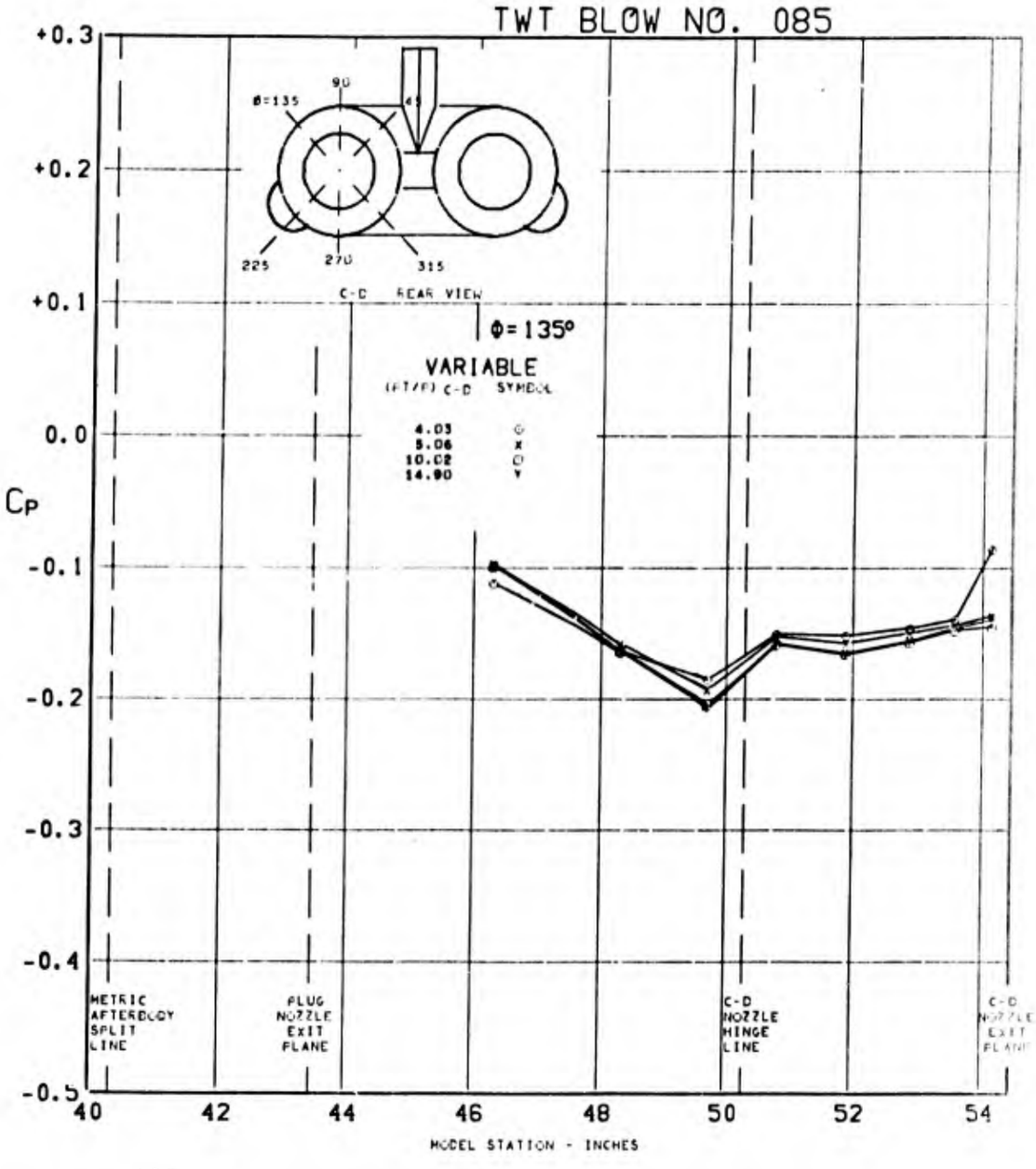

FIGURE 235. PRESSURE COEFFICIENTS ON C-D AFTERBODY (W1B1K1N1 P07 H1V1) $\Lambda_{LE}=70°$ AT 1.998 M_0, $(P_T/P_0)_{C-D}$=VARY, $(P_T/P_0)_{PLUG}=4.986$, $\alpha=2.9$

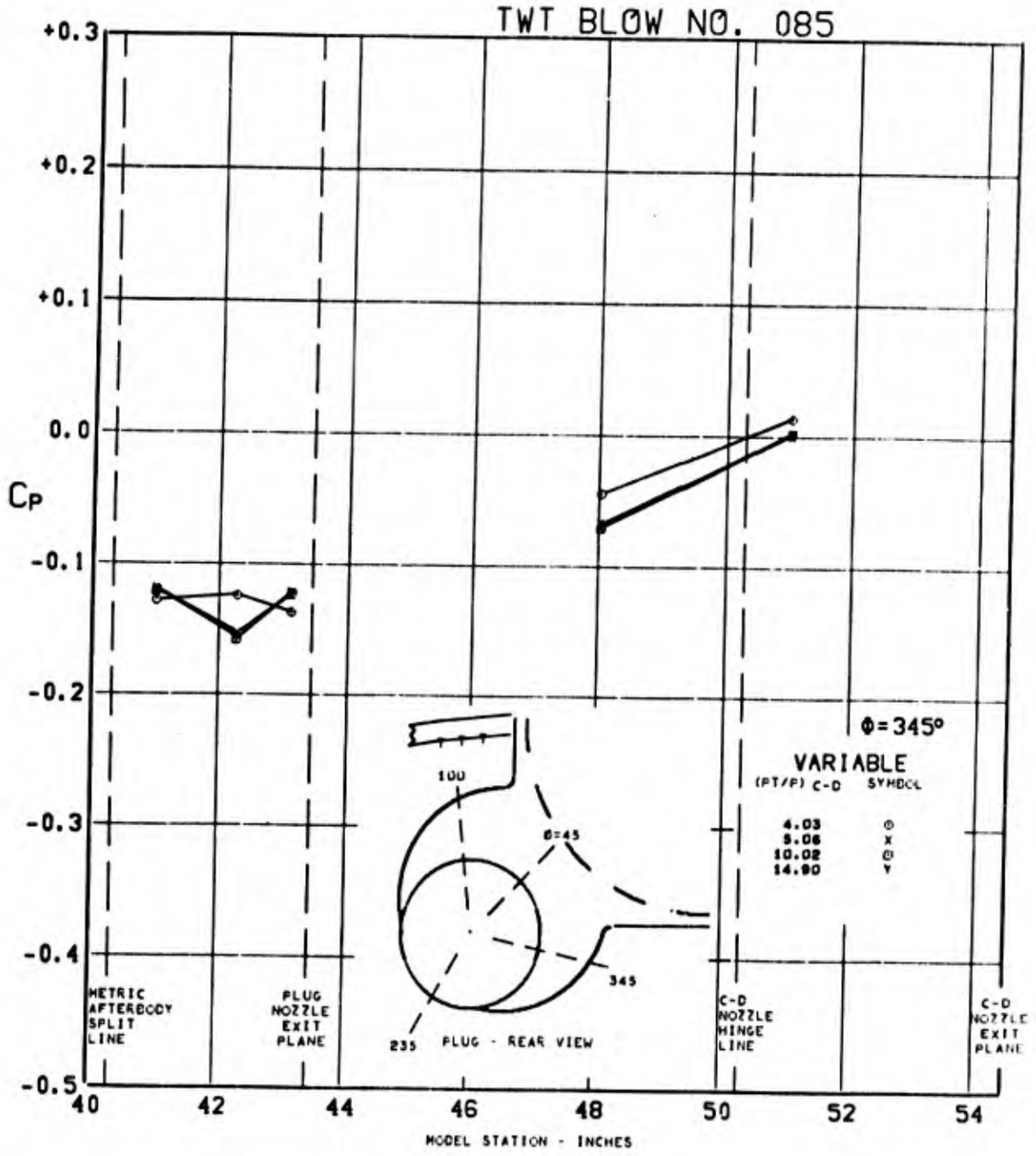

FIGURE 236. PRESSURE COEFFICIENTS ON TAIL & PLUG AFTERBODY (W1B1K1N1 P07 H1V1) $\Lambda_{LE}=70°$ AT 1.998 M_0, $(P_T/P_0)_{C-D}$=VARY, $(P_T/P_0)_{PLUG}$=4.986, α= 2.9

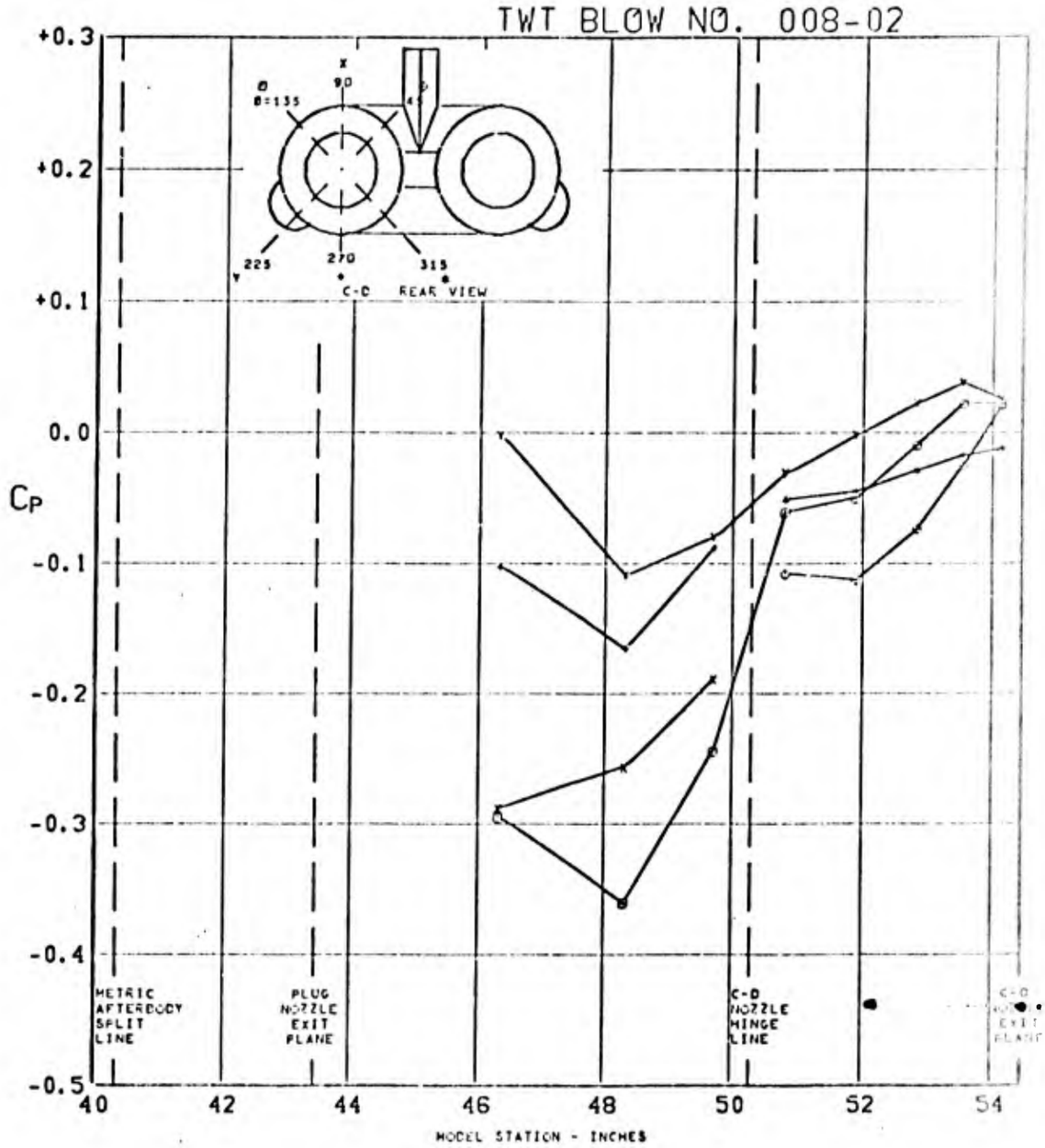

FIGURE 237. PRESSURE COEFFICIENTS ON C-D AFTERBODY (W1B1K1N1 P01 H1V1) Λ_{LE}=70° AT 0.850 M_0, $(P_T/P_0)_{C-D}$=CONE, $(P_T/P_0)_{PLUG}$=CONE, α= 2.

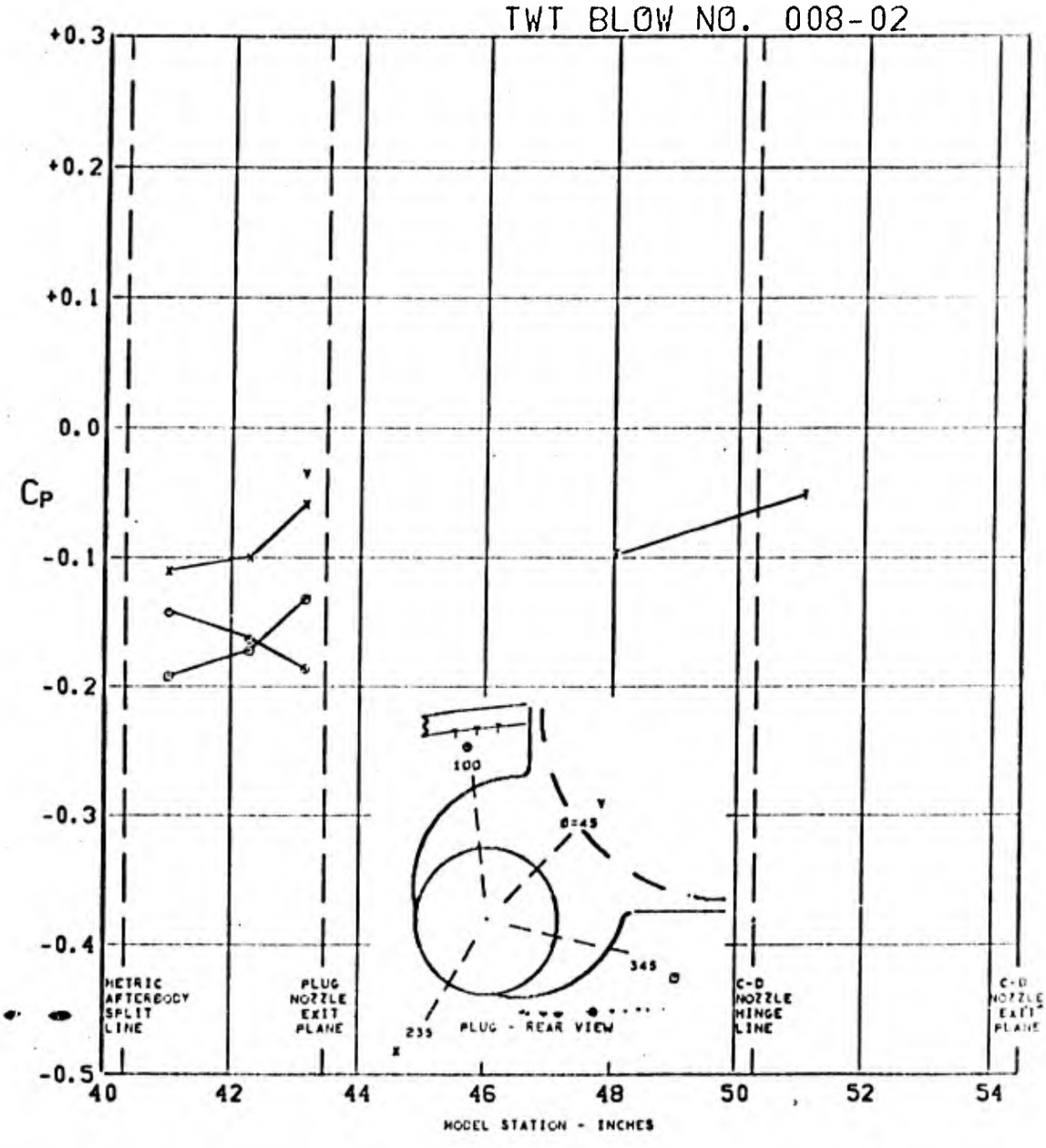

FIGURE 238. PRESSURE COEFFICIENTS ON TAIL & PLUG AFTERBODY (W1B1K1N1 P01 H1V1) $\Lambda_{LE}=70°$ AT 0.850 M_0, $(P_T/P_0)_{C-D}$=CONE, $(P_T/P_0)_{PLUG}$=CONE, α= 2.8

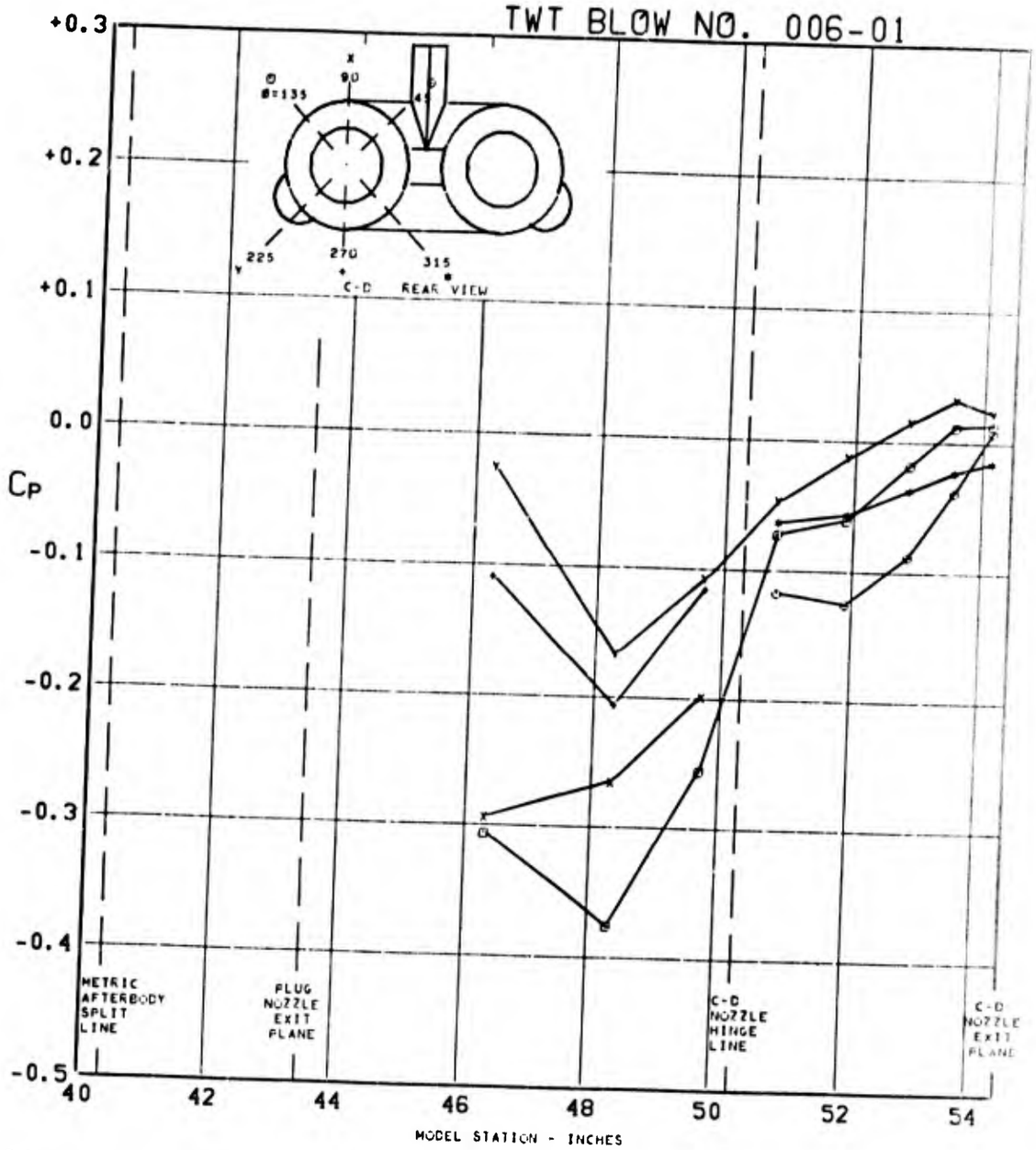

FIGURE 239. PRESSURE COEFFICIENTS ON C-D AFTERBODY (W1B1K1N1 P04 H1V1) $\Lambda_{LE}=70°$ AT 0.850 M_0, $(P_T/P_0)_{C-D}$=CONE, $(P_T/P_0)_{PLUG}=1.545$, $\alpha=$ 2.8

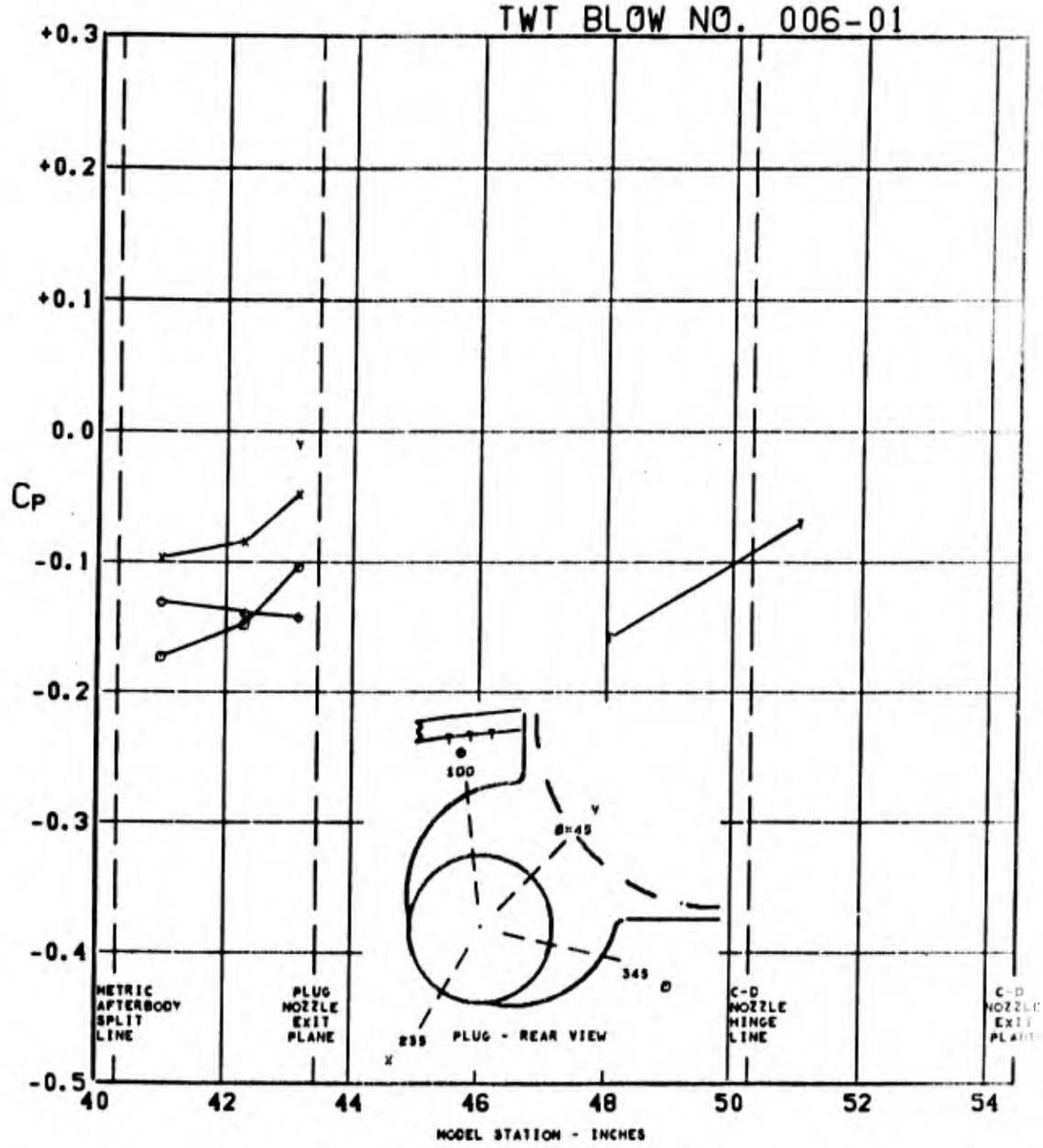

FIGURE 240. PRESSURE COEFFICIENTS ON TAIL & PLUG AFTERBODY (W1B1K1N1 P04 H1V1) Λ_{LE}=70° AT 0.850 M_0, $(P_T/P_0)_{C-D}$=CONE, $(P_T/P_0)_{PLUG}$=1.545, α= 2.8

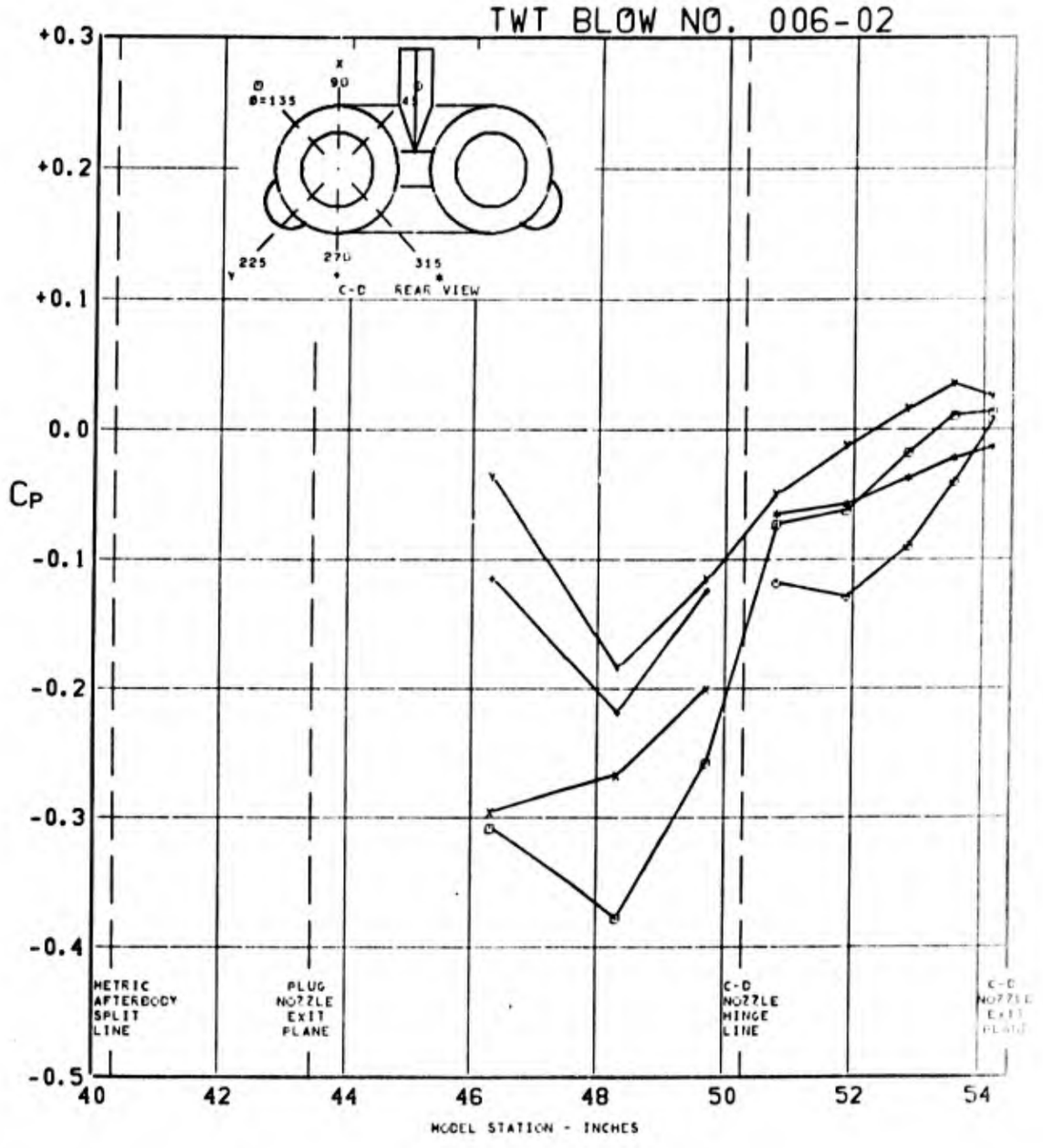

FIGURE 241. PRESSURE COEFFICIENTS ON C-D AFTERBODY (W1B1K1N1 P04 H1V1) $\Lambda_{LE}=70°$ AT 0.848 M_0, $(P_T/P_0)_{C-D}$=CONE, $(P_T/P_0)_{PLUG}=2.010$, $\alpha=$ 2.8

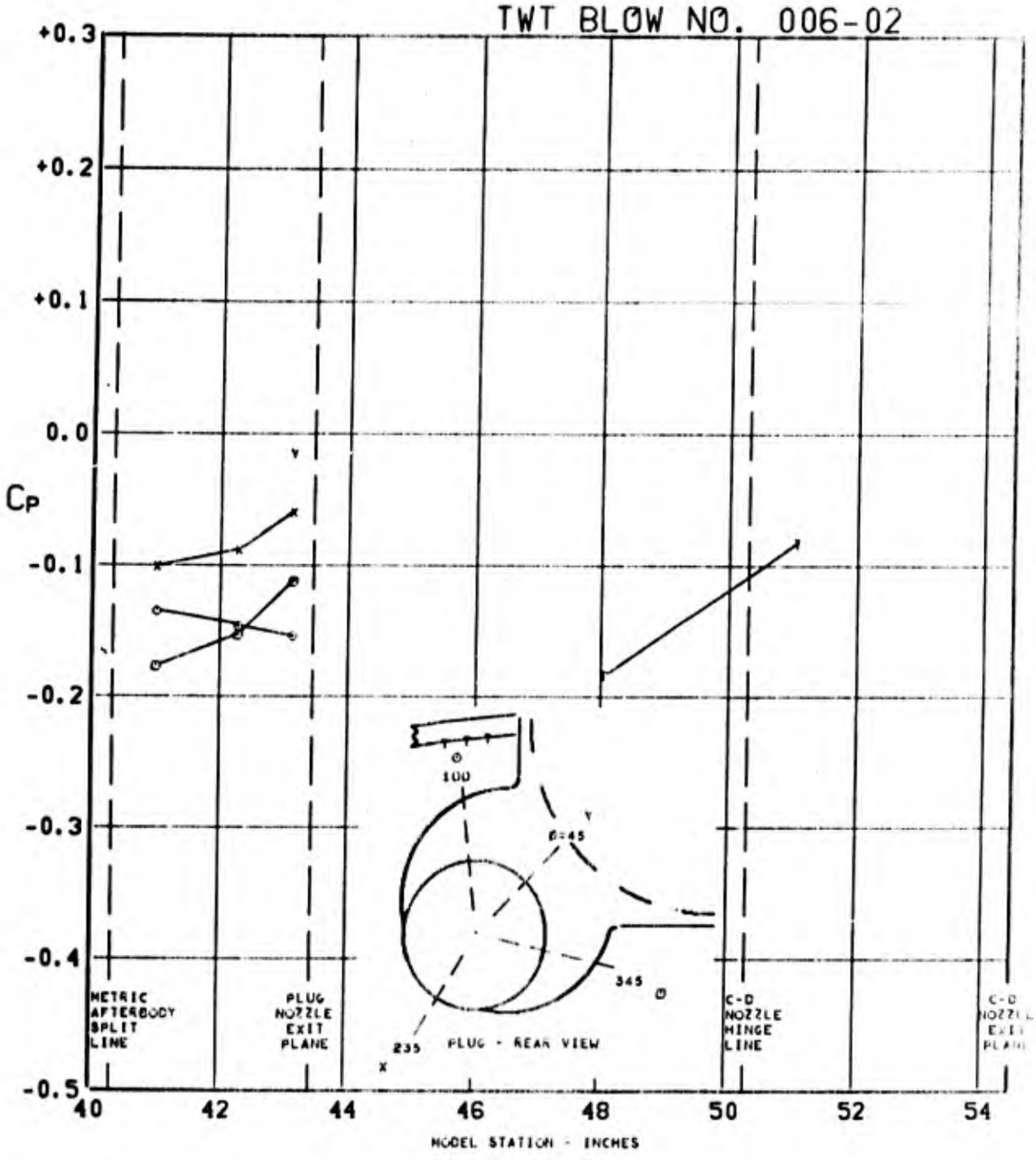

FIGURE 242. PRESSURE COEFFICIENTS ON TAIL & PLUG AFTERBODY (W1B1K1N1 P04 H1V1) Λ_{LE}=70° AT 0.848 M_0, $(P_T/P_0)_{C-D}$=CONE, $(P_T/P_0)_{PLUG}$=2.010, α= 2.8

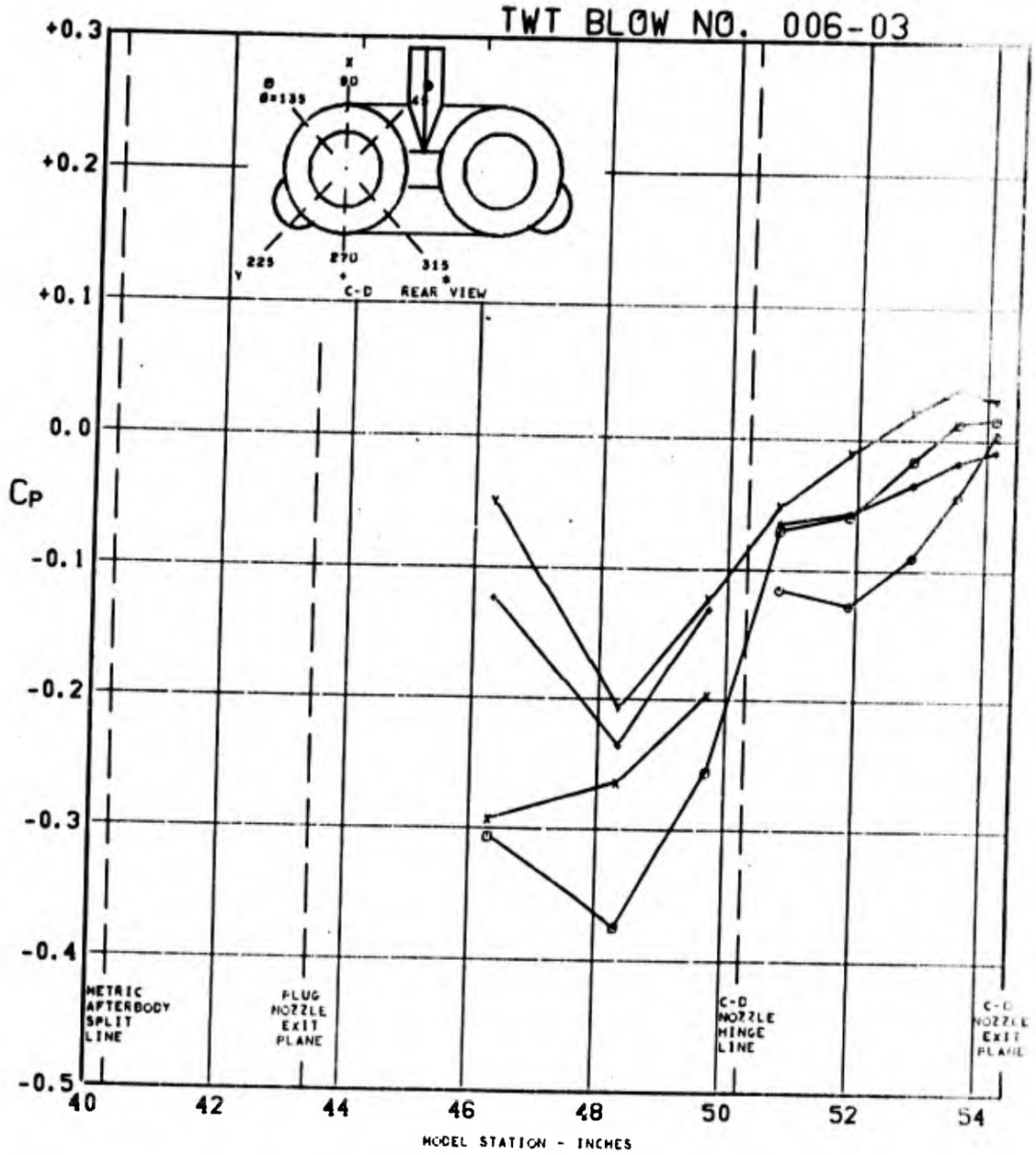

FIGURE 243. PRESSURE COEFFICIENTS ON C-D AFTERBODY (W1B1K1N1 P04 H1V1) $\Lambda_{LE}=70°$ AT 0.848 M_0, $(P_T/P_0)_{C-D}$=CONE, $(P_T/P_0)_{PLUG}$=2.981, α= 2.8

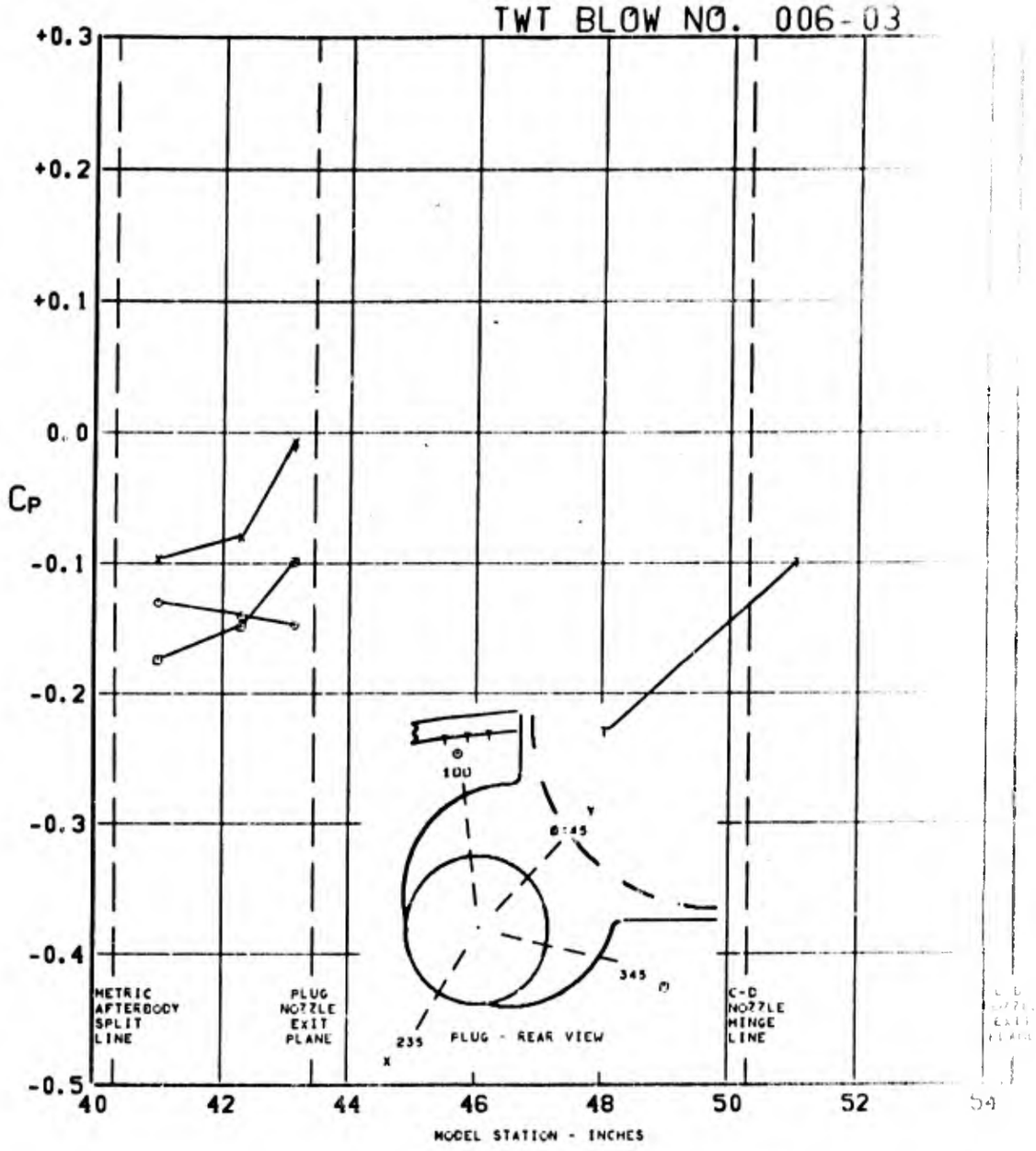

FIGURE 244. PRESSURE COEFFICIENTS ON TAIL & PLUG AFTERBODY (W1B1K1N1 P04 H1V1) $\Lambda_{LE}=70°$ AT 0.848 M_0, $(P_T/P_0)_{C-D}$=CONE, $(P_T/P_0)_{PLUG}=2.981$, $\alpha=$ 2.

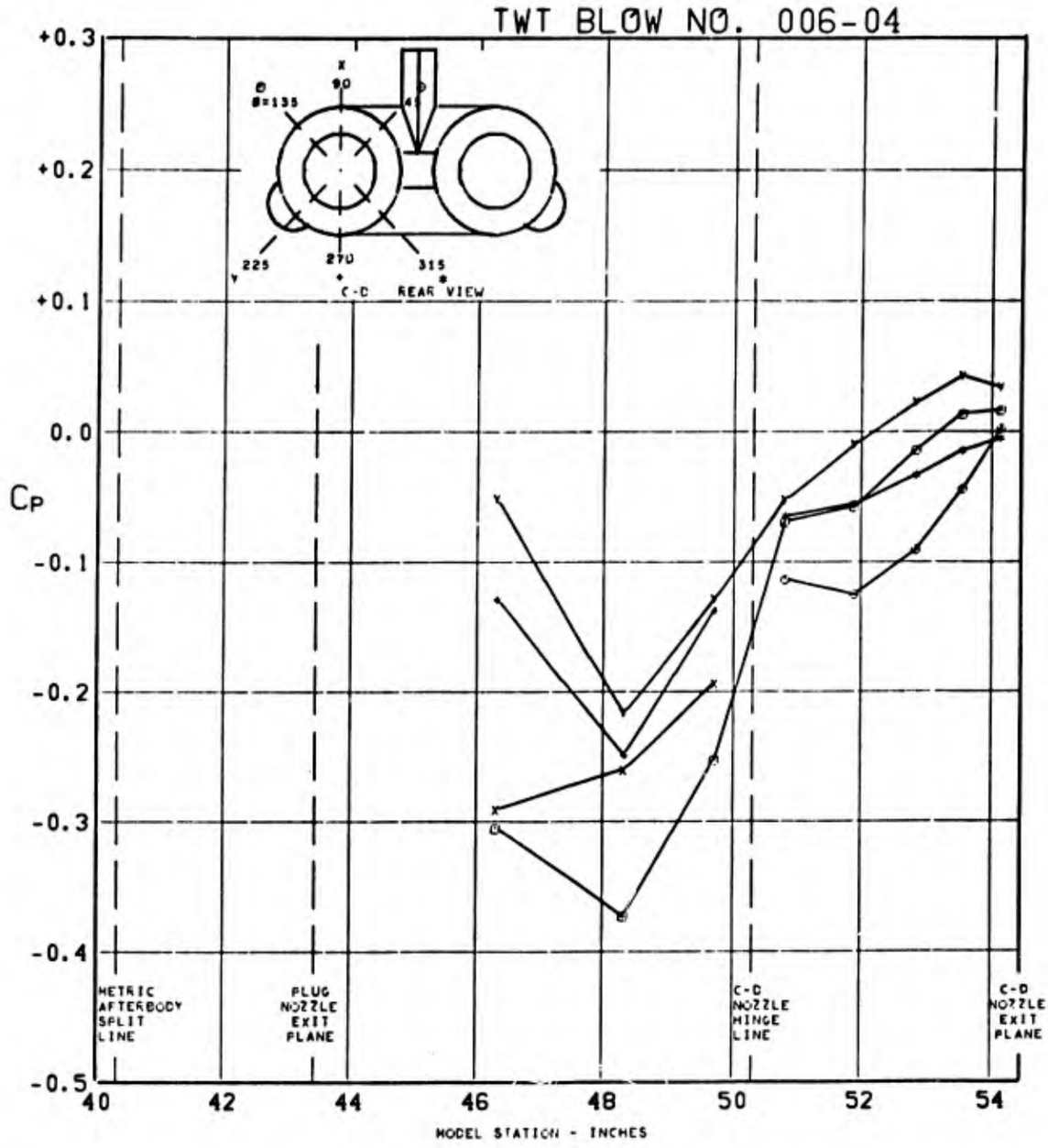

FIGURE 245. PRESSURE COEFFICIENTS ON C-D AFTERBODY (W1B1K1N1 P04 H1V1) Λ_{LE}=70° AT 0.848 M_0, $(P_T/P_0)_{C-D}$=CONE, $(P_T/P_0)_{PLUG}$=4.026, α= 2.8

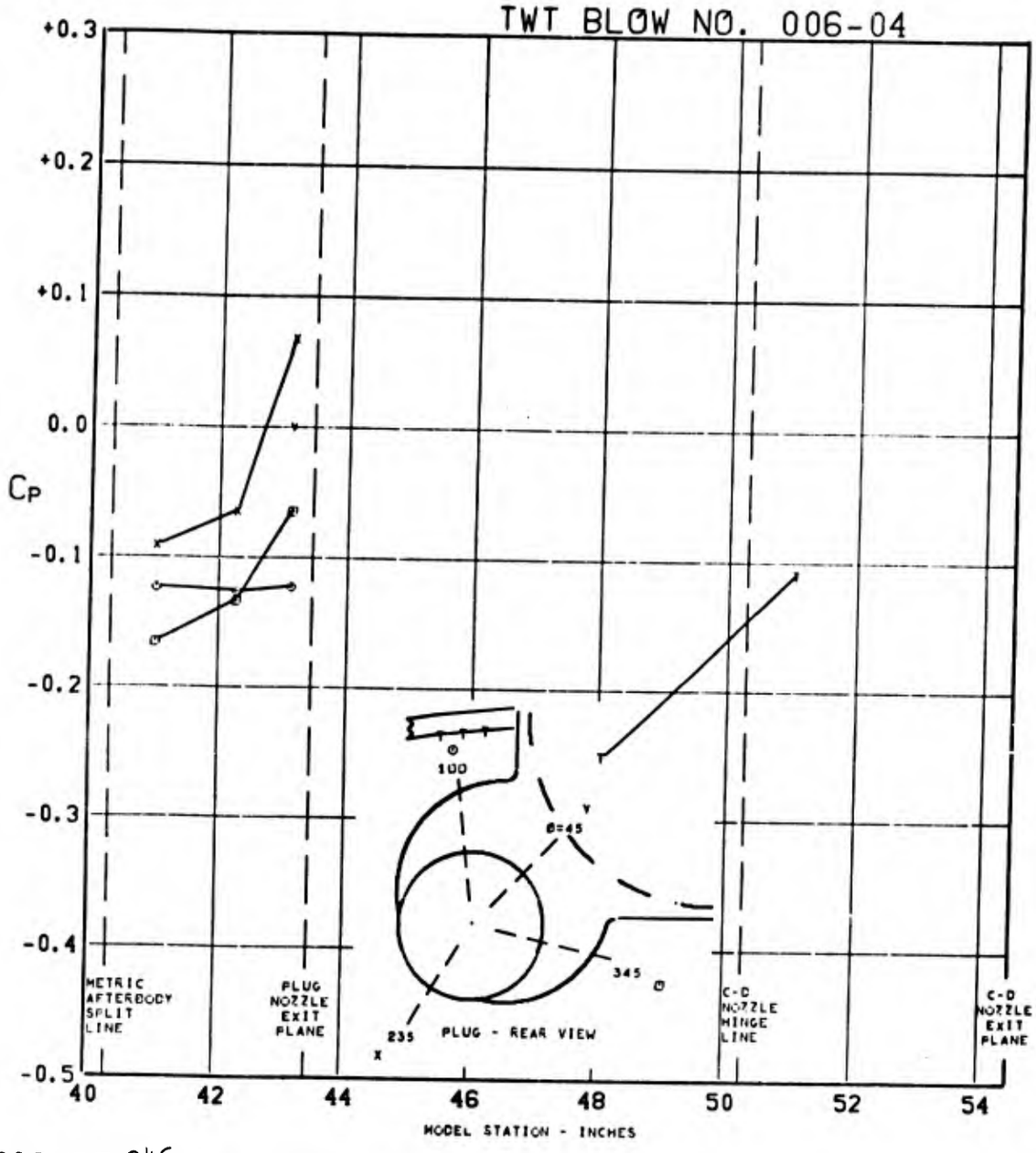

FIGURE 246. PRESSURE COEFFICIENTS ON TAIL & PLUG AFTERBODY (W1B1K1N1 P04 H1V1) $\Lambda_{LE}=70°$ AT 0.848 M_0, $(P_T/P_0)_{C-D}$=CONE, $(P_T/P_0)_{PLUG}=4.026$, $\alpha=2.8$

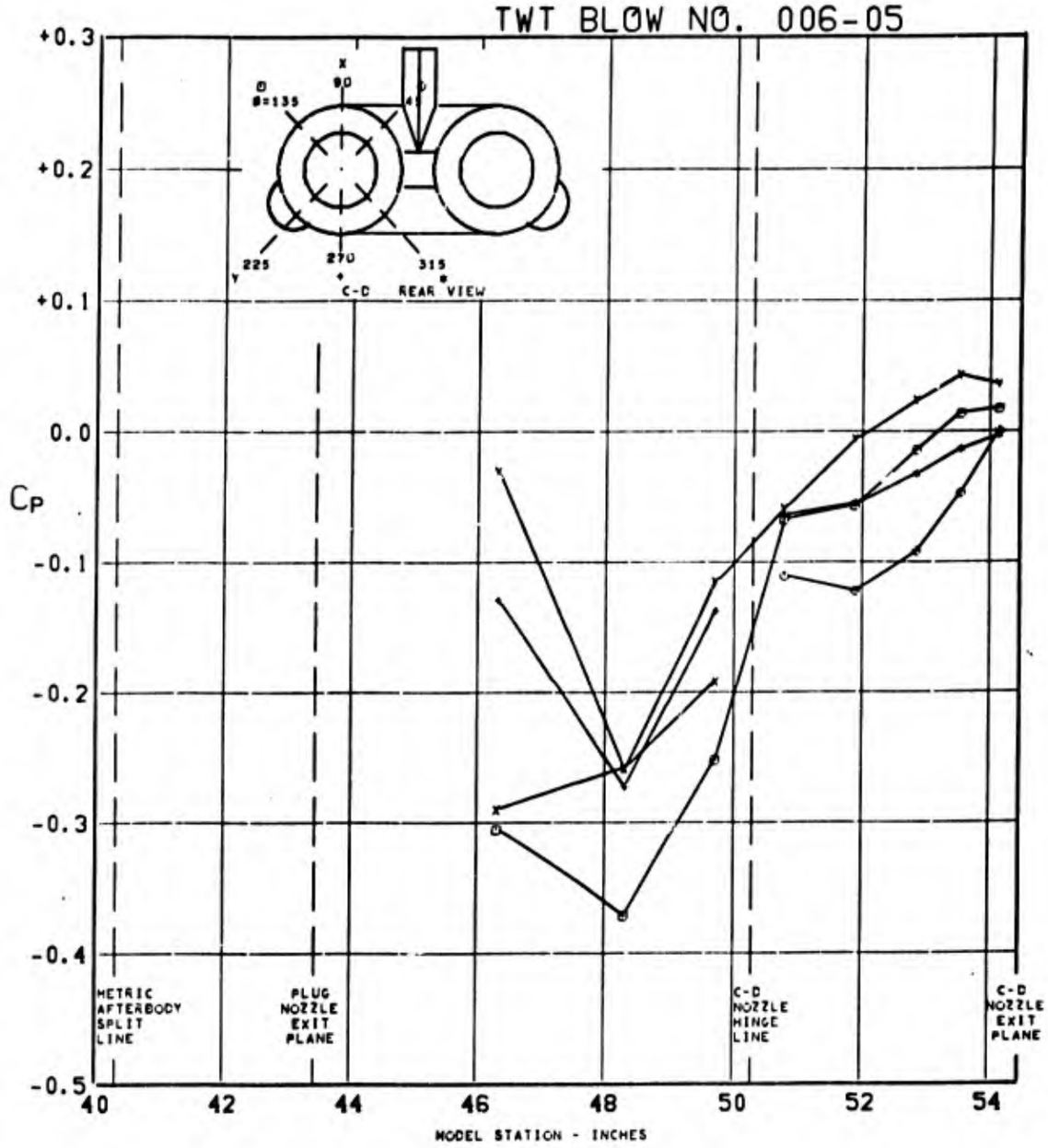

FIGURE 247. PRESSURE COEFFICIENTS ON C-D AFTERBODY (W1B1K1N1 P04 H1V1) Λ_{LE}=70° AT 0.848 M_0, $(P_T/P_0)_{C-D}$=CONE, $(P_T/P_0)_{PLUG}$=5.001, α= 2.8

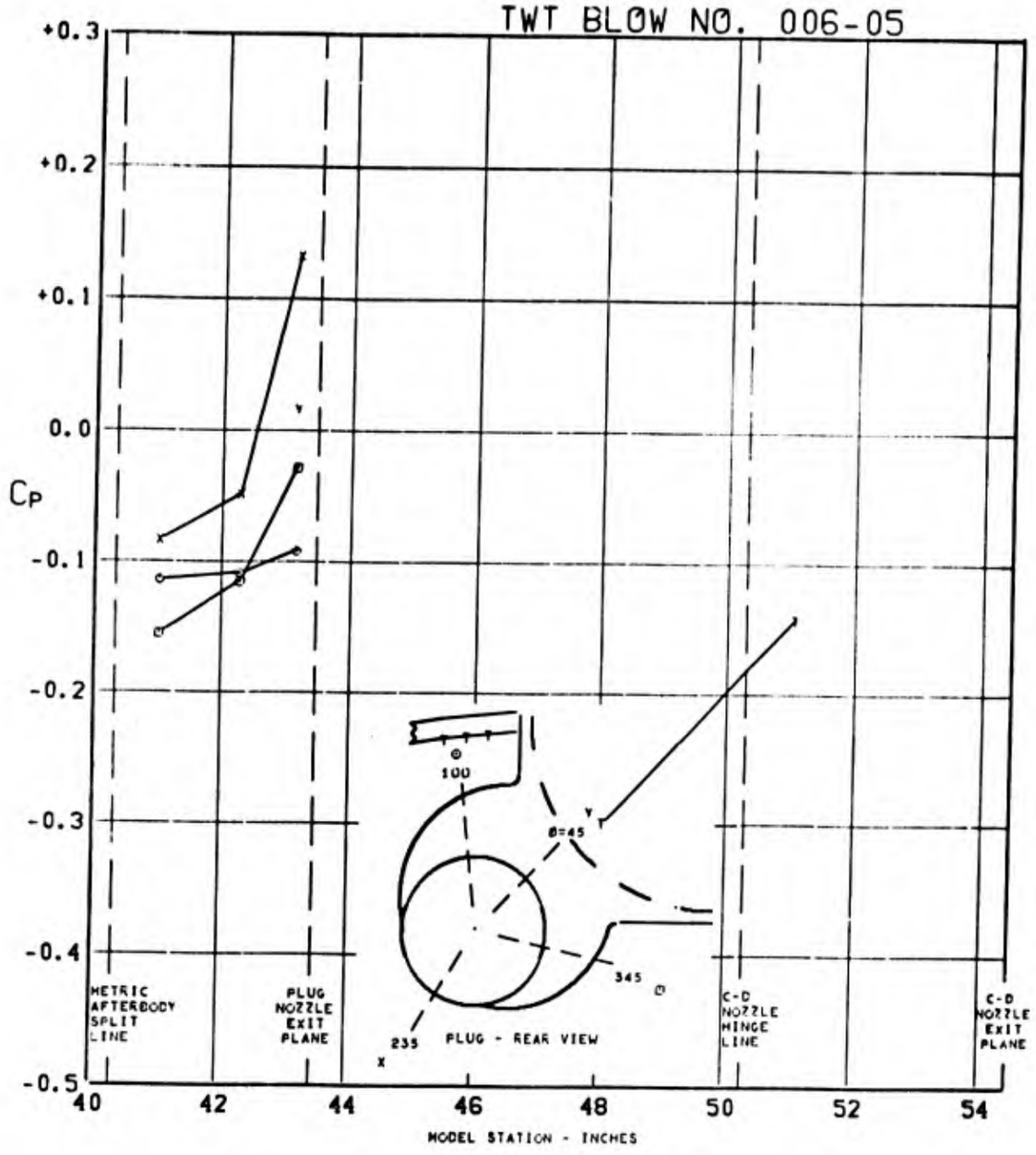

FIGURE 248. PRESSURE COEFFICIENTS ON TAIL & PLUG AFTERBODY (W1B1K1N1 P04 H1V1) $\Lambda_{LE}=70°$ AT 0.848 M_0, $(P_T/P_0)_{C-D}$=CONE, $(P_T/P_0)_{PLUG}$ =5.001, α= 2.8

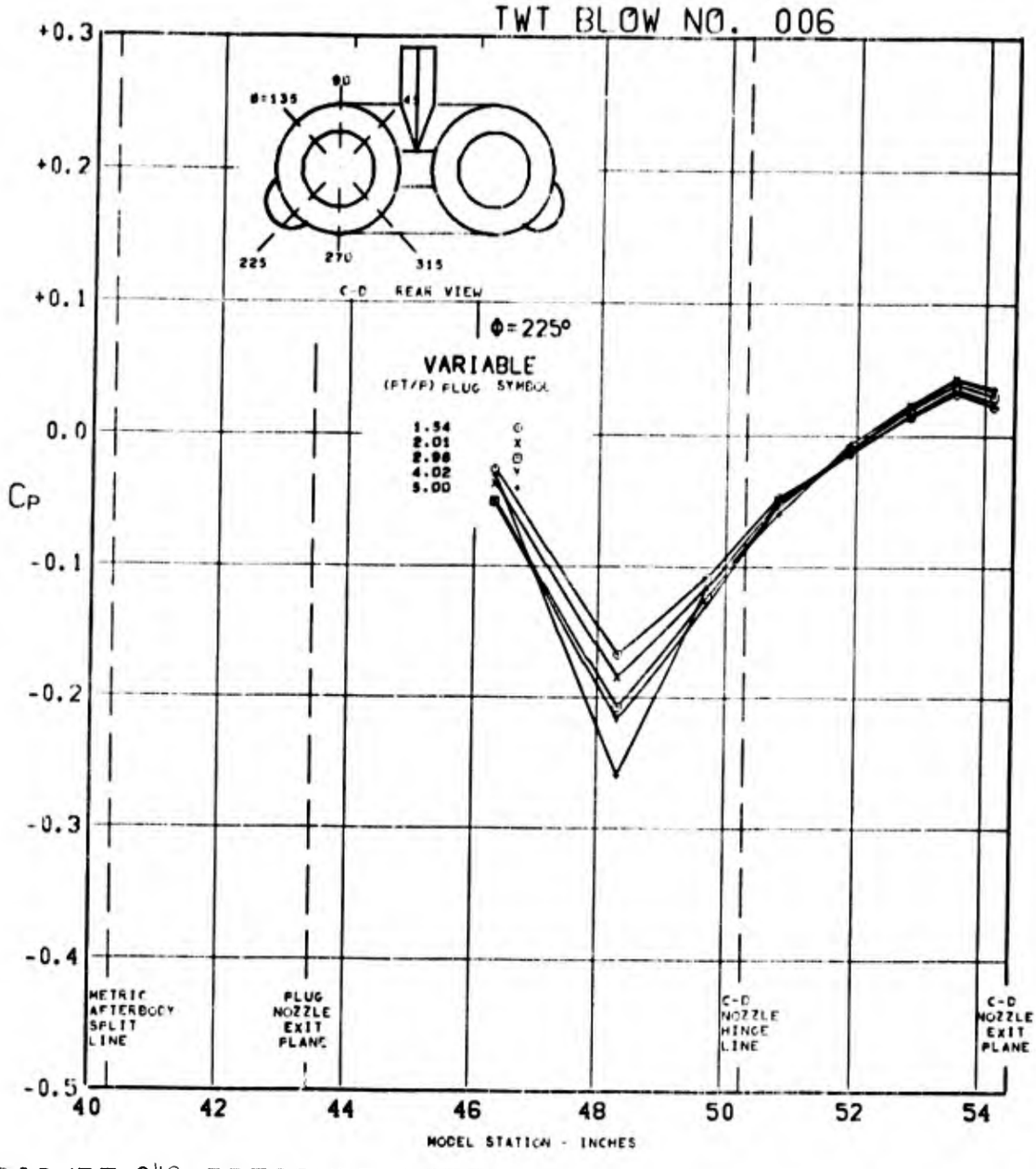

FIGURE 249. PRESSURE COEFFICIENTS ON C-D AFTERBODY (W1B1K1N1 P04 H1V1) Λ_{LE}=70° AT 0.848 M_0, $(P_T/P_0)_{C-D}$=CONE, $(P_T/P_0)_{PLUG}$=VARY, α= 2.8

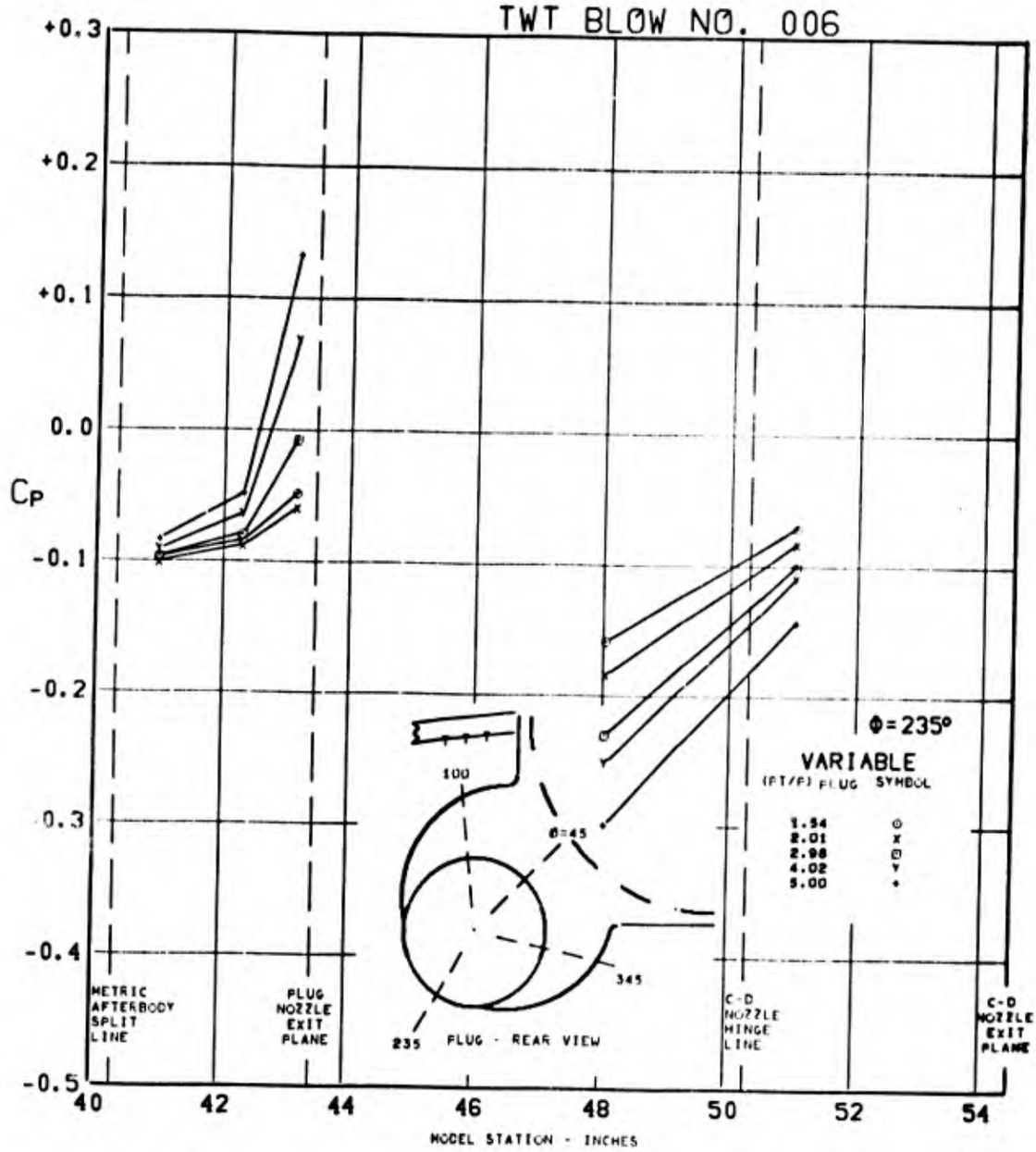

FIGURE 250. PRESSURE COEFFICIENTS ON TAIL & PLUG AFTERBODY (W1B1K1N1 P04 H1V1) $\Lambda_{LE}=70°$ AT 0.848 M_0, $(P_T/P_0)_{C-D}$=CONE, $(P_T/P_0)_{PLUG}$=VARY, α= 2.8

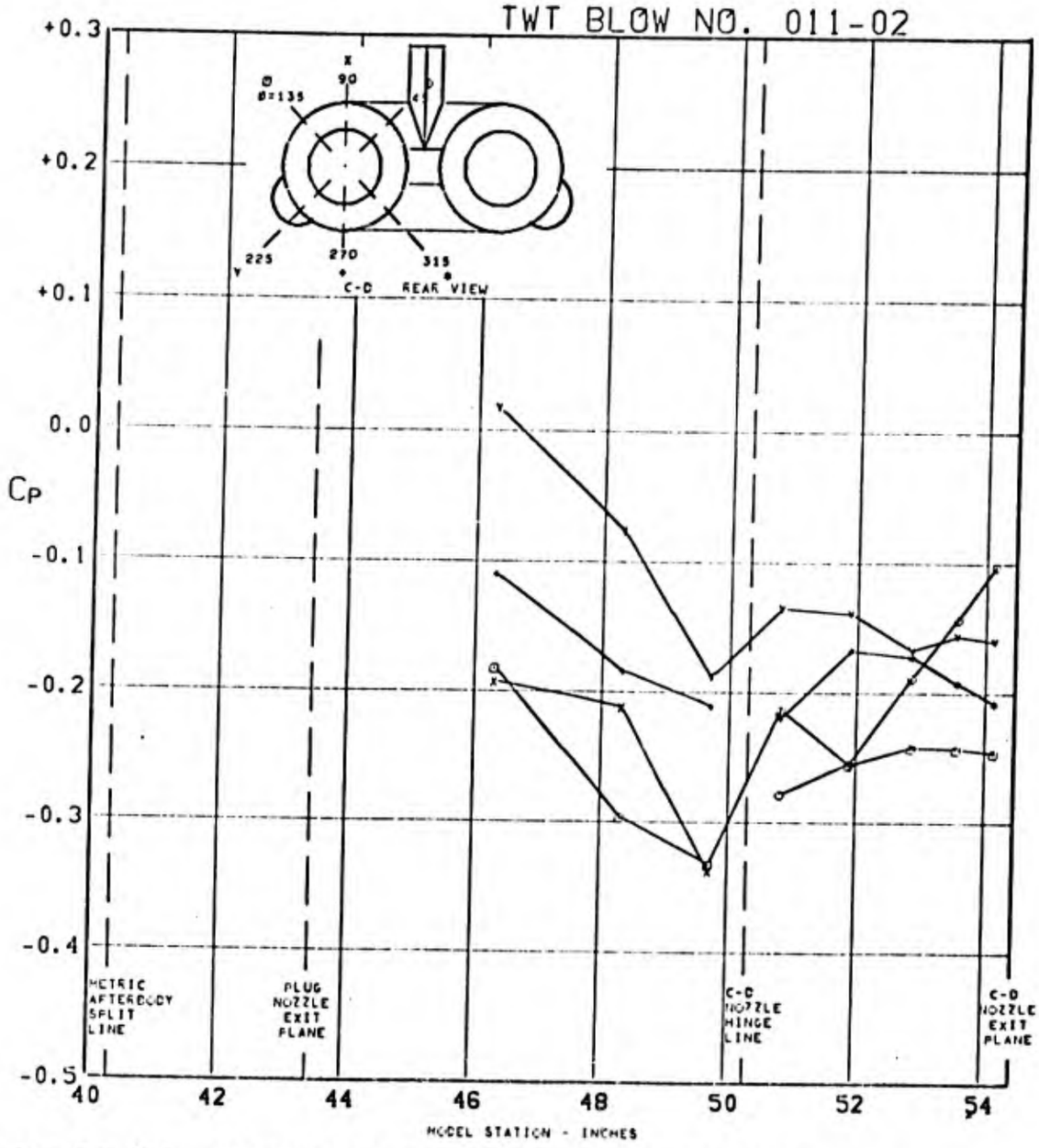

FIGURE 251. PRESSURE COEFFICIENTS ON C-D AFTERBODY (W1B1K1N1 P01 H1V1) Λ_{LE}=70° AT 1.271 M_0, $(P_T/P_0)_{C-D}$=CONE, $(P_T/P_0)_{PLUG}$=CONE, α= 2.8

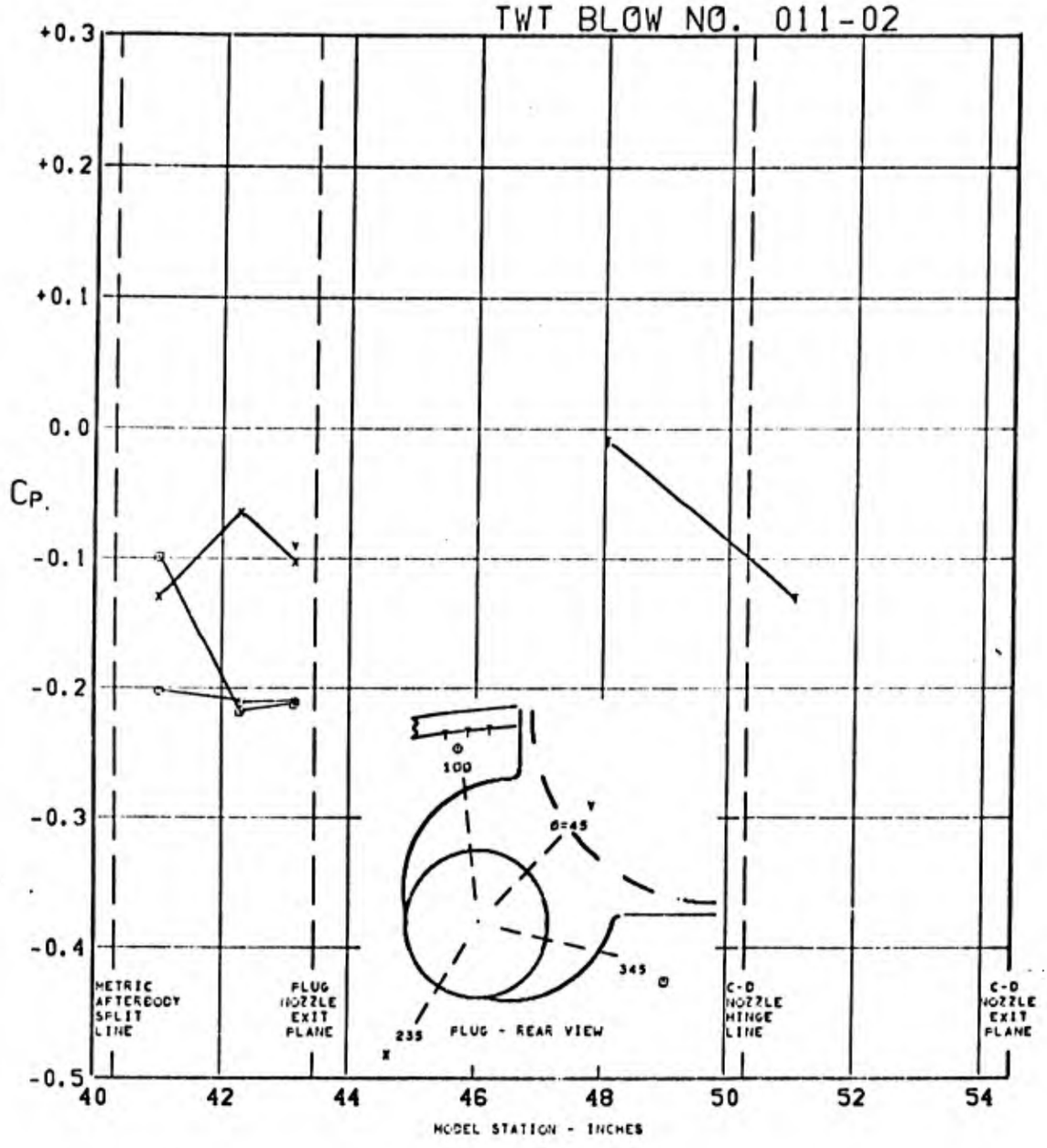

FIGURE 252. PRESSURE COEFFICIENTS ON TAIL & PLUG AFTERBODY (W1B1K1N1 P01 H1V1) Λ_{LE}=70° AT 1.271 M_0, $(P_T/P_0)_{C-D}$=CONE, $(P_T/P_0)_{PLUG}$=CONE, α= 2.8

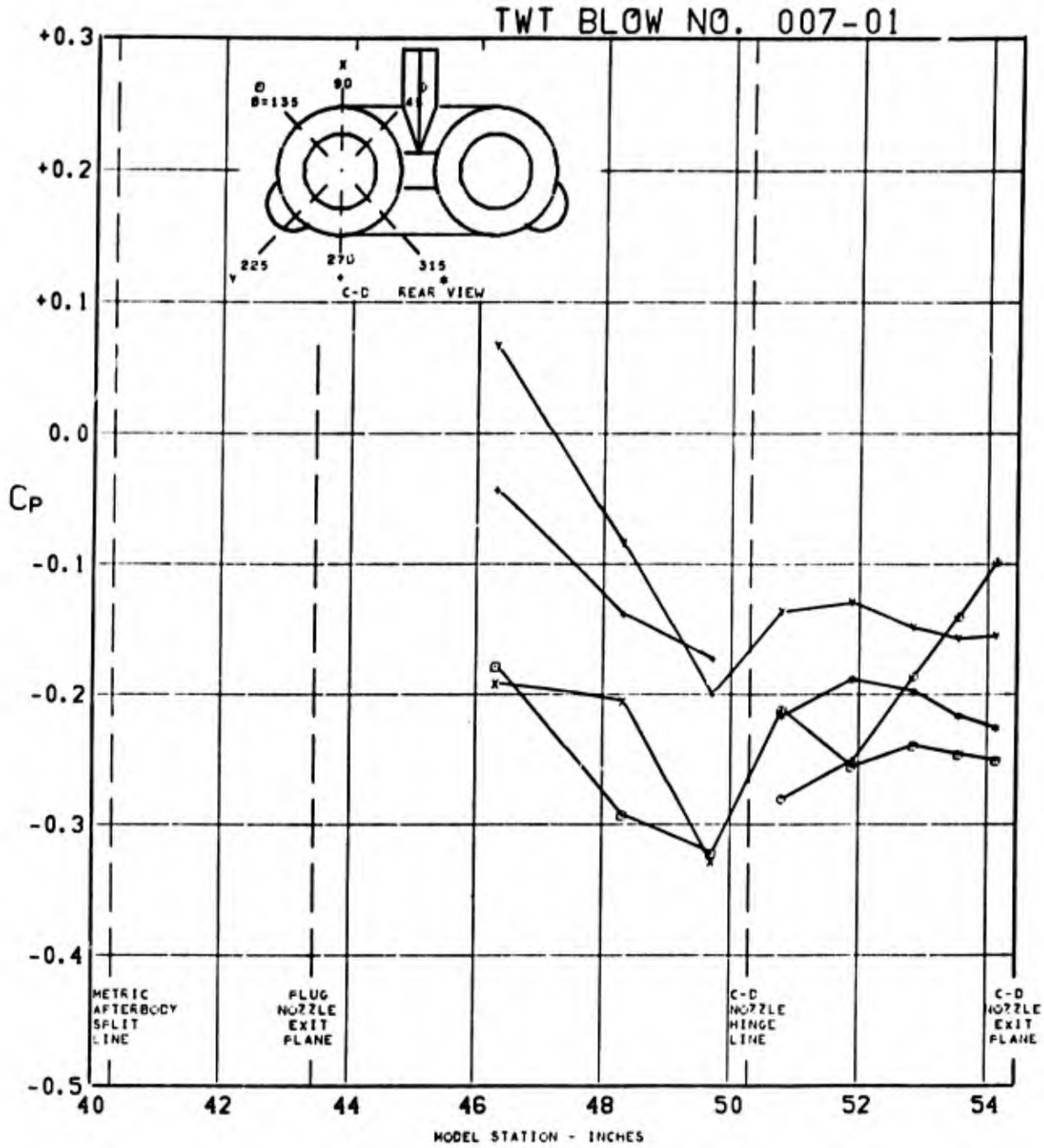

FIGURE 253. PRESSURE COEFFICIENTS ON C-D AFTERBODY (W1B1K1N1 P04 H1V1) Λ_{LE}=70° AT 1.269 M_0, $(P_T/P_0)_{C-D}$=CONE, $(P_T/P_0)_{PLUG}$=1.515, α= 2.9

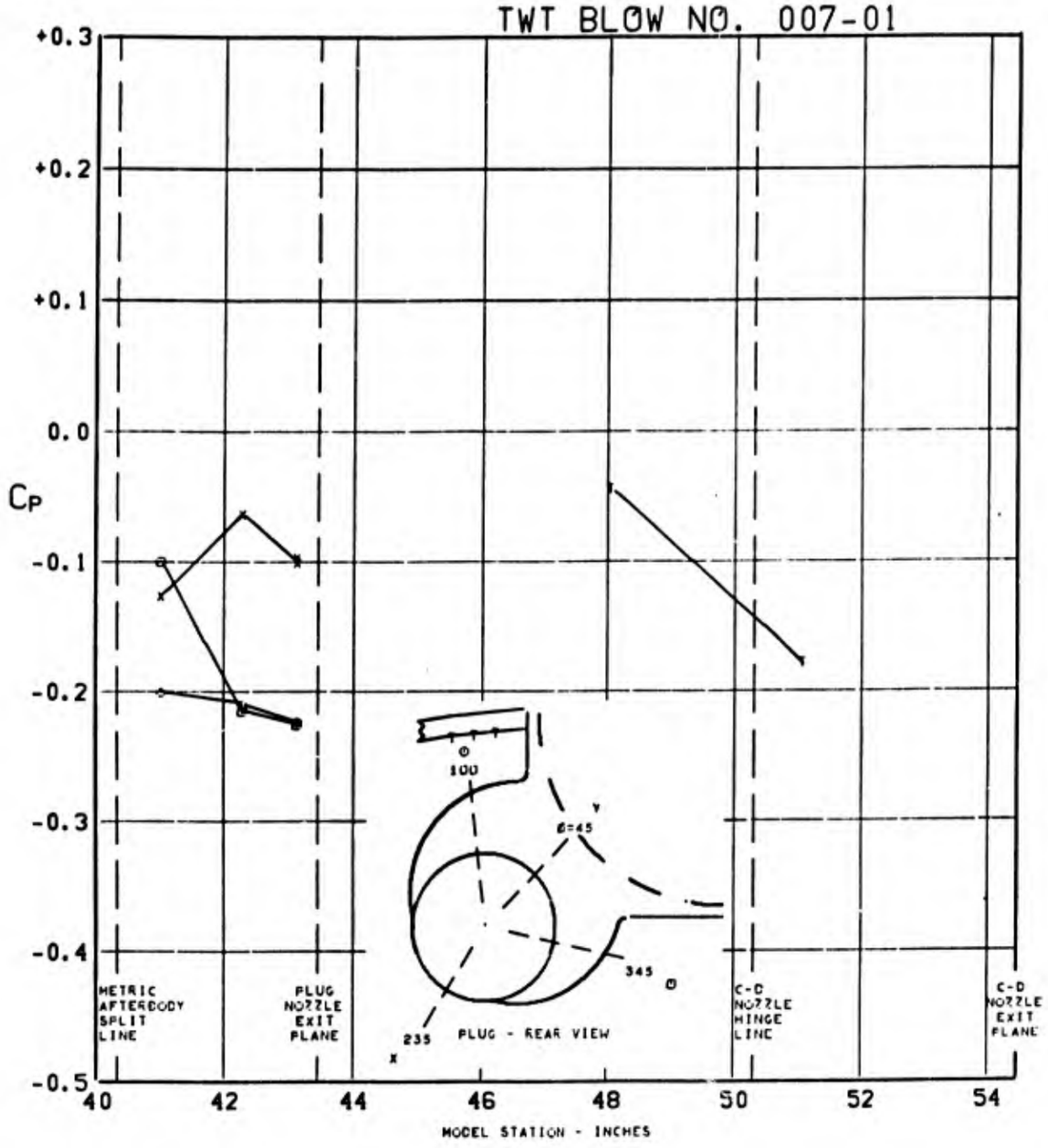

FIGURE 254. PRESSURE COEFFICIENTS ON TAIL & PLUG AFTERBODY (W1B1K1N1 P04 H1V1) Λ_{LE}=70° AT 1.269 M_0, $(P_T/P_0)_{C-D}$=CONE, $(P_T/P_0)_{PLUG}$=1.515, α= 2.9

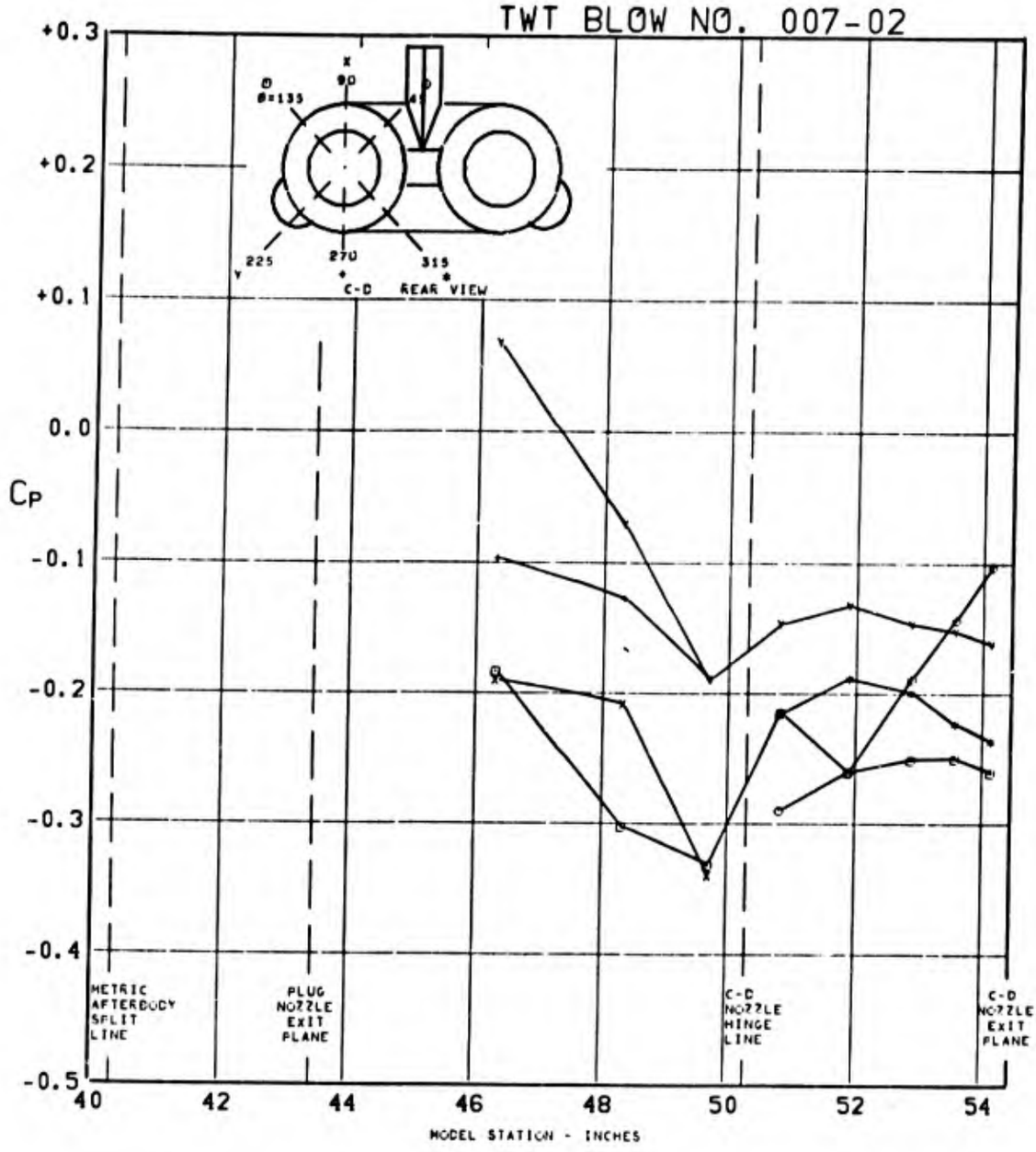

FIGURE 255. PRESSURE COEFFICIENTS ON C-D AFTERBODY (W1B1K1N1 P04 H1V1) $\Lambda_{LE}=70°$ AT 1.270 M_0, $(P_T/P_0)_{C-D}$=CONE, $(P_T/P_0)_{PLUG}=3.116$, $\alpha=2.9$

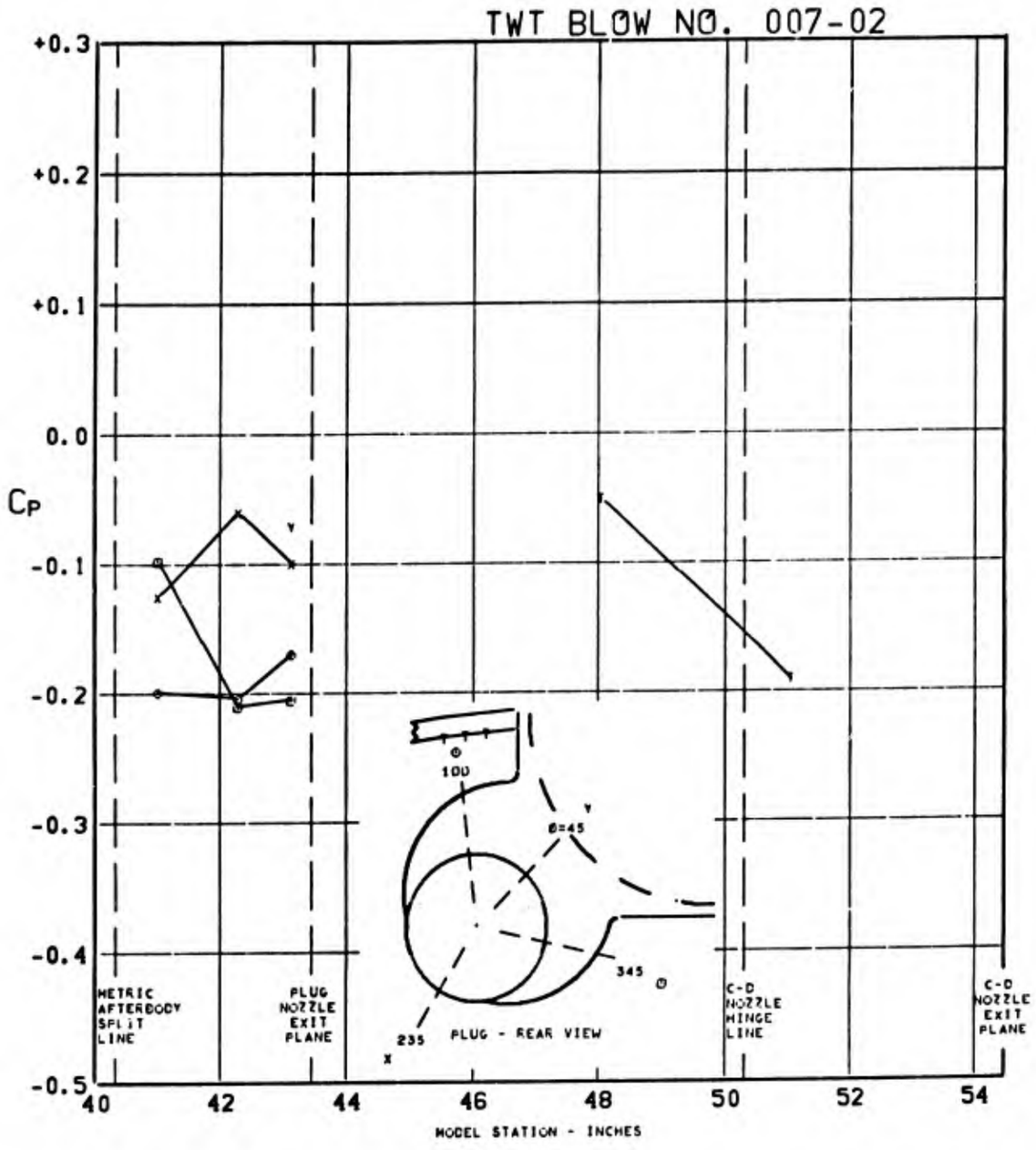

FIGURE 256. PRESSURE COEFFICIENTS ON TAIL & PLUG AFTERBODY (W1B1K1N1 P04 H1V1) Λ_{LE}=70° AT 1.270 M_0, $(P_T/P_0)_{C-D}$=CONE, $(P_T/P_0)_{PLUG}$=3.116, α= 2.9

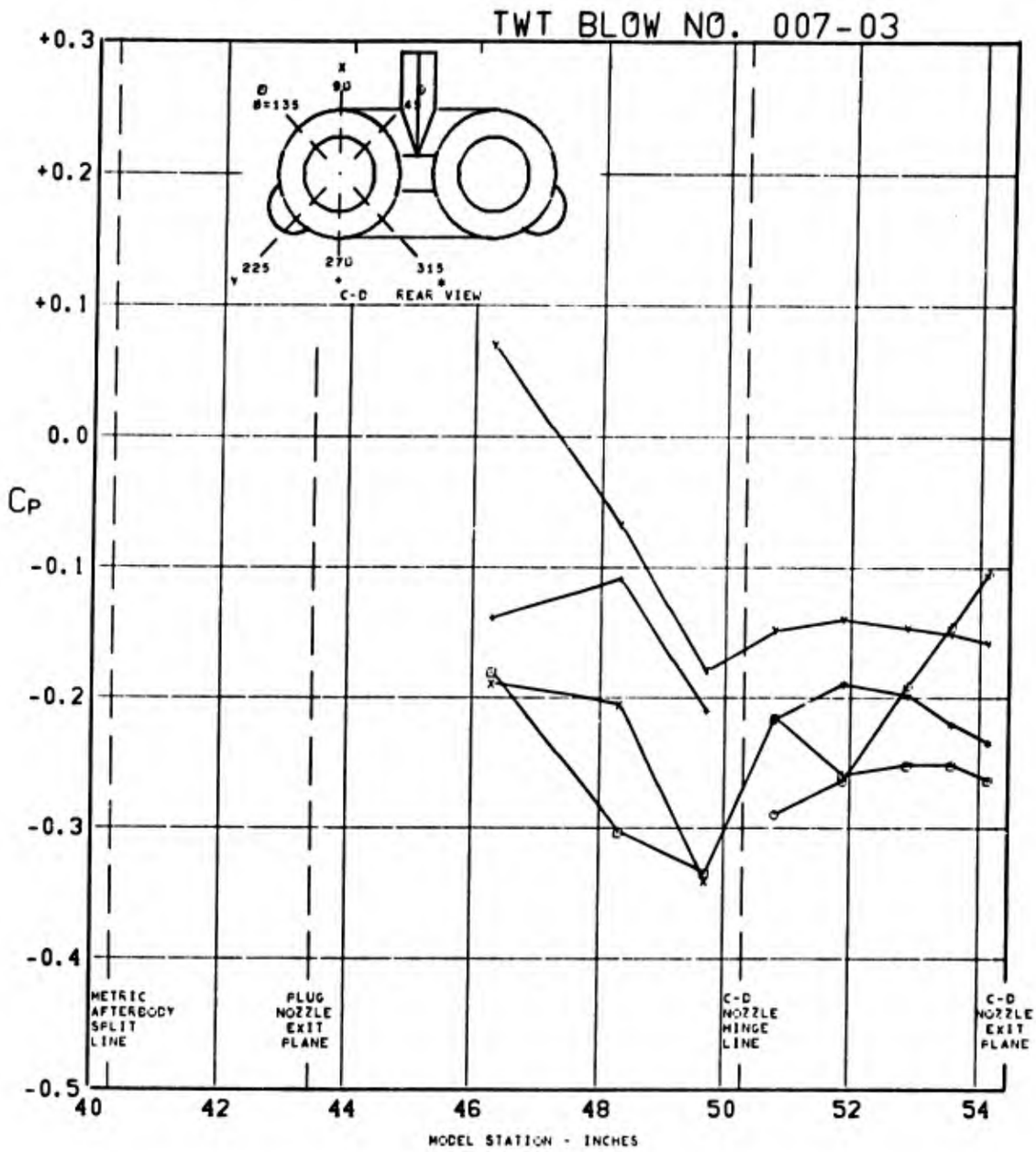

FIGURE 257. PRESSURE COEFFICIENTS ON C-D AFTERBODY (W1B1K1N1 P04 H1V1) Λ_{LE}=70° AT 1.270 M_0, $(P_T/P_0)_{C-D}$=CONE, $(P_T/P_0)_{PLUG}$=4.135, α= 2.9

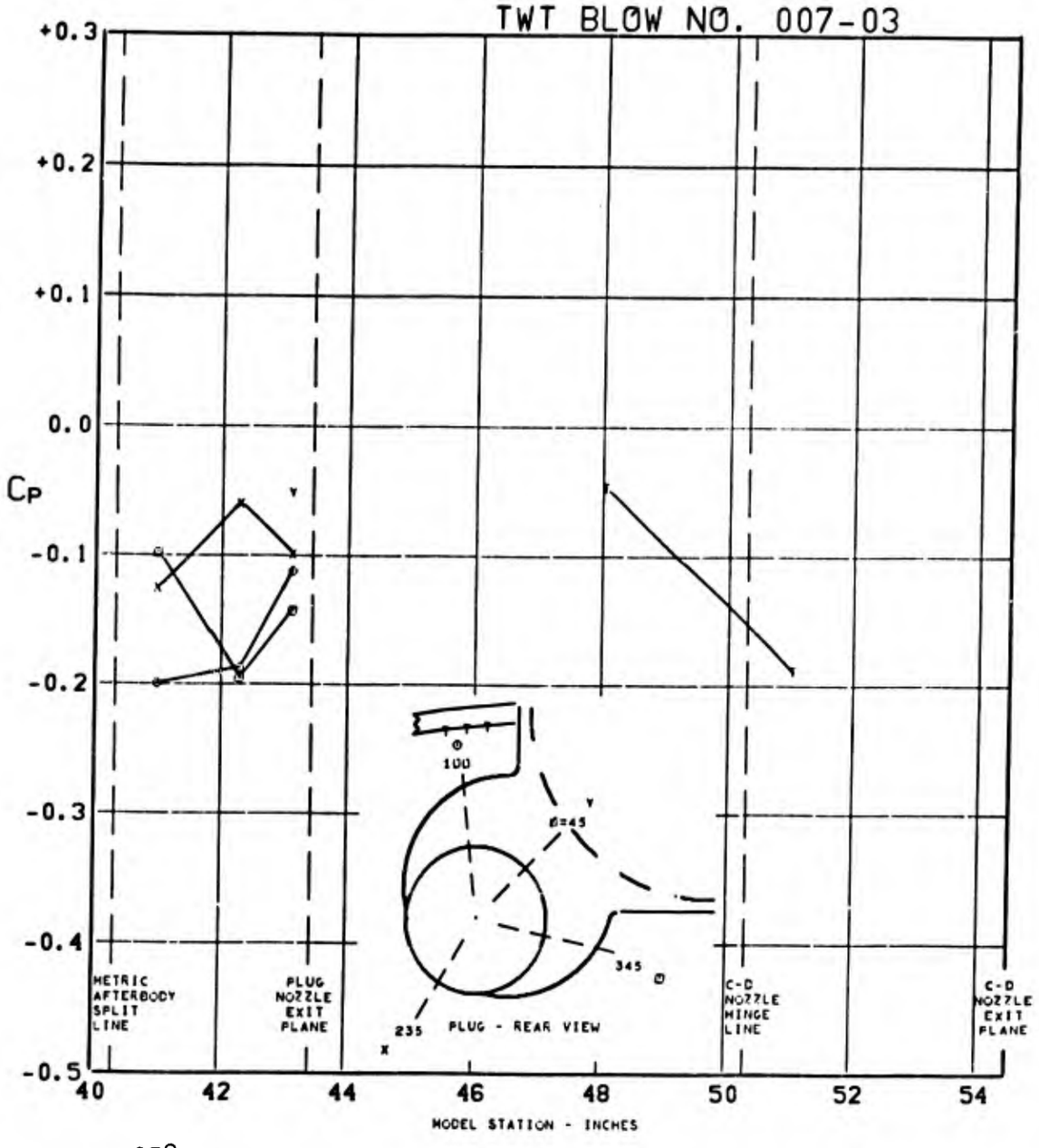

FIGURE 258. PRESSURE COEFFICIENTS ON TAIL & PLUG AFTERBODY (W1B1K1N1 P04 H1V1) Λ_{LE}=70° AT 1.270 M_0, $(P_T/P_0)_{C-D}$=CONE, $(P_T/P_0)_{PLUG}$=4.135, α= 2.9

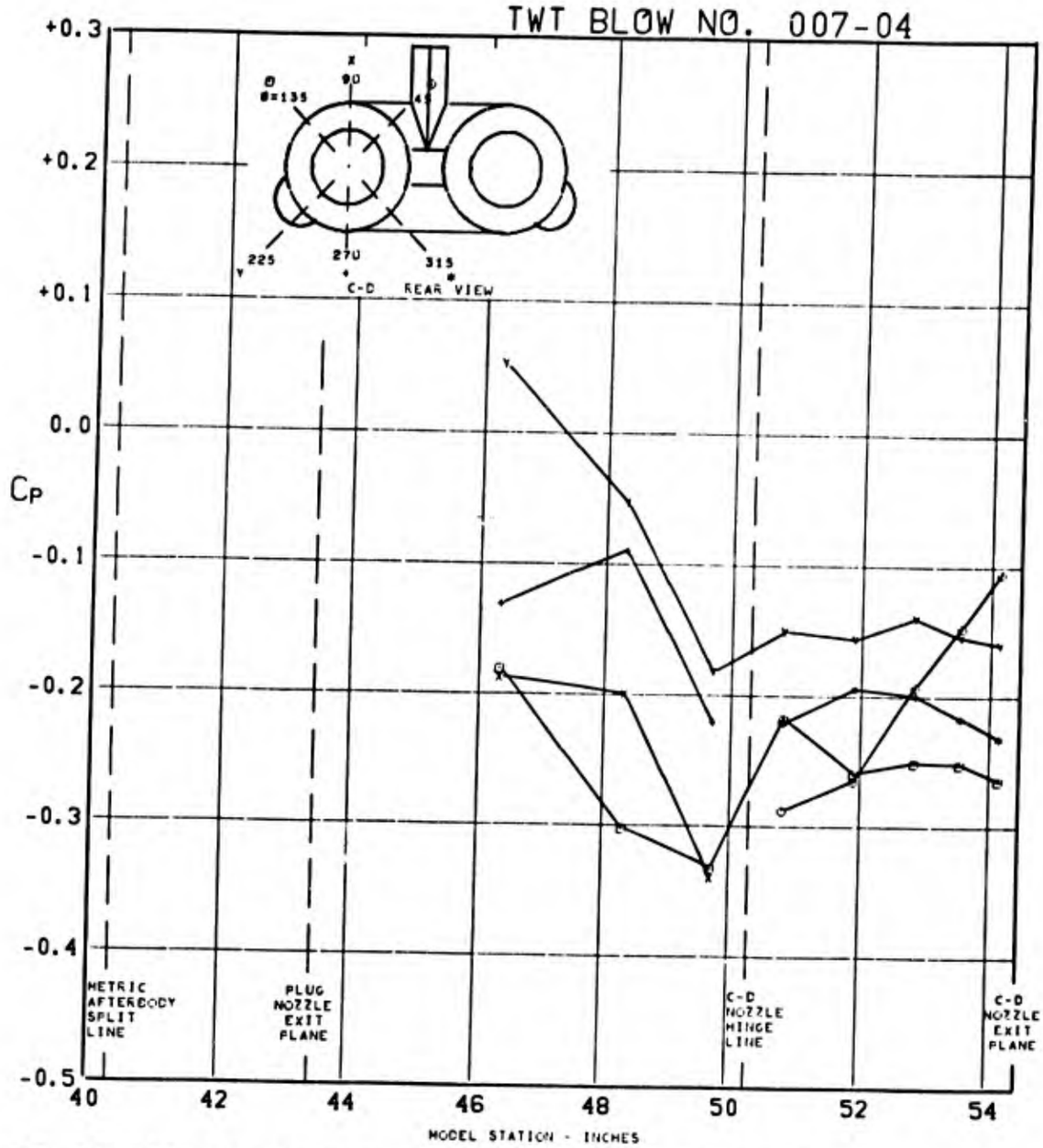

FIGURE 259. PRESSURE COEFFICIENTS ON C-D AFTERBODY (W1B1K1N1 P04 H1V1) $\Lambda_{LE}=70°$ AT 1.269 M_0, $(P_T/P_0)_{C-D}$=CONE, $(P_T/P_0)_{PLUG}=5.203$, $\alpha=2.9$

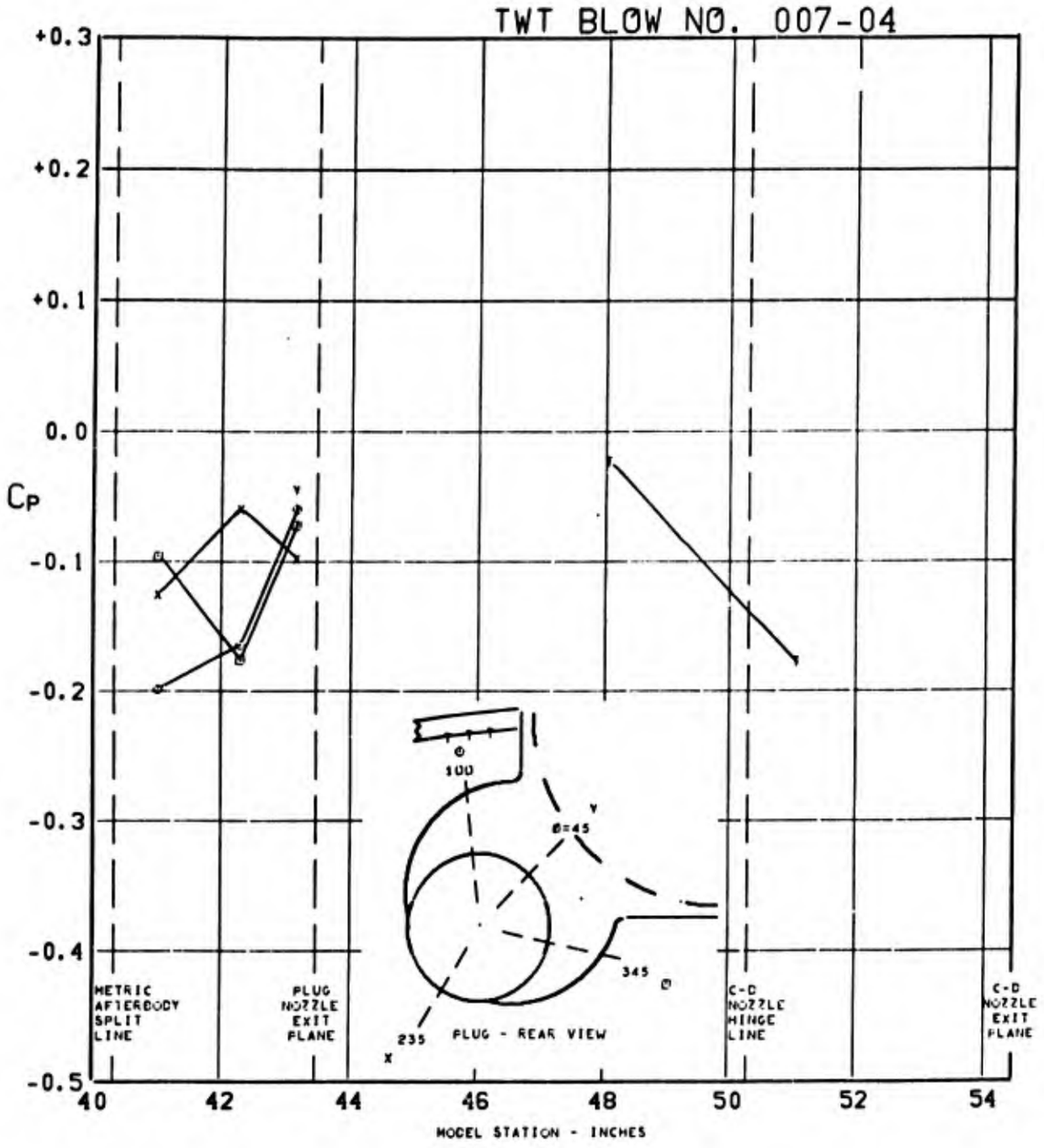

FIGURE 260. PRESSURE COEFFICIENTS ON TAIL & PLUG AFTERBODY (W1B1K1N1 P04 H1V1) $\Lambda_{LE}=70°$ AT 1.269 M_0, $(P_T/P_0)_{C-D}$=CONE, $(P_T/P_0)_{PLUG}$=5.203, α= 2.9

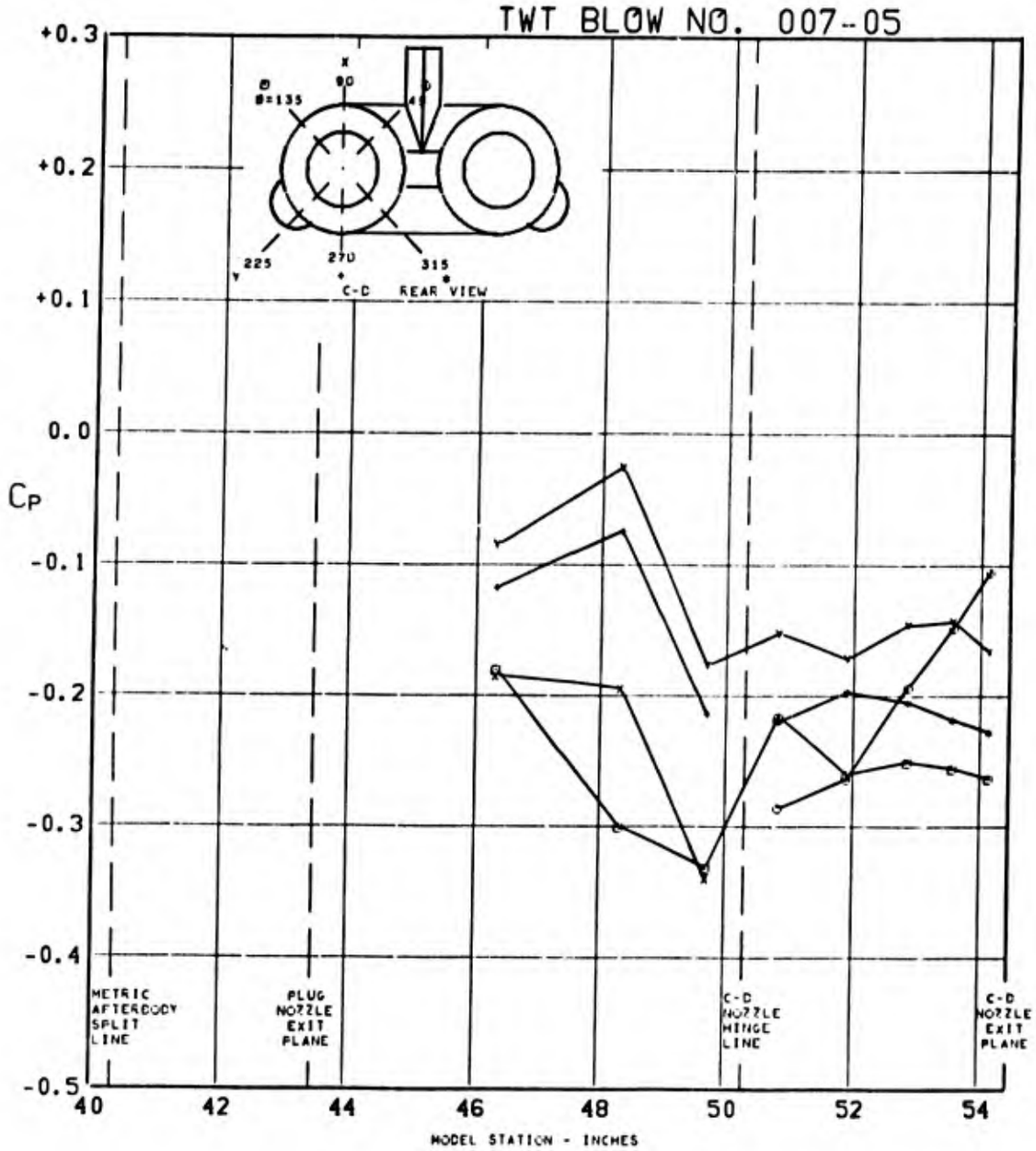

FIGURE 261. PRESSURE COEFFICIENTS ON C-D AFTERBODY (W1B1K1N1 P04 H1V1) $\Lambda_{LE}=70°$ AT 1.269 M_0, $(P_T/P_0)_{C-D}$=CONE, $(P_T/P_0)_{PLUG}$ =6.187, α= 2.9

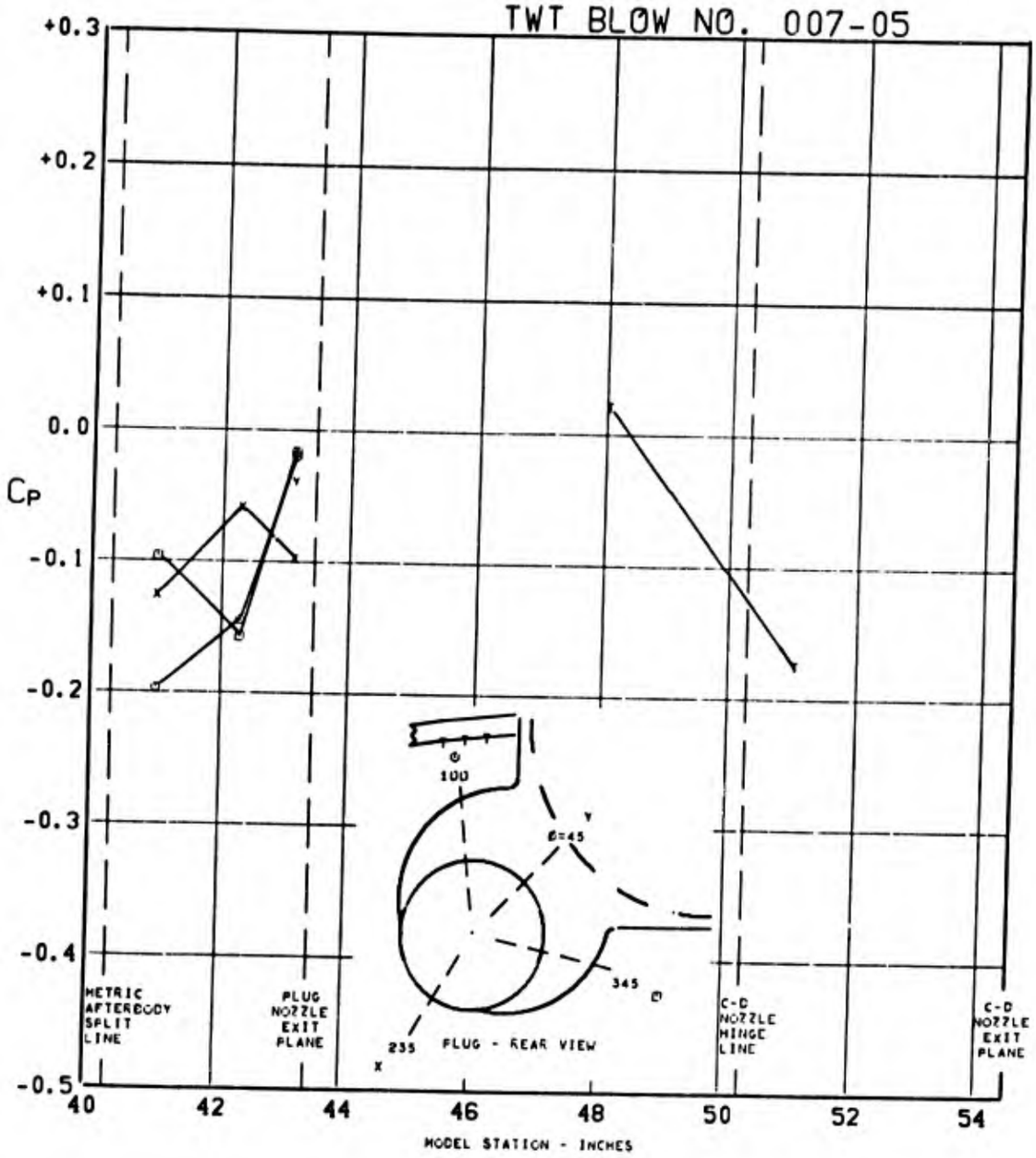

FIGURE 262. PRESSURE COEFFICIENTS ON TAIL & PLUG AFTERBODY (W1B1K1N1 P04 H1V1) $\Lambda_{LE}=70°$ AT 1.269 M_0, $(P_T/P_0)_{C-D}$=CONE, $(P_T/P_0)_{PLUG}$=6.187, α= 2.9

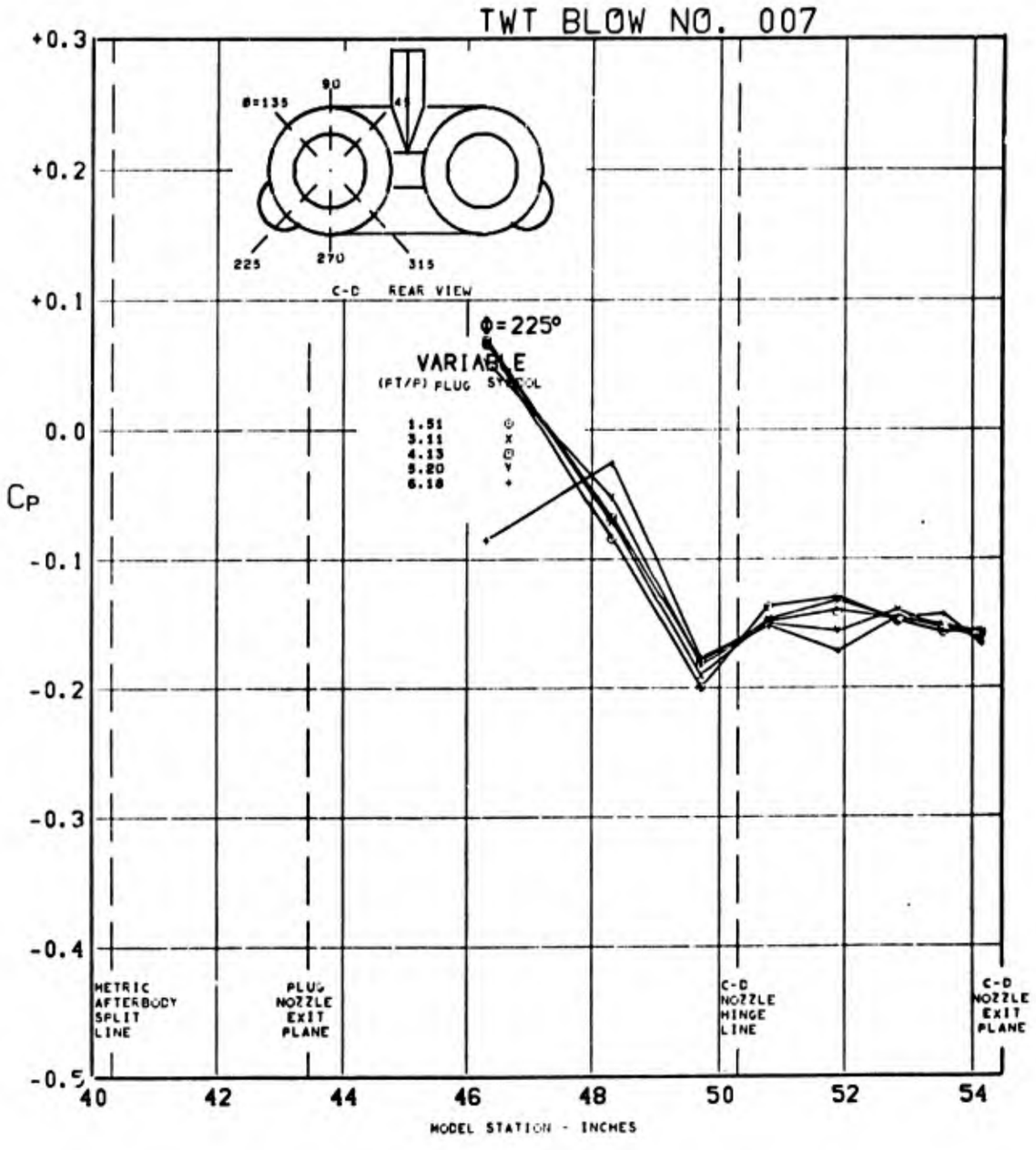

FIGURE 263. PRESSURE COEFFICIENTS ON C-D AFTERBODY (W1B1K1N1 P04 H1V1) Λ_{LE}=70° AT 1.269 M_0, $(P_T/P_0)_{C-D}$=CONE, $(P_T/P_0)_{PLUG}$=VARY, α= 2.9

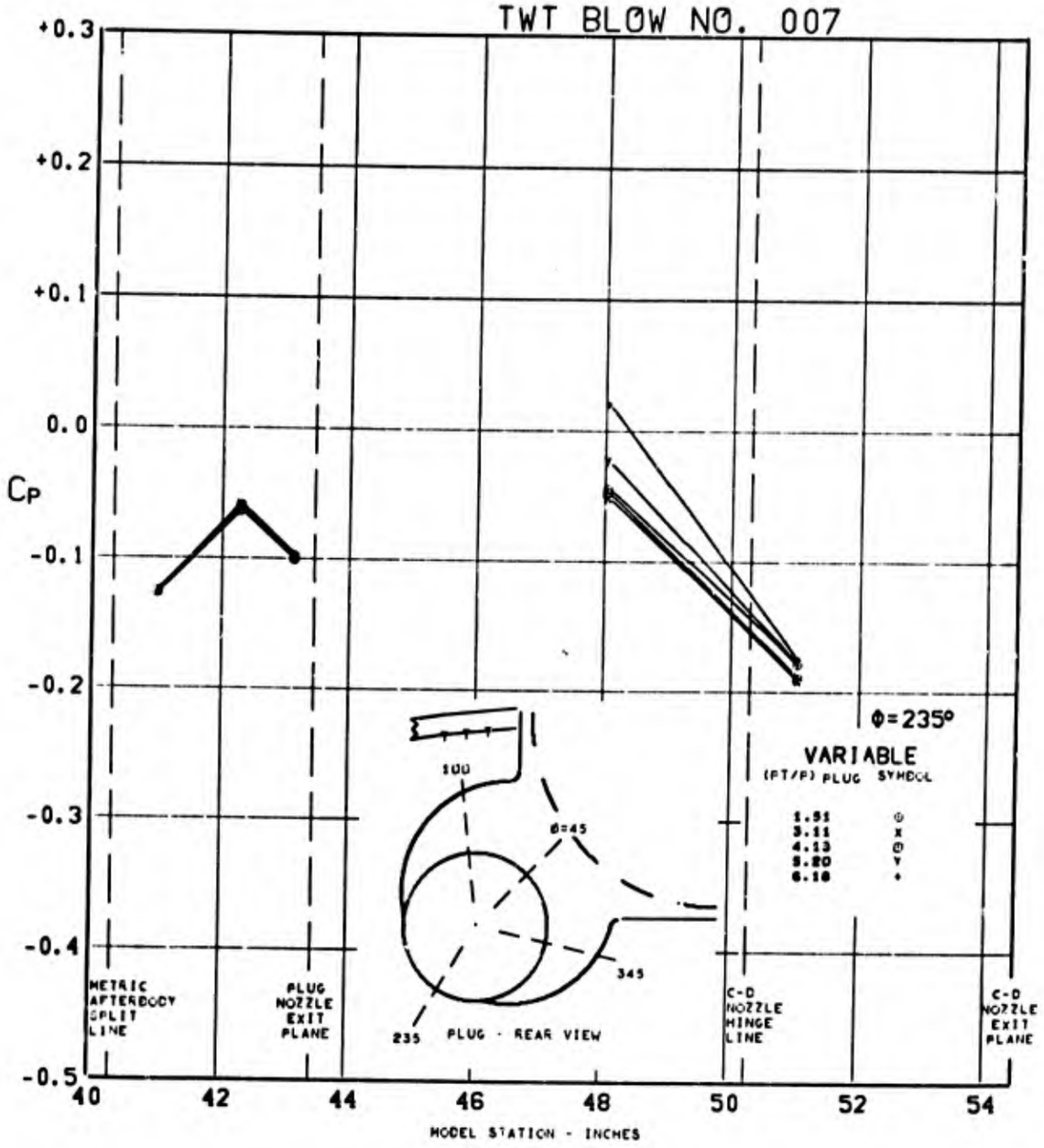

FIGURE 264. PRESSURE COEFFICIENTS ON TAIL & PLUG AFTERBODY (W1B1K1N1 P04 H1V1) Λ_{LE}=70° AT 1.269 M_0, $(P_T/P_0)_{C-D}$=CONE, $(P_T/P_0)_{PLUG}$=VARY, α= 2.9

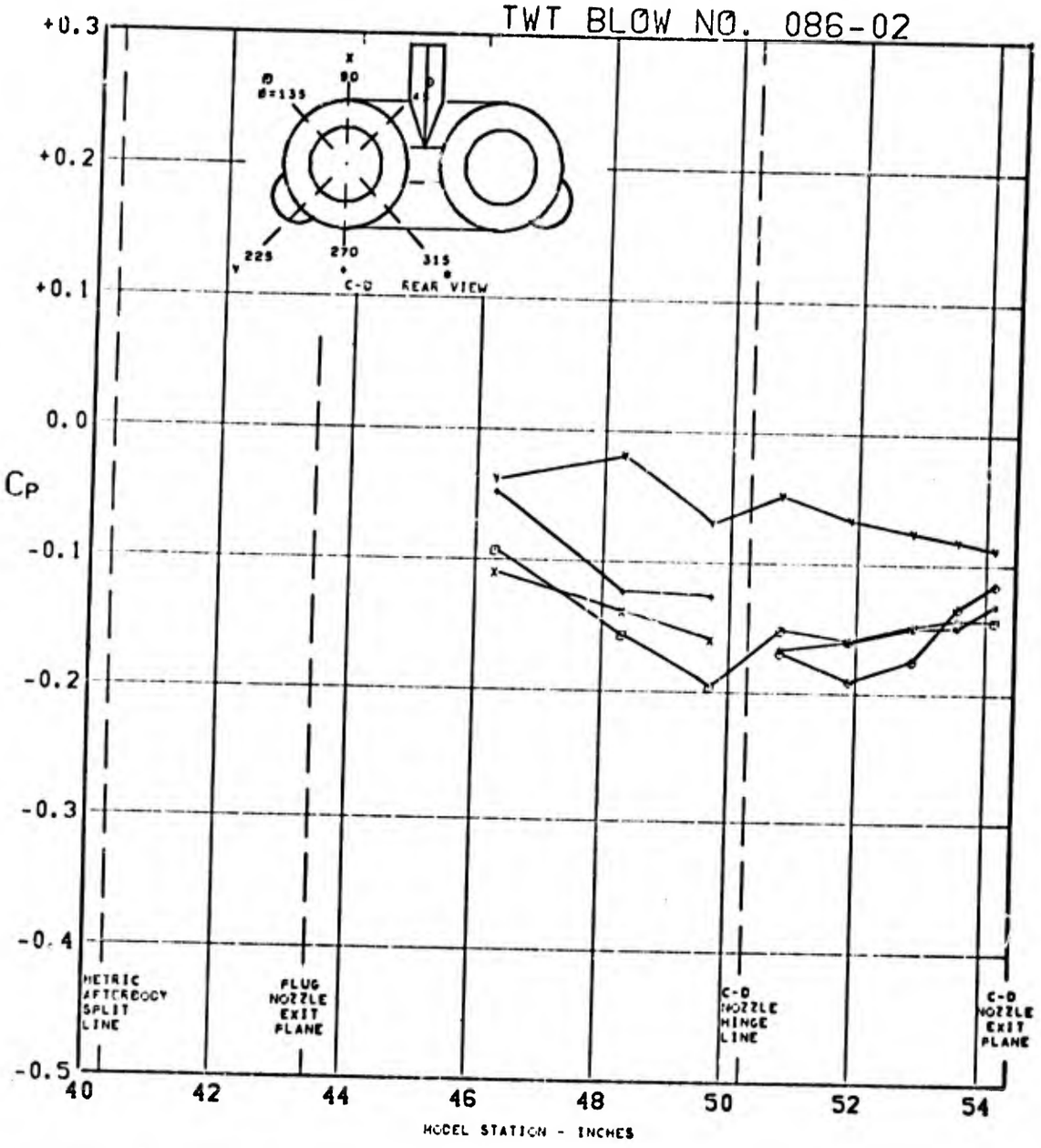

FIGURE 265. PRESSURE COEFFICIENTS ON C-D AFTERBODY (W1B1K1N1 P01 H1V1) Λ_{LE}=70° AT 1.998 M_0, $(P_T/P_0)_{C-D}$=CONE, $(P_T/P_0)_{PLUG}$=CONE, α= 2.8

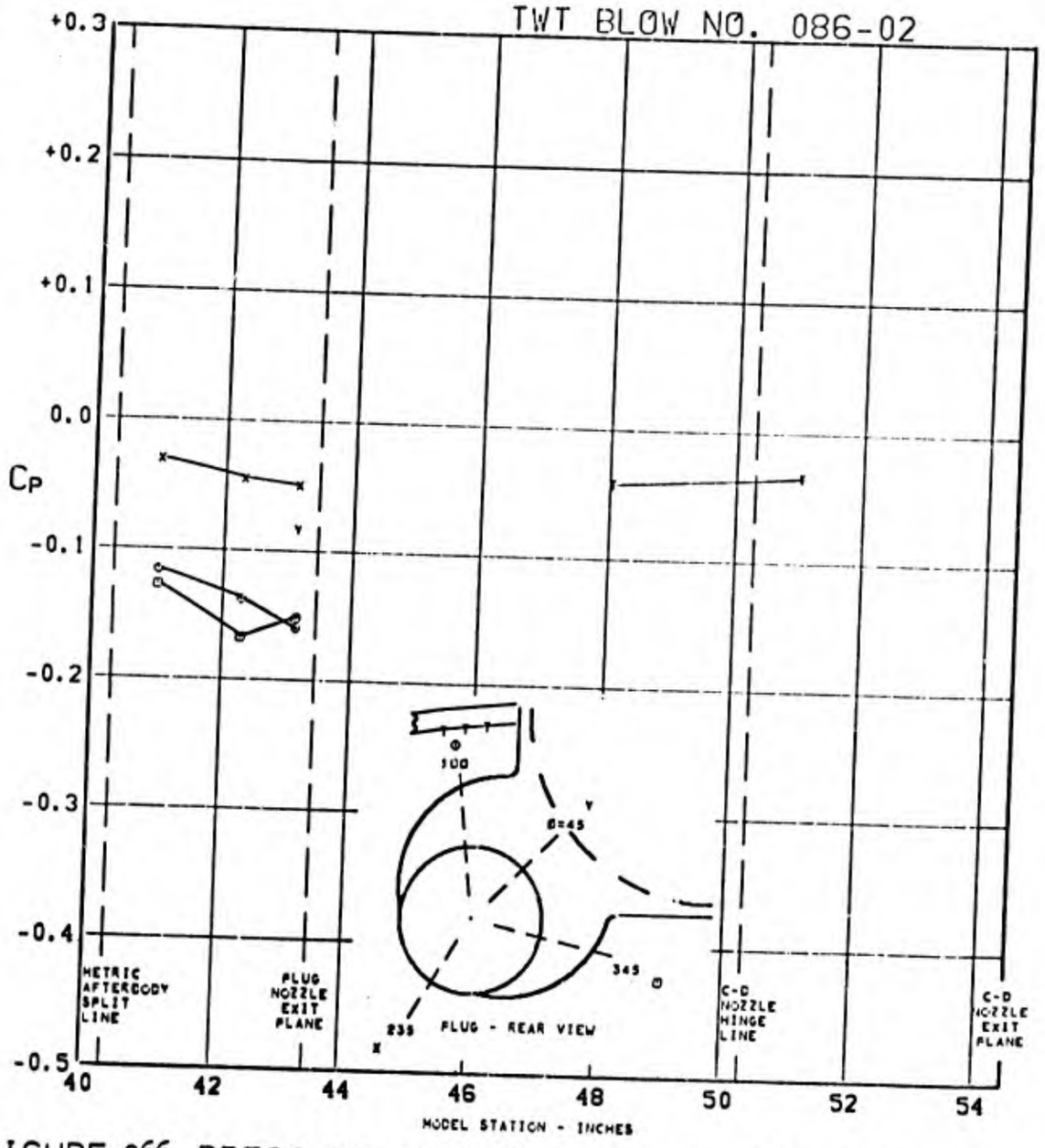

FIGURE 266. PRESSURE COEFFICIENTS ON TAIL & PLUG AFTERBODY (W1B1K1N1 P01 H1V1) $\Lambda_{LE}=70°$ AT 1.998 M_0, $(P_T/P_0)_{C-D}$=CONE, $(P_T/P_0)_{PLUG}$=CONE, α= 2.8

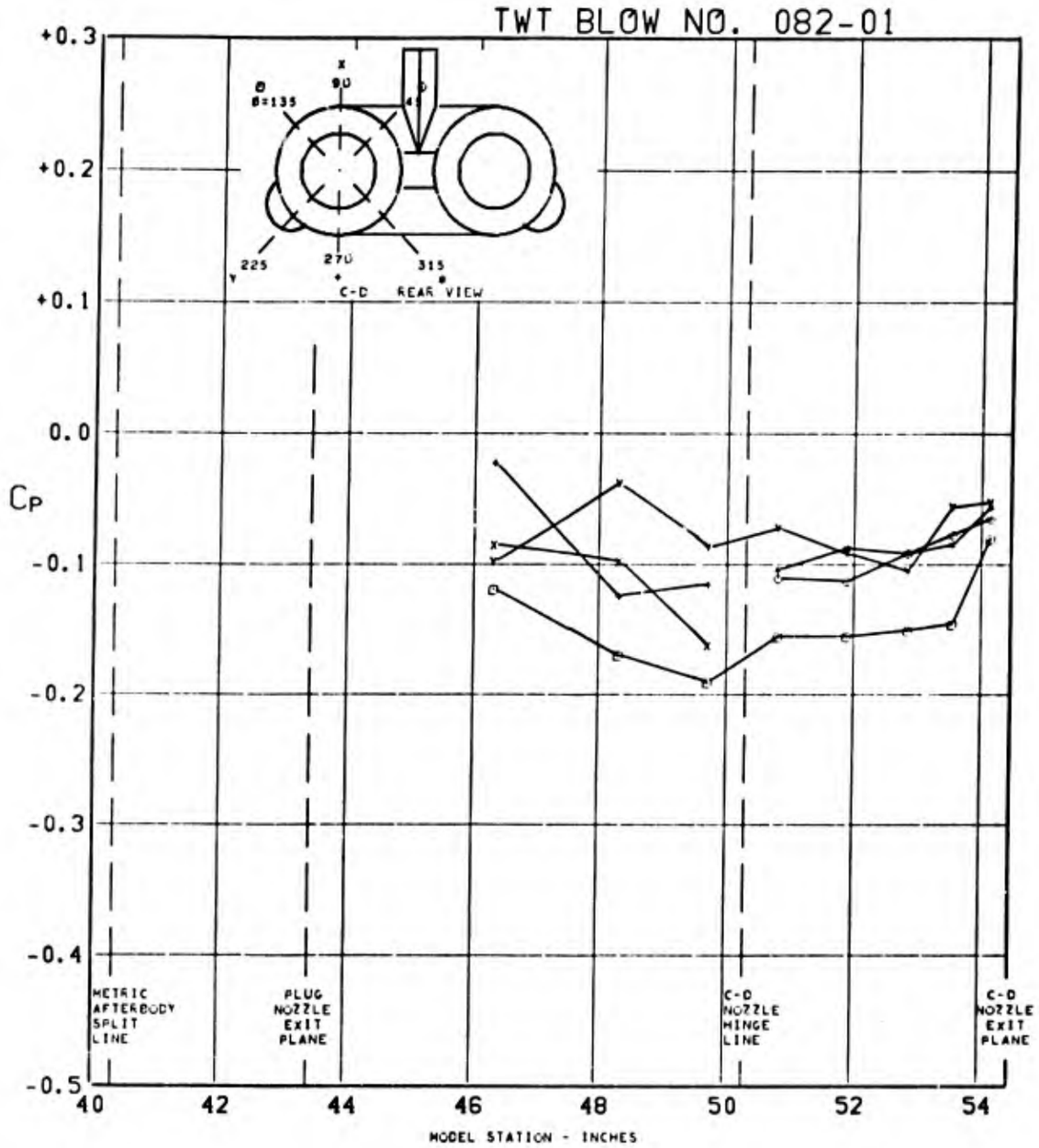

FIGURE 267. PRESSURE COEFFICIENTS ON C-D AFTERBODY (W1B1K1N1 P07 H1V1) $\Lambda_{LE}=70°$ AT 1.998 M_0, $(P_T/P_0)_{C-D}=0.965$, $(P_T/P_0)_{PLUG}=3.306$, $\alpha=2.9$

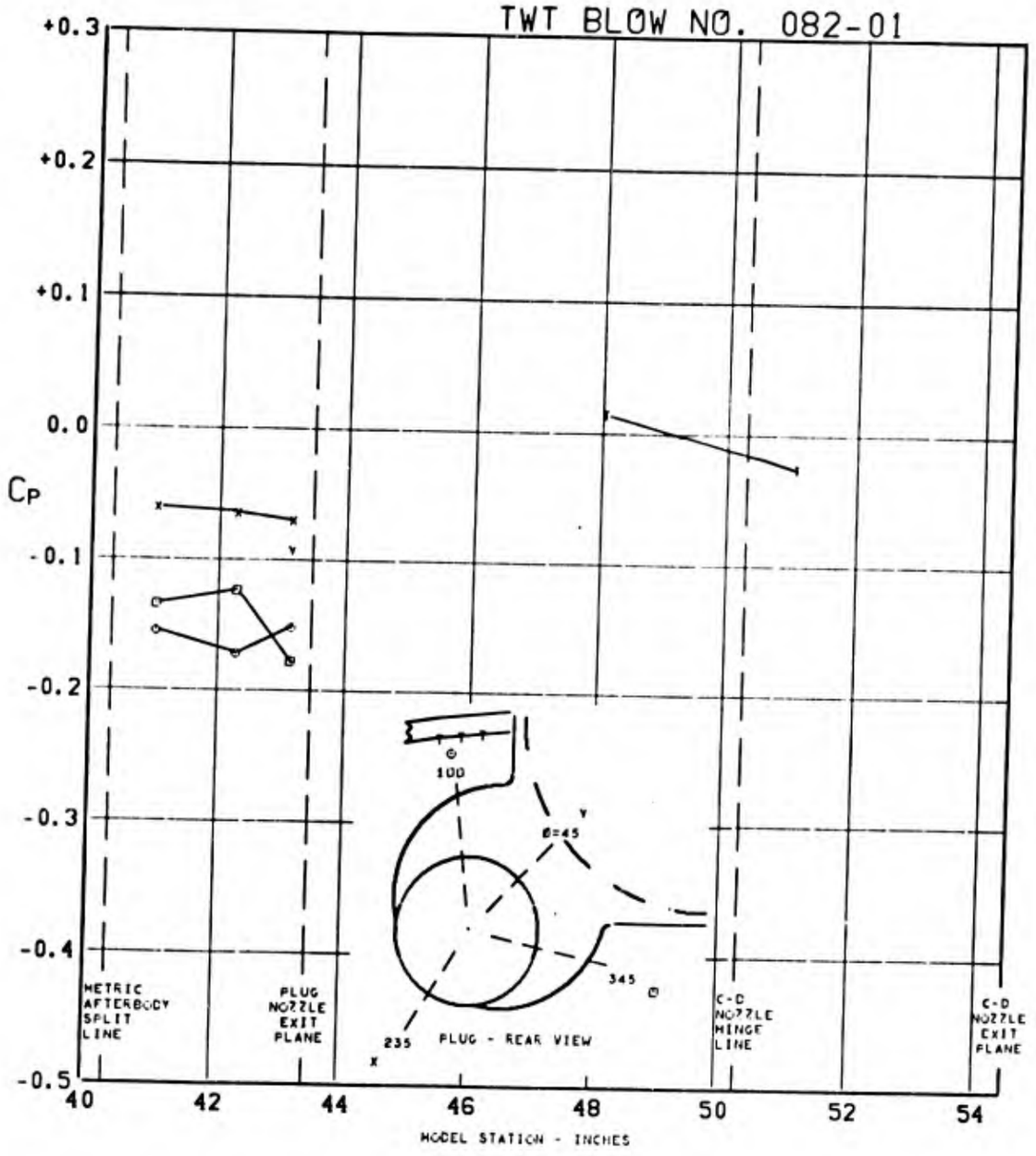

FIGURE 268. PRESSURE COEFFICIENTS ON TAIL & PLUG AFTERBODY (W1B1K1N1 P07 H1V1) $\Lambda_{LE}=70°$ AT 1.998 M_0, $(P_T/P_0)_{C-D}=0.965$, $(P_T/P_0)_{PLUG}=3.306$, $\alpha=2.9$

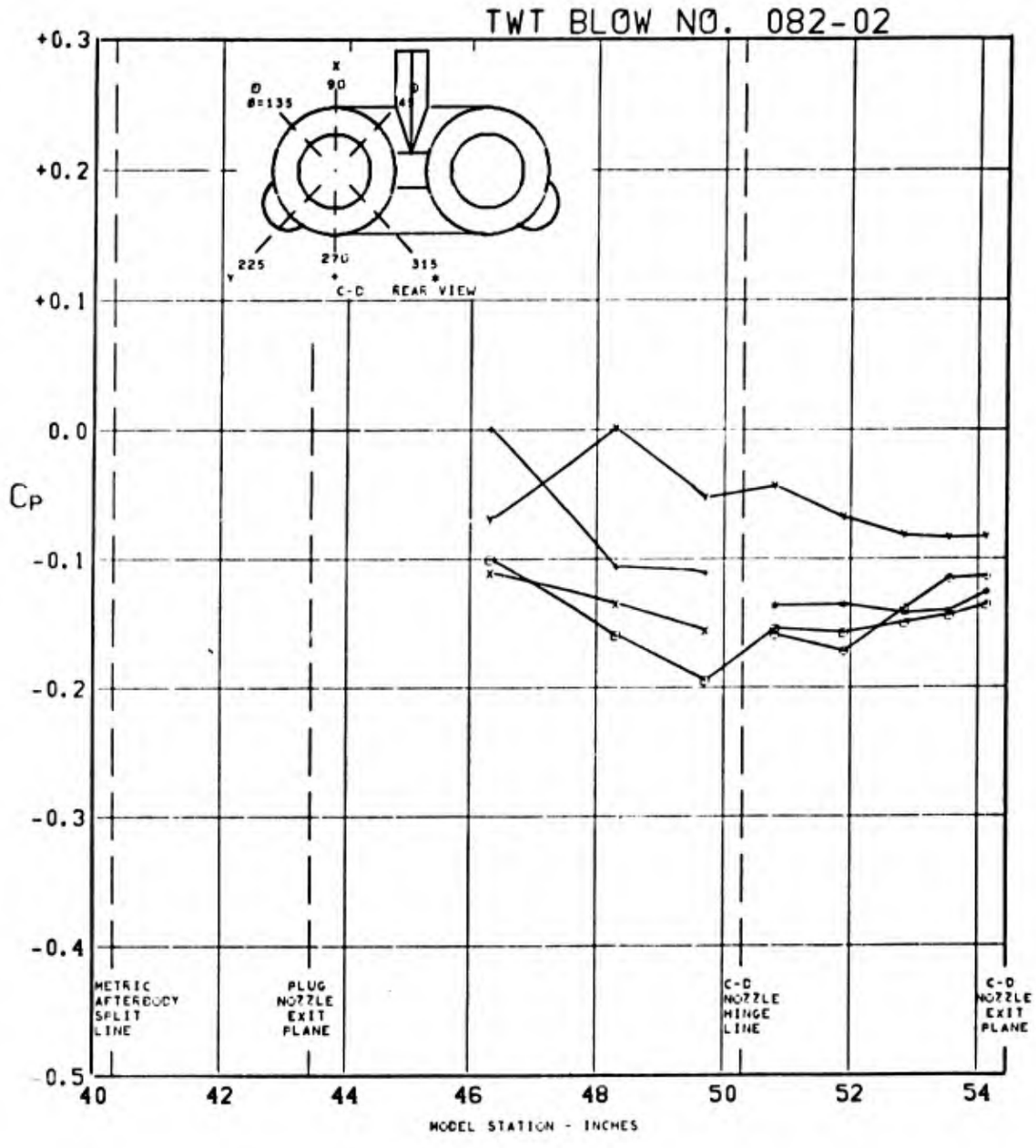

FIGURE 269. PRESSURE COEFFICIENTS ON C-D AFTERBODY (W1B1K1N1 P07 H1V1) $\Lambda_{LE}=70°$ AT 1.998 M_0, $(P_T/P_0)_{C-D}=0.741$, $(P_T/P_0)_{PLUG}=4.792$, $\alpha=2.9$

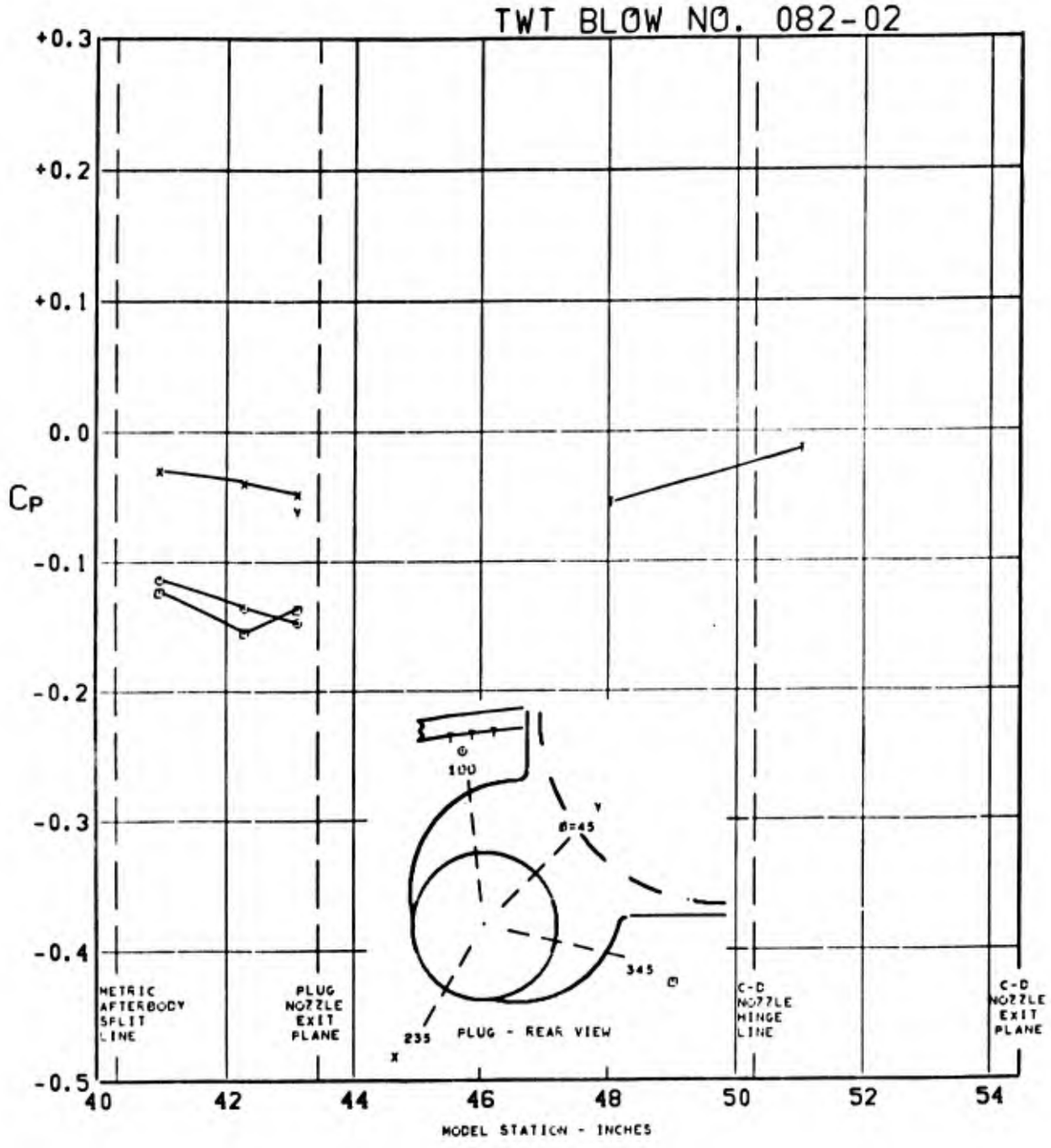

FIGURE 270. PRESSURE COEFFICIENTS ON TAIL & PLUG AFTERBODY (W1B1K1N1 P07 H1V1) Λ_{LE}=70° AT 1.998 M_0, $(P_T/P_0)_{C-D}$=0.741, $(P_T/P_0)_{PLUG}$=4.792, α= 2.9

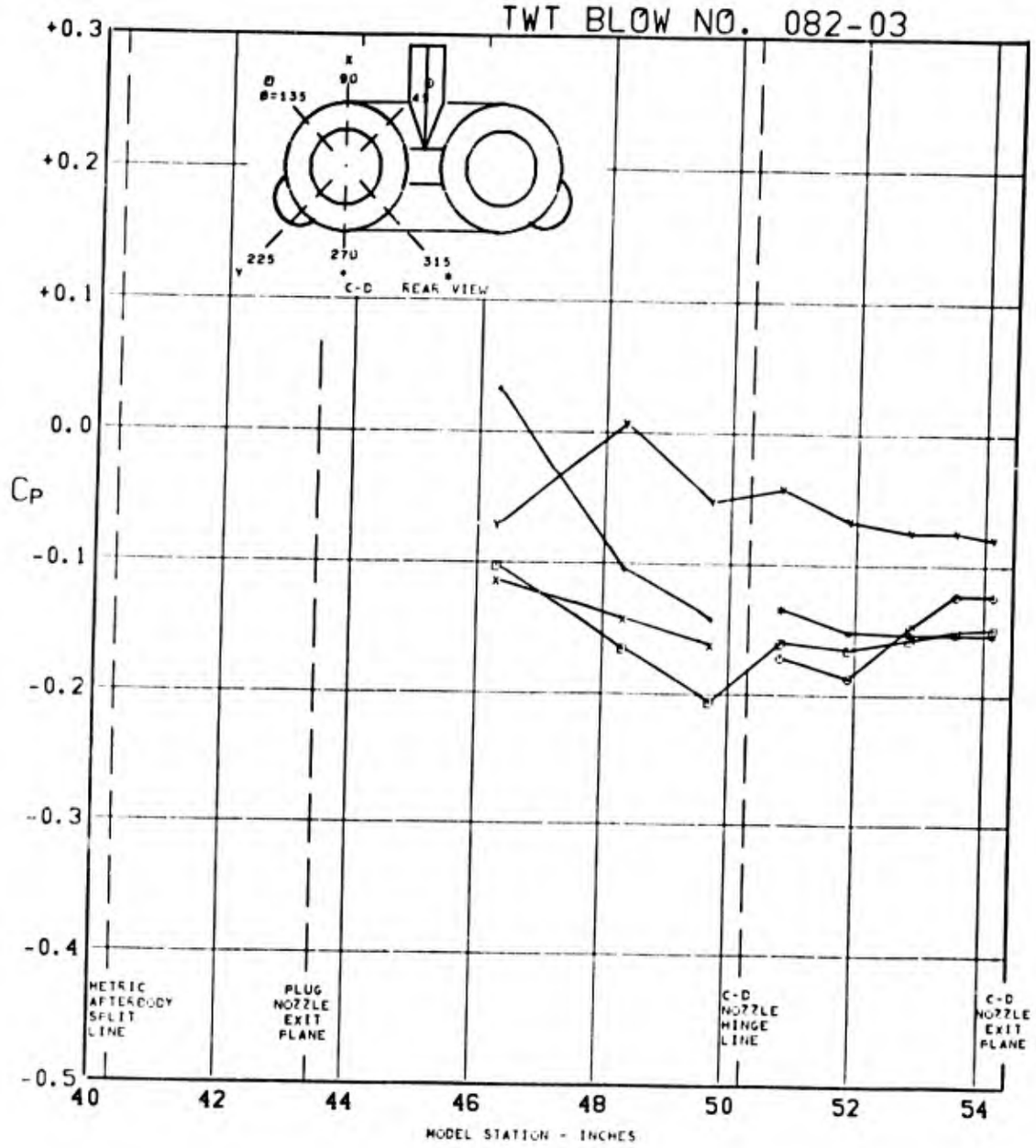

FIGURE 271. PRESSURE COEFFICIENTS ON C-D AFTERBODY (W1B1K1N1 P07 H1V1) $\Lambda_{LE}=70°$ AT 1.998 M_0, $(P_T/P_0)_{C-D}=0.678$, $(P_T/P_0)_{PLUG}=7.043$, $\alpha=2.9$

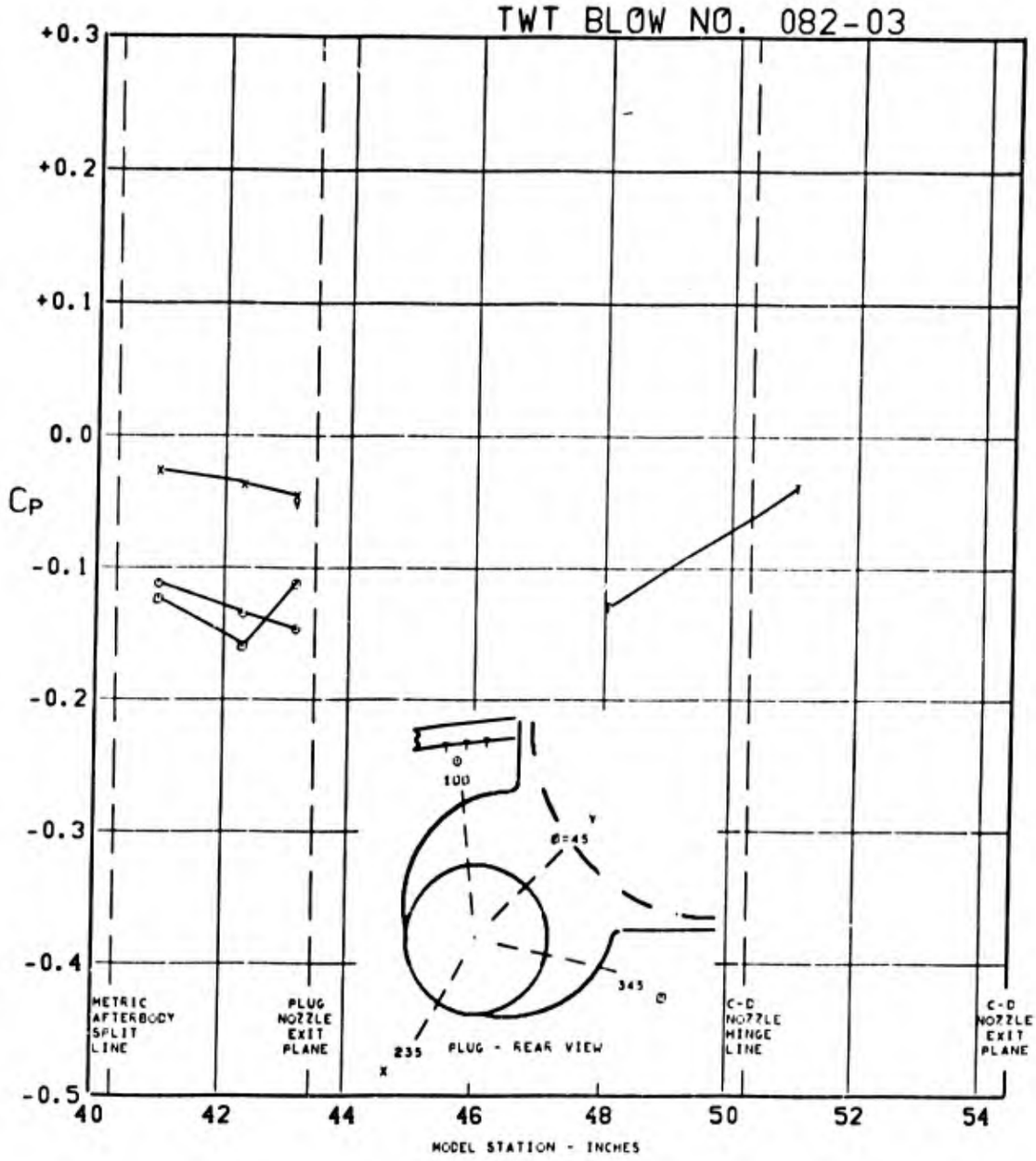

FIGURE 272. PRESSURE COEFFICIENTS ON TAIL & PLUG AFTERBODY (W1B1K1N1 P07 H1V1) $\Lambda_{LE}=70°$ AT 1.998 M_0, $(P_T/P_0)_{C-D}=0.678$, $(P_T/P_0)_{PLUG}=7.043$, $\alpha=2.9$

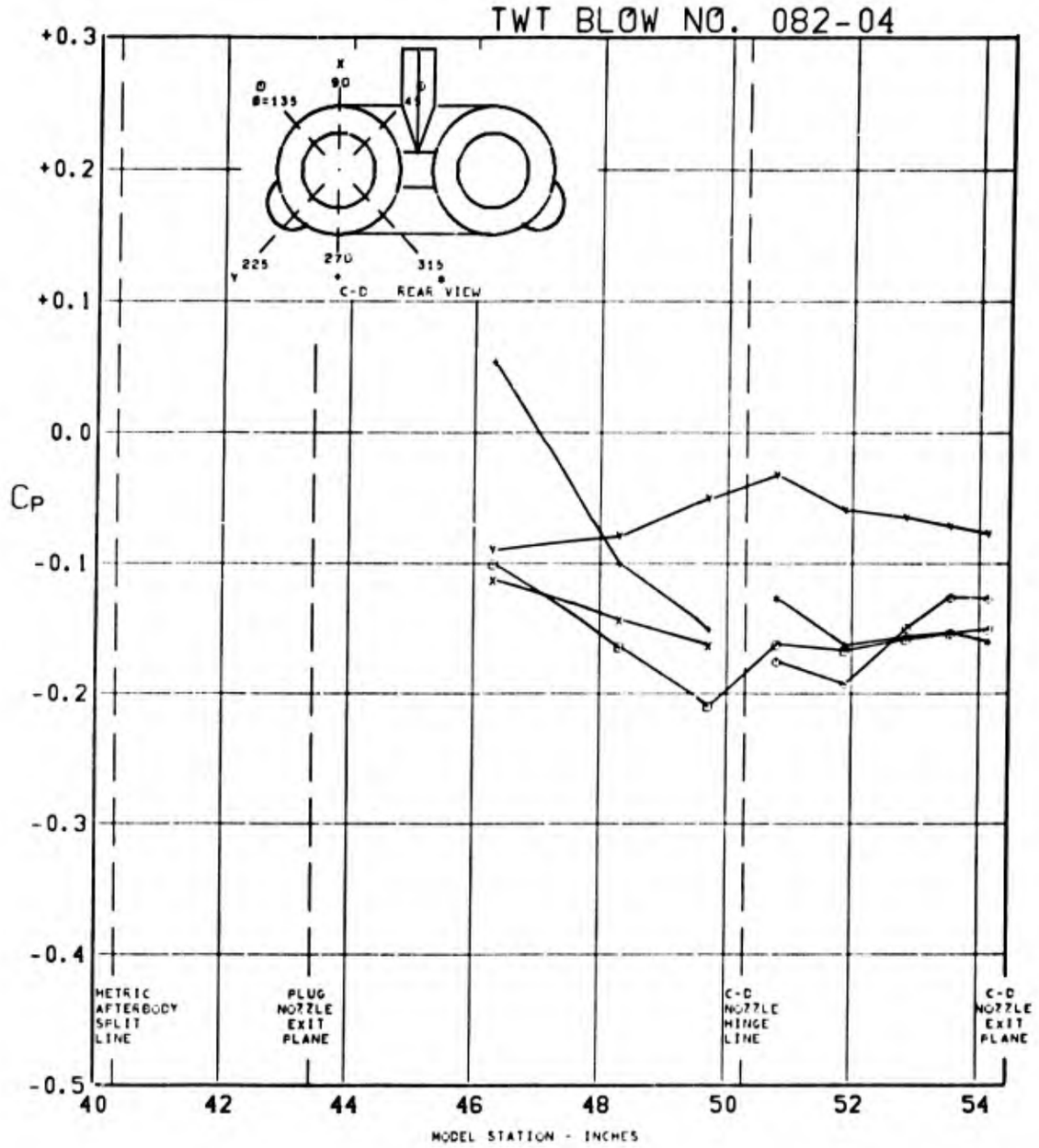

FIGURE 273. PRESSURE COEFFICIENTS ON C-D AFTERBODY (W1B1K1N1 P07 H1V1) $\Lambda_{LE}=70°$ AT 1.998 M_0, $(P_T/P_0)_{C-D}=0.658$, $(P_T/P_0)_{PLUG}=10.10$, $\alpha=2.9$

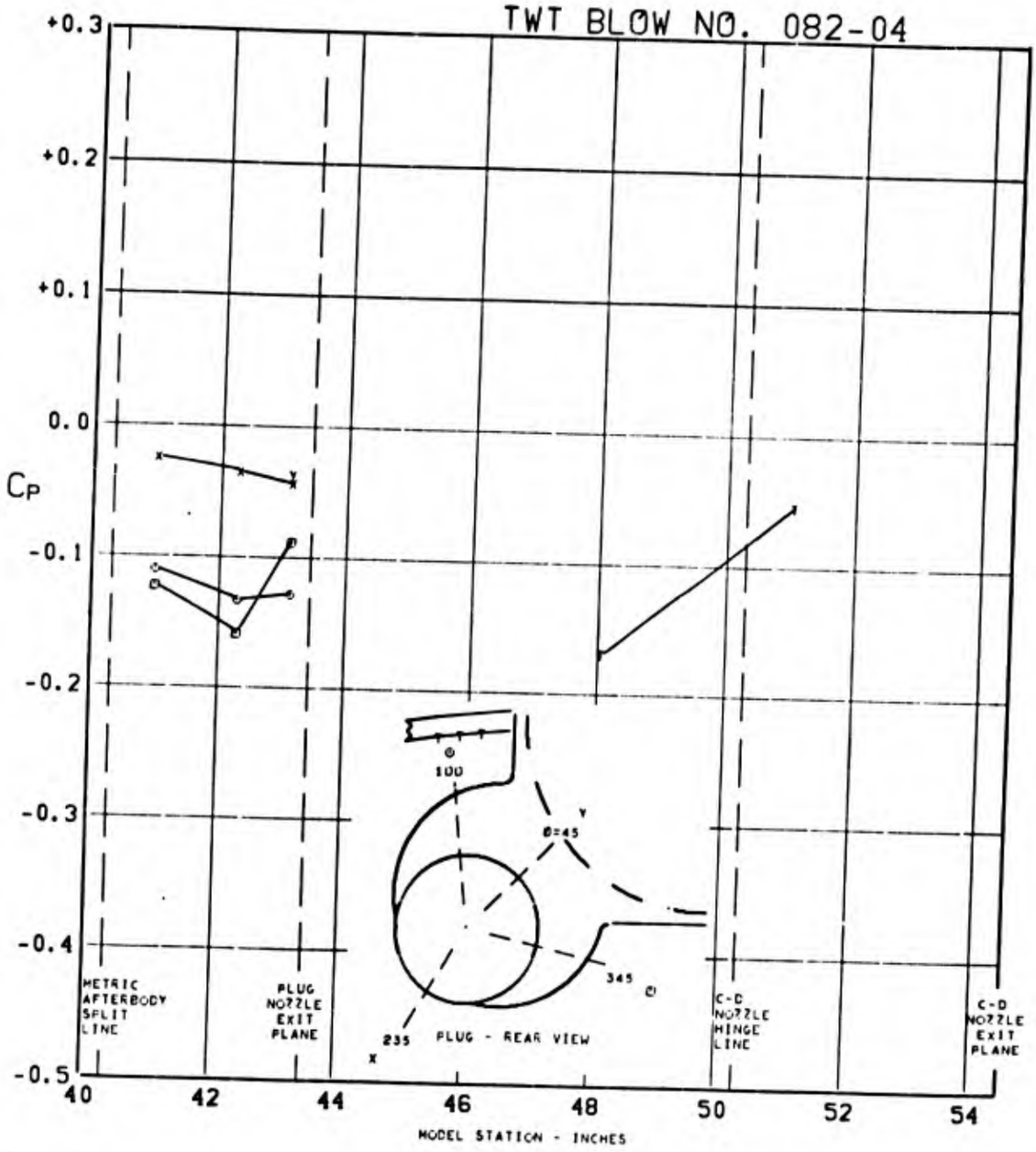

FIGURE 274. PRESSURE COEFFICIENTS ON TAIL & PLUG AFTERBODY (W1B1K1N1 P07 H1V1) $\Lambda_{LE}=70°$ AT 1.998 M_0, $(P_T/P_0)_{C-D}=0.658$, $(P_T/P_0)_{PLUG}=10.10$, $\alpha=2.9$

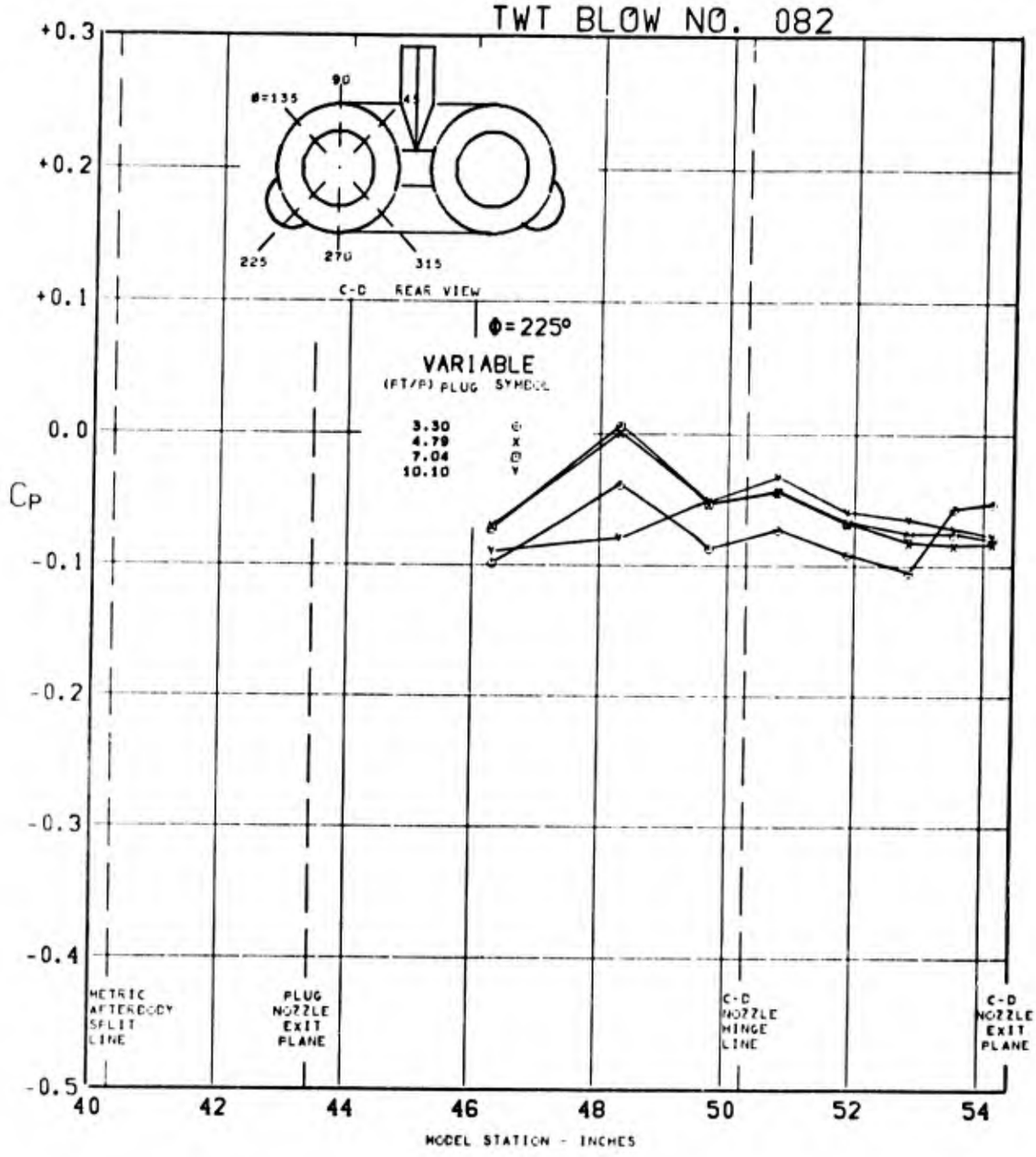

FIGURE 275. PRESSURE COEFFICIENTS ON C-D AFTERBODY (W1B1K1N1 P07 H1V1) $\Lambda_{LE}=70°$ AT 1.998 M_0, $(P_T/P_0)_{C-D}=0.658$, $(P_T/P_0)_{PLUG}$ = VARY, $\alpha=$ 2.9

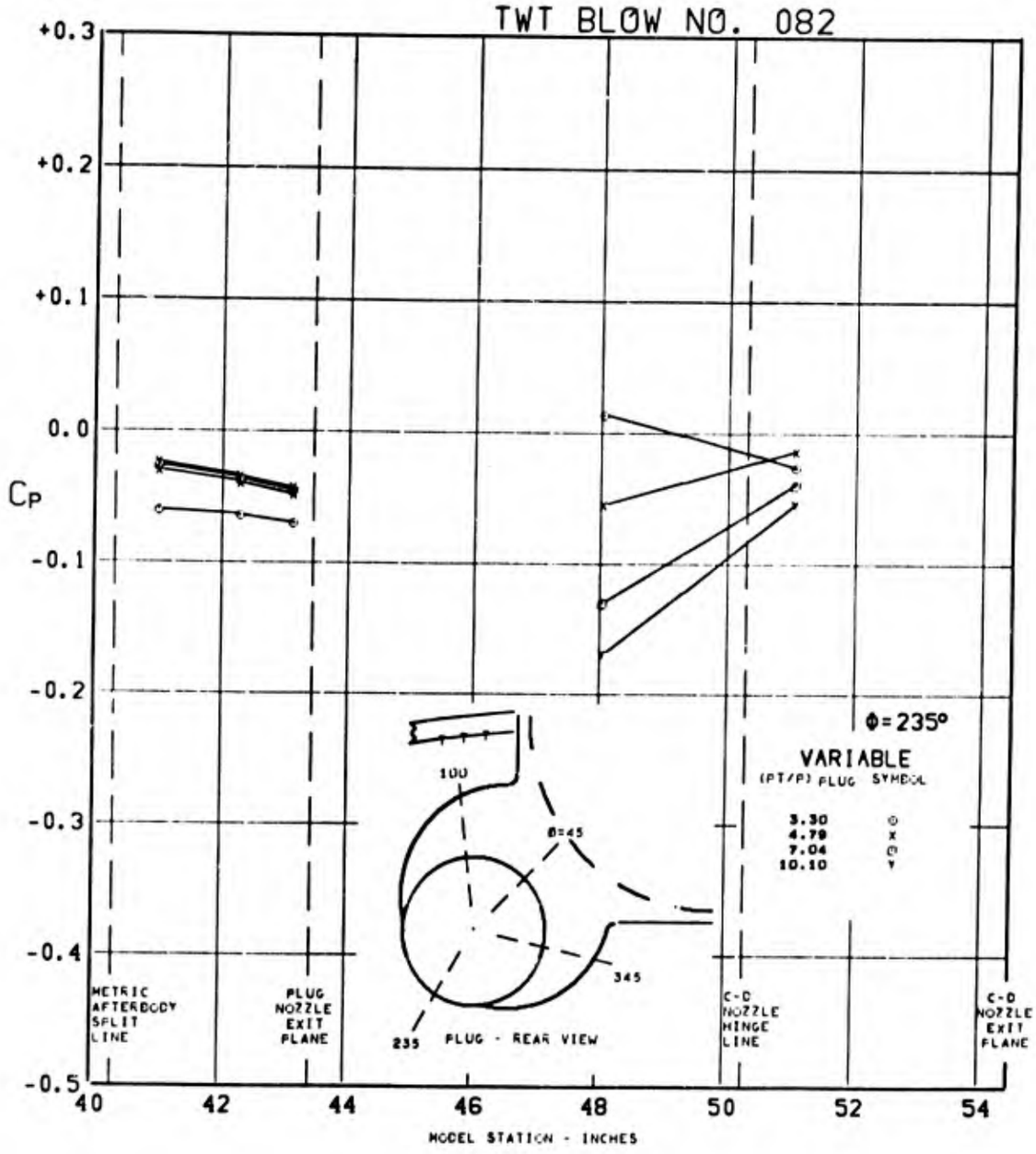

FIGURE 276. PRESSURE COEFFICIENTS ON TAIL & PLUG AFTERBODY (W1B1K1N1 P07 H1V1) $\Lambda_{LE}=70°$ AT 1.998 M_0, $(P_T/P_0)_{C-D}=0.658$, $(P_T/P_0)_{PLUG}$ =VARY, $\alpha=$ 2.9

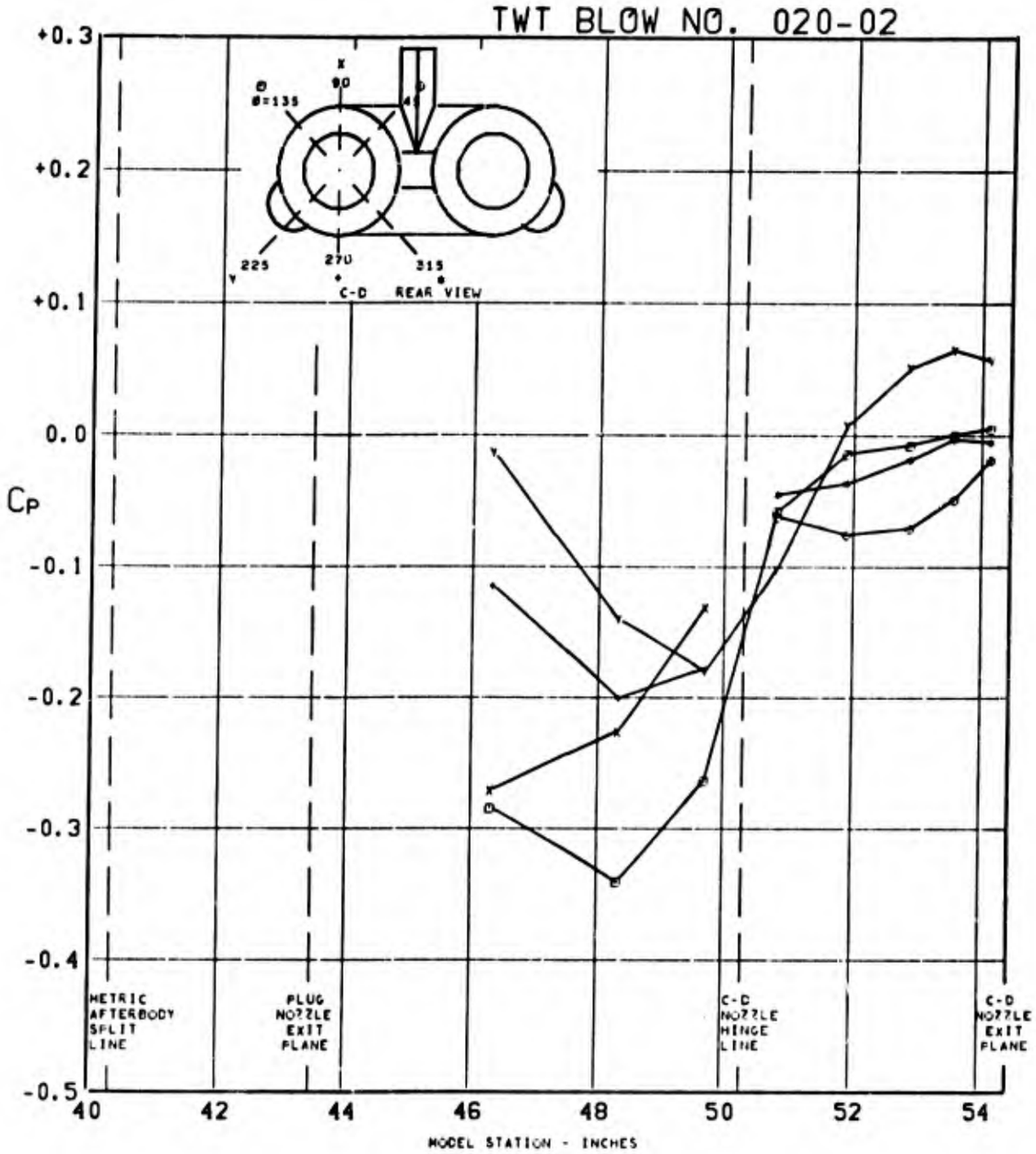

FIGURE 277. PRESSURE COEFFICIENTS ON C-D AFTERBODY (W1B1K1N1 P03 H1V1) $\Lambda_{LE}=70°$ AT 0.847 M_0, $(P_T/P_0)_{C-D}$=CONE, $(P_T/P_0)_{PLUG}$=CONE, α= 2.8

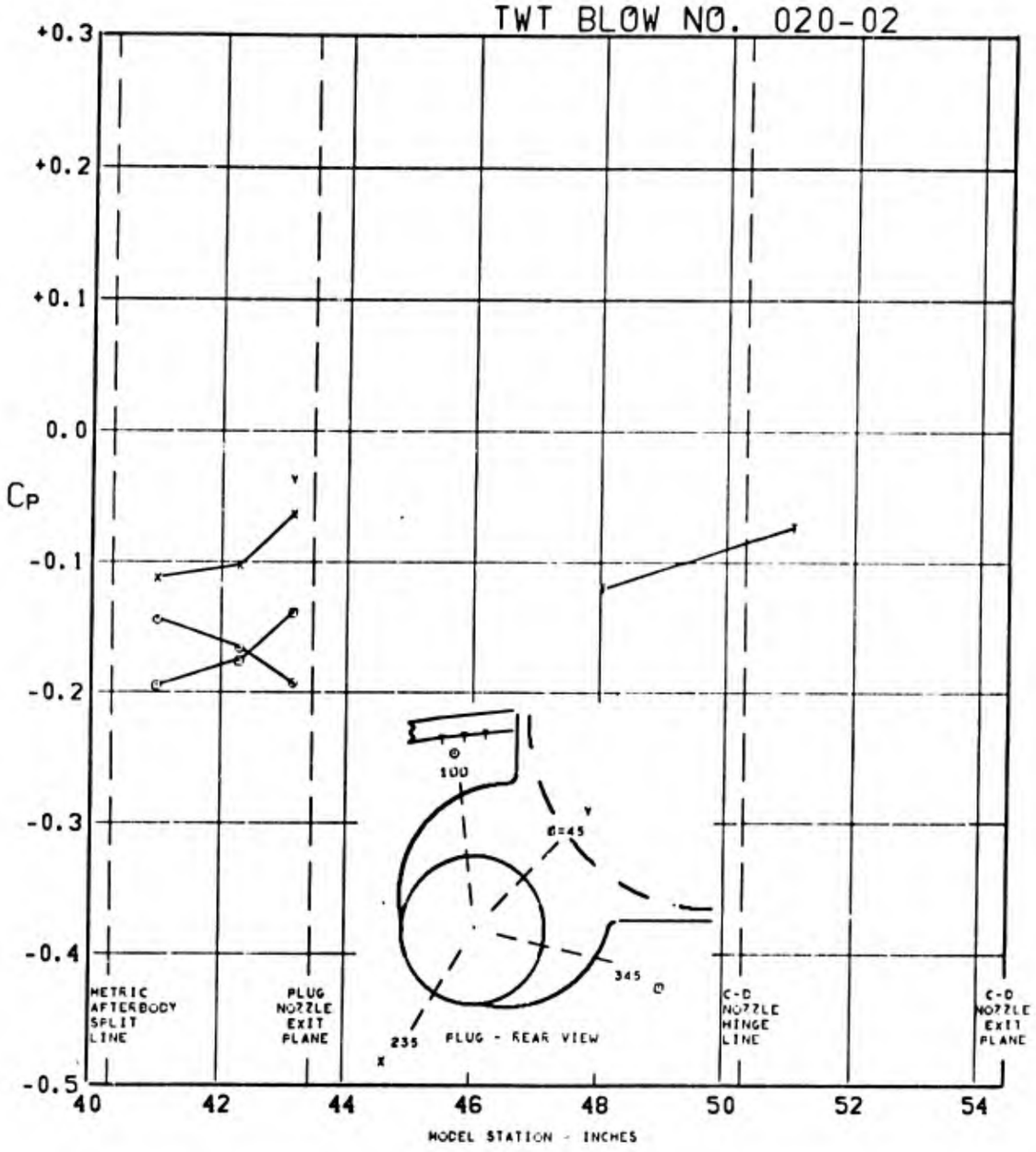

FIGURE 278. PRESSURE COEFFICIENTS ON TAIL & PLUG AFTERBODY (W1B1K1N1 P03 H1V1) $\Lambda_{LE}=70°$ AT 0.847 M_0, $(P_T/P_0)_{C-D}$=CONE, $(P_T/P_0)_{PLUG}$=CONE, α= 2.8

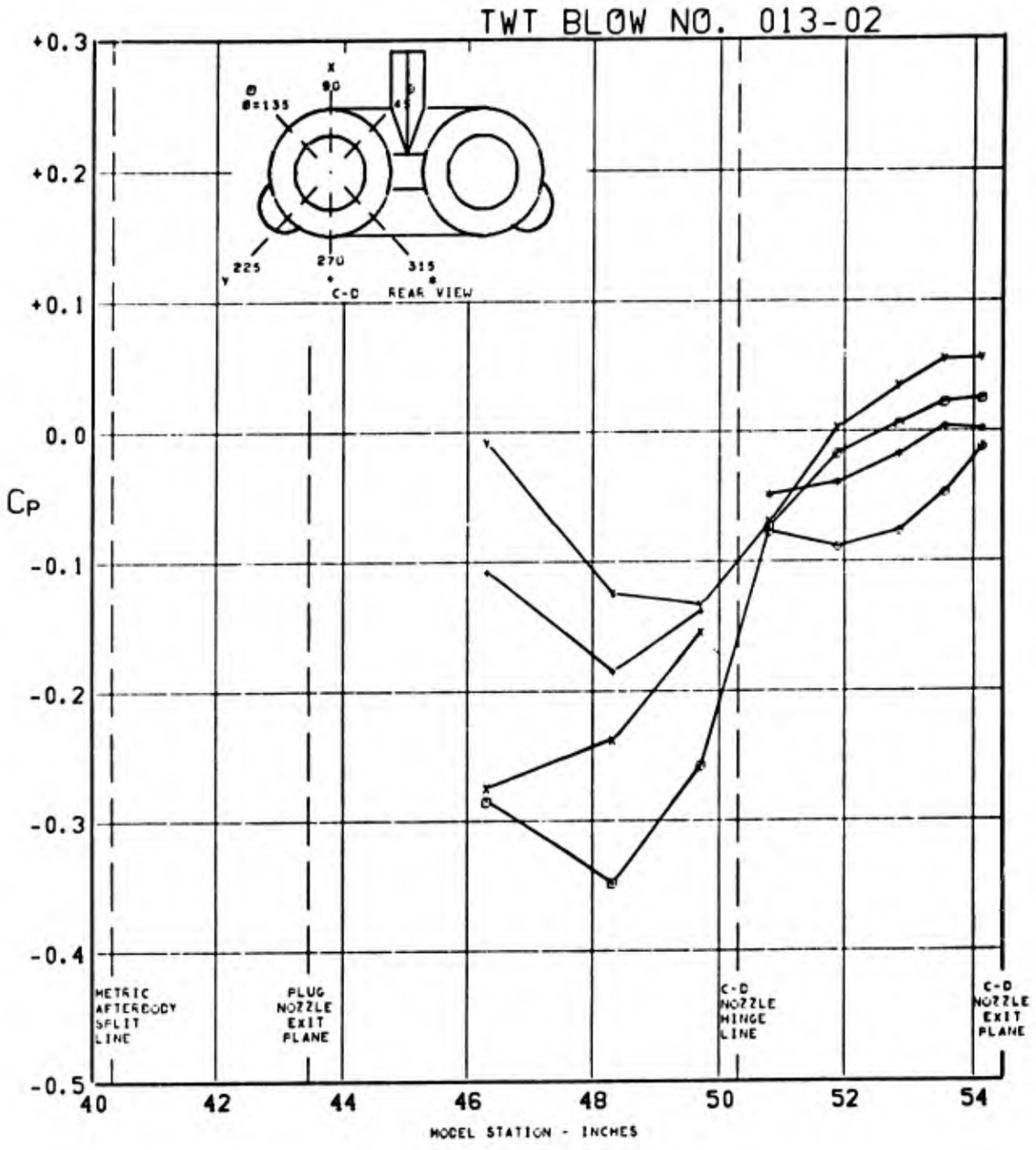

FIGURE 279. PRESSURE COEFFICIENTS ON C-D AFTERBODY (W1B1K1N1 P02 H1V1) Λ_{LE}=70° AT 0.850 M_0, $(P_T/P_0)_{C-D}$=CONE, $(P_T/P_0)_{PLUG}$=CONE, α= 2.7

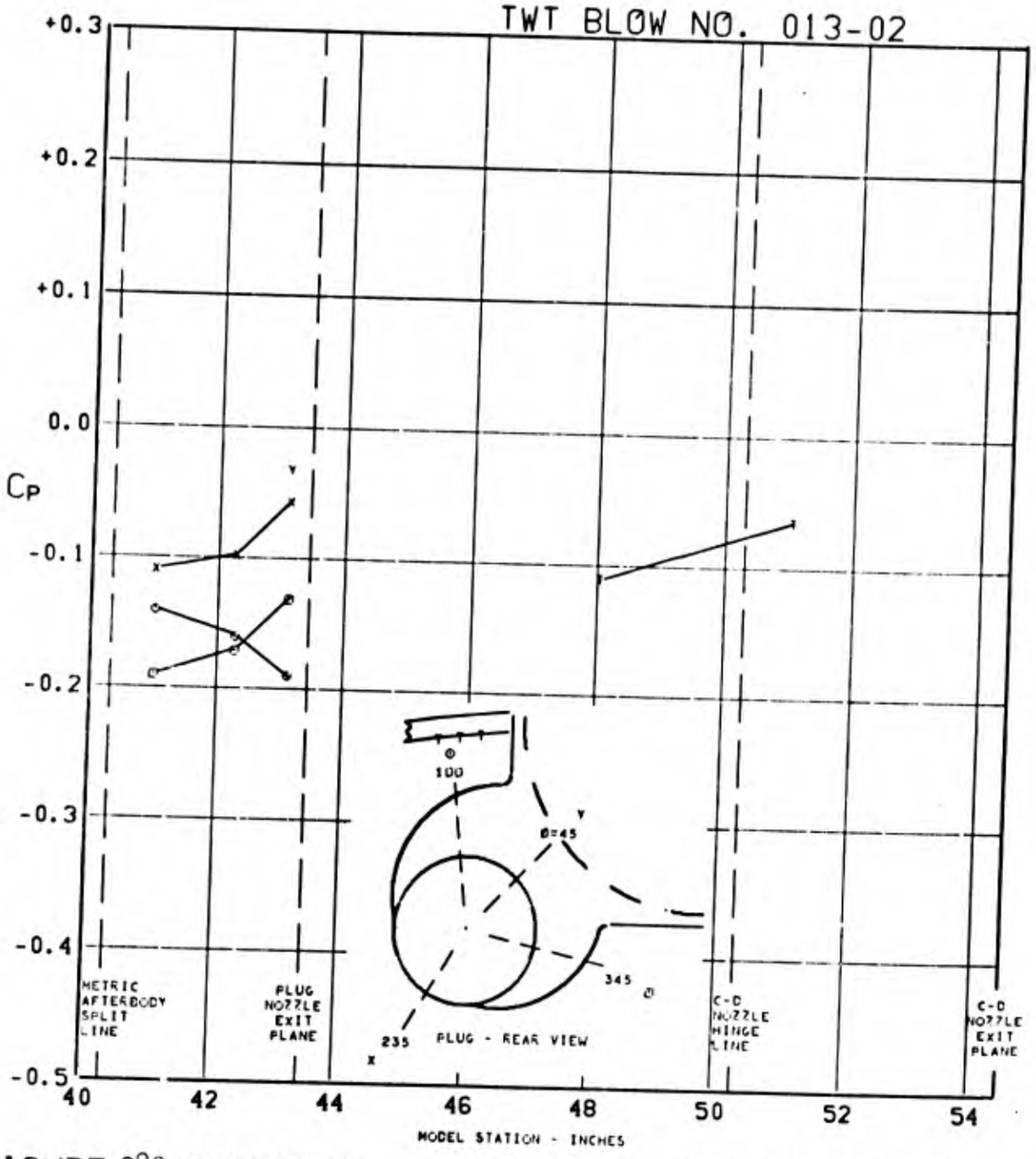

FIGURE 280. PRESSURE COEFFICIENTS ON TAIL & PLUG AFTERBODY (W1B1K1N1 P02 H1V1) $\Lambda_{LE}=70°$ AT 0.850 M_0, $(P_T/P_0)_{C-D}$=CONE, $(P_T/P_0)_{PLUG}$=CONE, α= 2.7

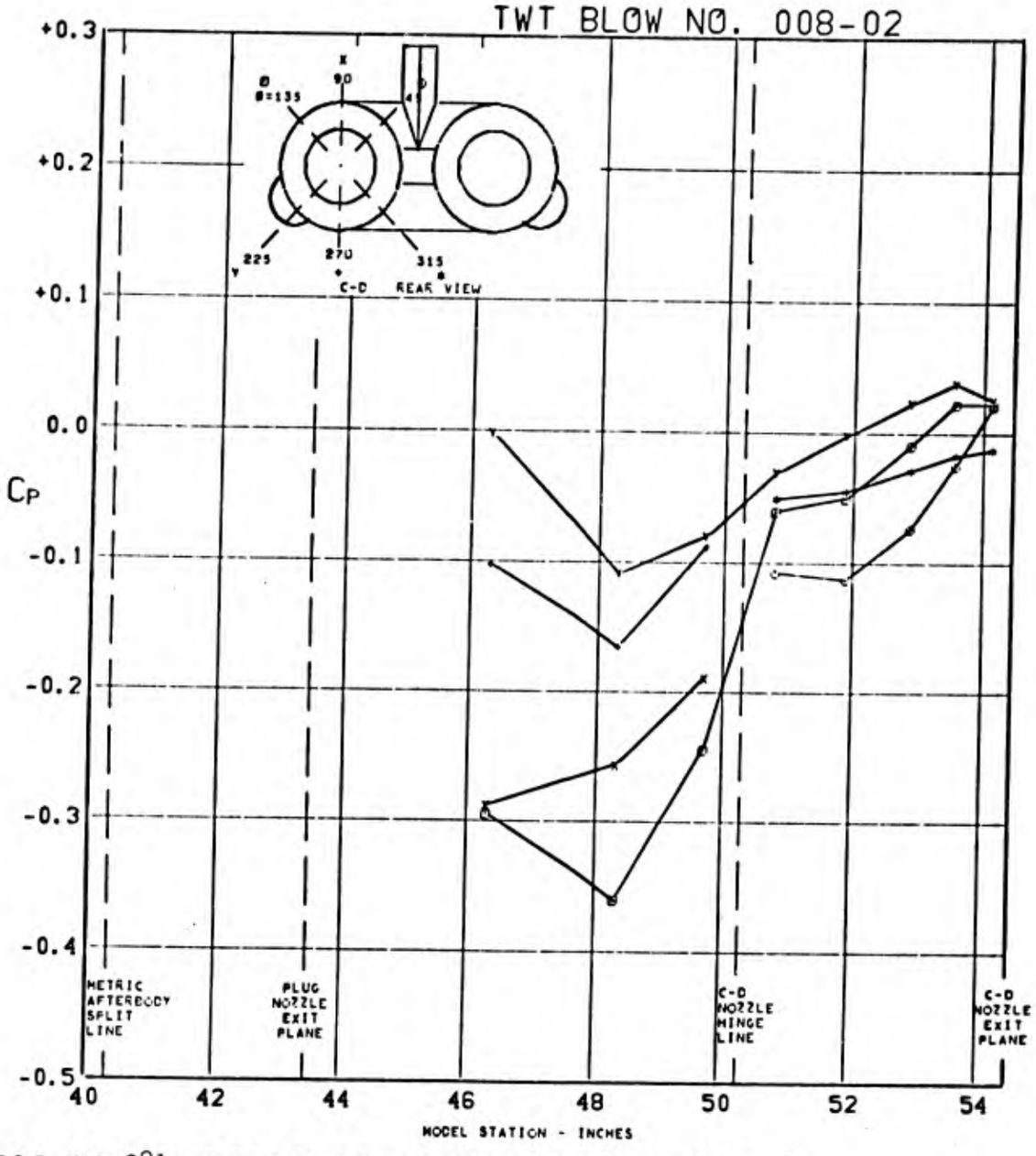

FIGURE 281. PRESSURE COEFFICIENTS ON C-D AFTERBODY (W1B1K1N1 P01 H1V1) Λ_{LE}=70° AT 0.850 M_0, $(P_T/P_0)_{C-D}$=CONE, $(P_T/P_0)_{PLUG}$=CONE, α= 2.8

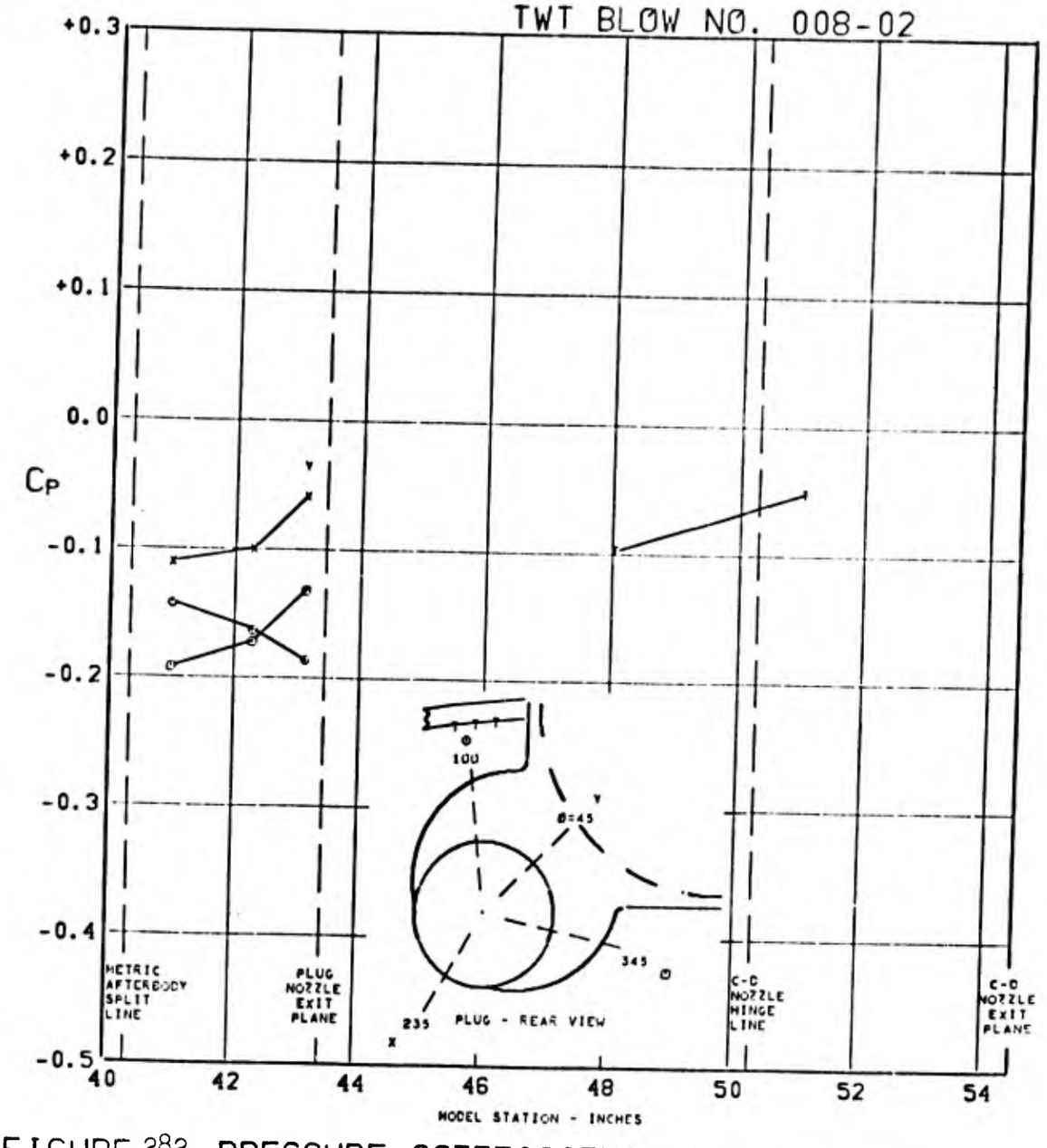

FIGURE 282. PRESSURE COEFFICIENTS ON TAIL & PLUG AFTERBODY (W1B1K1N1 P01 H1V1) $\Lambda_{LE}=70°$ AT 0.850 M_0, $(P_T/P_0)_{C-D}$=CONE, $(P_T/P_0)_{PLUG}$=CONE, α= 2.8

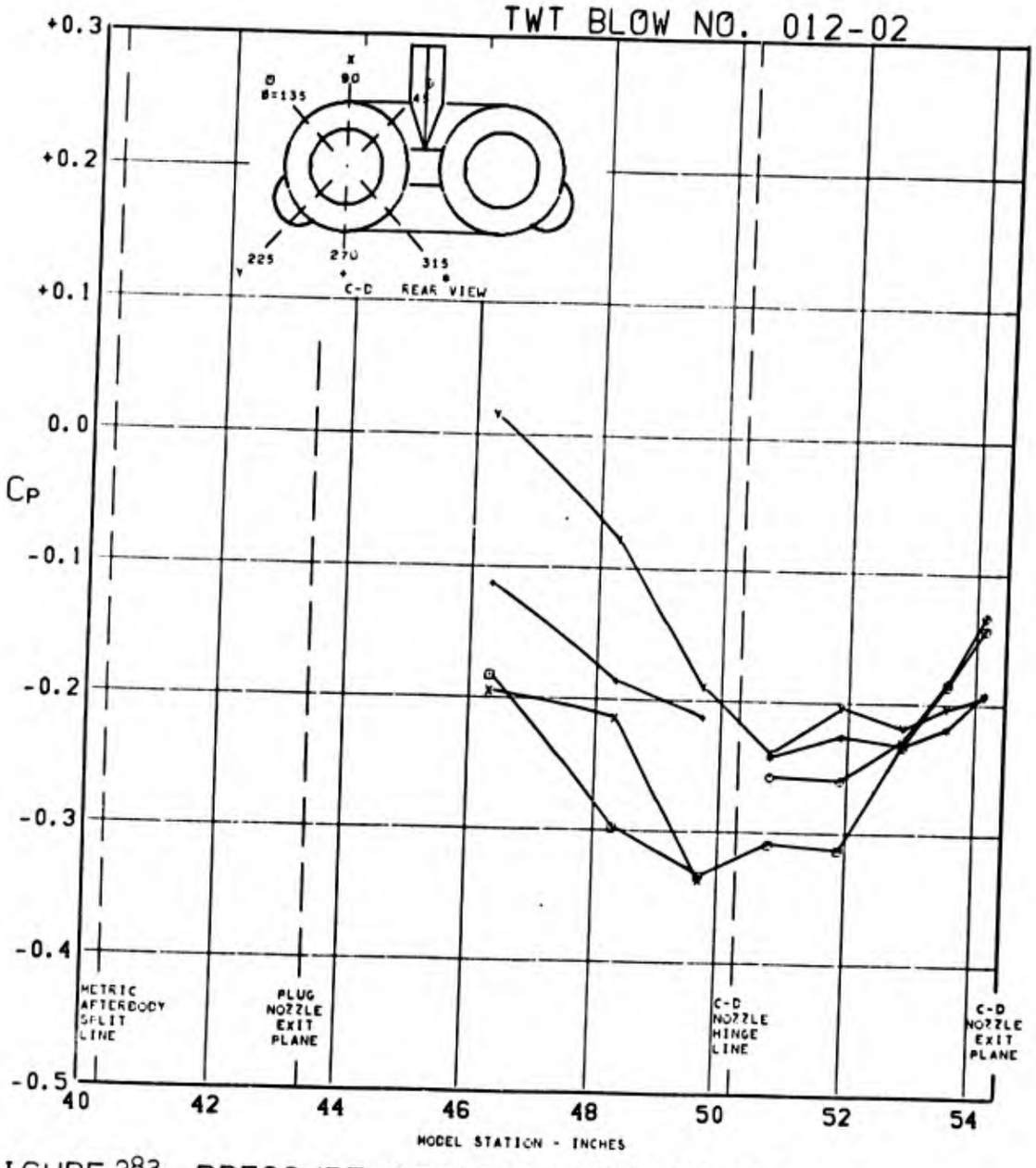

FIGURE 283. PRESSURE COEFFICIENTS ON C-D AFTERBODY (W1B1K1N1 P02 H1V1) $\Lambda_{LE}=70°$ AT 1.270 M_0, $(P_T/P_0)_{C-D}$=CONE, $(P_T/P_0)_{PLUG}$=CONE, α= 2.7

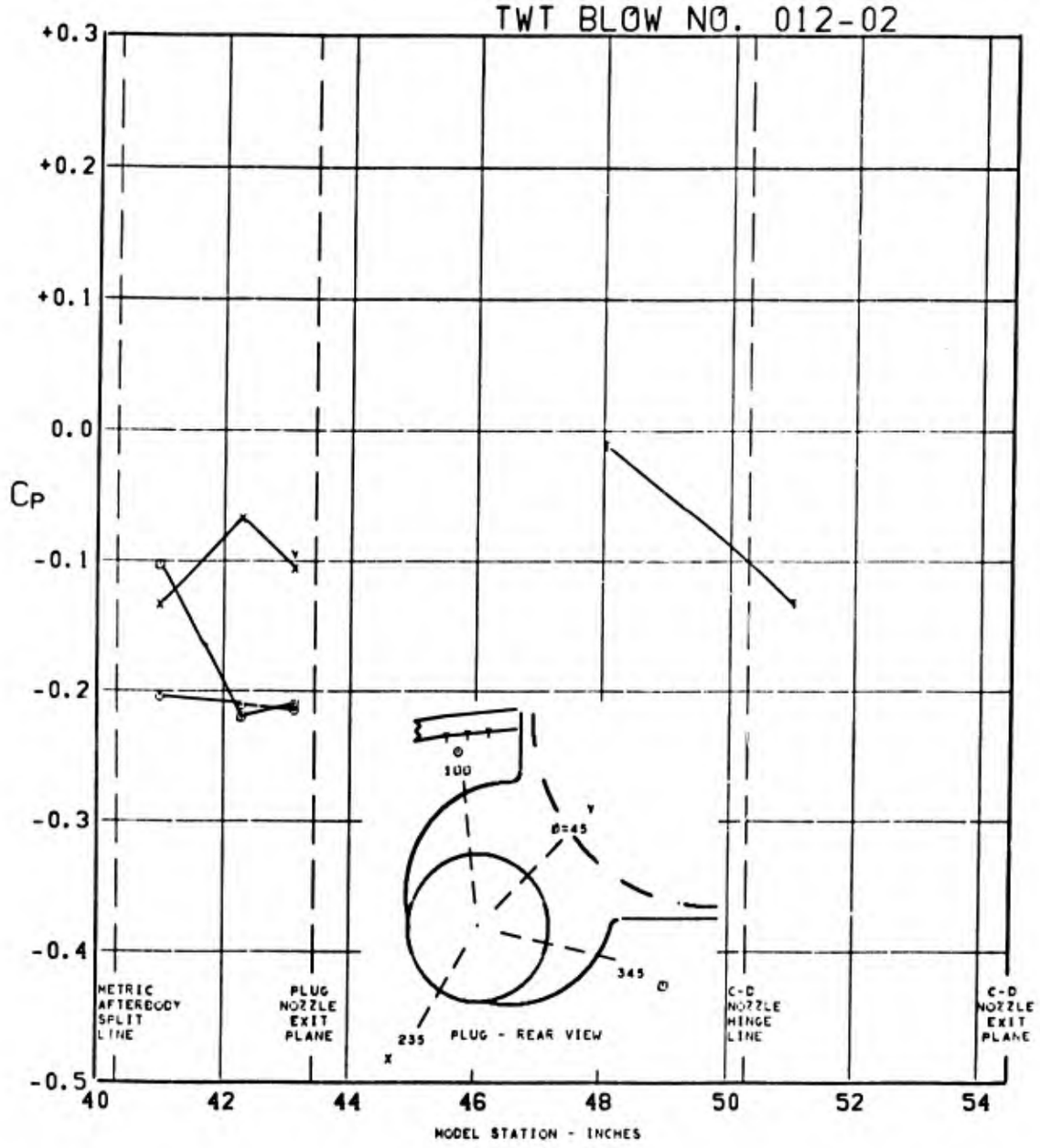

FIGURE 284. PRESSURE COEFFICIENTS ON TAIL & PLUG AFTERBODY (W1B1K1N1 P02 H1V1) Λ_{LE}=70° AT 1.270 M_0, $(P_T/P_0)_{C-D}$=CONE, $(P_T/P_0)_{PLUG}$=CONE, α= 2.7

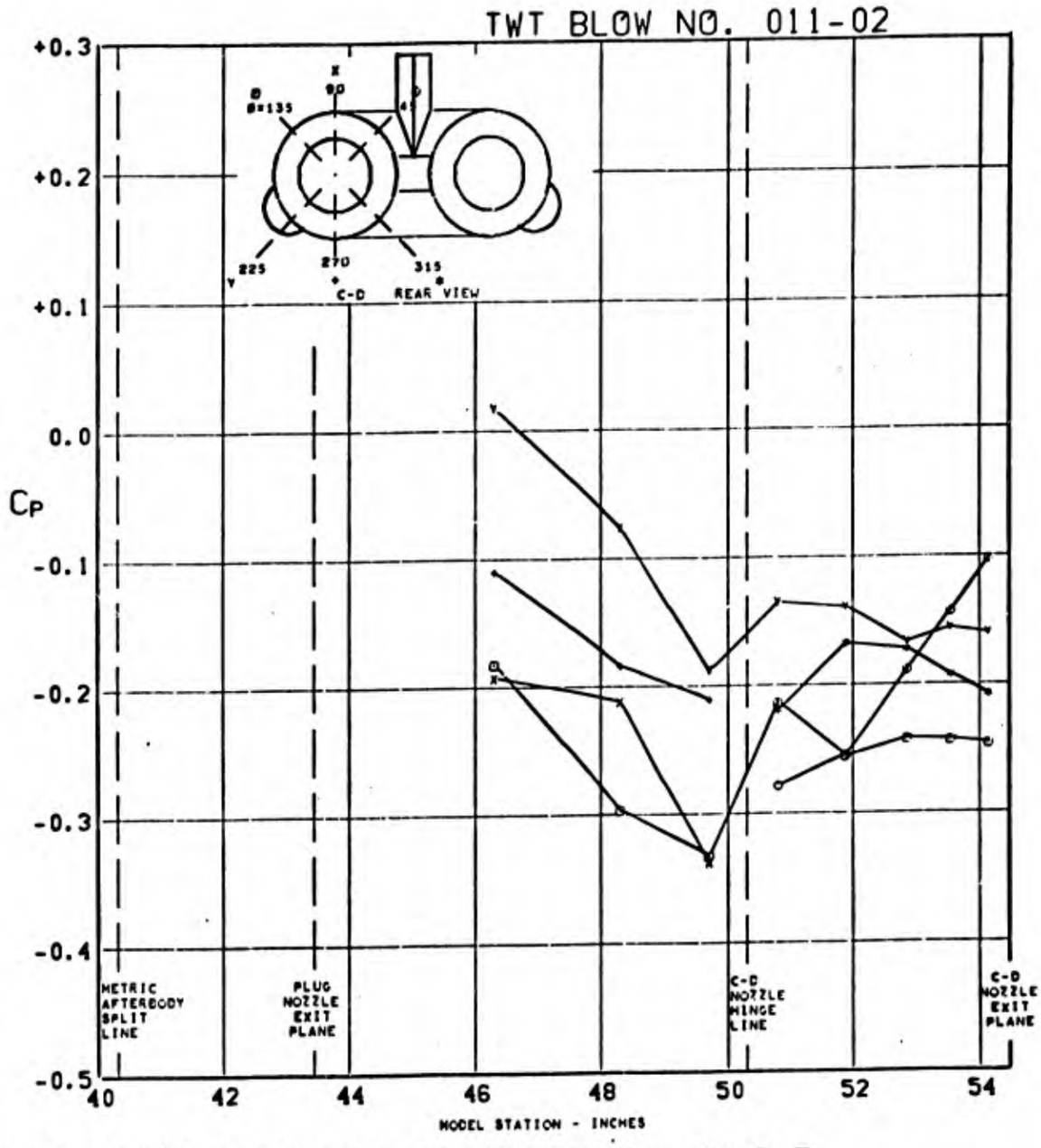

FIGURE 285. PRESSURE COEFFICIENTS ON C-D AFTERBODY (W1B1K1N1 P01 H1V1) $\Lambda_{LE}=70°$ AT 1.271 M_0, $(P_T/P_0)_{C-D}$=CONE, $(P_T/P_0)_{PLUG}$=CONE, α= 2.8

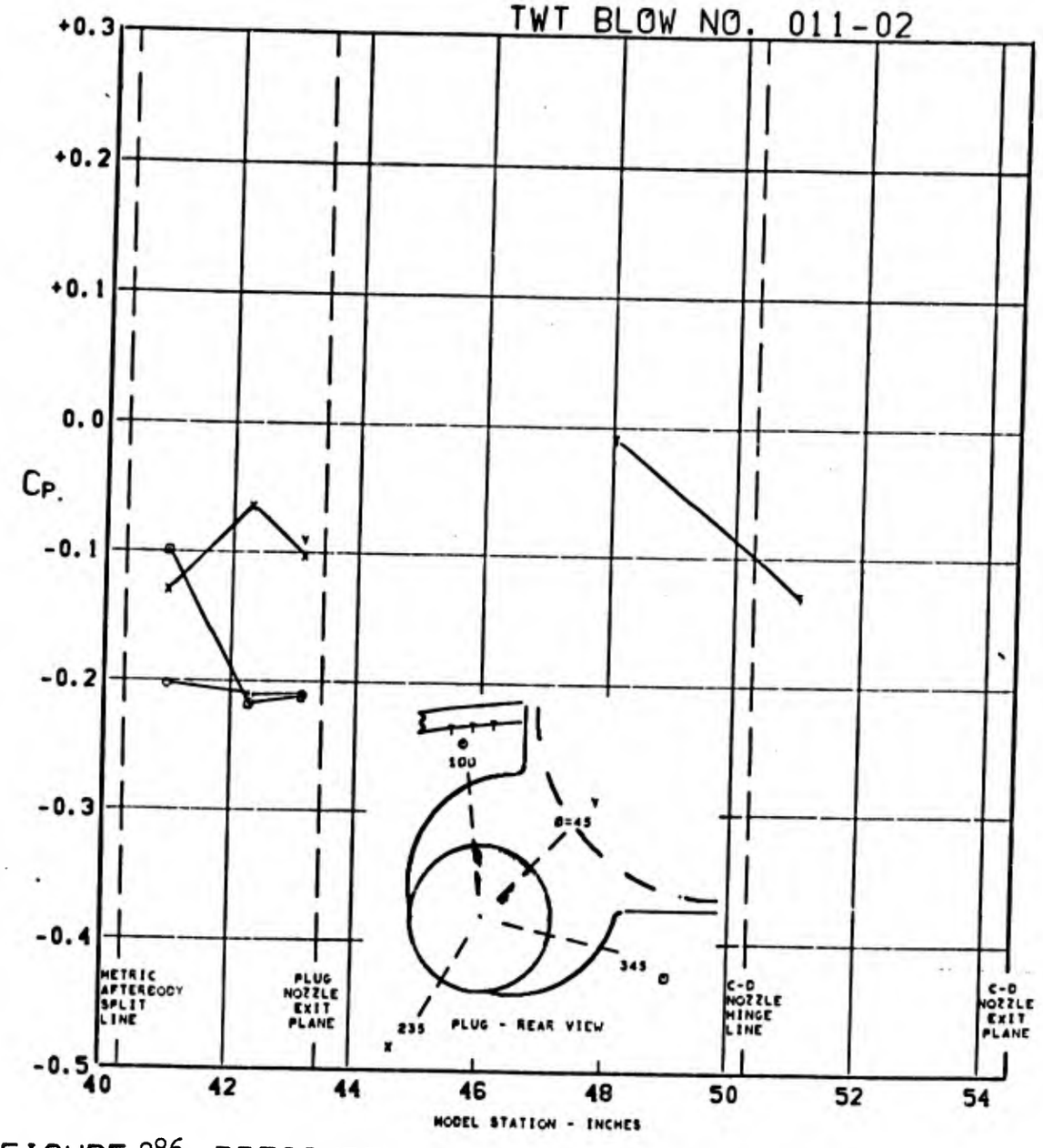

FIGURE 286. PRESSURE COEFFICIENTS ON TAIL & PLUG AFTERBODY (W1B1K1N1 P01 H1V1) $\Lambda_{LE}=70°$ AT 1.271 M_0, $(P_T/P_0)_{C-D}$=CONE, $(P_T/P_0)_{PLUG}$=CONE, α= 2.8

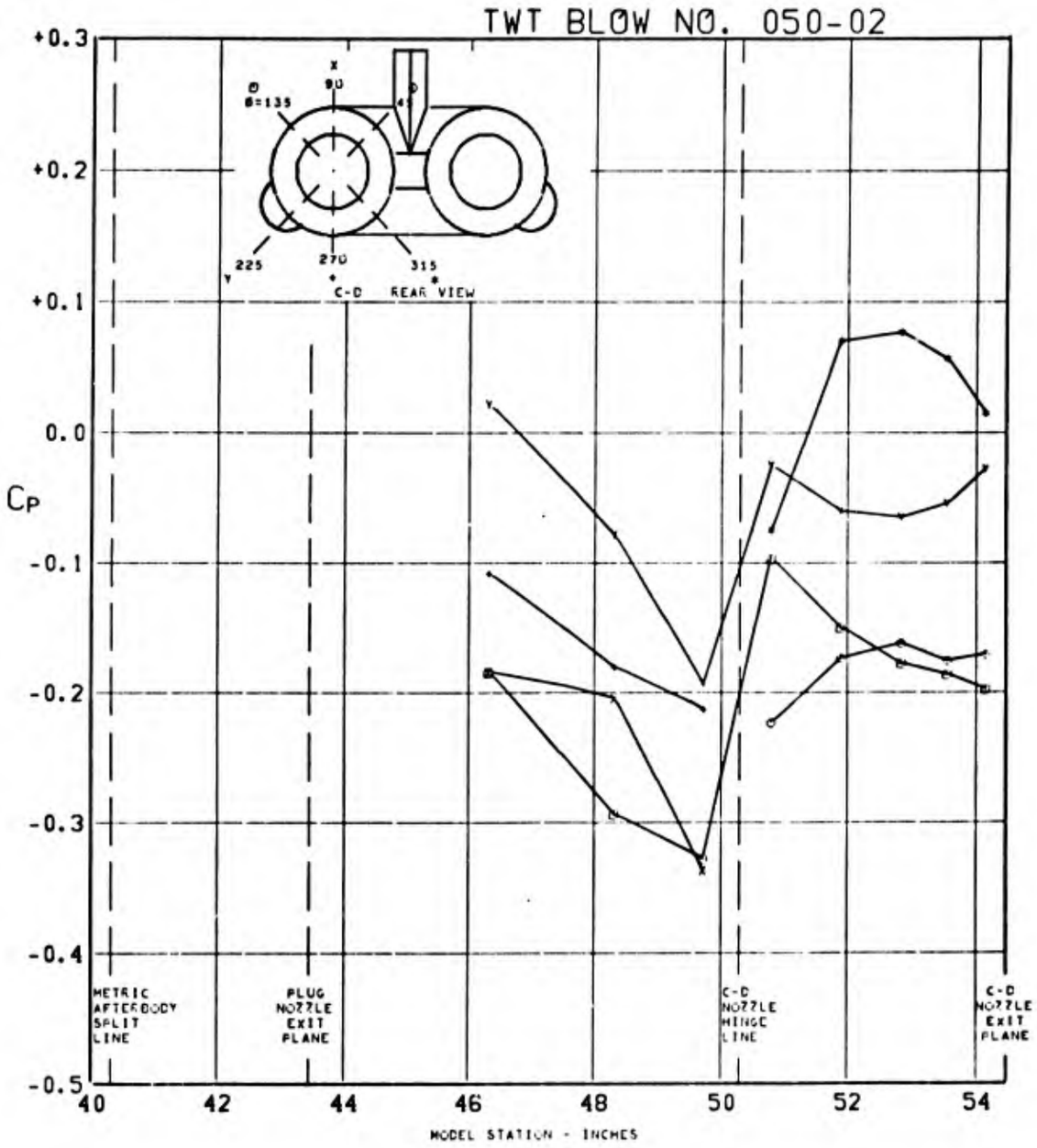

FIGURE 287. PRESSURE COEFFICIENTS ON C-D AFTERBODY (W1B1K1N1 P13 H1V1) Λ_{LE}=70° AT 1.269 M_0, $(P_T/P_0)_{C-D}$=0.848, $(P_T/P_0)_{PLUG}$=CONE, α= 2.9

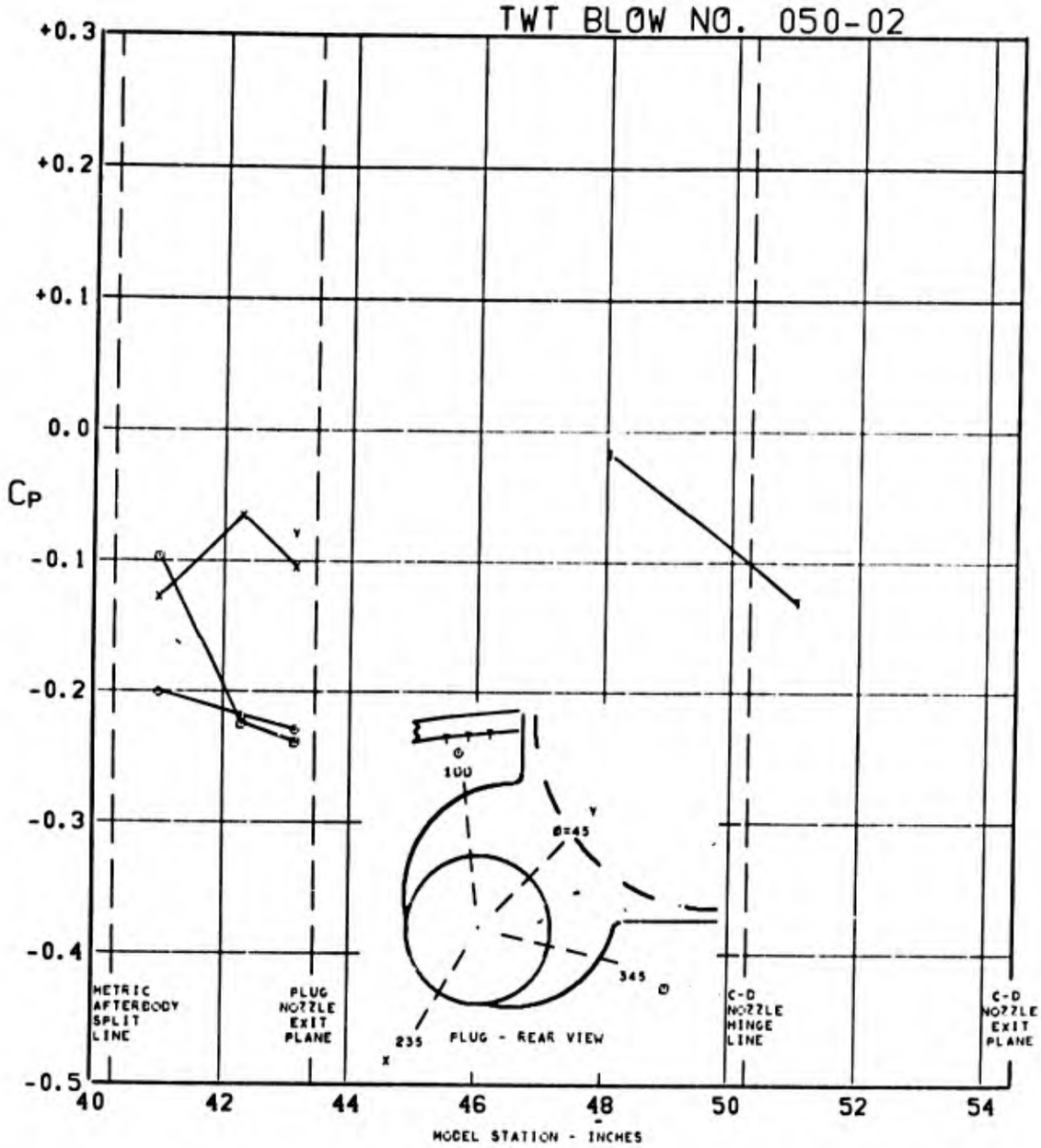

FIGURE 288. PRESSURE COEFFICIENTS ON TAIL & PLUG AFTERBODY (W1B1K1N1 P13 H1V1) $\Lambda_{LE}=70°$ AT 1.269 M_0, $(P_T/P_0)_{C-D}=0.848$, $(P_T/P_0)_{PLUG}$ =CONE , $\alpha=$ 2.9

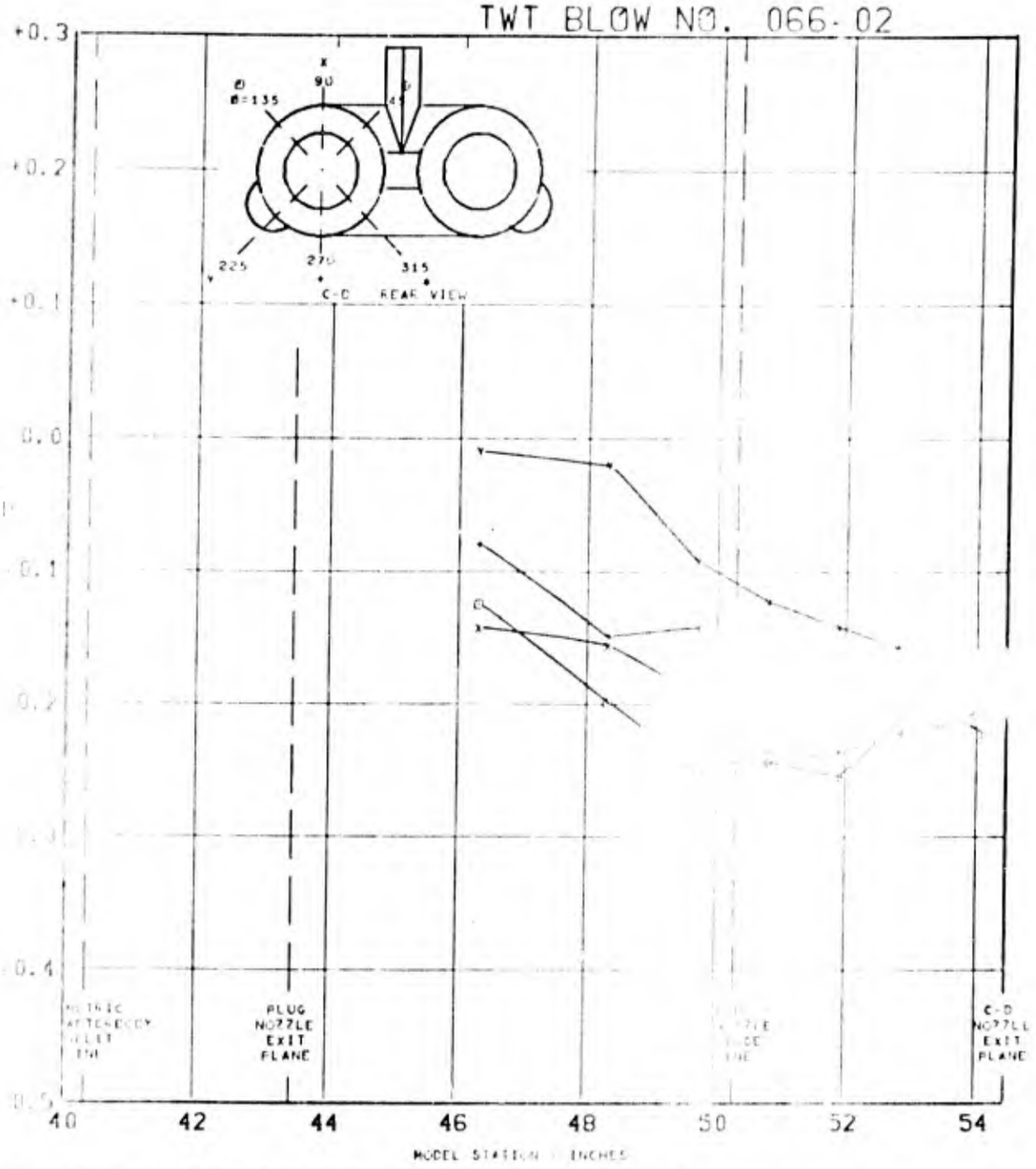

FIGURE 289. PRESSURE COEFFICIENTS ON C-D AFTERBODY (W1B1K1N1 P11 H1V1) $\Lambda_{LE}=70°$ AT .697 M_0, $(P_T/P_0)_{C-D}=0.753$, $(P_T/P_0)_{PLUG}$ =CONE, $\alpha=2.8$

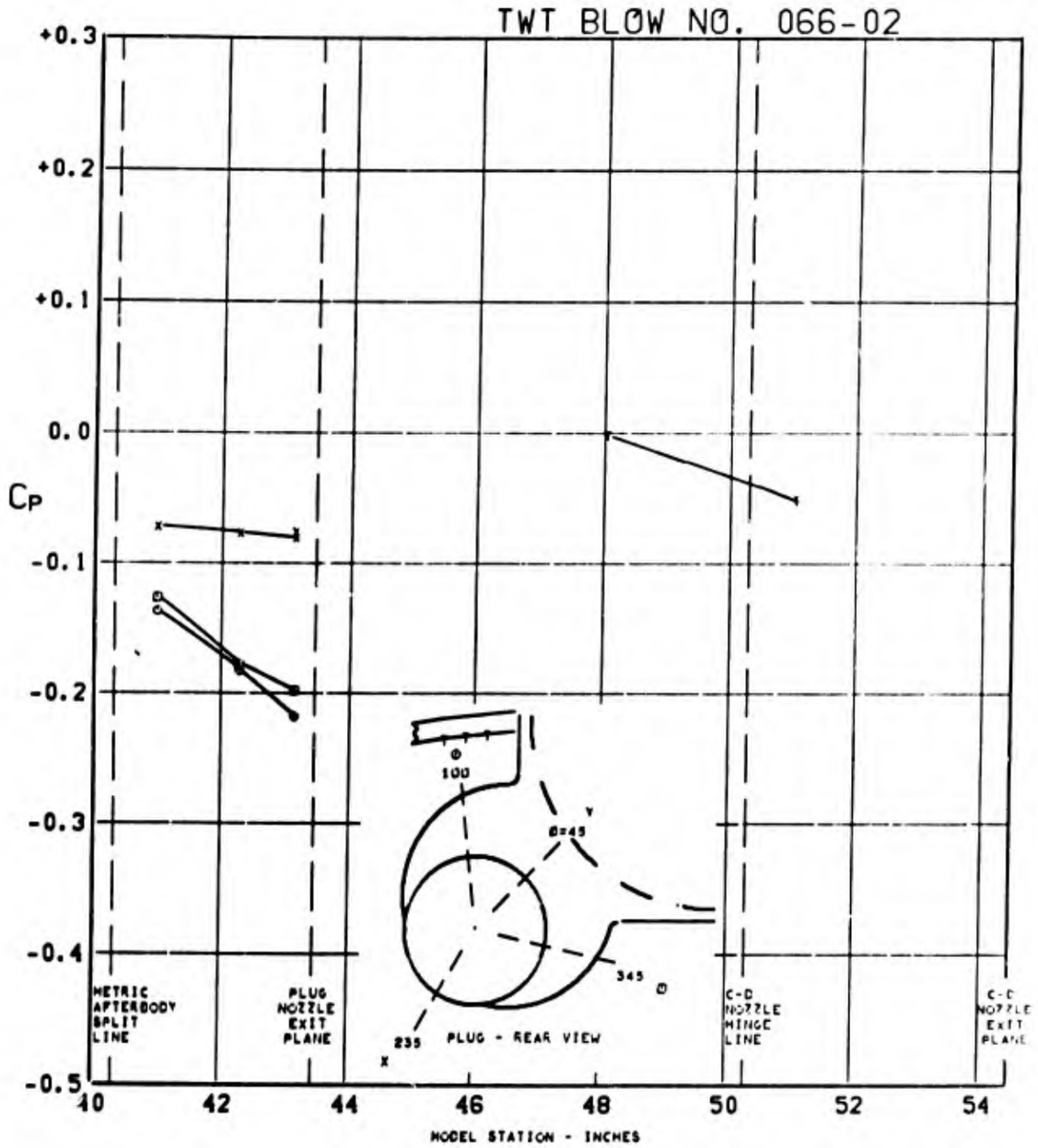

FIGURE 290. PRESSURE COEFFICIENTS ON TAIL & PLUG AFTERBODY (W1B1K1N1 P11 H1V1) Λ_{LE}=70° AT 1.697 M_0, $(P_T/P_0)_{C-D}$=0.753, $(P_T/P_0)_{PLUG}$ =CONE , α= 2.8

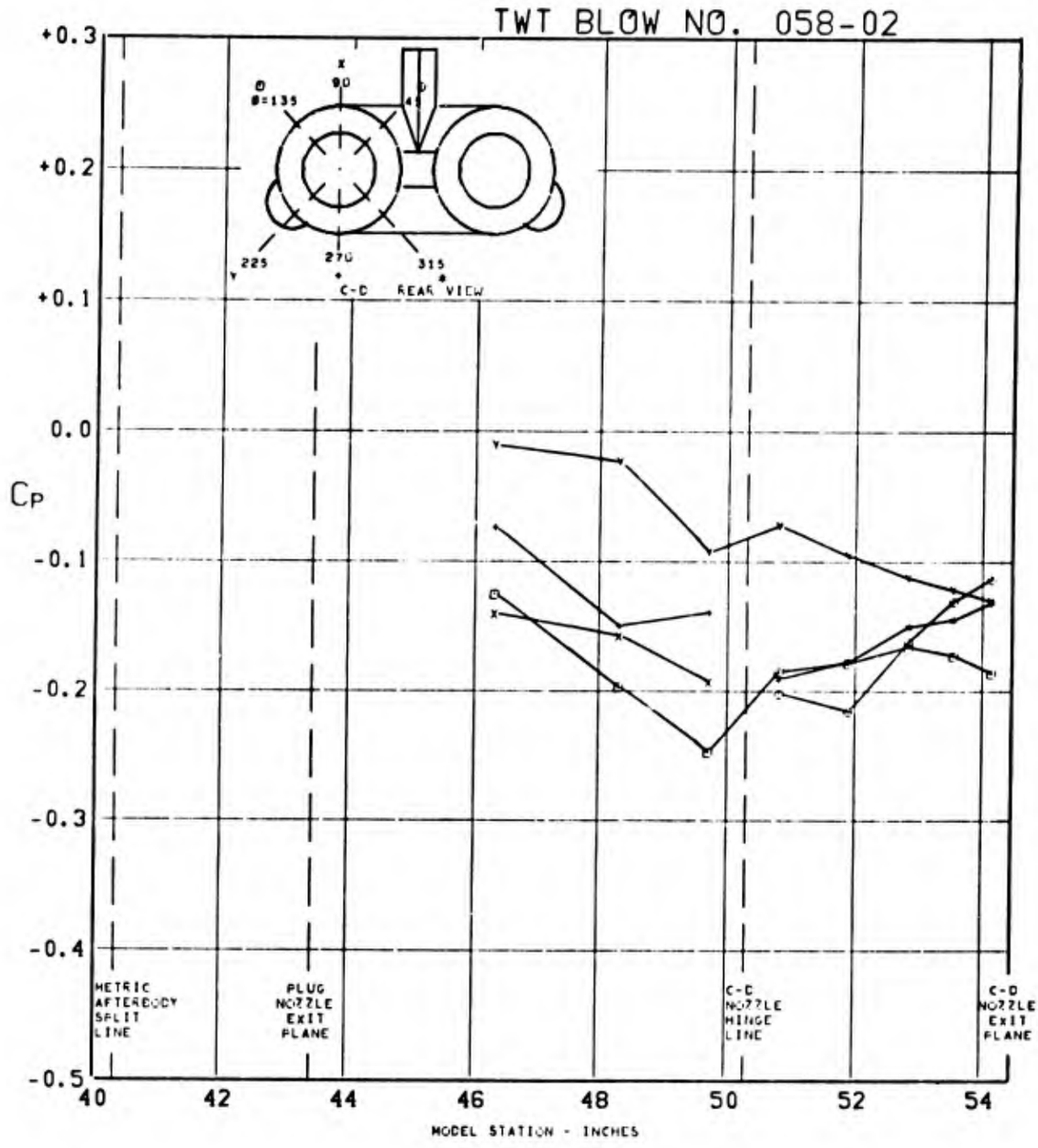

FIGURE 291. PRESSURE COEFFICIENTS ON C-D AFTERBODY (W1B1K1N1 P01 H1V1) $\Lambda_{LE}=70°$ AT 1.697 M_0 ; $(P_T/P_0)_{C-D}$=CONE , $(P_T/P_0)_{PLUG}$ =CONE , α= 2.9

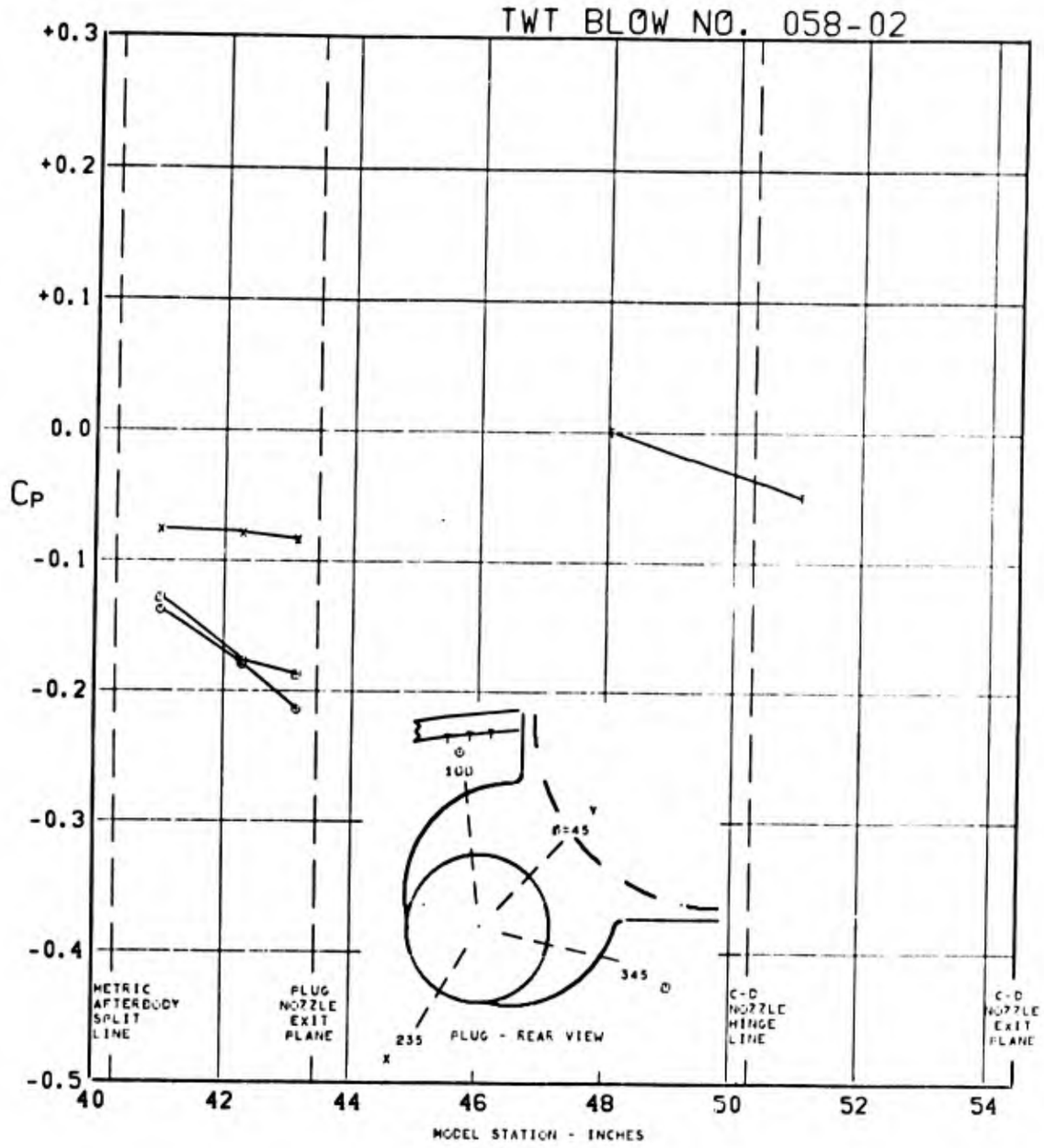

FIGURE 292. PRESSURE COEFFICIENTS ON TAIL & PLUG AFTERBODY (W1B1K1N1 P01 H1V1) $\Lambda_{LE}=70°$ AT 1.697 M_0, $(P_T/P_0)_{C-D}$=CONE, $(P_T/P_0)_{PLUG}$=CONE, α= 2.9

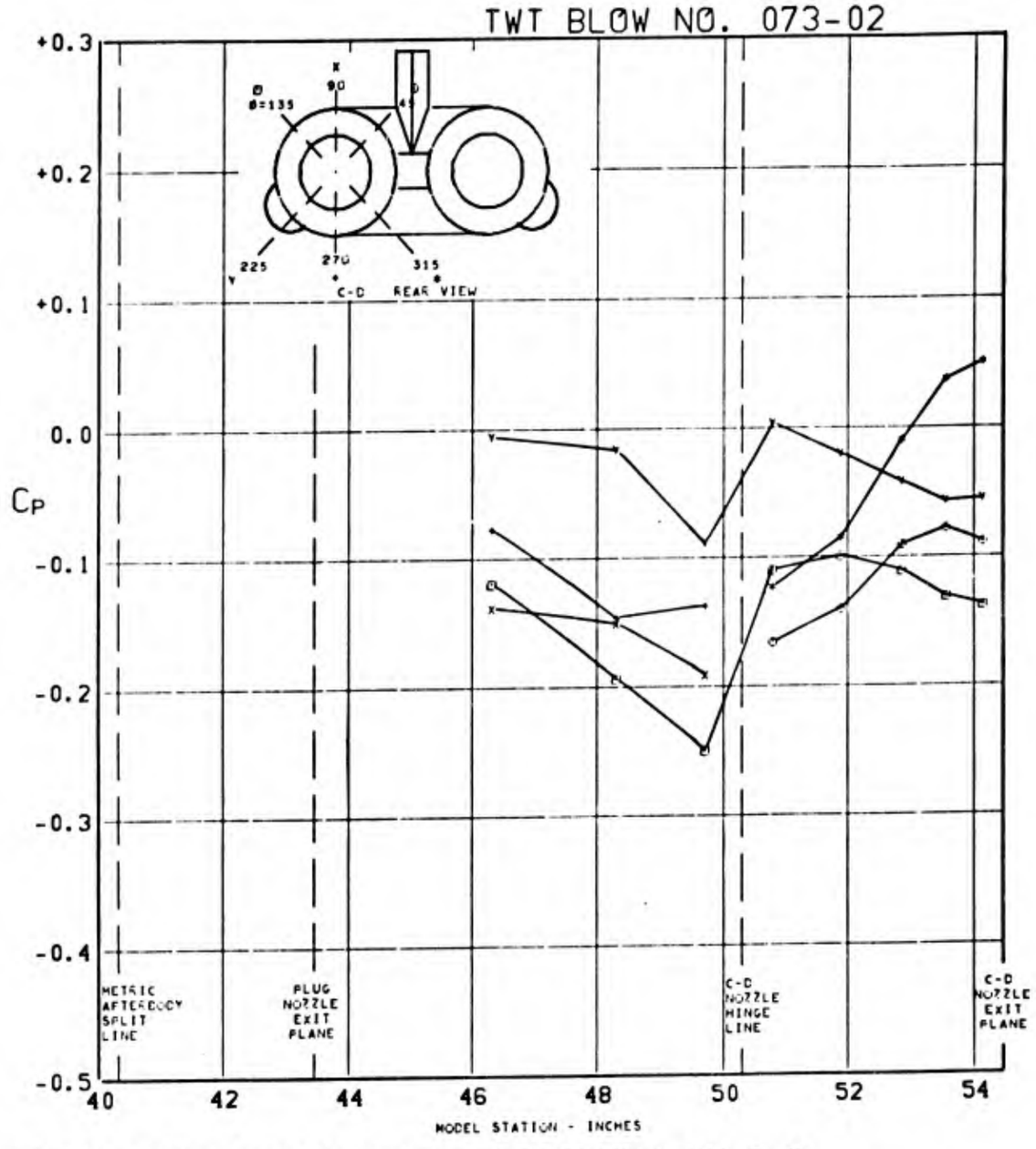

FIGURE 293. PRESSURE COEFFICIENTS ON C-D AFTERBODY (W1B1K1N1 P13 H1V1) Λ_{LE}=70° AT 1.697 M_0, $(P_T/P_0)_{C-D}$=0.636, $(P_T/P_0)_{PLUG}$ =CONE , α= 2.9

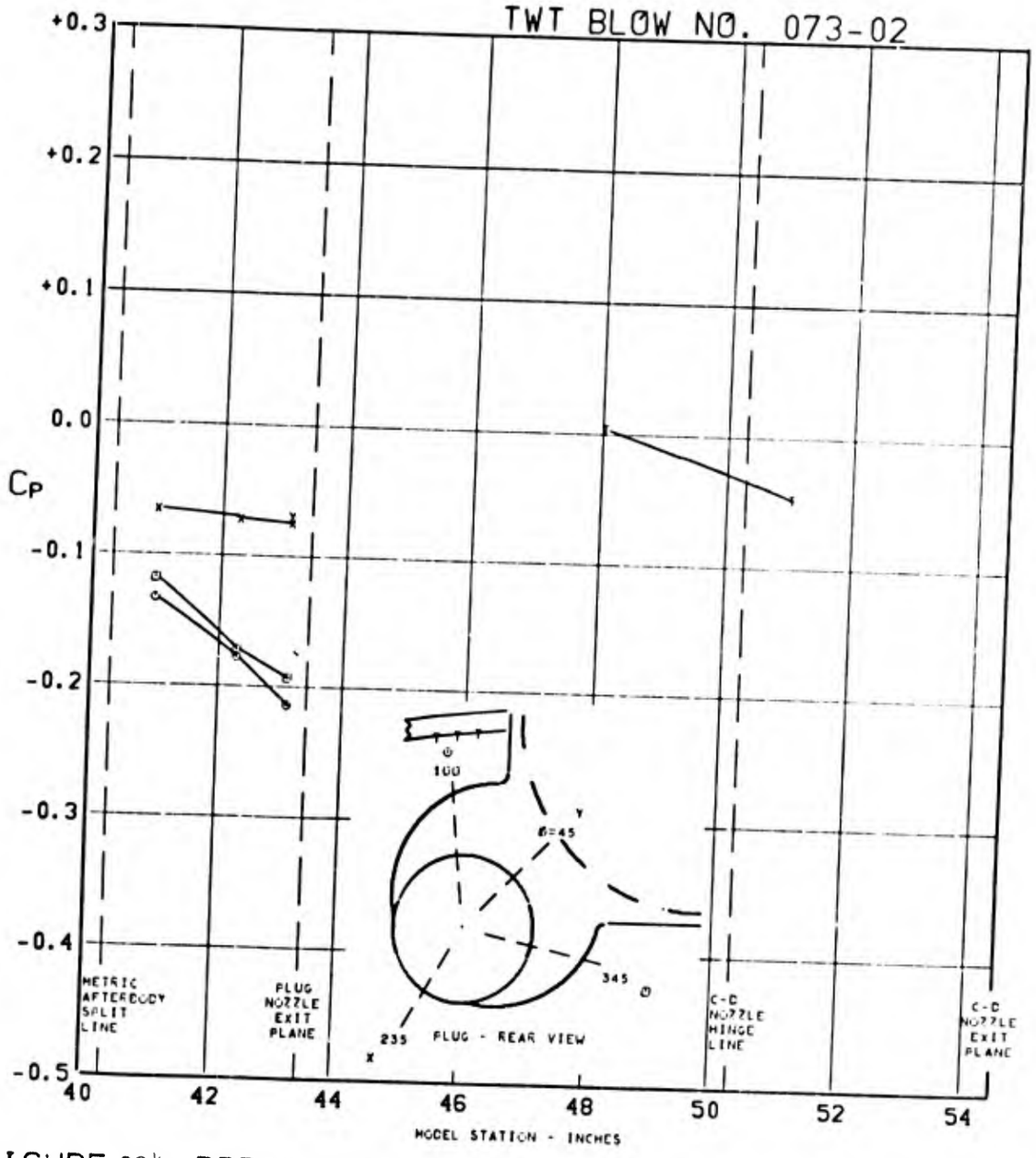

FIGURE 294. PRESSURE COEFFICIENTS ON TAIL & PLUG AFTERBODY (W1B1K1N1 P13 H1V1) $\Lambda_{LE}=70°$ AT 1.697 M_0, $(P_T/P_0)_{C-D}=0.636$, $(P_T/P_0)_{PLUG}$ =CONE , $\alpha=$ 2.9

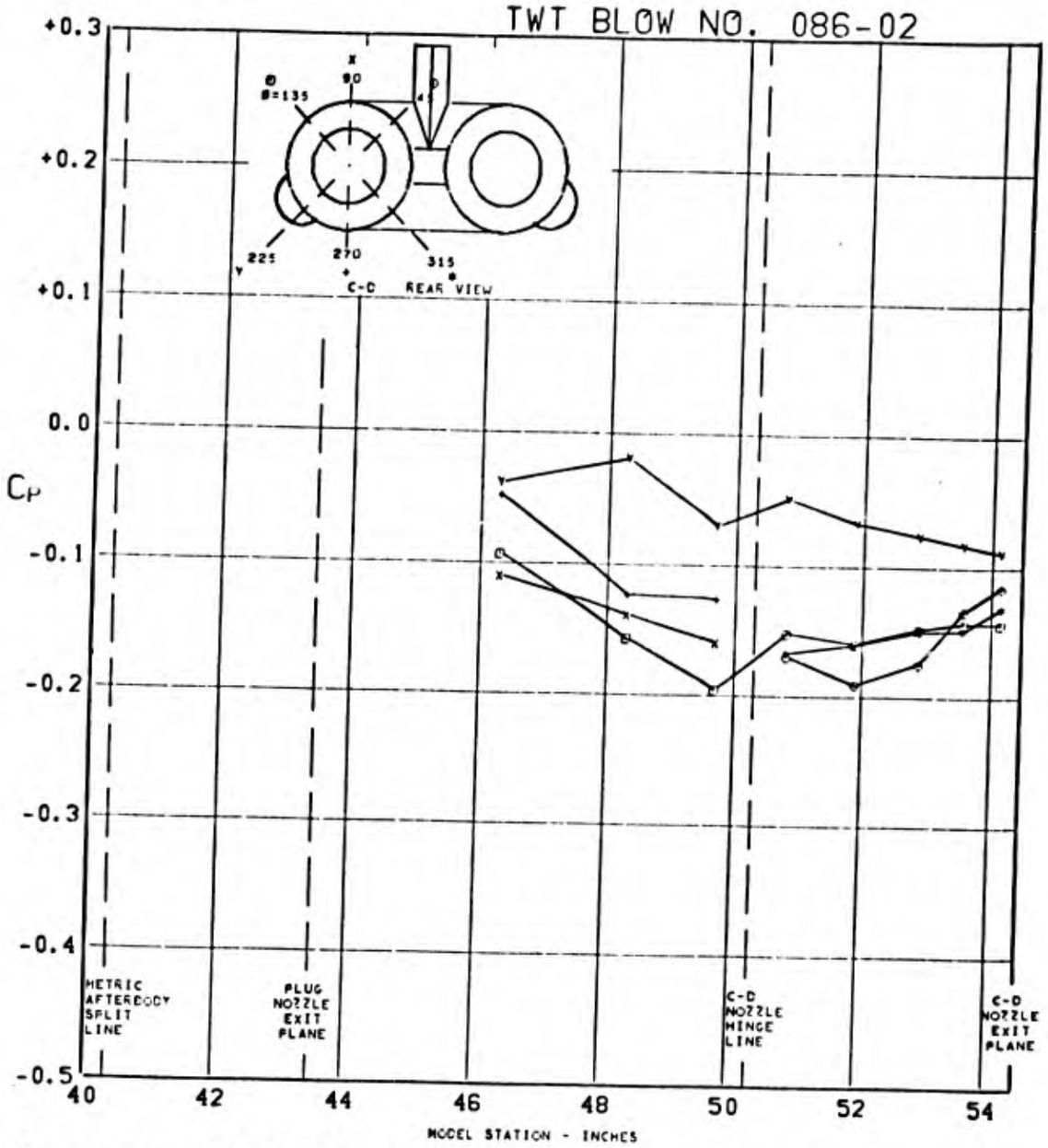

FIGURE 295. PRESSURE COEFFICIENTS ON C-D AFTERBODY (W1B1K1N1 P01 H1V1) $\Lambda_{LE}=70°$ AT 1.998 M_0, $(P_T/P_0)_{C-D}$=CONE, $(P_T/P_0)_{PLUG}$=CONE, α= 2.8

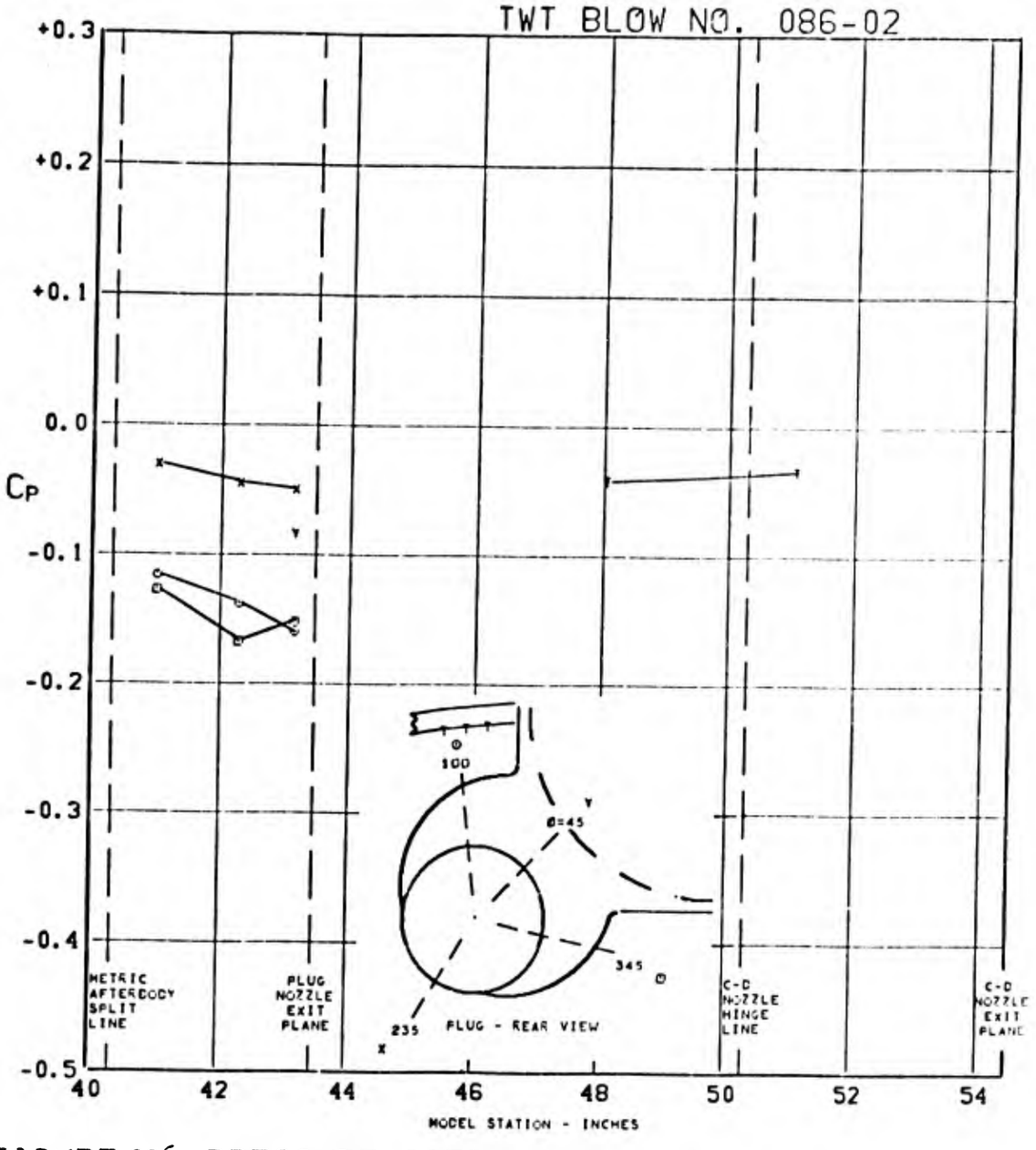

FIGURE 296. PRESSURE COEFFICIENTS ON TAIL & PLUG AFTERBODY (W1B1K1N1 P01 H1V1) Λ_{LE}=70° AT 1.998 M_0, $(P_T/P_0)_{C-D}$=CONE, $(P_T/P_0)_{PLUG}$=CONE, α= 2.8

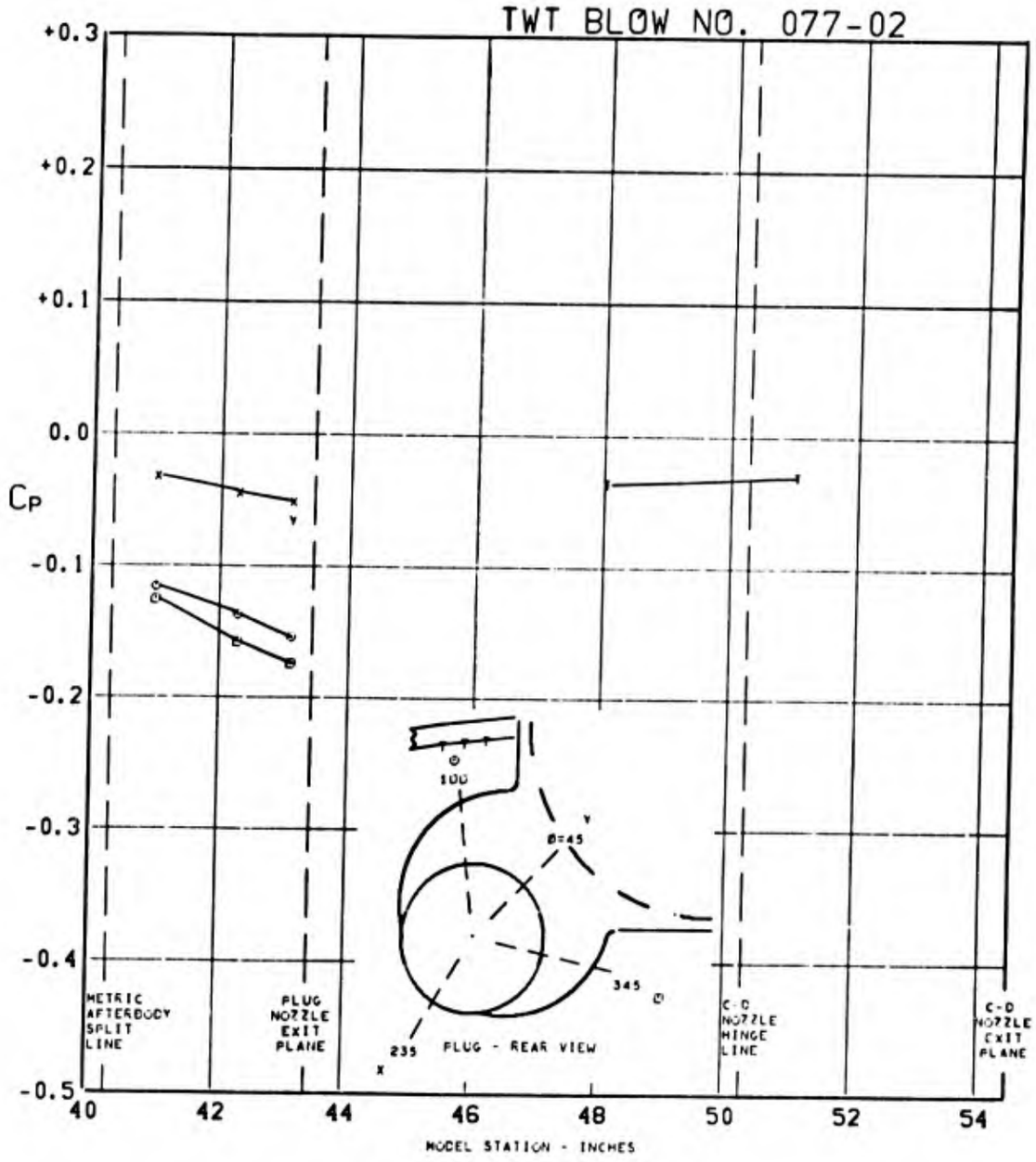

FIGURE 297. PRESSURE COEFFICIENTS ON TAIL & PLUG AFTERBODY (W1B1K1N1 P13 H1V1) $\Lambda_{LE}=70°$ AT 1.998 M_0, $(P_T/P_0)_{C-D}=0.721$, $(P_T/P_0)_{PLUG}$ =CONE, $\alpha=$ 3.0

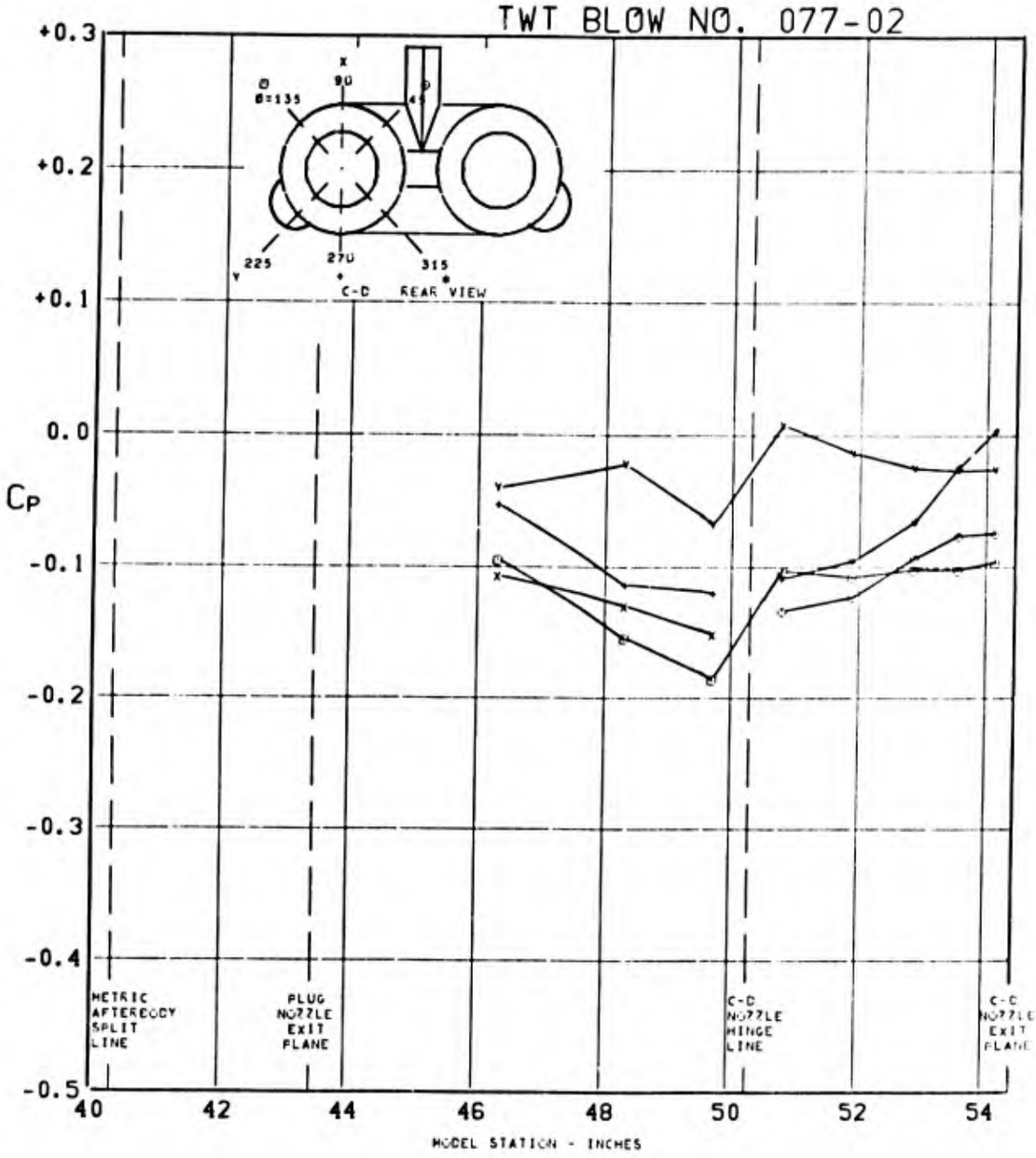

FIGURE 298. PRESSURE COEFFICIENTS ON C-D AFTERBODY (W1B1K1N1 P13 H1V1) $\Lambda_{LE}=70°$ AT 1.998 M_0, $(P_T/P_0)_{C-D}=0.721$, $(P_T/P_0)_{PLUG}$ =CONE , $\alpha=$ 3.0

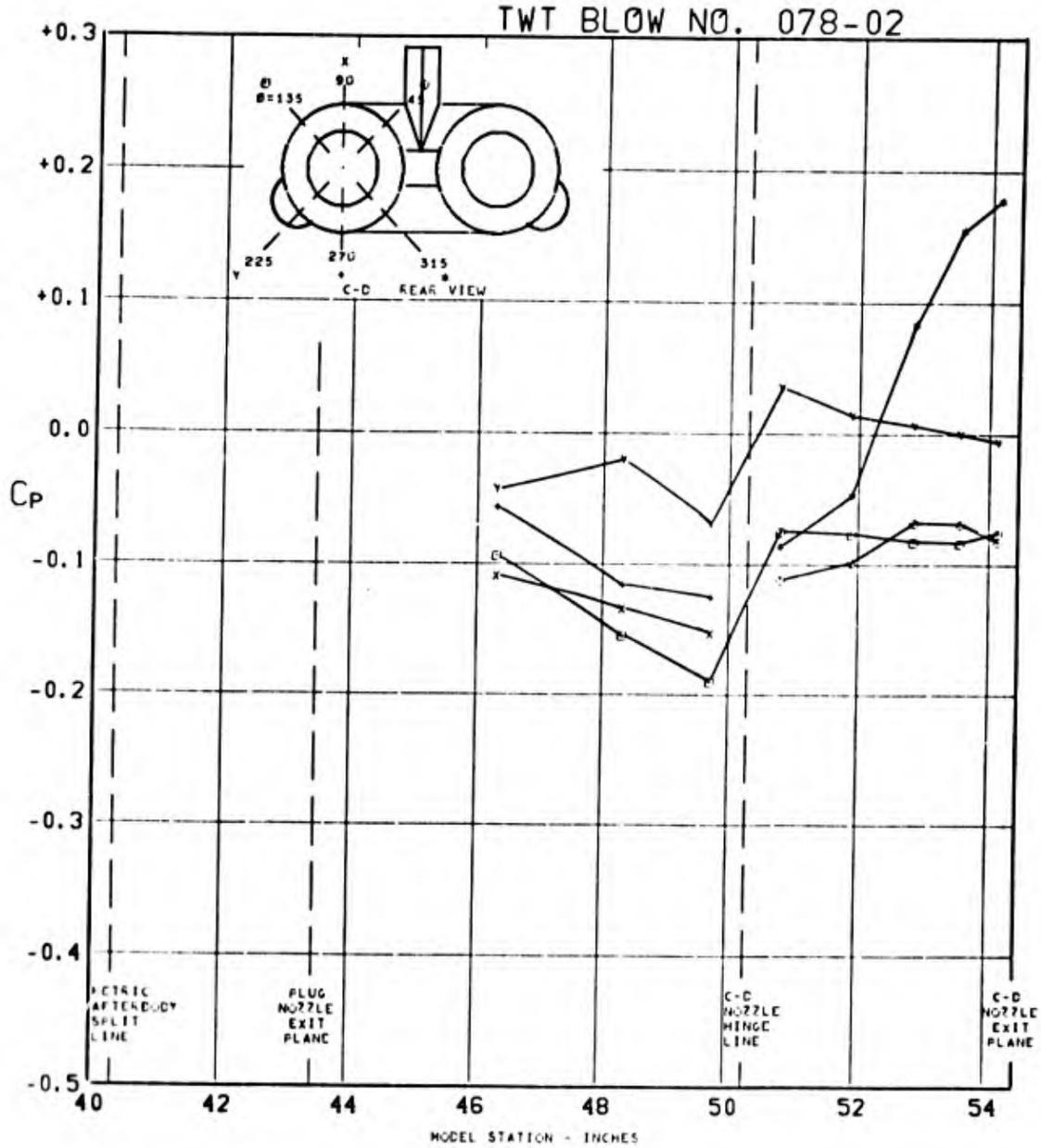

FIGURE 200. PRESSURE COEFFICIENTS ON C-D AFTERBODY (W1B1K1N1 P15 H1V1) Λ_{LE}=70° AT 1.998 M_0, $(P_T/P_0)_{C-D}$=0.665, $(P_T/P_0)_{PLUG}$ =CONE , α= 2.9

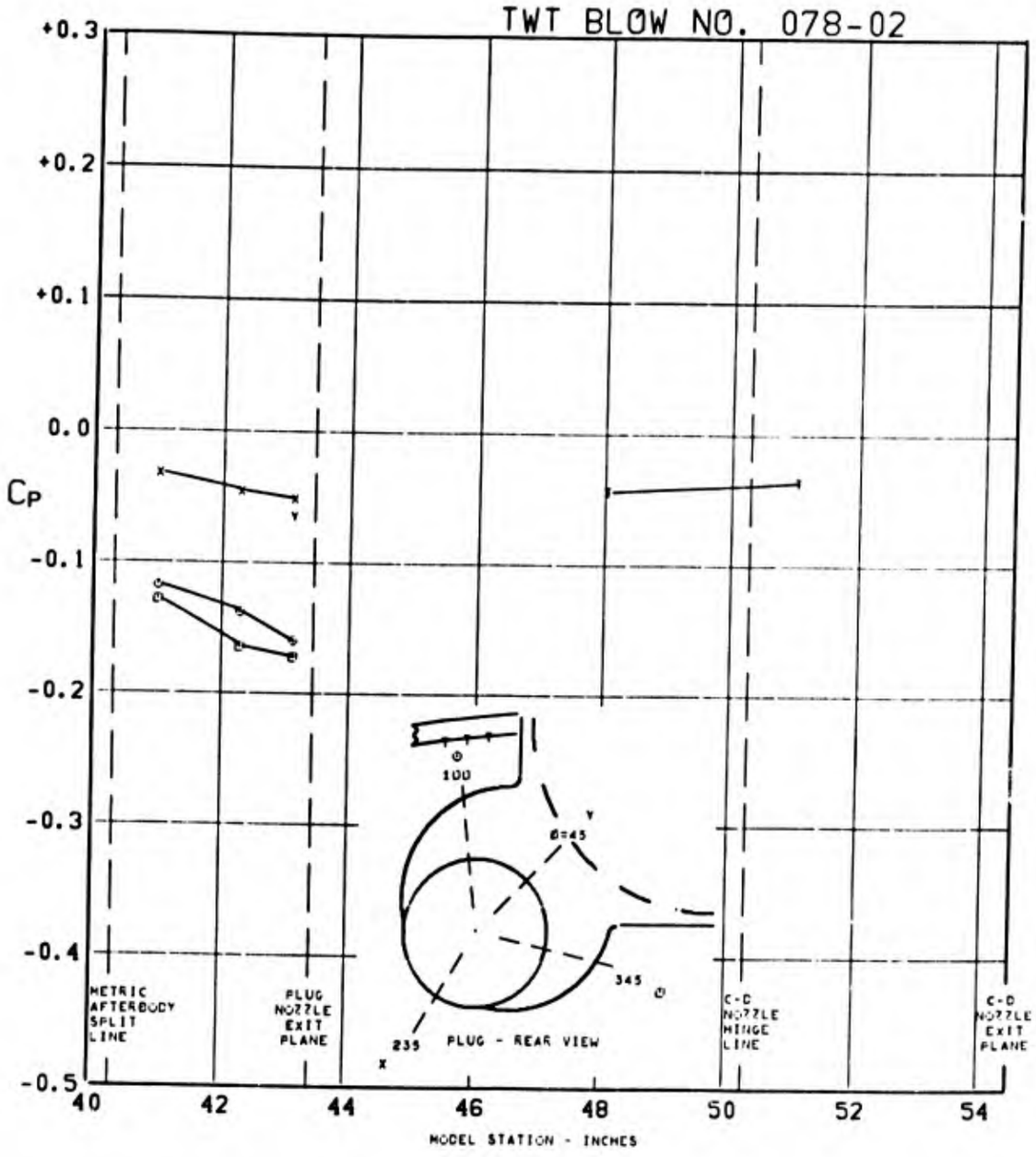

FIGURE 300. PRESSURE COEFFICIENTS ON TAIL & PLUG AFTERBODY (W1B1K1N1 P15 H1V1) $\Lambda_{LE}=70°$ AT 1.998 M_0, $(P_T/P_0)_{C-D}=0.665$, $(P_T/P_0)_{PLUG}$ =CONE , $\alpha=$ 2.9

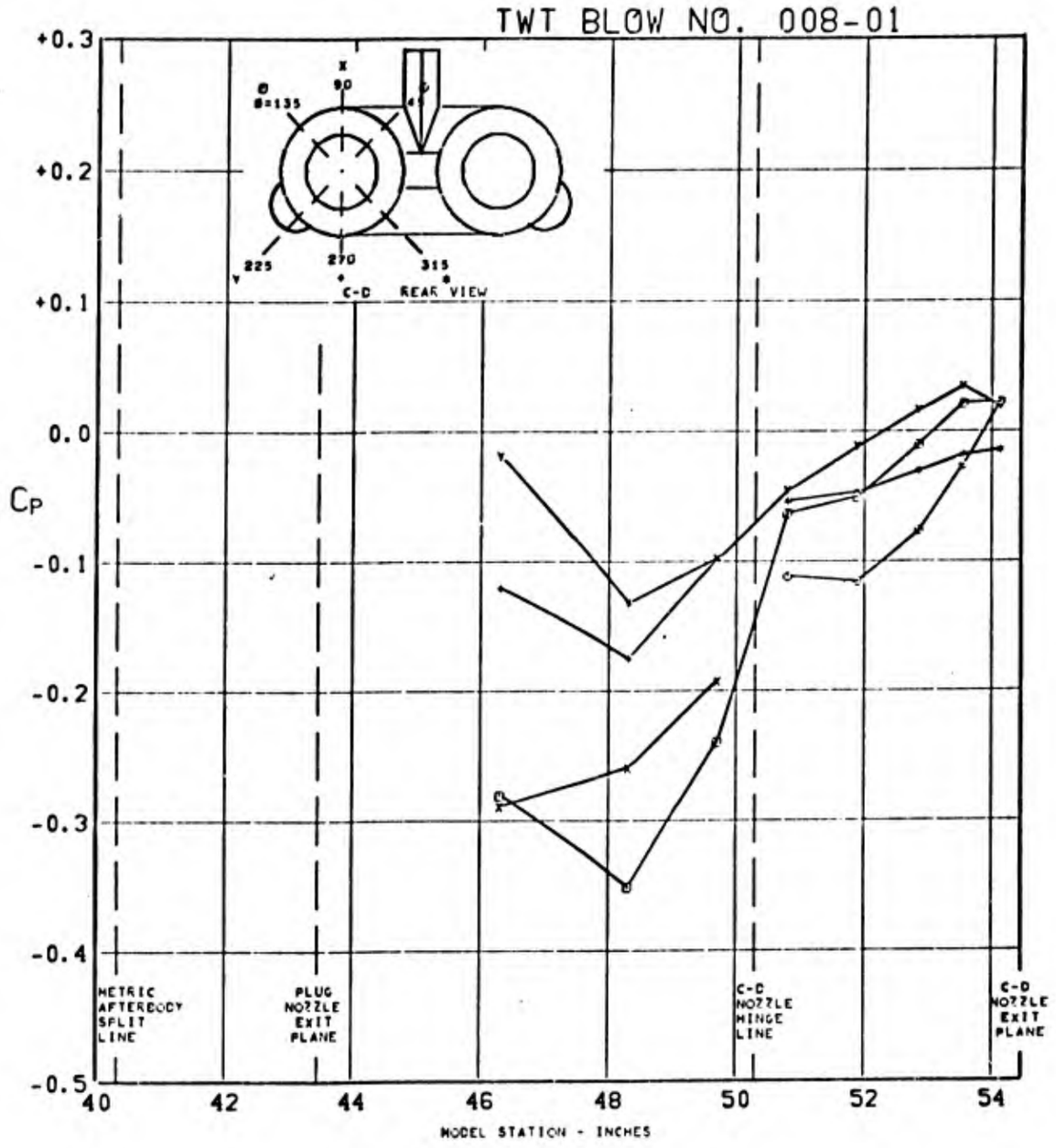

FIGURE 301. PRESSURE COEFFICIENTS ON C-D AFTERBODY (W1B1K1N1 P01 H1V1) Λ_{LE}=70° AT 0.852 M_0, $(P_T/P_0)_{C-D}$=CONE, $(P_T/P_0)_{PLUG}$=CONE, α= 0.0

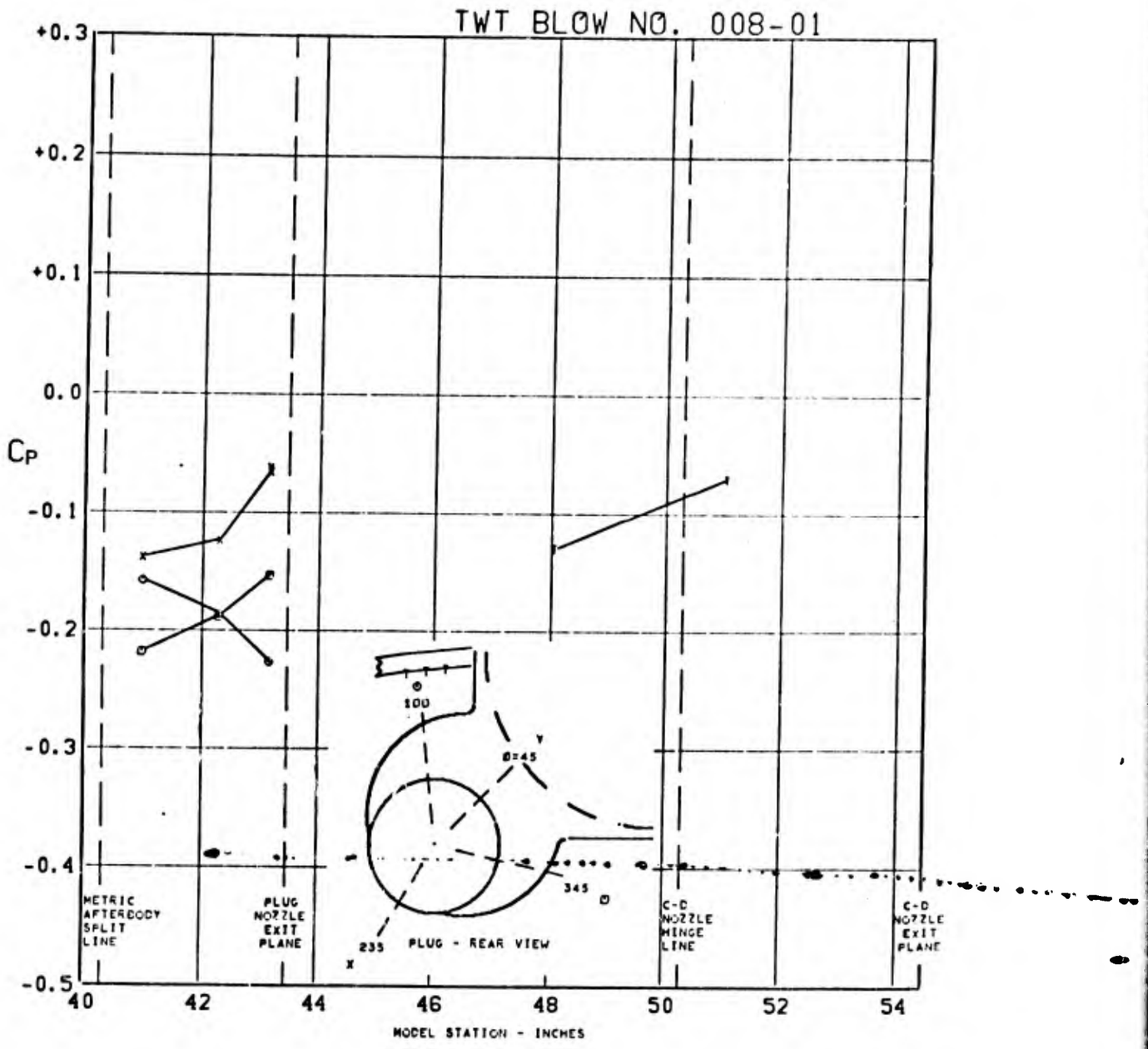

FIGURE 302. PRESSURE COEFFICIENTS ON TAIL & PLUG AFTERBODY (W1B1K1N1 P01 H1V1) Λ_{LE}=70° AT 0.852 M_0, $(P_T/P_0)_{C-D}$=CONE, $(P_T/P_0)_{PLUG}$=CONE, α= 0.0

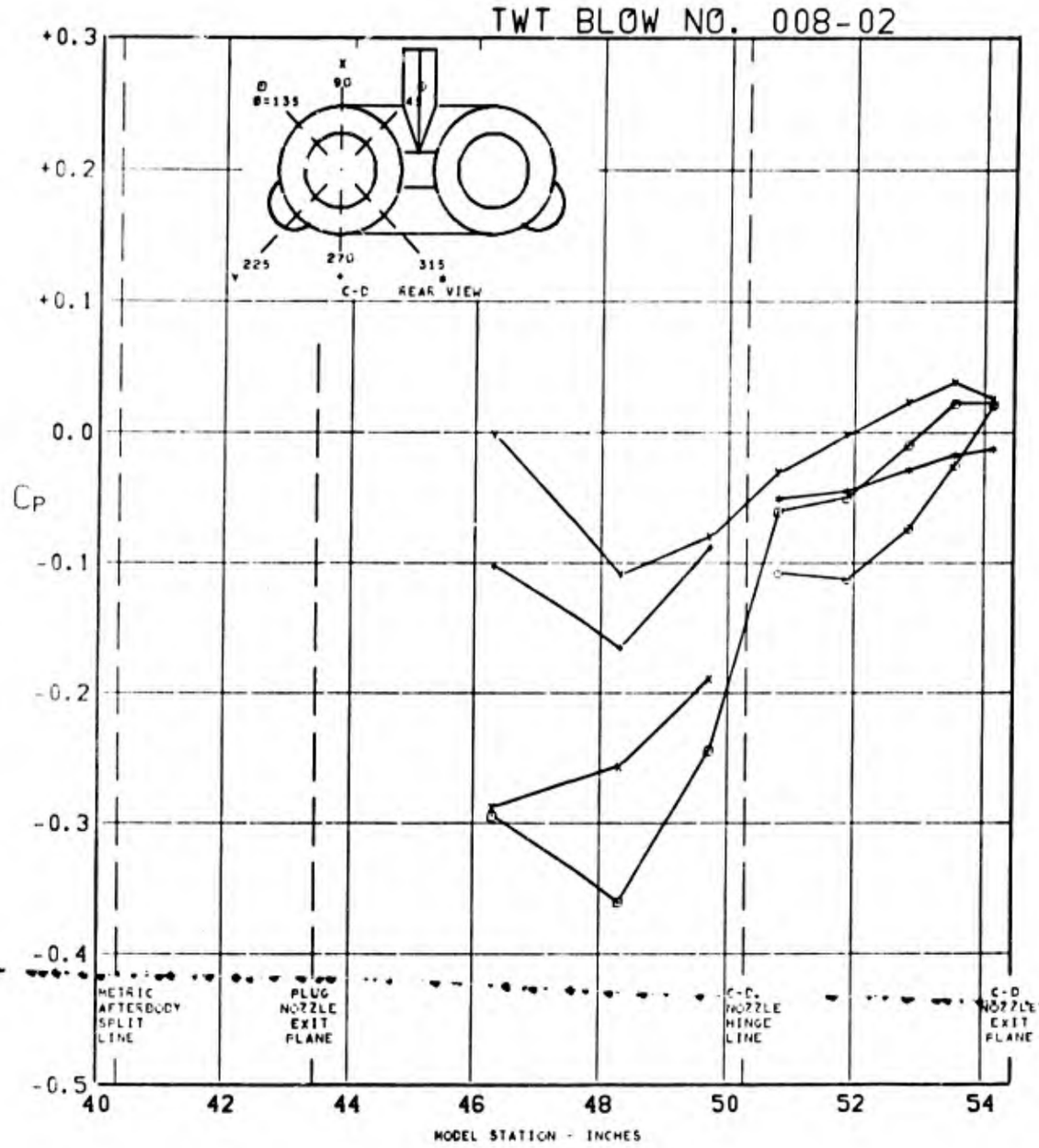

FIGURE 303. PRESSURE COEFFICIENTS ON C-D AFTERBODY (W1B1K1N1 P01 H1V1) Λ_{LE}=70° AT 0.850 M_0, $(P_T/P_0)_{C-D}$=CONE, $(P_T/P_0)_{PLUG}$=CONE, α= 2.8

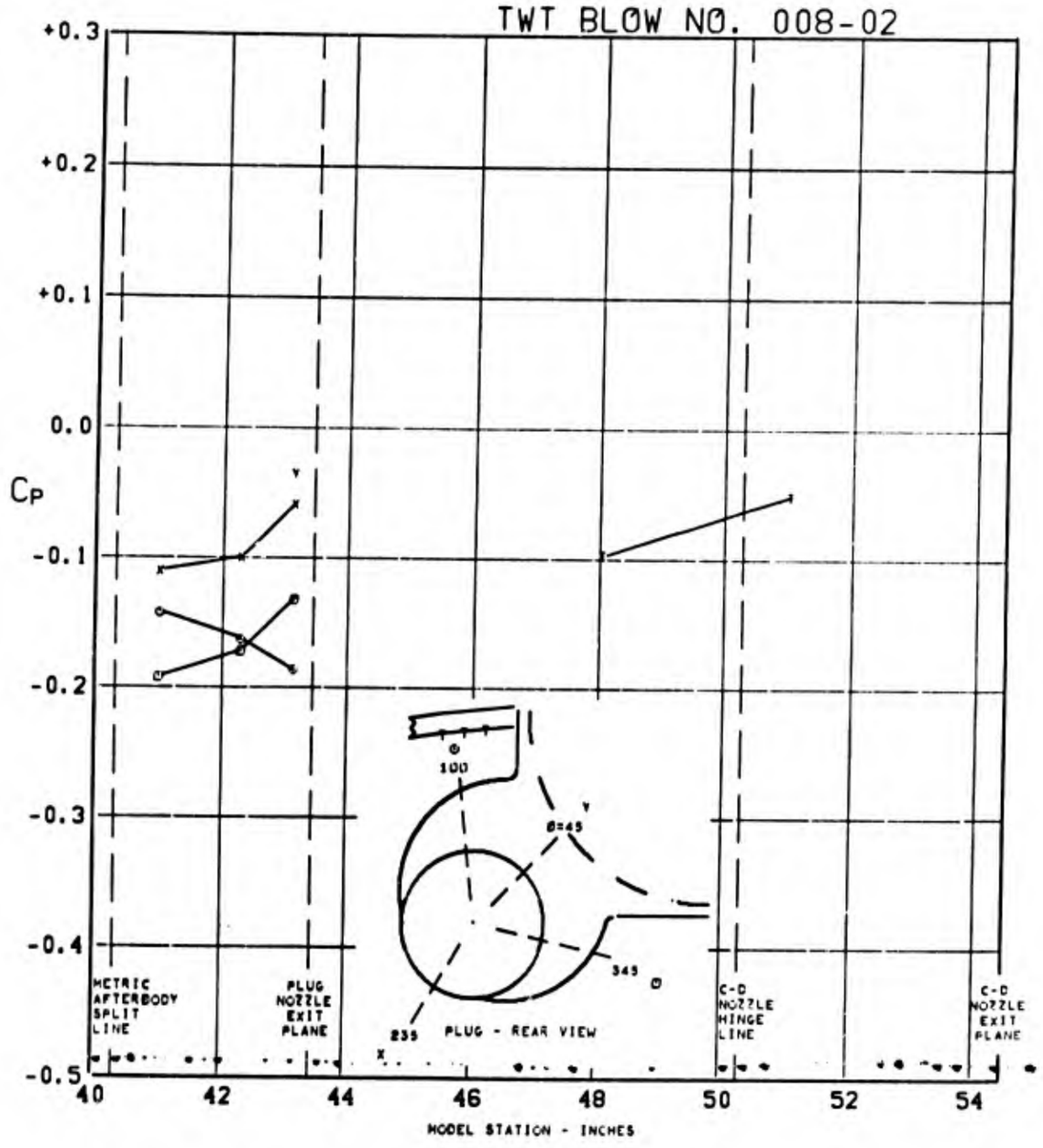

FIGURE 304. PRESSURE COEFFICIENTS ON TAIL & PLUG AFTERBODY (W1B1K1N1 P01 H1V1) Λ_{LE}=70° AT 0.850 M_0, $(P_T/P_0)_{C-D}$=CONE, $(P_T/P_0)_{PLUG}$=CONE, α= 2.8

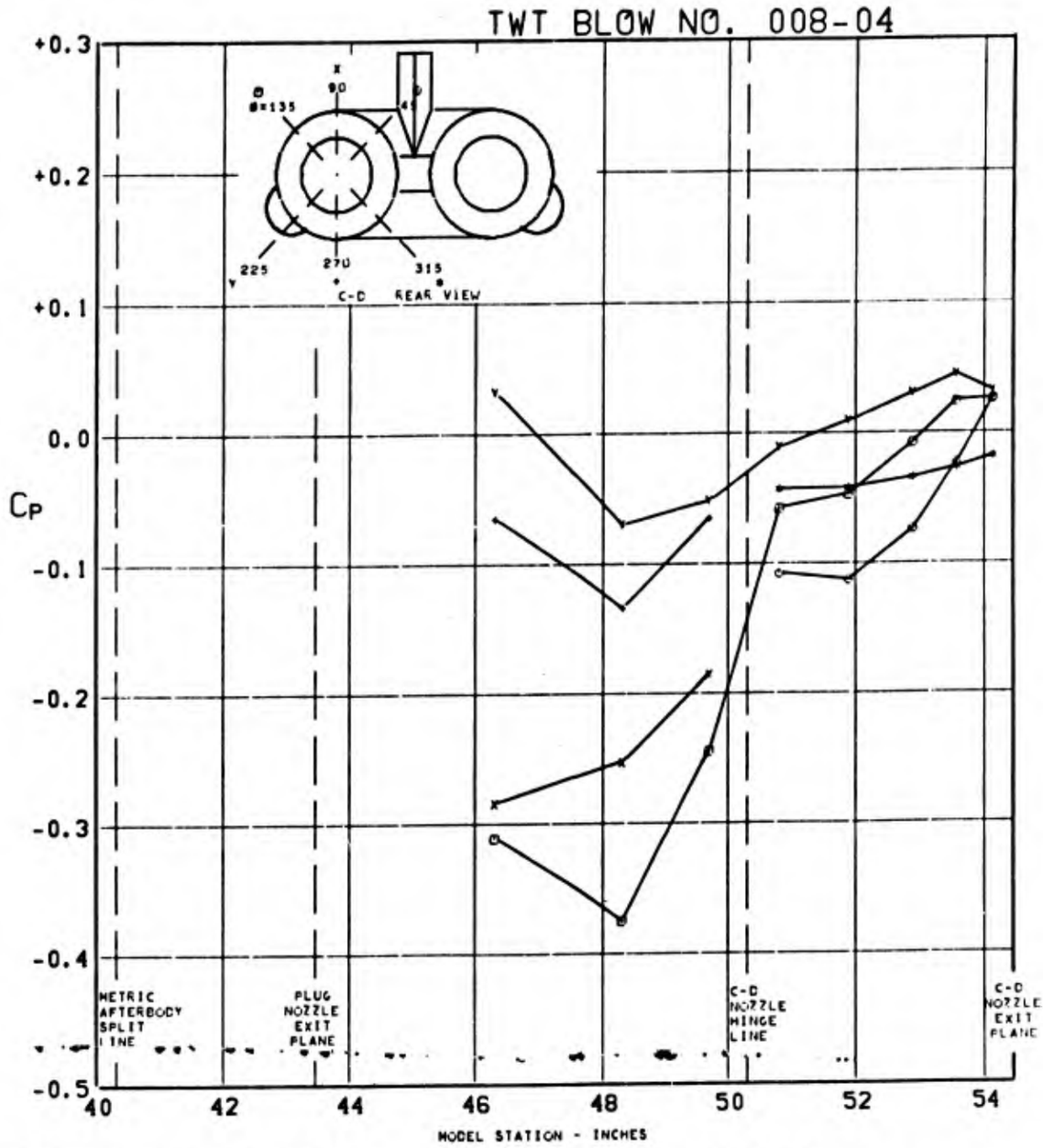

FIGURE 305. PRESSURE COEFFICIENTS ON C-D AFTERBODY (W1B1K1N1 P01 H1V1) $\Lambda_{LE}=70°$ AT 0.848 M_0, $(P_T/P_0)_{C-D}$=CONE, $(P_T/P_0)_{PLUG}$=CONE, α= 6.

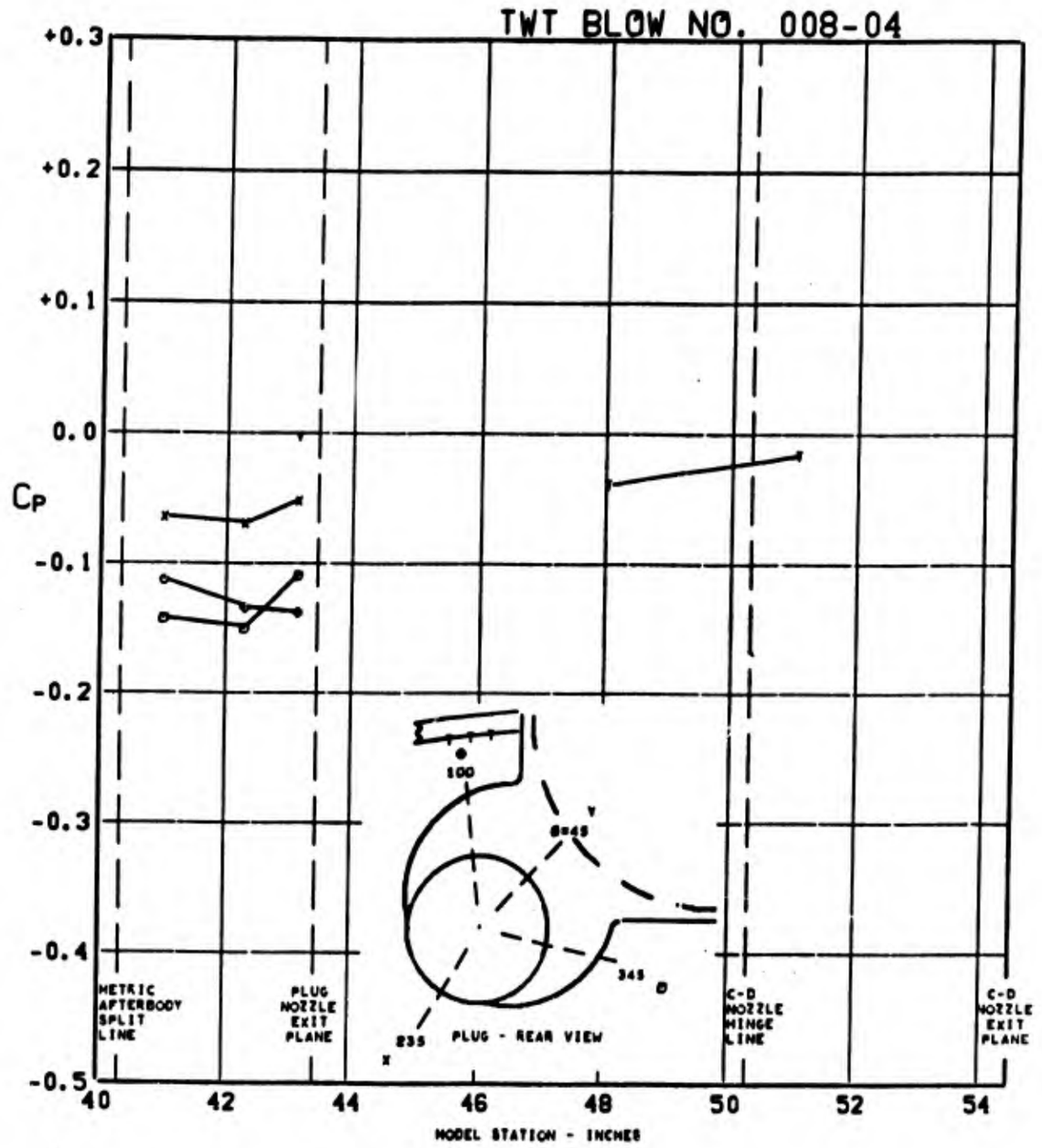

FIGURE 306. PRESSURE COEFFICIENTS ON TAIL & PLUG AFTERBODY (W1B1K1N1 P01 H1V1) Λ_{LE}=70° AT 0.848 M_0, $(P_T/P_0)_{C-D}$=CONE, $(P_T/P_0)_{PLUG}$=CONE, α= 6.8

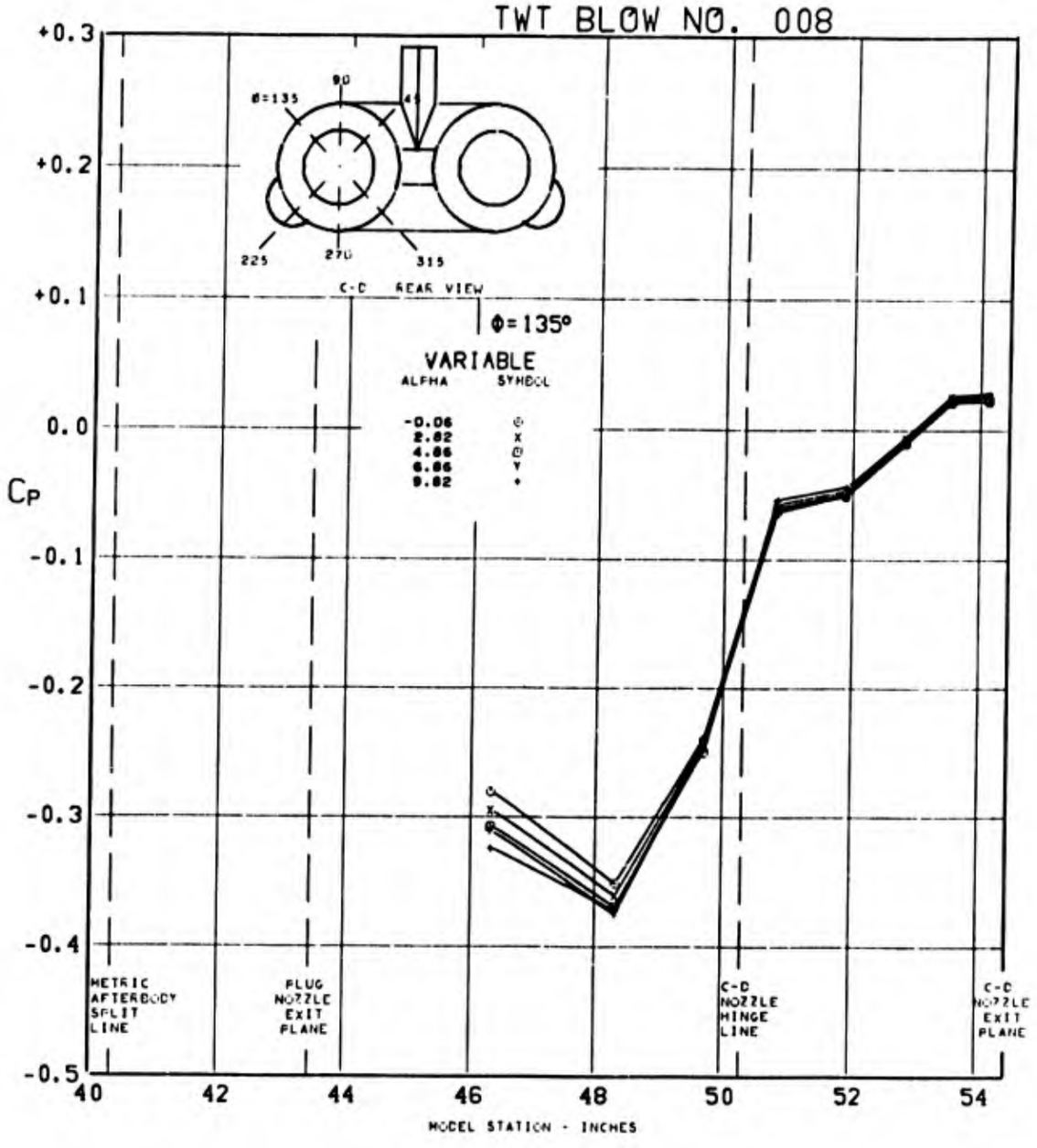

FIGURE 307. PRESSURE COEFFICIENTS ON C-D AFTERBODY (W1B1K1N1 P01 H1V1) $\Lambda_{LE}=70°$ AT 0.844 M_0, $(P_T/P_0)_{C-D}$=CONE, $(P_T/P_0)_{PLUG}$=CONE, α=VARY

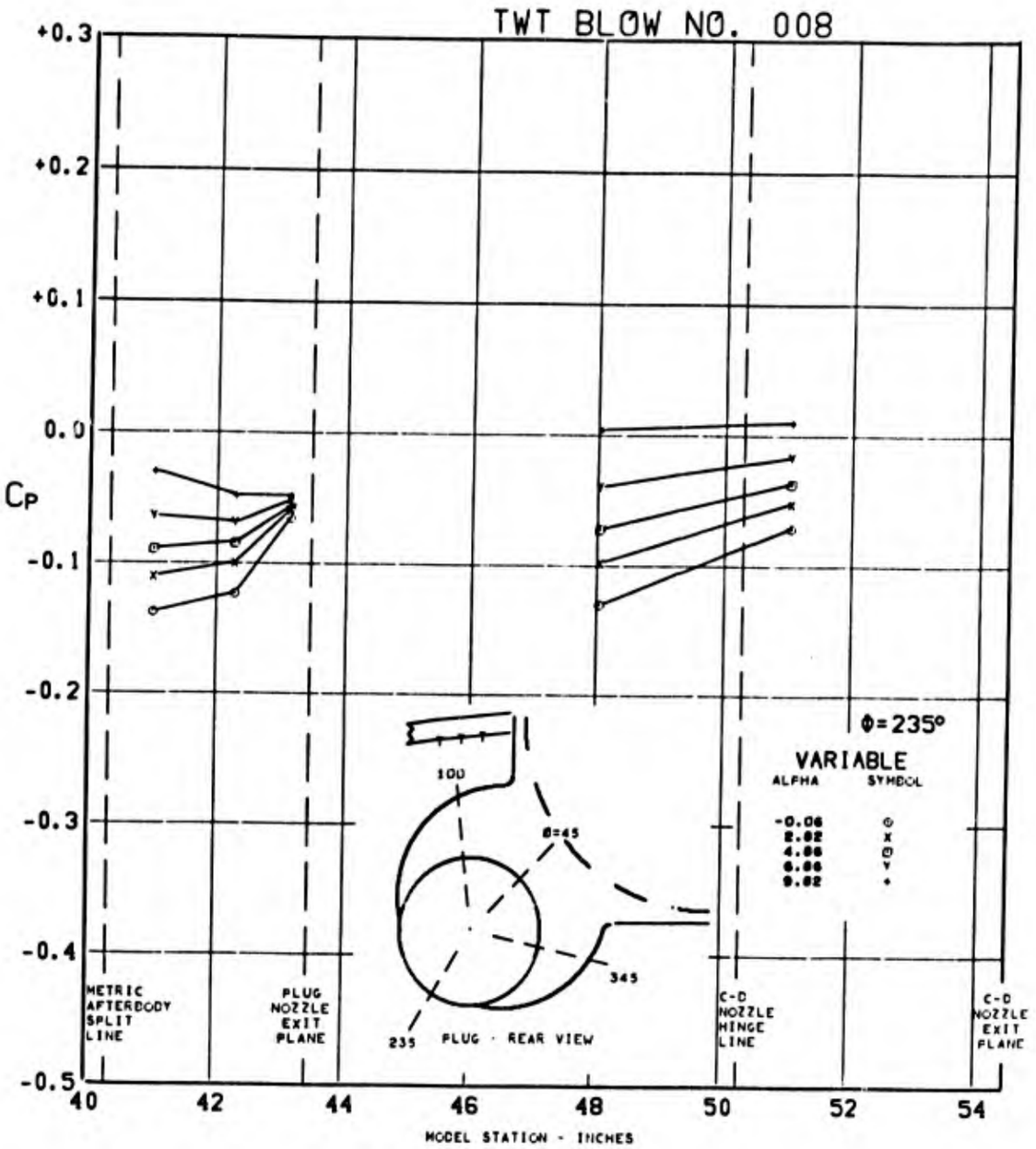

FIGURE 308. PRESSURE COEFFICIENTS ON TAIL & PLUG AFTERBODY (W1B1K1N1 P01 H1V1) Λ_{LE}=70° AT 0.844 M_0, $(P_T/P_0)_{C-D}$=CONE, $(P_T/P_0)_{PLUG}$=CONE, α=VARY

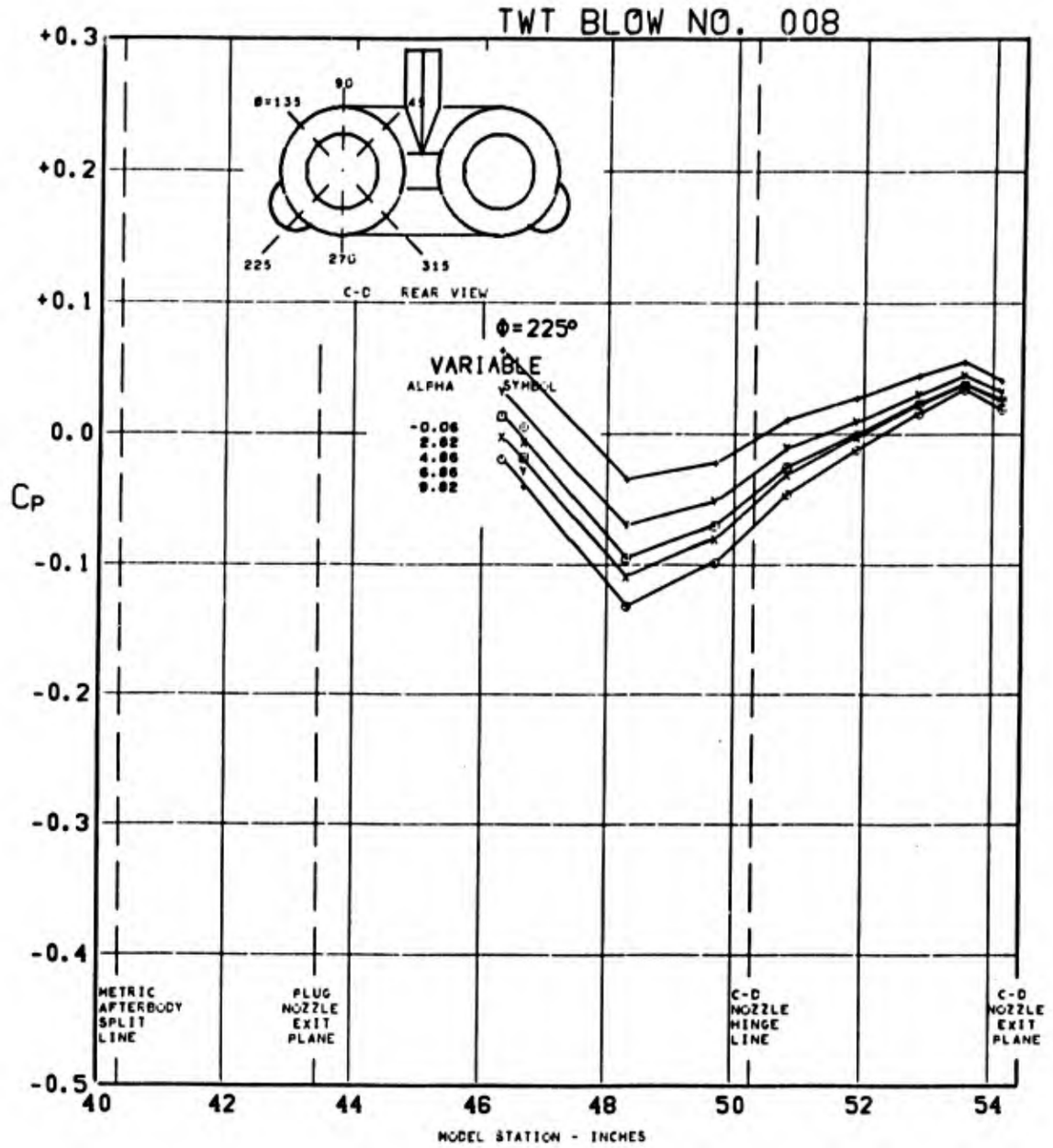

FIGURE 309. PRESSURE COEFFICIENTS ON C-D AFTERBODY (W1B1K1N1 P01 H1V1) $\Lambda_{LE}=70°$ AT 0.844 M_0, $(P_T/P_0)_{C-D}$=CONE, $(P_T/P_0)_{PLUG}$=CONE, α=VARY

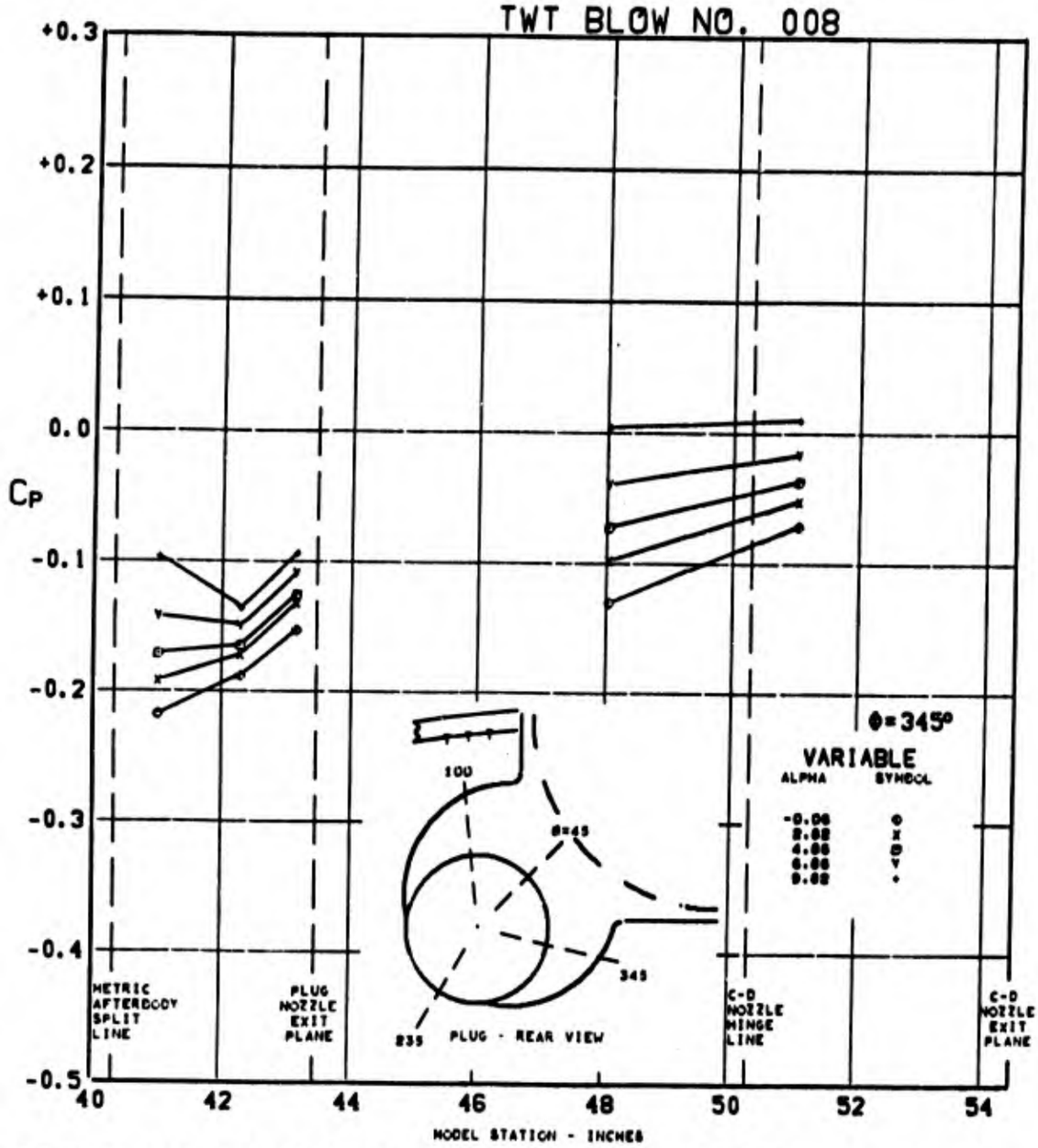

FIGURE 310. PRESSURE COEFFICIENTS ON TAIL & PLUG AFTERBODY (W1B1K1N1 P01 H1V1) Λ_{LE}=70° AT 0.844 M_0, $(P_T/P_0)_{C-D}$=CONE, $(P_T/P_0)_{PLUG}$=CONE, α=VARY

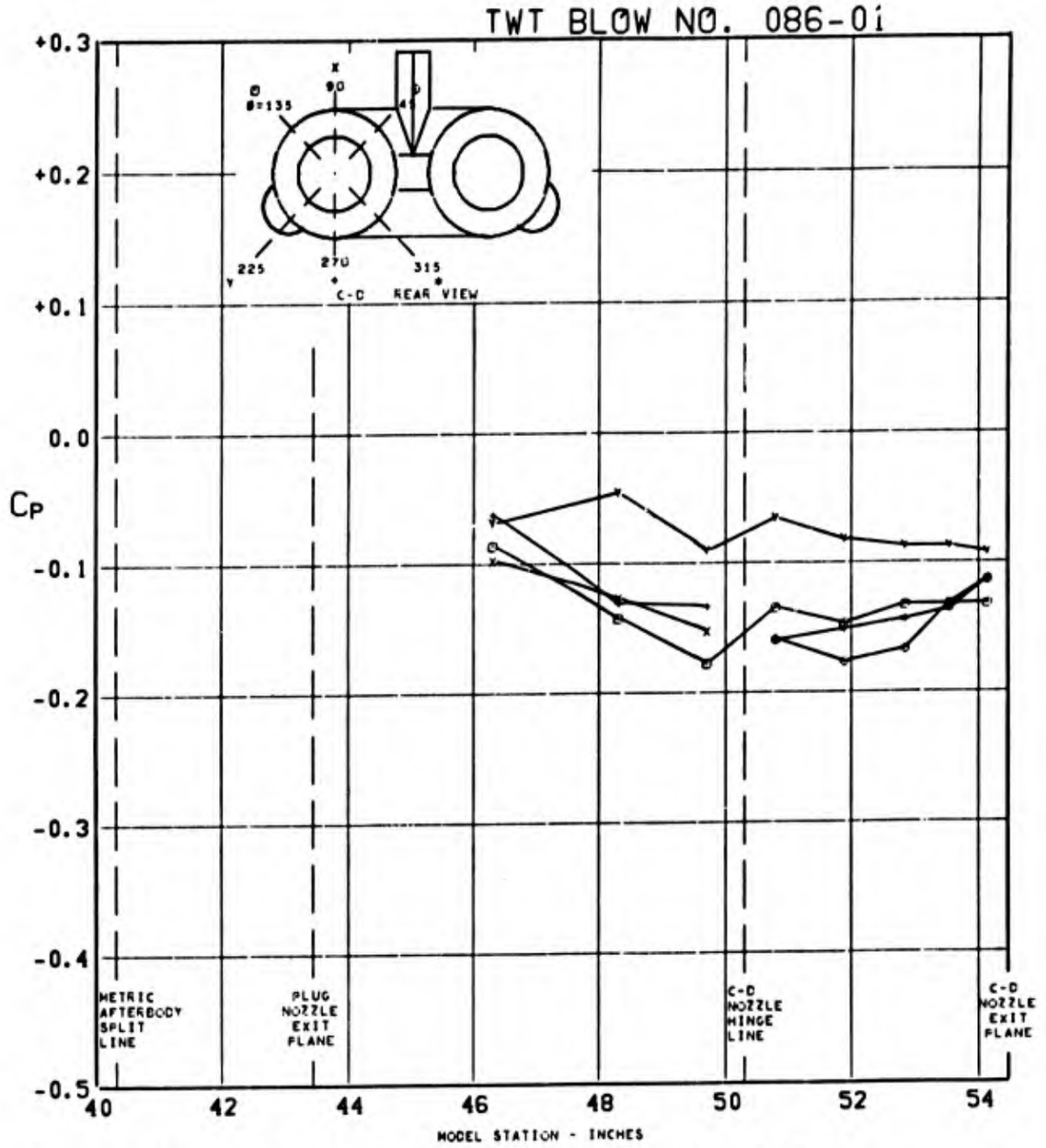

FIGURE 311. PRESSURE COEFFICIENTS ON C-D AFTERBODY (W1B1K1N1 P01 H1V1) Λ_{LE}=70° AT 1.998 M_0, $(P_T/P_0)_{C-D}$=CONE, $(P_T/P_0)_{PLUG}$=CONE, α= 0.0

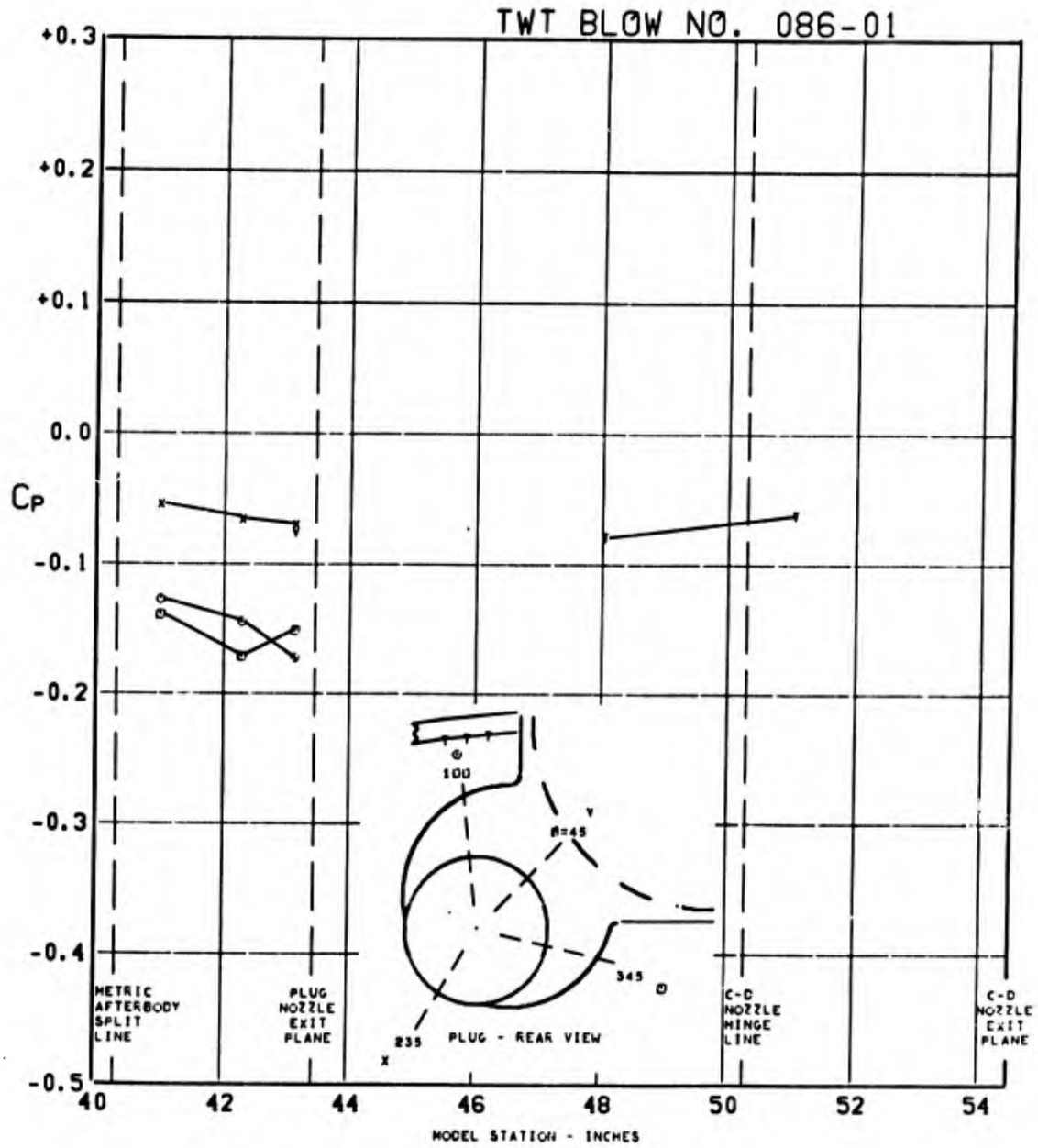

FIGURE 312. PRESSURE COEFFICIENTS ON TAIL & PLUG AFTERBODY (W1B1K1N1 P01 H1V1) Λ_{LE}=70° AT 1.998 M_0, $(P_T/P_0)_{C-D}$=CONE, $(P_T/P_0)_{PLUG}$=CONE, α= 0.0

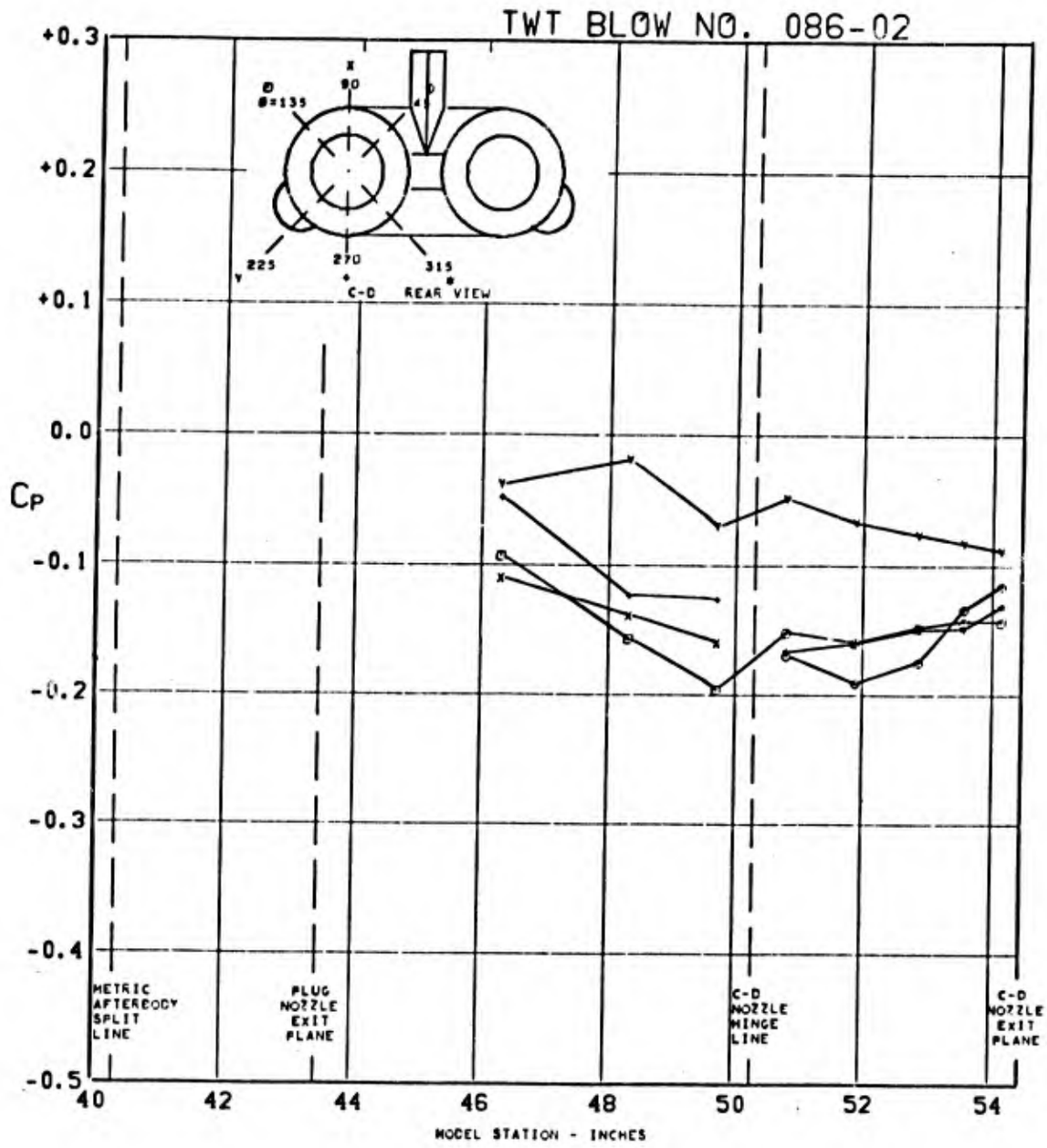

FIGURE 313. PRESSURE COEFFICIENTS ON C-D AFTERBODY (W1B1K1N1 P01 H1V1) $\Lambda_{LE}=70°$ AT 1.998 M_0, $(P_T/P_0)_{C-D}$=CONE, $(P_T/P_0)_{PLUG}$=CONE, α= 2.8

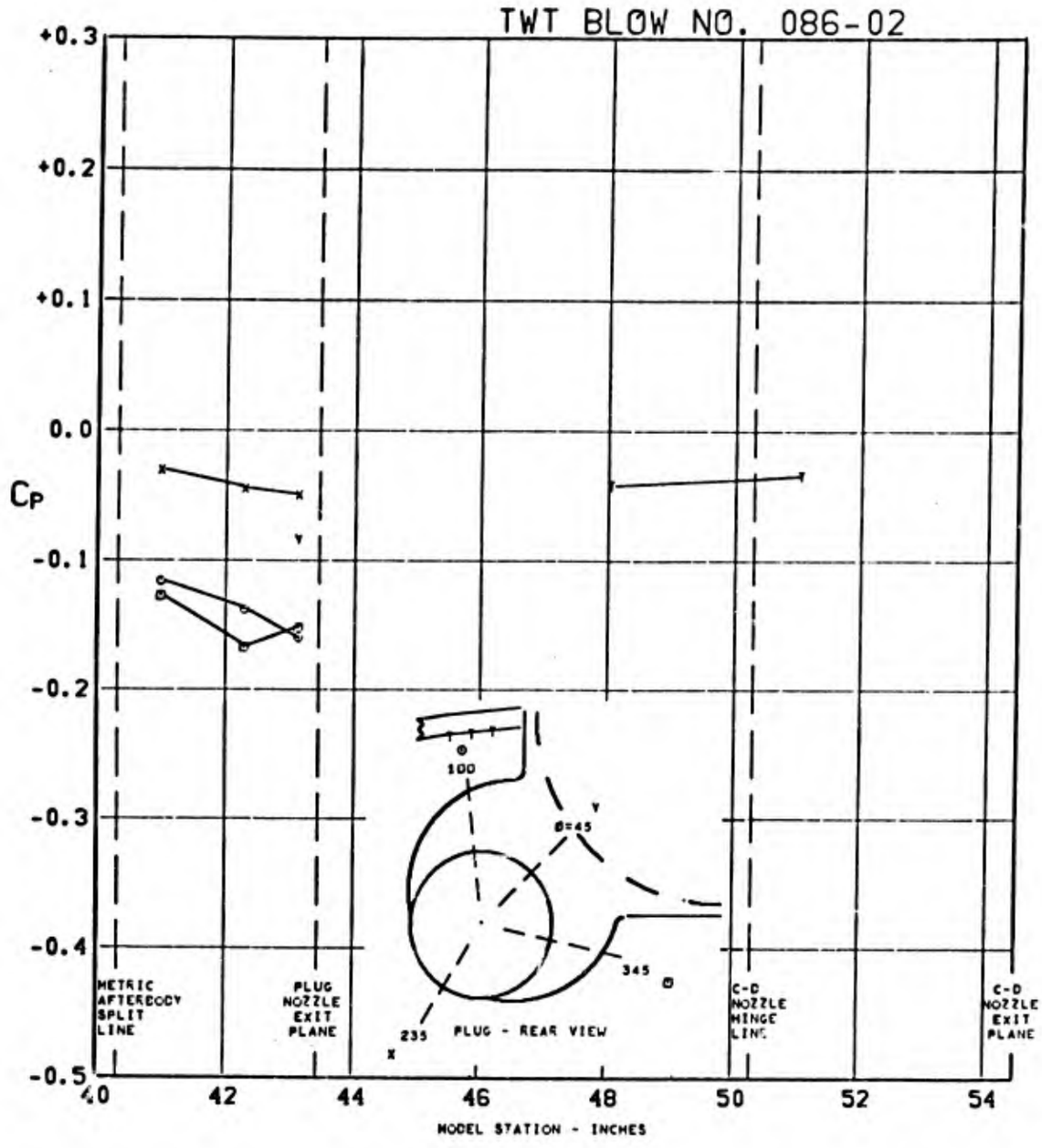

FIGURE 314. PRESSURE COEFFICIENTS ON TAIL & PLUG AFTERBODY (W1B1K1N1 P01 H1V1) Λ_{LE}=70° AT 1.998 M_0, $(P_T/P_0)_{C-D}$=CONE, $(P_T/P_0)_{PLUG}$=CONE, α= 2.8

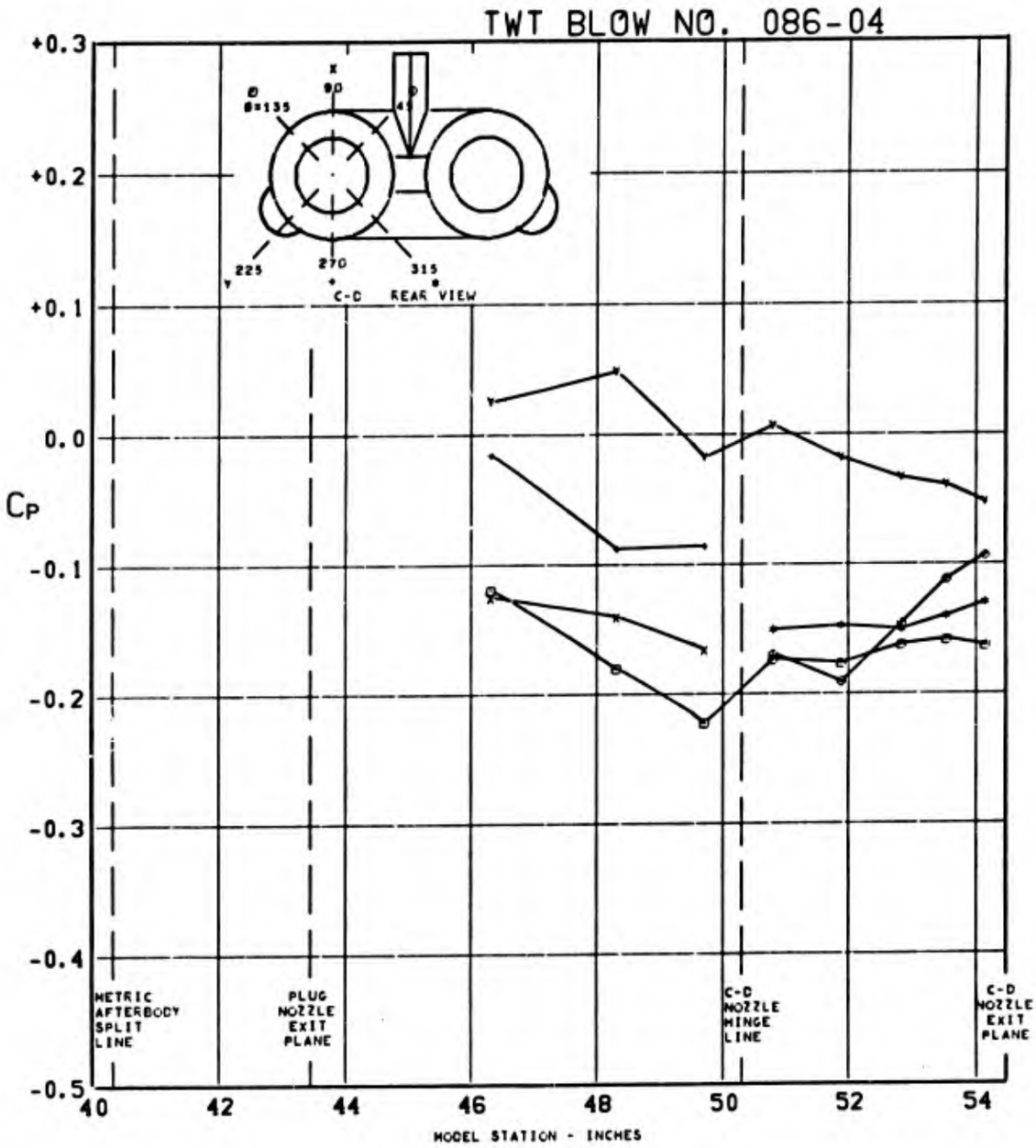

FIGURE 315. PRESSURE COEFFICIENTS ON C-D AFTERBODY (W1B1K1N1 P01 H1V1) Λ_{LE}=70° AT 1.998 M_0, $(P_T/P_0)_{C-D}$=CONE, $(P_T/P_0)_{PLUG}$=CONE, α= 6.8

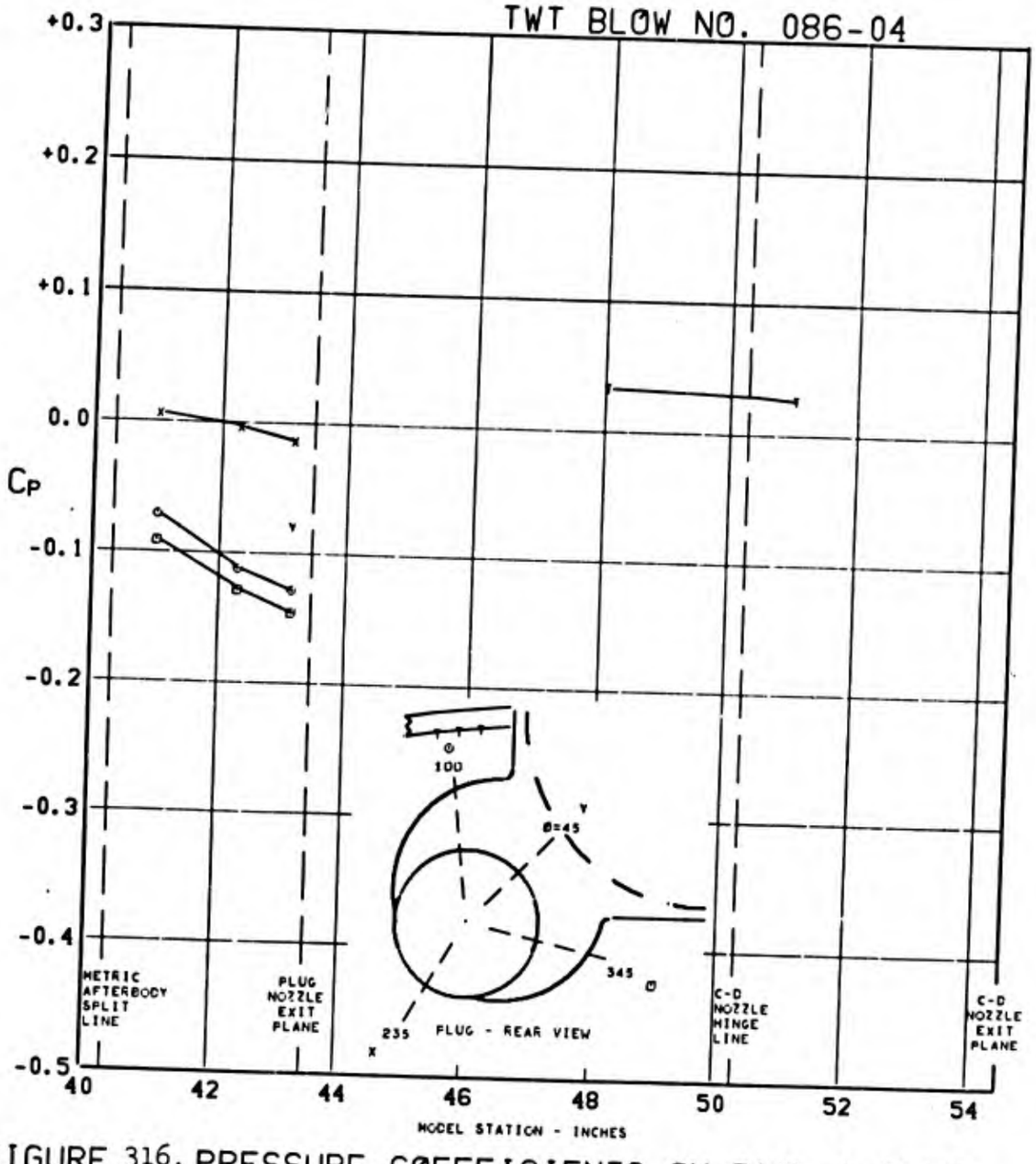

FIGURE 316. PRESSURE COEFFICIENTS ON TAIL & PLUG AFTERBODY (W1B1K1N1 P01 H1V1) Λ_{LE}=70° AT 1.998 M_0, $(P_T/P_0)_{C-D}$=CONE, $(P_T/P_0)_{PLUG}$=CONE, α= 6.8

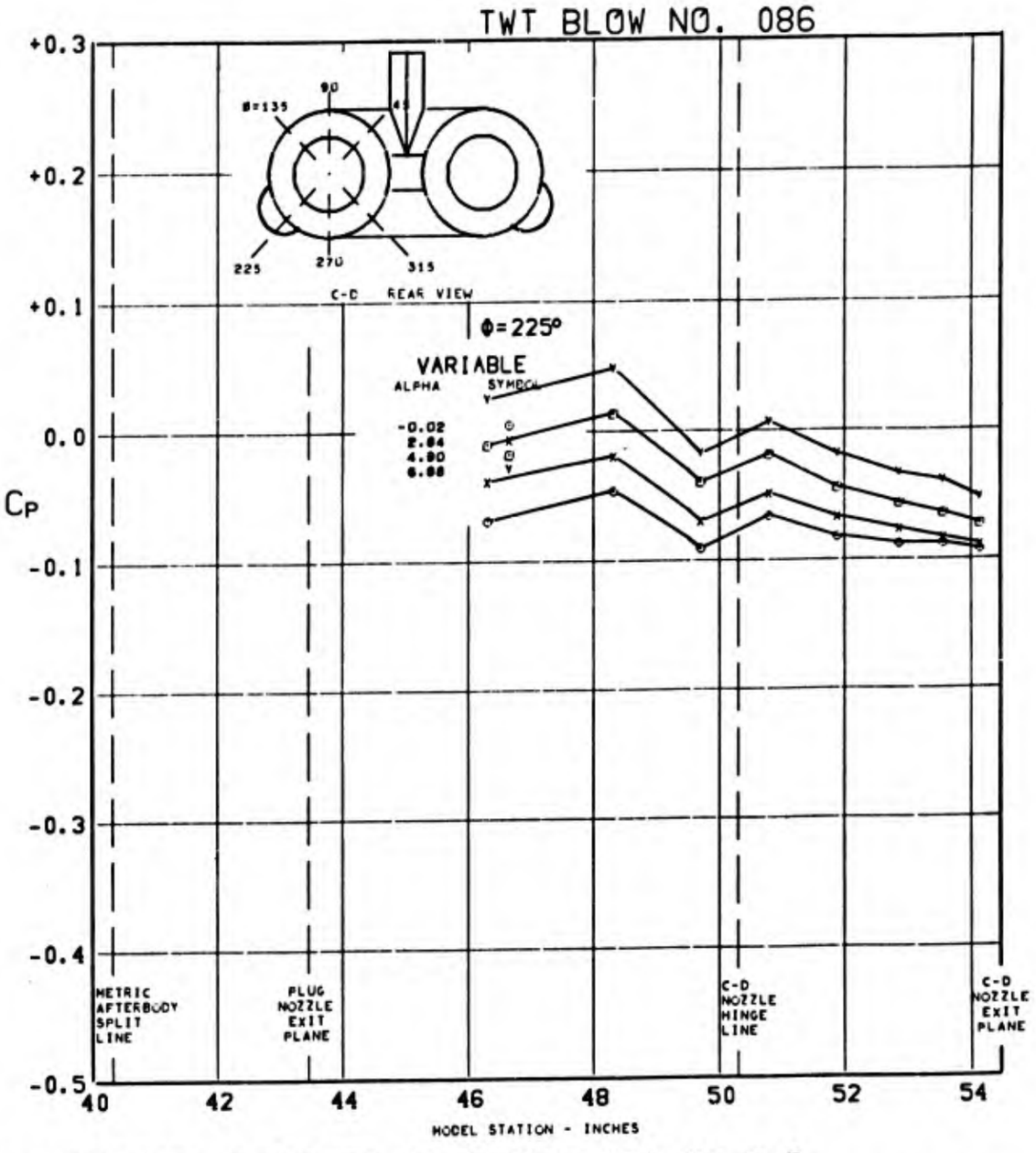

FIGURE 317. PRESSURE COEFFICIENTS ON C-D AFTERBODY (W1B1K1N1 P01 H1V1) Λ_{LE}=70° AT 1.998 M_0, $(P_T/P_0)_{C-D}$=CONE, $(P_T/P_0)_{PLUG}$=CONE, α=VARY

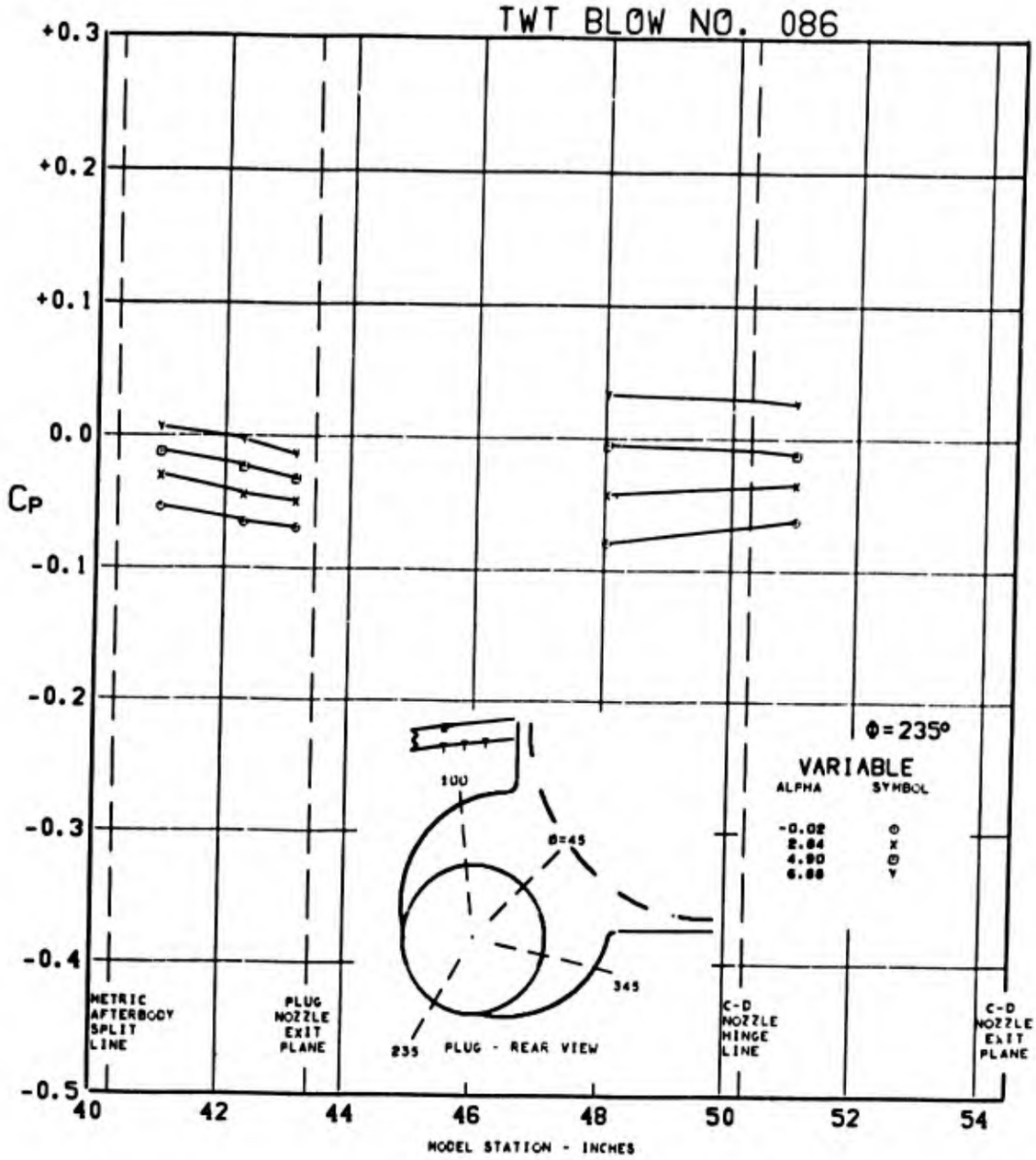

FIGURE 318. PRESSURE COEFFICIENTS ON TAIL & PLUG AFTERBODY (W1B1K1N1 P01 H1V1) $\Lambda_{LE}=70°$ AT 1.998 M_0, $(P_T/P_0)_{C-D}$=CONE, $(P_T/P_0)_{PLUG}$=CONE, α=VARY

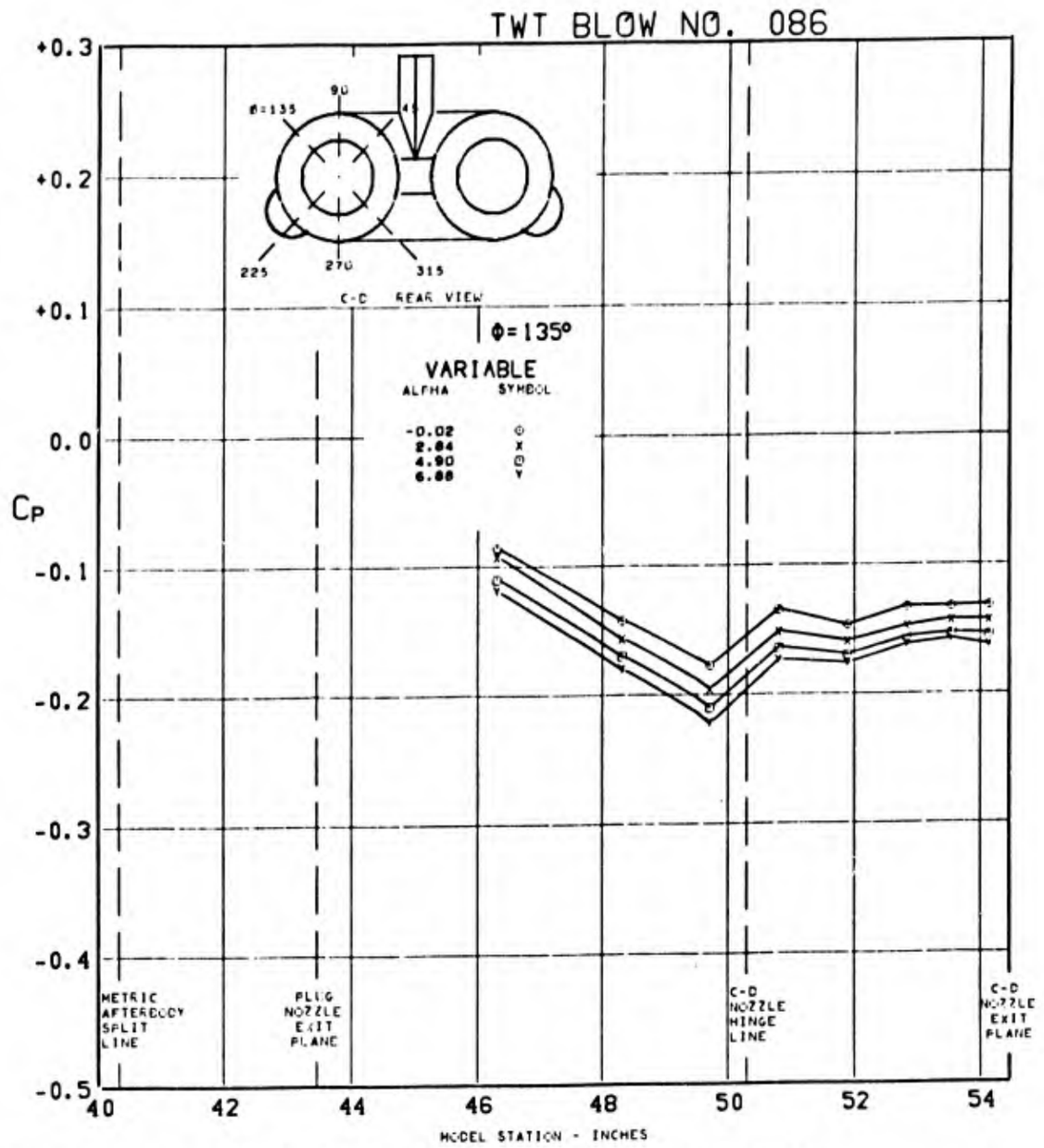

FIGURE 319. PRESSURE COEFFICIENTS ON C-D AFTERBODY (W1B1K1N1 P01 H1V1) Λ_{LE}=70° AT 1.998 M_0, $(P_T/P_0)_{C-D}$=CONE, $(P_T/P_0)_{PLUG}$=CONE, α=VARY

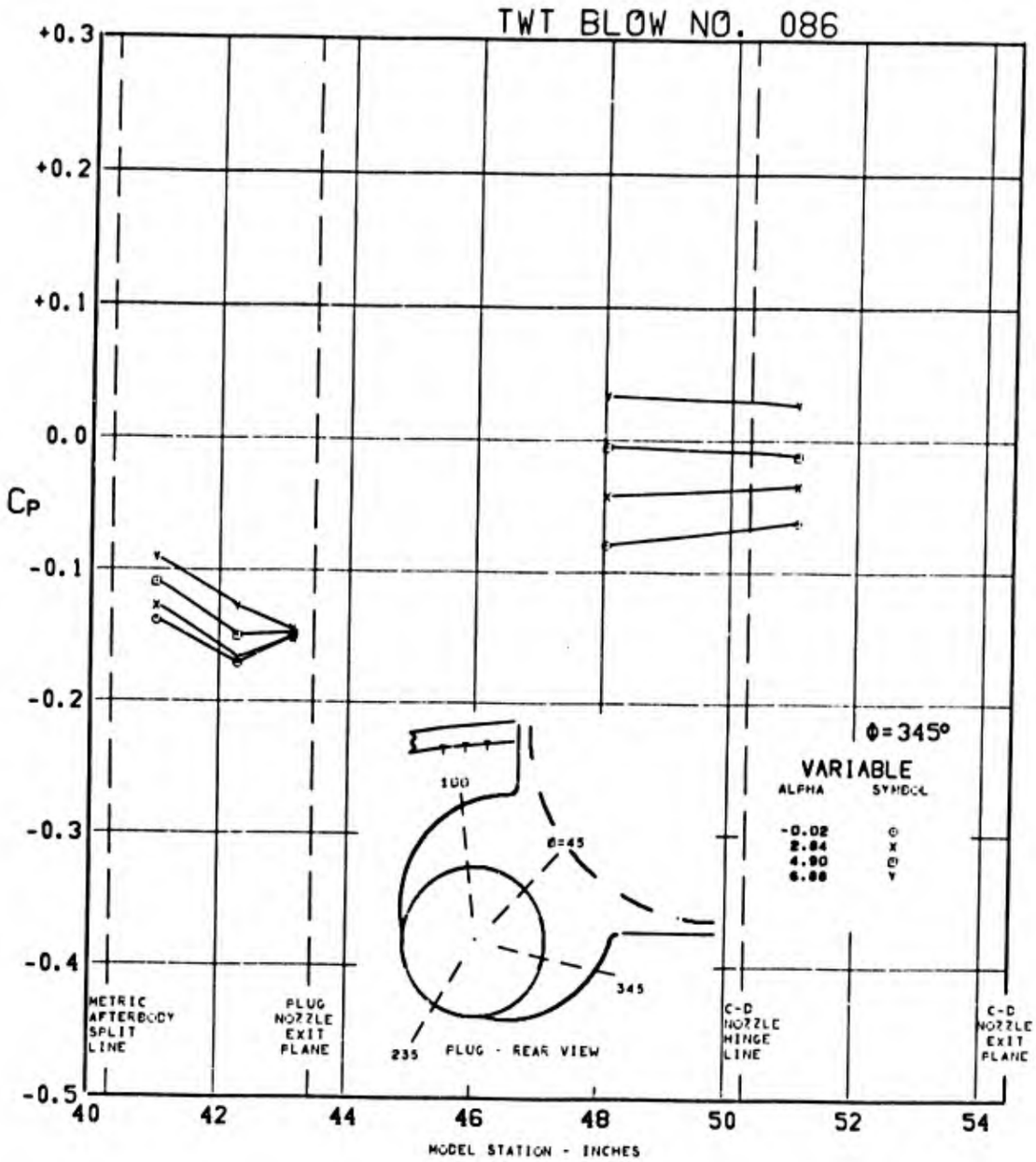

FIGURE 320 PRESSURE COEFFICIENTS ON TAIL & PLUG AFTERBODY (W1B1K1N1 P01 H1V1) $\Lambda_{LE}=70°$ AT 1.998 M_0, $(P_T/P_0)_{C-D}$=CONE, $(P_T/P_0)_{PLUG}$=CONE, α=VARY

APPENDIX

DISCUSSION OF CHORD FORCE BALANCE MEASUREMENTS

In section IV of this report, a discussion of chord force balance data was presented. It was stated in this section that the chord force balance data was somewhat questionable because of the corrections which must be applied to the basic balance measurement. The tare forces were caused by pressures acting on the inside of the C-D nozzle shroud. These pressures varied with C-D nozzle pressure ratio and were created at the internal split between the nozzle shroud and the nozzle liner (see figure 1). The split was located internally to avoid having a gap on the external surface near the aft end of the nozzle which might disturb the flow pattern. The pressures inside the shroud were measured during a blow and the pressure-area term was used to correct the measured chord force. It appears, however, that there were pressures acting on the shroud lip (see figure 7) that could not be measured during this test that were affecting the balance reading. When air was blown through the C-D nozzles with the tunnel air at rest, the corrected balance reading was still not zero. The actual reading, which is called a static correction, was applied to the corrected balance reading to adjust the balance data. The tare forces and the static correction forces were sometimes quite large, thus making these force data questionable.

Figures 321 through 326 show the chord force balance and pressure data for an A_9/A_M of .30 and .50 for three mach numbers: 85, 1.27 and 1.7. The data presented includes the baseline chord force value for both the balance and pressure data so that the change in incremental chord force may be seen. Uncorrected balance data shown in these figures is uncorrected in the sense that the static correction has not been included. The pressure-area corrections, however, have been included in this uncorrected data. Corrected balance data includes both the static correction plus the pressure-area correction.

Comparison of the chord force increment for the corrected balance data and the integrated pressure results indicates reasonably good agreement except for subsonic mach number conditions. At both subsonic and supersonic mach numbers, the chord force increment comparisons between the balance and pressure data deviate the greatest at pressure ratios approaching and including the nozzle separation region. This fact casts some doubt as to the validity of the pressure ratio correction for this range of pressure ratios.

(The reverse of this page is blank)

BLANK PAGE

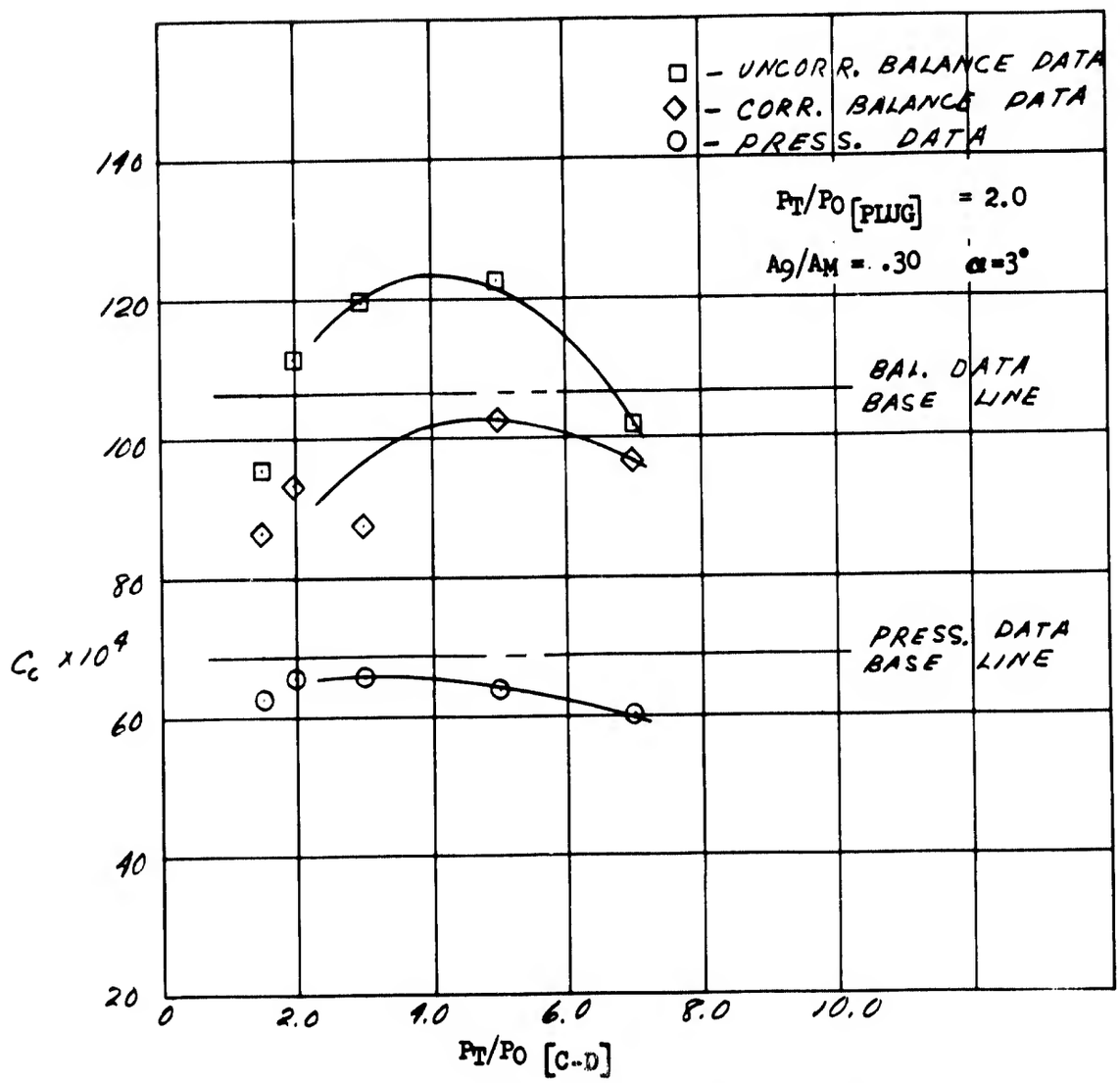

Figure 321. Chord Force Balance Measurements - M = .85

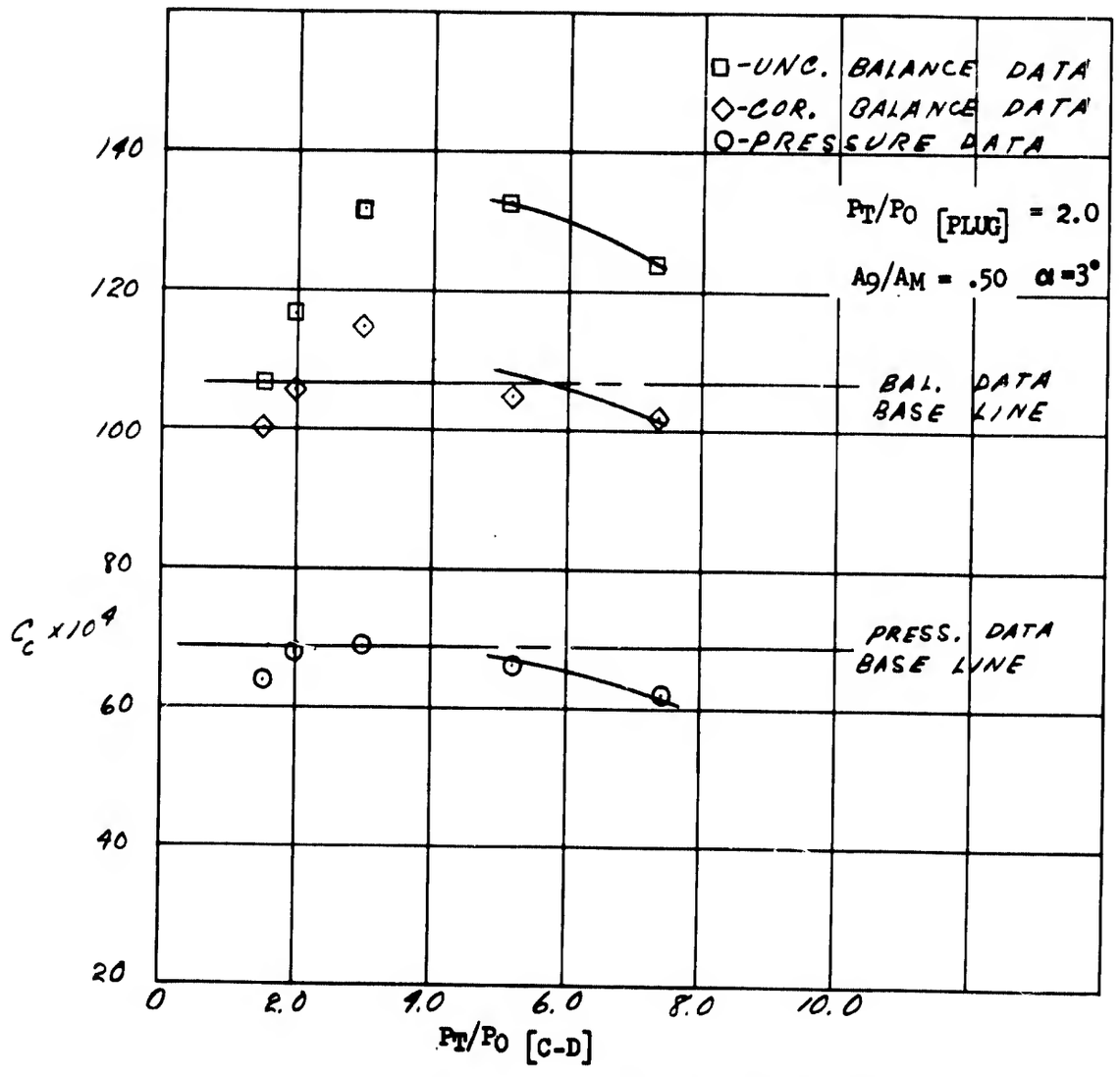

Figure 322. Chord Force Balance Measurements - M = .85

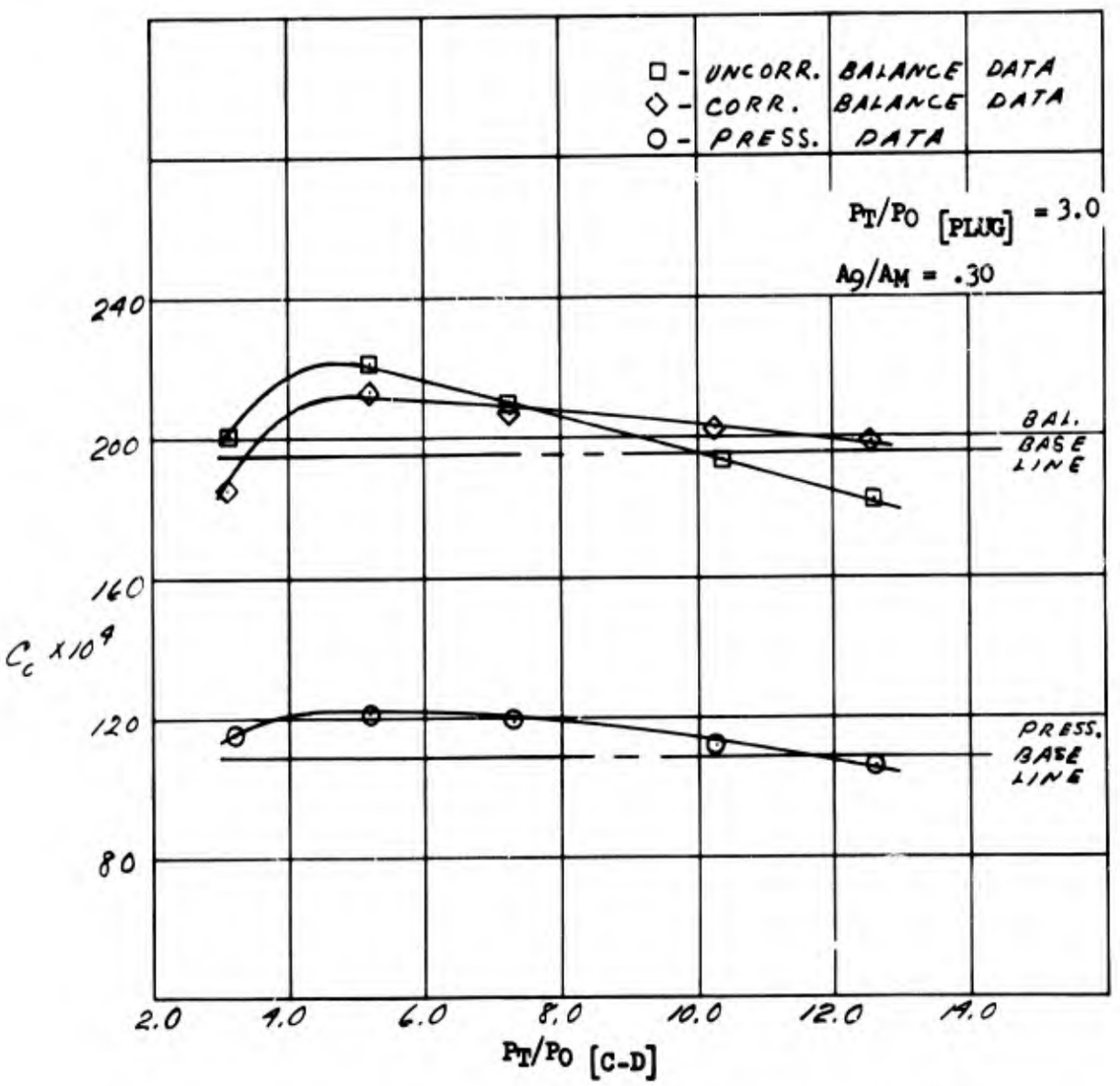

Figure 323. Chord Force Balance Measurements - M = 1.27

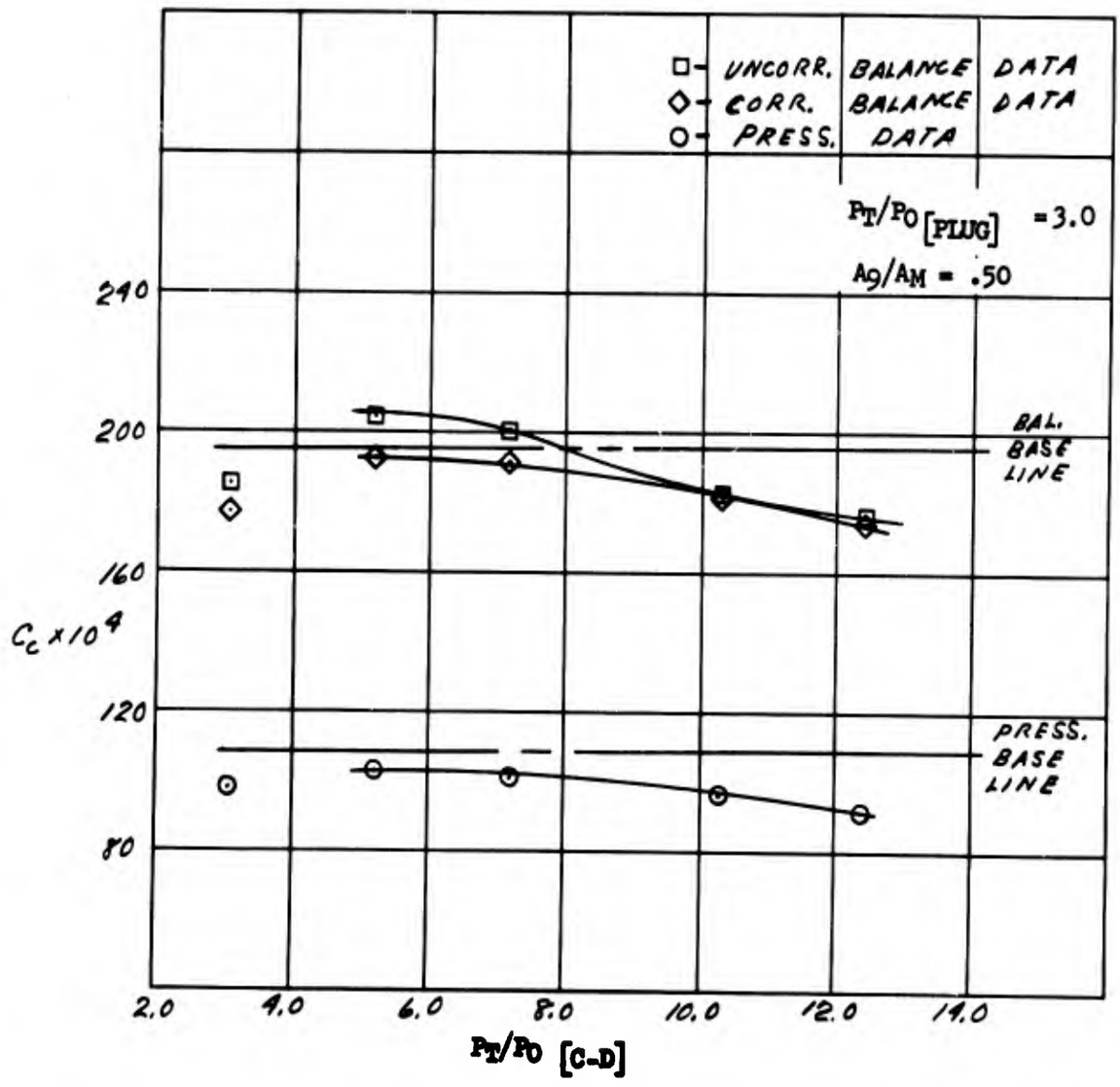

Figure 324. Chord Force Balance Measurements - M = 1.27

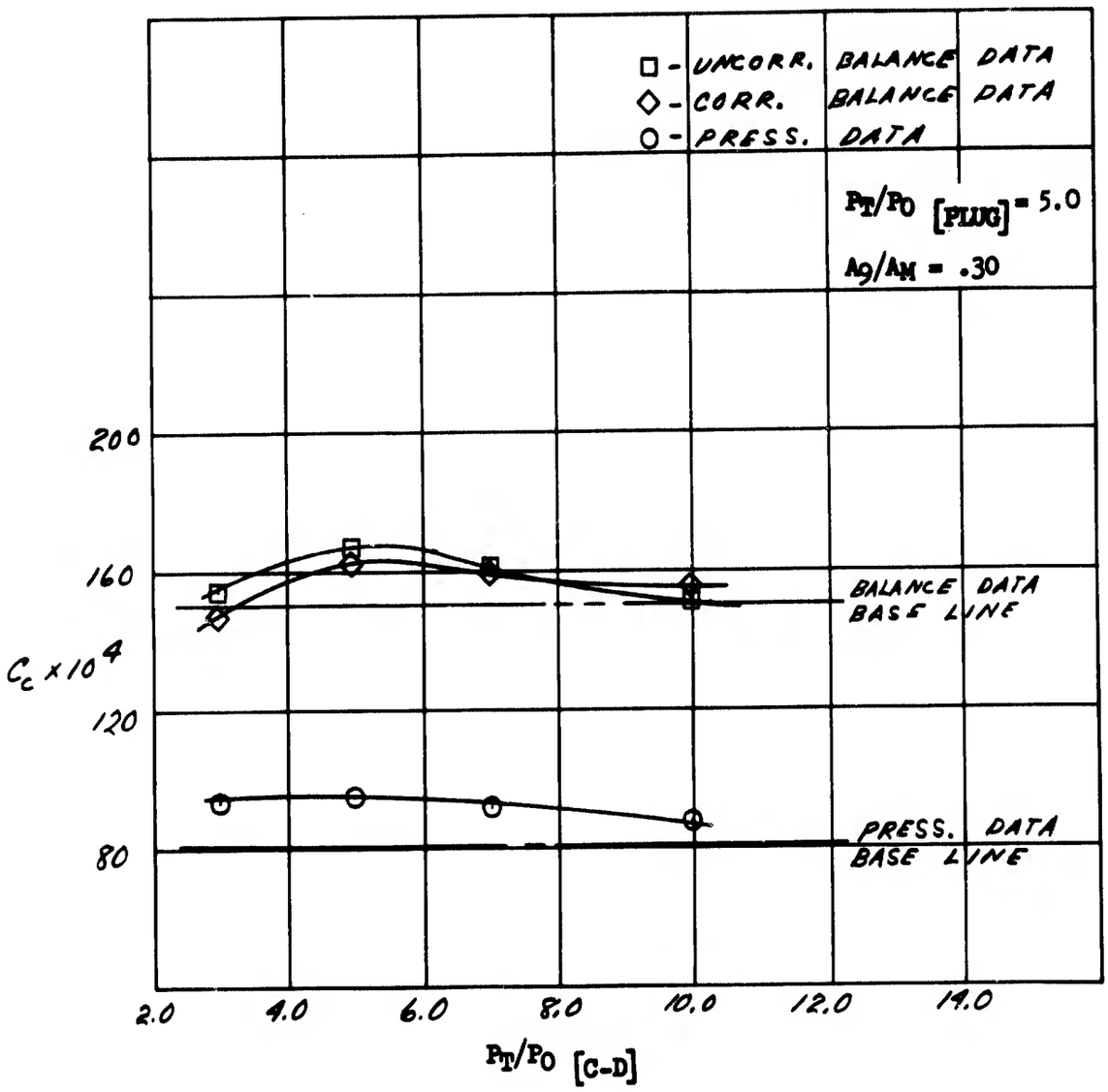

Figure 325. Chord Force Balance Measurements - M = 1.7

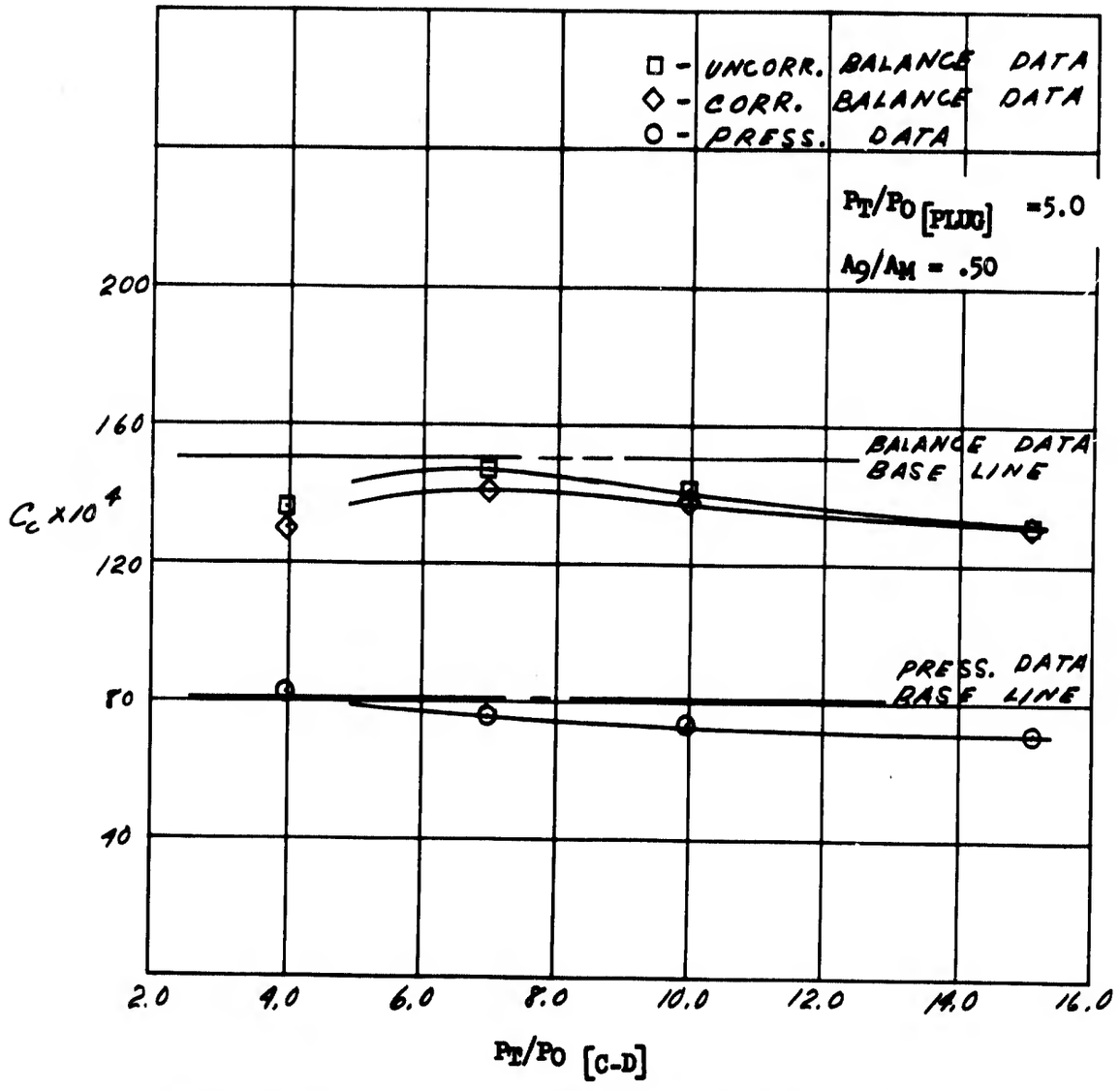

Figure 326. Chord Force Balance Measurements - M = 1.7

UNCLASSIFIED

Security Classification

DOCUMENT CONTROL DATA - R & D

(Security classification of title, body of abstract and indexing annotation must be entered when the overall report is classified)

1 ORIGINATING ACTIVITY (Corporate author)

Los Angeles Division
North American Rockwell Corporation

2a. REPORT SECURITY CLASSIFICATION

UNCLASSIFIED

2b. GROUP

- - -

3 REPORT TITLE

NOZZLE INTERACTION DRAG TESTS
PROPULSION SYSTEM INTEGRATION AND TEST PROGRAM (STEADY STATE)

4 DESCRIPTIVE NOTES *(Type of report and inclusive dates)*

Phase End Technical Report (6 January 1969 through 13 January 1969)

5 AUTHOR(S) *(First name, middle initial, last name)*

Robert C. Westphal and Robert H. Johnson

6 REPORT DATE	7a. TOTAL NO OF PAGES	7b. NO OF REFS
June 1969	384 + i through xiv	3

8a. CONTRACT OR GRANT NO.	9a. ORIGINATOR'S REPORT NUMBER(S)
F33615-67-C-1829	NA-68-939 Part III
b. PROJECT NO. 668A and 3066	
c.	9b. OTHER REPORT NO(S) *(Any other numbers that may be assigned this report)* AFAPL-TR-69-44, Part III
d.	

10 DISTRIBUTION STATEMENT This document is subject to special export controls and each transmittal to foreign governments or foreign nationals may be made only with prior approval of The Air Force Aero Propulsion Laboratory (APTA), Air Force Systems Command, Wright-Patterson Air Force Base, Ohio.

11 SUPPLEMENTARY NOTE	12 SPONSORING MILITARY ACTIVITY
None	Air Force Aero Propulsion Laboratory Air Force Systems Command Wright-Patterson Air Force Base, Ohio

13 ABSTRACT

Near wake and far wake nozzle jet effects on forces on the aft end of a .09 scale simulated fighter airplane were tested at mach numbers of .6, .85, 1.27, 1.7 and 2.0. Cold air was used for producing the simulated engine exhaust jets. Model configuration changes included various boattail angles, inlet bluntness, wing sweep, and horizontal tail on and off. Data obtained include chord force, normal force, and pitching moment from an internal balance, external static pressure distributions and chord force determined from integrated pressures, and schlieren and shadowgraph photographs of exhaust plumes. At subsonic mach numbers, the far wake jet effects of plug nozzles located forward on the afterbody were unfavorable. At supersonic mach numbers, the plug nozzle far-wake effects were favorable. Jet effects of the convergent-divergent nozzles located at the aft end of the model were favorable for all mach numbers.

DD FORM 1 NOV 68 1473

UNCLASSIFIED

Security Classification

14 KEY WORDS	LINK A		LINK B		LINK C	
	ROLE	WT	ROLE	WT	ROLE	WT
Nozzle performance						
Nozzle exhaust interaction						
Nozzle drag						
Wind tunnel nozzle tests						